antioxidants

Special Issue Reprint

# Ionizing Radiation, Antioxidant Response and Oxidative Damage

## Radiomodulators

Edited by
Elena Obrador and Alegria Montoro

www.mdpi.com/journal/antioxidants

MDPI

# Ionizing Radiation, Antioxidant Response and Oxidative Damage: Radiomodulators

# Ionizing Radiation, Antioxidant Response and Oxidative Damage: Radiomodulators

Editors

**Elena Obrador**
**Alegria Montoro**

MDPI • Basel • Beijing • Wuhan • Barcelona • Belgrade • Manchester • Tokyo • Cluj • Tianjin

*Editors*
Elena Obrador
University of Valencia
Valencia, Spain

Alegria Montoro
The University and
Politechnic La Fe Hospital
Valencia, Spain

*Editorial Office*
MDPI
St. Alban-Anlage 66
4052 Basel, Switzerland

This is a reprint of articles from the Special Issue published online in the open access journal *Antioxidants* (ISSN 2076-3921) (available at: https://www.mdpi.com/journal/antioxidants/special_issues/Radiation_Oxidative_Damage_Radiomodulators).

For citation purposes, cite each article independently as indicated on the article page online and as indicated below:

LastName, A.A.; LastName, B.B.; LastName, C.C. Article Title. *Journal Name* **Year**, *Volume Number*, Page Range.

**ISBN 978-3-0365-8188-0 (Hbk)**
**ISBN 978-3-0365-8189-7 (PDF)**

# Contents

# About the Editors

**Elena Obrador**

Honors degree in pharmacy and awarded with the First National Prize for University Studies (1994). Cum laude Ph.D. in physiology and Extraordinary Doctorate Award (1998). Full Professor of Physiology and Director of the Cell Pathophysiology Unit (UFC) at the University of Valencia. Professor in the master's degree of physiology (UV) and the master's degree of biomedical engineering (UV-UPV). My research work is focused on the development of strategies to selectively decrease the antioxidant defense against metastatic cancer cells in order to sensitize them to the antitumor effects of chemo- or radiotherapy. Some key milestones reached are: selective GSH depletion in cancer models in vivo, as well as the development of the molecular bases of therapeutic strategies that increase the efficacy of cancer treatments and eliminate melanoma metastases. Our group also works on the potential benefits of natural polyphenols in radioprotection, cancer and amyotrophic lateral sclerosis (ALS) treatment, and has filed 5 international patents. To date, I have published 58 scientific papers in international journals of the JCR ranking (ORCID 0000-0002-5934-5543) and several book chapters. Recently, we have set up a startup company (Scientia Biotech) to develop clinical applications of non-ionizing radiations in Oncotherapy.

**Alegría Montoro**

Bachelor in Biological Sciences by the University of Valencia (UV, 2001), cum laude Ph.D. and Extraordinary Doctorate Award by the Polytechnic University of Valencia (UPV, 2006). Master's degree in occupational hazard prevention, specialized in hygiene (2002) and security and in epidemiology and public health (2022). I am supervisor for Radioactive Facilities and Head of the Biodosimetry Laboratory in the Radiation Protection Service (RPS), University and Polytechnic La Fe Hospital, Valencia (Spain). My research work is focused on radiobiology, biodosimetry, radioprotectors and radiomitigators, radiosensitivity and nuclear/radiological emergencies. Some key milestones reached include the automation of biodosimetry techniques, with support from FEDER EU funding and the Valencian Government. To date, I have published 48 scientific papers in international journals of JCR ranking (ORCID 0000-0003-1662-1592) and have filed one international patent. Professor of radiobiology courses for the master's degree in radiation protection (UPV) and courses of medical countermeasures in the master's degree in personalized and community nutrition (UV). I am involved in international networks RENEB, REMPAN, BioDoseNet and EURAMED.

# Preface to "Ionizing Radiation, Antioxidant Response and Oxidative Damage: Radiomodulators"

Ionizing radiation (IR) can produce deleterious effects in living tissues, leading to significant morbidity and a potentially fatal illness that affects various organs in a dose-dependent manner. The term Radiomodulator includes Radioprotectors, Radiomitigators and Radiosensitizers. Radioprotectors and radiomitigators reduce or attenuate IR damages even when radiomitigators are administered after IR exposition. On the contrary, radiosensitizers potentiate the harmful effects of IR which can help to improve the efficacy of radiotherapy in the cancer treatment. IR has important applications in medicine, industry, agriculture, and research, being associates with an increased risk of accidental exposure, or unavoidable exposure in the case of space travel. Historical world events have highlighted the urgent need to develop predictive biomarkers of IR absorbed dose and radiation countermeasures to reduce or attenuate IR damage. Despite the strong economic and scientific efforts over the last decades, at present, clinical biomarkers of radiation-induced damage and drugs that can effectively protect against lethal IRs remain an unmet need. Additionally, the development of radiosensitizers that can protect healthy tissues is key to improving the survival and quality of life in cancer patients.

This Special Issue includes selected contributions that will help the readers to understand the mechanism involved in IR oxidative damage, as well as the importance of antioxidant and inflammatory responses in cellular and tissue recovery. This book includes an editorial and 15 scientific articles, of which 11 are original research papers and 4 are reviews. These outstanding contributions unravel the latest advancements in the bioefficacy and/or mechanisms of action of several promising radiomodulators, the capacity of hyperthermia to increase cancer treatment efficacy, clinical models to evaluate the radio-induced damages, and novel IR biomarker technologies.

As Guest Editors, we would like to acknowledge all authors for their valuable contributions and the reviewers for their constructive remarks. Special thanks go to the publishing team at *Antioxidants* for their professional assistance to complete this Special Issue.

**Elena Obrador and Alegria Montoro**
*Editors*

*antioxidants*

MDPI

*Editorial*

# Ionizing Radiation, Antioxidant Response and Oxidative Damage: Radiomodulators

**Elena Obrador [1,*] and Alegría Montoro [2]**

[1] Elena Obrador Department of Physiology, Faculty of Medicine and Odontology, University of Valencia, 46010 Valencia, Spain
[2] Alegría Montoro, Radiation Protection Service, University and Polytechnic Hospital La Fe, 46021 Valencia, Spain; almonpas@hotmail.com
* Correspondence: elena.obrador@uv.es

Ionizing radiation (IR) is the energy released by atoms in the form of electromagnetic waves (e.g., X or gamma rays) or particle radiation (alpha, beta, electrons, protons, neutrons, mesons, prions, and heavy ions) with sufficient energy to ionize atoms or molecules [1]. IR induces DNA breaks leading to direct molecular damages or even cell death, whereas in the case of cell survival, it can lead to carcinogenesis or other abnormalities [2,3]. The highly reactive free radicals formed by the radiolysis of water (superoxide anion ($O_2^{\bullet -}$), hydroxyl radical (•OH), hydrated electron ($e^-_{(aq)}$), and hydrogen peroxide ($H_2O_2$)) and the subsequent oxidative stress are the main cause of most of the molecular (DNA, lipids, proteins, etc.) damages [1,4]. In turn, cells injured by IR are responsible for inducing radiation bystander effects (RIBEs) in non-exposed tissues, manifested by changes including (but not limited to) gene expression alterations, chromosomal aberrations, micronuclei formation, secretion of miRNAs and or exosomes, and cell death/proliferation and/or transformation. In that sense, overproduced reactive oxygen species (ROS) and reactive nitrogen species (RNS) are considered initiators, whereas nitric oxide, the transforming growth factor beta (TGF-β), and other inflammatory cytokines are considered effectors involved in RIBE [5].

Radiation-induced biological effects are determined by the type of radiation, dose rate and total dose received, fractionation and protraction, penetration capacity, linear energy transfer, cell or tissue affected, and time of exposure [6]. The survival response can be modulated by different factors, e.g., DNA repair mechanisms, antioxidant defences, intrinsic radiosensibility of tissues, inflammatory response, RIBE, health condition, and/or the administration of radiomodulators. Radiomodulators include radioprotectors, radiomitigators, and molecules with radiosensitizing properties. The first ones reduce or prevent the damage induced by IR (generally acting as chelators of free radicals, antioxidants, . . . ), but to be effective, they must be administered before or at the same time as exposure [2]. In contrast, radiomitigators help to recover or attenuate radio-induced damages even when they are administered after radiation exposition [3,7], which represents an important strategic advantage. Mechanisms involved in the radiomitigating activity include the restoration of the cellular antioxidant defence mechanisms, the prevention of excessive inflammatory responses, and/or the repair of damaged tissues [5]. Finally, radiosensitizers can increase radio-induced damage in cells or tissues, and their use is mainly focused on cancer treatment, where it is especially important to induce cytotoxicity in the cancer cells without affecting healthy tissues [8–10].

Nuclear technology is becoming widely used in many diverse fields, i.e., industry, medicine, military, and basic research. Although a few years ago, exposure to IR was restricted to accidents at nuclear power plants or terrorist attacks, nowadays, the risk is increased by the improper and careless management of IR in the radiographic industry and in radiation oncology [11]. Moreover, IR exposure is unavoidable in the case of cancer

**Citation:** Obrador, E.; Montoro, A. Ionizing Radiation, Antioxidant Response and Oxidative Damage: Radiomodulators. *Antioxidants* **2023**, *12*, 1219. https://doi.org/10.3390/antiox12061219

Received: 16 May 2023
Revised: 16 May 2023
Accepted: 31 May 2023
Published: 5 June 2023

patients undergoing radiotherapy, and it will also be unavoidable for future aerospace ship crews [12]. All this raises the inexorable need to develop strategies that may allow rapid interventions to prevent or reduce radiation-induced damages. Significant advances have been made in public health and the clinical planning intended to prevent or improve the response to an accidental exposure [5]. However, despite the strong economic and scientific efforts over recent decades, at present, clinical biomarkers of radiation-induced damage and drugs that can effectively protect against lethal IRs are still an unmet need.

Overall, this Special Issue provides the readers with an understanding of the latest advancements in the bioefficacy and/or mechanisms of action of several promising radiomodulators [2,3,5,7,9,10,13–16], the capacity of hyperthermia to increase cancer treatment efficacy [17], a new clinical model to evaluate the radio-induced damages [15,18], and novel IR biomarker technologies [19,20].

N-acetyl-5-methoxytryptamine (melatonin), often referred to as a "sleep hormone", is produced by the pineal gland. Its free radical scavenger and antioxidant actions contribute to reducing nitric oxide formation, which facilitates the decrease in the inflammatory response after IR exposition [5]. According to the experiments concerning whole body irradiation, melatonin administered both before and after IR exposure increased the survival rate of examined animals, reduced symptoms of acute irradiation syndrome, and improved radio-induced oxidative stress and histopathological damages [21]. Animal studies have confirmed that melatonin can also alleviate radiation-induced cell death via inhibition of proapoptotic genes (e.g., Bax) and upregulation of antiapoptotic genes (e.g., Bcl-2) [22]. The radioprotective and radiomitigating efficacy of melatonin was confirmed by Abdullaev et al. in tissues (brain and spleen) that exhibit different proliferative activity and radiosensitivity [2].

Peroxiredoxins are capable of reducing a wide range of inorganic and organic peroxides. Novoselova et al. show that peroxiredoxin 6 treatment normalized p53 and NF-κB/p65 expression, p21 levels, DNA repair-associated genes, TLR expression, proinflammatory cytokine production (TNF-α and IL-6), and apoptosis in irradiated 3T3 cells cultures. Moreover, the IR-induced suppression of the Nrf2 activity (a key regulator of the antioxidant cellular response) could be restored by peroxiredoxin 6, even when it was administered after radiation exposure [3].

Wagle et al. evidenced that supplemented ferulic acid attenuates the total body irradiation-mediated bone marrow damages, stem cell senescence, and hematopoietic injury by enhancing the antioxidant defence. Thus pointing out its potential as a radioprotective countermeasure [13].

Lactoferrin is a multifunctional glycoprotein present in mammalian secretory fluids and in neutrophil granules. The study of Kopaeva et al. provided evidence for the radiomitigating potential of human Lactoferrin on mice subjected to sublethal irradiation. Their results show that treated mice increased their survival from 28% to 78%, attenuated weight loss, normalized their behaviour, and also increased the leukocyte account, serum homeostasis parameters, and structural organization of the spleen [7].

Pelvic irradiation-induced mucositis secondarily leads to changes in the composition of microbiota and reduces its diversity, all factors that contribute to radiation enteropathy [23,24]. Microbiome dysbiosis contributes to the overexpression of proinflammatory cytokines and weakens the function of the intestinal epithelial barrier [24]. Typical symptoms of gastrointestinal radiation injury, including vomiting, anorexia, abdominal pain, and diarrhoea, can seriously affects patients' quality of life after or during radiotherapy treatment [25,26]. Limiting the intestinal irradiation dose and using a lower fractionated dose helps to relieve symptoms, but compromises and reduces the anti-tumour efficacy of the treatment [27]. Probiotics can attenuate radiation-derived enteritis side effects by restoring microbiota, regulating the immune system, downregulating proinflammatory cytokines, regulating apoptosis, and reversing ecological dysregulation [28,29]. Thus, the development of probiotic therapy to prevent the radiotherapy-induced diarrhoea is a hot topic, but with contradictory efficacy according to several recent studies [30–32]. Although

some studies have proposed that *Lactobacillus rhamnosus* supplementation is efficacious for preventing radio-induced enteritis [33,34], Segers et al.'s results [14] evidence that, although supplementation with *Limnospira indica* PCC 8005 or *Lacticaseibacillus rhamnosus* GG ATCC prevented radio-induced dysbiosis, probiotic administration did not preserve the intestinal protective barrier or did not have significant immunomodulatory effects.

Radiotherapy failure and poor tumour prognosis are primarily attributed to radioresistance. In 1924, Otto Warburg observed that tumours consumed large quantities of glucose while secreting high levels of lactate, irrespective of the tissue oxygen concentration [35]. Since then, this "aerobic glycolysis" has been shown to benefit tumour growth by providing intermediates needed to maintain high rates of cellular division. Moreover, the link between glucose metabolism and redox stress is relevant for the cancer radiation response. Bian et al. present an interesting review exposing the mechanisms involved in mitochondrial metabolism and cancer radioresistance, targeting mitochondrial signalling pathways to reverse radiation insensitivity [36].

Planarians are invertebrate flatworms with stem cells constantly replacing old, damaged, or dying cells. Combined with new genomic technologies, the planarian sensitivity to IR provides an outstanding tool for the evaluation of potential radioprotective agents [18]. In this, Tsarkova et al.'s study on the planarian model confirms the antioxidant properties of Tameron against X-ray-induced and menadione-induced oxidative stress [15].

In cancer therapeutics, the development of radiosensitizers would represent a great advance, especially if treatment can also exert radioprotective effects on healthy tissues. Pacifico et al. evidence that a polyphenol-rich Olea europaea L. cv. Caiazzana Leaf extract mitigates radiation-induced DNA damage in normal cell lines, whereas it exacerbates radiation damage in cancer cells [9].

The prognosis of patients diagnosed with pancreatic cancer remains dismal, with a less than 3% survival at 5 years [37]. At supraphysiologic levels, ascorbate (vitamin C) acts as a pro-oxidant, donating electrons to form $H_2O_2$ and, thereby, causing selective cytotoxicity and oxidative stress in pancreatic cancer cells [38,39]. Thus, pharmacological ascorbate has potential as a radiosensitizer at the same time that several studies evidence its radioprotective potential in normal tissues [40]. During recent years, Auranofin has garnered interest for its anticancer potential, although its mechanisms of action are not completely elucidated. Steers et al. review the mechanism and effectiveness of auranofin alone and in combination with ascorbate and IR, in the treatment of pancreatic cancer [10].

Applying focused hyperthermia (HT), the temperature of the affected area is raised to around 40–45 °C using different methods, i.e., microwave, radiofrequency, ultrasound, or infrared radiations. In cancer therapy, a specific area is exposed to high temperatures to kill cancer cells or make them more sensitive to other cancer treatments, such as chemo and/or radiotherapy [17,41,42]. The tumour microenvironment is characterized by nutrient deprivation, limited oxygenation, and highly acidic conditions, properties associated with low effects on the tumour response to radiation [42]. HT increases tumour perfusion and re-oxygenation, drug uptake, and ROS production, inhibits the repair of radiation-induced damage, and induces cancer cell apoptosis [43,44]. In addition to the various thermoradiobiological effects, it has recently been shown that HT has immunostimulatory effects involving the innate and adaptive immune systems, thereby inducing systemic anti-tumour immune responses [45]. Kwon et al. review the latest advances regarding the efficacy of HT in the treatment of cancer and its possible synergistic effects with radiotherapy [17].

Sagkrioti et al. developed a database termed RadBioBase, which includes comprehensive transcriptomes of mammalian cells across healthy and non-healthy tissues when responding to a range of radiation types and doses. Their results evidence that the effects of high linear energy transfer (LET) radiation on cell transcriptomes significantly differ from those caused by low LET and, importantly, are consistent with immunomodulation, inflammation, oxidative stress responses, and cell death. The transcriptome changes also depend on the dose, since low doses up to 0.5 Gy mainly involve cytokine cascades, while

higher doses are mainly linked to ROS metabolism. Overall, their results suggest that different radiation types and doses can trigger distinct cell-intrinsic and cell-extrinsic pathways, which may facilitate manipulation to improving radiotherapy efficiency and reducing systemic toxicities [19].

The serum proteomic and oxidative modification profiling in mice exposed to total body X-Irradiation evidenced a dose-dependent and oxidation-related response involving six different serum proteins (angiotensinogen, odorant-binding protein 1a, serine protease inhibitor A3K, serum paraoxonase/arylesterase 1, prothrombin, and the epidermal growth factor receptor). Consequently, Yamaguchi et al. suggest the possible application of these changes as novel biomarkers to validate the radiation dose [20].

Electron radiation is widely used to ensure the microbiological safety of food and drugs. One of the most important advantages of this method is that it is carried out at low temperatures, which is important for heat-sensitive products. Many brands of nutraceuticals containing resveratrol are available, and Rosiak et al. show that, far from endangering the biological properties of resveratrol, electron beam radiation (even at a dose of 25 kGy) can increase the antioxidant properties of resveratrol [16].

Finally, Obrador et al. discuss the best choices for triage, dose assessment, and victim classification in the case of large-scale atomic or radiological events. Furthermore, our review focuses on the available medical countermeasures (radioprotectors, radiomitigators, radionuclide scavengers) that can implement the response to an accidental radiation exposure or can help to increase survival in cancer patients [5].

As a whole, these 11 research [2,3,7,9,13–16,18–20] and 4 review articles [5,10,17,36] from leading experts bring to the field exciting discussions on different aspects, new findings, and new perspectives, thus making this Special Issue an essential read for anyone interested in the impact of radiation exposure on human health.

**Funding:** This work was supported by the Project CPP2021-8817 funded by the MCIN/AEI/10.13039/501100011033/ and the European Union NextGenerationEU/PRTR.

**Conflicts of Interest:** The authors declare no conflict of interest.

## References

1. Obrador, E.; Salvador, R.; Villaescusa, J.I.; Soriano, J.M.; Estrela, J.M.; Montoro, A. Radioprotection and Radiomitigation: From the Bench to Clinical Practice. *Biomedicines* **2020**, *8*, 461. [CrossRef] [PubMed]
2. Abdullaev, S.A.; Glukhov, S.I.; Gaziev, A.I. Radioprotective and Radiomitigative Effects of Melatonin in Tissues with Different Proliferative Activity. *Antioxidants* **2021**, *10*, 1885. [CrossRef] [PubMed]
3. Novoselova, E.G.; Sharapov, M.G.; Lunin, S.M.; Parfenyuk, S.B.; Khrenov, M.O.; Mubarakshina, E.K.; Kuzekova, A.A.; Novoselova, T.V.; Goncharov, R.G.; Glushkova, O.V. Peroxiredoxin 6 Applied after Exposure Attenuates Damaging Effects of X-Ray Radiation in 3T3 Mouse Fibroblasts. *Antioxidants* **2021**, *10*, 1951. [CrossRef] [PubMed]
4. Reisz, J.A.; Bansal, N.; Qian, J.; Zhao, W.; Furdui, C.M. Effects of Ionizing Radiation on Biological Molecules–Mechanisms of Damage and Emerging Methods of Detection. *Antioxid. Redox Signal.* **2014**, *21*, 260–292. [CrossRef] [PubMed]
5. Obrador, E.; Salvador-Palmer, R.; Villaescusa, J.I.; Gallego, E.; Pellicer, B.; Estrela, J.M.; Montoro, A. Nuclear and Radiological Emergencies: Biological Effects, Countermeasures and Biodosimetry. *Antioxidants* **2022**, *11*, 1098. [CrossRef]
6. Russ, E.; Davis, C.M.; Slaven, J.E.; Bradfield, D.T.; Selwyn, R.G.; Day, R.M. Comparison of the Medical Uses and Cellular Effects of High and Low Linear Energy Transfer Radiation. *Toxics* **2022**, *10*, 628. [CrossRef]
7. Kopaeva, M.Y.; Alchinova, I.B.; Cherepov, A.B.; Demorzhi, M.S.; Nesterenko, M.V.; Zarayskaya, I.Y.; Karganov, M.Y. New Properties of a Well-Known Antioxidant: Pleiotropic Effects of Human Lactoferrin in Mice Exposed to Gamma Irradiation in a Sublethal Dose. *Antioxidants* **2022**, *11*, 1833. [CrossRef]
8. Kirsch, D.G.; Diehn, M.; Kesarwala, A.H.; Maity, A.; Morgan, M.A.; Schwarz, J.K.; Bristow, R.; Demaria, S.; Eke, I.; Griffin, R.J.; et al. The Future of Radiobiology. *J. Natl. Cancer Inst.* **2017**, *110*, 329–340. [CrossRef]
9. Pacifico, S.; Bláha, P.; Faramarzi, S.; Fede, F.; Michaličková, K.; Piccolella, S.; Ricciardi, V.; Manti, L. Differential Radiomodulating Action of Olea Europaea L. Cv. Caiazzana Leaf Extract on Human Normal and Cancer Cells: A Joint Chemical and Radiobiological Approach. *Antioxidants* **2022**, *11*, 1603. [CrossRef]
10. Steers, G.J.; Chen, G.Y.; O'Leary, B.R.; Du, J.; Van Beek, H.; Cullen, J.J. Auranofin and Pharmacologic Ascorbate as Radiomodulators in the Treatment of Pancreatic Cancer. *Antioxidants* **2022**, *11*, 971. [CrossRef]

11. Vinnikov, V.; Hande, M.P.; Wilkins, R.; Wojcik, A.; Zubizarreta, E.; Belyakov, O. Prediction of the Acute or Late Radiation Toxicity Effects in Radiotherapy Patients Using Ex Vivo Induced Biodosimetric Markers: A Review. *J. Pers. Med.* **2020**, *10*, 285. [CrossRef] [PubMed]
12. Lalkovicova, M. Neuroprotective Agents Effective against Radiation Damage of Central Nervous System. *Neural Regen. Res.* **2022**, *17*, 1885–1892. [CrossRef] [PubMed]
13. Wagle, S.; Sim, H.-J.; Bhattarai, G.; Choi, K.-C.; Kook, S.-H.; Lee, J.-C.; Jeon, Y.-M. Supplemental Ferulic Acid Inhibits Total Body Irradiation-Mediated Bone Marrow Damage, Bone Mass Loss, Stem Cell Senescence, and Hematopoietic Defect in Mice by Enhancing Antioxidant Defense Systems. *Antioxidants* **2021**, *10*, 1209. [CrossRef] [PubMed]
14. Segers, C.; Mysara, M.; Coolkens, A.; Wouters, S.; Baatout, S.; Leys, N.; Lebeer, S.; Verslegers, M.; Mastroleo, F. Limnospira Indica PCC 8005 Supplementation Prevents Pelvic Irradiation-Induced Dysbiosis but Not Acute Inflammation in Mice. *Antioxidants* **2023**, *12*, 572. [CrossRef] [PubMed]
15. Tsarkova, E.; Filippova, K.; Afanasyeva, V.; Ermakova, O.; Kolotova, A.; Blagodatski, A.; Ermakov, A. A Study on the Planarian Model Confirms the Antioxidant Properties of Tameron against X-Ray- and Menadione-Induced Oxidative Stress. *Antioxidants* **2023**, *12*, 953. [CrossRef]
16. Rosiak, N.; Cielecka-Piontek, J.; Skibiński, R.; Lewandowska, K.; Bednarski, W.; Zalewski, P. Antioxidant Potential of Resveratrol as the Result of Radiation Exposition. *Antioxidants* **2022**, *11*, 2097. [CrossRef]
17. Kwon, S.; Jung, S.; Baek, S.H. Combination Therapy of Radiation and Hyperthermia, Focusing on the Synergistic Anti-Cancer Effects and Research Trends. *Antioxidants* **2023**, *12*, 924. [CrossRef]
18. Ermakov, A.M.; Kamenskikh, K.A.; Ermakova, O.N.; Blagodatsky, A.S.; Popov, A.L.; Ivanov, V.K. Planarians as an In Vivo Experimental Model for the Study of New Radioprotective Substances. *Antioxidants* **2021**, *10*, 1763. [CrossRef]
19. Sagkrioti, E.; Biz, G.M.; Takan, I.; Asfa, S.; Nikitaki, Z.; Zanni, V.; Kars, R.H.; Hellweg, C.E.; Azzam, E.I.; Logotheti, S.; et al. Radiation Type- and Dose-Specific Transcriptional Responses across Healthy and Diseased Mammalian Tissues. *Antioxidants* **2022**, *11*, 2286. [CrossRef]
20. Yamaguchi, M.; Tatara, Y.; Nugraha, E.D.; Sato, Y.; Miura, T.; Hosoda, M.; Syaifudin, M.; Tokonami, S.; Kashiwakura, I. Serum Proteomic and Oxidative Modification Profiling in Mice Exposed to Total Body X-Irradiation. *Antioxidants* **2022**, *11*, 1710. [CrossRef]
21. Nuszkiewicz, J.; Woźniak, A.; Szewczyk-Golec, K. Ionizing Radiation as a Source of Oxidative Stress—The Protective Role of Melatonin and Vitamin D. *Int. J. Mol. Sci.* **2020**, *21*, 5804. [CrossRef] [PubMed]
22. Mohseni, M.; Mihandoost, E.; Shirazi, A.; Sepehrizadeh, Z.; Bazzaz, J.T.; Ghazi-khansari, M. Melatonin May Play a Role in Modulation of Bax and Bcl-2 Expression Levels to Protect Rat Peripheral Blood Lymphocytes from Gamma Irradiation-Induced Apoptosis. *Mutat. Res.* **2012**, *738–739*, 19–27. [CrossRef] [PubMed]
23. Segers, C.; Mysara, M.; Claesen, J.; Baatout, S.; Leys, N.; Lebeer, S.; Verslegers, M.; Mastroleo, F. Intestinal Mucositis Precedes Dysbiosis in a Mouse Model for Pelvic Irradiation. *ISME Commun.* **2021**, *1*, 24. [CrossRef] [PubMed]
24. Jian, Y.; Zhang, D.; Liu, M.; Wang, Y.; Xu, Z.-X. The Impact of Gut Microbiota on Radiation-Induced Enteritis. *Front. Cell Infect. Microbiol.* **2021**, *11*, 586392. [CrossRef] [PubMed]
25. Wang, A.; Ling, Z.; Yang, Z.; Kiela, P.R.; Wang, T.; Wang, C.; Cao, L.; Geng, F.; Shen, M.; Ran, X.; et al. Gut Microbial Dysbiosis May Predict Diarrhea and Fatigue in Patients Undergoing Pelvic Cancer Radiotherapy: A Pilot Study. *PLoS ONE* **2015**, *10*, e0126312. [CrossRef]
26. Ahmed, M.; Ahmed, R. Radiation in Gastroenterology. *Gastroenterol. Res.* **2022**, *15*, 285–296. [CrossRef]
27. Fan, J.; Lin, B.; Fan, M.; Niu, T.; Gao, F.; Tan, B.; Du, X. Research Progress on the Mechanism of Radiation Enteritis. *Front. Oncol.* **2022**, *12*, 888962. [CrossRef]
28. Linn, Y.H.; Thu, K.K.; Win, N.H.H. Effect of Probiotics for the Prevention of Acute Radiation-Induced Diarrhoea Among Cervical Cancer Patients: A Randomized Double-Blind Placebo-Controlled Study. *Probiotics Antimicrob. Proteins* **2019**, *11*, 638–647. [CrossRef]
29. Yang, Q.; Qin, B.; Hou, W.; Qin, H.; Yin, F. Pathogenesis and Therapy of Radiation Enteritis with Gut Microbiota. *Front. Pharmacol.* **2023**, *14*, 1116558. [CrossRef]
30. Segers, C.; Verslegers, M.; Baatout, S.; Leys, N.; Lebeer, S.; Mastroleo, F. Food Supplements to Mitigate Detrimental Effects of Pelvic Radiotherapy. *Microorganisms* **2019**, *7*, 97. [CrossRef]
31. Poonacha, K.N.T.; Villa, T.G.; Notario, V. The Interplay among Radiation Therapy, Antibiotics and the Microbiota: Impact on Cancer Treatment Outcomes. *Antibiotics* **2022**, *11*, 331. [CrossRef] [PubMed]
32. Eaton, S.E.; Kaczmarek, J.; Mahmood, D.; McDiarmid, A.M.; Norarfan, A.N.; Scott, E.G.; Then, C.K.; Tsui, H.Y.; Kiltie, A.E. Exploiting Dietary Fibre and the Gut Microbiota in Pelvic Radiotherapy Patients. *Br. J. Cancer* **2022**, *127*, 2087–2098. [CrossRef] [PubMed]
33. Riehl, T.E.; Alvarado, D.; Ee, X.; Zuckerman, A.; Foster, L.; Kapoor, V.; Thotala, D.; Ciorba, M.A.; Stenson, W.F. Lactobacillus Rhamnosus GG Protects the Intestinal Epithelium from Radiation Injury through Release of Lipoteichoic Acid, Macrophage Activation and the Migration of Mesenchymal Stem Cells. *Gut* **2019**, *68*, 1003–1013. [CrossRef] [PubMed]
34. Lee, S.U.; Jang, B.-S.; Na, Y.R.; Lee, S.H.; Han, S.; Chang, J.H.; Kim, H.J. Effect of Lactobacillus Rhamnosus GG for Regulation of Inflammatory Response in Radiation-Induced Enteritis. *Probiotics Antimicrob. Proteins* **2023**. [CrossRef] [PubMed]
35. Warburg, O. On Respiratory Impairment in Cancer Cells. *Science* **1956**, *124*, 269–270. [CrossRef] [PubMed]

36. Bian, C.; Zheng, Z.; Su, J.; Wang, H.; Chang, S.; Xin, Y.; Jiang, X. Targeting Mitochondrial Metabolism to Reverse Radioresistance: An Alternative to Glucose Metabolism. *Antioxidants* **2022**, *11*, 2202. [CrossRef]
37. Cieslak, J.A.; Cullen, J.J. Treatment of Pancreatic Cancer with Pharmacological Ascorbate. *Curr. Pharm. Biotechnol.* **2015**, *16*, 759–770. [CrossRef]
38. Du, J.; Martin, S.M.; Levine, M.; Wagner, B.A.; Buettner, G.R.; Wang, S.; Taghiyev, A.F.; Du, C.; Knudson, C.M.; Cullen, J.J. Mechanisms of Ascorbate-Induced Cytotoxicity in Pancreatic Cancer. *Clin. Cancer Res.* **2010**, *16*, 509–520. [CrossRef]
39. Du, J.; Cieslak, J.A.; Welsh, J.L.; Sibenaller, Z.A.; Allen, B.G.; Wagner, B.A.; Kalen, A.L.; Doskey, C.M.; Strother, R.K.; Button, A.M.; et al. Pharmacological Ascorbate Radiosensitizes Pancreatic Cancer. *Cancer Res.* **2015**, *75*, 3314–3326. [CrossRef]
40. Mehdi, Z.; Petronek, M.S.; Stolwijk, J.M.; Mapuskar, K.A.; Kalen, A.L.; Buettner, G.R.; Cullen, J.J.; Spitz, D.R.; Buatti, J.M.; Allen, B.G. Utilization of Pharmacological Ascorbate to Enhance Hydrogen Peroxide-Mediated Radiosensitivity in Cancer Therapy. *Int. J. Mol. Sci.* **2021**, *22*, 10880. [CrossRef]
41. Kampinga, H.H. Cell Biological Effects of Hyperthermia Alone or Combined with Radiation or Drugs: A Short Introduction to Newcomers in the Field. *Int. J. Hyperth.* **2006**, *22*, 191–196. [CrossRef] [PubMed]
42. Liebl, C.M.; Kutschan, S.; Dörfler, J.; Käsmann, L.; Hübner, J. Systematic Review about Complementary Medical Hyperthermia in Oncology. *Clin. Exp. Med.* **2022**, *22*, 519–565. [CrossRef] [PubMed]
43. Oei, A.L.; Kok, H.P.; Oei, S.B.; Horsman, M.R.; Stalpers, L.J.A.; Franken, N.A.P.; Crezee, J. Molecular and Biological Rationale of Hyperthermia as Radio- and Chemosensitizer. *Adv. Drug Deliv. Rev.* **2020**, *163*, 84–97. [CrossRef] [PubMed]
44. Vaupel, P.; Piazena, H.; Notter, M.; Thomsen, A.R.; Grosu, A.-L.; Scholkmann, F.; Pockley, A.G.; Multhoff, G. From Localized Mild Hyperthermia to Improved Tumor Oxygenation: Physiological Mechanisms Critically Involved in Oncologic Thermo-Radio-Immunotherapy. *Cancers* **2023**, *15*, 1394. [CrossRef] [PubMed]
45. Liu, P.; Ye, M.; Wu, Y.; Wu, L.; Lan, K.; Wu, Z. Hyperthermia Combined with Immune Checkpoint Inhibitor Therapy: Synergistic Sensitization and Clinical Outcomes. *Cancer Med.* **2023**, *12*, 3201–3221. [CrossRef]

*antioxidants*

MDPI

*Review*

# Nuclear and Radiological Emergencies: Biological Effects, Countermeasures and Biodosimetry

**Elena Obrador [1,*], Rosario Salvador-Palmer [1], Juan I. Villaescusa [2,3], Eduardo Gallego [4], Blanca Pellicer [1], José M. Estrela [1] and Alegría Montoro [2,3]**

[1] Department of Physiology, Faculty of Medicine and Odontology, University of Valencia, 46010 Valencia, Spain; rosario.salvador@uv.es (R.S.-P.); b.pellicerdegracia@gmail.com (B.P.); jose.m.estrela@uv.es (J.M.E.)
[2] Service of Radiological Protection, Clinical Area of Medical Image, La Fe University Hospital, 46026 Valencia, Spain; villaescusa_ign@gva.es (J.I.V.); almonpas@hotmail.com (A.M.)
[3] Biomedical Imaging Research Group GIBI230, Health Research Institute (IISLaFe), La Fe University Hospital, 46026 Valencia, Spain
[4] Energy Engineering Department, School of Industrial Engineering, Polytechnic University of Madrid, 28040 Madrid, Spain; eduardo.gallego@upm.es
* Correspondence: elena.obrador@uv.es; Tel.: +34-963864646

**Abstract:** Atomic and radiological crises can be caused by accidents, military activities, terrorist assaults involving atomic installations, the explosion of nuclear devices, or the utilization of concealed radiation exposure devices. Direct damage is caused when radiation interacts directly with cellular components. Indirect effects are mainly caused by the generation of reactive oxygen species due to radiolysis of water molecules. Acute and persistent oxidative stress associates to radiation-induced biological damages. Biological impacts of atomic radiation exposure can be deterministic (in a period range a posteriori of the event and because of destructive tissue/organ harm) or stochastic (irregular, for example cell mutation related pathologies and heritable infections). Potential countermeasures according to a specific scenario require considering basic issues, e.g., the type of radiation, people directly affected and first responders, range of doses received and whether the exposure or contamination has affected the total body or is partial. This review focuses on available medical countermeasures (radioprotectors, radiomitigators, radionuclide scavengers), biodosimetry (biological and biophysical techniques that can be quantitatively correlated with the magnitude of the radiation dose received), and strategies to implement the response to an accidental radiation exposure. In the case of large-scale atomic or radiological events, the most ideal choice for triage, dose assessment and victim classification, is the utilization of global biodosimetry networks, in combination with the automation of strategies based on modular platforms.

**Keywords:** nuclear and radiological emergencies; radioprotectors; radiomitigators; radionuclide scavengers; radiation biodosimetry

**Citation:** Obrador, E.; Salvador-Palmer, R.; Villaescusa, J.I.; Gallego, E.; Pellicer, B.; Estrela, J.M.; Montoro, A. Nuclear and Radiological Emergencies: Biological Effects, Countermeasures and Biodosimetry. *Antioxidants* **2022**, *11*, 1098. https://doi.org/10.3390/antiox11061098

Academic Editor: Stanley Omaye

Received: 8 May 2022
Accepted: 27 May 2022
Published: 31 May 2022



## 1. Introduction

Nuclear and radiological accidents can cause huge harm to individuals, the environment, and the economy. Chernobyl (USSR, 1986), Goiania (Brazil, 1987), and Fukushima Daiichi (2011, Japan) were awful catastrophes demonstrating how wrecking these mishaps can be. Moreover, since 11 September 2001, the danger of terrorism has become a public security concern in numerous nations. The number of known terrorist associations with worldwide reach, just like the expanded multiplication and transfer of technical data through the web, raises the chance of shocking assaults with chemical, biological, radiological, or even atomic weapons [1–3] (http://www.dni.gov/index.php/nctc-home, accessed on 15 December 2021; https://www.europol.europa.eu/about-europol/european-counter-terrorism-centre-ectc, accessed on 15 December 2021).

Radiation exposure is a danger from both potential "dirty bomb" terrorist events and industrial mishaps including problems with atomic reactors or misplaced radioactive sources. Calamities including exposure to radiological materials require technical planning and readiness to guarantee the health of first responders, the evacuation and clinical therapy of possibly contaminated casualties, and the management of the process of triage. Significant advances have been made throughout the most recent decade in public health and clinical planning intended to improve the response to an atomic explosion or a radiological episode [4–6].

A mass victim event would surpass the reaction capacity of the local responders and, subsequently, its methodology would require the mediation of exceptionally well prepared personnel and extensive public activity, based on a fast intervention plan arranged ahead of time. The best model (even though the most improbable) would be the explosion of an improvised nuclear device (IND), which would produce a fireball and a bright glimmer of irradiation followed by an impact wave and thermal pulse. That scenario would make it very hard to get supplies and personnel into the harmed areas, as well as the clearing of the injured to clinics. Mass screening of the affected people would be important to isolate those exposed from non-exposed and to take decisions based on the estimated dose received [7].

Exposure would result from irradiation close to the site of the explosion, which emits radiation at a high dose rate for a brief timeframe; and from deposited radioactivity (also known as aftermath), which has a lower dose rate. The absolute ingested dose would be reliant on the location of the people and the term of their exposure.

The number of individuals exposed, and the dosages received would likewise rely upon a number of factors, e.g., geological characteristics of the area (metropolitan or countryside, protection against radiation provided by buildings), environmental conditions, and the protection set up during the first hours.

Independent of the type of atomic or radiological crisis, explicit (pre-events) plans and reactions should incorporate innovative work in comprehending the pathophysiology of radiation injury, improvement of clinical countermeasures (MCM) (i.e., radioprotectors, radiomitigators, and radionuclide scavengers), and investigating a range of analytic tests to help the clinical decision-makers [8]. Ideally, planning should include energy, health, human management, security, work, transportation, ecology, aeronautics, and atomic guidelines.

## 2. Nuclear and Radiological Accidents

The scenario of the Chernobyl and Fukushima-Daiichi accidents comprised release of large amounts of radionuclides. In water reactors, vaporous and unpredictable splitting of items, specifically isotopes of iodine and cesium, would be determinant for the radiological issues off-site [9], as occurred in Fukushima (https://www.iaea.org, accessed on 15 December 2021). Less unpredictable splitting items or actinides would be critical in case of extreme reactivity accidents (like Chernobyl) in which fuel "hot particles" were delivered [10]. In the primary time frame during the crisis period of an atomic mishap, large amounts of iodine isotopes can reach individuals, with the thyroid being a basic target organ. Triage is critical to distinguish between individuals who need care because of their degree of exposure and those who need health observation. The characterization of the radiological circumstances of individuals and the environment is key to setting up protecting activities (https://www.icrp.org, accessed on 15 December 2021). In the more extended term, contamination of the environment with cesium and other seemingly perpetual radionuclides will influence life in the affected areas, where the external and interior exposure of people ought to be checked to implement effective countermeasures.

The scenario after a huge radiological accident, similar to that which occurred in Goiania (1987) with an enormous $^{137}$Cs source left in a closed oncologic facility, can likewise be difficult to oversee. In the Goiania accident, four deaths were recorded, 250 people suffered contamination, 62 of them were administered a radionuclide scavenger (Prussian blue), whereas more than 112,000 individuals were radiologically observed, and 3000 $m^3$

of radioactive wastes was generated (https://www.iaea.org, accessed on 15 December 2021). Another significant radiological event was that of the $^{210}$Po poisoning of Aleksandr Litvinenko in 2006 [11], which required follow up of the polonium pollution and screening of more than 750 individuals for their likely internal contamination, thus requiring a huge coordinated effort [12].

## 3. Main Radiations Associated to Nuclear and Radiological Emergencies

Injury from an atomic explosion will fluctuate contingent upon the exposure to various sorts of energy: heat, representing around 35% of total energy; blast, representing roughly half of total energy; and radiation, representing the leftover 15% of energy [13]. Here, the brief acute exposure would be promptly caused by emitted gamma rays combined with a subordinate dose of fast-moving neutrons. Neutrons can represent comprise 25 to 50% of the absolute radiation dose at a distance of approx. 1 km. This is important because, due to its high radiation biological effectiveness (RBE) and radiation weighting factors (WR) (www.icrp.org, accessed on 15 December 2021), the neutron dose can increase multiple times the harm of an equal photon absorbed dose.

The radiation dose received from an atomic blast will be prompt (that delivered with the impact wave), plus an additional relevant component due to fallout of fission and activation products that can be extended (from the aftermath) for a long time as polluted materials tumble to the earth [14]. The mean deadly dose of radiation that would kill half of the people in 60 days (LD50/60), after a total-body irradiation (TBI), is of approx. 3.25–4 Gy in individuals without supportive care; and 6–7 Gy when anti-infection agents and additional support are given [15,16].

In an IND-related event, gamma and neutron radiations will be released, and then gamma and beta radiations from items delivered by the blast [17–19].

In a radiological dispersal device (RDD or dirty bombs)-related event, the radiation exposure would be limited, as most likely just one sort of isotope would be utilized. In most RDD scenarios, even with the utilization of solid gamma-discharging radionuclides, huge radiation wounds should not to be normal. The dispersal impacts of the weapon would dissipate the radioactive source [20,21].

An individual exposed to radiation is not radioactive, while an individual contaminated with radionuclides (internal or remotely) may emit radioactivity that is perceptible with hand-held Geiger counters or whole-body scanners. Contamination results when a radioisotope (as gas, fluid, or solid) is delivered to the environment, and afterward ingested, inhaled, or deposited on the body's surface [22]. A prominent exemption is a neutron radiation exposure, where the cycle of neutron actuation can create biological radioactive material [23].

## 4. Triage and Categorization

The kind of triage varies with the type of radiological or atomic event. For instance, in the case of an atomic explosion, an enormous number of individuals should be assessed, including those affected by a high dose and those having negligible or no actual injury. The dose will be a critical boundary for a clinical triage. As of now, the most productive and available triage technique is the utilization of consecutive complete blood counts to evaluate lymphocyte exhaustion that is associated with assessed whole-body dose radiation exposure. If fast blood testing would not be conceivable, dose assessment can be at first evaluated dependent on basic boundaries, i.e., correlations between the extent of the body exposed to the radiation and the % of the radiation levels estimated in the environment; victim's shielding activities after the explosion; and signs and side effects from exposure to radiation or early radioactive particles' aftermath [24]. The radiation dose classes allude to dosages affecting the whole body or a large portion of the body (partial exposure). Notwithstanding the straightforward boundaries referenced above, the dose can be additionally be assessed dependent on: (a) the period until onset of early signs, (b) the seriousness of the signs (i.e., the acute radiation syndrome, ARS), and

(c) the biodosimetry methods [25–27]. Even though vomiting is a serious basic symptom after whole or huge partial body radiation exposure, it cannot be utilized to anticipate the radiation dose received. Vomiting can likewise be brought about by head injury, uneasiness, or other pathology [28].

It is key to point out that viable clinical triage can save numerous lives. In this, a fast reaction, sufficient coordination, and the accessibility of innovative biodosimetry is required. Clinical triage following an atomic explosion ought to be a stepwise cycle, where the principal point is abbreviated as "SALT"- Sort, Assess, Lifesaving Interventions, Treatment/Transport [29]. In the military, operational organizers use 'parts' to characterize the four levels where military clinical help is coordinated on a reformist premise to lead triage evaluation, quick treatment, evacuation, resupply, and capacities basic to the upkeep of health [30]. Stepwise triage should incorporate the point of care (POC) evaluation (blood counts, see above), followed by secondary evaluation, perhaps with high throughput screening to additionally characterize a person's dose (so that individuals considered in danger of showing ARS throughout the following weeks are identified). Also, assays which could be utilized for assessing long-haul malignant growth hazards (for example quality screening) ought to likewise be incorporated [31]. It is also imperative to consider that amid a radiological or atomic crisis, where the coordination of numerous individuals and management is fundamental, an unmistakable and agile command chain is vital.

## 5. Biological Effects in Nuclear and Radiological Accidents

### *5.1. Oxidative Stress and Inflammation at the Core of Ionizing Radiation-Induced Damage*

Ionizing radiation (IR) can break covalent bonds and cause oxidative harm to DNA, lipids, proteins, and numerous metabolites [32]. In experimental processes it is shown that the DNA molecule is more radiosensitive when it is irradiated in solution than in a dry environment [33]. The effects of IR on the DNA molecule are single and double chain fractures, structural alterations and elimination of the bases generating apurinic and apyrimidinic sites (AP sites), sugar damage, cross-links between DNA-DNA or between DNA-protein, and breaking of hydrogen bonds [34,35]. Moreover, overproduced reactive oxygen species (ROS) can react with cell membrane fatty acids and proteins impairing their function [36]. The primary event for the formation of a free radical in the radiolysis of water is the release of an electron in the interaction of low linear energy transfer (LET) ionizing radiation with the water molecule [37]. While the physicochemical events are a quick result of radiation exposure, the damage propagates the reaction by producing repeating waves of ROS, reactive nitrogen species (RNS), cytokines, chemokines, and other factors with related incendiary penetration [38].

During the radiolysis of water, ROS like superoxide anion ($O_2^{\bullet -}$), hydroxyl radical ($^{\bullet}OH$), hydrated electron and hydrogen peroxide ($H_2O_2$) are produced [39]. The release of nitric oxide ($NO^{\bullet}$) and its metabolites such as peroxynitrite ($ONOO^-$) and nitrogen dioxide ($NO_2^{\bullet}$) are also involved in IR genomic damage [5]. Overproduction of ROS and RNS is a harmful process that can cause damage to cellular biomolecules (DNA, proteins, and lipids), and affect the cell membrane, cellular signaling and genome integrity. These effects can influence numerous cellular processes linked to cell death, carcinogenesis, and cancer progression [40–42]. Indeed, oxidative stress, and the associated redox status shifts, can cause cell transition from quiescent to proliferative status, growth arrest or cell death activation according to the duration and extent of the redox imbalance [43]. In turn, cells injured by IR are responsible for inducing radiation bystander effects (RIBEs) in non-irradiated cell recipients, manifested by changes including (but not limited to) gene expression, protein synthesis, chromosomal aberrations, micronuclei formation, secretion of exosomes and miRNAs, and cell death/proliferation or transformation [44–46]. ROS are considered initiators, and NO, the transforming growth factor beta (TGF-β) and other inflammatory cytokines effectors are involved in RIBE [47,48]. Moreover, the inflammatory response generates recurring waves of ROS, cytokines, chemokines and growth factors with associated inflammatory infiltrates [49,50]. This represents a vicious circle where

both oxidative stress and inflammation induce each other. These concepts are supported because non-steroidal anti-inflammatory drugs and antioxidants decrease some of that latent damage, as well as the inflammation-associated mutations. This is a crucial point that determines that MCM to reduce the damage induced by IR is based on free radical scavengers, antioxidants, and anti-inflammatory agents [51–54].

### *5.2. Acute and Chronic Radiation Syndromes*

Biological impacts will fluctuate contingent upon the type and dose of radiation, and the time and recurrence (single or serial) of exposure [55]. The impacts of radiation on the body may show up rapidly (acute radiation syndrome, ARS) or require several years after exposure (deferred impacts, for example, fibrosis, sterility, genetic impacts, or malignancies). By and large, exposure to higher doses of radiation produces symptoms more quickly [54]. In the case of an atomic impact, radiation-derived wounds will be of different types, for example, injuries or thermal burns [56]. Heat and light cause thermal injury, including flash burns, fire burns, flash blindness (because of transitory loss of photopigments from retinal receptors), and retinal burns. The impact wave can cause breaks, slashes and cracks of the viscera, and aspiratory drain and edema [56].

Non-deadly harm (mis/unrepaired) may prompt genomic unsteadiness, for example, chromosomal variations, DNA mutations, and cell senescence. According to radiation assurance measures, radiation-prompted impacts are classified as (a) deterministic (tissue responses which require a threshold dose to exceed) which result from cell execution or the deficiency of cell capacity; and (b) stochastic or irregular (not relying upon such a limit, although its likelihood increases as the radiation dose expands) which are brought about by hereditary deviations and mutations setting off long term inherited impacts and malignancies [57].

The Life Span Study (LSS, https://www.rerf.or.jp, accessed on 7 January 2022) is an exploratory program examining deep-rooted health impacts dependent on epidemiologic (accomplice and case-control) considerations. Its most significant target is to explore the longer term impacts of bomb-derived radiation on reasons for death and the occurrence of malignancy. The examination has indicated that the danger of solid malignancy and leukemia among atomic specialists is steady with the dosage assessed, even if they get the radiation at low dose rates over numerous years [58]. The global INWORKS study has shown that in any event, when the combined dose of atomic industry laborers was under 100 mSv and the dose rate was under 10 mGy every year, the danger of solid malignancy is steady based on the dosage assessment [59]. A recent review [60] identified a large body of epidemiological data (published between 2006–2017) that assesses the evidence of an increase in solid cancer risks and/or leukemia, following low-dose IR exposure (<100 mGy).

ARS involves different phases of biological injury that may follow exposure (of the whole body or its majority) to a high dose of radiation (ordinarily in a brief timeframe). Its seriousness relies upon the radiation dose and normally includes syndromes whose term is directly correlated with the total dose received (and, ultimately, with the pace of exposure) [61–64]. Initially, a prodromal phase may show up with side effects, for example, sickness, spewing, and torpidity. This is continued (in hours to weeks) by various conceivable subsyndromes (related to various dose limits) for example the hematological (at doses of 1–2 Gy), gastrointestinal (GI) (dosages of 4–6 Gy), cutaneous (approx. 6 Gy), cerebrovascular (approx. 10 Gy) [65,66]. Lung wounds (approx. 8 Gy) may likewise show up half a month after exposure. An idle period of hematological ARS may infer a time of 1-3 weeks after getting a total dose of 2–4 Gy. Higher dosages may abbreviate or eliminate the inert phase [66].

Chronic radiation syndrome (CRS) results from long-term repeated exposure (external and/or radionuclide intake) to rather low doses [from 0.7–1.5 Gy (at rates > 0.1 Gy/year) to 2–3 Gy] and has a long-term intermittent course. It is worthwhile to point out that cancer induction can also be found at lower doses (<0.7 Gy). In the beginning, it was considered

that CRS manifestations could also include the chronic ARS damages, but as tissue reaction mechanisms of ARS and CRS differ, such association was recognized as incorrect [67]. The CRS term does not refer to the duration of disease (ARS manifestations can also remain for a long time, and develop chronic pathologies), but characterizes the result of protracted (chronic) radiation exposure [67–69].

Initial CRS symptoms are nonspecific, and can be reversible, if there is a decrease or a break in radiation exposure. If exposure continues, the initial symptoms grow progressively worse, and others may appear. The earliest manifestations of CRS are a dose-dependent inhibition of hematopoiesis and neurologic dysfunctions. Moderate but persistent leukopenia induced by neutropenia is one of the typical changes in peripheral blood, although in certain patients lymphopenia was also noted [68,70]. A severe degree of CRS is characterized by the development of bone marrow hypoplasia, persistent and marked granulocytopenia, profound thrombocytopenia, and moderate anemia. In these cases, hematopoiesis recovery is quite difficult or even impossible, even though the radiation exposure is discontinued [69]. Three sequential neurologic syndromes have been identified: vegetative dysfunction with impairment of neuro-visceral regulation, asthenic syndrome, and encephalomyelitis-type lesions of the central nervous system. Neurosensitive dysfunctions (olfactory and vestibular excitability decline, taste fatigue, etc.) sometimes precede the neuro-vegetative syndrome which is considered the earliest manifestation of the CRS [70]. Signs of vegetative dysfunction include: decrease in capillary tone (especially in skin vessels), an intense histamine-induced skin reaction, instability of the pulse with a tendency to hypotension, changes in the secretory and motor activity of the GI tract, etc. [70]. Some women develop changes in the sex hormone ratios (total estrogen levels were found at the lowest limit), in most cases accompanied by menstrual cycle disorders [69]; in animal models, a reduced number of follicles have been evidenced [71]. The rate of spontaneous abortions was five times higher than that without exposure [72]. The asthenic syndrome has a gradual progression, i.e., fatigue, headaches, dizziness, general weakness, hypersomnia, decreased working capacity and considerable memory deterioration [69,73]. At this stage patients can suffer cataracts, skin disorders such as a decrease in elasticity, dermatitis, xeroderma or hair loss [74]. Vascular dysfunction and thrombocytopenia play a key role in predisposition to hemorrhagic events like cutaneous petechial, mucosal, and visceral hemorrhages. Functional activity of organs and tissues, as well as structure, can undergo considerable changes (fibrosis, hypoplasia, malignant transformation, etc.). Radiation-related risk of cardiovascular disease is increased and can be associated with lung and heart fibrosis and atherosclerotic disorders [75]. Quite often, the CRS of medium severity is complicated by infections of respiratory and digestive systems [69,73]. When a demyelinating encephalomyelitis is developed, the patients' health status deteriorates dramatically, accompanied by general weakness and adynamy [69]. Although the brain has been classically regarded as a radioresistant organ, vascular lesions (edema, thrombosis, hemorrhage) and Blood-Brain Barrier (BBB) disruption are considered to be a precipitating factor for white matter necrosis [76]. Causes of death in the late period of CRS are sepsis and hemorrhages resulting from inhibition of hematopoiesis and immunity, malignant solid tumors and especially leukemia and chronic myeloleukemia [73]. There is evidence that relative risks are generally higher after radiation exposures in utero or during childhood [77].

Hereditary harm brought about by radiation is behind the expansion in the recurrence of malignant growths and can show both in the early phases and throughout the long term. As a reasonable model, notwithstanding acute ailments, numerous survivors of Chernobyl, Nagasaki, and Hiroshima additionally endured leukemia, and thyroid, stomach, and skin malignant growths (https://www.unscear.org, accessed on 7 January 2022) [74]. Studies on the nuclear bomb survivors in Japan revealed that the danger of mortality of solid malignant growth became apparent approximately ten years after detonation and expanded by half when the dose to which the colon was exposed arrived at 1 Gy; the danger of mortality from leukemia was quadrupled when the dose to which the red bone marrow was exposed reached 1 Gy [78–80].

## 6. Medical Countermeasures

It is critical to develop effective radioprotectors as a preventive measure for their application in planned radiation usage, such as radiation therapy, as well as unplanned exposure, such as natural background radiation, space travel, nuclear disasters, and nuclear warfare. The IR research program of the US National Cancer Institute proposed the following pharmacological classification of agents with IR protection properties according to the timing of administration: (a) protection, (b) mitigation, and (c) therapeutic agents [81]. In general, radioprotectors are used before IR exposure to protect cells and tissues from being damaged; radiomitigators are administered during or shortly after IR exposure, and attenuate damage and/or contribute to tissue recovery. Lastly, therapeutic agents are administered after symptoms have presented, acting as palliation or support [82]. As we will explain below, due to the capacity to scavenge free radicals, some antioxidants can be considered as radioprotectors, and many of them act also as radiomitigators for their capacity to enhance cellular antioxidant and repair mechanisms, during and after IR exposure. Finally, only a few can also be considered as therapeutic agents by reducing or palliating the clinical symptoms induced by exposure to IR.

The improvement of viable MCM to shield individuals from the unsafe impacts of normal radiation constitutes a neglected need [54]. Considering explicitly the radiological or atomic crises where earnest assistance is required, it is critical to plan separately for first responders, and for those directly presented to radiation during the mishap. First responders' vulnerability may be reduced by radioprotectors and radiomitigators, while those exposed to radiation may require radiomitigators, and of course, therapeutic support.

### *6.1. Radioprotectors*

An ideal radioprotective agent should fulfil several criteria, i.e., provide significant protection, be stable, offer the chance of a simple formulation, have an easy route of administration, and have no significant toxicity (mainly in particularly sensitive tissues, in which acute or late toxicity would be dose restricting). No single molecule so far has every one of these properties, and at this moment, radiation MCMs for ARS and other exposure-related injuries are assigned FDA orphan drug status [83].

Many different molecules have been assayed as potential radioprotectors. Some show promising properties but, considering pharmacokinetic properties and ease of in vivo administration, we might suggest the following for a potential radioprotective formula:

#### 6.1.1. Thiol-Containing Compounds

Since the detonation of the Hiroshima and Nagasaki bombs, the Walter Reed Army Research Institute (USA) enhanced its research program on radioprotective countermeasures and screened more than 4000 compounds [84]. Cysteine was the first one to confer radiation protection in mice subjected to total body radiation (TBI) [85], and since then many synthetic aminothiols have been developed and proved. Undoubtedly, the most effective was WR-2721 or amifostine, a sulfhydryl prodrug activated by alkaline phosphatase to the active WR-1065. Salivary glands and the epithelial cells of intestine are highly enriched in this activating enzyme, and thus oral administration of WR-2721 just before radiation results in localized high production of the bioactive derivate, preventing radio-induced mucositis and GI damage without significant systemic side effects [86–89]. The underlying mechanisms of action are free radical scavenging and hydrogen atom donation, along with DNA protection and repair; all coupled to an initial induction of cellular hypoxia [90–92]. WR-1065 has anti-mutagenic and anti-carcinogenic properties evidenced using in vitro testing systems [91], induces G1 cycle-arrest and p53 dependent-cytoprotection [52], up-regulates the expression of mitochondrial Mn-SOD2 and proteins responsible for DNA repair, and inhibits apoptosis through Bcl-2 and hypoxia-inducible factor-1$\alpha$ (HIF-1$\alpha$) [87]. Amifostine was the first Food and Drug Administration (FDA)-approved clinical radiation protector intended to reduce the impact of radiation on normal tissue, and more specifically, to decrease xerostomia in patients undergoing radiotherapy for head and neck cancers [92].

WR-1065 accumulates more rapidly in normal tissues than in malignant cells, due to the relative lower activity of alkaline phosphatase in cancer cells and acidic pH in the environment of many tumors. Amifostine is clinically used to prevent xerostomia, mucositis, dysphagia, dermatitis, and pneumonitis during radiotherapy of head and neck cancers, and a meta-analysis carried out in 2014 pointed out its beneficial effects [88]. However, a more recent randomized double-blind trial [89] does not support any benefit. Despite the heterogeneity, results appear to show some benefit to its use as radioprotector [87].

The glutathione redox status (GSH/GSSG) decreases after irradiation, mainly due to an increase in glutathione disulfide (GSSG) levels. Two reasons may explain the radiation-induced increase in blood GSSG: (a) GSH reacts with radiation-induced free radicals forming thiol radicals that react to produce GSSG; and (b) GSSG is released from different organs (e.g., the liver) into the blood. In fact, GSH is essential to prevent radiation damage and the glutathione redox ratio in the blood can be used as an index of radiation-induced oxidative stress [93]. The DNA single-strand breaks repair system is absent in GSH-deficient cells, and GSH is also essential to activate proliferation and repair of damaged tissues and to prevent cell death [94]. In fact, the main mechanism of action of most radioprotectors is to maintain intracellular levels of GSH. An illustrative example is *N*-acetylcysteine (NAC), a potent antioxidant and GSH precursor. NAC treatments (300 mg/kg, sc), starting either 4 h prior to or 2 h after radiation exposure, and with six subsequent daily injections over 7 days, reduced early deaths in abdominally irradiated (X-rays, 20 Gy) C57BL/6 mice [95]. More recently, radioprotective effects of NAC have been demonstrated in multiple studies [96,97], but the use of GSH or NAC with oncoradiotherapy cannot be supported because it may also favor cancer cell metastasis and radioresistance. Erdosteine (a homocysteine derivative) is a potent free radical scavenger, increases GPx and catalase (CAT) activities and GSH intracellular levels. Erdosteine treatment before γ-radiation ameliorated nephrotoxicity, and decreased IL-1, IL-6, and tumor necrosis factor alpha (TNF-α) blood levels, thus suggesting substantial protection against radiation-induced inflammatory damage [98].

Aminothiols and their phosphothioate derivatives, administered shortly before irradiation, exert radioprotection by one or a combination of effects: scavenging of radiation-induced free radicals; induction of hypoxia; formation of mixed disulfides; quenching of metals; repair of DNA and genome stabilization. However, radioprotectors of this type, including amifostine, have important side effects and a short pre-exposure time window of radioprotectiveness, which limit their use as radiation countermeasures [92,99]. Any strategy aimed at reducing toxicity, without reducing their radioprotective efficacy, would be a great advance. Rather novel approaches include: (a) slow-release delivery of drugs, (b) combined treatments with other radioprotectors/radiomitigators such as cytokines (G-CSF), selenium, metformin, antioxidants, etc.; (c) re-engineering better tolerated analogs like HL-003 or combining with antiemetic drugs; and (d) molecular conjugates and nanoparticle formulation designed to extend amifostine or WR1065 circulating half-life or to avoid intravenous administration. As reviewed by Singh y Seed [92], these approaches have proven to be useful but without a complete elimination of the toxicity or just increasing the radioprotection to a limited extent.

#### 6.1.2. Natural Phytochemicals

Over the last decades many phytochemicals, and especially polyphenols, have been broadly considered as radioprotectors and/or radiomitigators. The antioxidant activity of polyphenols depends, in part, on their ability to delocalize electron distribution, resulting in a more stable phenoxy group. Thereby, differences in ROS scavenging potential can be attributed to the different functional groups attached to the main nucleus [100]. Intercalation in DNA double helices induces stabilization and condensation of DNA structures making them less susceptible to free radicals' attack [100], reducing genotoxic damage induced by IR [101]. Xanthine oxidase and lipoxygenase are inhibited by many polyphenols, thus reducing the generation of free radicals. Finally, many polyphenols decrease the activation

of NF-κB and MAPK, thus reducing the release of inflammatory cytokines which play a role in the radiation-induced inflammatory response [102–104].

Genistein nanoparticles increase the expression of metallothionein genes and suppress the post-irradiation increase of cytokine production (IL-1-beta, IL-6) and cyclo-oxygenase-2 (COX-2) activity, thus preserving bone marrow progenitors and increasing survival on day 7 post-irradiation (9.25 Gy $^{60}$Co) [105]. The radioprotective effects of genistein are due to its ability to inhibit NF-κB, MMPs, and Bax/Bcl-2 signaling pathways and attenuate the inflammatory response induced by IR. In rodents, genistein has been shown to mitigate the effect of radiation on the lungs [106] and the intestinal tract [107]; used in combination with radiotherapy in prostate cancer patients, it can reduce intestinal, urinary, and sexual adverse effects.

The positive effects of curcumin as a radioprotector involve its free radical scavenging activity, antioxidant properties targeting the Nrf2 pathway [108], and its anti-inflammatory effects mediated by modulation of COX-2, IL-1, IL-6 [109], tumor necrosis factor alpha (TNF-α), TGF-β expression, release and/or activity [110,111]. Curcumin ameliorated radiation-induced pneumonitis and pulmonary fibrosis [112,113] and cognitive deficits (including learning and memory defects), exerted cardioprotective, neuroprotective, hepatoprotective, and renoprotective activities [108,110], and decreased pain severity [114]. Additionally, curcumin has antitumor effects [115] that can synergize with radiotherapy [116–118]; it should thus be considered a good option to increase the efficacy of radiotherapy on cancer cells, as well as to prevent the radiotherapy-induced adverse effects in normal tissues [112,114]. A few human studies have confirmed its efficacy for the management of radiotherapy induced dermatitis [119] and mucositis [120,121]. To modify the pharmacokinetic profile of curcumin and increase its bioefficacy, new formulations have been introduced [122].

Epigallocatechin-3-gallate (EGCG) and other flavonoids from green tea inhibited radiation-induced damage [123]. EGCG scavenges free radicals, increases the levels of several antioxidant enzymes, i.e., glutamate-cysteine ligase, SOD, and heme oxygenase-1 [124,125] and induces Nrf2 activation which, in turn, represses radiation-induced apoptosis and attenuates TBI-induced intestinal injury [126]. The inhibition of the proteasome, a regulator of inflammation, has been reported as well and, consequently, extracts of green tea decreased the release of pro-inflammatory cytokines, i.e., TNF-α, PGE2, IL-1β, IL-6 and IL-8 in vivo [127]. Epicatechin blocked ROS production and radiation-induced apoptosis via down-regulation of JNK and p-38, which ameliorated oral mucositis and survival rates [128], inhibited radiation-induced auditory cell death of rats [129], and enhanced the recovery of hematopoietic cells in mice [130].

Resveratrol (RES) has demonstrated potential anti-cancer, antioxidant, neuroprotective, anti-inflammatory and cardioprotective effects. It is noteworthy that RES serves as a scavenger of $O_2^{\bullet -}$, $^{\bullet}OH$ and metal-induced radicals, and increases the activity of many antioxidant enzymes [131]. RES significantly reduced radiation-induced chromosome aberration [132], DNA damage [133] and apoptosis, supported cell regeneration, and induced repression of the NLRP-3 inflammasome subset [134]. In mice, administration of RES attenuates radiation-induced intestinal damage via activation of sirtuin-1 [135], supporting lymphocyte [136] and intestinal functions recovery [137]. Under oxidative stress, RES promotes tyrosyl-tRNA synthetase acetylation, regulates relevant signaling proteins, and reduces apoptosis and DNA damage [138]. Clinical studies on RES as a normal tissue protector and potential tumor sensitizer are limited [139], mainly because RES possesses unfavorable bioavailability and pharmacokinetic properties. Synergistic effects with other polyphenols such as curcumin have also been evidenced and new formulations (hybrid molecules or nanoparticles) are being tested to increase its bioavailability and efficacy [140]. The use of derivatives, such as pterostilbene, with similar properties and a longer biological half-life, can significantly contribute to improve the radioprotective effects in vivo, as we have evidenced in our laboratory [141].

Oral silibinin treatment (100 mg/kg/day) reduced late-phase pulmonary inflammation and fibrosis in C57BL/6 mice after 13 Gy thoracic irradiation, via downregulation of NF-κB [142]. We have reported synergic radioprotective effects of silibinin with pterostilbene, resulting in 100% of the mice surviving, 30 days after TBI g-irradiation of 7.6 Gy (LD50/30) [141]. Silibinin can chelate thorium radionuclides ($^{232}$Th) preventing hemolysis and enhancing liver cells decorporation, which is important because those cells are the major targets of internalized $^{232}$Th [143].

Quercetin minimizes radio-induced oxidative damages and genotoxicity, preventing hematopoietic genomic instability and dysfunction [144] and skin fibrosis [145]. Quercetin pre-treatment attenuated ROS generation, downregulated NF-κB and reduced expression of proinflammatory cytokines (PGE2, IL-1β, IL6, IL-8 and TGF-β) [146]; it also reduced DNA double-strand breaks and cellular senescence in C57BL/6 mice exposed to a single-dose (25 Gy) or fractionated IR doses [147]. The anti-inflammatory effects of quercetin are also favored by its ability to reduce recruitment of neutrophils, myeloperoxidase and COX-2 activity, MAP kinases signaling and NLRP3 inflammasome activation in macrophages [148].

Recently, Faramarzi et al. [103] reviewed the radioprotective potential of natural polyphenols and, based on their dose-dependent antioxidant/pro-oxidant efficacy, concluded that they could represent a valuable alternative to synthetic compounds. Polyphenols provide protection to normal cells, with little or no protection to cancer cells, and in some cases, have the additional advantage of increasing cancer radiosensitivity. The potential use of polyphenols as radioprotectors is based on their low toxicity, the suitability of oral administration, and the possibility of combining several of them. Nevertheless, their low bioavailability due to poor absorption, rapid metabolism, and/or rapid systemic elimination, can compromise their efficacy. Thus, new pharmaceutical formulations (nanoparticles, vesicles, cocrystals . . . ) are being implemented and tested to facilitate oral administration and/or increase their effectiveness (see, e.g., https://www.circecrystal.com, accessed on 21 January 2022) [149–151].

The most promising non-polyphenolic phytochemicals with radioprotective effects are sesamol, gallic acid and caffeic acid derivates. The strong antioxidant activity of sesamol has been reported in comparison to standard antioxidants like vitamin C, curcumin, etc. Sesamol pre-treatment at 50 mg/kg (oral) was found to be the most effective dose in reducing mortality in irradiated Swiss albino mice exposed to 9.5 or 15 Gy γ-TBI [152]. The radiation-induced increase of apoptotic biomarkers and decrease in endogenous antioxidants (GSH, GST, CAT) was reduced by sesamol treatment, preserving crypt cells, villus height, and intestinal [152] and hematopoietic functions [153]. A recent study evidenced that daily oral consumption of sesamol is more effective than administration of a single dose before irradiation [154]. Similar results were observed using 100 mg/kg of gallic acid 1h prior to 10 Gy radiation exposure [155]. The cytoprotective effects of gallic acid are also due to its ability to enhance DNA repair, chelate metal ions, through the attenuation of MAPK and NF-κB/AP-1 signaling pathways, and reduce the release of inflammatory cytokines and adhesion molecules involved in leukocyte infiltration [156]. Caffeic acid (CA) and caffeic acid phenethyl ester (CAPE) act as free radical scavengers, compete with oxygen for IR-induced electrons, have antioxidant effects [151,157,158], decrease lipid peroxidation and increase antioxidant defenses in the heart and lung tissue of irradiated mice [159]. Treatment with CAPE prior to irradiation of rats effectively ameliorated intestinal [160], and hepatic [161] injuries. CA and CAPE inhibit activation of NF-kB, VEGF secretion and COX-2 activity, being considered potent anti-inflammatory agents [159,162]. In addition, CA stimulates cell cycle arrest and increases cell death in tongue, neck, and mouth cancer cells [158] and both molecules have anticarcinogenic properties attributed to their capacity to reduce tumoral angiogenesis, cancer growth and metastasis progression [158,162,163]. CAPE is a lipophilic agent, but incorporation into nanoparticles facilitates its administration. Moreover, nanoparticles can be modified to respond to different stimuli, such as pH, temperature, magnetic fields, oxidative stress, irradiation etc., thus facilitating the sustained release of drugs in selected tissues. That is the reason why even though CAPE-nanoparticles

showed a similar protective activity compared to CAPE under in vitro conditions, mice treated with nanoparticles had a longer survival after being exposed to IR [151].

Dietary sources of phytochemicals mentioned in this article and their radioprotective properties are detailed and reviewed in [102–104,164].

#### 6.1.3. Vitamins

With the understanding that free radicals perpetuate a significant amount of the damage caused by IR, vitamins with antioxidant potential (A, C, and E and its derivates) have been assayed as radioprotectors. Vitamin A and carotenes have antioxidant activity and capacity to enhance DNA repair, and in vivo reduced mortality and morbidity in mice exposed to partial or TBI [165]. Carotenoids such as crocin and crocetin (isolated from saffron) have antioxidant, anti-inflammatory and antiapoptotic effects [166]. In mice bearing pancreatic tumors, crocin significantly reduced tumor burden and radiation-induced hepatic damage [167], while crocetin reduced in vitro radiation injury in intestinal epithelial cells [168] and testis injury in pubertal mice exposed to 2 Gy X-rays [169]. Lycopene is the carotene isomer with the highest antioxidant potential and capacity to reduce proinflammatory cytokines expression such as IL-8 and IL-6 or NF-κB. Pre-clinical studies evidenced its radioprotective efficacy, particularly, if it is administered previously to or as soon as possible after radiation exposure [170,171] which is very interesting because lycopene has also anti-cancer activity, as recently reviewed in [172].

Administration of vitamin C (ascorbic acid, AA) before g-irradiation prevents chromosomal damage in bone marrow cells, mainly due to its antioxidant activity [173], reduces the GIS severity [174] and the adverse effects of TBI in the liver and kidney [175]. Moreover, intraperitoneal administration of 3 g AA/kg, up to 24 h after TBI (7.5 Gy), significantly increased survival in mice, reduced radiation-induced apoptosis in bone marrow cells, and restored hematopoietic function [176]. Nevertheless, administration of less than 3 g AA/kg was ineffective, and doses of 4 or more g/kg were harmful to mice. Moreover, treatments beyond 36 h were ineffective [176]. These facts highlight the limited efficacy margins of the treatment and compromise its use as a radioprotective measure.

Vitamin E is an essential fat-soluble nutrient with antioxidant, anti-inflammatory and neuroprotective properties. Eight vitamers are included in the vitamin E family, four saturated (α, β, γ, and δ) called tocopherols, and four unsaturated analogs (α, β, γ, and δ) referred as tocotrienols [177]. All of them are collectively known as tocols, and α-tocopherol is the most abundant in human tissues. Tocols are free radical scavengers, potent antioxidants and anti-inflammatory agents with capacity to attenuate fibrosis in tissues exposed to IR [177–179]. α-tocopherol succinate inhibited radiation-induced apoptosis and DNA damage, increased antioxidant enzymes activity, protected active mitotic tissues, and inhibited the expression of oncogenes in irradiated mice [180]. Moreover, when α-tocopherol was administered 24 h before $^{60}$Co γ-radiation, there was a significatively increase in the survival rate of mice, attributed to the capacity to restore crypt cellularity and inhibit bacterial translocation from the gut to the bloodstream [181]. Further studies revealed that α-tocopherol succinate significantly reduced thrombocytopenia, neutropenia, and monocytopenia, an effect mediated through induction of high levels of granulocyte colony-stimulating factor (G-CSF) [182]. Moreover, pre-clinical studies provided evidence that tocotrienols radioprotection is exerted, in part, via induction of G-CSF [183,184], suppressing expression of TNF-α, IL-6, IL-8, inducible nitric oxide synthase (iNOS), and NF-κB signaling [179]. IR downregulates the expression of thrombomodulin (TM) and increases endothelial surface expression of adhesion molecules which allow the attachment of immune cells and, thereby, contribute to inflammation and activation of the coagulation cascade. In this regard, the efficacy of tocotrienols is attributed to their higher antioxidant potential, their ability to inhibit HMG-CoA reductase activity [185], and increase TM expression in endothelial cells [186], which result in anti-permeability, anti-inflammatory and anti-thrombotic response [179]. Promising radioprotective results of γ-tocotrienol (GT3) have been demonstrated in mice [187] and primate models, by preserving the hematopoi-

etic stem and progenitor cells, and recovery from γ-irradiation (5.8 or 6.5 Gy)-induced neutropenia and thrombocytopenia [188,189]. Recent preclinical studies evidenced that GT3 may be a potential countermeasure against late degenerative tissue effects of high-LET radiation in the heart [190] and lung radiation injury [191]. Tocotrienols accumulate in the intestine to a greater level than tocopherols, and this can be involved in its greater ability to attenuate GIS [192]. γ-tocotrienols seem to have a greater efficacy as radioprotectors attributed [189] to their: (a) higher antioxidant potential [191], (b) capacity to downregulate proapoptotic/antiapoptotic ratio [193], (c) ability to accumulate in endothelial cells and intestinal epithelium which facilitates the recovery of mesenchymal immune cells [192], and (d) ability to inhibit HMG-CoA reductase, helping to avoid chronic inflammatory responses associated to radio-induced vascular and intestinal damage [185]. Moreover, recent studies have also evidenced the anti-cancer properties of γ-tocotrienols [179] and, although their low bioavailability is an important limiting factor [177], new formulations may help to overcome this pitfall. In this sense, a novel water-soluble liposomal formulation of γ-tocotrienol selectively targets the spleen and bone marrow with high efficiency, and facilitates rapid recovery of hematopoietic components after lethal TBI radiation in mouse models [194]. High doses of tocols are required to exert radioprotective effects, which increase the risk of toxic accumulative side effects. To ameliorate this risk, several trials have assayed and evidenced additive/synergistic effects with other radioprotectants such us aminofostine [195], simvastin [196], and others. For instance, pentoxifylline (a xanthine derivative approved by the FDA as a phosphodiesterase inhibitor, with antioxidant and anti-inflammatory effects) improved survival and enhanced the radioprotective properties of γ-tocotrienol on the hematopoietic, GI and vascular systems in mice subjected to 12 Gy $^{60}$Co γ-irradiation [197]. A Phase II clinical trial also demonstrated the radioprotective efficacy of the combination pentoxifylline+vitamin E to attenuate radiation-induced fibrosis [198]. Two randomized controlled trials provided evidence that dietary supplementation of alpha-tocopherol and beta-carotene during radiation therapy could reduce the severe adverse effects of treatment, but also warned that high doses might compromise radiation treatment efficacy [199,200]. Other radioprotective combinations, such as α-tocopherol acetate and AA, had the additional advantage of enhancing apoptosis in irradiated cancer cells [201,202].

Calcitriol upregulates the expression of SirT1, SODs and GPxs and induces the synthesis of metallothioneins in vitro [203,204]. Jain et al. (2013) showed a positive link between vitamin D and GSH concentrations, as well as a reduction in the levels of pro-inflammatory cytokines [205]. Inhabitants of contaminated regions near Chernobyl had lower vitamin D blood levels compared to those living in uncontaminated regions [206]. Therefore, oral supplementation with vitamin D during radiotherapy or in professionals chronically exposed to low IR doses could be doubly useful, preventing radioinduced oxidative stress and osteoporosis [207]. Recent studies evidence that calcitriol selectively radiosensitizes cancer cells by activating the NADPH/ROS pathway [208].

#### 6.1.4. Antioxidant Enzyme Activities and Oligoelements

Many antioxidant/defense enzymes, such as SODs, GPxs, and metalloproteins require trace elements as cofactors (e.g., Cu, Mn, or Se), thus, their dietary supplementation has been widely evaluated as a radioprotective strategy [54,209]. As cofactor for selenoenzymes, i.e., GPxs, thioredoxin reductase-1 and ribonucleotide reductase, Se supplementation enhances GPxs activity, thus reducing intracellular $H_2O_2$ and organic peroxide levels. Both sodium selenite and selenomethionine, i.p. injected before or shortly after (+15 min) radiation exposure ($^{60}$Co, 9 Gy), enhance the survival of irradiated mice, but selenomethionine had lower toxicity [210]. Se treatment enhances Nrf2 transcription and upregulates the adaptive response to IR in bone marrow and hematopoietic precursors [211]. 3,3′-diselenodipropionic acid (DSePA) had maximum absorption in the lung, suppressed NF-kB/IL-17/G-CSF/neutrophil axis and significantly reduced infiltration of neutrophils and levels of IL1-β, ICAM-1, E-selectin, IL-17 and TGF-β in the bronchoalveolar fluid,

prevented pneumonitis and increased survival of irradiated mice without affecting radiation sensitivity of tumors [212]. During the reaction with oxidizing free radicals DSePA generates intermediates with GPx like activity that reduce lipid peroxidation, apoptosis and excessive inflammatory response in radiosensitive tissues such as lung, liver, spleen, and GI tract, increasing survival against supra-lethal doses of γ-radiation [213]. Se compounds are less effective than aminofostine as radioprotectors, but have also lower toxicity and can be used in combined treatments [214].

Two consecutive systematic reviews, carried out between 1987 and 2012 [215] and 2013 and 2019 [216] evidenced that cancer patients tend to have low Se blood levels, which is aggravated by radiotherapy and/or its side effects (vomiting, etc.), and associates to a decrease in the activity of different antioxidant enzymes. Based on the results from clinical trials in patients who underwent radiotherapy, it was concluded that Se supplementation prevented or reduced the side effects of radiotherapy without compromising its anticancer efficacy; and consequently, authors highly recommend sodium selenite (200–500 µg/daily) oral supplementation [216]. On the other hand, it is paradoxical that several studies have demonstrated Se can act as prooxidant in a dose dependent fashion and can attenuate DNA repair mechanisms as well as antiapoptotic genes in some cancer cells, being nowadays assayed as a radiosensitizer in oncoradiotherapy. In vivo, the variability in redox potential gradients, the lower pH and the redox imbalance existing in the cancer microenvironment can facilitate the conversion of Se nanoparticles (SeNPs) into a pro-oxidant agent causing mitochondrial dysfunction, cell cycle arrest, and ultimately cancer cell death [217]. Organic Se compounds and especially SeNPs are better candidates as radioprotectors and radiosentitizers for their lower toxicity and higher cancer cell selectivity compared to sodium selenite [217,218].

SODs exist as CuZnSOD (cytosolic and nuclear fraction) and mitochondrial MnSOD, and both scavenge $O_2^{\bullet -}$ by accelerating its conversion to $H_2O_2$. Attempts to supplement the activity of endogenous SOD include the induction of in vivo gene expression using adenovirus or plasmid liposomes, and administration of nanozymes with SOD-like activity [219]. A porphyrin-mimetic of the human MnSOD (BMX-001), which crosses the BBB, protected the brain's white matter at the same time that it increased the sensitivity of the cancer cells to IR [220]. BMX-001 can potentially interact with numerous redox-sensitive pathways, such as those involving NF-κB and Nrf2, thus having an impact on their transcriptional activity [219]. The ability of BMX-001 to reduce the toxic effects of radiotherapy in cancer patients is being evaluated in phase II clinical trials (www.clinicaltrials.gov, accessed on 3 February 2022), e.g., NCT05254327 (rectal Cancer), NCT03608020 (brain metastases), NCT02655601 (high-grade glioma) and NCT02990468 (head and neck cancer) [54], and initial results seem to indicate that BMX-001 reduces side effects of radiotherapy.

#### 6.1.5. Cyclic Nitroxides

Synthetic cyclic stable nitroxide radicals (NRs), such as Tempo, Tempol, XJB-5-131, TK649.030, JRS527.084 or JP4-039, contain a nitroxyl group with an unpaired electron (-NO) and are stabilized by methyl groups, which prevent radical-radical dismutation. In vivo, NRs undergo a very rapid, one-electron reaction to the corresponding hydroxylamine, which has also antioxidant activity. NRs stabilize free radicals, easily diffuse through the cell membranes, have SOD and CAT-like activity, prevent the Fenton and Haber–Weiss reactions and are capable of protecting cells from radical induced damage [54,221].

Gramicidin *S*-nitroxide JP4-039 is a free radical scavenger and antioxidant targeting mitochondria through a segment of a cyclopeptide gramicidin that abrogates mitochondrial oxidative stress and cardiolipin oxidation, playing a pivotal role in the execution of apoptosis. JP4-039 effectively protects and mitigates TBI-induced hematopoietic, GI syndrome and skin damage even when it is delivered intravenously up to 72 h after exposure [222,223]. JP4-039 treatment ameliorated head and neck radiation-induced mucositis and marrow suppression in mice [224]. In a comparative study with other four nitroxides, JP4-039 demonstrated the best median survival after radiation exposition [225]. Based on these

properties, Luo et al. have synthesized and analyzed a series of nitronyl nitroxide radical spin-labeled RES derivatives that have also shown important radioprotective effects [226].

#### 6.1.6. Melatonin

*N*-acetyl-5-methoxytryptamine (melatonin), the main secretory product of the pineal gland, is a free radical scavenger with strong antioxidant properties, related to its chemical structure (specifically, the aromatic ring indole rich in delocalized electrons). Melatonin indirectly affects the oxidative–antioxidant balance, stimulating the expression of genes encoding for SODs, GPxs and GR, and ameliorates inflammatory responses. Such protection is evidenced by the capacity of melatonin to reduce 8-hydroxy-2′-deoxyguanosine levels and associated DNA lesions [227,228]. Moreover, animal studies confirmed that melatonin is able to alleviate radiation-induced cell death via inhibiting proapoptotic genes (e.g., Bax) and upregulating antiapoptotic genes (e.g., Bcl-2) [229]. Its radioprotective efficacy in pre-clinical models has been recently reviewed in [230]. Melatonin has some characteristics of an ideal radioprotector (multiple ways of action, low toxicity, and ability to cross biological barriers), and also has anti-cancer properties, i.e., apoptotic, antiangiogenic, antiproliferative, and metastasis-inhibitory effects reviewed in [231]. A meta-analysis of eight randomized controlled trials concluded that melatonin (20 mg, orally administered, once a day) led to substantial improvements regarding tumor remission, 1-year survival, and alleviation of therapy-related side effects [232].

### *6.2. Radiomitigators*

Radiomitigators minimize the toxicity of IR even when they are administered after radiation exposure, which differentiates them from radioprotectors that almost prevent/reduce the direct damages. Since most radiological and atomic mishaps are unexpected events, decision-making specialists should consider the use of radiomitigators that can most assist with limiting the destructive impacts of radiation exposure in those already affected. In this technical sense, ideal radiomitigators ought to be anti-inflammatory, enhance antioxidant defenses, have antimutagenic properties, upregulate the DNA repair mechanisms, activate mitotic processes, cell growth and differentiation to promote the regeneration of damaged tissues, and forestall or reduce ARS and CRS. At present, no molecule under study meets all these prerequisites, but there are a large number of choices [54,233,234], which may be combined, for quick administration to affected individuals. For such situations, we may recommend the following:

#### 6.2.1. Antiemetic Drugs, Probiotics, Prebiotics, and Toll-like Receptor Agonists

The pathophysiology of radioinduced GI toxicity is mediated by enterocyte loss, vascular injury, and bacterial translocation. The symptoms involve nausea, vomiting and diarrhea that aggravate electrolyte and fluid loss and lead to morbidity/mortality. Anti-emetics are useful for the stabilization of affected patients, with 5-hydroxytryptamine-3 receptor antagonists (granisetron and ondansetron) often being the first choice of treatment, whereas the addition of dexamethasone provides a modest improvement in prophylaxis [235]. Higher half-life and effectivity make granisetron a better option. The disadvantage of the preventive antiemetic treatment is that prodromal symptoms will be masked and they are useful bioindicators of ARS [235,236].

Gut microbiota dysbiosis aggravates radiation enteritis, reduces the absorbing surface of intestinal epithelial cells, weakens the intestinal epithelial barrier function, and promotes inflammatory factor expression, thus leading to a persistent mucositis, diarrhea and bacteremia [237]. Cancer patients exposed to radiation therapy exhibit marked alterations in gut microbiota composition, with a decrease in protecting *Bifidobacterium* and *Lactobacillus* spp. together with an excessive growth of Gram-negative pathogen bacilli [238]. Maintenance of normal microbiota using probiotics exerts nutrient competition and avoids binding of intestinal pathogens to host mucosa, thus preventing bacterial translocation. Gut microbiota produces short-chain fatty acids (SCFAs), mainly composed of acetate, propionate and

butyrate, that are the main energy source of colon cells and prevent intestinal inflammation by reducing the production of chemokines or adhesion molecules. Butyrate, in particular, is reported to stimulate a variety of colonic mucosal functions and to induce the expansion of Treg lymphocytes [239]. SCFAs play an important role in relieving intestinal injury induced by radiotherapy, whereas propionate [240] and valeric acid [241] have shown long-term radiomitigation of hematopoietic and GI syndromes by reducing the release of ROS, DNA damage and proinflammatory responses.

Prebiotics, fecal microbiota transplantation and, especially, probiotics prevent and improve radiation-induced enteritis [242,243]. In preclinical and clinical studies, probiotic interventions with *Lactobacilli* and/or *Bifidobacteria* ameliorate micro-intestinal atrophy and diarrheal symptoms [244], and exert cancer protection [245]. Commensal bacteria and probiotics interaction with Toll-like receptors (TLRs) activate the NF-κB, ensuring the development of innate immune responses, maintaining the barrier function, and promoting wound repair and tissue regeneration [237]. Several TLR2 and TLR4 agonists reduce radiation-induced apoptosis in epithelial stem cells, alleviating intestinal damage [246,247]. In clinical trials, probiotics reduce the incidence of diarrhea [242,243,248] and mucositis in cancer patients treated with radiotherapy [238], even though results are difficult to evaluate as they vary with the type of cancer, radiotherapy modality used, and type of probiotic used [246]. A recently published systematic review concludes that *Bifidobacterium longum*, *Lactobacillus acidophilus*, *Bifidobacterium breve*, *Bifidobacterium infantis* and *Saccharomyces boulardii* could be a good combination to prevent mucositis or ameliorate side effects of radiotherapy [249].

β-glucans (constituents of the cell wall in bacteria and plants) administered prior to and after irradiation exposition, prevent intestinal pathogen bacterial translocation, stimulate hematopoiesis and enhance survival in radiation-exposed animals [233,250]. Urolithin A (UroA), a metabolite generated from the transformation of ellagitannins by the gut, shows immunomodulatory and anti-inflammatory activities, and markedly upregulated the survival of irradiated mice. UroA improved the intestine's morphology architecture and the regeneration of enterocytes, and significantly decreased radiation-induced p53-mediated apoptotic cell death [251].

#### 6.2.2. Cytokines and Growth Factors

Any radiation dose >2 Gy results in bone marrow depletion, decreased blood cell counts, hemorrhage, and immunosuppression, leading to secondary infections. In the absence of treatment, death may occur in 2–8 weeks post-irradiation. Clinical therapy can help, and should not be limited to the use of antibiotics, blood, and platelet transfusions [236].

Cytokines like IL-1, IL-6, or TNFα promote inflammation, recruit leukocytes into damaged tissues and have restorative effects on the bone marrow. For that reason, earlier studies considered them as radioprotectors [252,253]. Nowadays, this hypothesis has changed since the proinflammatory states exacerbate IR toxicity.

The bone marrow recovery has been highlighted by the FDA, and in fact, some radioprotectants have been approved act in this sense, i.e., Filgrastim (a recombinant DNA type of the physiological G-CSF), Pegfilgrastim (a PEGlylated type of the previous), Sargramostim (a recombinant granulocyte-macrophage colony-stimulating factor, GM-CSF) and recently (2021) romiplostim (a Fc-peptide fusion protein that activates the thrombopoietin receptor) [54,234,254]. G-CSF and pegylated G-CSF promote proliferation, differentiation and maturation, and enhance blood neutrophil recovery and the survival rate. In 2009, The World Health Organization convened a panel of experts to develop recommendations for MCM in the management of H-ARS in a hypothetical scenario involving the hospitalization of 100–200 patients exposed to IR. According to this First Global Consensus, WHO strongly endorsed cytokine therapy (G-CSF or GM-CSF) within 24 h of exposure, above 2 Gy, for affected individuals with significant lymphopenia or when neutropenia (<500 cells/mm$^3$) persists for more than 7 days [236,255]. Pegylated G-CSF can be used as an alternative to G-CSF, with the advantage that it can be administered weekly (daily in the case of G-CSF),

but it appears to be less efficacious in treating injuries combined with skin burns. Treatment should be maintained until the neutrophil count maintains over 1000 cells/$mm^3$ in the absence of infection. Individuals with prolonged anemia can be treated with erythropoietin to avoid transfusions, considering the option of iron supplementation.

GM-CSF, administered as late as 48 h after radiation exposure, accelerates recovery from neutropenia and thrombocytopenia and decreases infection rates [256]. Lung injury (RILI) is a common complication of thoracic cancer radiotherapy, and currently, it has no effective treatment. GM-CSF reduced the occurrence of both pneumonia and pulmonary fibrosis. Moreover, an analysis of the clinicopathological characteristics of 41 patients, undergoing radiotherapy, evidenced that RILI remission was significantly correlated with GM-CSF treatment [257].

Keratinocyte growth factor (KGF) produced by mesenchymal cells protects and repairs epithelial tissues. KGF promotes the recovery of the mucosa, improves intestinal barrier functions and limits bacterial translocation and subsequent sepsis after irradiation. In clinical studies Palifermin®, a human recombinant KFG with analogous activity and higher stability, reduced the incidence, duration and severity of oral mucositis and esophagitis in cancer patients, and stimulated immune recovery following hematopoietic stem cell transplantation [258].

Epidermal growth factor (EGF) promotes epithelial and hematopoietic stem cells regeneration [259]. Bone marrow-derived hematopoietic stem cells (HSCs) express the EGF receptor in response to radiation and, in turn, EGF promotes HSCs regeneration in vivo. Mechanistically, EGF reduced radiation-induced apoptosis through repression of PUMA proapoptotic protein, and EGF receptor signaling was needed for DNA repair and for HSCs regeneration [259,260]. rhNRG-1β is an EGF-like protein that maintained mitochondrial integrity and ATP production in irradiated cardiomyocytes and preserves cardiac function via the ErbB2-ERK-SIRT1 signaling pathway [261]. Cotreatment with G-CSF led to a further increase in survival (20% in controls, 67% in EGF, 86% in EGF+G-CSF) [260].

A decrease in fibroblast growth factor (FGF) blood levels is found after irradiation, and a human recombinant derivative (FGF-P) improved duodenal functions and increased survival in GI-ARS mouse models. After been exposed to IR, FGF-P treated animals showed less hemorrhages and cutaneous ulcerations. FGF-P also holds promise for the treatment of burns, wounds and stem-cell regeneration [262].

It must be pointed out that the increased activity of many of these cytokines can be associated with prolonged ROS and RNS generation, a fact that favors the development of chronic inflammatory problems, and thereby the development of fibrosis and/or carcinogenesis [50]. Moreover, many cancer cells (glioblastoma, lung cancer, etc.) increase expression of EGF and other cytokine receptors, which makes the use of these radioprotectors unfeasible in cancer patients undergoing radiotherapy.

Bleeding due to thrombocytopenia is a common cause of death in ARS patients. Several agents have been assessed, including recombinant human thrombopoietin (TPO) and TPO mimetics like romiplostim (Nplate®) and eltrombopag [263]. Unfortunately, alloimmunization was developed after TPO administration, and it is no longer manufactured [264]. Nplate® (injectable) activates the TPO receptor on megakaryocyte precursors promoting cell proliferation and platelet production. It has been clinically assayed successfully for the treatment of thrombocytopenia and is approved by the FDA and European Medicine Agency for the treatment of idiopathic purpura and immune thrombocytopenia [265]. Romiplostim (administered for 3 consecutive days) increases survival to 100% in C57BL/6J mice exposed to a γ-TBI (7 Gy) and, at day 30, blood cells, hematopoietic progenitors and the histological appearance of the intestine were similar to non-irradiated controls [266]. Furthermore, a single dose of Nplate® (30 μg/kg) enhanced the survival to 40% [267]; combined with G-CSF and EPO, it increased survival to 100% (0% survival in controls 30 days after exposure), recovering hematological parameters to the levels of non-irradiated mice [268]. In non-human primates, Nplate® and pegfilgrastim combined treatment had much greater effects on platelet and neutrophil recovery following γ-irradiation compared

to single agents alone [269]. HemaMax® (human recombinant IL-12) restored all cell progenitor types in the bone marrow, decreased thrombocytopenia, leukopenia and infection rates and preserved GI functions, induced recovery of body weight and increased survival, when administered 24 h post-TBI (8.0 Gy) to mice and rhesus monkeys [270]. Pegylated IL-11 (Neumega®) is FDA approved to treat thrombocytopenia in cancer patients, although it has limited use as a radiomitigator, due to the need to be administered daily. To circumvent this problem, another mono-PEGylated IL-11 analog (BBT-059) was designed and showed higher bioavailability and potency in vivo. In a mouse model, BBT-059 led to multi-lineage hematopoietic reconstitution and appears to increase survival more than PEG-G-CSF and PEG-GM-CSF at high TBI doses [259,271].

HSCs and mesenchymal stem cells (MSCs) have also been proven to be effective in treating ARS in preclinical models. Hematopoietic stem cell therapy is recommended for patients with complete aplasia assessed by bone marrow biopsies [255], but in Chernobyl and other accident scenarios, survival was more likely among individuals that did not received bone marrow transplant [272]. Most recipients died shortly after transplantation due to the rapidly progressing insults to skin, lung and gut, complicated by serious bacterial, fungal and/or viral infections [264]. For that reason, Radiation Emergency Assistance Center/Training Site provides recommendations for the administration of antibiotic and/or other antimicrobial agents [264]. The WHO expert group (2011) recommend "wait and see" for a spontaneous or cytokine induction of hematopoiesis recovery, and to consider the administration of hematopoietic stem cells only after 2–3 weeks, and only in the absence of non-hematopoietic organ failure [255]. This recommendation has not changed as a result of the analysis of more recent studies [264]. Mesenchymal stem cells (MSC) are abundant resources (umbilical cord, bone marrow, blood, adipose tissue, and placental tissue), can differentiate into cells of the mesodermal lineage [273], and have demonstrated capacity to regenerate damaged tissues [274]. Despite this promise, translating the potential into actual clinical practice needs to solve many barriers, including immune-rejection, teratogenesis, and others [275]. A clinical trial is evaluating the efficacy of MSC injections for the treatment of chronic radiotherapy-induced complications (PRISME, NCT02814864) [273].

#### 6.2.3. Inhibitors of the Inflammatory Response

Excess of intracellular ROS, hypoxia and microvascular injury induced early activation of HIF-1α is a powerful stimulator of various pro-fibrotic mediators such as TGF-β, chemokines (e.g., MCP-1 and MIP-1beta), vascular endothelial growth factor (VEGF), and platelet-derived growth factor [276,277]. TGF-β stimulates apoptosis through Smad and Rho/Rock pathways, upregulates enzymes such as NOX2, NOX4, COX-2 and iNOS, inducing oxidative stress and proinflammatory responses that may persist and are associated with vascular damages and fibrosis RIBE [278–280]. Consequently, it is not surprising that halofuginone (an inhibitor of the TGF-β signaling pathway) and bevacizumab (an anti-VEGF antibody) have been shown to prevent or reduce radiation-induced fibrosis [281,282], with the additional advantage of inhibiting tumor angiogenesis and consequently tumor growth and metastasis formation. Different phase I/II clinical trials in women with metastatic breast cancer have shown more successful radiotherapy response if combined with a TGF-β inhibitor (LY2157299, NCT02538471). In fact, reduction of the plasma levels of TGF-β is associated with greater efficacy of radiotherapy on different types of cancer [283]. Some inflammatory polyphenols (genistein, curcumin, resveratrol or quercetin) downregulate TGF-β expression or signaling pathways attenuating radio-induced skin, pulmonary and/or myocardial fibrosis [102,112,113,145,277].

Radiation exposure enhances COX and iNOS activity, increasing the production of PGE2 and NO (respectively), both involved in the activation of the inflammatory response [284,285]. NSAIDs assayed as radiomitigators include non-selective COX inhibitors, e.g., acetylsalicylic acid (aspirin), ibuprofen, indomethacin, diclofenac, and flurbiprofen. Aspirin ameliorates radiation-induced kidney and lung damage and reduces post-irradiation chromosomal aberrations [286]. A recent meta-analysis of randomized controlled trials

indicates that acetylsalicylic acid reduces the overall risk of recurrence and mortality of colorectal cancer and/or colorectal adenomas, which increases the interest in its possible use as a radioprotector/radiosensitizer [287]. Flurbiprofen showed radioprotection in clinical studies, e.g., delaying the onset of mucositis and reducing its severity after radiotherapy in head and neck cancer patients, although the overall severity or duration of mucositis was not improved [288]. Benzydamine (a prostaglandin synthetase inhibitor) decreased the incidence and severity of oral mucositis associated to radiotherapy exposure [289].

Selective COX-2 inhibitors have the advantage of having less undesirable side effects, whereas promote myelopoiesis, thus avoiding the negative feedback control exerted by PGE2 [285]. Meloxicam alone, and in combination with IB-MECA (an adenosine A3 receptor agonist), has been reported to stimulate endogenous production of G-CSF and hematopoiesis, increasing the survival of mice exposed to lethal doses of radiation [290]. Celecoxib (a selective COX-2 inhibitor) attenuated severe skin reactions after a high single dose of 50 Gy and, in rats, reduced brain injury maintaining the integrity of the BBB and reducing inflammation [291]. In a glioblastoma model, the combined effect of radiation and celecoxib increased tumor cell necrosis, showing a significant reduction in tumor microvascular density and prolonged survival compared to irradiation alone [292]. It should be added that the analgesic effects of COX inhibitors can contribute to the well-being of of people affected by exposure to IR.

The mainstay of treatment in acute radiation pneumonitis consists of the systemic administration of glucocorticoids at high doses, aiming to reduce inflammation and inhibit TNFα-induced nitric oxide-mediated endothelial cell and lymphocyte toxicity. The use of inhaled corticosteroids ensures the highest dose deposition in the airway, thus decreasing side effects and ameliorating pulmonary fibrosis [293]. Nevertheless, systematic prophylactic use of corticosteroids to prevent toxic pulmonary edema is not recommended in China or Germany [294] and there is no evidence of a significant long-term benefit based on the use of corticosteroids.

#### 6.2.4. Statins

These 3-hydroxy-3-methyl-glutaryl-coenzyme A reductase inhibitors are commonly used to treat hypercholesterolemia and atherosclerosis. Statins also possess other biological effects, i.e., improving endothelial function, decreasing oxidative stress and inflammation, and regulating the immune system. Statins lessen the mRNA expression of pro-inflammatory and pro-fibrotic cytokines, accelerate the repair of DNA double-strand breaks and mitigate DNA damage [295]. Simvastatin, in particular, has been shown to mitigate radiation-induced enteric injury [296], to prevent radiation-induced marrow adipogenesis [297], to attenuate radiation-induced salivary gland dysfunction in mice [298], and to reduce cardiac dysfunction and capsular fibrosis [299]. GT3 and simvastin provide synergic protection against radiation-induced lethality, hematopoietic and bone marrow injury compared to the single treatments [196]. Pravastatin [300] and atorvastatin [301] have also shown radiomitigative efficacy.

#### 6.2.5. Angiotensin Axis Modifying Agents

There is some evidence that IR upregulates angiotensin II (AngII) expression in a dose-dependent manner, and AngII can increase ROS production through activation of the NADPH oxidase, upregulating inflammatory and profibrogenic pathways involved in long-term radiation injury [302,303]. Moreover, local synthesis of Ang II has been observed in fibrotic plaques and lung myofibroblasts, whereas apoptosis of alveolar epithelial was completely abrogated by an AngII receptor antagonist or by anti-AngII antibodies [304]. In pre-clinical models ACEi (angiotensin-converting enzyme inhibitors) and AngII antagonists, widely used as antihypertensive agents, have been shown to mitigate nephrotoxicity [305], pneumonitis [306,307] and other hematopoietic radio-inducted toxicities [308]. ACEi increases Ang-(1–7) levels which seems to have radioprotective [309] and antitumoral effects [310]. Several retrospective studies reported that ACEi decreased

the risk of radiation pneumonitis in lung cancer patients [311]. In a randomized controlled trial in patients exposed to 14 Gy TBI (9 equal fractions for 3 days) captopril mitigated renal nephropathy—increasing survival but not significantly [312], although a subsequent study by the same authors indicated significant differences in survival were attributable to radiomitigating effects on the respiratory system [313]. Captopril has been shown to be a better mitigator than lisinopril, enalapril, or ramipril [234], but a large prospective study in lung cancer patients treated with captopril and radiotherapy was halted due to insufficient accrual [302]. However, a recent meta-analysis seems to evidence that the use of ACEi decreased the incidence of symptomatic radiation-induced pneumonitis in lung cancer patients, especially in those older than 70 years, while those treated with angiotensin receptor blockers had a slight (non-significant) trend towards developing pneumonitis [314]. In addition, recent studies using ramipril and lorsartan showed reduced neuronal apoptosis, enhanced BBB integrity, and improved cognitive and motor function after TBI [315,316], major side effects of cranial radiotherapy in adult and pediatric cancer survivors.

#### 6.2.6. Molecular Hydrogen ($H_2$)

The antioxidant advantages of $H_2$ gas include [317,318]: (a) selectively scavenging the deleterious $ONOO^-$ and $^{\bullet}OH$ radicals, preserving other important ROS and NIS for normal signaling regulation, (b) stronger reductive activity than other dietetic antioxidants as C or E vitamins, (c) enhanced Nrf2 transcription and SOD, CAT and GPx expression [319] and (d) reduced NADPH oxidase activity [320]. In addition to reducing oxidative stress, $H_2$ increases the expression of antiapoptotic proteins (Bcl-xL and Bcl-2) [321], which could be helpful to attenuate damage induced by IR. In addition, $H_2$ downregulates the expression of adhesion molecules, reduces the infiltration of neutrophils and macrophages [322], inhibits NF-κB and reduces serum IL-1β, IL-6, and TNF-α levels, which could prevent RIBE and alleviate inflammatory response [323]. Most of these properties have been evidenced in a recent human clinical trial [324].

Hirano et al. [325] have recently published an interesting review on the potential radioprotective effects of $H_2$ on cognitive function, testis, lungs, heart, skin, cartilage, GI system, hematopoietic organs and the immune system. A randomized placebo-controlled study showed that consumption of $H_2$-supplemented water improved the quality of life of patients treated with radiotherapy for liver tumors [326]. $H_2$ mitigated radio-induced bone marrow damage in cancer patients without compromising the anti-tumor effects of radiotherapy according to a retrospective observational study [327]. In vitro and in vivo, $H_2$-rich water promoted tritium elimination (Table 1), reducing serum levels and tissue-bound tritium, and attenuated the genetic damage [328]. In addition to its antioxidant, anti-inflammatory and antiapoptotic effects, $H_2$ can be easily administered through various routes with little adverse effects and great efficacy [317,318,325]. These results show promising potential for the use of $H_2$ as a potential radiomitigator that should be studied in more depth.

#### 6.2.7. Metformin

Metformin is one of the most commonly used anti-diabetic drugs and has shown potential antioxidant, radioprotective, and anticarcinogenic properties [329,330]. It is a hydrogen-rich agent able to neutralize free radicals, increase GSH, and upregulate the activity of SOD and CAT [331], which all favor the antioxidant cell defense. Metformin stimulates DNA repair via non-homologous end joining or homologous recombination, and nucleotide excision repair [50]. Some studies showed that metformin exhibited a radioprotective effect only when administered to mice after radiation exposure; and others evidenced that it can also be considered a radiomitigator, because it reduced chronic production of ROS and pro-fibrotic cytokines such as TGF-β, and attenuated fibrosis through modulation of pro-oxidant genes such as NOX4, if administered after radiation exposure [332]. Metformin can also induce several redox-related genes, such as the PRKAA2 (which encodes the AMPK), a mechanism that helps in protecting cells from the accumu-

lation of unrepaired DNA and attenuates inflammation and pro-fibrotic pathways [329]. Metformin also ameliorates IR hematopoietic stem cell injury in mice [333]. Cardiovascular disease is a pivotal disorder after radiotherapy and the administration of metformin to γ-irradiated (5 Gy) rats significantly ameliorated the increase in plasma of cardiac disease-related biomarkers such as, LDH and CK-MB, NF-κB, IL-6 and TNF-α levels compared to the control group, which suggests that concomitant administration of metformin during radiotherapy can act as an efficient heart protector from oxidative stress and inflammatory damages, and endothelial dysfunction-derived damage [334]. Furthermore, several studies have evidenced the synergistic action of metformin when it is administered with sulfhydryl containing drugs [335] or with melatonin [332,336], although in others the synergy was not evidenced and melatonin was shown to be a better radioprotector [337]. It is also worth mentioning that metformin improves tumor oxygenation and the response to radiotherapy in tumor xenograft models. Thus, it can be considered a potential radiosensitizer to improve the outcome of radiotherapy [338,339]. In this regard, the use of metformin in patients with hepatocellular carcinoma and receiving radiotherapy has been associated with a higher overall survival [340]. Metformin's anticancer effects are well documented in preclinical studies, along with early phase clinical trials, but there is a significant lack of late phase clinical trials [341].

As we noted previously, we do not have any molecule that meets the requirements of an ideal radioprotector or radiomitigator. However, a combination of molecules may accomplish summation of protective/mitigating mechanisms and, in the end, synergies. Moreover, it is basic to have MCM that can be effective and that can also be immediately administered to the people in need. Such combinations should be assayed in standard clinical trials. Fortunately, most of the alternatives referenced above have had such preclinical and clinical examinations performed for various indications (see e.g., https://www.clinicaltrials.gov, accessed on 3 February 2022).

### *6.3. Radionuclide Scavengers*

Table 1 summarizes the diverse radionuclides that might be encountered in contamination events. Clinical countermeasures and treatments, their route of administration and main mechanisms of action, as well as the organs or tissues where those agents may accumulate are also indicated. Radiation exposure brought about by radionuclide contamination only stops if the radionuclide is completely disposed from the body, with or without therapy.

**Table 1.** Contamination by radionuclides and medical countermeasures.

| Ionizing Radiation Type | Element | Radioactive Half-Life | Major Exposure Pathways | Focal Accumulation | Medical Countermeasure for Internal Contamination | Mechanism of Action | Route of Management | References |
|---|---|---|---|---|---|---|---|---|
| α | **Americium** ($^{241}$**Am**) | 432.7 years | Inhalation<br>Skin | Lung<br>Liver<br>Bone<br>Bone marrow | Calcium-diethylenetriaminepentaacetate (Ca-DTPA) | Ca-DTPA is 10 times more effective than Zn-DTPA, thus Zn-DTPA is considered a second choice. It is also a good option for long term treatment. | IV (single infusion, do not fractionate the dose).<br>Nebulized inhalation (only in adults)<br>Wound irrigation can be accompanied by IV DTPA.<br>Within the first 24 h. Drink a lot and void frequently. | [11,342,343] |
| | | | | | Zinc-diethylenetriaminepentaacetate (Zn-DTPA) | | | |
| | **Plutonium** ($^{238}$**Pu**, $^{239}$**Pu** and $^{240}$**Pu**) | 88, 24,100 and 6563 years, respectively | Inhalation (Limited absorption) | Lung<br>Bone<br>Bone marrow<br>Liver<br>Gonads | Ca-DTPA/Zn-DTPA | Chelating agent (see above). | IV (daily bolus or single infusion, do not fractionate the dose).<br>Nebulized inhalation (only in adults). | [175,343–345] |
| | | | | | Deferoxamine (DFOA) (methanesulphonate of deferoxamine B) | Pu–deferoxamine complex is urinary excreted. | IM (preferred route)<br>IV (slow infusion) | |
| | | | | | Hydroxypyridinonate ligand 3,4,3-LI(1,2-HOPO) | Quelating agent, with increased urinary and predominant biliary Pu excretion. | Oral or IV. Not approved in humans, but it has a wider window of use and is more effective than DTPA. | |
| | **Polonium** ($^{210}$**Po**) | 138.4 days | Inhalation<br>Ingestion<br>Skin | Spleen<br>Kidneys<br>Lymph nodes<br>Bone marrow<br>Liver<br>Lung mucosa | Dimercaprol (BAL) (First choice) | $^{210}$Po reacts with thiol groups, so chelating agents containing these (BAL or DMPS) increase its renal excretion. | IM, but do not continue for too long. Repeated doses of BAL in combination with DMSA reduce the retention more than BAL alone. | [173,174,346] |
| | | | | | Dimercaptosuccinic acid (DMSA) | Forms water soluble chelates and, consequently, increases the urinary excretion of $^{210}$Po. | Oral. Safety/efficacy in children <12 years is not established. | |
| | | | | | Deferoxamine | $^{210}$Po-chelates are excreted in the urine. | IM (preferred route) or IV (slow infusion) | |
| | | | | | D-Penicillamine | | Oral, avoid if case of penicillin allergy | |
| | | | | | Dimercaptopropansulphonate (DMPS) | | Oral or IV | |
| | | | | | Gastric aspiration or lavage | Reduce intestinal absorption in case of ingestion | It only has some effect within 2 h of intake. | |
| | | | | | Magnesium sulfate, aluminum hydroxide, or barium sulfate | | Oral | |
| | **Thorium** ($^{232}$**Th**) | $1.41 \times 10^{10}$ years | Inhalation<br>Ingestion | Bone | Ca-DTPA/Zn-DTPA | Chelating agent (see $^{241}$Am) | (See $^{241}$Am) | [143] |

**Table 1.** *Cont.*

| Ionizing Radiation Type | Element | Radioactive Half-Life | Major Exposure Pathways | Focal Accumulation | Medical Countermeasure for Internal Contamination | Mechanism of Action | Route of Management | References |
|---|---|---|---|---|---|---|---|---|
| | **Uranium** ($^{235}$**U** and $^{238}$**U**) | $7.1 \times 10^8$ and $4.5 \times 10^9$ years respectively | Inhalation Ingestion | Kidneys Bone | Sodium bicarbonate ($NaHCO_3$) | Alkalinization leads to the formation of $UO_2(CO_3)_3^{4-}$ which is quickly eliminated by the urine, preventing toxic nephritis. Chelating agents must not be used. | IV (until urine pH is 8–9, and then mantain for 3 days) | [347–349] |
| | | | | Kidneys | Acetazolamide | Reduces uranium tubular reabsorption accelerating renal excretion. 3 times more effective than $NaHCO_3$, but without effect on skeletal retention | Oral | [350] |
| β | **Phosphorus** ($^{32}$**P**) | 14.3 days | Inhalation Ingestion Skin | Bone Bone marrow Rapidly replicating cells | Aluminum carbonate | Phosphate binder | Oral (for 5 days) | [351] |
| | | | | | Sodium glycerophosphate | Phosphate competition | Oral | |
| | | | | | Sodium phosphate | | Oral | |
| | | | | | Potassium phosphate | | Oral | |
| | | | | | Potassium phosphate, dibasic | | Oral (with a glass of water) | |
| | | | | | Sevelamer carbonate | Phosphate binder | Oral | |
| | | | | | Aluminum hydroxide | Competitive inhibition of intestinal absorption. | Oral | |
| | **Strontium** ($^{89}$**Sr** and $^{90}$**Sr**) | 51 days and 28 years, respectively | Inhalation Ingestion | Bone | Stabile strontium | Competitive inhibition of intestinal absorption. | Oral or IV | [352–356] |
| | | | | | Ammonium chloride (First choice) | Acidification of the medium favors the formation of anionic forms and their renal excretion. | | |
| | | | | | Calcium gluconate (First choice) | Competes for bone binding sites based on chemical analogy. | IV (within 12 h, if it is possible) | |
| | | | | | Sodium alginate, for digestive contamination. | Used for the treatment of gastro-oesophageal reflux. It forms a high viscosity gel and block intestinal absorption. | Oral (with a full glass of water) | |
| | | | | | Calcium carbonate | Ca interferes with intestinal absorption of Sr and Ra, increases fecal excretion, and compete with their bone deposition | Oral (within 12 h of radionuclide intake if it is possible) | |
| | | | | | Calcium phosphate | Phosphate decreases intestinal absorption, whereas Ca increases urinary excretion of Sr-90. | Oral (single dose within 24 h of radionuclide intake) | |

**Table 1.** *Cont.*

| Ionizing Radiation Type | Element | Radioactive Half-Life | Major Exposure Pathways | Focal Accumulation | Medical Countermeasure for Internal Contamination | Mechanism of Action | Route of Management | References |
|---|---|---|---|---|---|---|---|---|
| β (cont.) | **Strontium** (**$^{89}$Sr** and **$^{90}$Sr**) | 51 days and 28 years, respectively | Inhalation Ingestion | Bone | Barium sulfate | Reduces the intestinal absorption by forming insoluble sulfates. | Oral (single dose within 24 h) | [327,357] |
| | | | | | Aluminum phosphate | Reduces intestinal absorption. | Oral | |
| | | | | | Aluminum hydroxide | Reduces intestinal absorption. | Oral | |
| | **Tritium** (**$^{3}$H**) | 12.5 years | Inhalation Ingestion Skin | Whole-body | Water | Facilitates urinary excretion. The effectiveness of dilution will be greater, the sooner it is applied. | Oral (>3–4 L/day, for 3 weeks). $H_2$-rich water accelerates $^{3}$H renal excretion. | |
| | | | | | Chlorthalidone | Diuretic. Increase the renal elimination of $^{3}$H and other radionuclides. | Oral | |
| | | | | | Furosemide | Diuretic. Increase the renal elimination of $^{3}$H and other radionuclides | Oral | |
| | **Yttrium** (**$^{90}$Y**) | 64 h | Inhalation | Bone | Ca-DTPA/Zn-DTPA | Chelating agent (See $^{241}$Am) | See $^{241}$Am, but the administration must be done within 4 h | |
| | | | | | EDTA | Chelates are urinary excreted | IV (single dose) or IM (divided dose) | |
| β, γ | **Cesium** (**$^{134}$Cs and $^{137}$Cs**) | 2 and 30 years, respectively | Inhalation Ingestion | Whole-body (especially kidney) | Prussian Blue (Ferric hexacyanoferrate) | Traps Cs in gut minimizing intestinal absorption and reabsorption (in the case of Cs radionuclides excreted in the bile). | Oral | [358–361] |
| | **Cobalt** (**$^{57}$Co, $^{58}$Co** and **$^{60}$Co**) | 272 days, 71 days, and 5.26 years, respectively | Inhalation | Whole-body (especially liver) | EDTA | Chelates are urinary excreted | IV (Single dose) or IM (divided dose) | [362–364] |
| | | | | | Dimercaprol | Forms chelates by competing with endogenous sulfhydryl groups. | IM | |
| | | | | | Ca-DTPA/Zn-DTPA | Chelating agent (see $^{241}$Am) | (See $^{241}$Am) | |
| | | | | | Cobalt gluconate | Isotopic dilution. | IM or sublingual | |
| | **Iodine** (**$^{131}$I**) | 8.1 days | Inhalation Ingestion Skin | Thyroid | Potassium iodide (KI) | Competitive inhibition of NIS reduces thyroid deposition. Iodide blocks 98% of I-131 thyroid uptake if it is administered several minutes before incorporation. | Oral. Single dose that must be administered less than 24 h prior to, and up to 2 h after exposure. | [343,359,365] |
| | | | | | Potassium perchlorate ($KClO_4$) | Competitive inhibition of NIS reduces thyroid deposition. Not recommended in pregnant and newborns | Oral. Alternative option for iodine sensitivity. In Japanese is more effective than IK. | [365,366] |
| | **Iridium** (**$^{192}$Ir**) | 74 days | N/A | Spleen | EDTA | Chelating agent (see cobalt). | IV (single dose) IM (divided dose) | [367,368] |
| | | | | | Ca-DTPA/Zn-DTPA | Chelating agent (see $^{241}$Am) | (See $^{241}$Am) | |

**Table 1.** *Cont.*

| Ionizing Radiation Type | Element | Radioactive Half-Life | Major Exposure Pathways | Focal Accumulation | Medical Countermeasure for Internal Contamination | Mechanism of Action | Route of Management | References |
|---|---|---|---|---|---|---|---|---|
| α, γ | **Californium** ($^{252}$**Cf**) | 2.6 years | Inhalation Ingestion | Bone Liver | Ca-DTPA/Zn-DTPA | Chelating agent (see $^{241}$Am) | (See $^{241}$Am) | [369] |
| α, γ, neutron | **Curium** ($^{244}$**Cm**) | 18 years | Inhalation Ingestion | Liver Bone | Ca-DTPA/Zn-DTPA | Chelating agent (see $^{241}$Am) | (See $^{241}$Am) | [175,343,369,370] |
| α, β, γ | **Radium** ($^{226}$**Ra**) | 1602 years | Ingestion | Bone | Aluminum hydroxide | Blocks intestinal absorption. | Oral | [355,371–373] |
| | | | | | Calcium gluconate | Competes for bone binding sites based on chemical analogy. | IV (within 12 h, if it is possible) | |
| | | | | | Calcium carbonate | (See above in $^{90}$Sr) | Oral | |
| | | | | | Calcium phosphate | (See above in $^{90}$Sr) | Oral | |
| | | | | | Sodium alginate | (See above in $^{90}$Sr) | Oral (with a full glass of water) | |
| | | | | | Barium sulfate | Reduces the intestinal absorption of $^{226}$Ra by forming insoluble sulfates | Oral | |

MCM as listed have been suggested as treatments for internal contamination with radioisotopes by: Hickman, D. P. Management of persons contaminated with radionuclides: NCRP Report No. 161 (Volume 1) [374]. *Medical Management of Persons Internally Contaminated with Radionuclides in a Nuclear or Radiological Emergency*; Emergency Preparedness and Response; International Atomic Energy Agency: Vienna, 2018 [375]. Hübner, K.F.; Watson, E.E. Management of Persons Accidentally Contaminated with Radionuclides: NCRP Report No. 65. Washington, D.C. 1980 [376]. Managing Internal Radiation Contamination—Radiation Emergency Medical Management Available online: https://remm.hhs.gov/int_contamination.htm (accessed on 5 May 2022) [377]. Ammerich, M.; Giraud, J.M.; Helfer, N.; Menetrier, F.; Schoulz, D.; Blanc, J.; Vilain, D.; Boll, H.; Bourguignon, M.; Chappe, P.; et al. Medical Intervention in Case of a Nuclear or Radiological Event—National Guide, Release V36, 2008 [378].

### *6.4. Biological Dosimetry*

Despite the fact that there are many approved and expected biomarkers to survey the harmful impacts of IR [54], which biomarkers ought to be suggested in the instance of a radiological or atomic crisis? In these scenarios, speed, reliability, and traceability should be the prevailing criteria. These needs rouse us to choose, as the most suitable, those presented below.

#### 6.4.1. Lymphocyte Depletion Kinetic (LDK) Assay

This measure is utilized to gauge the dose following whole or incomplete body outer radiation exposure which was absorbed over minutes to hours. Methodologically, serial complete blood counts are acquired, and the outright lymphocyte check is determined and followed over time. The typical reach for outright lymphocyte count can be impacted by numerous variables, including the hardware utilized, and the ethnicity, age, health, and sex of the examined reference population. In addition, lymphocyte counts can be decreased or expanded by medications, contamination, and numerous clinical problems disconnected from radiation. What is key is that the lymphocyte exhaustion rate is directly identified with radiation assimilated dose (dose range 0.5–14 Gy). For example, a dose of 2–4 Gy associates with lymphocyte atrophy happening over ~4–6 days, while for a dose of 4–6 Gy the lymphocyte decrease requires ~2–4 days [379]. The US Armed Forces Radiobiology Research Institute (AFRRI) BAT (biodosimetry assessment tool) program (https://www.remm.nlm.gov, accessed on 15 February 2022) proposes acquiring a blood cell count as soon as possible after radiation exposure, and suggests that if the absorbed dose is known or suspected to be $\geq$5 Gy, blood counts ought to be obtained each 9–12 h for 2 to 3 days after irradiation and afterward at regular intervals of 24 h for 3 to 9 days. Other than this, a >5 Gy gamma-ray equivalent dose can be estimated based on biological end points like initial vomiting <2 h after exposure, or other dosimetric end points like physical dosimetry. If the retained dose is known or suspected to be <5 Gy, blood counts ought to be acquired at regular intervals of 24 h for 9 days. A straightforward dose-prediction algorithm based on lymphocyte kinetics as documented in prior radiation accidents was proposed by Goans et al. [380], where results are determined in gamma dose (Gy) whole body counterparts. Notwithstanding, this technique has impediments since it is not appropriate for surveying fractional body exposures or internally deposited radioisotopes.

In developed nations confronting a large-scale radiation crisis, biodosimetry dependent on LDK, clinical signs and indications, and dose estimated from geographic data are probably going to be accessible more quickly than biodosimetry dependent on cytogenetics [31].

#### 6.4.2. Neutrophils-to-Lymphocytes (NLR) Ratio

The neutrophil-to-lymphocyte ratio (NLR) is a valuable marker of host inflammation, which mirrors the connection between circulating neutrophils and lymphocyte counts (dose rage 0.5–10 Gy). It may conveniently be determined from routine complete blood counts (CBCs) with differentiation. It has been indicated that an increase in NLR throughout radiotherapy has a negative impact on survival in breast cancer patients, putting these patients with radiotherapy-susceptible host immunity at a higher risk of tumor recurrence [381]. An essential investigation of the prognostic estimation of the NLR compared with human whole-body irradiation was published after the mishap at the Chernobyl Nuclear Power Station [382].

#### 6.4.3. Cytogenetics

Cytogenetic dosimetry is a significant dose evaluation strategy, especially when there are challenges in deciphering the information, in scenarios where there is reason to believe that people not wearing dosimeters have been exposed to radiation, in instances of cases claiming for compensation after suffering radiation harms that are not upheld by unequivocal dosimetric proof, or in instances of exposure over a person's working lifetime

(https://www.iaea.org, accessed on 24 February 2022). This incorporates [383,384] the examination of:

1. DNA lesions. IR can cause a wide range of harm in DNA including base damage (BD), single-strand breaks (SSB), abasic sites (AS), DNA-protein cross-links (DPC), and DNA twofold strand breaks (DSB).
2. Chromosome-type abnormalities, i.e., dicentrics (DC, the worldwide standard for cytogenetic biodosimetry after radiation exposure; the dicentric yield is utilized to assess the radiation exposure measurements as per a measurably inferred and predetermined dose-reaction plot) [385]; centric rings; acentrics; rogue cells; reciprocal, non-reciprocal and interstitial translocations (dose range 0.5–5 Gy).
3. Chromatid-type aberrations i.e., terminal and interstitial deletions; achromatic injuries; isochromatic deletions; asymmetrical interchanges; symmetrical interchanges; triradials.
4. Premature chromosome condensation (PCC). The G0-PCC can be a valuable instrument for high dose biodosimetry with a speedy evaluation of fragment recurrence (dose range 0.2–20 Gy). Further, it holds the potential for multi-parametric dosimetry in combination with fluorescent in situ hybridization (FISH) [386].
5. Micronuclei framed from slacking chromosomal fragments or whole chromosomes at anaphase which are excluded from the nuclei of daughter cells (dose range 0.2–5 Gy). The cytokinesis-blocked micronucleus test (CBMN) is a biodosimetric technique to gauge chromosomal harm in mitogen-stimulated human lymphocytes [387]. While this procedure produces dose-reaction information that fits a straight quadratic model for exposures to low LET radiation and dosages up for 5 Gy, restrictions to the precision of this technique emerge at bigger doses. Precision at higher dosages is restricted by the number of cells at mitosis.

In this way, thinking about the technical conditions around a radiological or atomic crisis, it appears reasonable to suggest DSB, DC, and CBMN tests as the most ideal choices. For example, Nakamura et al. [388] considered the causal connection between DNA harm acceptance in bovine lymphocytes and the Fukushima mishap. DNA harm was assessed by evaluating the degrees of DNA DSB in peripheral blood lymphocytes by immunocytofluorescence-based measurement of γ-H2AX foci (dose range 0.5–5 Gy (microscopy) or 0.5–10 Gy (cytometry)). A more than two-fold increment in the fraction of harmed lymphocytes was seen in all animal cohorts within the evacuation zone. These outcomes set up a clear relationship between exposure and elevated levels of harm to DNA in animals living in the area of the atomic power plant mishap.

#### 6.4.4. Other Options

Other likely biomarkers of IR-induced harm incorporate (but are not restricted to) oxidative stress markers (e.g., 8-hydroxy-2′-deoxyguanosine, isoprostanes and protein carbonyls), immune and inflammatory mediators (various cytokines and chemokines), altered gene expression and mutations (e.g., NF-κB activation, GADD45, CDKN1A, genes related with the nucleotide excision repair mechanism, TP53, PPP1R14C, TNFAIP8L1, DNAJC1, PRTFDC1, KLF10, TNFAIP8L1, Slfn4, Itgb5, Smim3, Tmem40, Litaf, Gp1bb, Cxx1c, FDXR), epigenetic markers (gene methylation and repetitive components), metabolomics-related markers (e.g., urine glyoxylate, threonate, thymine, uracil, citrate,2-oxoglutarate, thymidine, 2′-deoxyuridine, 2′-deoxyxanthosine; blood serum inositol, serine, lysine, glycine, threonine, glycerol, isocitrate, gluconic acid, stearic acid, methylglutarylcarnitine), proteomics-related markers (e.g., plasma ferredoxin reductase, α-2-macroglobulin, chromogranin-A, GPx-3, lipidomics-related markers (e.g., blood serum linoleic acid, palmitic acid, phosphatidylcholines, glycerolipids, glycerophospholipids and esterified sterols), and miRNAs (e.g., miR-150, miR-30a, miR-30c, miR-34a, miR-200b, miR-29a, miR-29b, miR-144-5p, miR-144-3p). As of now, the hardware required, the need for automation (see for example [54]), and the absence of explicit investigations of this topic, do not prompt us to recommend any of these choices as satisfactory in a radiological or nuclear mishap scenario.

6.4.5. Networks

The WHO set up in 1987 the REMPAN organization (Radiation Emergency Medical Preparedness and Assistance Network) in light of the tasks assigned to it in the conventions on early notice and help with the event of atomic mishaps, for which the International Atomic Energy Agency (IAEA, https://www.iaea.org, accessed on 1 March 2022) is the responsible association. In 2007, WHO directed an overview of biological dosimetry laboratories and their crisis reaction abilities in chosen districts. The outcomes demonstrated a robust capacity, although there were not many local or public organizations set up. WHO BioDoseNet was then implemented as a worldwide organization of biodosimetry laboratories whose job is to help in management and decision-making in instances of big radiation crisis events where the capacity of individual labs is likely to be overwhelmed. Global biodosimetry networks have been set up, such as the Latin American Biological Dosimetry Network (LBDNet), the organization from Canada and The United States of America (North American BD Network), the Chromosome Network Council coordinated by Japan, the Asian Network of Biological Dosimetry (ARADOS), the Biological Dose Network in China and the European Network for Biological and Retrospective Physical Dosimetry (RENEB). At global level, worldwide organizations have been set up by the WHO (BioDoseNet), the IAEA (within RANET), EURADOS, and the Global Health Security Initiative (GHSI). This speaks to coordinated worldwide action to organise dose assessment. As an illustration of systems management efficacy, the MULTIBIODOSE project (multi-disciplinary biodosimetric instruments to oversee high scale radiological victims), established as a feature of the FP7 Euratom program in May 2010, showed genuinely similar outcomes among various research centers, with reliable dose estimates [389].

Systems management should give: (1) agility, by offering permanent support, every day/365 days a year, (2) prompt admittance to a facilitated server with stand-up capacity for integration, and (3) use of same equipment and supplies, standard operating procedures (SOPs), alignment curves and scoring rules for validated tests. Well built-up coordination can give the upgraded capacity to react to either demand for help from entities without dose assessment capability, or those who may be overwhelmed due to an abrupt surge of patients with suspected or known exposures. Consequently, in the event that one research center gets overwhelmed, tests can be shipped off to different labs within the network with certainty that the dose assessments will be reliable and equivalent.

6.4.6. Advances in Automation

An ideal reaction to radiological or nuclear crises (large-scale specifically) suggests the need for multi-parametric examination combined with a quality assurance/control, speed in collecting samples, high-throughput technology for test planning and analysis, right linkage with clinical triage and treatment surge, and proficient data management frameworks.

The US Biomedical Advanced Research and Development Authority (BARDA) program (https://www.phe.gov, accessed on 7 March 2022) is currently financing two correlative classifications of biodosimetry innovations: (1) A point of care test for a brisk triage of an exposed populace, categorized as having a biological dose above or under 2-Gy to determine the danger of suffering ARS. This test is intended to be managed by an individual with next to zero clinical preparation in a field hospital or triage station. Preferably, results would be accessible in less than 15 min after getting the sample with minimal sample handling. The point of this test is to isolate the people with radiation-related clinical necessities from the individuals who may not need explicit therapy. (2) A lab based high-throughput assay to quantitatively evaluate the dose retained by a person. The framework being created is fit for evaluating the assimilated dose in the range of 0.5–10 Gy with a superior exactness contrasted with the point-of-care devices [390]. This framework is required to be capable of processing up to 400,000 samples per week with a high level of lab computerization. Automation in obtaining results after sample assortment would in a perfect world be under 8 h. Over time, the utilization of robotized platforms and the improvement of research facility surge capacity networks can help customary cytogenetic

evaluation techniques. In this sense, enhancements incorporate the utilization of barcoded test compartments, mechanical fluid handlers, and computerized metaphase cell collectors, metaphase cell spreaders, slide stainers, and coverslippers [385]. Two primary methodologies have been utilized to diminish the time expected to gauge a dose—first, the work of robotized metaphase finders, and second, decreases in the number of metaphases scored. A few programming platforms have been created for triage management utilizing existing biodosimetry procedures; for example, time to emesis, LDK, and DCA (dicentric chromosome assay) have been implemented for use in the point-of-care setting. The BAT program (see above) is a model. The DCA QuickScan strategy further speeds up scoring [391]. Additionally, the RABIT-II-DCA is a completely computerized DCA in multiwell plates. All activities, from test stacking to chromosome scoring, are performed, without human mediation, by the second generation Rapid Automated Biodosimetry Tool II (RABiT-II) mechanical framework, a plate imager, and custom programming, FluorQuantDic. The framework requires small volumes of blood (30 µL per individual) to appraise the radiation dose received because of a radiation mishap or terrorist assault [392].

The CBMN is a biodosimetric instrument to measure chromosomal harm in mitogen-stimulated human lymphocytes. A scanning and image processing system with a robotized micronucleus scoring, the Radometer MN-Series (RS-MN) microscopic system designed by Radosys (Budapest, Hungary, https://www.radosys.com, accessed on 15 March 2022), has been presented for triage [393]. A similar model is the CytoRadx Assay (https://asell.com, accessed on 15 March 2022).

The FAST-DOSE (Fluorescent Automated Screening Tool for Dosimetry) is an immunofluorescent, biomarker-based framework intended to reproduce assimilated radiation dose in blood tests from possibly exposed people. This framework is intended to evaluate intracellular protein changes in blood leukocytes, and has been shown to effectively differentiate beneath or over 2 Gy as long as 8 days after complete body exposure in non-human primates [394].

The G0-PCC (G0-Phase Premature Chromosome Condensation) permits chromosome aberration analysis within the space of hours after blood assortment. Among all deviations, the examination of chromosomal fragments is the fastest [386]. Significantly, this approach holds potential for multi-parametric dosimetry in combination with FISH.

Mechanization of sample analysis by flow cytometry may overcome the time restrictions connected to the utilization of magnifying instrument-based examination (e.g., γ-H2AX identification [395]). This a phosphorylated type of the H2A histone family member X forming when twofold strand breaks show up, and it has been proposed for screening radiation-initiated DNA harm [396].

The DosiKit is a field-radiation biodosimetry immunoassay for fast triage of people exposed to outer TBI, which was validated in human blood cell extracts 0.5 h after in vitro exposure to $^{137}$Cs γ rays, utilizing γ-H2AX analysis. DosiKit can appraise absolute body irradiation doses from 0.5 to 10 Gy with a solid linear dose-dependent signal and can be utilized to differentiate possibly exposed people into three dose ranges: under 2 Gy, in the range of 2 to 5 Gy, and above 5 Gy (DCA permits exact estimation of dosages under 5 Gy). The fundamental preferred position is a brisk test that can be performed directly in the field by operational personnel with minimal preparation [397]. The DosiKit framework was completely integrated into a deployable radiological crisis research lab, and the reaction to operational necessities was exceptionally favorable [398].

The REDI-Dx Biodosimetry Test System (https://www.redidx.com, accessed on 15 March 2022) has been created as an in vitro analytic test, which uses blood collected into DxCollect® Blood Collection Tubes (BCT) for the quantitative assessment of the absorbed IR dose. Test outcomes are analyzed with the ABI 3500xL Dx Genetic Analyzer (Rancho Dominguez, CA, USA) and the REDI-Dx Interpretive Analysis Software (Rancho Dominguez, CA, USA), for the gene expression of a set of radiation responsive genes based on the DxDirect® genomic platform. REDI-Dx has been demonstrated to be a good indicator of dosage, for deciding treatment classification dependent on either 2.0 or 6.0 Gy [399].

The HemoDose is a software device, which estimates absorbed doses based on blood counts (https://www.remm.nlm.gov, accessed on 21 March 2022) [400]. The dose assessed by HemoDose dependent on lymphocyte counts and DC chromosome indicated an equivalent correlation with hematological ARS degrees 1 and 4 (in light of the clinical therapy protocols for radiation mishap casualties, METREPOL) [401,402].

### *6.5. Biophysical Dosimetry*

#### 6.5.1. External Exposure

##### Personal Dosimetry

These devices should be utilized when individuals are in danger of exposure to IR. The chest or stomach locations are predominant. Dosimeters can be additionally positioned in a limb for the scenario where the assessed dose received could be higher in the limb than in the rest of the body [403]. A standard individual dosimeter ought to be fit for giving data on ingested dosages from photons of at least 10 Gy (https://www.iaea.org, accessed on 21 March 2022). Naito et al. [404] estimated individual external doses during the recovery phase in a town after the Fukushima Daiichi atomic power plant mishap. They utilized an individual dosimeter (D-Shuttle) combined with a global positioning system gadget to quantify, and subsequently comprehend, individual outer doses relying upon the resident's area. At the point when a mishap happens outside the controlled territory, exposed people not wearing dosimeters cannot be checked for radiation exposure.

##### Area Monitoring

This is not expected to survey individual doses, but to give a rough estimate of the dose rate at the mishap site [405]. The requirement for exact and fair-minded radiation monitoring is exemplified by the disarray with respect to radiation levels around the Fukushima nuclear site [406]. Examinations may include different likely areas and hotspots for the evaluation of the presence and power of radioactivity in the environment and for the affected people. Region monitors ought to work dependent on explicit measures for the required level of precision, considering the reliance on radiation energy, direction of incidence, temperature, radiofrequency interference, as well as other expected factors.

Instruments used in screening a territory can include: (a) instruments for photons; (b) instruments to detect β particles and low energy photons; (c) instruments for neutrons; (d) passive γ monitors; (e) passive neutron survey meters; and (f) spectrometers (https://www.iaea.org, accessed on 21 March 2022). For example, after the Fukushima fiasco, most information with respect to the diminishing of biological radioactivity was estimated utilizing a NaI (Tl) scintillation meter (Hitachi Aloca Medical, Ltd., TCS-172B), aligned according to the International Electrotechnical Commission's norms (IEC 60846-1:2009) [407].

##### Dose Reconstruction

Dose reproduction is a review assessment of radiation dose(s) received by recognizable or representative people from a specific exposure. Much of the time, it is the only strategy to assess γ radiation or low dose exposure. Numerous factors, e.g., distance from the source, exposure length, irradiation geometry, and shielding, should be considered in dose assurance, making this technique a tedious system (https://www.icrp.org, accessed on 21 March 2022).

As depicted by [408], scientific issues in radiation dose recreation can be assembled into three distinct classifications: (a) information issues, for example, demographic data, changes in site tasks over the long run, characterization of intermittent versus persistent exposures, and the utilization of colleagues' information; (b) dosimetry issues, for example, strategies for evaluation of exposures, missed dose, unmonitored dose, and clinical radiation dose brought about as a condition of the workplace; (c) explicit issues identified with outer dose, such as affectability, precision and energy reliance of individual monitors, exposure geometries, and ongoing uncertainties. Issues identified with inner dose incor-

porate sensitivity of bioassay techniques, uncertainties in biokinetic models, suitable dose coefficients, and modelling uncertainties.

As instances of this strategy, Ivanova et al. [409] built up a system for the reproduction of individualized exposure doses for people dwelling at Chernobyl at the hour of the mishap. The strategy depends on the information of radio-biological (ground, meal) and dosimetric (whole body estimations) checking held in Ukraine during the period 1986–2013. Related to the Fukushima atomic mishap, Technical Report No. 162 (2012) gives a thorough record of the estimations and studies undertaken by the Australian Radiation Protection and Nuclear Health Agency (https://www.arpansa.gov.au, accessed on 1 April 2022) to survey the effect on the health of people and the environment in Australia. This report incorporates radiation observations of the environment and seas and testing of imported food and merchandise.

Electron Paramagnetic Resonance (EPR)

EPR dosimetry depends on the evaluation by EPR spectroscopy of dose subordinate changes in the concentration of free radicals, defects, or any species with paramagnetic properties that is shaped in a given material under exposure to IR [410]. The capacity of electron paramagnetic reverberation to quantify radiation-derived paramagnetic species, which persist in specific tissues (e.g., teeth, fingernails, toenails, bone, and hair), has made this procedure a noteworthy technique for screening significantly exposed people [411] for dose range 1–30 Gy.

Optically Stimulated Luminescence (OSL)

Luminescence signals utilized in dosimetry comprise light emitted under stimulation by a material able to store energy from radiation. Such materials incorporate insulators and semi-conductors [410]. The standard method for estimating OSL is to illuminate the sample with a steady power incitement source and measure the resulting luminiscence (identified as CW-OSL). The OSL signal arrives at the greatest outflow very quickly after the irradiation is turned on, and from that point decays dramatically as the snares are discharged [412]. The essential points of interest when contrasted with EPR are that there is no spectral deconvolution required and the equipment needed is considered less complex and more suited to field events. The applicable dose range is 0.03–10 Gy.

Thermoluminescent (TL) Material

TL-detectors were used for cosmic radiation dosimetry in early 1960s, and since then they have been applied in numerous space missions for personal dosimetry, for biological experiments and for medical applications [413].

The TL material has the capacity of storing energy when presented to IR. This energy is re-discharged as visible light when the material is heated to a suitable temperature. The unadulterated materials with ideal grid structure are not considered as TL materials; however, when certain materials are added (which serve as activators), they display thermoluminescence [414]. TL materials can demonstrate the environment radiation dose at the site of a mishap but not the assimilated dose of a victim.

Dose computation utilizing luminescence of solid-state dosimeter has become a significant field of innovative work, and has been effectively applied in territories affected by the Hiroshima and Nagasaki bombs [415], at the Nevada test site [416], and the Semipalatinsk test site [417]. The strategy was additionally utilized for areas affected by the Chernobyl mishap [418] and in contaminated settlements of the upper Techa River in the Southern Urals [419]. The applicable dose range is 0.01 mSv–10 Sv.

6.5.2. Internal Exposure

Whole-Body Counters (WBC)

A WBC is a gadget to measure principally γ-rays emitted by radioactive material present in the body, which may vary contingent upon the radionuclide. Alpha particle decaysa can likewise be identified by their coincident γ radiation [420]. Detection can be accomplished by utilizing either a scintillation indicator or a semiconductor locator set in proximity to the body. A fundamental constraint of this strategy is that WBC might not be able to distinguish radioisotopes that have comparable γ energies.

Thyroid Monitoring

After the Chernobyl mishap, thyroid malignancy expanded, a problem that was particularly evident among children who had internal exposure to radioiodine through milk consumption [365,421]. This was expected due to the inclination of radioactive iodine to collect in the thyroid and children's thyroids having a higher susceptability to radiation than adults. For that reason, radiological prophylaxis must be dedicated primarily to ensuring that the measure reaches, in optimal conditions, children and young people under 18 years of age, pregnant and lactating women [365].

$^{131}$I has a short half-life of around 8 days; however, once it enters the body, a high percentage will accumulate in the thyroid, and the gland will thus be directly exposed to β-particles and γ-beams. A reduction of radioiodine uptake into the thyroid can be achieved by administering a large dose of IK (130 mg, in adolescents older than 12 years and adults) shortly before and up to 2 h after, the expected onset of radiation exposure [365,366]. Saturation of the sodium/iodide symporter (NIS) and the Wolff–Chaikoff effect are the main mechanisms involved in transient blockage of $^{131}$I uptake in the thyroid [422]. As indicated in Table 1, stable iodine blocks about 98% of $^{131}$I thyroid uptake if it is given several minutes before incorporation. If the administration is simultaneous, the efficacy drops to 90%, being of the order of 50% when the iodine is administered 4–6 h later. Administering IK 24 h after exposure can even be counterproductive, because it prolongs the biological half-life of $^{131}$I that is already accumulated in the thyroid [365]. A single administration of IK is normally enough, although repetitive administrations might be required in the case of prolonged or repeated exposures. The latter is not recommended in neonates orpregnant and breastfeeding women due to the risk of adverse effects [365,366].

NIS transports other monovalent anions, with the following decreasing activity: $TcO_4^- > ClO_4^- > I^- > Br^-$. Perchlorate has a higher affinity to the NIS than iodide, thus it can be a good alternative in case of iodine sensitivity [365,366]. The Japanese have a delayed responsiveness to iodine transport saturation; thus, potassium perchlorate confers a much better protection in acute $^{131}$I exposure. In case of longer or repeated exposures, preference should be given to perchlorate in both Caucasians and Japanese [366].

Lung Monitoring

Lung checking is desirable not long after the intake, as it gives a more precise estimation of lung deposition and retention than whole-body estimation [423]. Suggestions have been made for computation of radiation dosages to the respiratory tract of laborers exposed to airborne radionuclides (Human Respiratory Tract Model for Radiological Protection, https://www.icrp.org, accessed on 1 April 2022). The retention is given for the complete body (for example, activity in all compartments of the biokinetic model, including respiratory tract and the thoracic lymph nodes). These capacities are determined several times after an acute intake (for example, inhalation or ingestion).

Lung counting is the sort of in vivo estimation suggested for radionuclides with long residence times in the lung, for example, uranium oxides, plutonium, and $^{241}$Am oxides. In vivo estimations of radionuclides in the lung commonly include the detection of X rays as well as photons with energies < 200 keV (https://www.iaea.org, accessed on 1 April 2022).

Bioassays

Concerning contamination, a bioassay is characterized as the assurance of amounts of radioactive material in the human body, regardless of whether by direct estimation, in vivo checking, or by measuring materials discharged or eliminated from the human body (for example the utilization of nasal swipes and swabs to evaluate for inhalation; stools and urine to survey for ingestion; and excisional biopsies of cutaneous scraped spots, slashes, and soft tissue wounds to evaluate for transdermal retention or absorption through injuries) [424].

After the Fukushima mishap in 2011, it was decided at the National Radiation Triage Medical Center (NREMC) of the Korea Institute of Radiological and Medical Sciences that mobile units for inward contamination checking would be more effective than the utilization of fixed-type WBCs to screen individuals. Accordingly, the NREMC developed a Mobile Radiobioassay Laboratory (MRL) for fast field-based checking of internal contamination following atomic or radiological crises [425].

#### 6.5.3. Body Surface Contamination

In the early phases of an atomic mishap, it is important to screen the surface radioactive contamination of everyone living and working around the accident site (https://www.irpa.net, accessed on 1 April 2022). Proper survey meters ought to be utilized. In such a situation, radiation type, size of contaminated territory, and strength and compactness of the detector itself are key determinants. Surface contamination is estimated by surface review meters, for example, a Geiger–Müller (G-M) counter, which is valuable for the concentration level, adequacy of the disinfecting method, and skin dose [426]. During evacuation following the Fukushima mishap, evacuees were screened for body surface contamination utilizing a G-M meter [201]. Body surface contamination levels should be related to inhaled thyroid dosages.

#### 6.5.4. Neutron Exposure

The neutron activation strategy is based on the measurement of radiation released by the decay of radioactive nuclei formed by neutron irradiation of the samples (body organs or tissues). At the point when radioactive atoms decay in the sample, $\gamma$ rays with traceable energies are emitted by each nuclide. Utilizing a $\gamma$-ray spectroscope, the amount and energy of radiated $\gamma$ rays can be estimated. For a mishap associated with neutron emission, neutron activation is the best technique to assessing the dose [204]. Ekendahl et al. [427] assessed neutron exposure to radioactivity in body tissues utilizing samples of human blood and hair dependent on neutron-spectrum calculations.

## 7. Conclusions

Biological and biophysical dosimetry is fundamental in distinguishing the individuals who need prompt clinical mediation from those with a possibility for postponed therapy, those who only require long follow up, and those potentially requiring no medical care. However, as of now, biomarkers and procedures do not appropriately fit a triage scenario. As no single biodosimetry method is adequate for dose prediction, time points, and exposure conditions, use of a combination of various methodologies is essential. Biomarker research likewise faces constraints, notably, on experimentation with humans, albeit sometimes the clinical exposure to therapeutic radiation has created informative outcomes. Moreover, most investigations have been performed utilizing a single type of radiation. Nonetheless, e.g., photon and neutron dosages in mixed exposure scenarios ought to be evaluated independently, since this may be key to assessing the danger of radiation-induced clinical syndromes. Lab information is basic to help decision-making, yet biomarker data are not sufficient for a health evaluation, triage, therapy, and clinical management. Research on biomarkers for dose assessment ought to incorporate exposure to mixed field radiation (synchronous exposure to various sorts of radiation), internal exposures from inhalation or ingestion of radionuclides, accumulated serial exposures,

and combined injury (as the inflammatory reaction will occur in organs/tissues affected by injuries, which will confound the assessment). Finally, the utilization of radiation biomarkers to anticipate levels of exposure should address the characteristic differences in radiosensitivities across a population. As a supplement to the biodosimetry procedures, we additionally recommend the option of utilizing biobanks to safeguard samples that do not need prompt examination. Consequently, a multiparametric approach based on physical, biological, and clinical strategies appears the most proper decision. For instance, Figure 1 lays outs the dosimetry/assessment measures that, with the available technology, ought to be performed in the event of a nuclear explosion.

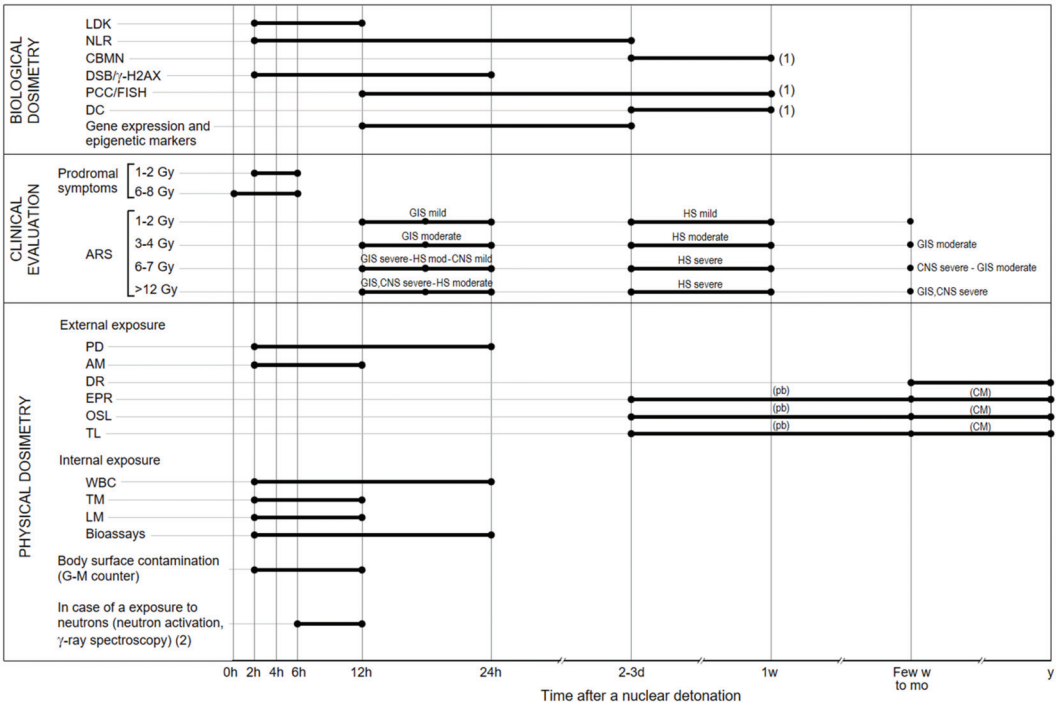


**Figure 1.** Stepwise dosimetry and evaluation after a nuclear detonation. (1) Results can be obtained more quickly if automation systems are available. GIS, gastrointestinal syndrome; HS, hematopoietic syndrome; CNS, central nervous system syndrome; mod, moderate; (pb), personal belongings; CM, construction materials. (2) Samples of human blood and hair. These cytogenetic techniques require 48–72 h to process the samples (not indicated). We have focused on the specific case of samples which are processed right after the accident, in a scenario where triage is rapid to avoid deterministic effects. If there is no option, samples can be processed later, and the results used in a retrospective manner. A recognized drawback of the dicentric (DC) and cytokinesis-block micronucleus (CBMN) assays is that the damage is unstable and therefore can be eliminated from the peripheral blood lymphocyte pool. Nevertheless, some lymphocytes containing aberrations continue to exist in the peripheral circulation for many years after an irradiation, although a high dose exposure or a long delay between irradiation and sampling can reduce the aberration yield. Sevan'kaev et al. remark that "the pattern of decline was biphasic with a more rapid first phase, with a half-life of 4 months, followed by a slower decline with half-lives around 2–4 years. It is usually assumed that for biological dosimetry purposes, where delayed sampling requires an extrapolation to zero time, the yield of DIC decreases with a half-life of about 3 years" [428]. Therefore, DIC and CBMN are useful for dose assessment from 2–3 days to 3 years after the accident, whereas FISH, as a stable alteration, has a time window of more years. It is recommended to run these assays within the first year after harmful radiation exposure.

During an accidental radiation exposure, MCM should separate first responders and individuals directly exposed to radiation. Ideal radioprotectors or radiomitigators for such scenarios have not been found. Based on recent advances and studied mechanisms, in this review we have discussed those that in our opinion appear most promising. Radioprotectors include derivatives of aminothiols and cyclic nitroxides (which, despite having toxic effects, have been shown to have greater radioprotective efficacy), natural products (vitamin antioxidants, trace elements such as Se, phytochemicals, etc.), and antioxidant enzyme mimetics, among others. Much more has been achieved in terms of increasing the knowledge about the mechanisms related to RIBE and in reducing side effects of radiotherapy in cancer patients. These advances will help in the development of new radiomitigating strategies. Among the most promising therapies are those aimed at activating recovery of the tissues (cytokines and growth factors), preventing side effects (probiotics, prebiotics, etc.), reducing the inflammatory response (bevacizumab, COXi, angiotensin axis modifying agents, statins) and, thereby, radio-induced chronic side effects such as fibrosis or others. The combination of antioxidant and anti-inflammatory effects of many of them prevents DNA damage and reduces the risk of developing tumors and/or cancers. Some molecules (e.g., melatonin, metformin, curcumin, caffeic acid, bevacizumab, etc.) offer the additional advantage of increasing the efficacy of radiotherapy on cancer cells, and thus can be used as radiosensitizers in cancer cells. Given that none of the tested molecules have total radioprotective/radiomitigating effects, it is evident that more work is needed to implement combined strategies aiming to find synergistic and/or additive effects. The development of new formulations (nanoparticles, nanocrystals, nanovesicles) will facilitate oral administration or the release of said molecules in especially sensitive tissues, thereby contributing to effective radioprotective/mitigating doses and reducing possible toxic effects. In the event of a nuclear emergency, the protocols and time sequence for selecting/caring for the affected exposed, as well as the appropriate treatments (radioprotectants/radiomitigators), including doses and route of administration, need to be implemented. MCM are still assigned FDA orphan drug status, and thus many of these radioprotective strategies could be considered by FDA under "fast track" approval process.

The utilization of complementary tools, preferably shaping parts of automated equipment and established networks, is the future of radioprotection research. Furthermore, in practice, clinical evaluation faces restrictions for large scale screening, i.e., the need of uniquely prepared medical care workers or the low throughput due to the short time available to finish a correct evaluation. Straightforward strategies such as an early lymphocyte count are needed to set up a baseline. However, this may not be conceivable in a large-scale event because of time limitations and the absence of enough technical personnel.

Therefore, despite the many advances discussed in this review, there are many challenges that still need to be addressed to deal effectively with nuclear and radiological accidents.

**Author Contributions:** Conceptualization, E.O. and A.M.; methodology, E.O. and A.M.; software, R.S.-P. and B.P.; validation, E.O., R.S.-P. and A.M.; formal analysis, R.S.-P. and J.I.V.; investigation, all authors; resources, all authors; data curation, R.S.-P.; writing—original draft preparation, E.O., J.M.E. and A.M.; writing—review and editing, E.O. and R.S.-P.; visualization, R.S.-P. and E.G.; supervision, J.M.E.; project administration, E.O.; funding acquisition, E.O. and J.M.E. All authors have read and agreed to the published version of the manuscript.

**Funding:** This research was funded by the MINECO (Ministerio de Economía y Competitividad), Spain (grant number SAF2017-83458-R); Elysium Health Inc., NY, USA (grant number OTR2017-17899INVES); and the Agencia Valenciana de Innovación (grant number INNVA1/2021/22).

**Conflicts of Interest:** The authors declare no conflict of interest.

## Abbreviations

AA, acid ascorbic; ACEi, angiotensin-converting enzyme inhibitors; AFRRI, United States armed powers radiobiology research institute; AngII, angiotensine II; AP sites, apyrimidinic sites; ARADOS, Asian network of biological dosimetry; ARS, acute radiation syndrome; AS, abasic sites; ASA; acetylsalicylic acid; BARDA, United States biomedical advanced research and development authority; BAT, biodosimetry assessment tool; BBB, Blood-Brain Barrier; BBT-059, PEGylated interleukin-11; BCT, Blood Collection Tubes; BD, base damage; CA, caffeic acid; CAPE, caffeic acid phenethyl ester; CAT, catalase; CBCs, complete blood counts; CBMN, cytokinesis-blocked micronucleus assay; COX, cyclooxygenase; CNS, central nervous system syndrome; CRS, chronic radiation syndrome; DC, dicentric chromosome; DPC, DNA-protein cross-links; DSB, double strand breaks; EGCG, Epigallocatechin-3-gallate; EGF, epidermal growth factor; EPR, electron paramagnetic resonance; FAST-DOSE, fluorescent automated screening tool for dosimetry; FDA, Food and Drug Administration; FGF, fibroblast growth factor; FISH, fluorescent in situ hybridization; G-CSF, granulocyte colony-stimulating factor; GHSI, global health security initiative; GI, gastrointestinal; GI-ARS, gastrointestinal ARS; GIS, gastrointestinal syndrome; GM-CSF, granulocyte macrophage colony-stimulating factor; G-m, Geiger-Müller; GPx, Glutathione peroxidase; GSH, L-γ-glutamyl-L-cysteinyl-glycine; GSSG, oxidized glutathione; GT3, γ-tocotrienol; H-ARS, hematopoietic acute radiation syndrome; HIF-1α, hypoxia-inducible factor-1α; IAEA, international atomic energy agency; IEC, international electrotechnical commission; IND, improvised nuclear devices; iNOS, inducible nitric oxide synthase; IR, ionizing radiation; JP4-039, Gramicidin *S*-derived nitroxide; KGF, Keratinocyte growth factor; LBDnet, latin American biological dosimetry network; LDK, lymphocyte depletion kinetic assay; LET, linear energy transfer; LSS, Life Span Study; MCM, medical countermeasures; Melatonin, *N*-acetyl-5-methoxytryptamine; MRL, mobile radiobioassay laboratory; NAC, *N*-acetylcysteine; NF-κB, nuclear factor kappa-light-chain-enhancer of activated B cells; NIS, sodium/iodide symporter; NREMC, national radiation Triage medical center; Nrf2, Nuclear factor erythroid 2-related factor 2; NRL, neutrophils-to-lymphocytes ratio; OSL, optically stimulated luminescence; PCC, premature chromosome condensation; POC, point of care; PPARs, peroxisome proliferator-activated receptors; RABIT-II, rapid automated biodosimetry tool II; RED, radiation exposure devices; RDD, radiological dispersal devices; REMPAN, radiation Triage medical preparedness and assistance; RENEB, European network for biological and retrospective physical dosimetry; RES, resveratrol; RILI, Radiation-induced lung injury; RNS, reactive nitrogen species; ROS, reactive oxygen species; RS-MN, radiometer MN-series; SALT, Sort Assess Lifesaving Interventions Treatment/Transport; SCFAs, short-chain fatty acids; SOD, superoxide dismutase; SOP, standard operating procedure; SSB, single strand breaks; TNF-α, tumor necrosis factor alpha; TGF-β, transforming growth factor beta; TBI, total body irradiation; TL, thermoluminiscent material; TLRs, Toll-like receptors; TM, thrombomodulin; UroA, urolithin A; VEGF, vascular endothelial growth factor; WBC, whole body counters.

## References

1. Rubin, G.J.; Chowdhury, A.K.; Amlôt, R. How to Communicate with the Public About Chemical, Biological, Radiological, or Nuclear Terrorism: A Systematic Review of the Literature. *Biosecur. Bioterror. Biodef. Strat. Pract. Sci.* **2012**, *10*, 383–395. [CrossRef] [PubMed]
2. Socol, Y.; Gofman, Y.; Yanovskiy, M.; Brosh, B. Assessment of probable scenarios of radiological emergency and their consequences. *Int. J. Radiat. Biol.* **2020**, *96*, 1390–1399. [CrossRef] [PubMed]
3. Williams, M.; Armstrong, L.; Sizemore, D.C. Biologic, Chemical, and Radiation Terrorism Review. In *StatPearls*; StatPearls Publishing: Treasure Island, FL, USA, 2020.
4. Drell, S.D.; Shultz, G.P.; Andreasen, S.P. Nuclear Safety. A Safer Nuclear Enterprise. *Science* **2012**, *336*, 1236. [CrossRef] [PubMed]
5. Bomanji, J.B.; Novruzov, F.; Vinjamuri, S. Radiation Accidents and Their Management: Emphasis on the Role of Nuclear Medicine Professionals. *Nucl. Med. Commun.* **2014**, *35*, 995–1002. [CrossRef] [PubMed]
6. Ohba, T.; Liutsko, L.; Schneider, T.; Barquinero, J.F.; Crouaïl, P.; Fattibene, P.; Kesminiene, A.; Laurier, D.; Sarukhan, A.; Skuterud, L.; et al. The SHAMISEN Project: Challenging historical recommendations for preparedness, response and surveillance of health and well-being in case of nuclear accidents: Lessons learnt from Chernobyl and Fukushima. *Environ. Int.* **2020**, *146*, 106200. [CrossRef]
7. Korir, G.; Karam, P.A. A Novel Method for Quick Assessment of Internal and External Radiation Exposure in the Aftermath of a Large Radiological Incident. *Health Phys.* **2018**, *115*, 235–251. [CrossRef]

8. Dainiak, N.; Albanese, J.; Kaushik, M.; Balajee, A.S.; Romanyukha, A.; Sharp, T.J.; Blakely, W.F. Concepts of Operations for a US Dosimetry and Biodosimetry Network. *Radiat. Prot. Dosim.* **2019**, *186*, 130–138. [CrossRef]
9. Sehgal, B.R. *Nuclear Safety in Light Water Reactors: Severe Accident Phenomenology*; Academic Press: Cambridge, MA, USA, 2011; ISBN 978-0-12-391906-9.
10. Kortov, V.; Ustyantsev, Y. Chernobyl accident: Causes, consequences and problems of radiation measurements. *Radiat. Meas.* **2013**, *55*, 12–16. [CrossRef]
11. Harrison, J.; Fell, T.; Leggett, R.; Lloyd, D.; Puncher, M.; Youngman, M. The polonium-210 poisoning of Mr Alexander Litvinenko. *J. Radiol. Prot.* **2017**, *37*, 266–278. [CrossRef]
12. Miller, R.G.; Mitchell, J.D.; Moore, D.H. Riluzole for amyotrophic lateral sclerosis (ALS)/motor neuron disease (MND). *Cochrane Database Syst. Rev.* **2012**, *65*, CD001447. [CrossRef]
13. Reeves, G.I. Biophysics and Medical Effects of Enhanced Radiation Weapons. *Health Phys.* **2012**, *103*, 150–158. [CrossRef]
14. Kraus, T.; Foster, K. Analysis of Fission and Activation Radionuclides Produced by a Uranium-fueled Nuclear Detonation and Identification of the Top Dose-producing Radionuclides. *Health Phys.* **2014**, *107*, 150–163. [CrossRef]
15. Baverstock, K.F.; Ash, P.J.N.D. A review of radiation accidents involving whole body exposure and the relevance to the LD50/60 for man. *Br. J. Radiol.* **1983**, *56*, 837–849. [CrossRef]
16. DiCarlo, A.L.; Maher, C.; Hick, J.L.; Hanfling, D.; Dainiak, N.; Chao, N.; Bader, J.L.; Coleman, C.N.; Weinstock, D.M. Radiation Injury After a Nuclear Detonation: Medical Consequences and the Need for Scarce Resources Allocation. *Disaster Med. Public Health Prep.* **2011**, *5*, S32–S44. [CrossRef]
17. Conklin, W.C.; Liotta, P.L. radiological threat assessment and the federal response plan—A gap analysis. *Health Phys.* **2005**, *89*, 457–470. [CrossRef]
18. Forum on Medical and Public Health Preparedness for Catastrophic Events; Board on Health Sciences Policy; Institute of Medicine. *Nationwide Response Issues after an Improvised Nuclear Device Attack. Workshop Summary*; Davis, M., Reeve, M., Altevogt, B., Eds.; The National Academies Collection: Reports funded by National Institutes of Health; National Academies Press (US): Washington, DC, USA, 2013; ISBN 978-0-309-28601-5.
19. Yeddanapudi, N.; Clay, M.A.; Durham, D.P.; Hoffman, C.M.; Homer, M.J.; Appler, J.M. Informing CONOPS and medical countermeasure deployment strategies after an improvised nuclear device detonation: The importance of delayed treatment efficacy data. *Int. J. Radiat. Biol.* **2018**, *96*, 4–11. [CrossRef]
20. Musolino, S.V.; Harper, F.T. Emergency response guidance for the first 48 hours after the outdoor detonation of an explosive radiological dispersal device. *Health Phys.* **2006**, *90*, 377–385. [CrossRef]
21. Wolbarst, A.B.; Wiley, A.L.; Nemhauser, J.B.; Christensen, D.M.; Hendee, W.R. Medical Response to a Major Radiologic Emergency: A Primer for Medical and Public Health Practitioners. *Radiology* **2010**, *254*, 660–677. [CrossRef]
22. Breitenstein, B.D., Jr. The medical management of unintentional radionuclide intakes. *Radiat. Prot. Dosim.* **2003**, *105*, 495–497. [CrossRef]
23. Cherniavskiy, I.Y.; Vinnikov, V.A. The assessment of radiation hazardous areas considering the spectral analysis of the neutron component of a tactical neutron bomb detonation. *Appl. Radiat. Isot.* **2019**, *149*, 152–158. [CrossRef]
24. Hick, J.L.; Bader, J.L.; Coleman, C.N.; Ansari, A.J.; Chang, A.; Salame-Alfie, A.; Hanfling, D.; Koerner, J.F. Proposed "Exposure And Symptom Triage" (EAST) Tool to Assess Radiation Exposure After a Nuclear Detonation. *Disaster Med. Public Health Prep.* **2017**, *12*, 386–395. [CrossRef]
25. Obrador, E.; Carretero, J.; Esteve, J.M.; Pellicer, J.A.; Pascual, A.; Petschen, I.; Estrela, J.M. Glutamine Potentiates TNF-Alpha-Induced Tumor Cytotoxicity. *Free Radic. Biol. Med.* **2001**, *31*, 642–650. [CrossRef]
26. Zeegers, D.; Venkatesan, S.; Koh, S.W.; Low, G.K.M.; Srivastava, P.; Sundaram, N.; Sethu, S.; Banerjee, B.; Jayapal, M.; Belyakov, O.; et al. Biomarkers of Ionizing Radiation Exposure: A Multiparametric Approach. *Genome Integr.* **2017**, *8*, 6. [CrossRef]
27. Nugis, V.Y.; Kozlova, M.G.; Nadejina, N.M.; Galstyan, I.A.; Nikitina, V.A.; Khvostunov, I.K.; Golub, E.V. Cytogenetic biodosimetry of accidental exposures in the long terms after irradiation. *Radiat. Prot. Dosim.* **2019**, *186*, 31–36. [CrossRef]
28. Camarata, A.S.; Switchenko, J.M.; Demidenko, E.; Flood, A.B.; Swartz, H.M.; Ali, A.N. Emesis as a Screening Diagnostic for Low Dose Rate (LDR) Total Body Radiation Exposure. *Health Phys.* **2016**, *110*, 391–394. [CrossRef]
29. Hartman, E.N.; Daines, B.; Seto, C.; Shimshoni, D.; Feldman, M.E.; LaBrunda, M. Sort, Assess, Life-Saving Intervention, Triage With Drone Assistance in Mass Casualty Simulation: Analysis of Educational Efficacy. *Cureus* **2020**, *12*, e10572. [CrossRef]
30. Blakely, W.F.; Romanyukha, A.; Hayes, S.M.; Reyes, R.A.; Stewart, H.M.; Hoefer, M.H.; Williams, A.; Sharp, T.; Huff, L.A. U.S. Department of Defense Multiple-Parameter Biodosimetry Network. *Radiat. Prot. Dosim.* **2016**, *172*, 58–71. [CrossRef]
31. Sullivan, J.M.; Prasanna, P.G.S.; Grace, M.B.; Wathen, L.K.; Wallace, R.L.; Koerner, J.F.; Coleman, C.N. Assessment of Biodosimetry Methods for a Mass-Casualty Radiological Incident: Medical Response and Management Considerations. *Health Phys.* **2013**, *105*, 540–554. [CrossRef]
32. Einor, D.; Bonisoli-Alquati, A.; Costantini, D.; Mousseau, T.; Møller, A. Ionizing radiation, antioxidant response and oxidative damage: A meta-analysis. *Sci. Total Environ.* **2016**, *548–549*, 463–471. [CrossRef] [PubMed]
33. Watanabe, R.; Saito, K. Monte Carlo simulation of strand-break induction on plasmid DNA in aqueous solution by monoenergetic electrons. *Radiat. Environ. Biophys.* **2002**, *41*, 207–215. [CrossRef]
34. Wallace, S.S. DNA Damages Processed by Base Excision Repair: Biological Consequences. *Int. J. Radiat. Biol.* **1994**, *66*, 579–589. [CrossRef] [PubMed]

35. Prise, K.M.; Pinto, M.; Newman, H.C.; Michael, B.D. A review of studies of ionizing radiation-induced double-strand break clustering. *Radiat. Res.* **2001**, *156*, 572–576. [CrossRef]
36. Sies, H. Oxidative stress: A concept in redox biology and medicine. *Redox Biol.* **2015**, *4*, 180–183. [CrossRef] [PubMed]
37. Ramos-Méndez, J.; LaVerne, J.A.; Domínguez-Kondo, N.; Milligan, J.; Štěpán, V.; Stefanová, K.; Perrot, Y.; Villagrasa, C.; Shin, W.-G.; Incerti, S.; et al. TOPAS-nBio validation for simulating water radiolysis and DNA damage under low-LET irradiation. *Phys. Med. Biol.* **2021**, *66*, 175026. [CrossRef] [PubMed]
38. Schaue, D.; Micewicz, E.D.; Ratikan, J.A.; Xie, M.W.; Cheng, G.; McBride, W.H. Radiation and Inflammation. *Semin. Radiat. Oncol.* **2014**, *25*, 4–10. [CrossRef] [PubMed]
39. Sies, H.; De Groot, H. Role of reactive oxygen species in cell toxicity. *Toxicol. Lett.* **1992**, *64–65*, 547–551. [CrossRef]
40. Milkovic, L.; Siems, W.; Siems, R.; Zarkovic, N. Oxidative Stress and Antioxidants in Carcinogenesis and Integrative Therapy of Cancer. *Curr. Pharm. Des.* **2014**, *20*, 6529–6542. [CrossRef]
41. Gill, J.G.; Piskounova, E.; Morrison, S.J. Cancer, Oxidative Stress, and Metastasis. *Cold Spring Harb. Symp. Quant. Biol.* **2016**, *81*, 163–175. [CrossRef]
42. Pouget, J.-P.; Georgakilas, A.G.; Ravanat, J.-L. Targeted and Off-Target (Bystander and Abscopal) Effects of Radiation Therapy: Redox Mechanisms and Risk/Benefit Analysis. *Antioxid. Redox Signal.* **2018**, *29*, 1447–1487. [CrossRef]
43. Azzam, E.I.; Jay-Gerin, J.-P.; Pain, D. Ionizing radiation-induced metabolic oxidative stress and prolonged cell injury. *Cancer Lett.* **2012**, *327*, 48–60. [CrossRef]
44. Klammer, H.; Mladenov, E.; Li, F.; Iliakis, G. Bystander effects as manifestation of intercellular communication of DNA damage and of the cellular oxidative status. *Cancer Lett.* **2015**, *356*, 58–71. [CrossRef]
45. Burdak-Rothkamm, S.; Rothkamm, K. Radiation-induced bystander and systemic effects serve as a unifying model system for genotoxic stress responses. *Mutat. Res. Mutat. Res.* **2018**, *778*, 13–22. [CrossRef]
46. Yahyapour, R.; Motevaseli, E.; Rezaeyan, A.; Abdollahi, H.; Farhood, B.; Cheki, M.; Najafi, M.; Villa, V. Mechanisms of Radiation Bystander and Non-Targeted Effects: Implications to Radiation Carcinogenesis and Radiotherapy. *Curr. Radiopharm.* **2018**, *11*, 34–45. [CrossRef]
47. Mikkelsen, R.B.; Wardman, P. Biological chemistry of reactive oxygen and nitrogen and radiation-induced signal transduction mechanisms. *Oncogene* **2003**, *22*, 5734–5754. [CrossRef]
48. Olivares, A.; Alcaraz-Saura, M.; Achel, D.; Berná-Mestre, J.; Alcaraz, M. Radiation-Induced Bystander Effect: Loss of Radioprotective Capacity of Rosmarinic Acid In Vivo and In Vitro. *Antioxidants* **2021**, *10*, 231. [CrossRef]
49. Frey, B.; Hehlgans, S.; Rödel, F.; Gaipl, U.S. Modulation of inflammation by low and high doses of ionizing radiation: Implications for benign and malign diseases. *Cancer Lett.* **2015**, *368*, 230–237. [CrossRef]
50. Najafi, M.; Motevaseli, E.; Shirazi, A.; Geraily, G.; Rezaeyan, A.; Norouzi, F.; Rezapoor, S.; Abdollahi, H. Mechanisms of inflammatory responses to radiation and normal tissues toxicity: Clinical implications. *Int. J. Radiat. Biol.* **2018**, *94*, 335–356. [CrossRef]
51. Michalowski, A.S. Anti-inflammatory drug treatment of radiation injuries. *Adv. Exp. Med. Biol.* **1997**, *400B*, 873–877.
52. Lee, T.K.; Stupans, I. Radioprotection: The non-steroidal anti-inflammatory drugs (NSAIDs) and prostaglandins. *J. Pharm. Pharmacol.* **2002**, *54*, 1435–1445. [CrossRef]
53. Martin, O.A.; Yin, X.S.; Forrester, H.B.; Sprung, C.N.; Martin, R.F. Potential strategies to ameliorate risk of radiotherapy-induced second malignant neoplasms. *Semin. Cancer Biol.* **2016**, *37–38*, 65–76. [CrossRef]
54. Obrador, E.; Salvador, R.; Villaescusa, J.; Soriano, J.; Estrela, J.; Montoro, A. Radioprotection and Radiomitigation: From the Bench to Clinical Practice. *Biomedicines* **2020**, *8*, 461. [CrossRef] [PubMed]
55. Stewart, F.A.; Akleyev, A.; Hauerjensen, M.; Hendry, J.; Kleiman, N.; MacVittie, T.; Aleman, B.; Edgar, A.; Mabuchi, K.; Muirhead, C.; et al. ICRP publication 118: ICRP Statement on Tissue Reactions and Early and Late Effects of Radiation in Normal Tissues and Organs—Threshold Doses for Tissue Reactions in a Radiation Protection Context. *Ann. ICRP* **2012**, *41*, 1–322. [CrossRef] [PubMed]
56. Reed-Schrader, E.; Hayoun, M.A.; Kropp, A.M.; Goldstein, S. EMS Weapons of Mass Destruction and Related Injury. In *StatPearls*; StatPearls Publishing: Treasure Island, FL, USA, 2020.
57. Rajaraman, P.; Hauptmann, M.; Bouffler, S.; Wojcik, A. Human individual radiation sensitivity and prospects for prediction. *Ann. ICRP* **2018**, *47*, 126–141. [CrossRef] [PubMed]
58. Qu, S.; Gao, J.; Tang, B.; Yu, B.; Shen, Y.; Tu, Y. Low-dose ionizing radiation increases the mortality risk of solid cancers in nuclear industry workers: A meta-analysis. *Mol. Clin. Oncol.* **2018**, *8*, 703–711. [CrossRef]
59. Laurier, D.; Richardson, D.B.; Cardis, E.; Daniels, R.; Gillies, M.; O'Hagan, J.; Hamra, G.B.; Haylock, R.; Leuraud, K.; Moissonnier, M.; et al. The International Nuclear Workers Study (Inworks): A Collaborative Epidemiological Study to Improve Knowledge About Health Effects of Protracted Low-Dose Exposure. *Radiat. Prot. Dosim.* **2016**, *173*, 21–25. [CrossRef]
60. De Gonzalez, A.B.; Daniels, R.D.; Cardis, E.; Cullings, H.M.; Gilbert, E.; Hauptmann, M.; Kendall, G.; Laurier, D.; Linet, M.S.; Little, M.P.; et al. Epidemiological Studies of Low-Dose Ionizing Radiation and Cancer: Rationale and Framework for the Monograph and Overview of Eligible Studies. *J. Natl. Cancer Inst. Monogr.* **2020**, *2020*, 97–113. [CrossRef]
61. Vorobiev, A.I. Acute radiation disease and biological dosimetry in 1993. *Stem Cells* **1997**, *15* (Suppl. 2), 269–274. [CrossRef]
62. Leibowitz, B.J.; Wei, L.; Zhang, L.; Ping, X.; Epperly, M.; Greenberger, J.; Cheng, T.; Yu, J. Ionizing irradiation induces acute haematopoietic syndrome and gastrointestinal syndrome independently in mice. *Nat. Commun.* **2014**, *5*, 3494. [CrossRef]
63. Hu, S. Linking Doses with Clinical Scores of Hematopoietic Acute Radiation Syndrome. *Health Phys.* **2016**, *111*, 337–347. [CrossRef]

64. King, G.L.; Sandgren, D.J.; Mitchell, J.M.; Bolduc, D.L.; Blakely, W.F. System for Scoring Severity of Acute Radiation Syndrome Response in Rhesus Macaques (Macaca mulatta). *Comp. Med.* **2018**, *68*, 474–488. [CrossRef]
65. López, M.; Martín, M. Medical management of the acute radiation syndrome. *Rep. Pract. Oncol. Radiother.* **2011**, *16*, 138–146. [CrossRef]
66. Stenke, L.; Lindberg, K.; Lindberg, M.L.; Lewensohn, R.; Valentin, J.; Powles, R.; Dainiak, N. Coordination of management of the acute radiation syndrome. *Radiat. Prot. Dosim.* **2018**, *182*, 80–84. [CrossRef]
67. Kurshakov, N.A. Chronic Radiation Sickness. *Bull. Radiat. Med.* **1956**, *4*, 3–20.
68. Veremeyeva, G.; Akushevich, I.; Pochukhailova, T.; Blinova, E.; Varfolomeyeva, T.; Ploshchanskaya, O.; Khudyakova, O.; Vozilova, A.; Kozionova, O.; Akleyev, A. Long-term cellular effects in humans chronically exposed to ionizing radiation. *Health Phys.* **2010**, *99*, 337–346. [CrossRef]
69. Akleyev, A.V. Clinical Manifestations of Chronic Radiation Syndrome. In *Chronic Radiation Syndrome*; Akleyev, A.V., Ed.; Springer: Berlin/Heidelberg, Germany, 2014; pp. 145–245. ISBN 978-3-642-45117-1.
70. Akleyev, A.V. Early signs of chronic radiation syndrome in residents of the Techa riverside settlements. *Radiat. Environ. Biophys.* **2021**, *60*, 203–212. [CrossRef]
71. Kimler, B.F.; Briley, S.M.; Johnson, B.W.; Armstrong, A.G.; Jasti, S.; Duncan, F.E. Radiation-induced ovarian follicle loss occurs without overt stromal changes. *Reproduction* **2018**, *155*, 553–562. [CrossRef]
72. Akleyev, A. Normal tissue reactions to chronic radiation exposure in man. *Radiat. Prot. Dosim.* **2016**, *171*, 107–116. [CrossRef]
73. Azizova, T.V.; Bannikova, M.V.; Zhuntova, G.V.; Grigoryeva, E.S.; Moseeva, M.B.; Bragin, E.V. Registry for chronic radiation syndrome in a worker cohort of the Russian nuclear enterprise, Mayak Production Association. *J. Radiol. Prot.* **2019**, *39*, 890–905. [CrossRef]
74. Hamada, N.; Fujimichi, Y. Classification of radiation effects for dose limitation purposes: History, current situation and future prospects. *J. Radiat. Res.* **2014**, *55*, 629–640. [CrossRef]
75. Ozasa, K.; Takahashi, I.; Grant, E. Radiation-related risks of non-cancer outcomes in the atomic bomb survivors. *Ann. ICRP* **2016**, *45*, 253–261. [CrossRef]
76. Hinksman, C.A.; Haylock, R.G.E.; Gillies, M. Cerebrovascular Disease Mortality after occupational Radiation Exposure among the UK National Registry for Radiation Workers Cohort. *Radiat. Res.* **2022**, *197*, 459–470. [CrossRef] [PubMed]
77. Little, M.P.; Wakeford, R.; Bouffler, S.D.; Abalo, K.; Hauptmann, M.; Hamada, N.; Kendall, G.M. Review of the risk of cancer following low and moderate doses of sparsely ionising radiation received in early life in groups with individually estimated doses. *Environ. Int.* **2021**, *159*, 106983. [CrossRef] [PubMed]
78. Little, M.P. Cancer and non-cancer effects in Japanese atomic bomb survivors. *J. Radiol. Prot.* **2009**, *29*, A43–A59. [CrossRef] [PubMed]
79. Rühm, W.; Laurier, D.; Wakeford, R. Cancer risk following low doses of ionising radiation–Current epidemiological evidence and implications for radiological protection. *Mutat. Res. Toxicol. Environ. Mutagen.* **2021**, *873*, 503436. [CrossRef]
80. Leuraud, K.; Richardson, D.B.; Cardis, E.; Daniels, R.D.; Gillies, M.; Haylock, R.; Moissonnier, M.; Schubauer-Berigan, M.K.; Thierry-Chef, I.; Kesminiene, A.; et al. Risk of cancer associated with low-dose radiation exposure: Comparison of results between the INWORKS nuclear workers study and the A-bomb survivors study. *Radiat. Environ. Biophys.* **2021**, *60*, 23–39. [CrossRef]
81. Citrin, D.; Cotrim, A.P.; Hyodo, F.; Baum, B.J.; Krishna, M.C.; Mitchell, J.B. Radioprotectors and Mitigators of Radiation-Induced Normal Tissue Injury. *Oncologist* **2010**, *15*, 360–371. [CrossRef]
82. Bourgier, C.; Levy, A.; Vozenin, M.-C.; Deutsch, E. Pharmacological strategies to spare normal tissues from radiation damage: Useless or overlooked therapeutics? *Cancer Metastasis Rev.* **2012**, *31*, 699–712. [CrossRef] [PubMed]
83. Singh, V.K.; Romaine, P.L.; Seed, T.M. Medical Countermeasures for Radiation Exposure and Related Injuries: Characterization of Medicines, FDA-Approval Status and Inclusion into the Strategic National Stockpile. *Health Phys.* **2015**, *108*, 607–630. [CrossRef]
84. Weiss, J.F.; Landauer, M.R. Protection against ionizing radiation by antioxidant nutrients and phytochemicals. *Toxicology* **2003**, *189*, 1–20. [CrossRef]
85. Patt, H.M.; Tyree, E.B.; Straube, R.L.; Smith, D.E. Cysteine Protection against X Irradiation. *Science* **1949**, *110*, 213–214. [CrossRef]
86. Molkentine, J.M.; Fujimoto, T.N.; Horvath, T.D.; Grossberg, A.J.; Garcia, C.J.G.; Deorukhkar, A.; Bonilla, M.D.L.C.; Lin, D.; Samuel, E.L.G.; Chan, W.K.; et al. Enteral Activation of WR-2721 Mediates Radioprotection and Improved Survival from Lethal Fractionated Radiation. *Sci. Rep.* **2019**, *9*, 1949. [CrossRef] [PubMed]
87. King, M.; Joseph, S.; Albert, A.; Thomas, T.V.; Nittala, M.R.; Woods, W.C.; Vijayakumar, S.; Packianathan, S. Use of Amifostine for Cytoprotection during Radiation Therapy: A Review. *Oncology* **2019**, *98*, 61–80. [CrossRef] [PubMed]
88. Gu, J.; Zhu, S.; Li, X.; Wu, H.; Li, Y.; Hua, F. Effect of Amifostine in Head and Neck Cancer Patients Treated with Radiotherapy: A Systematic Review and Meta-Analysis Based on Randomized Controlled Trials. *PLoS ONE* **2014**, *9*, e95968. [CrossRef] [PubMed]
89. Lee, M.G.; Freeman, A.R.; Roos, D.E.; Milner, A.D.; Borg, M.F. Randomized double-blind trial of amifostine versus placebo for radiation-induced xerostomia in patients with head and neck cancer. *J. Med. Imaging Radiat. Oncol.* **2018**, *63*, 142–150. [CrossRef]
90. Kouvaris, J.R.; Kouloulias, V.E.; Vlahos, L.J. Amifostine: The First Selective-Target and Broad-Spectrum Radioprotector. *Oncol.* **2007**, *12*, 738–747. [CrossRef]
91. Grdina, D.; Kataoka, Y.; Murley, J. Amifostine: Mechanisms of action underlying cytoprotection and chemoprevention. *Drug Metab. Drug Interact.* **2000**, *16*, 237–280. [CrossRef]

92. Singh, V.K.; Seed, T.M. The efficacy and safety of amifostine for the acute radiation syndrome. *Expert Opin. Drug Saf.* **2019**, *18*, 1077–1090. [CrossRef]
93. Navarro, J.; Obrador, E.; Pellicer, J.A.; Asensi, M.; Vina, J.; Estrela, J.M. Blood Glutathione as an Index of Radiation-Induced Oxidative Stress in Mice and Humans. *Free Radic. Biol. Med.* **1997**, *22*, 1203–1209. [CrossRef]
94. Estrela, J.M.; Ortega, A.; Obrador, E. Glutathione in Cancer Biology and Therapy. *Crit. Rev. Clin. Lab. Sci.* **2006**, *43*, 143–181. [CrossRef]
95. Jia, D.; Koonce, N.A.; Griffin, R.J.; Jackson, C.; Corry, P.M. Prevention and Mitigation of Acute Death of Mice after Abdominal Irradiation by the Antioxidant *N*-Acetyl-cysteine (NAC). *Radiat. Res.* **2010**, *173*, 579–589. [CrossRef]
96. Li, J.; Meng, Z.; Zhang, G.; Xing, Y.; Feng, L.; Fan, S.; Fan, F.; Buren, B.; Liu, Q. *N*-acetylcysteine relieves oxidative stress and protects hippocampus of rat from radiation-induced apoptosis by inhibiting caspase-3. *Biomed. Pharm.* **2014**, *70*, 1–6. [CrossRef]
97. Mercantepe, T.; Topcu, A.; Rakici, S.; Tumkaya, L.; Yilmaz, A.; Mercantepe, F. The radioprotective effect of *N*-acetylcysteine against x-radiation-induced renal injury in rats. *Environ. Sci. Pollut. Res.* **2019**, *26*, 29085–29094. [CrossRef]
98. Elkady, A.A.; Ibrahim, I.M. Protective effects of erdosteine against nephrotoxicity caused by gamma radiation in male albino rats. *Hum. Exp. Toxicol.* **2015**, *35*, 21–28. [CrossRef]
99. Rades, D.; Fehlauer, F.; Bajrovic, A.; Mahlmann, B.; Richter, E.; Alberti, W. Serious adverse effects of amifostine during radiotherapy in head and neck cancer patients. *Radiother. Oncol.* **2004**, *70*, 261–264. [CrossRef]
100. Wang, Q.; Xie, C.; Xi, S.; Qian, F.; Peng, X.; Huang, J.; Tang, F. Radioprotective Effect of Flavonoids on Ionizing Radiation-Induced Brain Damage. *Molecules* **2020**, *25*, 5719. [CrossRef]
101. Alcaraz, M.; Olivares, A.; Achel, D.G.; García-Gamuz, J.A.; Castillo, J.; Alcaraz-Saura, M. Genoprotective Effect of Some Flavonoids against Genotoxic Damage Induced by X-rays In Vivo: Relationship between Structure and Activity. *Antioxidants* **2021**, *11*, 94. [CrossRef]
102. Fischer, N.; Seo, E.-J.; Efferth, T. Prevention from radiation damage by natural products. *Phytomedicine* **2017**, *47*, 192–200. [CrossRef]
103. Faramarzi, S.; Piccolella, S.; Manti, L.; Pacifico, S. Could Polyphenols Really Be a Good Radioprotective Strategy? *Molecules* **2021**, *26*, 4969. [CrossRef]
104. Jit, B.P.; Pradhan, B.; Dash, R.; Bhuyan, P.P.; Behera, C.; Behera, R.K.; Sharma, A.; Alcaraz, M.; Jena, M. Phytochemicals: Potential Therapeutic Modulators of Radiation Induced Signaling Pathways. *Antioxidants* **2021**, *11*, 49. [CrossRef]
105. Ha, C.T.; Li, X.-H.; Fu, D.; Xiao, M.; Landauer, M.R. Genistein Nanoparticles Protect Mouse Hematopoietic System and Prevent Proinflammatory Factors after Gamma Irradiation. *Radiat. Res.* **2013**, *180*, 316–325. [CrossRef]
106. Calveley, V.L.; Jelveh, S.; Langan, A.; Mahmood, J.; Yeung, I.W.T.; Van Dyk, J.; Hill, R.P. Genistein Can Mitigate the Effect of Radiation on Rat Lung Tissue. *Radiat. Res.* **2010**, *173*, 602–611. [CrossRef]
107. Zhang, J.; Pang, Z.; Zhang, Y.; Liu, J.; Wang, Z.; Xu, C.; He, L.; Li, W.; Zhang, K.; Zhang, W.; et al. Genistein From Fructus sophorae Protects Mice From Radiation-Induced Intestinal Injury. *Front. Pharmacol.* **2021**, *12*, 655652. [CrossRef]
108. Ashrafizadeh, M.; Ahmadi, Z.; Mohamamdinejad, R.; Farkhondeh, T.; Samarghandian, S. Curcumin Activates the Nrf2 Pathway and Induces Cellular Protection Against Oxidative Injury. *Curr. Mol. Med.* **2020**, *20*, 116–133. [CrossRef] [PubMed]
109. Derosa, G.; Maffioli, P.; Simental-Mendía, L.E.; Bo, S.; Sahebkar, A. Effect of curcumin on circulating interleukin-6 concentrations: A systematic review and meta-analysis of randomized controlled trials. *Pharmacol. Res.* **2016**, *111*, 394–404. [CrossRef] [PubMed]
110. Akbari, A.; Jelodar, G.; Nazifi, S.; Afsar, T.; Nasiri, K. Oxidative Stress as the Underlying Biomechanism of Detrimental Outcomes of Ionizing and Non-Ionizing Radiation on Human Health: Antioxidant Protective Strategies. *Zahedan J. Res. Med. Sci.* **2019**, *21*, e85655. [CrossRef]
111. Farhood, B.; Mortezaee, K.; Goradel, N.H.; Khanlarkhani, N.; Salehi, E.; Nashtaei, M.S.; Najafi, M.; Sahebkar, A. Curcumin as an anti-inflammatory agent: Implications to radiotherapy and chemotherapy. *J. Cell. Physiol.* **2018**, *234*, 5728–5740. [CrossRef]
112. Amini, P.; Saffar, H.; Nourani, M.R.; Motevaseli, E.; Najafi, M.; Taheri, R.A.; Qazvini, A. Curcumin Mitigates Radiation-induced Lung Pneumonitis and Fibrosis in Rats. *Int. J. Mol. Cell Med.* **2019**, *7*, 212–219. [CrossRef]
113. Johnson, S.; Shaikh, S.; Muneesa, F.; Rashmi, B.; Bhandary, Y.P. Radiation induced apoptosis and pulmonary fibrosis: Curcumin an effective intervention? *Int. J. Radiat. Biol.* **2020**, *96*, 709–717. [CrossRef] [PubMed]
114. Sahebkar, A.; Henrotin, Y. Analgesic Efficacy and Safety of Curcuminoids in Clinical Practice: A Systematic Review and Meta-Analysis of Randomized Controlled Trials. *Pain Med.* **2015**, *17*, 1192–1202. [CrossRef]
115. Verma, V. Relationship and interactions of curcumin with radiation therapy. *World J. Clin. Oncol.* **2016**, *7*, 275–283. [CrossRef]
116. Sebastià, N.; Montoro, A.; Hervás, D.; Pantelias, G.; Hatzi, V.; Soriano, J.; Villaescusa, J.; Terzoudi, G. Curcumin and trans-resveratrol exert cell cycle-dependent radioprotective or radiosensitizing effects as elucidated by the PCC and G2-assay. *Mutat. Res. Mol. Mech. Mutagen.* **2014**, *766–767*, 49–55. [CrossRef]
117. Yu, C.; Yang, B.; Najafi, M. Targeting of cancer cell death mechanisms by curcumin: Implications to cancer therapy. *Basic Clin. Pharmacol. Toxicol.* **2021**, *129*, 397–415. [CrossRef]
118. Zoi, V.; Galani, V.; Tsekeris, P.; Kyritsis, A.P.; Alexiou, G.A. Radiosensitization and Radioprotection by Curcumin in Glioblastoma and Other Cancers. *Biomedicines* **2022**, *10*, 312. [CrossRef]
119. Wolf, J.R.; Heckler, C.E.; Guido, J.J.; Peoples, A.R.; Gewandter, J.S.; Ling, M.; Vinciguerra, V.P.; Anderson, T.; Evans, L.; Wade, J.; et al. Oral curcumin for radiation dermatitis: A URCC NCORP study of 686 breast cancer patients. *Supportive Care Cancer* **2018**, *26*, 1543–1552. [CrossRef]
120. Sonis, S.T. Superoxide Dismutase as an Intervention for Radiation Therapy-Associated Toxicities: Review and Profile of Avasopasem Manganese as a Treatment Option for Radiation-Induced Mucositis. *Drug Des. Dev. Ther.* **2021**, *15*, 1021–1029. [CrossRef]

121. Adhvaryu, M.; Vakharia, B.; Reddy, N. Curcumin Prevents Mucositis and Improves Patient Compliance in Head & Neck Cancer Patients Undergoing Radio-Chemotherapy. *Ann. Med. Chem. Res.* **2018**, *4*, 1022.
122. Xie, J.; Yong, Y.; Dong, X.; Du, J.; Guo, Z.; Gong, L.; Zhu, S.; Tian, G.; Yu, S.; Gu, Z.; et al. Therapeutic Nanoparticles Based on Curcumin and Bamboo Charcoal Nanoparticles for Chemo-Photothermal Synergistic Treatment of Cancer and Radioprotection of Normal Cells. *ACS Appl. Mater. Interfaces* **2017**, *9*, 14281–14291. [CrossRef]
123. Zhao, X.; Liu, X.; Wang, G.; Wen, X.; Zhang, X.; Hoffman, A.R.; Li, W.; Hu, J.-F.; Cui, J. Loss of insulin-like growth factor II imprinting is a hallmark associated with enhanced chemo/radiotherapy resistance in cancer stem cells. *Oncotarget* **2016**, *7*, 51349–51364. [CrossRef]
124. Richi, B.; Kale, R.K.; Tiku, A.B. Radio-modulatory effects of Green Tea Catechin EGCG on pBR322 plasmid DNA and murine splenocytes against gamma-radiation induced damage. *Mutat. Res.* **2012**, *747*, 62–70. [CrossRef]
125. Zhu, W.; Xu, J.; Ge, Y.; Cao, H.; Ge, X.; Luo, J.; Xue, J.; Yang, H.; Zhang, S.; Cao, J. Epigallocatechin-3-gallate (EGCG) protects skin cells from ionizing radiation via heme oxygenase-1 (HO-1) overexpression. *J. Radiat. Res.* **2014**, *55*, 1056–1065. [CrossRef]
126. Xie, N.; Zhang, L.; Gao, W.; Huang, C.; Huber, P.E.; Zhou, X.; Li, C.; Shen, G.; Zou, B. NAD+ metabolism: Pathophysiologic mechanisms and therapeutic potential. *Signal Transduct. Target. Ther.* **2020**, *5*, 1–37. [CrossRef] [PubMed]
127. Pajonk, F.; Riedisser, A.; Henke, M.; McBride, W.H.; Fiebich, B. The effects of tea extracts on proinflammatory signaling. *BMC Med.* **2006**, *4*, 28. [CrossRef] [PubMed]
128. Shin, Y.S.; Shin, H.A.; Kang, S.U.; Kim, J.-H.; Oh, Y.-T.; Park, K.H.; Kim, C.-H. Effect of Epicatechin against Radiation-Induced Oral Mucositis: In Vitro and In Vivo Study. *PLoS ONE* **2013**, *8*, e69151. [CrossRef] [PubMed]
129. Pyun, J.; Kang, S.; Hwang, H.; Oh, Y.; Lim, Y.; Choo, O.; Kim, C. Epicatechin inhibits radiation-induced auditory cell death by suppression of reactive oxygen species generation. *Neuroscience* **2011**, *199*, 410–420. [CrossRef]
130. Shimura, T.; Koyama, M.; Aono, D.; Kunugita, N. Epicatechin as a promising agent to countermeasure radiation exposure by mitigating mitochondrial damage in human fibroblasts and mouse hematopoietic cells. *FASEB J.* **2019**, *33*, 6867–6876. [CrossRef]
131. Salehi, S.; Bayatiani; Yaghmaei, P.; Rajabi, S.; Goodarzi, M.; Mashayekhi, F.J. Protective effects of resveratrol against X-ray irradiation by regulating antioxidant defense system. *Radioprotection* **2018**, *53*, 293–298. [CrossRef]
132. Carsten, R.E.; Bachand, A.M.; Bailey, S.M.; Ullrich, R.L. Resveratrol Reduces Radiation-Induced Chromosome Aberration Frequencies in Mouse Bone Marrow Cells. *Radiat. Res.* **2008**, *169*, 633–638. [CrossRef]
133. Koohian, F.; Shanei, A.; Shahbazi-Gahrouei, D.; Hejazi, S.H.; Moradi, M.-T. The Radioprotective Effect of Resveratrol Against Genotoxicity Induced by γ-Irradiation in Mice Blood Lymphocytes. *Dose Response* **2017**, *15*, 1559325817705699. [CrossRef]
134. Sun, H.; Cai, H.; Fu, Y.; Wang, Q.; Ji, K.; Du, L.; Xu, C.; Tian, L.; He, N.; Wang, J.; et al. The Protection Effect of Resveratrol Against Radiation-Induced Inflammatory Bowel Disease via NLRP-3 Inflammasome Repression in Mice. *Dose Response* **2020**, *18*, 1559325820931292. [CrossRef]
135. Zhang, H.; Yan, H.; Zhou, X.; Wang, H.; Yang, Y.; Zhang, J.; Wang, H. The protective effects of Resveratrol against radiation-induced intestinal injury. *BMC Complement. Altern. Med.* **2017**, *17*, 1–8. [CrossRef]
136. Ocolotobiche, E.E.; Banegas, Y.C.; Güerci, A.M. Modulation of ionizing radiation-induced damage in human blood lymphocytes by in vivo treatment with resveratrol. *Int. J. Radiat. Biol.* **2019**, *95*, 1220–1225. [CrossRef]
137. Radwan, R.R.; Karam, H.M. Resveratrol attenuates intestinal injury in irradiated rats via PI3K/Akt/mTOR signaling pathway. *Environ. Toxicol.* **2019**, *35*, 223–230. [CrossRef]
138. Gao, P.; Li, N.; Ji, K.; Wang, Y.; Xu, C.; Liu, Y.; Wang, Q.; Wang, J.; He, N.; Sun, Z.; et al. Resveratrol targets TyrRS acetylation to protect against radiation-induced damage. *FASEB J.* **2019**, *33*, 8083–8093. [CrossRef]
139. Mortezaee, K.; Najafi, M.; Farhood, B.; Ahmadi, A.; Shabeeb, D.; Musa, A.E. Resveratrol as an Adjuvant for Normal Tissues Protection and Tumor Sensitization. *Curr. Cancer Drug Targets* **2020**, *20*, 130–145. [CrossRef]
140. Micale, N.; Molonia, M.; Citarella, A.; Cimino, F.; Saija, A.; Cristani, M.; Speciale, A. Natural Product-Based Hybrids as Potential Candidates for the Treatment of Cancer: Focus on Curcumin and Resveratrol. *Molecules* **2021**, *26*, 4665. [CrossRef]
141. Obrador, E.; Salvador-Palmer, R.; Pellicer, B.; López-Blanch, R.; Sirerol, J.A.; Villaescusa, J.I.; Montoro, A.; Dellinger, R.W.; Estrela, J.M. Combination of natural polyphenols with a precursor of NAD+ and a TLR2/6 ligand lipopeptide protects mice against lethal γ radiation. *J. Adv. Res.* **2022**, *in press*. [CrossRef]
142. Son, Y.; Lee, H.J.; Rho, J.K.; Chung, S.Y.; Lee, C.G.; Yang, K.; Kim, S.H.; Lee, M.; Shin, I.S.; Kim, J.S. The ameliorative effect of silibinin against radiation-induced lung injury: Protection of normal tissue without decreasing therapeutic efficacy in lung cancer. *BMC Pulm. Med.* **2015**, *15*, 68. [CrossRef]
143. Ali, M.; Sadhu, B.; Boda, A.; Tiwari, N.; Das, A.; Ali, S.M.; Bhattacharya, D.; Pandey, B.N.; Kumar, A. Thorium decorporation efficacy of rationally-selected biocompatible compounds with relevance to human application. *J. Hazard. Mater.* **2018**, *365*, 952–961. [CrossRef]
144. Verma, S.; Dutta, A. Quercetin 3 Rutinoside Facilitates Protection Against Radiation Induced Genotoxic and Oxidative Damage A Study in C57bl 6 Mice. *Def. Life Sci. J.* **2021**, *6*, 128–137. [CrossRef]
145. Horton, J.A.; Li, F.; Chung, E.J.; Hudak, K.; White, A.; Krausz, K.; Gonzalez, F.; Citrin, D. Quercetin Inhibits Radiation-Induced Skin Fibrosis. *Radiat. Res.* **2013**, *180*, 205–215. [CrossRef]
146. De Siqueira, W.N.; Dos Santos, F.T.J.; De Souza, T.F.; Lima, M.D.V.; Silva, H.A.M.F.; De Oliveira, P.S.S.; Pitta, M.G.D.R.; Bezerra, M.B.C.F.; Fernandes, T.D.S.E.; De França, E.J.; et al. Study of the Potential Radiomitigator Effect of Quercetin on Human Lymphocytes. *Inflammation* **2018**, *42*, 124–134. [CrossRef] [PubMed]

147. Zhang, J.; Hong, Y.; Liuyang, Z.; Li, H.; Jiang, Z.; Tao, J.; Liu, H.; Xie, A.; Feng, Y.; Dong, X.; et al. Quercetin Prevents Radiation-Induced Oral Mucositis by Upregulating BMI-1. *Oxidative Med. Cell. Longev.* **2021**, *2021*, 1–16. [CrossRef] [PubMed]
148. Ferraz, C.R.; Carvalho, T.T.; Manchope, M.F.; Artero, N.A.; Rasquel-Oliveira, F.S.; Fattori, V.; Casagrande, R.; Verri, W.A. Therapeutic Potential of Flavonoids in Pain and Inflammation: Mechanisms of Action, Pre-Clinical and Clinical Data, and Pharmaceutical Development. *Molecules* **2020**, *25*, 762. [CrossRef] [PubMed]
149. Bolla, G.; Nangia, A. Pharmaceutical cocrystals: Walking the talk. *Chem. Commun.* **2016**, *52*, 8342–8360. [CrossRef]
150. Xie, J.; Wang, C.; Zhao, F.; Gu, Z.; Zhao, Y. Application of Multifunctional Nanomaterials in Radioprotection of Healthy Tissues. *Adv. Health Mater.* **2018**, *7*, e1800421. [CrossRef]
151. Choi, S.-H.; Lee, D.-Y.; Kang, S.; Lee, M.-K.; Lee, J.-H.; Lee, S.-H.; Lee, H.-L.; Lee, H.-Y.; Jeong, Y.-I. Caffeic Acid Phenethyl Ester-Incorporated Radio-Sensitive Nanoparticles of Phenylboronic Acid Pinacol Ester-Conjugated Hyaluronic Acid for Application in Radioprotection. *Int. J. Mol. Sci.* **2021**, *22*, 6347. [CrossRef]
152. Parihar, V.K.; Prabhakar, K.; Veerapur, V.P.; Kumar, M.S.; Reddy, Y.R.; Joshi, R.; Unnikrishnan, M.K.; Rao, C.M. Effect of sesamol on radiation-induced cytotoxicity in Swiss albino mice. *Mutat. Res.* **2006**, *611*, 9–16. [CrossRef]
153. Khan, S.; Kumar, A.; Adhikari, J.S.; Rizvi, M.A.; Chaudhury, N.K. Protective effect of sesamol against $^{60}$Co γ-ray-induced hematopoietic and gastrointestinal injury in C57BL/6 male mice. *Free Radic. Res.* **2015**, *49*, 1344–1361. [CrossRef]
154. Majdaeen, M.; Banaei, A.; Abedi-Firouzjah, R.; Gorji, K.E.; Ataei, G.; Momeni, F.; Zamani, H. Investigating the radioprotective effect of sesamol oral consumption against gamma irradiation in mice by micronucleus and alkaline comet assays. *Appl. Radiat. Isot.* **2020**, *159*, 109091. [CrossRef]
155. Nair, G.G.; Nair, C.K.K. Radioprotective Effects of Gallic Acid in Mice. *BioMed. Res. Int.* **2013**, *2013*, 1–13. [CrossRef]
156. Bai, J.; Zhang, Y.; Tang, C.; Hou, Y.; Ai, X.; Chen, X.; Zhang, Y.; Wang, X.; Meng, X. Gallic acid: Pharmacological activities and molecular mechanisms involved in inflammation-related diseases. *Biomed. Pharm.* **2020**, *133*, 110985. [CrossRef]
157. Sim, H.-J.; Bhattarai, G.; Lee, J.; Lee, J.-C.; Kook, S.-H. The Long-lasting Radioprotective Effect of Caffeic Acid in Mice Exposed to Total Body Irradiation by Modulating Reactive Oxygen Species Generation and Hematopoietic Stem Cell Senescence-Accompanied Long-term Residual Bone Marrow Injury. *Aging Dis.* **2019**, *10*, 1320–1327. [CrossRef]
158. Alam, M.; Ashraf, G.M.; Sheikh, K.; Khan, A.; Ali, S.; Ansari, M.; Adnan, M.; Pasupuleti, V.R.; Hassan, I. Potential Therapeutic Implications of Caffeic Acid in Cancer Signaling: Past, Present, and Future. *Front. Pharmacol.* **2022**, *13*, 845871. [CrossRef]
159. Mansour, H.H.; Tawfik, S.S. Early treatment of radiation-induced heart damage in rats by caffeic acid phenethyl ester. *Eur. J. Pharmacol.* **2012**, *692*, 46–51. [CrossRef]
160. Jin, L.-G.; Chu, J.-J.; Pang, Q.-F.; Zhang, F.-Z.; Wu, G.; Zhou, L.-Y.; Zhang, X.-J.; Xing, C.-G. Caffeic acid phenethyl ester attenuates ionize radiation-induced intestinal injury through modulation of oxidative stress, apoptosis and p38MAPK in rats. *Environ. Toxicol. Pharmacol.* **2015**, *40*, 156–163. [CrossRef]
161. Chu, J.; Zhang, X.; Jin, L.; Chen, J.; Du, B.; Pang, Q. Protective effects of caffeic acid phenethyl ester against acute radiation-induced hepatic injury in rats. *Environ. Toxicol. Pharmacol.* **2015**, *39*, 683–689. [CrossRef]
162. Alam, M.; Ahmed, S.; Elasbali, A.M.; Adnan, M.; Alam, S.; Hassan, I.; Pasupuleti, V.R. Therapeutic Implications of Caffeic Acid in Cancer and Neurological Diseases. *Front. Oncol.* **2022**, *12*, 860508. [CrossRef]
163. Kuo, Y.-Y.; Jim, W.-T.; Su, L.-C.; Chung, C.-J.; Lin, C.-Y.; Huo, C.; Tseng, J.-C.; Huang, S.-H.; Lai, C.-J.; Chen, B.-C.; et al. Caffeic Acid Phenethyl Ester Is a Potential Therapeutic Agent for Oral Cancer. *Int. J. Mol. Sci.* **2015**, *16*, 10748–10766. [CrossRef]
164. Mun, G.-I.; Kim, S.; Choi, E.; Kim, C.S.; Lee, Y.-S. Pharmacology of natural radioprotectors. *Arch. Pharmacal Res.* **2018**, *41*, 1033–1050. [CrossRef]
165. Changizi, V.; Haeri, S.A.; Abbasi, S.; Rajabi, Z.; Mirdoraghi, M. Radioprotective effects of vitamin A against gamma radiation in mouse bone marrow cells. *MethodsX* **2019**, *6*, 714–717. [CrossRef]
166. Song, Y.-N.; Wang, Y.; Zheng, Y.-H.; Liu, T.-L.; Zhang, C. Crocins: A comprehensive review of structural characteristics, pharmacokinetics and therapeutic effects. *Fitoterapia* **2021**, *153*, 104969. [CrossRef] [PubMed]
167. Bakshi, H.; Zoubi, M.; Faruck, H.; Aljabali, A.; Rabi, F.; Hafiz, A.; Al-Batanyeh, K.; Al-Trad, B.; Ansari, P.; Nasef, M.; et al. Dietary Crocin is Protective in Pancreatic Cancer while Reducing Radiation-Induced Hepatic Oxidative Damage. *Nutrients* **2020**, *12*, 1901. [CrossRef] [PubMed]
168. Zhang, C.; Chen, K.; Wang, J.; Zheng, Z.; Luo, Y.; Zhou, W.; Zhuo, Z.; Liang, J.; Sha, W.; Chen, H. Protective Effects of Crocetin against Radiation-Induced Injury in Intestinal Epithelial Cells. *BioMed Res. Int.* **2020**, *2020*, 2906053. [CrossRef] [PubMed]
169. Rossi, G.; Placidi, M.; Castellini, C.; Rea, F.; D'Andrea, S.; Alonso, G.; Gravina, G.; Tatone, C.; Di Emidio, G.; D'Alessandro, A. Crocetin Mitigates Irradiation Injury in an In Vitro Model of the Pubertal Testis: Focus on Biological Effects and Molecular Mechanisms. *Molecules* **2021**, *26*, 1676. [CrossRef]
170. Gajowik, A.; Dobrzyńska, M.M. The evaluation of protective effect of lycopene against genotoxic influence of X-irradiation in human blood lymphocytes. *Radiat. Environ. Biophys.* **2017**, *56*, 413–422. [CrossRef]
171. Motallebnejad, M.; Zahedpasha, S.; Moghadamnia, A.A.; Kazemi, S.; Moslemi, D.; Pouramir, M.; Asgharpour, F. Protective effect of lycopene on oral mucositis and antioxidant capacity of blood plasma in the rat exposed to gamma radiation. *Casp. J. Intern. Med.* **2020**, *11*, 419–425. [CrossRef]
172. Puah, B.-P.; Jalil, J.; Attiq, A.; Kamisah, Y. New Insights into Molecular Mechanism behind Anti-Cancer Activities of Lycopene. *Molecules* **2021**, *26*, 3888. [CrossRef]

173. Jefferson, R.D.; Goans, R.E.; Blain, P.G.; Thomas, S.H. Diagnosis and treatment of polonium poisoning. *Clin. Toxicol.* **2009**, *47*, 379–392. [CrossRef]
174. Ansoborlo, E.; Berard, P.; Auwer, C.D.; Leggett, R.; Menetrier, F.; Younes, A.; Montavon, G.; Moisy, P. Review of Chemical and Radiotoxicological Properties of Polonium for Internal Contamination Purposes. *Chem. Res. Toxicol.* **2012**, *25*, 1551–1564. [CrossRef]
175. Foltin, G.L.; Schonfeld, D.J. *Shannon MW Pediatric Terrorism and Disaster Preparedness: A Resource for Pediatricians*; Agency for Healthcare Research and Quality: Rockville, MD, USA, 2006.
176. Sato, T.; Kinoshita, M.; Yamamoto, T.; Ito, M.; Nishida, T.; Takeuchi, M.; Saitoh, D.; Seki, S.; Mukai, Y. Treatment of Irradiated Mice with High-Dose Ascorbic Acid Reduced Lethality. *PLoS ONE* **2015**, *10*, e0117020. [CrossRef]
177. Nukala, U.; Thakkar, S.; Krager, K.J.; Breen, P.J.; Compadre, C.M.; Aykin-Burns, N. Antioxidant Tocols as Radiation Countermeasures (Challenges to be Addressed to Use Tocols as Radiation Countermeasures in Humans). *Antioxidants* **2018**, *7*, 33. [CrossRef] [PubMed]
178. Singh, V.K.; Beattie, L.A.; Seed, T.M. Vitamin E: Tocopherols and tocotrienols as potential radiation countermeasures. *J. Radiat. Res.* **2013**, *54*, 973–988. [CrossRef]
179. Aykin-Burns, N.; Pathak, R.; Boerma, M.; Kim, T.; Hauer-Jensen, M. Utilization of Vitamin E Analogs to Protect Normal Tissues While Enhancing Antitumor Effects. *Semin. Radiat. Oncol.* **2018**, *29*, 55–61. [CrossRef] [PubMed]
180. Singh, V.K.; Singh, P.K.; Wise, S.Y.; Posarac, A.; Fatanmi, O.O. Radioprotective properties of tocopherol succinate against ionizing radiation in mice. *J. Radiat. Res.* **2012**, *54*, 210–220. [CrossRef] [PubMed]
181. Singh, P.K.; Wise, S.Y.; Ducey, E.J.; Fatanmi, O.O.; Elliott, T.B.; Singh, V.K. α-Tocopherol Succinate Protects Mice against Radiation-Induced Gastrointestinal Injury. *Radiat. Res.* **2012**, *177*, 133–145. [CrossRef] [PubMed]
182. Singh, P.K.; Wise, S.Y.; Ducey, E.J.; Brown, D.S.; Singh, V.K. Radioprotective efficacy of tocopherol succinate is mediated through granulocyte-colony stimulating factor. *Cytokine* **2011**, *56*, 411–421. [CrossRef] [PubMed]
183. Kulkarni, S.; Singh, P.K.; Ghosh, S.P.; Posarac, A.; Singh, V.K. Granulocyte colony-stimulating factor antibody abrogates radioprotective efficacy of gamma-tocotrienol, a promising radiation countermeasure. *Cytokine* **2013**, *62*, 278–285. [CrossRef]
184. Singh, V.K.; Wise, S.Y.; Scott, J.R.; Romaine, P.L.; Newman, V.L.; Fatanmi, O.O. Radioprotective efficacy of delta-tocotrienol, a vitamin E isoform, is mediated through granulocyte colony-stimulating factor. *Life Sci.* **2014**, *98*, 113–122. [CrossRef]
185. Berbee, M.; Fu, Q.; Boerma, M.; Wang, J.; Kumar, K.S.; Hauer-Jensen, M. γ-Tocotrienol Ameliorates Intestinal Radiation Injury and Reduces Vascular Oxidative Stress after Total-Body Irradiation by an HMG-CoA Reductase-Dependent Mechanism. *Radiat. Res.* **2009**, *171*, 596–605. [CrossRef]
186. Pathak, R.; Shao, L.; Ghosh, S.P.; Zhou, D.; Boerma, M.; Weiler, H.; Hauer-Jensen, M. Thrombomodulin Contributes to Gamma Tocotrienol-Mediated Lethality Protection and Hematopoietic Cell Recovery in Irradiated Mice. *PLoS ONE* **2015**, *10*, e0122511. [CrossRef]
187. Rosen, E.; Fatanmi, O.O.; Wise, S.Y.; Rao, V.A.; Singh, V.K. Gamma-tocotrienol, a radiation countermeasure, reverses proteomic changes in serum following total-body gamma irradiation in mice. *Sci. Rep.* **2022**, *12*, 3387. [CrossRef]
188. Singh, V.K.; Kulkarni, S.; Fatanmi, O.O.; Wise, S.Y.; Newman, V.L.; Romaine, P.L.P.; Hendrickson, H.; Gulani, J.; Ghosh, S.P.; Kumar, K.S.; et al. Radioprotective Efficacy of Gamma-Tocotrienol in Nonhuman Primates. *Radiat. Res.* **2016**, *185*, 285–298. [CrossRef]
189. Singh, V.K.; Hauer-Jensen, M. γ-Tocotrienol as a Promising Countermeasure for Acute Radiation Syndrome: Current Status. *Int. J. Mol. Sci.* **2016**, *17*, 663. [CrossRef]
190. Nemec-Bakk, A.S.; Sridharan, V.; Landes, R.D.; Singh, P.; Cao, M.; Seawright, J.W.; Liu, X.; Zheng, G.; Dominic, P.; Pathak, R.; et al. Mitigation of late cardiovascular effects of oxygen ion radiation by γ-tocotrienol in a mouse model. *Life Sci. Space Res.* **2021**, *31*, 43–50. [CrossRef]
191. Kumar, V.P.; Stone, S.; Biswas, S.; Sharma, N.; Ghosh, S.P. Gamma Tocotrienol Protects Mice from Targeted Thoracic Radiation Injury. *Front. Pharmacol.* **2020**, *11*, 587970. [CrossRef]
192. Garg, S.; Sadhukhan, R.; Banerjee, S.; Savenka, A.V.; Basnakian, A.G.; McHargue, V.; Wang, J.; Pawar, S.A.; Ghosh, S.P.; Ware, J.; et al. Gamma-Tocotrienol Protects the Intestine from Radiation Potentially by Accelerating Mesenchymal Immune Cell Recovery. *Antioxidants* **2019**, *8*, 57. [CrossRef]
193. Suman, S.; Datta, K.; Chakraborty, K.; Kulkarni, S.S.; Doiron, K.; Fornace, A.; Kumar, K.S.; Hauer-Jensen, M.; Ghosh, S.P. Gamma tocotrienol, a potent radioprotector, preferentially upregulates expression of anti-apoptotic genes to promote intestinal cell survival. *Food Chem. Toxicol.* **2013**, *60*, 488–496. [CrossRef]
194. Lee, S.-G.; Kalidindi, T.M.; Lou, H.; Gangangari, K.; Punzalan, B.; Bitton, A.; Lee, C.J.; Park, S.; Bodei, L.; Kharas, M.G.; et al. Gamma-Tocotrienol loaded liposomes as radioprotection from hematopoietic side effects caused by radiotherapeutic drugs. *J. Nucl. Med.* **2020**, *62*, 584–590. [CrossRef]
195. Singh, V.K.; Fatanmi, O.O.; Wise, S.Y.; Newman, V.L.; Romaine, P.L.; Seed, T.M. The potentiation of the radioprotective efficacy of two medical countermeasures, gamma-tocotrienol and amifostine, by a combination prophylactic modality. *Radiat. Prot. Dosim.* **2016**, *172*, 302–310. [CrossRef]
196. Pathak, R.; Kumar, V.P.; Hauer-Jensen, M.; Ghosh, S.P. Enhanced Survival in Mice Exposed to Ionizing Radiation by Combination of Gamma-Tocotrienol and Simvastatin. *Mil. Med.* **2019**, *184*, 644–651. [CrossRef]
197. Berbee, M.; Fu, Q.; Garg, S.; Kulkarni, S.; Kumar, K.S.; Hauer-Jensen, M. Pentoxifylline Enhances the Radioprotective Properties of γ-Tocotrienol: Differential Effects on the Hematopoietic, Gastrointestinal and Vascular Systems. *Radiat. Res.* **2011**, *175*, 297–306. [CrossRef]

198. Haddad, P.; Kalaghchi, B.; Amouzegar-Hashemi, F. Pentoxifylline and vitamin E combination for superficial radiation-induced fibrosis: A phase II clinical trial. *Radiother. Oncol.* **2005**, *77*, 324–326. [CrossRef]
199. Bairati, I.; Meyer, F.; Gélinas, M.; Fortin, A.; Nabid, A.; Brochet, F.; Mercier, J.-P.; Têtu, B.; Harel, F.; Abdous, B.; et al. Randomized Trial of Antioxidant Vitamins to Prevent Acute Adverse Effects of Radiation Therapy in Head and Neck Cancer Patients. *J. Clin. Oncol.* **2005**, *23*, 5805–5813. [CrossRef]
200. Meyer, F.; Bairati, I.; Jobin, E.; Gélinas, M.; Fortin, A.; Nabid, A.; Têtu, B. Acute Adverse Effects of Radiation Therapy and Local Recurrence in Relation to Dietary and Plasma Beta Carotene and Alpha Tocopherol in Head and Neck Cancer Patients. *Nutr. Cancer* **2007**, *59*, 29–35. [CrossRef]
201. Ohba, T.; Hasegawa, A.; Kohayagawa, Y.; Kondo, H.; Suzuki, G. Body Surface Contamination Levels of Residents under Different Evacuation Scenarios after the Fukushima Daiichi Nuclear Power Plant Accident. *Health Phys.* **2017**, *113*, 175–182. [CrossRef]
202. Vasil'Eva, I.N.; Bespalov, V.G.; Baranenko, D.A. Radioprotective and Apoptotic Properties of a Combination of α-Tocopherol Acetate and Ascorbic Acid. *Bull. Exp. Biol. Med.* **2016**, *161*, 248–251. [CrossRef]
203. Marampon, F.; Gravina, G.L.; Festuccia, C.; Popov, V.M.; Colapietro, E.A.; Sanità, P.; Musio, D.; De Felice, F.; Lenzi, A.; Jannini, E.A.; et al. Vitamin D protects endothelial cells from irradiation-induced senescence and apoptosis by modulating MAPK/SirT1 axis. *J. Endocrinol. Investig.* **2015**, *39*, 411–422. [CrossRef] [PubMed]
204. Farhood, B.; Ghorbani, M.; Goushbolagh, N.A.; Najafi, M.; Geraily, G. Different Methods of Measuring Neutron Dose/Fluence Generated During Radiation Therapy with Megavoltage Beams. *Health Phys.* **2020**, *118*, 65–74. [CrossRef] [PubMed]
205. Jain, S.K.; Micinski, D. Vitamin D upregulates glutamate cysteine ligase and glutathione reductase, and GSH formation, and decreases ROS and MCP-1 and IL-8 secretion in high-glucose exposed U937 monocytes. *Biochem. Biophys. Res. Commun.* **2013**, *437*, 7–11. [CrossRef] [PubMed]
206. Kaminskyi, O.V.; Pankiv, V.I.; Pankiv, I.V.; Afanasyev, D.E. Vitamin D content in population of radiologically contaminated areas in chernivtsi oblast (Pilot Project). *Probl. Radiac. Med. Radiobiol.* **2018**, *23*, 442–451. [CrossRef] [PubMed]
207. Yaprak, G.; Gemici, C.; Temizkan, S.; Ozdemir, S.; Dogan, B.C.; Seseogullari, O.O. Osteoporosis development and vertebral fractures after abdominal irradiation in patients with gastric cancer. *BMC Cancer* **2018**, *18*, 972. [CrossRef]
208. Ji, M.-T.; Nie, J.; Nie, X.-F.; Hu, W.-T.; Pei, H.-L.; Wan, J.-M.; Wang, A.-Q.; Zhou, G.-M.; Zhang, Z.-L.; Chang, L.; et al. 1α,25(OH)2D3 Radiosensitizes Cancer Cells by Activating the NADPH/ROS Pathway. *Front. Pharmacol.* **2020**, *11*, 945. [CrossRef]
209. Hosseinimehr, S.J. The protective effects of trace elements against side effects induced by ionizing radiation. *Radiat. Oncol. J.* **2015**, *33*, 66–74. [CrossRef]
210. Weiss, J.; Srinivasan, V.; Kumar, K.; Landauer, M. Radioprotection by metals: Selenium. *Adv. Space Res.* **1992**, *12*, 223–231. [CrossRef]
211. Bartolini, D.; Tew, K.D.; Marinelli, R.; Galli, F.; Wang, G.Y. Nrf2-modulation by seleno-hormetic agents and its potential for radiation protection. *BioFactors* **2019**, *46*, 239–245. [CrossRef]
212. Gandhi, K.; Goda, J.; Gandhi, V.; Sadanpurwala, A.; Jain, V.; Joshi, K.; Epari, S.; Rane, S.; Mohanty, B.; Chaudhari, P.; et al. Oral administration of 3,3′-diselenodipropionic acid prevents thoracic radiation induced pneumonitis in mice by suppressing NF-kB/IL-17/G-CSF/neutrophil axis. *Free Radic. Biol. Med.* **2019**, *145*, 8–19. [CrossRef]
213. Kunwar, A.; Bansal, P.; Kumar, S.J.; Bag, P.; Paul, P.; Reddy, N.; Kumbhare, L.; Jain, V.; Chaubey, R.; Unnikrishnan, M. In vivo radioprotection studies of 3,3′-diselenodipropionic acid, a selenocystine derivative. *Free Radic. Biol. Med.* **2010**, *48*, 399–410. [CrossRef]
214. Kunwar, A.; Priyadarsini, K.I.; Jain, V.K. 3,3′-Diselenodipropionic acid (DSePA): A redox active multifunctional molecule of biological relevance. *Biochim. Biophys. Acta (BBA)-Gen. Subj.* **2020**, *1865*, 129768. [CrossRef]
215. Puspitasari, I.M.; Abdulah, R.; Yamazaki, C.; Kameo, S.; Nakano, T.; Koyama, H. Updates on clinical studies of selenium supplementation in radiotherapy. *Radiat. Oncol.* **2014**, *9*, 125. [CrossRef]
216. Handa, E.; Puspitasari, I.M.; Abdulah, R.; Yamazaki, C.; Kameo, S.; Nakano, T.; Koyama, H. Recent advances in clinical studies of selenium supplementation in radiotherapy. *J. Trace Elem. Med. Biol.* **2020**, *62*, 126653. [CrossRef]
217. Zhao, G.; Wu, X.; Chen, P.; Zhang, L.; Yang, C.S.; Zhang, J. Selenium nanoparticles are more efficient than sodium selenite in producing reactive oxygen species and hyper-accumulation of selenium nanoparticles in cancer cells generates potent therapeutic effects. *Free Radic. Biol. Med.* **2018**, *126*, 55–66. [CrossRef]
218. Kim, S.J.; Choi, M.C.; Park, J.M.; Chung, A.S. Antitumor Effects of Selenium. *Int. J. Mol. Sci.* **2021**, *22*, 11844. [CrossRef]
219. Batinic-Haberle, I.; Tovmasyan, A.; Spasojevic, I. Mn Porphyrin-Based Redox-Active Drugs: Differential Effects as Cancer Therapeutics and Protectors of Normal Tissue Against Oxidative Injury. *Antioxid. Redox Signal.* **2018**, *29*, 1691–1724. [CrossRef]
220. Weitzel, D.H.; Tovmasyan, A.; Ashcraft, K.A.; Rajic, Z.; Weitner, T.; Liu, C.; Li, W.; Buckley, A.F.; Prasad, M.R.; Young, K.H.; et al. Radioprotection of the Brain White Matter by Mn(III) *N*-Butoxyethylpyridylporphyrin–Based Superoxide Dismutase Mimic MnTnBuOE-2-PyP$^{5+}$. *Mol. Cancer Ther.* **2014**, *14*, 70–79. [CrossRef]
221. Lewandowski, M.; Gwozdzinski, K. Nitroxides as Antioxidants and Anticancer Drugs. *Int. J. Mol. Sci.* **2017**, *18*, 2490. [CrossRef]
222. Patyar, R.R.; Patyar, S. Role of drugs in the prevention and amelioration of radiation induced toxic effects. *Eur. J. Pharmacol.* **2018**, *819*, 207–216. [CrossRef]
223. Wei, L.; Leibowitz, B.J.; Epperly, M.; Bi, C.; Li, A.; Steinman, J.; Wipf, P.; Li, S.; Zhang, L.; Greenberger, J.; et al. The GS-nitroxide JP4-039 improves intestinal barrier and stem cell recovery in irradiated mice. *Sci. Rep.* **2018**, *8*, 2072. [CrossRef] [PubMed]
224. Willis, J.; Epperly, M.W.; Fisher, R.; Zhang, X.; Shields, N.; Hou, W.; Wang, H.; Li, S.; Wipf, P.; Parmar, K.; et al. Amelioration of Head and Neck Radiation-Induced Mucositis and Distant Marrow Suppression in Fanca−/− and Fancg−/− Mice by Intraoral Administration of GS-Nitroxide (JP4-039). *Radiat. Res.* **2018**, *189*, 560–578. [CrossRef] [PubMed]

225. Epperly, M.W.; Sacher, J.R.; Krainz, T.; Zhang, X.; Wipf, P.; Liang, M.; Fisher, R.; Li, S.; Wang, H.; Greenberger, J.S. Effectiveness of Analogs of the GS-Nitroxide, JP4-039, as Total Body Irradiation Mitigators. *In Vivo* **2017**, *31*, 39–44. [CrossRef]
226. Luo, G.; Sun, L.; Li, H.; Chen, J.; He, P.; Zhao, L.; Tang, W.; Qiu, H. The potent radioprotective agents: Novel nitronyl nitroxide radical spin-labeled resveratrol derivatives. *Fitoterapia* **2021**, *155*, 105053. [CrossRef] [PubMed]
227. Galano, A.; Tan, D.-X.; Reiter, R.J. Melatonin: A Versatile Protector against Oxidative DNA Damage. *Molecules* **2018**, *23*, 530. [CrossRef]
228. Shirazi, A.; Esmaely, F.; Mahmoudzadeh, A.; Cheki, M. The radioprotective effect of melatonin against radiation-induced DNA double-strand breaks in radiology. *J. Cancer Res. Ther.* **2020**, *16*, S59–S63. [CrossRef]
229. Mohseni, M.; Mihandoost, E.; Shirazi, A.; Sepehrizadeh, Z.; Bazzaz, J.T.; Ghazi-Khansari, M. Melatonin may play a role in modulation of bax and bcl-2 expression levels to protect rat peripheral blood lymphocytes from gamma irradiation-induced apoptosis. *Mutat. Res. Mol. Mech. Mutagen.* **2012**, *738–739*, 19–27. [CrossRef]
230. Nuszkiewicz, J.; Woźniak, A.; Szewczyk-Golec, K. Ionizing Radiation as a Source of Oxidative Stress—The Protective Role of Melatonin and Vitamin D. *Int. J. Mol. Sci.* **2020**, *21*, 5804. [CrossRef]
231. Gurunathan, S.; Qasim, M.; Kang, M.-H.; Kim, J.-H. Role and Therapeutic Potential of Melatonin in Various Type of Cancers. *OncoTargets Ther.* **2021**, *14*, 2019–2052. [CrossRef]
232. Wang, Y.-M.; Jin, B.-Z.; Ai, F.; Duan, C.-H.; Lü, Y.-Z.; Dong, T.-F.; Fu, Q.-L. The efficacy and safety of melatonin in concurrent chemotherapy or radiotherapy for solid tumors: A meta-analysis of randomized controlled trials. *Cancer Chemother. Pharmacol.* **2012**, *69*, 1213–1220. [CrossRef]
233. Hofer, M.; Hoferová, Z.; Falk, M. Pharmacological Modulation of Radiation Damage. Does It Exist a Chance for Other Substances than Hematopoietic Growth Factors and Cytokines? *Int. J. Mol. Sci.* **2017**, *18*, 1385. [CrossRef]
234. Singh, V.K.; Seed, T.M. Repurposing Pharmaceuticals Previously Approved by Regulatory Agencies to Medically Counter Injuries Arising Either Early or Late Following Radiation Exposure. *Front. Pharmacol.* **2021**, *12*, 1103. [CrossRef]
235. Li, W.S.; Van der Velden, J.M.; Ganesh, V.; Vuong, S.; Raman, S.; Popovic, M.; Lam, H.; Wong, K.H.; Ngan, R.K.; Burbach, J.P.M.; et al. Prophylaxis of radiation-induced nausea and vomiting: A systematic review and meta-analysis of randomized controlled trials. *Ann. Palliat. Med.* **2017**, *6*, 104–117. [CrossRef]
236. Singh, V.K.; Seed, T.M. Pharmacological management of ionizing radiation injuries: Current and prospective agents and targeted organ systems. *Expert Opin. Pharm.* **2020**, *21*, 317–337. [CrossRef]
237. Touchefeu, Y.; Montassier, E.; Nieman, K.; Gastinne, T.; Potel, G.; Varannes, S.B.D.; Le Vacon, F.; De La Cochetière, M.F. Systematic review: The role of the gut microbiota in chemotherapy- or radiation-induced gastrointestinal mucositis-current evidence and potential clinical applications. *Aliment. Pharmacol. Ther.* **2014**, *40*, 409–421. [CrossRef]
238. Jian, Y.; Zhang, D.; Liu, M.; Wang, Y.; Xu, Z.-X. The Impact of Gut Microbiota on Radiation-Induced Enteritis. *Front. Cell. Infect. Microbiol.* **2021**, *11*, 586392. [CrossRef]
239. Sivaprakasam, S.; Prasad, P.D.; Singh, N. Benefits of short-chain fatty acids and their receptors in inflammation and carcinogenesis. *Pharmacol. Ther.* **2016**, *164*, 144–151. [CrossRef]
240. Guo, H.; Chou, W.-C.; Lai, Y.; Liang, K.; Tam, J.W.; Brickey, W.J.; Chen, L.; Montgomery, N.D.; Li, X.; Bohannon, L.M.; et al. Multi-omics analyses of radiation survivors identify radioprotective microbes and metabolites. *Science* **2020**, *370*, eaay9097. [CrossRef]
241. Li, Y.; Dong, J.; Xiao, H.; Zhang, S.; Wang, B.; Cui, M.; Fan, S. Gut commensal derived-valeric acid protects against radiation injuries. *Gut Microbes* **2020**, *11*, 789–806. [CrossRef]
242. Liu, M.-M.; Li, S.-T.; Shu, Y.; Zhan, H.-Q. Probiotics for prevention of radiation-induced diarrhea: A meta-analysis of randomized controlled trials. *PLoS ONE* **2017**, *12*, e0178870. [CrossRef]
243. Segers, C.; Verslegers, M.; Baatout, S.; Leys, N.; Lebeer, S.; Mastroleo, F. Food Supplements to Mitigate Detrimental Effects of Pelvic Radiotherapy. *Microorganisms* **2019**, *7*, 97. [CrossRef]
244. Zhao, T.-S.; Xie, L.-W.; Cai, S.; Xu, J.-Y.; Zhou, H.; Tang, L.-F.; Yang, C.; Fang, S.; Li, M.; Tian, Y. Dysbiosis of Gut Microbiota Is Associated With the Progression of Radiation-Induced Intestinal Injury and Is Alleviated by Oral Compound Probiotics in Mouse Model. *Front. Cell. Infect. Microbiol.* **2021**, *11*, 717636. [CrossRef]
245. De Almeida, C.V.; De Camargo, M.R.; Russo, E.; Amedei, A. Role of diet and gut microbiota on colorectal cancer immunomodulation. *World J. Gastroenterol.* **2019**, *25*, 151–162. [CrossRef]
246. Liu, J.; Liu, C.; Yue, J. Radiotherapy and the gut microbiome: Facts and fiction. *Radiat. Oncol.* **2021**, *16*, 1–15. [CrossRef]
247. Stenson, W.F.; Ciorba, M.A. Nonmicrobial Activation of TLRs Controls Intestinal Growth, Wound Repair, and Radioprotection. *Front. Immunol.* **2021**, *11*, 617510. [CrossRef] [PubMed]
248. Devaraj, N.K.; Suppiah, S.; Veettil, S.K.; Ching, S.M.; Lee, K.W.; Menon, R.K.; Soo, M.J.; Deuraseh, I.; Hoo, F.K.; Sivaratnam, D. The Effects of Probiotic Supplementation on the Incidence of Diarrhea in Cancer Patients Receiving Radiation Therapy: A Systematic Review with Meta-Analysis and Trial Sequential Analysis of Randomized Controlled Trials. *Nutrients* **2019**, *11*, 2886. [CrossRef] [PubMed]
249. Picó-Monllor, J.A.; Mingot-Ascencao, J.M. Search and Selection of Probiotics That Improve Mucositis Symptoms in Oncologic Patients. A Systematic Review. *Nutrients* **2019**, *11*, 2322. [CrossRef] [PubMed]
250. Hofer, M.; Pospíšil, M. Modulation of Animal and Human Hematopoiesis by β-Glucans: A Review. *Molecules* **2011**, *16*, 7969–7979. [CrossRef]

251. Zhang, Y.; Dong, Y.; Lu, P.; Wang, X.; Li, W.; Dong, H.; Fan, S.; Li, D. Gut metabolite Urolithin A mitigates ionizing radiation-induced intestinal damage. *J. Cell. Mol. Med.* **2021**, *25*, 10306–10312. [CrossRef]
252. Dalmau, S.R.; Freitas, C.S.; Tabak, D.G. Interleukin-1 and tumor necrosis factor-alpha as radio- and chemoprotectors of bone marrow. *Bone Marrow Transpl.* **1993**, *12*, 551–563.
253. MacVittie, T.J.; Farese, A.M.; Patchen, M.L.; Myers, L.A. Therapeutic Efficacy of Recombinant Interleukin-6 (IL-6) Alone and Combined with Recombinant Human IL-3 in a Nonhuman Primate Model of High-Dose, Sublethal Radiation-Induced Marrow Aplasia. *Blood* **1994**, *84*, 2515–2522. [CrossRef]
254. DiCarlo, A.L. Scientific research and product development in the United States to address injuries from a radiation public health emergency. *J. Radiat. Res.* **2021**, *62*, 752–763. [CrossRef]
255. Dainiak, N.; Gent, R.N.; Carr, Z.; Schneider, R.; Bader, J.; Buglova, E.; Chao, N.; Coleman, C.N.; Ganser, A.; Gorin, C.; et al. First Global Consensus for Evidence-Based Management of the Hematopoietic Syndrome Resulting From Exposure to Ionizing Radiation. *Disaster Med. Public Health Prep.* **2011**, *5*, 202–212. [CrossRef]
256. Singh, V.K.; Seed, T.M. BIO 300: A promising radiation countermeasure under advanced development for acute radiation syndrome and the delayed effects of acute radiation exposure. *Expert Opin. Investig. Drugs* **2020**, *29*, 429–441. [CrossRef]
257. Hu, Q.; Zhou, Y.; Wu, S.; Wu, W.; Deng, Y.; Shao, A. Molecular hydrogen: A potential radioprotective agent. *Biomed. Pharm.* **2020**, *130*, 110589. [CrossRef]
258. Vadhan-Raj, S.; Goldberg, J.D.; Perales, M.-A.; Berger, D.P.; Brink, M.R.M.V.D. Clinical applications of palifermin: Amelioration of oral mucositis and other potential indications. *J. Cell. Mol. Med.* **2013**, *17*, 1371–1384. [CrossRef]
259. Dicarlo, A.L.; Horta, Z.P.; Aldrich, J.T.; Jakubowski, A.A.; Skinner, W.K.; Case, C.M. Use of Growth Factors and Other Cytokines for Treatment of Injuries During a Radiation Public Health Emergency. *Radiat. Res.* **2019**, *192*, 99–120. [CrossRef]
260. Doan, P.L.; Himburg, H.A.; Helms, K.; Russell, J.L.; Fixsen, E.; Quarmyne, M.; Harris, J.R.; Deoliviera, D.; Sullivan, J.M.; Chao, N.J.; et al. Epidermal growth factor regulates hematopoietic regeneration after radiation injury. *Nat. Med.* **2013**, *19*, 295–304. [CrossRef]
261. Gu, A.; Jie, Y.; Sun, L.; Zhao, S.; E, M.; You, Q. RhNRG-1β Protects the Myocardium against Irradiation-Induced Damage via the ErbB2-ERK-SIRT1 Signaling Pathway. *PLoS ONE* **2015**, *10*, e0137337. [CrossRef]
262. Casey-Sawicki, K.; Zhang, M.; Kim, S.; Zhang, A.; Zhang, S.B.; Zhang, Z.; Singh, R.; Yang, S.; Swarts, S.; Vidyasagar, S.; et al. A Basic Fibroblast Growth Factor Analog for Protection and Mitigation against Acute Radiation Syndromes. *Health Phys.* **2014**, *106*, 704–712. [CrossRef]
263. Yamaguchi, M.; Hirouchi, T.; Yoshioka, H.; Watanabe, J.; Kashiwakura, I. Diverse functions of the thrombopoietin receptor agonist romiplostim rescue individuals exposed to lethal radiation. *Free Radic. Biol. Med.* **2019**, *136*, 60–75. [CrossRef]
264. Dainiak, N. Medical management of acute radiation syndrome and associated infections in a high-casualty incident. *J. Radiat. Res.* **2018**, *59*, ii54–ii64. [CrossRef]
265. Gilreath, J.; Lo, M.; Bubalo, J. Thrombopoietin Receptor Agonists (TPO-RAs): Drug Class Considerations for Pharmacists. *Drugs* **2021**, *81*, 1285–1305. [CrossRef]
266. Yamaguchi, M.; Hirouchi, T.; Yokoyama, K.; Nishiyama, A.; Murakami, S.; Kashiwakura, I. The thrombopoietin mimetic romiplostim leads to the complete rescue of mice exposed to lethal ionizing radiation. *Sci. Rep.* **2018**, *8*, 10659. [CrossRef]
267. Bunin, D.I.; Bakke, J.; Green, C.E.; Javitz, H.S.; Fielden, M.; Chang, P.Y. Romiplostim (Nplate®) as an effective radiation countermeasure to improve survival and platelet recovery in mice. *Int. J. Radiat. Biol.* **2019**, *96*, 145–154. [CrossRef] [PubMed]
268. Hirouchi, T.; Ito, K.; Nakano, M.; Monzen, S.; Yoshino, H.; Chiba, M.; Hazawa, M.; Nakano, A.; Ishikawa, J.; Yamaguchi, M.; et al. Mitigative Effects of a Combination of Multiple Pharmaceutical Drugs on the Survival of Mice Exposed to Lethal Ionizing Radiation. *Curr. Pharm. Biotechnol.* **2015**, *17*, 190–199. [CrossRef] [PubMed]
269. Wong, K.; Chang, P.Y.; Fielden, M.; Downey, A.M.; Bunin, D.; Bakke, J.; Gahagen, J.; Iyer, L.; Doshi, S.; Wierzbicki, W.; et al. Pharmacodynamics of romiplostim alone and in combination with pegfilgrastim on acute radiation-induced thrombocytopenia and neutropenia in non-human primates. *Int. J. Radiat. Biol.* **2019**, *96*, 155–166. [CrossRef] [PubMed]
270. Basile, L.A.; Ellefson, D.; Gluzman-Poltorak, Z.; Junes-Gill, K.; Mar, V.; Mendonca, S.; Miller, J.D.; Tom, J.; Trinh, A.; Gallaher, T.K. HemaMax™, a Recombinant Human Interleukin-12, Is a Potent Mitigator of Acute Radiation Injury in Mice and Non-Human Primates. *PLoS ONE* **2012**, *7*, e30434. [CrossRef]
271. Plett, P.A.; Chua, H.L.; Sampson, C.H.; Katz, B.P.; Fam, C.M.; Anderson, L.J.; Cox, G.N.; Orschell, C.M. PEGylated G-CSF (BBT-015), GM-CSF (BBT-007), AND IL-11 (BBT-059) Analogs Enhance Survival and Hematopoietic Cell Recovery in a Mouse Model of the Hematopoietic Syndrome of the Acute Radiation Syndrome. *Health Phys.* **2014**, *106*, 7–20. [CrossRef]
272. Baranov, A.; Gale, R.P.; Guskova, A.; Piatkin, E.; Selidovkin, G.; Muravyova, L.; Champlin, R.E.; Danilova, N.; Yevseeva, L.; Petrosyan, L.; et al. Bone Marrow Transplantation after the Chernobyl Nuclear Accident. *N. Engl. J. Med.* **1989**, *321*, 205–212. [CrossRef]
273. Wang, K.-X.; Cui, W.-W.; Yang, X.; Tao, A.-B.; Lan, T.; Li, T.-S.; Luo, L. Mesenchymal Stem Cells for Mitigating Radiotherapy Side Effects. *Cells* **2021**, *10*, 294. [CrossRef]
274. Yang, S.-J.; Wang, X.-Q.; Jia, Y.-H.; Wang, R.; Cao, K.; Zhang, X.; Zhong, J.; Tan, D.-M.; Tan, Y. Human Umbilical Cord Mesenchymal Stem Cell Transplantation Restores Hematopoiesis in Acute Radiation Disease. *Am. J. Transl. Res.* **2021**, *13*, 8670–8682.

275. Benderitter, M.; Caviggioli, F.; Chapel, A.; Coppes, R.P.; Guha, C.; Klinger, M.; Malard, O.; Stewart, F.; Tamarat, R.; Van Luijk, P.; et al. Stem Cell Therapies for the Treatment of Radiation-Induced Normal Tissue Side Effects. *Antioxid. Redox Signal.* **2014**, *21*, 338–355. [CrossRef]
276. Ahamed, J.; Laurence, J. Role of Platelet-Derived Transforming Growth Factor-β1 and Reactive Oxygen Species in Radiation-Induced Organ Fibrosis. *Antioxid. Redox Signal.* **2017**, *27*, 977–988. [CrossRef]
277. Wang, B.; Wang, H.; Zhang, M.; Ji, R.; Wei, J.; Xin, Y.; Jiang, X. Radiation-induced myocardial fibrosis: Mechanisms underlying its pathogenesis and therapeutic strategies. *J. Cell. Mol. Med.* **2020**, *24*, 7717–7729. [CrossRef]
278. Farhood, B.; Goradel, N.H.; Mortezaee, K.; Khanlarkhani, N.; Salehi, E.; Nashtaei, M.S.; Shabeeb, D.; Musa, A.E.; Fallah, H.; Najafi, M. Intercellular communications-redox interactions in radiation toxicity; potential targets for radiation mitigation. *J. Cell Commun. Signal.* **2018**, *13*, 3–16. [CrossRef]
279. Cheki, M.; Yahyapour, R.; Farhood, B.; Rezaeyan, A.; Shabeeb, D.; Amini, P.; Rezapoor, S.; Najafi, M. COX-2 in Radiotherapy: A Potential Target for Radioprotection and Radiosensitization. *Curr. Mol. Pharmacol.* **2018**, *11*, 173–183. [CrossRef]
280. Monceau, V.; Pasinetti, N.; Schupp, C.; Pouzoulet, F.; Opolon, P.; Vozenin, M.-C. Modulation of the Rho/ROCK pathway in heart and lung after thorax irradiation reveals targets to improve normal tissue toxicity. *Curr. Drug Targets* **2010**, *11*, 1395–1404. [CrossRef]
281. Lin, R.; Yi, S.; Gong, L.; Liu, W.; Wang, P.; Liu, N.; Zhao, L.; Wang, P. Inhibition of TGF-β signaling with halofuginone can enhance the antitumor effect of irradiation in Lewis lung cancer. *OncoTargets Ther.* **2015**, *8*, 3549–3559. [CrossRef]
282. Zhuang, H.; Shi, S.; Yuan, Z.; Chang, J.Y. Bevacizumab treatment for radiation brain necrosis: Mechanism, efficacy and issues. *Mol. Cancer* **2019**, *18*, 21. [CrossRef]
283. Liu, J.; Liao, S.; Diop-Frimpong, B.; Chen, W.; Goel, S.; Naxerova, K.; Ancukiewicz, M.; Boucher, Y.; Jain, R.K.; Xu, L. TGF-β blockade improves the distribution and efficacy of therapeutics in breast carcinoma by normalizing the tumor stroma. *Proc. Natl. Acad. Sci. USA* **2012**, *109*, 16618–16623. [CrossRef]
284. Yahyapour, R.; Amini, P.; Rezapoor, S.; Rezaeyan, A.; Farhood, B.; Cheki, M.; Fallah, H.; Najafi, M. Targeting of Inflammation for Radiation Protection and Mitigation. *Curr. Mol. Pharmacol.* **2018**, *11*, 203–210. [CrossRef]
285. Laube, M.; Kniess, T.; Pietzsch, J.; Laube, M.; Kniess, T.; Pietzsch, J. Development of Antioxidant COX-2 Inhibitors as Radioprotective Agents for Radiation Therapy—A Hypothesis-Driven Review. *Antioxidants* **2016**, *5*, 14. [CrossRef]
286. Demirel, C.; Kilciksiz, S.C.; Gurgul, S.; Erdal, N.; Yigit, S.; Tamer, L.; Ayaz, L. Inhibition of Radiation-Induced Oxidative Damage in the Lung Tissue: May Acetylsalicylic Acid Have a Positive Role? *Inflammation* **2015**, *39*, 158–165. [CrossRef]
287. Ma, S.; Jin, Z.; Liu, Y.; Liu, L.; Feng, H.; Li, P.; Tian, Z.; Ren, M.; Liu, X. Furazolidone Increases Survival of Mice Exposed to Lethal Total Body Irradiation through the Antiapoptosis and Antiautophagy Mechanism. *Oxidative Med. Cell. Longev.* **2021**, *2021*, e6610726. [CrossRef]
288. Stokman, M.A.; Spijkervet, F.K.L.; Burlage, F.R.; Roodenburg, J.L.N. Clinical effects of flurbiprofen tooth patch on radiation-induced oral mucositis. A pilot study. *Support. Care Cancer* **2004**, *13*, 42–48. [CrossRef]
289. Kazemian, A.; Kamian, S.; Aghili, M.; Hashemi, F.; Haddad, P. Benzydamine for prophylaxis of radiation-induced oral mucositis in head and neck cancers: A double-blind placebo-controlled randomized clinical trial. *Eur. J. Cancer Care* **2009**, *18*, 174–178. [CrossRef]
290. Hofer, M.; Pospíšil, M.; Dušek, L.; Hoferová, Z.; Komůrková, D. Agonist of the adenosine A3 receptor, IB-MECA, and inhibitor of cyclooxygenase-2, meloxicam, given alone or in a combination early after total body irradiation enhance survival of γ-irradiated mice. *Radiat. Environ. Biophys.* **2013**, *53*, 211–215. [CrossRef] [PubMed]
291. Xu, X.; Huang, H.; Tu, Y.; Sun, J.; Xiong, Y.; Ma, C.; Qin, S.; Hu, W.; Zhou, J. Celecoxib Alleviates Radiation-Induced Brain Injury in Rats by Maintaining the Integrity of Blood-Brain Barrier. *Dose Response* **2021**, *19*, 15593258211024392. [CrossRef]
292. Kang, K.B.; Wang, T.T.; Woon, C.T.; Cheah, E.S.; Moore, X.L.; Zhu, C.; Wong, M.C. Enhancement of glioblastoma radioresponse by a selective COX-2 inhibitor celecoxib: Inhibition of tumor angiogenesis with extensive tumor necrosis. *Int. J. Radiat. Oncol.* **2007**, *67*, 888–896. [CrossRef]
293. Arroyo-Hernández, M.; Maldonado, F.; Lozano-Ruiz, F.; Muñoz-Montaño, W.; Nuñez-Baez, M.; Arrieta, O. Radiation-induced lung injury: Current evidence. *BMC Pulm. Med.* **2021**, *21*, 9. [CrossRef]
294. Yan, T.-T.; Lin, G.-A.; Wang, M.-J.; Lamkowski, A.; Port, M.; Rump, A. Pharmacological treatment of inhalation injury after nuclear or radiological incidents: The Chinese and German approach. *Mil. Med. Res.* **2019**, *6*, 10. [CrossRef]
295. McLaughlin, M.F.; Donoviel, D.B.; Jones, J.A. Novel Indications for Commonly Used Medications as Radiation Protectants in Spaceflight. *Aerosp. Med. Hum. Perform.* **2017**, *88*, 665–676. [CrossRef]
296. Zhao, X.; Yang, H.; Jiang, G.; Ni, M.; Deng, Y.; Cai, J.; Li, Z.; Shen, F.; Tao, X. Simvastatin attenuates radiation-induced tissue damage in mice. *J. Radiat. Res.* **2013**, *55*, 257–264. [CrossRef]
297. Bajaj, M.S.; Ghode, S.S.; Kulkarni, R.S.; Limaye, L.S.; Kale, V.P. Simvastatin improves hematopoietic stem cell engraftment by preventing irradiation-induced marrow adipogenesis and radio-protecting the niche cells. *Haematologica* **2015**, *100*, e323–e327. [CrossRef] [PubMed]
298. Sun, X.; Yang, X.; Chen, J.; Ge, X.-L.; Qin, Q.; Zhu, H.; Zhang, C.; Xu, L. Simvastatin attenuates radiation-induced salivary gland dysfunction in mice. *Drug Des. Dev. Ther.* **2016**, *10*, 2271–2278. [CrossRef] [PubMed]
299. Parsamanesh, N.; Karami-Zarandi, M.; Banach, M.; Penson, P.E.; Sahebkar, A. Effects of statins on myocarditis: A review of underlying molecular mechanisms. *Prog. Cardiovasc. Dis.* **2021**, *67*, 53–64. [CrossRef]

300. Doi, H.; Matsumoto, S.; Odawara, S.; Shikata, T.; Kitajima, K.; Tanooka, M.; Takada, Y.; Tsujimura, T.; Kamikonya, N.; Hirota, S. Pravastatin reduces radiation-induced damage in normal tissues. *Exp. Ther. Med.* **2017**, *13*, 1765–1772. [CrossRef]
301. Amiri, F.T.; Hamzeh, M.; Naeimi, R.A.; Ghasemi, A.; Hosseinimehr, S.J. Radioprotective effect of atorvastatin against ionizing radiation-induced nephrotoxicity in mice. *Int. J. Radiat. Biol.* **2018**, *94*, 106–113. [CrossRef]
302. Pinter, M.; Kwanten, W.J.; Jain, R.K. Renin–Angiotensin System Inhibitors to Mitigate Cancer Treatment–Related Adverse Events. *Clin. Cancer Res.* **2018**, *24*, 3803–3812. [CrossRef]
303. Lu, L.; Sun, C.; Su, Q.; Wang, Y.; Li, J.; Guo, Z.; Chen, L.; Zhang, H. Radiation-induced lung injury: Latest molecular developments, therapeutic approaches, and clinical guidance. *Clin. Exp. Med.* **2019**, *19*, 417–426. [CrossRef]
304. Wang, J.; Zheng, H.; Sung, C.-C.; Hauer-Jensen, M. The synthetic somatostatin analogue, octreotide, ameliorates acute and delayed intestinal radiation injury. *Int. J. Radiat. Oncol.* **1999**, *45*, 1289–1296. [CrossRef]
305. Moulder, J.E.; Cohen, E.P.; Fish, B.L. Mitigation of experimental radiation nephropathy by renin-equivalent doses of angiotensin converting enzyme inhibitors. *Int. J. Radiat. Biol.* **2014**, *90*, 762–768. [CrossRef]
306. Medhora, M.; Gao, F.; Wu, Q.; Molthen, R.C.; Jacobs, E.R.; Moulder, J.E.; Fish, B.L. Model Development and Use of ACE Inhibitors for Preclinical Mitigation of Radiation-Induced Injury to Multiple Organs. *Radiat. Res.* **2014**, *182*, 545–555. [CrossRef]
307. Mungunsukh, O.; George, J.; McCart, E.A.; Snow, A.L.; Mattapallil, J.J.; Mog, S.R.; Panganiban, R.A.M.; Bolduc, D.L.; Rittase, W.B.; Bouten, R.M.; et al. Captopril reduces lung inflammation and accelerated senescence in response to thoracic radiation in mice. *J. Radiat. Res.* **2021**, *62*, 236–248. [CrossRef]
308. McCart, E.A.; Lee, Y.H.; Jha, J.; Mungunsukh, O.; Rittase, W.B.; Summers, T.A., Jr.; Muir, J.; Day, R.M. Delayed Captopril Administration Mitigates Hematopoietic Injury in a Murine Model of Total Body Irradiation. *Sci. Rep.* **2019**, *9*, 2198. [CrossRef] [PubMed]
309. Rodgers, K.E.; Espinoza, T.; Roda, N.; Meeks, C.J.; Hill, C.; Louie, S.G.; Dizerega, G.S. Accelerated hematopoietic recovery with angiotensin-(1–7) after total body radiation. *Int. J. Radiat. Biol.* **2012**, *88*, 466–476. [CrossRef]
310. Willey, J.S.; Bracey, D.N.; Gallagher, P.E.; Tallant, E.A.; Wiggins, W.F.; Callahan, M.F.; Smith, T.L.; Emory, C.L. Angiotensin-(1-7) Attenuates Skeletal Muscle Fibrosis and Stiffening in a Mouse Model of Extremity Sarcoma Radiation Therapy. *J. Bone Jt. Surg.* **2016**, *98*, 48–55. [CrossRef]
311. Alite, F.; Balasubramanian, N.; Adams, W.; Surucu, M.; Mescioglu, I.; Harkenrider, M.M. Decreased Risk of Radiation Pneumonitis With Coincident Concurrent Use of Angiotensin-converting Enzyme Inhibitors in Patients Receiving Lung Stereotactic Body Radiation Therapy. *Am. J. Clin. Oncol.* **2018**, *41*, 576–580. [CrossRef]
312. Cohen, E.P.; Irving, A.A.; Drobyski, W.R.; Klein, J.P.; Passweg, J.R.; Talano, J.-A.; Juckett, M.B.; Moulder, J.E. Captopril to Mitigate Chronic Renal Failure After Hematopoietic Stem Cell Transplantation: A Randomized Controlled Trial. *Int. J. Radiat. Oncol.* **2008**, *70*, 1546–1551. [CrossRef]
313. Cohen, E.P.; Bedi, M.; Irving, A.A.; Jacobs, E.; Tomic, R.; Klein, J.; Lawton, C.A.; Moulder, J.E. Mitigation of Late Renal and Pulmonary Injury After Hematopoietic Stem Cell Transplantation. *Int. J. Radiat. Oncol.* **2012**, *83*, 292–296. [CrossRef]
314. Sun, F.; Sun, H.; Zheng, X.; Yang, G.; Gong, N.; Zhou, H.; Wang, S.; Cheng, Z.; Ma, H. Angiotensin-converting Enzyme Inhibitors Decrease the Incidence of Radiation-induced Pneumonitis Among Lung Cancer Patients: A Systematic Review and Meta-analysis. *J. Cancer* **2018**, *9*, 2123–2131. [CrossRef]
315. Erpolat, O.P.; Demircan, N.V.; Sarıbas, G.S.; Kuzucu, P.; Senturk, E.; Elmas, C.; Borcek, A.; Kurt, G. A Comparison of Ramipril and Bevacizumab to Mitigate Radiation-Induced Brain Necrosis: An Experimental Study. *World Neurosurg.* **2020**, *144*, e210–e220. [CrossRef]
316. Xiong, J.; Gao, Y.; Li, X.; Li, K.; Li, Q.; Shen, J.; Han, Z.; Zhang, J. Losartan Treatment Could Improve the Outcome of TBI Mice. *Front. Neurol.* **2020**, *11*, 992. [CrossRef]
317. Qian, L.; Shen, J.; Chuai, Y.; Cai, J. Hydrogen as a New Class of Radioprotective Agent. *Int. J. Biol. Sci.* **2013**, *9*, 887–894. [CrossRef] [PubMed]
318. Tian, Y.; Zhang, Y.; Wang, Y.; Chen, Y.; Fan, W.; Zhou, J.; Qiao, J.; Wei, Y. Hydrogen, a Novel Therapeutic Molecule, Regulates Oxidative Stress, Inflammation, and Apoptosis. *Front. Physiol.* **2021**, *12*, 789507. [CrossRef] [PubMed]
319. Barancik, M.; Kura, B.; LeBaron, T.W.; Bolli, R.; Buday, J.; Slezak, J. Molecular and Cellular Mechanisms Associated with Effects of Molecular Hydrogen in Cardiovascular and Central Nervous Systems. *Antioxidants* **2020**, *9*, 1281. [CrossRef] [PubMed]
320. Zhao, M.; Liu, M.-D.; Pu, Y.-Y.; Wang, D.; Xie, Y.; Xue, G.-C.; Jiang, Y.; Yang, Q.-Q.; Sun, X.-J.; Cao, L. Hydrogen-rich water improves neurological functional recovery in experimental autoimmune encephalomyelitis mice. *J. Neuroimmunol.* **2016**, *294*, 6–13. [CrossRef]
321. Qiu, X.; Dong, K.; Guan, J.; He, J. Hydrogen attenuates radiation-induced intestinal damage by reducing oxidative stress and inflammatory response. *Int. Immunopharmacol.* **2020**, *84*, 106517. [CrossRef]
322. Chen, M.; Zhang, J.; Chen, Y.; Qiu, Y.; Luo, Z.; Zhao, S.; Du, L.; Tian, D. Hydrogen protects lung from hypoxia/re-oxygenation injury by reducing hydroxyl radical production and inhibiting inflammatory responses. *Sci. Rep.* **2018**, *8*, 8004. [CrossRef]
323. Shao, A.; Wu, H.; Hong, Y.; Tu, S.; Sun, X.; Wu, Q.; Zhao, Q.; Zhang, J.; Sheng, J. Hydrogen-Rich Saline Attenuated Subarachnoid Hemorrhage-Induced Early Brain Injury in Rats by Suppressing Inflammatory Response: Possible Involvement of NF-κB Pathway and NLRP3 Inflammasome. *Mol. Neurobiol.* **2015**, *53*, 3462–3476. [CrossRef]
324. Sim, M.; Kim, C.-S.; Shon, W.-J.; Lee, Y.-K.; Choi, E.Y.; Shin, D.-M. Hydrogen-rich water reduces inflammatory responses and prevents apoptosis of peripheral blood cells in healthy adults: A randomized, double-blind, controlled trial. *Sci. Rep.* **2020**, *10*, 12130. [CrossRef]

325. Hirano, S.-I.; Ichikawa, Y.; Sato, B.; Yamamoto, H.; Takefuji, Y.; Satoh, F. Molecular Hydrogen as a Potential Clinically Applicable Radioprotective Agent. *Int. J. Mol. Sci.* **2021**, *22*, 4566. [CrossRef]
326. Kang, K.-M.; Kang, Y.-N.; Choi, I.-B.; Gu, Y.; Kawamura, T.; Toyoda, Y.; Nakao, A. Effects of drinking hydrogen-rich water on the quality of life of patients treated with radiotherapy for liver tumors. *Med. Gas Res.* **2011**, *1*, 11. [CrossRef]
327. Takefuji, Y.; Hirano, S.-I.; Aoki, Y.; Li, X.-K.; Ichimaru, N.; Takahara, S. Protective effects of hydrogen gas inhalation on radiation-induced bone marrow damage in cancer patients: A retrospective observational study. *Med. Gas Res.* **2021**, *11*, 104–109. [CrossRef]
328. Li, H.; Yin, Y.; Liu, J.; Lu, B.; Wan, H.; Yang, L.; Wang, W.; Li, R. Hydrogen-rich water attenuates the radiotoxicity induced by tritium exposure in vitro and in vivo. *J. Radiat. Res.* **2020**, *62*, 34–45. [CrossRef]
329. Mortezaee, K.; Shabeeb, D.; Musa, A.E.; Najafi, M.; Farhood, B. Metformin as a Radiation Modifier; Implications to Normal Tissue Protection and Tumor Sensitization. *Curr. Clin. Pharmacol.* **2019**, *14*, 41–53. [CrossRef]
330. Adalsteinsson, J.A.; Muzumdar, S.; Waldman, R.; Wu, R.; Ratner, D.; Feng, H.; Ungar, J.; Silverberg, J.I.; Olafsdottir, G.H.; Kristjansson, A.K.; et al. Metformin is associated with decreased risk of basal cell carcinoma: A whole-population case-control study from Iceland. *J. Am. Acad. Dermatol.* **2021**, *85*, 56–61. [CrossRef]
331. Chukwunonso Obi, B.; Okoye, T.C.; Okpashi, V.E.; Igwe, C.N.; Alumanah, E.O. Comparative Study of the Antioxidant Effects of Metformin, Glibenclamide, and Repaglinide in Alloxan-Induced Diabetic Rats. *J. Diabetes Res.* **2016**, *2016*, 1635361. [CrossRef]
332. Farhood, B.; Aliasgharzadeh, A.; Amini, P.; Rezaeyan, A.; Tavassoli, A.; Motevaseli, E.; Shabeeb, D.; Musa, A.E.; Najafi, M. Mitigation of Radiation-Induced Lung Pneumonitis and Fibrosis Using Metformin and Melatonin: A Histopathological Study. *Medicina* **2019**, *55*, 417. [CrossRef]
333. Xu, G.; Wu, H.; Zhang, J.; Li, D.; Wang, Y.; Wang, Y.; Zhang, H.; Lu, L.; Li, C.; Huang, S.; et al. Metformin ameliorates ionizing irradiation-induced long-term hematopoietic stem cell injury in mice. *Free Radic. Biol. Med.* **2015**, *87*, 15–25. [CrossRef]
334. Karam, H.M.; Radwan, R.R. Metformin modulates cardiac endothelial dysfunction, oxidative stress and inflammation in irradiated rats: A new perspective of an antidiabetic drug. *Clin. Exp. Pharmacol. Physiol.* **2019**, *46*, 1124–1132. [CrossRef]
335. Miller, R.C.; Murley, J.S.; Grdina, D.J. Metformin exhibits radiation countermeasures efficacy when used alone or in combination with sulfhydryl containing drugs. *Radiat. Res.* **2014**, *181*, 464–470. [CrossRef]
336. Tajabadi, E.; Javadi, A.; Azar, N.A.; Najafi, M.; Shirazi, A.; Shabeeb, D.; Musa, A.E. Radioprotective effect of a combination of melatonin and metformin on mice spermatogenesis: A histological study. *Int. J. Reprod. Biomed.* **2020**, *18*, 1073–1080. [CrossRef]
337. Najafi, M.; Cheki, M.; Hassanzadeh, G.; Amini, P.; Shabeeb, D.; Musa, A.E. Protection from Radiation-induced Damage in Rat's Ileum and Colon by Combined Regimens of Melatonin and Metformin: A Histopathological Study. *Antiinflamm. Antiallergy Agents Med. Chem.* **2020**, *19*, 180–189. [CrossRef]
338. Chen, L.; Liao, F.; Jiang, Z.; Zhang, C.; Wang, Z.; Luo, P.; Jiang, Q.; Wu, J.; Wang, Q.; Luo, M.; et al. Metformin mitigates gastrointestinal radiotoxicity and radiosensitises P53 mutation colorectal tumours via optimising autophagy. *Br. J. Pharmacol.* **2020**, *177*, 3991–4006. [CrossRef]
339. Sun, X.; Dong, M.; Gao, Y.; Wang, Y.; Du, L.; Liu, Y.; Wang, Q.; Ji, K.; He, N.; Wang, J.; et al. Metformin increases the radiosensitivity of non-small cell lung cancer cells by destabilizing NRF2. *Biochem. Pharmacol.* **2022**, *199*, 114981. [CrossRef]
340. Jang, W.I.; Kim, M.-S.; Lim, J.S.; Yoo, H.J.; Seo, Y.S.; Han, C.J.; Park, S.C.; Kay, C.S.; Kim, M.; Jang, H.S.; et al. Survival Advantage Associated with Metformin Usage in Hepatocellular Carcinoma Patients Receiving Radiotherapy: A Propensity Score Matching Analysis. *Anticancer Res.* **2015**, *35*, 5047–5054.
341. Ahmed, Z.S.O.; Golovoy, M.; Abdullah, Y.; Ahmed, R.S.I.; Dou, Q.P. Repurposing of Metformin for Cancer Therapy: Updated Patent and Literature Review. *Recent Patents Anticancer Drug Discov.* **2021**, *16*, 161–186. [CrossRef]
342. Kazzi, Z.N.; Heyl, A.; Ruprecht, J. Calcium and zinc DTPA administration for internal contamination with plutonium-238 and americium-241. *Curr. Pharm. Biotechnol.* **2012**, *13*, 1957–1963. [CrossRef]
343. Yamamoto, L.G. Risks and Management of Radiation Exposure. *Pediatr. Emerg. Care* **2013**, *29*, 1016–1026. [CrossRef]
344. Volf, V. Chelation Therapy of Incorporated Plutonium-238 and Americium-241: Comparison of LICAM(C), DTPA and DFOA in Rats, Hamsters and Mice. *Int. J. Radiat. Biol. Relat. Stud. Phys. Chem. Med.* **1985**, *49*, 449–462. [CrossRef]
345. Ruggiero, C.E.; Matonic, J.H.; Reilly, S.D.; Neu, M.P. Dissolution of Plutonium(IV) Hydroxide by Desferrioxamine Siderophores and Simple Organic Chelators. *Inorg. Chem.* **2002**, *41*, 3593–3595. [CrossRef] [PubMed]
346. Nurchi, V.M.; Andersen, O. Clinical Therapy of Patients Contaminated with Polonium or Plutonium. *Curr. Med. Chem.* **2021**, *28*, 7238–7246. [CrossRef]
347. Joksić, A.; Katz, S.A. Chelation therapy for treatment of systemic intoxication with uranium: A review. *J. Environ. Sci. Health Part A Tox. Hazard Subst. Environ. Eng.* **2015**, *50*, 1479–1488. [CrossRef] [PubMed]
348. Ohmachi, Y.; Imamura, T.; Ikeda, M.; Shishikura, E.; Kim, E.; Kurihara, O.; Sakai, K. Sodium bicarbonate protects uranium-induced acute nephrotoxicity through uranium-decorporation by urinary alkalinization in rats. *J. Toxicol. Pathol.* **2015**, *28*, 65–71. [CrossRef] [PubMed]
349. Yue, Y.-C.; Li, M.-H.; Wang, H.-B.; Zhang, B.-L.; He, W. The toxicological mechanisms and detoxification of depleted uranium exposure. *Environ. Health Prev. Med.* **2018**, *23*, 18. [CrossRef] [PubMed]
350. Destombes, C.; Laroche, P.; Cazoulat, A.; Gérasimo, P. Réduction de La Fixation Rénale de l'uranium Par l'acétazolamide: Importance de l'élimination Urinaire Du Bicarbonate. In *Annales Pharmaceutiques Françaises*; Elsevier: Amsterdam, The Netherlands, 1999; Volume 57, pp. 397–400.

351. Simons, C.S.; Meyers, M.C.; Cobau, C.D. Accidental Overdosage with Radiophosphorus: Therapy by Induced Phosphate Diuresis. *Am. J. Med. Sci.* **1967**, *54*, 451–463. [CrossRef]
352. Durakovic, A. Internal Contamination with Medically Significant Radionuclides. *Arh. Hig. Rada I Toksikol.* **1986**, *37*, 67–99. [CrossRef]
353. Spencer, H.; Feldstein, A.; Samachson, J.; Feldstkin, A. Effect of Combined Use of Calcium Gluconate and Ammonium Chloride on Removal of Sr85 in Man Two Weeks after Exposure. *Exp. Biol. Med.* **1961**, *108*, 308–312. [CrossRef]
354. Danetskaia, E.V.; Lavrent'ev, L.N.; Zapol'skaia, N.A.; Teplykh, L.A. Evaluation of the protective effect of Prussian blue, sodium alginate and calcium phosphate according to tumor development after single and chronic exposure to strontium 90 and cesium 137 mixture. *Vopr. Onkol.* **1977**, *23*, 57–61.
355. Volf, V. First Aid After Internal Radiostrontium Contamination Using Oral Barium Sulphate. *Phys. Med. Biol.* **1961**, *6*, 287–294. [CrossRef]
356. Jäggi, M.; Eikenberg, J. Separation of 90Sr from radioactive waste matrices—Microwave versus fusion decomposition. *Appl. Radiat. Isot.* **2009**, *67*, 765–769. [CrossRef]
357. Chen, W.; Li, H.; Wang, K.; Bian, H.; Wang, Y.; Cui, F.; Liu, Y.; Chen, Q. Medical Treatment and Dose Estimation of a Person Exposed to Tritium. *Dose Response* **2019**, *17*, 1559325819880670. [CrossRef]
358. Tanaka, I.; Ishihara, H.; Yakumaru, H.; Tanaka, M.; Yokochi, K.; Tajima, K.; Akashi, M. Comparison of Absorbents and Drugs for Internal Decorporation of Radiocesium: Advances of Polyvinyl Alcohol Hydrogel Microsphere Preparations Containing Magnetite and Prussian Blue. *Biol. Pharm. Bull.* **2016**, *39*, 353–360. [CrossRef]
359. Aaseth, J.; Nurchi, V.M.; Andersen, O. Medical Therapy of Patients Contaminated with Radioactive Cesium or Iodine. *Biomolecules* **2019**, *9*, 856. [CrossRef]
360. Carniato, F.; Gatti, G.; Vittoni, C.; Katsev, A.M.; Guidotti, M.; Evangelisti, C.; Bisio, C. More Efficient Prussian Blue Nanoparticles for an Improved Caesium Decontamination from Aqueous Solutions and Biological Fluids. *Molecules* **2020**, *25*, 3447. [CrossRef]
361. Rump, A.; Ostheim, P.; Eder, S.; Hermann, C.; Abend, M.; Port, M. Preparing for a "dirty bomb" attack: The optimum mix of medical countermeasure resources. *Mil. Med. Res.* **2021**, *8*, 3. [CrossRef]
362. Goldfrank, L.R.; Flomenbaum, N.E.; Lewin, N.A.; Howland, M.A.; Hoffman, R.S.; Nelson, L.S. Cobalt. In *Goldfrank's Toxicologic Emergencies*; Appleton and Lange: Norwalk, CT, USA, 1990; pp. 654–655.
363. Malinen, L.K.; Koivula, R.; Harjula, R. Removal of radiocobalt from EDTA-complexes using oxidation and selective ion exchange. *Water Sci. Technol.* **2009**, *60*, 1097–1101. [CrossRef]
364. Fisher, D.R.; Dunavant, B.G. Internal Decontamination of Radiocobalt. *Health Phys.* **1978**, *35*, 279–285. [CrossRef]
365. World Health Organization (WHO) Iodine Thyroid Blocking. *Guidelines for Use in Planning for and Responding to Radiological and Nuclear Emergencies 2017*; World Health Organization: Geneva, Switzerland, 2017.
366. Rump, A.; Eder, S.; Hermann, C.; Lamkowski, A.; Kinoshita, M.; Yamamoto, T.; Abend, M.; Shinomiya, N.; Port, M. A comparison of thyroidal protection by iodine and perchlorate against radioiodine exposure in Caucasians and Japanese. *Arch. Toxicol.* **2021**, *95*, 2335–2350. [CrossRef]
367. Peterson, J.; MacDonell, M.; Haroun, L.; Monette, F.; Hildebrand, R.; Taboas, A. Radiological and Chemical Fact Sheets to Support Health Risk Analyses for Contaminated Areas. Available online: /paper/Radiological-and-Chemical-Fact-Sheets-to-Support-Peterson-MacDonell/f86865b29ed10353dfae5db4aaa7f64fe75ee05e (accessed on 18 December 2020).
368. Brodsky, A.; Wald, N. Experiences with Early Emergency Response and Rules of Thumb. In *Public Protection from Nuclear, Chemical, and Biological Terrorism*; Brodsky, A., Johnson, R.H., Jr., Goans, R.E., Eds.; CRC Press: Madison, WI, USA, 2004; pp. 335–371.
369. Laurent, B.; Florence, M. Treatment of radiological contamination: A review. *J. Radiol. Prot.* **2021**, *41*, S427–S437. [CrossRef]
370. Guilmette, R.A.; Muggenburg, B.A. Effectiveness of Continuously Infused Dtpa Therapy in Reducing the Radiation Dose From Inhaled 244Cm2O3 Aerosols. *Health Phys.* **1992**, *62*, 311–318. [CrossRef]
371. Garla, V.V.; Salim, S.; Kovvuru, K.R.; Subauste, A. Hungry bone syndrome secondary to prostate cancer successfully treated with radium therapy. *BMJ Case Rep.* **2018**, *2018*, bcr-2018. [CrossRef]
372. Van Der Borght, O.; Van Puymbroeck, S.; Colard, J. Intestinal Absorption and Body Retention of 226-Radium and 47-Calcium in Mice: Effect of Sodium Alginate, Measured in Vivo with a Ge(Li) Detector. *Health Phys.* **1971**, *21*, 181–196. [CrossRef] [PubMed]
373. Alabdula'Aly, A.I.; Maghrawy, H.B. Radon emanation from radium specific adsorbents. *Water Res.* **2010**, *44*, 177–184. [CrossRef] [PubMed]
374. Hickman, D.P. Management of persons contaminated with radionuclides: NCRP report no. 161 (Volume 1). *Radiat. Prot. Dosim.* **2010**, *141*, 215–216. [CrossRef]
375. IAEA. *Medical Management of Persons Internally Contaminated with Radionuclides in a Nuclear or Radiological Emergency*; Emergency Preparedness and Response; International Atomic Energy Agency: Vienna, Austria, 2018.
376. HÜbner, K.F.; Watson, E.E. Management of Persons Accidentally Contaminated with Radionuclides: NCRP Report No. 65. Washington, D.C., National Council on Radiation Protection and Mesasurements, 1980, 205 Pp, $8.00. *J. Nucl. Med.* **1981**, *22*, 397.
377. Managing Internal Radiation Contamination-Radiation Emergency Medical Management. Available online: https://remm.hhs.gov/int_contamination.htm (accessed on 5 May 2022).
378. Ammerich, M.; Giraud, J.M.; Helfer, N.; Menetrier, F.; Schoulz, D.; Blanc, J.; Vilain, D.; Boll, H.; Bourguignon, M.; Chappe, P.; et al. *Medical Intervention in Case of a Nuclear or Radiological Event-National Guide*; Release V36; International Atomic Energy Agency: Vienna, Austria, 2008; p. 170.

379. Goans, R.E.; Holloway, E.C.; Berger, M.E.; Ricks, R.C. Early dose assessment in criticality accidents. *Health Phys.* **2001**, *81*, 446–449. [CrossRef]
380. Gowns, R.E.; Holloway, E.C.; Berger, M.E.; Ricks, R.C. Early Dose Assessment Following Severe Radiation Accidents. *Health Phys.* **1997**, *72*, 513–518. [CrossRef]
381. Yoon, C.I.; Kim, D.; Ahn, S.G.; Bae, S.J.; Cha, C.; Park, S.; Park, S.; Kim, S.I.; Lee, H.S.; Park, J.Y.; et al. Radiotherapy-Induced High Neutrophil-to-Lymphocyte Ratio is a Negative Prognostic Factor in Patients with Breast Cancer. *Cancers* **2020**, *12*, 1896. [CrossRef]
382. Konchalovskiĭ, M.V.; Baranov, A.E.; Solov'Ev, V.I. [Neutrophil and lymphocyte dose curves in relatively uniform human whole body irradiation (based on data of the accident at the Chernobyl AES)]. *Med. Radiol. (Mosk.)* **1991**, *36*, 29–33.
383. Wong, K.F.; Siu, L.L.P.; Ainsbury, E.; Moquet, J. Cytogenetic biodosimetry: What it is and how we do it. *Hong Kong Med. J.* **2013**, *19*, 168–173.
384. Ainsbury, E.; Badie, C.; Barnard, S.; Manning, G.; Moquet, J.; Abend, M.; Antunes, A.C.; Barrios, L.; Bassinet, C.; Beinke, C.; et al. Integration of new biological and physical retrospective dosimetry methods into EU emergency response plans–joint RENEB and EURADOS inter-laboratory comparisons. *Int. J. Radiat. Biol.* **2016**, *93*, 99–109. [CrossRef]
385. Shirley, B.C.; Knoll, J.H.M.; Moquet, J.; Ainsbury, E.; Pham, N.-D.; Norton, F.; Wilkins, R.C.; Rogan, P.K. Estimating partial-body ionizing radiation exposure by automated cytogenetic biodosimetry. *Int. J. Radiat. Biol.* **2020**, *96*, 1492–1503. [CrossRef]
386. Yadav, U.; Bhat, N.N.; Shirsath, K.B.; Mungse, U.S.; Sapra, B. Multifaceted applications of pre-mature chromosome condensation in radiation biodosimetry. *Int. J. Radiat. Biol.* **2020**, *96*, 1274–1280. [CrossRef]
387. Pujol-Canadell, M.; Perrier, J.R.; Cunha, L.; Shuryak, I.; Harken, A.; Garty, G.; Brenner, D.J. Cytogenetically-based biodosimetry after high doses of radiation. *PLoS ONE* **2020**, *15*, e0228350. [CrossRef]
388. Nakamura, A.J.; Suzuki, M.; Redon, C.E.; Kuwahara, Y.; Yamashiro, H.; Abe, Y.; Takahashi, S.; Fukuda, T.; Isogai, E.; Bonner, W.M.; et al. The Causal Relationship between DNA Damage Induction in Bovine Lymphocytes and the Fukushima Nuclear Power Plant Accident. *Radiat. Res.* **2017**, *187*, 630–636. [CrossRef]
389. Voisin, P. Standards in biological dosimetry: A requirement to perform an appropriate dose assessment. *Mutat. Res. Genet Toxicol. Environ. Mutagen.* **2015**, *793*, 115–122. [CrossRef]
390. Homer, M.J.; Raulli, R.; DiCarlo-Cohen, A.L.; Esker, J.; Hrdina, C.; Maidment, B.W.; Moyer, B.; Rios, C.; Macchiarini, F.; Prasanna, P.G.; et al. United states department of health and human services biodosimetry and radiological/nuclear medical countermeasure programs. *Radiat. Prot. Dosim.* **2016**, *171*, 85–98. [CrossRef]
391. Flegal, F.N.; DeVantier, Y.; Marro, L.; Wilkins, R. Validation of QuickScan Dicentric Chromosome Analysis for High Throughput Radiation Biological Dosimetry. *Health Phys.* **2012**, *102*, 143–153. [CrossRef]
392. Royba, E.; Repin, M.; Pampou, S.; Karan, C.; Brenner, D.J.; Garty, G. RABiT-II-DCA: A Fully-automated Dicentric Chromosome Assay in Multiwell Plates. *Radiat. Res.* **2019**, *192*, 311–323. [CrossRef]
393. Hülber, T.; Kocsis, Z.S.; Kis, E.; Sáfrány, G.; Pesznyák, C. A scanning and image processing system with integrated design for automated micronucleus scoring. *Int. J. Radiat. Biol.* **2020**, *96*, 628–641. [CrossRef]
394. Wang, G.; Ren, X.; Yan, H.; Gui, Y.; Guo, Z.; Song, J.; Zhang, P. Neuroprotective Effects of Umbilical Cord-Derived Mesenchymal Stem Cells on Radiation-Induced Brain Injury in Mice. *Ann. Clin. Lab. Sci.* **2020**, *50*, 57–64.
395. Firsanov, D.; Solovjeva, L.; Lyublinskaya, O.; Zenin, V.; Kudryavtsev, I.; Serebryakova, M.; Svetlova, M. Rapid Detection of γ-H2AX by Flow Cytometry in Cultured Mammalian Cells. *Methods Mol. Biol.* **2017**, *1644*, 129–138. [CrossRef] [PubMed]
396. Ivashkevich, A.; Redon, C.E.; Nakamura, A.J.; Martin, R.F.; Martin, O.A. Use of the γ-H2AX assay to monitor DNA damage and repair in translational cancer research. *Cancer Lett.* **2012**, *327*, 123–133. [CrossRef] [PubMed]
397. Etzol, J.B.; Valente, M.; Altmeyer, S.; Bettencourt, C.; Bouvet, S.; Cosler, G.; Desangles, F.; Drouet, M.; Entine, F.; Hérodin, F.; et al. DosiKit, a New Portable Immunoassay for Fast External Irradiation Biodosimetry. *Radiat. Res.* **2017**, *190*, 176–185. [CrossRef] [PubMed]
398. Entine, F.; Etzol, J.B.; Bettencourt, C.; Dondey, M.; Michel, X.; Gagna, G.; Gellie, G.; Corre, Y.; Ugolin, N.; Chevillard, S.; et al. Deployment of the DosiKit System Under Operational Conditions: Experience From a French Defense National Nuclear Exercise. *Health Phys.* **2018**, *115*, 185–191. [CrossRef]
399. Jacobs, A.R.; Guyon, T.; Headley, V.; Nair, M.; Ricketts, W.; Gray, G.; Wong, J.Y.C.; Chao, N.; Terbrueggen, R. Role of a high throughput biodosimetry test in treatment prioritization after a nuclear incident. *Int. J. Radiat. Biol.* **2018**, *96*, 57–66. [CrossRef]
400. Hu, S.; Blakely, W.F.; Cucinotta, F.A. HEMODOSE: A Biodosimetry Tool Based on Multi-Type Blood Cell Counts. *Health Phys.* **2015**, *109*, 54–68. [CrossRef]
401. Port, M.; Pieper, B.; Dörr, H.D.; Hübsch, A.; Majewski, M.; Abend, M. Correlation of Radiation Dose Estimates by DIC with the METREPOL Hematological Classes of Disease Severity. *Radiat. Res.* **2018**, *189*, 449–455. [CrossRef]
402. Haupt, J.; Ostheim, P.; Port, M.; Abend, M. Using dicentric dose estimates and early radiation-induced blood cell count changes of real case histories for validation of the hemodose biodosimetry tool. *Radiat. Prot. Dosim.* **2020**, *189*, 428–435. [CrossRef]
403. Szewczak, K.; Jednorog, S.; Krajewski, P. Individual dose monitoring of the nuclear medicine departments staff controlled by Central Laboratory for Radiological Protection. *Nucl. Med. Rev.* **2013**, *16*, 62–65. [CrossRef]
404. Naito, W.; Uesaka, M.; Kurosawa, T.; Kuroda, Y. Measuring and assessing individual external doses during the rehabilitation phase in Iitate village after the Fukushima Daiichi nuclear power plant accident. *J. Radiol. Prot.* **2017**, *37*, 606–622. [CrossRef]

405. Raskob, W.; Schneider, T.; Gering, F.; Charron, S.; Zheleznyak, M.; Andronopoulos, S.; Heriard-Dubreuil, G.; Camps, J. PREPARE: Innovative integrated tools and platforms for radiological emergency preparedness and post-accident response in Europe. *Radiat. Prot. Dosim.* **2014**, *164*, 170–174. [CrossRef] [PubMed]
406. Strand, P.; Sundell-Bergman, S.; Brown, J.; Dowdall, M. On the divergences in assessment of environmental impacts from ionising radiation following the Fukushima accident. *J. Environ. Radioact.* **2017**, *169–170*, 159–173. [CrossRef] [PubMed]
407. Yoshimura, K.; Saegusa, J.; Sanada, Y. Initial decrease in the ambient dose equivalent rate after the Fukushima accident and its difference from Chernobyl. *Sci. Rep.* **2020**, *10*, 3859. [CrossRef] [PubMed]
408. Toohey, R.E. Scientific issues in radiation dose reconstruction. *Health Phys.* **2008**, *95*, 26–35. [CrossRef] [PubMed]
409. Ivanova, O.M.; Kovgan, L.M.; Masiuk, S.V. Methodology of Reconstruction of Individualized Exposure Doses for Persons Residing at Radioactively Contaminated Territories of Ukraine. *Probl. Radiac. Med. Radiobiol.* **2018**, *23*, 164–187. [CrossRef]
410. Trompier, F.; Burbidge, C.; Bassinet, C.; Baumann, M.; Bortolin, E.; De Angelis, C.; Eakins, J.; DELLA Monaca, S.; Fattibene, P.; Quattrini, M.C.; et al. Overview of physical dosimetry methods for triage application integrated in the new European network RENEB. *Int. J. Radiat. Biol.* **2016**, *93*, 65–74. [CrossRef]
411. Swartz, H.M.; Flood, A.B.; Williams, B.B.; Dong, R.; Swarts, S.G.; He, X.; Grinberg, O.; Sidabras, J.; Demidenko, E.; Gui, J.; et al. Electron Paramagnetic Resonance Dosimetry for a Large-Scale Radiation Incident. *Health Phys.* **2012**, *103*, 255–267. [CrossRef]
412. Yukihara, E.G.; McKeever, S.W.S. *Optically Stimulated Luminescence: Fundamentals and Applications*; John Wiley & Sons: Hoboken, NJ, USA, 2011; ISBN 978-0-470-97721-7.
413. Kron, T.; Lonski, P.; Yukihara, E.G. THERMOLUMINESCENCE DOSIMETRY (TLD) IN MEDICINE: FIVE 'W'S AND ONE HOW. *Radiat. Prot. Dosim.* **2020**, *192*, 139–151. [CrossRef]
414. Duragkar, A.; Muley, A.; Pawar, N.; Chopra, V.; Dhoble, N.; Chimankar, O.; Dhoble, S. Versatility of thermoluminescence materials and radiation dosimetry—A review. *Luminescence* **2019**, *34*, 656–665. [CrossRef]
415. Roesch, W.C. *US-Japan Joint Reassessment of Atomic Bomb Radiation Dosimetry in Hiroshima and Nagasaki: Final Report*; Radiation Effects Research Foundation: Hiroshima, Japan, 1987.
416. Haskell, E.H.; Bailiff, I.K.; Kenner, G.H.; Kaipa, P.L.; Wrenn, M.E. Thermoluminescence Measurements of Gamma-ray Doses Attributable to Fallout from the Nevada Test Site Using Building Bricks As Natural Dosimeters. *Health Phys.* **1994**, *66*, 380–391. [CrossRef]
417. Göksu, H.Y.; Bailiff, I.K. Luminescence dosimetry using building materials and personal objects. *Radiat. Prot. Dosim.* **2006**, *119*, 413–420. [CrossRef]
418. Bailiff, I.K.; Stepanenko, V.; Göksu, H.Y.; Bøtter-Jensen, L.; Brodski, L.; Chumak, V.; Correcher, V.; Delgado, A.; Golikov, V.; Jungner, H.; et al. Comparison of retrospective luminescence dosimetry with computational modeling in two highly contaminated settlements downwind of the chernobyl NPP. *Health Phys.* **2004**, *86*, 25–41. [CrossRef]
419. Bougrov, N.G.; Baturin, V.A.; Goeksu, H.Y.; Degteva, M.O.; Jacob, P. Investigations of thermoluminescence dosimetry in the Techa river flood plain: Analysis of the new results. *Radiat. Prot. Dosim.* **2002**, *101*, 225–228. [CrossRef]
420. Miyazaki, M.; Ohtsuru, A.; Ishikawa, T. An overview of internal dose estimation using whole-body counters in fukushima prefecture. *Fukushima J. Med. Sci.* **2014**, *60*, 95–100. [CrossRef]
421. Weiss, W. Chernobyl thyroid cancer: 30 years of follow-up overview. *Radiat. Prot. Dosim.* **2018**, *182*, 58–61. [CrossRef]
422. Eder, S.; Hermann, C.; Lamkowski, A.; Kinoshita, M.; Yamamoto, T.; Abend, M.; Shinomiya, N.; Port, M.; Rump, A. A comparison of thyroidal protection by stable iodine or perchlorate in the case of acute or prolonged radioiodine exposure. *Arch. Toxicol.* **2020**, *94*, 3231–3247. [CrossRef]
423. Yoder, R.C.; Dauer, L.T.; Balter, S.; Boice, J.D.; Grogan, H.A.; Mumma, M.T.; Passmore, C.N.; Rothenberg, L.N.; Vetter, R.J. Dosimetry for the study of medical radiation workers with a focus on the mean absorbed dose to the lung, brain and other organs. *Int. J. Radiat. Biol.* **2019**, *98*, 619–630. [CrossRef]
424. Anigstein, R.; Erdman, M.C.; Ansari, A. Use of Transportable Radiation Detection Instruments to Assess Internal Contamination from Intakes of Radionuclides Part I: Field Tests and Monte Carlo Simulations. *Health Phys.* **2016**, *110*, 612–622. [CrossRef]
425. Ha, W.-H.; Kwon, T.-E.; Kim, J.; Jin, Y.W. Rapid monitoring of internal contamination using a mobile radiobioassay laboratory following radiation emergencies. *Radiat. Prot. Dosim.* **2018**, *182*, 104–106. [CrossRef]
426. Tatsuzaki, H. [Assessment, diagnosis and treatment of internal or body surface contamination]. *Nihon rinsho. Jpn. J. Clin. Med.* **2012**, *70*, 446–450.
427. Ekendahl, D.; Rubovič, P.; Žlebčík, P.; Hupka, I.; Huml, O.; Bečková, V.; Malá, H. Neutron dose assessment using samples of human blood and hair. *Radiat. Prot. Dosim.* **2019**, *186*, 202–205. [CrossRef]
428. Sevan'Kaev, A.V.; Lloyd, D.C.; Edwards, A.A.; Khvostunov, I.; Mikhailova, G.F.; Golub, E.V.; Shepel, N.N.; Nadejina, N.M.; Galstian, I.A.; Nugis, V.Y.; et al. A cytogenetic follow-up of some highly irradiated victims of the Chernobyl accident. *Radiat. Prot. Dosim.* **2004**, *113*, 152–161. [CrossRef]

antioxidants

MDPI

*Article*

# Radioprotective and Radiomitigative Effects of Melatonin in Tissues with Different Proliferative Activity

**Serazhutdin A. Abdullaev *, Sergey I. Glukhov and Azhub I. Gaziev**

Institute of Theoretical and Experimental Biophysics, Russian Academy of Sciences, Pushchino, 142290 Moscow Region, Russia; s.glukhov@iteb.ru (S.I.G.); gaziev@iteb.ru (A.I.G.)
* Correspondence: abdullaev@iteb.ru; Tel.: +7-(4967)739364

**Abstract:** We used various markers to analyze damage to mouse tissues (spleen and cerebral cortex) which have different proliferative activity and sensitivity to ionizing radiation (IR). We also assessed the degree of modulation of damages that occurs when melatonin is administered to mice prior to and after their X-ray irradiation. The data from this study showed that lesions in nuclear DNA (nDNA) were repaired more actively in the spleen than in the cerebral cortex of mice irradiated and treated with melatonin (N-acetyl-5-methoxytryptamine). Mitochondrial biogenesis involving mitochondrial DNA (mtDNA) synthesis was activated in both tissues of irradiated mice. A significant proportion of the newly synthesized mtDNA molecules were mutant copies that increase oxidative stress. Melatonin reduced the number of mutant mtDNA copies and the level of $H_2O_2$ in both tissues of the irradiated mice. Melatonin promoted the restoration of ATP levels in the tissues of irradiated mice. In the mouse tissues after exposure to X-ray, the level of malondialdehyde (MDA) increased and melatonin was able to reduce it. The MDA concentration was higher in the cerebral cortex tissue than that in the spleen tissue of the mouse. In mouse tissues following irradiation, the glutathione (GSH) level was low. The spleen GSH content was more than twice as low as that in the cerebral cortex. Melatonin helped restore the GSH levels in the mouse tissues. Although the spleen and cerebral cortex tissues of mice differ in the baseline values of the analyzed markers, the radioprotective and radiomitigative potential of melatonin was observed in both tissues.

**Keywords:** radiation; melatonin; nDNA-repair; mtDNA-mutations; oxidation stress; protection; mitigation; $H_2O_2$; ATP; MDA; GSH

**Citation:** Abdullaev, S.A.; Glukhov, S.I.; Gaziev, A.I. Radioprotective and Radiomitigative Effects of Melatonin in Tissues with Different Proliferative Activity. *Antioxidants* **2021**, *10*, 1885. https://doi.org/10.3390/antiox10121885

Academic Editors: Elena Obrador Pla and Alegria Montoro

Received: 8 October 2021
Accepted: 24 November 2021
Published: 25 November 2021



## 1. Introduction

Ionizing radiation is often used in the treatment of various tumor diseases. However, healthy tissues may also be damaged by radiation, including the induction of short-term and long-term effects and the appearance of secondary tumors [1]. Medical staff who use IR sources for diagnosis and therapy and professionals involved in the production of nuclear technologies can be exposed to radiation. A significant number of people can be exposed to IR during radiological or nuclear technology incidents or accidents. The impact of cosmic irradiation on astronauts is also a critical factor for space flights outside the Earth's orbit [2]. Therefore, the search for and study of radioprotectors, radiomitigators, and means of treating radiation injuries remain rather topical problems. The development of such drugs has been the focus of attention of radiobiologists and radiologists for decades [3]. Antioxidant compounds account for a significant proportion of preclinical studies of radioprotectors and radiomitigators, since radiation exposure to cells is associated with the induction of prolonged intracellular oxidative stress [4]. Melatonin (N-acetyl-5-methoxytryptamine) was found to be extremely effective among the numerous compounds that passed preclinical tests as radioprotectors as it reduced the in vitro and in vivo effects of IR [5,6]. Currently, melatonin (MEL) is widely used clinically as an adaptogenic drug that normalizes circadian rhythms and is increasingly finding clinical use as an adjuvant in the radiotherapy of tumors [7–9]. According to the analysis of data from a large number of studies, the provisions

on the possibility to use melatonin to protect astronauts from hard cosmic irradiation have been substantiated [10]. In this case, it happens that the main risks are mostly associated with the possible consequences of cosmic irradiation's effects on the central nervous system and spleen, which lead to potential neurological disorders, degenerative effects, and decrease in the immune system and affect many aspects of the crew's health [11,12]. As is known, that brain and spleen tissues exhibit different radiosensitivity [3]. Many years ago (in 1906) J. Bergonié and L. Tribondeau proposed a "rule" stating that ionizing radiation is more harmful to cells with a faster turnover. Therefore, there is a relationship between the radiosensitivity and proliferative activity of various tissues [13]. According to this rule, the brain can be considered a radioresistant tissue, and the spleen can be considered a radiosensitive tissue. Today, it is a generally accepted understanding [3]. We can agree with this only based on data on structural disorders and cell death in these tissues, since functional physiological disorders in the brain are observed even under the action of small doses of radiation [14]. It should also be noted that a significant amount of research is devoted to the study of the modulation of radiation damage to the brain under the action of various compounds, including MEL, while similar studies devoted to the modulation of spleen damage are rather limited.

This study is devoted to the comparative assessment on a number of markers, damages in the cerebral cortex and spleen tissues of mice after irradiation of their whole bodies with X-rays, and the modulation of these damages when MEL was administered before and after irradiation. Nuclear DNA (nDNA) and mitochondrial DNA (mtDNA) damage and repair, change in the number of mtDNA copies, $H_2O_2$, ATP, reduced glutathione (GSH) as a marker of the antioxidant system, and malondialdehyde (MDA) as a marker of oxidative stress were used as markers.

## 2. Materials and Methods

### *2.1. Chemicals*

All chemicals were of the "high purity" category from the Alamed company, Moscow, Russia and from the Sigma-Aldrich company, St. Louis, MO, USA. All solutions were prepared in deionized water obtained from the Milli-Q system (Millipore, Bedford, MA, USA). Melatonin (MEL) was obtained from Sigma-Aldrich, St. Louis, MO, USA.

### *2.2. Animals and Their Irradiation*

Male mice C57BL/6 at the age of 2 months weighing 20–22 g were obtained from Stolbovaya nursery (Settlement Stolbovaya; Moscow, Russia). The mice were used in experiments after 7 days of acclimatization in the animal room. All experiments with animals were performed in accordance with the European Convention for the protection of vertebrate animals used for experimental and other scientific purposes, Directive 2010/63/EU. The protocol was approved by the Committee on Biomedical Ethics of the Institute of Theoretical and Experimental Biophysics of the Russian Academy of Sciences/the Physiology Section of the Russian Committee on Bioethics (Protocol N° 20 dated 9 February 2021). The animals were fed a special diet for mice and rats and had free access to clean drinking water. The animals were irradiated at the Research Equipment Sharing Center, a group of radiation sources of the Institute of Cell Biophysics of the Russian Academy of Sciences, on a RUT-250-15-1 X-ray machine (280 kVp, 20 mA) with AL and Cu filters of 1 mm with a dose rate of 1 Gy/min. The animals were irradiated in plastic containers at a dose of 5 Gy. The irradiation of mice was carried out for 5 min.

### *2.3. Administration of Melatonin to Mice and Collection of Tissues for Analysis*

A freshly prepared MEL solution was used for administration. To do this, 250 mg of MEL was dissolved in boiled drinking water (at room temperature) containing 0.1% dimethyl sulfoxide (DMSO). The final concentrations of this solution were 2.5% MEL and 0.1% DMSO. Mice were orally treated with 100 μL of this solution, corresponding to doses of MEL of 125 mg/kg and DMSO of 0.1 mg/kg of a mouse's body weight [15]. A 0.1%

DMSO solution was also prepared separately for administration to control groups of mice. The solutions were administered to groups of mice 30 min before irradiation or 20 min after irradiation. Each individual analysis group consisted of 5–6 mice. The preparation was additionally injected into drinking water (0.3 mg/mL) within 24 and 48 h for mice that were treated with MEL after irradiation, given the short clearance of MEL [15]. To isolate the cerebral cortex and spleen tissues, mice were sacrificed by decapitation 15 min and 24 and 48 h after irradiation. Groups of unirradiated and irradiated mice not treated with MEL were used as controls. The spleen and brain tissue (cortex) were separated with a scalpel on ice immediately after decapitation, then were frozen and stored at −80 °C until analysis.

### *2.4. DNA Isolation and Purification*

Tissues were homogenized in a glass homogenizer and DNA was isolated using the QIAGEN Genomic-tip Kit and Genomic DNA Buffer (QIAGEN, Hilden, Germany). The amount of DNA in all cases was determined by its reaction with the PicoGreen reagent according to the manufacturer's protocol (Molecular Probes Inc., Eugene, OR, USA) and fluorescence was registered on an NanoQuant Infinite M200 instrument (Tecan Group Ltd., Grödig/Salzburg, Austria). DNA samples for mitochondrial genome PCR-analysis were incubated within 20 min at 25 °C in TE buffer with XhoI restriction endonuclease (New England Biolabs, Ipswich, MA, USA). XhoI endonuclease initiates a break at the site of the CTCGAG hexamer of the supercoiled mtDNA outside the amplified region and leads to relaxation of the mtDNA, making the selected region available for PCR [16].

### *2.5. Analysis of Damage and Repair of Mitochondrial DNA and Nuclear DNA*

To determine the damage and repair of nDNA and mtDNA, we used the long amplicon quantitative polymerase chain reaction (LA-QPCR) method [17] taking into account our previous experience [18]. In these analyses, we used (2U/μL) KAPA Long Range Hot Start Kit (KAPA Biosystems, Humboldt County, CA, USA). LA-QPCR was used to amplify a 8.7 kb region of nDNA and 10.9 kb of mtDNA. For amplification of a long fragment of mtDNA (10.9 kb), the standard thermocycler program included initial denaturation at 94 °C for 5 min, with 18 cycles of 94 °C for 30 s and 68 °C for 12.5 min, and with a final extension at 72 °C for 10 min. To amplify a long fragment of nDNA (8.7 kb), the thermocycler profile included initial denaturation at 94 °C for 5 min, and 28 cycles of 94 °C for 30 s and 68 °C for 12 min, with a final extension at 72 °C for 10 min. Preliminary assays were carried out to ensure the linearity of PCR amplification with respect to the number of cycles and DNA concentration. Since the amplification of a small region would be relatively independent of oxidative DNA damage (low probability), a small DNA fragment for nDNA (110 bp) and for mtDNA (117 bp) was also amplified for normalization of the data obtained with the large fragments, as described previously [18,19]. PCR analyses were performed in triplicate for each DNA sample. All of the amplified products were resolved and visualized using agarose gel electrophoresis and quantitated with an Image Quant (Molecular Dynamics, Waukesha, WI, USA) or VarsaDoc (Bio-Rad, Hercules, CA, USA). The data were plotted as histograms with relative amplification, such as the *y*-axis, which was calculated by comparing the values of exposed samples with the control. All primers are presented in Table 1.

**Table 1.** Primers and probes used in the current study.

| Locus | Primer, Probes | Accession Number | 5′→3′ Sequence | Size |
|---|---|---|---|---|
| mtDNA | for<br>rev | NC_005089.1 | Primers for LA-QPCR<br>GCCAGCCTGACCCATAGCCATAATAT<br>GAGAGATTTTATGGGTGTAATGCGG | 10.9 kb |
| nDNA | for<br>rev | NC_000073.7<br>X14061.1 | TTGAGACTGTGATTGGCAATGCCT<br>CCTTTAATGCCCATCCCGGACT | 8.7 kb |
| mtDNA | for<br>rev | NC_005089.1 | CCCAGCTACTACCATCATTCAAGT<br>GATGGTTTGGGAGATTGGTTGATGT | 117 bp |
| nDNA | for<br>rev | NC_000071.7<br>NM_007393.5 | CTGCCTGACGGCCAGG<br>GGAAAAGAGCCTCAGGGCAT | 110 bp |
| ND4 | for<br>rev<br>probe | NC_005089.1 | Primers for quantitative analysis of mtDNA/nDNA<br>ATTATTATTACCCGATGAGGGAACC<br>ATTAAGATGAGGGCAATTAGCAGT<br>FAM-ACGCCTAAACGCAGGGATTTATTTCCTA-BHQ1 | 115 bp |
| GAPDH | for<br>rev<br>probe | NC_000072.7<br>NM_001289726.1 | GTGAGGGAGATGCTCAGTGT<br>CTGGCATTGCTCTCAATGAC<br>ROX-TAAGAAACCCTGGACCACCCACCCC-BHQ2 | 214 bp |
| ND3 | for<br>rev | NC_005089.1 | Primers for mtDNA mutant copies<br>AGCTCTCCATTTATTGATGAGG<br>GAGGTTGAAGAAGGTAGATGGC | 534 bp |

### *2.6. Quantitative Analysis of Mitochondrial DNA Copies Relative to the Nuclear DNA*

Quantitative analysis of mtDNA was carried out by real-time PCR with TaqMan oligonucleotides on a Prism 7500 thermal cycler (Applied Biosystems, Foster City, CA, USA) [20]. The changes in the relative quantity of mtDNA with respect to nDNA were determined as a ratio between the number of copies of the mitochondrial *ND4* gene and that of the *GAPDH* gene of nDNA in the same test tube. The $2^{-\Delta\Delta CT}$ method was used for analysis. PCR tests were carried out in triplicate for each DNA sample. The following PCR program was used: 5 min at 95 °C followed by 40 cycles (95 °C for 30 s, annealing and elongation at 60 °C for 1 min). The results are presented as a percentage of data compared to unirradiated mice (taken as 100%). The PCR primers used in this study are given in Table 1.

### *2.7. Surveyor Nuclease Assay of mtDNA Mutant Copies*

To evaluate the relative level of mutant copies of mtDNA isolated from brain tissue, we used the Surveyor® Mutation Detection Kit (Transgenomic, Omaha, NE, USA), as described in [21,22]. To estimate mutations in mtDNA, a region including the *ND3* gene (534 bp) was chosen for amplification. The PCR primers employed in this study are given in Table 1. PCR was carried out by a programmed thermocycler Thermal Cycler 2720 (Applied Biosystems, Foster City, CA, USA). PCR was performed in a 25 µL volume containing 1.0 ng of total DNA, 75 mM of Tris-HCl, a pH of 8.8, 20 mM of $(NH_4)_2SO_4$, 2.5 mM of $MgCl_2$, 200 µM of each dNTP, 250 nM of each primer, 0.01% tween-20, and 1.0 unit of total mixture of Taq and Pfu polymerases (Thermo Scientific, Pittsburgh, PA, USA). PCR was initiated by a "hot start" after initial denaturation for 4 min at 94 °C. The amplification was carried out in 40 cycles under the following conditions: 30 s at 94 °C, 30 s at 62 °C, and 1 min at 72 °C; the final extension step of 4 min was at 72 °C. After the PCR was completed, all amplification products were diluted to an equal concentration. To obtain heteroduplex DNA, equal volumes (7 µL) of PCR products of mtDNA amplification from control and exposed mice were mixed. The mixtures were heated at 95 °C for 10 min and cooled slowly to 40 °C for 70 min at a rate of 0.3 °C/min. Then, 1/10 volume of 0.15 M $MgCl_2$ solution, 1 µL of Surveyor Enhancer S, and 1 µL of Surveyor Nuclease S were added to the heteroduplex mixture. The mixture was incubated at 42 °C for 60 min. The reaction was stopped by adding 1/10 volume of stop solution. Nuclease digestion products were

analyzed by electrophoresis in a 2.0% agarose gel stained with ethidium bromide. PCR tests of heteroduplexes were carried out in triplicate for each DNA sample. The fluorescence intensity of DNA bands in the gels was registered by the AlphaImager Mini System (Alpha Innotech, Santa Clara, CA, USA). The ratio of the cleavage products' fluorescence to the total intensity of fluorescence of DNA bands in the gel (% of Surveyor Nuclease cleaved DNA) was calculated using the ImageJ software package (Wayne Rasband, Kensington, MD, USA).

### *2.8. Determination of Hydrogen Peroxide Level*

A Fluorimetric Hydrogen Peroxide Assay Kit 165 (Sigma-Aldrich Co., St. Louis, MO, USA) was used for the quantitative measurement of hydrogen peroxide ($H_2O_2$) in mice tissues. This kit uses peroxidase substrate that generates a red fluorescent product that can be analyzed in 96-well black transparent bottom microplates. All analyses were performed in accordance with the recommendations of the manufacturer. The amount of $H_2O_2$ was calculated on the basis of a standard curve obtained using a concentration range of an $H_2O_2$ solution obtained by diluting a 30% $H_2O_2$ solution with ultrapure water. Each test sample was run in triplicate. Data were obtained from 6 mice in each group. The amount of $H_2O_2$ was expressed in nmol per mg of protein using a standard curve. Protein was assessed in these and other analyses by the method of Lowry et al. [23] using bovine serum albumin as a standard.

### *2.9. ATP Analysis*

The ATP content was determined following the recommendations indicated in [24]. ATP was extracted from tissue homogenates after the removal of proteins with TE buffer saturated with phenol. ATP level was measured using a luciferin–luciferase kit with a Glo-Max 96 Microplate Luminometer (Promega, E6521, Madison, WI, USA). ATP concentration was assessed using a standard curve in nmol per mg of protein. Data were normalized to total protein, and tissue ATP levels were expressed in μmol per 100 mg of protein.

### *2.10. Determination of Lipid Peroxidation*

The lipid peroxidation level was judged by changes in malondialdehyde (MDA) content after reaction with thiobarbituric acid (TBA) by the method of Buget and Aoust [25]. For this purpose, the cerebral cortex and spleen tissues of mice were homogenized in lysis buffer (50 mM Tris-Cl, 1% NP-40, 0.2% sodium deoxycholate, 0.1% SDS, 150 mM NaCl, and 1 mM EDTA). Then, one volume of tissue lysate was mixed with two volumes of TBA reagent (15% TCA, 0.375% TBA, and 0.25 N HCl), followed by incubation at 90 °C for 30 min. After cooling, the reaction mixture was centrifuged at 10,000 rpm for 15 min. The supernatant absorbance was measured at 533 nm with respect to the blank. The amount of lipid peroxidation was calculated from the MDA level in nmol per milligram of protein (nmol/mg of protein).

### *2.11. Determination of Glutathione Level (GSH)*

Tissues were homogenized in lysis buffer (50 mM Tris-Cl, 1% NP-40, 0.2% sodium deoxycholate, 0.1% SDS, 150 mM NaCl, and 1 mM EDTA) as indicated in the determination of lipid oxidation [25]. A total of 1.8 mL of 0.05 M EDTA and 3 mL of a precipitator (containing 1.67 g of $HPO_3$, 0.2 g of disodium EDTA salt, and 30 g of NaCl per liter of water) were added to 0.2 mL of tissue homogenate. After thorough mixing, the solution was kept for 5–7 min and then centrifuged. This step promotes the separation of GSH (in the supernatant) from the rest of the proteins and other cellular elements (in the sediment). Then, two volumes of 0.3 M $Na_2HPO_4$ solution and 0.5 volumes of 4 mM DTNB (5,5′-dithiobis-2-nitrobenzoic acid) were added to one volume of the supernatant [26]. Absorbance was determined at 412 nm against a mixture of solutions without biomaterial additives (blank). GSH was expressed in nmol per mg of protein using a standard curve.

### *2.12. Statistical Analysis*

All numerical results are expressed as the mean ± SEM of 5–6 independent experiments and $p < 0.05$ was considered statistically significant. The statistical analyses were performed using GraphPad Prism 8.0 software (San Diego, CA, USA).

## 3. Results

### *3.1. Damage and Repair of Nuclear DNA and Mitochondrial DNA following Irradiation*

**1.** As established in a number of studies, exogenous melatonin is a powerful antioxidant and has *in vitro* and *in vivo* radioprotective and radiomitigator effects [5,6]. Melatonin also exhibits a wide range of antioxidant defense reactions at various cellular levels. It helps to reduce oxidative stress caused by active forms of oxygen and nitrogen (RONS) and acts as an absorber of free radicals [27,28]. Therefore, it is of interest to elucidate changes in the most important markers of radiation damage in tissues with different radiosensitivity and proliferative activity in animals when they are administered with melatonin. In our study on mice, the spleen and cerebral cortex were taken as such tissues. In this study, mice were irradiated on a RUT-250-15-1 X-ray machine (280 kVp, 20 mA) with AL and Cu filters of 1 mm with a dose rate of 1 Gy/min. As is known, the most important marker of radiation exposure to living organisms is DNA damage. To determine nDNA and mtDNA damage, we used the method of quantitative PCR with a long amplicon (LA-QPCR) [17]. The presence of damage such as modified bases, single-strand and double-strand breaks, or DNA–protein crosslinking can block the activity of KAPA Biosystems' DNA polymerase. Thus, this method allowed us to assess the overall level of DNA damage.

**2.** The amplification products of long sections of nDNA and mtDNA from the tissues of unirradiated mice were taken as 100% control. It can be seen that the level of synthesized products of nDNA and mtDNA LA-QPCR from the mice's spleens and cerebral cortexes 15 min after irradiation was significantly lower than that of the unirradiated mice (Figure 1). Such a reduction in LA-QPCR products indicates that these amplifiable areas of nDNA and mtDNA contained damages capable of blocking KAPA Long Range Rapid PCR DNA polymerase (KAPA Biosystems, Wilmington, MA, USA). The preservation of low levels of amplification of nDNA and mtDNA regions indicates the presence of non-repaired damages in them. However, there was an increase in LA-QPCR products by 24 and 48 h post-radiation time, which indicates the functioning of DNA damage repair processes. According to the results obtained, nDNA and mtDNA from the tissues of mice treated with MEL before IR-radiation and after irradiation had significantly less damages capable of blocking KAPA Long Range DNA polymerase. As can be expected, this shows that MEL contributes to the DNA damage reduction (Figure 1). nDNA and mtDNA from the tissues of mice treated with MEL before irradiation and after irradiation had significantly less damages capable of blocking KAPA Long Range DNA polymerase. As can be expected, this also shows that MEL contributes to the DNA damage reduction. The results obtained show that the nDNA repair occurs more actively in the spleen and cerebral cortex tissues of mice treated with MEL after irradiation. When comparing the LA-QPCR amplification data of nDNA from two tissues of mice irradiated and treated with MEL, it seems that the nDNA repair in the spleen tissue for the indicated periods of post-radiation time was more active than in the cerebral cortex (Figure 1).

**3.** According to the experiment results, we can also conclude that mtDNA in the spleen and the cerebral cortex was actively restored, especially in mice that were treated with MEL after irradiation (Figure 1). However, if the increase in the synthesis of the LA-QPCR product of nDNA during the post-irradiation period was due to the repair of nDNA damages that inhibited KAPA Long Range DNA polymerase, this is unlikely to be the reason for the sharp increase in the synthesis of LA-QPCR products of mtDNA from the same tissues of mice. It is known that only base excision repair (BER) effectively functions in mammalian mitochondria [29]. Other pathway of repairing mutagenic mtDNA damage do not function in mammalian mitochondria. Moreover, double-strand breaks (DSBs) of mtDNA in mammalian cells are not repaired [30,31], and damaged mtDNA can

undergo degradation [32]. In this experiment, we most likely registered the activation of mitochondrial biogenesis with the mtDNA synthesis (Figure 1). To test this assumption, we decided to continue experiments to elucidate the effect of MEL on the quantitative content of mtDNA relative to nDNA in the spleen and cerebral cortex tissues of mice exposed to radiation.

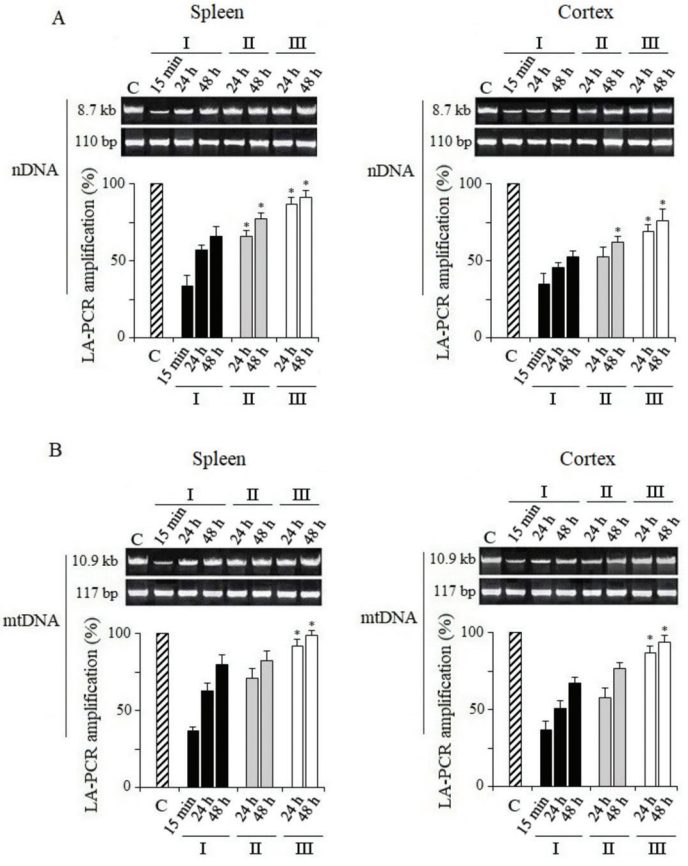


**Figure 1.** Analysis of damage and repair of nuclear DNA and recovery of mitochondrial DNA. Long fragments of nDNA (8.7 kb) and mtDNA (10.9 kb) were measured. These data were normalized by the measured levels of the short fragment of nDNA (110 bp) and mtDNA (117 bp), obtained using the same DNA sample. (**A**) Quantitative analysis of the LA-QPCR amplicons of nDNA extracted from spleen and cerebral cortex. (**B**) Quantitative analysis of the LA-QPCR amplicons of mtDNA extracted from spleen and cerebral cortex. Data are presented in % to control (C). Here and in other figures: the dose of X-ray irradiation of mice was 5 Gy and MEL was administered to mice before and after irradiation as a single dose of 125 mg/kg. Electropherogram samples of synthesized amplicons are presented above the histograms. The numbers (15 min, 24 h, 48 h) above and below indicate the time after irradiation. I—mice without MEL administration; II—MEL administration before irradiation; III—MEL administration after irradiation. The data are presented as mean ± SEM of 5–6 independent experiments. Statistical significance was set at * $p < 0.05$.

### *3.2. Effect of Melatonin on Mitochondrial Biogenesis in Tissues of X-Irradiated Mice*

A change in the number of mtDNA copies or the ratio of mtDNA/nDNA is the most important criterion for assessing mitochondrial biogenesis in tissues or cells [30,31]. The

results of the analyses obtained by the real-time PCR method show that the number of mtDNA copies increased in the spleen and cerebral cortex tissues of mice 24 and 48 h after their irradiation with a dose of 5 Gy in comparison with the data of the control (non-irradiated) animals group (Figure 2). As judged from the number of mtDNA copies, the enhancement of mtDNA synthesis was more pronounced in the spleen tissue than in the cerebral cortex of the irradiated mice. It should also be noted that the content of mtDNA in the tissues of mice, for a 15-min time after irradiation, remained at the level of the data from the control non-irradiated mice. These results indicate that mtDNA synthesis and, accordingly, mitochondrial biogenesis were activated much later; we registered their increase 24 and 48 h after irradiation. At the same time, we can see that when MEL was administered, the synthesis of mtDNA molecules occurred less actively than in the data obtained in irradiated mice without the administration of MEL. This gives the impression that MEL partially suppresses IR-induced mtDNA synthesis in the tissues of the spleen and cerebral cortex. In fact, most likely, this is the result of a decrease in the level of RONS generated by dysfunctional mitochondria under the influence of MEL. At the same time, the inhibition effect of IR-induced mtDNA synthesis upon administration of MEL to animals after irradiation was more pronounced in comparison with the data of the group of mice treated with MEL before irradiation. Based on the data obtained, it can be assumed that upon initiation of replicative synthesis involving a damaged mtDNA template and with the participation of DNA polymerase γ and DNA polymerase θ in mitochondria [32,33], the appearance of new copies of mtDNA with mutations and deletions in the tissues of mice after irradiation with IR can be expected.

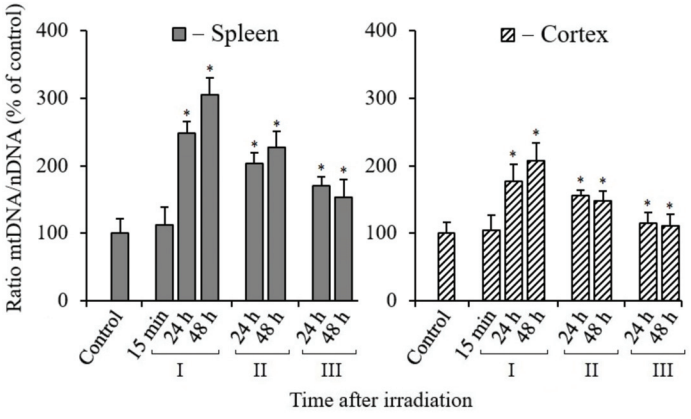


**Figure 2.** Ratio of mtDNA/nDNA in the tissues of the spleen and cerebral cortex of mice after their irradiation. The *y*-axis shows the percentage (%) of the change in mtDNA to nDNA ratio relative to control. The numbers (15 min, 24 h, 48 h) on *X*-axis indicate the time after irradiation. I—mice without MEL administration; II—MEL administration before irradiation; III—MEL administration after irradiation. The data are presented as mean ± SEM of 5–6 independent experiments. Statistical significance was set at * $p < 0.05$.

### 3.3. *Analysis of Mitochondrial DNA Mutant Copies*

As noted above, with the exception of BER, other DNA repair pathways are not involved in repairing mtDNA damage in mammalian cells [26]. Therefore, the observed increase in the number of mtDNA copies in the tissues of irradiated mice (Figure 2) suggested that it was associated with increased mtDNA mutagenesis. Our subsequent analyses confirmed this assumption. Electropherograms of the Surveyor nuclease digestion products of mtDNA PCR amplicon heteroduplexes and their quantitative analysis are shown in Figure 3. The quantitative analysis of the cleavage products of heteroduplexes showed that the level of mtDNA mutant copies significantly increased in the spleen and

cerebral cortex tissues of mice within 24–48 h after irradiation (Figure 3B). The number of mutant copies in the spleen tissue increased to 30% by 48 h post-radiation time, and it also increased to 20% in the cerebral cortex tissue relative to the control. On the other hand, the data from the analysis of the mtDNA mutant copies number in the tissues of mice treated with MEL before and after irradiation were significantly lower than those from mice that were not treated with MEL. It should also be noted that a significant decrease in the mtDNA mutant copies number was recorded, as can be seen, in the cerebral cortex tissue when MEL was administered into mice after irradiation in comparison with data from the spleens of groups of irradiated mice that were treated with MEL.

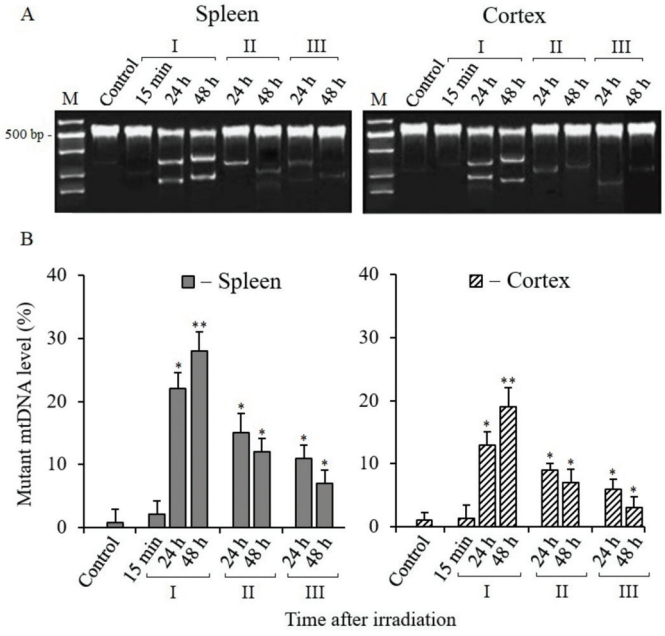


**Figure 3.** Detection of mtDNA mutant copies of spleen and cerebral cortex tissues in mice 15 min, 24, and 48 h after X-ray irradiation. (**A**) Electrophoresis of cleavage products obtained by Surveyor nuclease digestion of heteroduplexes of mtDNA PCR amplicons from spleen and cerebral cortex tissues. (**B**) Percentage of Surveyor nuclease cleaved heteroduplexes of PCR amplicons of mtDNA (ND3 gene, 534 bp). I—mice without MEL administration; II—MEL administration before irradiation; III—MEL administration after irradiation. The data are presented as mean ± SEM of 5–6 independent experiments. Statistical significance was set at * $p < 0.05$, ** $p < 0.01$.

### *3.4. Changes in $H_2O_2$ Content in Tissues of X-Irradiated Mice*

As is known, mitochondria and a number of extramitochondrial oxidases generate various reactive oxygen and nitrogen species (RONS). However, not all RONS can diffuse through the membranes of mitochondria or other organelles and reach the cell nucleus, since most of them migrate only over short distances. $H_2O_2$ molecules are the most stable and capable of migrating over long distances (1 μm or more) [34,35]. Therefore, we decided to determine changes in oxidative stress in the spleen and cerebral cortex tissues of irradiated mice by the level of hydrogen peroxide. The analysis results are shown in Figure 4. The data show that $H_2O_2$ production increased more sharply in the spleen tissue of mice during 24–48 h of the post-radiation period. At the same time, with the introduction of MEL, the level of $H_2O_2$ in the spleen significantly decreased. In the tissue of the cerebral cortex, the tendency for changes in the content of $H_2O_2$ is the same as in the spleen, but less pronounced. Here (Figure 4) it can be seen that, after the irradiation of mice, the $H_2O_2$

level increased immediately after 15 min and this level remained for 24 and 48 h. At the same time, we observed a decrease in the $H_2O_2$ level after only 48 h in the cerebral cortex tissue of mice treated with MEL after irradiation.

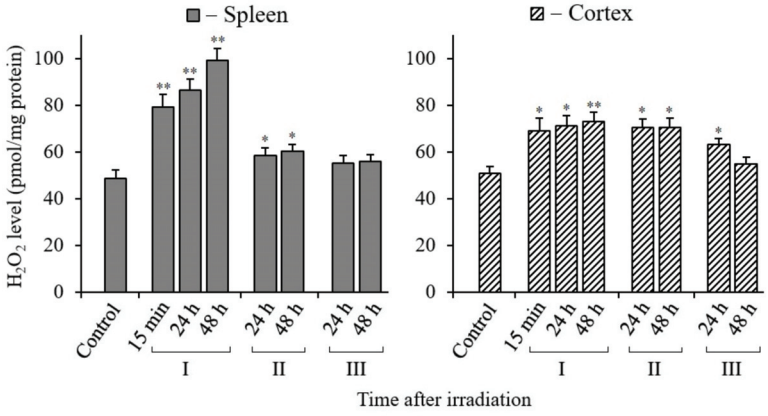


**Figure 4.** Changes in the $H_2O_2$ content in spleen and cerebral cortex tissues of mice 15 min, 24, and 48 h after their exposure to X-rays. I—mice groups without MEL administration; II—MEL administration before irradiation; III—MEL administration after irradiation. The data are presented as mean ± SEM of 5–6 independent experiments. Statistical significance was set at * $p < 0.05$; ** $p < 0.01$.

### *3.5. Changes in ATP Content in Tissues of X-Irradiated Mice*

Maximum energy support is required for DNA repair and cell recovery. This can ensure the synthesis of ATP in functionally active mitochondria [36]. Therefore, it is very important to evaluate the change in the ATP content in the tissues of irradiated mice and the effect of MEL on the correction of its synthesis level. The results of our analyses show that the content of ATP in the spleen tissue was approximately two times less per unit mass of tissue compared to its content in the cerebral cortex tissue of control and irradiated mice (Figure 5). The observed difference was obviously due to the unequal content of mitochondria in these tissues. Nevertheless, the post-radiation changes in the ATP content in both tissues were relatively similar. It can be seen that the ATP content in both tissues sharply decreased in the initial period after irradiation, especially after 15 min. However, a tendency towards restoration of the ATP content in both tissues of the irradiated mice was observed after 24 and 48 h of post-radiation time. Moreover, the restoration of the ATP content in the tissues of the mice that were treated with MEL before and after irradiation was more active. This is best seen in the results obtained on the cerebral cortex tissues. Thus, we can conclude that MEL contributes to the maintenance of mitochondrial functions and the synthesis of the required level of ATP in the spleen and cerebral cortex tissues of irradiated mice.

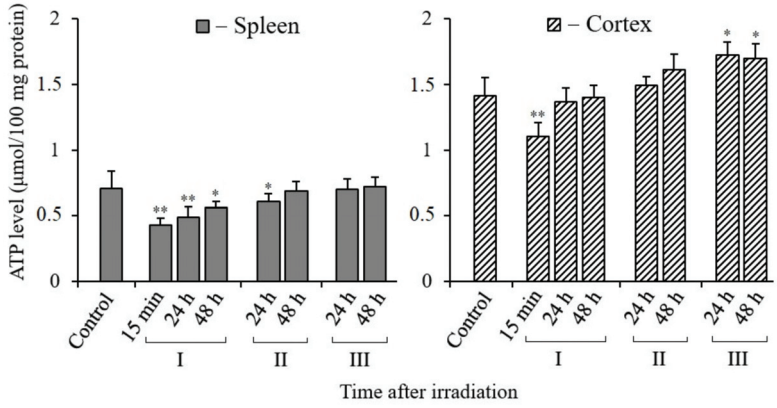


**Figure 5.** Changes in the ATP content in spleen and cerebral cortex tissues of mice 15 min, 24, and 48 h after their irradiation. I—mice groups without MEL administration; II—MEL administration before irradiation; III—MEL administration after irradiation. The data are presented as mean ± SEM of 5–6 independent experiments. Statistical significance was set at * $p < 0.05$; ** $p < 0.01$.

### *3.6. Changes in MDA Content in Tissues of X-Irradiated Mice*

In radiation biology, an increase in the level of the lipid oxidation product malondialdehyde (MDA) in cells or tissues is considered as one of the most important markers of radiation damage. This marker indicates the occurrence of oxidative stress.

The results of our analyses gave quite different results of the content of MDA in the tissues of the spleen and cerebral cortex of mice exposed to X-rays (Figure 6).

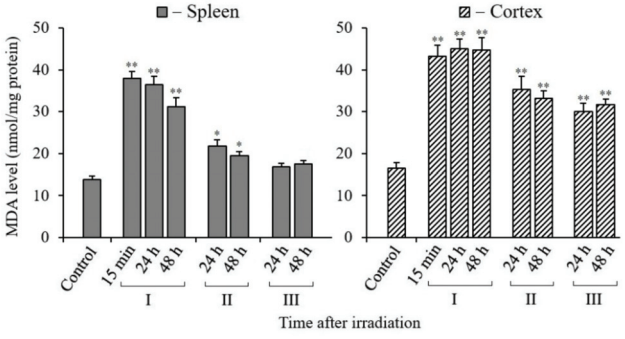


**Figure 6.** Changes in the MDA content in spleen and cerebral cortex tissues of mice 15 min, 24, and 48 h after their exposure to X-rays. I—mice without MEL administration; II—MEL administration before irradiation; III—MEL administration after irradiation. The data are presented as mean ± SEM of 5–6 independent experiments. Statistical significance was set at * $p < 0.05$, ** $p < 0.01$.

Administration of MEL to mice before and after irradiation promoted a significant decrease in MDA in the spleen tissue. Similar results were obtained by MDA analyses in the cerebral cortex tissue of the same mice. However, the results of the brain tissue analyses were quantitatively different from those of the spleen tissue analyses. First of all, the MDA level in the cerebral cortex tissue was higher in comparison with the data of the spleen analyses. Moreover, the administration of MEL to mice before and after irradiation in the brain tissue retained an increased content of MDA, although it was significantly lower than that in the analysis data from the tissues of mice that were not treated with MEL. It can also be noted that the data obtained from MDA analyses both in the spleen tissue and in the

brain tissue of irradiated mice that were treated with MEL after irradiation were lower than the results obtained in the tissues of mice that were treated with MEL before irradiation.

### *3.7. Changes in Glutathione Content in Tissues of X-Irradiated Mice*

Reduced glutathione (GSH) is an essential non-enzymatic antioxidant that plays a prominent part in determining cell radiosensitivity. A decrease in the content of GSH in tissues or in the blood is considered as a marker of a decrease in the level of antioxidants in the body as a result of radiation exposure. The results of our analyses show that there was a sharp decrease in glutathione in the spleen and cerebral cortex tissues of mice after irradiation of the whole body with X-rays (Figure 7). These data also show that the content of GSH in the spleen was more than two times less than that in the cerebral cortex tissue. At the same time, reduced levels of GSH were retained in both tissues during the post-radiation time (up to 48 h). We observed an active increase in the content of reduced GSH in the tissues of these mice only after oral administration of MEL to mice before or after irradiation. At the same time, the results show that the restoration of GSH level in the cerebral cortex tissue occurred more actively in mice treated with MEL after irradiation.

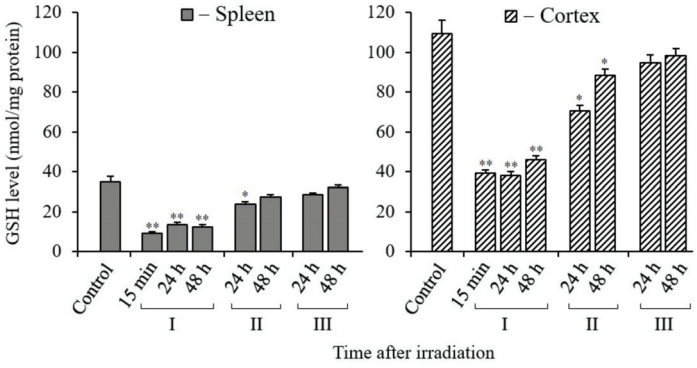


**Figure 7.** Changes in the GSH in spleen and cerebral cortex tissues of mice 15 min, 24, and 48 h after their irradiation. I—mice without MEL administration; II—MEL administration before irradiation; III—MEL administration after irradiation. The data are presented as mean ± SEM of 5–6 independent experiments. Statistical significance was set at * $p < 0.05$, ** $p < 0.01$.

## 4. Discussion

In a normally functioning cell, DNA is constantly subject to oxidation and "spontaneous" hydrolytic degradation [37]. RONS cause a lot of damage in DNA, including base modifications, the destruction of deoxyribose, formation of apurinic/apyrimidinic sites and single-strand breaks (SSBs) [38]. In addition, double-strand breaks (DSBs) can also form in DNA as a result of a close match of SSBs or in the process of repair of closely spaced damaged bases on complementary strands of a double helix [39]. When IR is exposed to cells, DNA damage is induced much more (depending on the dose of IR). Moreover, there is a sharp increase in the production of RONS in irradiated cells, which can last from several minutes to tens of days, depending on the radiation dose [40]. Therefore, supporting the activity of DNA repair systems and the level of antioxidants play a crucial role in the fate of the irradiated organism. It is obvious that in the regulation of these processes, along with other protective systems of the cell, melatonin can play a primary role [41].

The review article by Galano et al. [41] analyzes the data of many studies on the role of MEL in protecting DNA from oxidative damage. It is shown here that MEL provides cleaning of free radicals and other forms of RONS from cells and activates enzymes involved in the BER. MEL activates the expression of genes encoding DNA repair enzymes and antioxidant enzymes, but suppresses the activity of pro oxidant enzymes. Thus, it is clear that MEL provides protection of the nuclear genome in different directions [41].

It has recently been reported that MEL not only protects DNA, to a large extent, from mutagenic damage, but also from the induction of DNA DSBs, which are lethal events for the cell if they are not repaired. Thus, in patients undergoing computed tomography (CT), DNA DSBs induction was recorded in blood lymphocytes. Moreover, in the group who received a single oral dose of 100 mg of MEL 5–10 min before and 30 min after CT examination, these DNA damages was not recorded [42]. These results are confirmed in another study. The authors observed DNA DSBs in lymphocytes when exposed to IR at doses of 10 mGy and 100 mGy. Administration of 100 mg of MEL to patients before irradiation caused a decrease in DNA DSBs levels [43]. In another study, when incubating human blood lymphocytes in an environment with the addition of radioactive iodine $I^{131}$ for 2 h in the presence of MEL, the number of induced DNA DSBs decreased by 40% relative to the control (lymphocytes incubated with $I^{131}$ without MEL) [44].

As described above, for a comparative assessment of damage and repair of nDNA and mtDNA in different tissues, we used the method of quantitative PCR with a long amplicon (LA-QPCR) [17]. The presence of damage such as modified bases, SSBs, DSBs, or DNA–protein crosslinking can block the activity of KAPA Biosystems DNA polymerase and, accordingly, reduce the PCR synthesis product. The results of our analyses indicate that the repair of nDNA total damage capable of blocking KAPA Long Range DNA polymerase in the spleen and cerebral cortex of irradiated mice proceeds rather slowly within 48 h after total body irradiation, and occurs more slowly in the brain cells (Figure 1). It is known that in postmitotic cells, different DNA repair pathways are less active than in dividing cells [45]. Recently, it was shown that after irradiation of the rat head with X-rays, DSBs nDNA in the cortical neurons persisted for a long post-radiation time [46]. We also recently reported that DNA damage repair in irradiated rats is slower in cortical tissue than in hippocampal tissue [18].

The spleen is an organ of the reticuloendothelial system with proliferative activity [47]. The nDNA damage repair in the spleen tissue is more active, although it could not be completed by 48 h without the administration of MEL.

It is possible that the observed slow DNA repair within 24–48 h in the tissues of irradiated mice without the introduction of MEL was due to the occurrence of additional damage in the same DNA. These additional damages may occur as a result of the action of RONS, generated in the dysfunctional mitochondria of the same cells. With the introduction of MEL, obviously, there is a significant cleaning of these RONS. Exposure to ionizing radiation can not only cause acute radiation syndrome, but also increase the risk of developing long-term consequences. IR stimulates RONS production by mitochondria for a few hours to a few days after irradiation. This prolonged RONS generation in mitochondria can induce additional damage to nDNA and mtDNA cells after radiation exposure [40]. It has long been established that the cause of increased oxidative stress in the cells of irradiated mammals is mitochondrial dysfunction [48]. At the same time, the antioxidant activity in the tissues and blood of irradiated rodents sharply decreases [49,50].

We found increased mtDNA synthesis in mouse tissues after irradiation, clearly associated with mitochondrial biogenesis. This well-known phenomenon is the induction of biogenesis with the synthesis of mtDNA under radiation exposure to the cells of animals [51–53]. It is caused by the occurrence of mitochondrial dysfunction, increased oxidative stress, and a decrease in ATP synthesis, along with the emergence of increased energy needs in damaged cells.

As noted above, the processes of mtDNA damage repair occur with low efficiency in mammalian mitochondria. In these organelles, only the pathway of the BER functions efficiently [29]. The results of our analyses (Figure 2) showed an increased mtDNA synthesis in the spleen and cerebral cortex cells by 24–48 h after irradiation. As might be expected, the activity of mtDNA synthesis decreased in both tissues when mice were treated with MEL before and after irradiation, which lowered the RONS content. Various mammalian tissue cells may exhibit tissue-specific features in the activation of mitochondrial biogenesis and mtDNA synthesis, associated with their activity in the generation of ATP and RONS [54].

The subsequent results of our studies showed that in the post-radiation mitochondrial biogenesis, some of the synthesized mtDNA molecules were mutant copies. Obviously, mutations in the newly synthesized mtDNA molecules appeared during the replication of damaged mtDNA matrixes with the participation of DNA polymerase γ and DNA polymerase θ in mitochondria [35,36]. The increased levels of mtDNA mutant copies were observed in the spleen and cerebral cortex tissues of irradiated mice; however, their number significantly decreased upon the administration of MEL before and after irradiation (Figure 3). Therefore, it can be assumed that the antimutagenic effect of MEL is due to both the interception of initial RONS (the administration of MEL before irradiation) and the neutralization of RONS generated in the cells of irradiated mice (the administration of MEL after irradiation) [55]. These results are consistent with the previously obtained data of Tan et al. [56], who concluded that MEL protects mitochondria, has a regulatory effect on mitochondrial biogenesis and dynamics, and contributes to the preservation of the functions of these organelles. The increased level of mutant mtDNA copies in mammalian tissues after irradiation is due to both the low efficiency of the mtDNA repair systems and the effect of RONS; their production in the mitochondria of mammalian cells can continue over a long post-radiation period [40].

The results of a number of studies show that the mitochondrial dysfunction detected in human and animal cells after irradiation is largely associated with the induction of mutations in mtDNA genes encoding proteins of electron transport chain complexes, which continue to operate with the overproduction of RONS [57,58]. Obviously, the expression of mtDNA mutation genes leads to the synthesis of aberrant proteins. The latter can lead to perturbation of the oxidative phosphorylation system in mitochondria, with prolongs the increased generation of ROSNS and increased oxidative stress. This causes even more damage to macromolecules in the organelles and the entire cell, including nDNA. A "vicious cycle" is formed for a long period. This cycle operates in the various mammalian tissue cells at different rates and leads to the differential accumulation of mutant mtDNA copies, which, in turn, increase oxidative stress for a long post-radiation period. Thus, it can be assumed that, when IR is exposed to mammalian tissues, mitochondria containing mtDNA mutant copies become dysfunctional with enhanced RONS generation, which supports the induction of additional nDNA damage and genome instability of surviving cells, the development of degenerative diseases, aging, and oncogenesis for a long post-radiation period [59]. The mitochondrial respiratory chain is considered to be the most important cellular source providing most of the RONS in the cells of an aerobic organism [60]. However, there are other sources of RONS in mammalian cells that can be activated by radiation exposure. These include peroxisomes and many oxidases [61]. NADPH oxidases, a family of NOX enzymes that are located in various cellular compartments, can make a significant contribution to the enhancement of oxidative stress [62]. NADPH oxidases catalyze the one-electron reduction of $O_2$ to produce a superoxide anion ($O_2^{\bullet -}$) followed by the formation of $H_2O_2$ and hydroxyl radicals ($OH^{\bullet}$) [62].

Although all types of RONS are generated in irradiated cells, the greatest contribution to nDNA damage and other macromolecules is made by $H_2O_2$, $OH^{\bullet}$, and ONOO, which can diffuse over long distances. Especially $H_2O_2$ molecules capable of diffusing over distances are attainable by nDNA [63]. It has been noted that in physiological conditions, the level of $H_2O_2$ can reach 1–10 nM, whereas at "supraphysiological" concentrations, its content will be higher (>100 nM) [62].

In our analyses, the increase in the $H_2O_2$ level in the spleen may have been due to the low level of antioxidants compared to the cerebral cortex tissue (Figure 4). It was also reported that with an increase in the frequency of mtDNA mutations, the level of RONS may raise in the spleen [64]. Due to the specificity of this tissue, it can be noted that iron ions are released in the spleen after irradiation, which can increase the level of RONS with the induction of cell ferroptosis [65]. However, the increased $H_2O_2$ level in the spleen tissue of irradiated mice can be significantly reduced by the administration of MEL before and after irradiation. It is possible to observe not only an increase in $H_2O_2$, but also a decrease in ATP synthesis

with a loss of mitochondrial membrane potential (ΔΨm) in the initial period in the cells' mitochondria after IR exposure [61]. The ATP content decreases unevenly in different tissues of mice. We found that the decrease in ATP was more actively manifested in the spleen (by 80%) than in the brain tissue (by 20%) (Figure 5) [60]. First of all, the reason for this is that the number of mitochondria in the brain tissue of two-month-old mice is three times greater than in the spleen [62]. The content of ATP in the spleen tissue decreases after irradiation of the mice, however, unlike the cerebral cortex, with the introduction of MEL it increases only to the control level. Perhaps this is a manifestation of the tissue specificity of the mitochondrial reaction [63]. After a short-term decrease in the content of ATP in the tissues of irradiated mice in the post-radiation period, its synthesis is restored. MEL has an active effect on the restoration of ATP synthesis, as well as on the biogenesis of mitochondria in the tissues of irradiated mice.

In radiation biology, the levels of MDA (a marker of oxidative stress) and antioxidant enzymes or reduced GSH (a marker of the antioxidant system) are often used to assess changes in the redox status of cells after irradiation. There are a number of publications in the literature which show that the radioprotective effect of MEL, observed in experiments on animals, is associated with the decreased MDA and increased GSH levels in their tissues [66–68]. According to the results of our study, the MDA levels in the spleen and cerebral cortex tissues of mice 48 h after irradiation remain elevated compared to the non-irradiated control tissues (Figure 6). As might be expected, the data of the GSH content analyses show decreased values. The GSH level in the spleen of the control mice was much lower than in the cerebral cortex tissue (Figure 7). There is a tendency to restore the MDA and GSH content to their reference values after the administration of MEL to mice before and after irradiation. There is still an increased MDA level in the cerebral cortex tissue after the administration of MEL, although the GSH level increases more noticeably to the reference values. The high MDA level in the cerebral cortex tissue might be due to the increased content of lipids in this tissue.

## 5. Conclusions

Numerous studies show that MEL is a strong antioxidant that exhibits radioprotective and radiomitigative effects. The results of our study on the evaluation of the effect of MEL on tissues with different proliferative activity and radiosensitivity in mice exposed to IR confirm this position. The results showed that, although the tissues of the spleen and cerebral cortex of mice differ in the initial control values of the analyzed markers, the potential of radiation protection of MEL is successfully implemented in both tissues.

It should also be noted that the issue of the expediency of splenectomy in radiotherapy of tumors of intra-abdominal organs or in astronauts during long-term space flights outside the protection of the Earth's magnetosphere is currently being discussed. Of course, the data obtained by exposure to X-rays on the body is difficult to completely extrapolate to damage to normal tissues during hadron therapy of tumors or to the effects of cosmic radiation on astronauts. Nevertheless, since oxidative stresses of different levels occur when cells are exposed to different IR ($^{56}$Fe, protons, and X-rays) [69], it seems possible to suppress them by MEL and refrain from splenectomy.

**Author Contributions:** Conceptualization, A.I.G.; methodology, S.A.A. and A.I.G.; conducting all analyses, S.A.A., S.I.G. and A.I.G.; writing—review and editing, A.I.G. and S.A.A.; funding acquisition, A.I.G., S.A.A. and S.I.G.; statistical analysis, S.A.A. and A.I.G. All authors have read and agreed to the published version of the manuscript.

**Funding:** The study was supported by the Russian government contract N° 075-00381-21-00 (2021–2023) of the Institute of Theoretical and Experimental Biophysics, Russian Academy of Sciences, and with the support of the Russian Foundation for Basic Research under grant N° 17-29-01007.

**Institutional Review Board Statement:** The study was approved by the Committee on Biomedical Ethics of the Institute of Theoretical and Experimental Biophysics of the Russian Academy of Sci-

ences/the Physiology Section of the Russian Committee on Bioethics (Protocol N° 20/2021 dated 9 February 2021).

**Informed Consent Statement:** Not applicable.

**Data Availability Statement:** Data is contained within the article.

**Acknowledgments:** The authors express their gratitude to A.V. Pisakov for carrying out work on the irradiation of mice and to T. Hilscher for technical support during a number of analyses and for working with animals.

**Conflicts of Interest:** All authors declare no conflict of interest.

## References

1. Karri, J.; Lachman, L.; Hanania, A.; Marathe, A.; Singh, M.; Zacharias, N.; Orhurhu, V.; Gulati, A.; Abd-Elsayed, A. Radiotherapy-specific chronic pain syndromes in the cancer population: An evidence-based narrative review. *Adv. Ther.* **2021**, *38*, 1425–1446. [CrossRef] [PubMed]
2. Chancellor, J.C.; Scott, G.B.; Sutton, J.P. Space radiation: The number one risk to astronaut health beyond low Earth orbit. *Life* **2014**, *4*, 491–510. [CrossRef]
3. Hall, E.J.; Giaccia, A.J. *Radiobiology for the Radiologist*, 8th ed.; Wolters Kluwer: Philadelphia, PA, USA, 2019.
4. Rosen, E.M.; Day, R.; Singh, V.K. New approaches to radiation protection. *Front. Oncol.* **2015**, *4*, 381. [CrossRef]
5. Reiter, R.J.; Tan, D.X.; Herman, T.S.; Thomas, C.R., Jr. Melatonin as a radioprotective agent: A review. *Int. J. Radiat. Oncol. Biol. Phys.* **2004**, *59*, 639–653.
6. Zetner, D.; Andersen, L.P.; Rosenberg, J. Melatonin as protection against radiation injury: A systematic review. *Drug Res.* **2016**, *66*, 281–296. [CrossRef] [PubMed]
7. Zharinov, G.M.; Bogomolov, O.A.; Chepurnaya, I.V.; Neklasova, N.Y.; Anisimov, V.N. Melatonin increases overall survival of prostate cancer patients with poor prognosis after combined hormone radiation treatment. *Oncotarget* **2020**, *11*, 3723–3729. [CrossRef]
8. Gurunathan, S.; Qasim, M.; Kang, M.H.; Kim, J.H. Role and therapeutic potential of melatonin in various type of cancers. *Onco Targets Ther.* **2021**, *14*, 2019–2052. [CrossRef]
9. Moloudizargari, M.; Moradkhani, F.; Hekmatirad, S.; Fallah, M.; Asghari, M.H.; Reiter, R.J. Therapeutic targets of cancer drugs: Modulation by melatonin. *Life Sci.* **2021**, *267*, 118934. [CrossRef]
10. Liu, M.T.; Reiter, R.J. Melatonin protection against ionizing radiation in space. *J. Cell. Sci. Apo.* **2019**, *2*, 112.
11. Simonsen, L.C.; Slaba, T.C.; Guida, P.; Rusek, A. NASA's first ground-based galactic cosmic ray simulator: Enabling a new era in space radiobiology research. *PLoS Biol.* **2020**, *18*, e3000669. [CrossRef] [PubMed]
12. Laiakis, E.C.; Shuryak, I.; Deziel, A.; Wang, Y.-W.; Barnette, B.L.; Yu, Y.; Ullrich, R.L.; Fornace, A.J., Jr.; Emmett, M.R. Effects of low dose space radiation exposures on the splenic metabolome. *Int. J. Mol. Sci.* **2021**, *22*, 3070. [CrossRef] [PubMed]
13. Bergonié, J.; Tribondeau, L. De quelques résultats de la radiotherapie et essai de fixation d'une technique rationnelle. *CR Acad. Sci.* **1906**, *143*, 983–985.
14. Betlazar, C.; Middleton, R.J.R.; Banati, B.; Liu, G.-J. The impact of high and low dose ionizing radiation on the central nervous system. *Redox Biol.* **2016**, *9*, 144–156. [CrossRef]
15. Choudharya, S.; Kumara, A.; Sahac, N.; Chaudhury, N.K. PK-PD based optimal dose and time for orally administered supraphar-macological dose of melatonin to prevent radiation induced mortality in mice. *Life Sci.* **2019**, *219*, 31–39. [CrossRef]
16. Gonzalez-Hunt, C.P.; Rooney, J.P.; Ryde, I.T.; Anbalagan, C.; Joglekar, R.; Meyer, J.N. PCR-based analysis of mitochondrial DNA copy number, mitochondrial DNA damage, and nuclear DNA damage. *Curr. Protoc. Toxicol.* **2016**, *67*, 1–34. [CrossRef] [PubMed]
17. Furda, A.; Santos, J.H.; Meyer, J.N.; Van Houten, B. Quantitative PCR-based measurement of nuclear and mitochondrial DNA damage and repair in mammalian cells. *Methods Mol. Biol.* **2014**, *1105*, 419–437. [PubMed]
18. Abdullaev, S.; Gubina, N.; Bulanova, T.; Gaziev, A.I. Assessment of nuclear and mitochondrial DNA, expression of mitochondria-related genes in different brain regions in rats after whole-body X-ray irradiation. *Int. J. Mol. Sci.* **2020**, *21*, 1196. [CrossRef] [PubMed]
19. Sanders, L.H.; Rouanet, J.P.; Howlett, E.H.; Leuthner, T.C.; Rooney, J.P.; Greenamyre, J.T.; Meyer, J.N. Newly revised protocol for quantitative PCR-based assay to measure mitochondrial and nuclear DNA damage. *Curr. Protoc. Toxicol.* **2018**, *76*, e50. [CrossRef]
20. Rooney, J.P.; Ryde, I.T.; Sanders, L.H.; Howlett, E.H.; Colton, M.D.; Germ, K.E.; Mayer, G.D.; Greenamyre, J.T.; Meyer, J.N. PCR based determination of mitochondrial DNA copy number in multiple species. *Methods Mol. Biol.* **2015**, *1241*, 23–38.
21. Bannwarth, S.; Procaccio, V.; Paquis-Flucklinger, V. Rapid identification of unknown heteroplasmic mitochondrial DNA mutations with mismatch-specific surveyor nuclease. *Methods Mol. Biol.* **2009**, *554*, 301–313.
22. Abdullaev, S.; Bulanova, T.; Timoshenko, G.; Gaziev, A.I. Increase of mtDNA number and its mutant copies in rat brain after exposure to 150 MeV protons. *Mol. Biol. Rep.* **2020**, *47*, 4815–4820. [CrossRef] [PubMed]
23. Lowry, O.H.; Rosebrough, N.J.; Farr, A.L.; Randall, R.J. Protein measurement with the Folin phenol reagent. *J. Biol. Chem.* **1951**, *193*, 265–275. [CrossRef]

24. Chida, J.; Kido, H. Extraction and quantification of adenosine triphosphate in mammalian tissues and cells. *Methods Mol. Biol.* **2014**, *1098*, 21–32. [PubMed]
25. Buege, J.A.; Aust, S.D. Microsomal lipid peroxidation. *Methods Enzymol.* **1978**, *52*, 302–310.
26. Ellman, G.L. Tissue sulfhydryl groups. *Arch. Biochem. Biophys.* **1959**, *8*, 70–77. [CrossRef]
27. Galano, A.; Reiter, R.J. Melatonin and its metabolites vs oxidative stress: From individual actions to collective protection. *J. Pineal Res.* **2018**, *65*, e12514. [CrossRef]
28. Majidinia, M.; Reiter, R.J.; Shakouri, S.K.; Yousefi, B. The role of melatonin,a multitasking molecule, in retarding the processes of ageing. *Ageing Res. Rev.* **2018**, *47*, 198–213. [CrossRef]
29. Van Houten, B.; Hunter, S.E.; Meyer, J.N. Mitochondrial DNA damage induced autophagy, cell death, and disease. *Front. Biosci.* **2016**, *21*, 42–54. [CrossRef]
30. Moretton, A.; Morel, F.; Macao, B.; Lachaume, P.; Ishak, L.; Lefebvre, M.; Garreau-Balandier, I.; Vernet, P.; Falkenberg, M.; Farge, G. Selective mitochondrial DNA degradation following double strand breaks. *PLoS ONE* **2017**, *12*, e0176795. [CrossRef]
31. Peeva, V.; Blei, D.; Trombly, G.; Corsi, S.; Szukszto, M.J.; Rebelo-Guiomar, P.; Gammage, P.A.; Kudin, A.P.; Becker, C.; Altmüller, J.; et al. Linear mitochondrial DNA is rapidly degraded by components of the replication machinery. *Nat. Commun.* **2018**, *9*, 1727. [CrossRef]
32. Zhao, L. Mitochondrial DNA degradation: A quality control measure for mitochondrial genome maintenance and stress response. *Enzymes* **2019**, *45*, 311–341. [PubMed]
33. Lee, H.C.; Wei, Y.H. Mitochondrial biogenesis and mitochondrial DNA maintenance of mammalian cells under oxidative stress. *Int. J. Biochem. Cell Biol.* **2005**, *37*, 822–834. [CrossRef]
34. Andres, A.M.; Tucker, K.C.; Thomas, A.; Taylor, D.J.; Sengstock, D.; Jahania, S.M.; Dabir, R.; Pourpirali, S.; Brown, J.A.; Westbrook, D.G.; et al. Mitophagy and mitochondrial biogenesis in atrial tissue of patients undergoing heart surgery with cardiopulmonary bypass. *JCI Insight* **2017**, *2*, e89303. [CrossRef] [PubMed]
35. DeBalsi, K.L.; Hoff, K.E.; Copeland, W.C. Role of the mitochondrial DNA replication machinery in mitochondrial DNA mutagenesis, aging and age-related diseases. *Ageing Res. Rev.* **2017**, *33*, 89–104. [CrossRef] [PubMed]
36. Wisnovsky, S.; Sack, T.; Pagliarini, D.J.; Laposa, R.R.; Kelley, S.O. DNA polymerase θ increases mutational rates in mitochondrial DNA. *ACS Chem. Biol.* **2018**, *13*, 900–908. [CrossRef]
37. Lindahl, T. Instability and decay of the primary structure of DNA. *Nature* **1993**, *362*, 709–715. [CrossRef] [PubMed]
38. Evans, M.D.; Dizdaroglu, M.; Cooke, M.S. Oxidative DNA damage and disease: Induction, repair and significance. *Mutat. Res.* **2004**, *567*, 1–61. [CrossRef]
39. Lieber, M.R. The mechanism of double-strand DNA break repair by the nonhomologous DNA end-joining pathway. *Annu. Rev. Biochem.* **2010**, *79*, 181–211. [CrossRef]
40. Azzam, E.I.; Jay-Gerin, J.P.; Pain, D. Ionizing radiation-induced metabolic oxidative stress and prolonged cell injury. *Cancer Lett.* **2011**, *327*, 48–60. [CrossRef] [PubMed]
41. Galano, A.; Tan, D.-X.; Reiter, R.J. Melatonin: A versatile protector against oxidative DNA damage. *Molecules* **2018**, *23*, 530. [CrossRef]
42. Eskandari, A.; Mahmoudzadeh, A.; Shirazi, A.; Esmaely, F.; Carnovale, C.; Cheki, M. Melatonin a promising candidate for DNA double-stranded breaks reduction in patients undergoing abdomen-pelvis computed tomography examinations. *Anticancer Agents Med. Chem.* **2020**, *2*, 859–864. [CrossRef] [PubMed]
43. Esmaely, F.; Mahmoudzadeh, A.; Cheki, M.; Shirazi, A. The radioprotective effect of melatonin against radiation-induced DNA double-strand breaks in radiology. *J. Cancer Res. Ther.* **2020**, *16*, 59–63.
44. Jafarpour, S.M.; Shekarchi, B.; Bagheri, H.; Farhood, B. The Radioprotective effects of melatonin and nanoselenium on DNA double-strand breaks in peripheral lymphocytes caused by I-131. *Indian J. Nucl. Med.* **2021**, *36*, 134–139.
45. Iyama, T.; Wilson, D.M., III. DNA repair mechanisms in dividing and non-dividing cells. *DNA Repair* **2013**, *12*, 620–636. [CrossRef]
46. Mata-Garrido, J.; Tapia, O.; Casafont, I.; Berciano, M.T.; Cuadrado, A.; Lafarga, M. Persistent accumulation of unrepaired DNA damage in rat cortical neurons: Nuclear organization and ChIP-seq analysis of damaged DNA. *Acta Neuropathol. Commun.* **2018**, *6*, 68. [CrossRef]
47. Mebius, R.E.; Kraal, G. Structure and function of the spleen. *Nat. Rev. Immunol.* **2005**, *5*, 606–616. [CrossRef] [PubMed]
48. Yoshida, T.; Goto, S.; Kawakatsu, M.; Urata, Y.; Li, T.-S. Mitochondrial dysfunction, a probable cause of persistent oxidative stress after exposure to ionizing radiation. *Free Radic. Res.* **2012**, *46*, 147–153. [CrossRef] [PubMed]
49. Sun, L.; Inaba, Y.; Sogo, Y.; Ito, A.; Bekal, M.; Chida, K.; Moritake, T. Total body irradiation causes a chronic decrease in antioxidant levels. *Sci. Rep.* **2021**, *11*, 6716. [CrossRef] [PubMed]
50. Sun, L.; Inaba, Y.; Sato, K.; Hirayama, A.; Tsuboi, K.; Okazaki, R.; Chida, K.; Moritake, T. I Dose-dependent decrease in antioxidant capacity of whole blood after irradiation: A novel potential marker for biodosimetry. *Sci. Rep.* **2018**, *8*, 7425. [CrossRef]
51. Malakhova, L.V.; Bezlepkin, V.G.; Antipova, V.N.; Gaziev, A.I. The increase in copy number of mitochondrial DNA in tissues of γirradiated mice. *Cell. Mol. Biol. Lett.* **2005**, *10*, 592–603.
52. Nugent, S.M.; Mothersill, C.E.; Seymour, C.; McClean, B.; Lyng, F.M.; Murphy, J.E. Increased mitochondrial mass in cells with functionally compromised mitochondria after exposure to both direct gamma radiation and bystander factors. *Radiat. Res.* **2007**, *168*, 134–142. [CrossRef]

53. Yamamori, T.; Sasagawa, T.; Ichii, O.; Hiyoshi, M.; Bo, T.; Yasui, H.; Kon, Y.; Inanami, O. Analysis of the mechanism of radiation-induced upregulation of mitochondrial abundance in mouse fibroblasts. *J. Radiat. Res.* **2017**, *58*, 292–301. [CrossRef] [PubMed]
54. Herbers, E.; Kekäläinen, N.J.; Hangas, A.; Pohjoismäki, J.L.; Goffart, S. Tissue specific differences in mitochondrial DNA maintenance and expression. *Mitochondrion* **2019**, *44*, 85–92. [CrossRef] [PubMed]
55. Anisimov, V.N.; Popovich, I.G.; Zabezhinski, M.A.; Anisimov, S.V.; Vesnushkin, G.M.; Vinogradova, I.A. Melatonin as antioxidant, geroprotector and anticarcinogen. *Biochim. Biophys. Acta* **2006**, *1757*, 573–589. [CrossRef]
56. Tan, D.-X.; Manchester, L.C.; Qin, L.; Reiter, R.J. Melatonin: A mitochondrial targeting molecule involving mitochondrial protection and dynamics. *Int. J. Mol. Sci.* **2016**, *17*, 2124. [CrossRef]
57. Slane, B.G.; Aykin-Burns, N.; Smith, B.J.; Kalen, A.L.; Goswami, P.C.; Domann, F.E.; Spitz, D.R. Mutation of succinate dehydrogenase subunit C results in increased, oxidative stress, and genomic instability. *Cancer Res.* **2006**, *66*, 7615–7620. [CrossRef]
58. Kulkarni, R.; Marples, B.; Balasubramaniam, M.; Thomas, R.; Tucker, J. Mitochondrial gene expression changes in normal and mitochondrial mutant cells after exposure to ionizing radiation. *Radiat. Res.* **2010**, *173*, 635–644. [CrossRef] [PubMed]
59. Lawless, C.; Greaves, L.; Reeve, A.K.; Turnbull, D.M.; Vincent, A.E. The rise and rise of mitochondrial DNA mutations. *Open Biol.* **2020**, *10*, 200061. [CrossRef]
60. Murphy, M.P. How mitochondria produce reactive oxygen species. *Biochem. J.* **2009**, *417*, 1–13. [CrossRef]
61. Sies, H.; Jones, D.P. Reactive oxygen species (ROS) as pleiotropic physiological signaling agents. *Nat. Rev. Mol. Cell Biol.* **2020**, *21*, 363–383. [CrossRef]
62. Bedard, K.; Krause, K.H. The NOX family of ROS-generating NADPH oxidases: Physiology and pathophysiology. *Physiol. Rev.* **2007**, *87*, 245–313. [CrossRef]
63. Sies, H. Hydrogen peroxide as a central redox signaling molecule in physiological oxidative stress: Oxidative eustress. *Redox Biol.* **2017**, *11*, 613–619. [CrossRef] [PubMed]
64. Zhang, X.; Liu, H.; Xing, X.; Tian, M.; Hu, X.; Liu, F.; Feng, J.; Chang, S.; Liu, P.; Zhang, H. Ionizing radiation induces ferroptosis in splenic lymphocytes of mice. *Int. J. Radiat. Res.* **2021**, *19*, 99–111. [CrossRef]
65. Masuyama, M.; Iida, R.; Takatsuka, H.; Yasuda, T.; Matsuki, T. Quantitative change in mitochondrial DNA content in various mouse tissues during aging. *Biochim. Biophys. Acta* **2005**, *1723*, 302–308. [CrossRef]
66. Erol, F.S.; Topsakal, C.; Ozveren, M.F.; Kaplan, M.; Ilhan, N.; Ozercan, I.H.; Yildiz, O.G. Protective effects of melatonin and vitamin E in brain damage due to gamma radiation. *Neurosurg. Rev.* **2004**, *27*, 65–69. [CrossRef]
67. Shirazi, A.R.; Fardid, R.; Mihandoost, E. Protective effect of low dose melatonin on radiation-induced damage to rat liver. *J. Biomed. Phys. Eng.* **2012**, *2*, 66–70.
68. Tahamtan, R.; Shabestani, M.A.; Tahamtani, Y.; Tavassoli, A.R.; Akmali, M.; Mosleh-Shirazi, M.A.; Naghizadeh, M.M.; Ghasemi, D.; Tahamtan, R.; Keshavarz, M.; et al. Radioprotective effect of melatonin on radiation-induced lung injury and lipid peroxidation in rats. *Cell J.* **2015**, *17*, 111–120.
69. Limoli, L.; Giedzinski, E.; Baure, J.; Rola, R.; Fike, J.R. Redox changes induced in hippocampal precursor cells by heavy ion irradiation. *Radiat. Environ. Biophys.* **2007**, *46*, 167–172. [CrossRef]

*antioxidants*

MDPI

*Article*

# Peroxiredoxin 6 Applied after Exposure Attenuates Damaging Effects of X-ray Radiation in 3T3 Mouse Fibroblasts

**Elena G. Novoselova *, Mars G. Sharapov, Sergey M. Lunin , Svetlana B. Parfenyuk, Maxim O. Khrenov, Elvira K. Mubarakshina, Anna A. Kuzekova, Tatyana V. Novoselova, Ruslan G. Goncharov and Olga V. Glushkova**

Institute of Cell Biophysics of the Russian Academy of Sciences, 142290 Pushchino, Russia; sharapov.mg@yandex.ru (M.G.S.); lunin@rambler.ru (S.M.L.); lana_kras2@rambler.ru (S.B.P.); xpehob2004@mail.ru (M.O.K.); mubarakshina_e@rambler.ru (E.K.M.); 13krevetka@gmail.com (A.A.K.); novossulova_t@rambler.ru (T.V.N.); ruslangoncharov071@gmail.com (R.G.G.); glushckova@mail.ru (O.V.G.)
* Correspondence: elenanov_06@mail.ru

**Abstract:** Although many different classes of antioxidants have been evaluated as radioprotectors, none of them are in widespread clinical use because of their low efficiency. The goal of our study was to evaluate the potential of the antioxidant protein peroxiredoxin 6 (Prdx6) to increase the radioresistance of 3T3 fibroblasts when Prdx6 was applied after exposure to 6 Gy X-ray. In the present study, we analyzed the mRNA expression profiles of genes associated with proliferation, apoptosis, cellular stress, senescence, and the production of corresponding proteins from biological samples after exposure of 3T3 cells to X-ray radiation and application of Prdx6. Our results suggested that Prdx6 treatment normalized p53 and NF-κB/p65 expression, p21 levels, DNA repair-associated genes (XRCC4, XRCC5, H2AX, Apex1), TLR expression, cytokine production (TNF-α and IL-6), and apoptosis, as evidenced by decreased caspase 3 level in irradiated 3T3 cells. In addition, Prdx6 treatment reduced senescence, as evidenced by the decreased percentage of SA-β-Gal positive cells in cultured 3T3 fibroblasts. Importantly, the activity of the NRF2 gene, an important regulator of the antioxidant cellular machinery, was completely suppressed by irradiation but was restored by post-irradiation Prdx6 treatment. These data support the radioprotective therapeutic efficacy of Prdx6.

**Keywords:** X-ray radiation; 3T3 fibroblasts; proliferation; apoptosis; cellular stress; senescence; peroxiredoxin 6; Prdx6; radioprotector

**Citation:** Novoselova, E.G.; Sharapov, M.G.; Lunin, S.M.; Parfenyuk, S.B.; Khrenov, M.O.; Mubarakshina, E.K.; Kuzekova, A.A.; Novoselova, T.V.; Goncharov, R.G.; Glushkova, O.V. Peroxiredoxin 6 Applied after Exposure Attenuates Damaging Effects of X-ray Radiation in 3T3 Mouse Fibroblasts. *Antioxidants* **2021**, *10*, 1951. https://doi.org/10.3390/antiox10121951

Academic Editors: Elena Obrador Pla and Alegria Montoro

Received: 28 October 2021
Accepted: 3 December 2021
Published: 5 December 2021



## 1. Introduction

It is well-known that ionizing radiation (IR) leads to the formation of free radicals and reactive oxygen species (ROS). Ionizing radiation induces cellular stress and damage mediated through either direct changes in DNA or indirect effects on DNA via generation of ROS [1]. Exposure of cells to IR may have various consequences, including cell death, mutations, transformation, and cell cycle arrest. Radiation-induced ROS cause single- and double-stranded DNA breaks and extensive base modifications. To evaluate cellular responses to IR, many different approaches have been used, ranging from chromosomal changes visualization to cell viability analysis, assessments of cell activity, and transcription profiling with an expression analysis of a large array of genes. Overall, this allows researchers to gain insight into the molecular mechanisms underlying the response to IR exposure.

The fate of irradiated cells is influenced by the activities of various transcription factors and interactions between them during the cell response to irradiation. Based on the fact that IR induces the active production of ROS in cells, it is reasonable to study effects of antioxidant enzymes, including peroxiredoxins, as radioprotectors. We have previously shown the beneficial effects of recombinant peroxiredoxin 6 (Prdx6, EC:1.11.1.27) in various pathologies associated with oxidative stress, such as mechanical and thermal skin injuries, chemical burns

of the respiratory tract, ischemia-reperfusion injuries [2–4], and type 1 diabetes mellitus [5]. In the latter study, we demonstrated that Prdx6 protected RIN-m5F (rat insulinoma) beta cells cultured with high glucose levels through a mechanism that leads to a reduction in ROS production and apoptosis. It was shown that peroxiredoxins (Prdxs), an evolutionarily ancient family of peroxidases capable of reducing a wide range of inorganic and organic peroxide substrates, may play an important role in radioprotection [6,7]. It should be noted that we have recently demonstrated penetration of exogenous Prdx6 into the cells using FITC-labeled Prdx6 [8].

We also studied the radioprotective activity of Prdx6 in different models in vivo and in vitro, and these studies were associated with the prophylactic application of Prdx6 before exposure to IR [9–12]. In addition, we recently demonstrated that preliminarily applied Prdx6 protected 3T3 mouse fibroblasts against LD50 X-ray irradiation in vitro. Thus, pretreatment with Prdx6 increased cell survival, stimulated proliferation, normalized the level of ROS in the culture, and suppressed apoptosis and necrosis in 3T3 fibroblasts [8]. We believe that it is equally important to test whether Prdx6 is capable of exerting a radioprotective effect when applied several hours after irradiation.

The effects of IR are the result of the activation of complex signaling pathway networks in response to DNA damage, which may lead either to recovery that is DNA repair and cell cycle arrest or cell death. These pathways are triggered by the activation of transcription factors, such as p53, nuclear erythroid-derived 2-related factor 2 (Nrf2), nuclear factor kappa B (NF-κB), and activating protein 1 (AP-1). Different radiation doses [13,14] and types of radiation produce different effects on gene expression [15]. High radiation doses are associated with increased severity of DNA damage, accompanied by responses to genotoxic stress, including the recognition of DNA damage, as well as altered repair mechanisms and immunological changes [16].

Among the transcription factors, nuclear factor kappa B (NF-κB) has been recognized as a key agent for the protection of cells against apoptosis in most cell types [17]. Both p53 and NF-κB are activated after exposure to IR, whereas activating protein 1 (AP-1) may control proliferation, aging, differentiation, and apoptosis, and Nrf2 may stimulate cellular antioxidant defense systems [18]. In addition, p21 was originally identified as a common inhibitor of cyclin-dependent kinases, transcriptionally modulated by p53, as well as a marker of cellular senescence. Earlier, p21 was considered a tumor suppressor that acted mainly by arresting the cell cycle and leading to the suppression of tumor growth. However, detailed studies of p21 have shown that p21 regulates responses to many cellular processes, including cell cycle arrest, apoptosis, DNA repair, aging, and autophagy [19].

In contrast, NF-κB has been shown to induce the activation of inflammatory and oxidative mediators, thus causing increased oxidative stress in cells [20,21]. Additionally, the transcription factor Nrf2, via the regulation of many antioxidant enzymes, such as glutathione peroxidase, may protect cells and tissues against inflammatory damage, mainly by inhibiting NF-κB signaling and suppressing the expression of several inflammatory and oxidative mediators [22,23].

Thus, the aim of this work was to study the effects of Prdx6 added to 3T3 fibroblasts several hours after irradiation of cells at a dose of 6 Gy. Thereby, the main subject of the work was not to identify the preventive effect of Prdx6, which has been demonstrated, but to investigate the possibility of its therapeutic activity when the enzyme is applied after irradiation. For this purpose, we analyzed mRNA expression profiles for genes associated with proliferation, apoptosis, senescence, and the production of corresponding proteins from biological samples after exposure to high doses of X-ray radiation and application of Prdx6. Finally, the aim of this study was to assess the role of Prdx6 in the regulation of therapeutic targets, such as NF-κB, Nrf2, TLR, p53, and p21, in irradiated fibroblasts to elucidate the therapeutic value of Prdx6 in counteracting X-ray toxicity. In parallel, we studied the responses of 3T3 cells by determining the production of cytokines IL-6 and TNF-α, expression of toll-like receptors (TLR1, TLR2, and TLR4), as well as the JNK

pathway and SA-β-Gal activity. In addition, the stress response of the 3T3 cells was assessed using the heat shock protein system, including Hsp70, Hsp90α, and Hsp90β.

## 2. Materials and Methods

### *2.1. Cell Culture and Evaluation of Cell Proliferation*

Cells of BALB/3T3 lineage (American Type Culture Collection) were seeded into 25 $cm^2$ culture flasks (volume 5 mL), at concentration $1 \times 10^6$ cells/flask, in DMEM (PanEco, Moscow, Russia) with addition of 10% fetal calf serum (Thermo, Swindon, UK) and an antibiotic/antimycotic solution (Sigma, Ronkonkoma, NY, USA). Cells were cultivated in a $CO_2$ incubator at 37 °C and 5% $CO_2$. For the experiments, cells of 5th–8th passages were used. Cells were allowed to attach for 24 h and then exposed to X-ray irradiation or a sham-irradiation (the same manipulations, excluding the X-ray device activation). Then, four hours later, 0.15 mg/mL Prdx6 was added.

Four groups of cells were used: (1) "control", sham-irradiated 3T3 cells; (2) "Prdx6", sham-irradiated 3T3 cells incubated in presence of Prdx6; (3) "6 Gy", 3T3 cells irradiated with X-ray in dosage 6 Gy; (4) "6 Gy + Prdx6", 3T3 cells irradiated with X-ray in dosage 6 Gy incubated in presence of Prdx6.

To assess survival, cells of 4 groups were placed into 96-well plates at concentration of $1 \times 10^4$ cells/well and maintained at 37 °C and 5% $CO_2$ for 24, 48, 72, or 120 h for subsequent survival evaluation, which included staining the cells with 0.05% Crystall Violet and counting using a Crystal Viollet counting (measure OD 595 nm) [5].

### *2.2. X-ray Treatment*

Irradiation was performed using a RUT-15 therapeutic X-ray device (focal length 8.5 cm, current 20 mA, voltage 200 kV) (Mosrentgen, Moscow, Russia) at a dose rate of 1 Gy/min. 3T3 cells were irradiated in culture flask, or 24, or 96-well plates at ambient temperature, and the accumulated dose was 6Gy. Sham-exposed cells were kept in the same conditions, excluding X-ray irradiation.

### *2.3. Isolation and Purification of the PRDX6*

Genetic constructions encoding human Prdx6 enzymes were expressed in E. coli, strain BL21 (DE3), as described earlier [24]. The obtained recombinant proteins included a His-tag. The proteins were purified by affinity chromatography on Ni-NTA-agarose (Thermo Fisher Scientific, Waltham, MA, USA), as described in the manufacturer's instructions. Isolation of proteins was performed as previously described [10]. The purity of the enzymes as measured by electrophoresis in 12% SDS/PAGE was at least 98%. Prdx6 diluted in phosphate buffer (1.7 mmol/L $KH_2PO_4$, 5.2 mmol/L $Na_2HPO_4$, 150 mmol/L NaCl, pH 7.4) at a concentration of 10 mg/mL was stored at −20 °C. Two months storage time at the above conditions produced no reduction in enzymatic activity. A peroxidase activity of Prdx6 in relation to hydrogen peroxide ($H_2O_2$) or tert-butyl hydroperoxide (t-BOOH) was according to Kang, with minor modifications. The peroxidase activity of recombinant Prdx6 was 230 nmol/min/mg of protein (in relation to $H_2O_2$) and 100 nmol/min/mg of protein (in relation to t-BOOH).

### *2.4. Senescence-Associated Beta-Galactosidase Staining*

Cellular senescence of 3T3 cells exposed to X-ray radiation was detected using a senescence-associated β-galactosidase (SA-β-gal) assay. 3T3 cells cultured in 24-well plates at $1 \times 10^4$ cells/well at 37 °C and 5% $CO_2$ were treated as previously described [25]. After 120 h, the cells were washed with PBS and fixed in 2% formaldehyde/0.2% glutaraldehyde solution. The fixed cells were maintained overnight at 37 °C (without $CO_2$) with SA-β-Gal staining solution. Finally, green blue–colored cells were counted (at least 100-200 cells per microscopic field in six fields) as a percentage of the total cell number and displayed as a percentage of cell senescence.

### *2.5. Electrophoresis and Immunoblotting*

3T3 cells were seeded into cell culture flasks (T25) at concentration of $1 \times 10^6$ cells/flask, allowed to attach for 24 h and then exposed to X-ray irradiation or sham-irradiation. After irradiation (sham exposure) cells maintained at 37 °C and 5% $CO_2$ for 120 h. Proteins from 3T3 cells were isolated using a lysis buffer as described previously [26]. The total protein concentration was measured using a spectrophotometer NanoDrop2000c (ThermoFisher Scientific, Wilmington, DE, USA). Equal quantities of total protein from samples were applied onto 10% SDS-PAGE and separated by electrophoresis. Then, a semi-dry transfer onto PVDF Hybond-P membranes (Amersham, Buckinghamshire, UK) was performed. Afterwards, the membranes were blocked using 5% fat milk in Tris-HCl buffer (pH 7.4) with 0.05% Tween 20 for 1 h, and monoclonal primary antibodies (1:1000) were applied, followed by incubation overnight at 4 °C. Following three washes with Tris-buffered saline/Tween 20, the membranes were maintained with an HRP-conjugated secondary goat anti-rabbit IgG antibody (P-GAR Iss, IMTEK, Moscow, Russia) (1:1000) for 1 h at ambient conditions. Primary monoclonal rabbit antibodies against GAPDH (14C10, #2118), NF-κB p65(C22B4, #4764), Phospho-NF-kB p65 Ser536 (93H1, #3033), Phospho-NF-kB p65 (Ser276) (93H1, #3037), Phospho-SAPK/JNK (Thr183/Tyr185 (#9251), Phospho-p53 (Ser46, #2521), Phospho-p53 (Ser15, #9284), p21 (#64016), Phospho-H2AX Ser139 (#2577), HSP70 (#4872), HSP90α (D1A7, #8165), HSP90β (#5087), Caspase-3 (#9662) (Cell Signaling Technology, USA) were used. GAPDH was used as a loading control. To develop blots, ECL Plus chemiluminescent cocktail (Amersham/GE) was used according to the manufacturer's instructions. The blots were photographed using WL transilluminator (Vilber Lourmat, Collégien, France). Quantification of the protein bands was performed densitometrically with Image Studio Software ver. 5.2.5 (Li-COR, USA). The averaged results normalized to the corresponding loading control (GAPDH) were expressed in relative units.

### *2.6. Gene Expression Analysis*

3T3 cells were seeded into cell culture flasks (T25) at concentration of $1 \times 10^6$ cells/flask, allowed to attach for 24 h, and then exposed to X-ray irradiation or sham-irradiation. After irradiation (sham exposure) cells maintained at 37 °C and 5% $CO_2$ for 120 h. The gene expression level was determined by reverse transcription real-time PCR. Total RNA was isolated from 3T3 cells with ExtractRNA reagent (Evrogen, Moscow, Russia). RNA quality was estimated electrophoretically in 1.5% agarose gel. RNA concentration was determined using NanoDrop 1000c spectrophotometer (Thermo Fisher Scientific, Waltham, MA, USA). Two micrograms of total RNA were used for reverse transcription with MMLV reverse transcriptase and standard dT15 oligonucleotide ("Evrogen", Russia). The synthesized cDNA was used for real-time PCR with qPCRmix-HS SYBR kit ("Evrogen", Russia) and 200 nM gene-specific primers (Table S1). The genes expression related to the cellular antioxidant response system (SOD3, PRDX1, PRDX2, PRDX3, PRDX4, PRDX5, PRDX6), apoptosis (CASP3, p53), DNA repair system (APEX1, XRCC4, XRCC5, and Ogg1), senescence marker (CDKN1), some transcription factors (p65/NF-κB, NRF2, AP-1), Toll-like receptors (TLR1, TLR2, TLR4), heat shock proteins (HSP90 and HSP70), and cytokine IL-6 were analyzed. Real-time PCR was carried out using DNA amplifier DTlite (DNA-Technology, Moscow, Russia) with cycling mode: (1) «hot-start»: 95 °C, 5 min; (2) denaturation, 95 °C, 15 s; (3) primer annealing and DNA synthesis at 60°C, 30 s. Stages (2–3) were repeated 40 times. The expression levels of genes studied was normalized to that of the housekeeping gene-β-actin (ACTB). The $2^{-\Delta\Delta Ct}$ method was used to calculate differences in genes expression [27].

### *2.7. Measurement of Cytokine Production*

3T3 cells of all groups were cultured in 24-well plates at $2 \times 10^5$ cells/well at 37 °C and 5% $CO_2$ for 120 h (for ELISA assay). The cytokine concentrations were determined in the cell lysates by ELISA method in 96-well plates. Commercial reagent kits for quantification of murine interleukin-6 (IL-6) or tumor necrosis factor (TNFα) were used (Peprotech, Rocky Hill, NJ, USA) as described earlier [28].

### *2.8. Statistical Analysis*

Statistical data analysis was carried out using the Sigma Plot 11 software package (Systat Software Inc., San Jose, CA, USA). Statistical significance between experimental groups was determined using two-way ANOVA with Bonferroni post-hoc tests for survival analysis or unpaired Student's *t*-tests for all other analyses. $p < 0.05$ was considered statistically significant. The results are presented as mean value ± standard error (SE).

## 3. Results

### *3.1. Effects of Prdx6 on the Survival, Proliferation, and Antioxidant Status of Irradiated 3T3 Cells*

Prdx6 added to the 3T3 cell culture in vitro 4 h after irradiation of the cells with a dose of 6 Gy significantly reduced the radiation-induced cell's death. A significant increase in cell survival was especially pronounced in the first two days after exposure to X-ray radiation in the group with the application of exogenous Prdx6 (4 h after irradiation). The number of viable cells in the Prdx6-treated irradiated group was 15–20% higher than in the irradiated control group (Figure 1A). The cyclin-dependent kinase inhibitor 1 (mRNA-CDKN1, protein-p21) was also increased after irradiation, while the presence of Prdx6 almost completely abolished this effect. At the same time, the application of exogenous Prdx6 to the culture of unirradiated 3T3 cells did not significantly affect the level of p21 expression (Figure 1B,C).

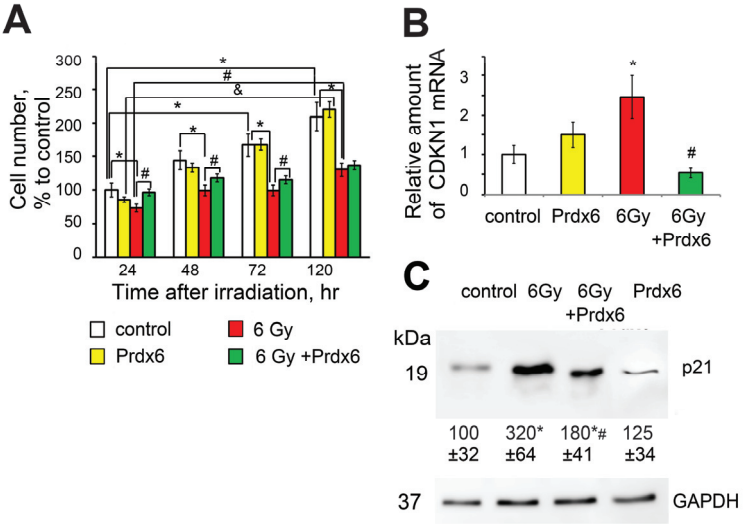


**Figure 1.** Effects of X-ray irradiation and Prdx6 addition on (**A**) cell proliferation ($F_{time}(9.105) = 18.569$, $p < 0.001$; $F_{exposure}(3.105) = 240.29$, $p < 0.001$; $F_{time*exposure}(3.105) = 133.92$, $p < 0.001$); (**B**) mRNA level of CDKN1 in the 3T3 cells; (**C**) p21 protein level in 3T3 cells measured by Western blot analysis. Equal amounts of total proteins were analyzed with the corresponding antibodies with normalization to a GAPDH loading control (bottom). Blot images show a single representative experiment, while values below the protein bands show protein level in relative units corresponding to the internal GAPDH control calculated from 3 independent experiments, and all mRNA evaluation experiments were performed in 6 repetitions. * Significantly different from the sham-irradiated control, $p < 0.05$, & significantly different from the irradiated cells, $p < 0.05$, # significantly different from the irradiated cells, $p < 0.05$.

Thus, the addition of Prdx6 prevented an increase of the senescence marker in irradiated 3T3 cells. In addition, evidence was obtained that the X-ray irradiation increased the percentage of SA-β-Gal positive cells, confirming the post-radiation oxidative stress and the activation of cell senescence mechanisms (Figure 2). In contrast, the addition of Prdx6

to the culture medium of the irradiated 3T3 cells led to a relative decrease in the percentage of SA-β-Gal-positive cells in comparison with non-treated irradiated cells. Meanwhile, the introduction of Prdx6 into the culture of non-irradiated cells did not affect the number of SA-β-Gal positive cells (Figure 2).

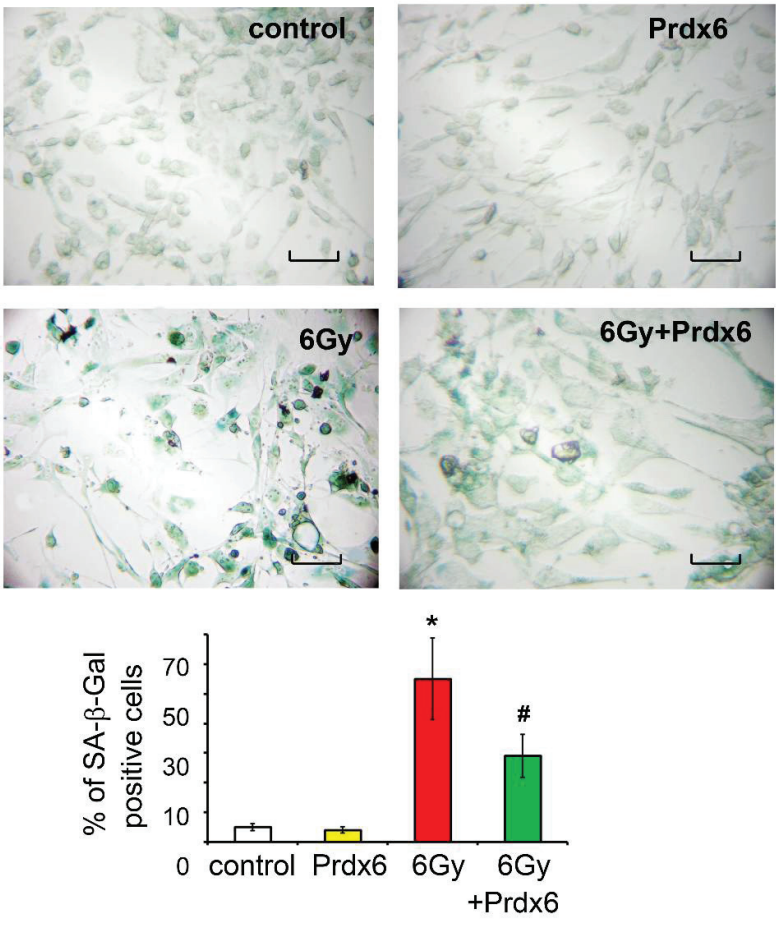


**Figure 2.** Representative images of effects of X-ray irradiation and Prdx6on SA-β-gal staining and the quantification of SA-β-gal-positive 3T3 cells. Data are percentages of total amounts of cells counted in the microscope's field of vision, $n = 300$ or more ± SEM. Scale bars are 100 μm. * Significantly different from the sham-irradiated control, $p < 0.05$, # significantly different from the irradiated cells, $p < 0.05$.

The expression of some antioxidant response system genes, for which the most significant change in expression after irradiation of 3T3 cells was previously shown, was assessed [8]. Interestingly, X-ray irradiation with a dose of 6 Gy resulted in a prolonged activation of the expression of isoforms PRDX2, PRDX3, and PRDX4, while the expression level of PRDX1, PRDX5, and PRDX6 did not differ significantly from the control values (Figure 3A). The addition of Prdx6 to the culture medium of 3T3 cells significantly normalized the expression of endogenous peroxiredoxins. The evaluation of SOD3 gene expression showed significant post-irradiation stimulation of the expression of this gene, whereas, in the presence of Prdx6, the expression of SOD3 in irradiated cells was almost normalized

(Figure 3B). Opposite effects of radiation and Prdx6 were found for the expression of the NRF2 gene (Figure 3C).

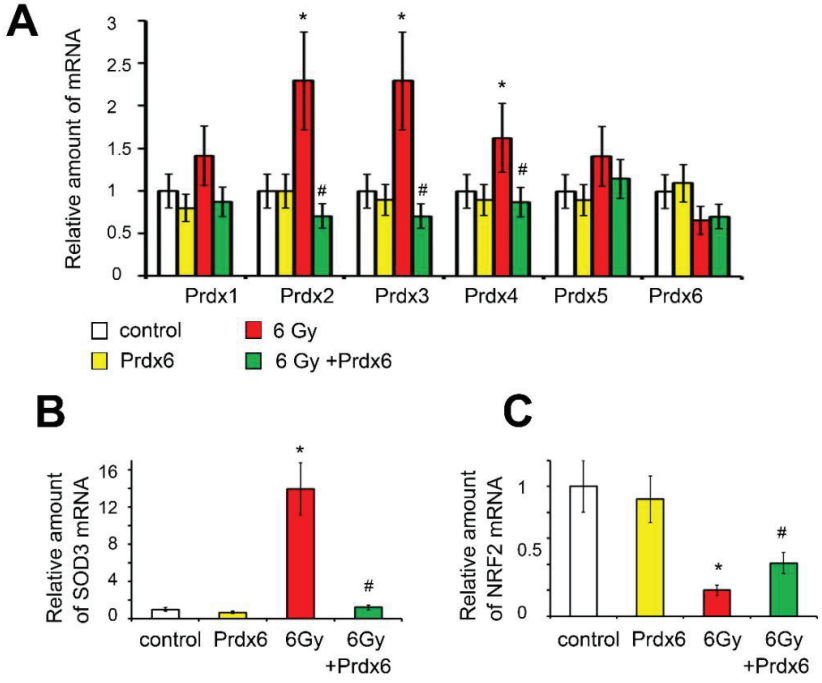


**Figure 3.** Effects of X-ray irradiation and Prdx6 addition on expression of genes regulating antioxidant status in 3T3 cells: (**A**) Peroxiredoxins; (**B**) SOD3; (**C**) NRF2. The mRNA evaluation experiments were performed in 6 repetitions. * Significantly different from the sham-irradiated control, $p < 0.05$, # significantly different from the irradiated cells, $p < 0.05$.

### *3.2. Post-Irradiation Effects of Prdx6 on Cytokine Production, TLR's Expression, Apoptosis, and Cellular Stress in Irradiated 3T3 Cells*

By evaluating the effects of radiation on the 3T3 cell's activity, we observed that X-ray radiation with a dose of 6 Gy led to the activation of the NF-κB pathway, increased the production of pro-inflammatory cytokines IL-6 and TNF-α, and increased the expression of toll-like receptors TLR1, TLR2, and TLR4 (Figure 4). Notably, the administration of Prdx6 after irradiation removed the pro-inflammatory effects of radiation, both at the gene and protein levels. The only exception was a JNK signaling cascade, whose activity did not increase, but decreased by almost 10 times after irradiation, while the addition of Prdx6 did not change the effect of radiation on JNK activity (Figure 4B).

Apoptosis in irradiated 3T3 fibroblasts was assessed by the expression and activity of caspase 3 (Figure 5A,B). The results showed that IR sharply accelerated apoptosis in 3T3 cells, and the addition of Prdx6 to the cell culture medium decreased the expression of the gene regulating the production of caspase 3 below the control level, which indicated the ability of Prdx6 to protect cells from radiation-induced apoptosis. Additionally, the production of the p53 protein was assessed in 3T3 cells, as well as levels of phosphorylated forms of this protein, ph-p53 (S46) and ph-p53 (S15), which have different roles in the cell. It was shown that IR significantly increased the total level of p53 in the cells, as well as the phosphorylation of p53 at Ser 46 and Ser 15 (Figure 5B,C). In addition, the Prdx6 added to the cells 4 h after irradiation demonstrated an obvious protective effect, manifesting in the normalization of the p53 level, as well as in a tendency to restoring of ph-p53 (S46) and ph-p53 (S15) levels, especially the ph-p53 (S15) form, which promotes cell survival [29].

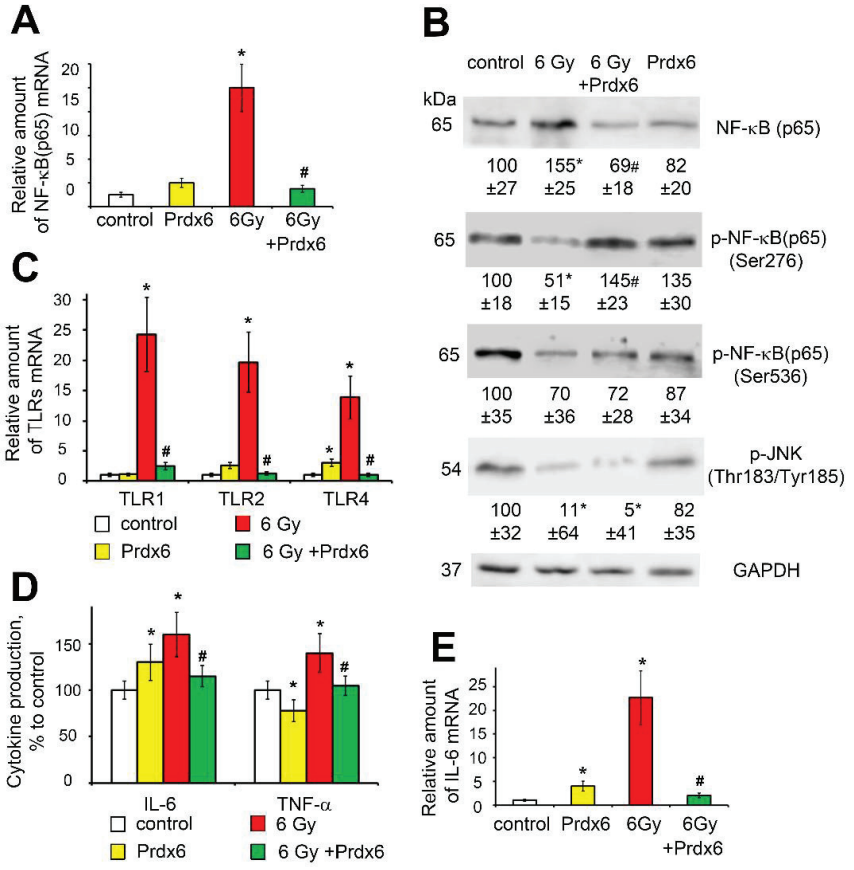


**Figure 4.** Effects of X-ray irradiation and Prdx6 addition on expression of genes and levels of proteins regulating and characterizing the immune status in the 3T3 cells: (**A**) NF-κB mRNA level; (**B**) NF-κB, p-NF-κB (Ser276 and Ser536, were normalized with total p65) and JNK proteins level; (**C**) TLRs mRNA level; (**D**) IL-6 mRNA level and TNF-α and IL-6 production in the 3T3 cells; (**E**) mRNA IL-6 level. The explanations for Western blot and mRNA analysis as in the legend for Figure 1. * Significantly different from the sham-irradiated control, $p < 0.05$, # significantly different from the irradiated cells, $p < 0.05$.

We also evaluated the expression of a panel of DNA repair-associated genes (such as XRCC4, XRCC5, Apex1, and Ogg1) (Figure 6). The results showed that IR stimulates the expression of these genes, indicating DNA damage in the 3T3-irradiated cells. In addition, irradiation led to increase in phosphorylation of H2AX which is a clear indication of DNA damage. Along with that, IR modulated the expression of H2AX that may indicate its effects on global histone regulation. Prdx6 protein added to the culture medium after irradiation exerted a protective effect in cells, which was indicated by a decrease in the expression of these genes associated with DNA damage and cell senescence, as well as a decrease in p-H2AX level, an important marker of IR-induced double-strand DNA breaks [30,31].

The expression of genes regulating the production of heat shock proteins HSP90α, HSP90β, and HSP70 is a direct indicator of cellular stress. We found that the irradiation of 3T3 fibroblasts led to the significant activation of genes that regulate the production of the inducible form of the heat shock proteins HSP90α, HSP90β, and HSP70 (Figure 7). The presence of Prdx6 in the cell culture medium prevented the stress response of 3T3 cells to X-ray irradiation.

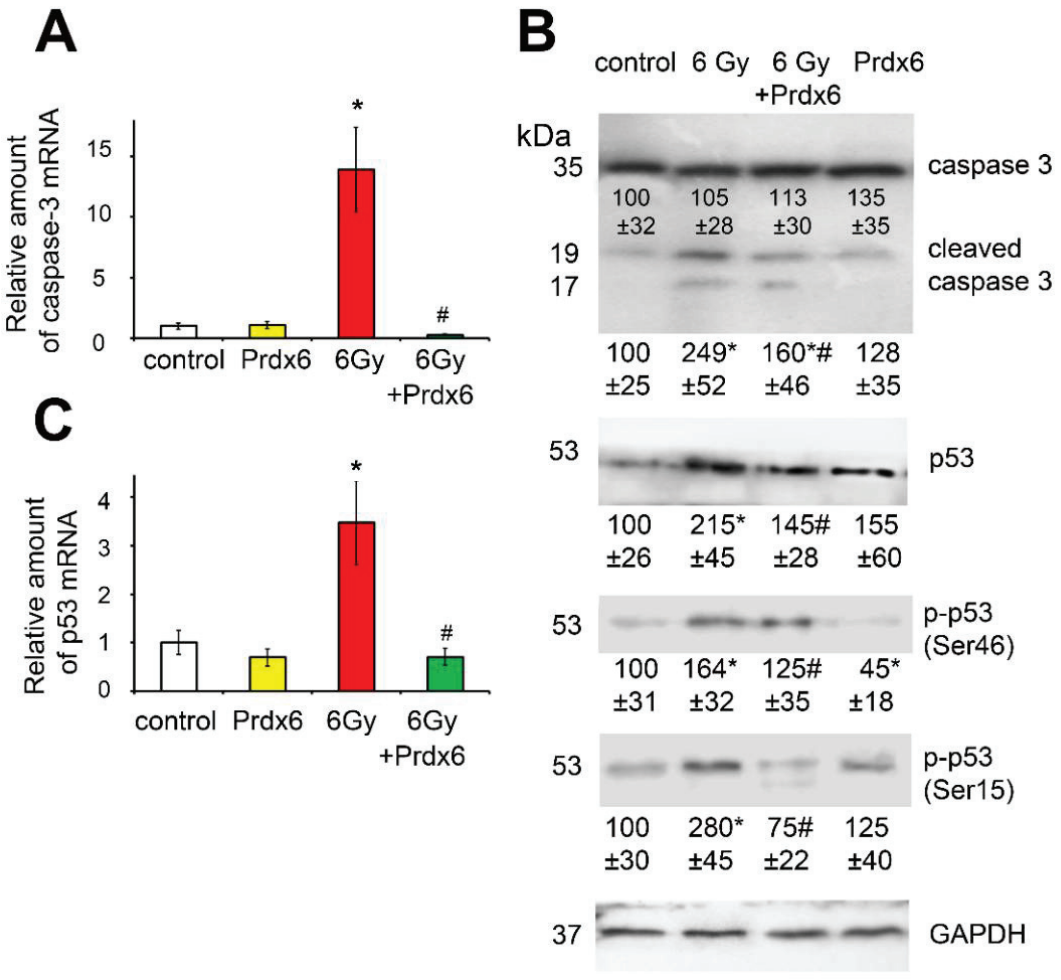


**Figure 5.** Effects of X-ray irradiation and Prdx6 addition on expression of genes and levels of proteins regulating and characterizing apoptosis in 3T3 cells: (**A**) mRNA of caspase 3; (**B**) p53, p-p53 (was normalized with total p53), and caspase 3 protein level; (**C**) mRNA of p53. The explanations for Western blot and mRNA analysis as in the legend for Figure 1. * Significantly different from the sham control cells, $p < 0.05$, # significantly different from the irradiated cells, $p < 0.05$.

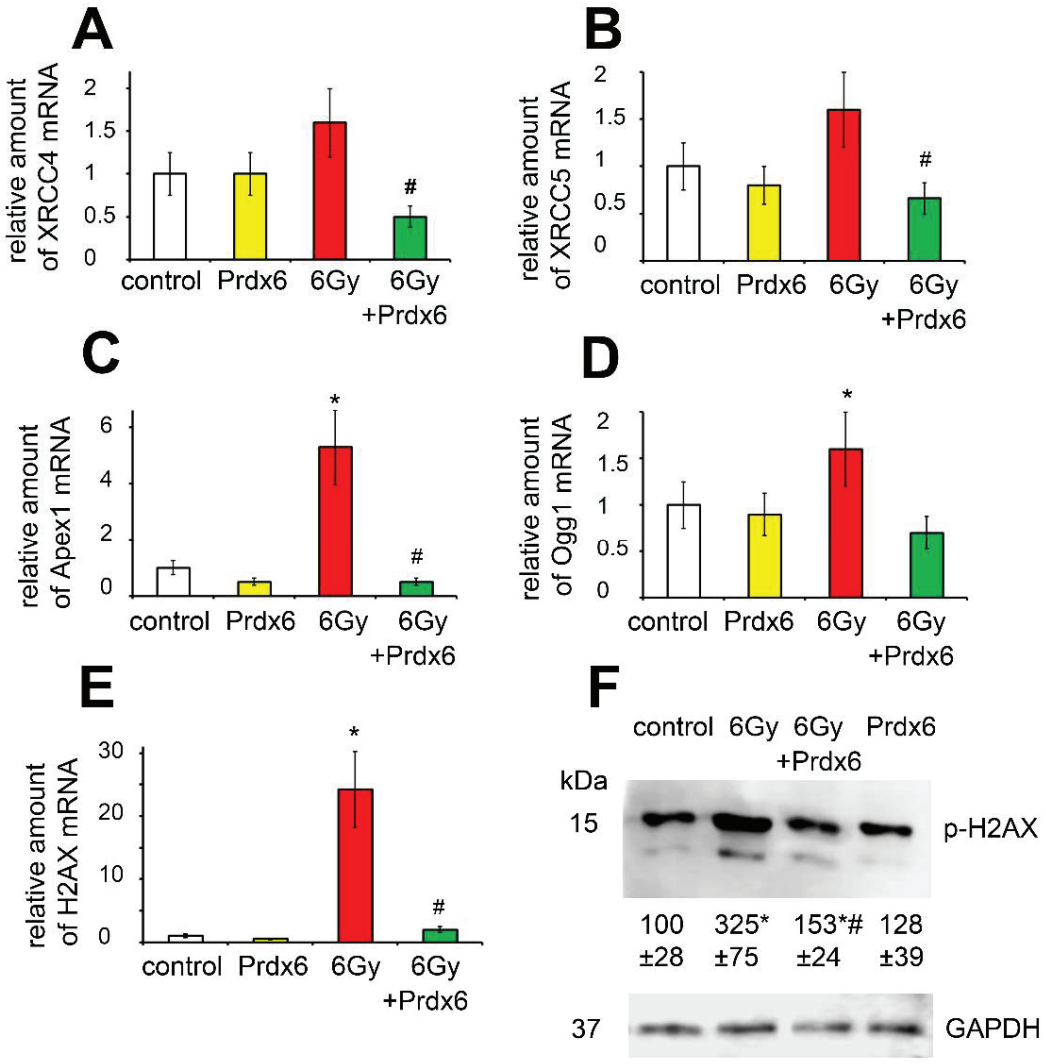


**Figure 6.** Effects of X-ray irradiation and Prdx6 addition on expression of genes and level of proteins regulating and characterizing DNA reparation in the 3T3 cells: (**A**) mRNA of XRCC4; (**B**) mRNA of XRCC5; (**C**) mRNA of Apex 1; (**D**) mRNA of Apex 1; (**E**) mRNA of H2AX; (**F**) The level of p-H2AX protein. The explanations for Western blot and mRNA analysis as in the legend for Figure 1. * Significantly different from the sham-irradiated control, $p < 0.05$, # significantly different from the irradiated cells, $p < 0.05$.

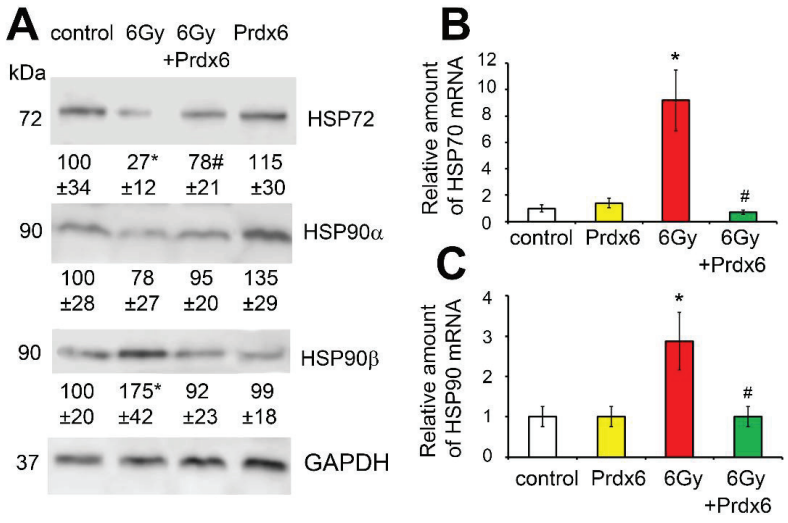


**Figure 7.** Effects of X-ray irradiation and Prdx6 addition on expression of genes and levels of proteins, regulating and characterizing heat shock proteins in the 3T3 cells: (**A**) HSP90α and HSP90β proteins levels; (**B**) mRNA of HSP70; (**C**) mRNA of HSP90. The explanations for Western blot and mRNA analysis as in the legend for Figure 1. * Significantly different from the sham-irradiated cells, $p < 0.05$, # significantly different from the irradiated cells, $p < 0.05$.

## 4. Discussion

Earlier, we demonstrated that preliminary administration of exogenous Prdx6 before irradiation of cells [8] and animals [10] provided a radioprotective effect. The radioprotective effect of Prdx6 approximately for 80% was due to its peroxidase activity, and, for 20%, due to stimulation of the TLR4 receptor [8]. It should be noted that exposure to ionizing radiation produces a long-term oxidative stress. In particular, after irradiation, a prolonged (hours-days) increase in the level of lipid peroxidation was observed [32], as well as formation of long-lived reactive protein species [33] that were shown to be effectively eliminated by Prdx6 [10]. In addition, after exposure to radiation, a dysfunction of the electron transport chain of mitochondria and the activation of a number of oxidases (NAD (P) H-oxidase, xanthine oxidase, cyclooxygenase etc.) were observed, which also contribute to an increase in the level of intracellular ROS and the progression of oxidative stress [34]. In this regard, it was interesting to test the effects of antioxidant enzyme Prdx6 applied after exposure to X-rays. Therefore, the purpose of this study was to evaluate the radiomitigating properties of recombinant Prdx6 in the culture of 3T3 embryonic fibroblasts.

Prdx6 can neutralize the broadest range of hydroperoxides and, unlike other members of the Prdx family, is able to reduce phospholipid peroxides and peroxynitrite, as well as phospholipase A2 activity (aiPLA2) under certain conditions [35]. Apparently, due to the aiPLA2 activity, Prdx6 may penetrate into cells, thereby directly affecting their redox status [8].

In cells that survive X-ray irradiation, changes in the expression of genes associated with DNA repair, cell cycle, inflammation, and immune responses are usually observed [36]. To study the effects of recombinant Prdx6 protein on irradiated 3T3 cells, we measured the key regulators of cellular processes. Among them, nuclear transcription factor kappa B (NF-κB) is a key factor in the regulation of metabolic pathways in most cell types. NF-κB is a central transcription factor in the immune system and influences cell survival. Moreover, the induction of radioresistance is mediated by several NF-κB regulated genes [17]. The p53 protein plays an important role in the regulation of the cell cycle, DNA repair, and apoptosis and is an attractive therapeutic target for cancer treatment [37]. Surprisingly,

we have shown that both p53 and NF-κB are activated in 3T3 cells after exposure to IR, whereas the presence of Prdx6 significantly reduced the effect of X-ray irradiation.

When studying the expression of PRDX1-6, which are considered the most important intracellular hydroperoxidases, it was found that isoform-specific expression of peroxiredoxins was induced on 5th day after irradiation (Figure 3), which may be explained by adaptation to the changing spectrum of hydroperoxides in the cell, because peroxiredoxin isoforms have different efficacy towards different peroxide substrates. However, in general, the induction of the expression of these genes was several times lower than in the first 6 h after irradiation of 3T3 cells [8], which may be due to the suppression of NRF2 (Figure 3), which regulates the expression of genes of many antioxidants' enzymes [38,39]. It should be noted that suppression of NRF2 may be mediated via activation of the transcription factor NF-κB (Figure 4), which is shown to suppress NRF2 activity [40]. The activation of NF-κB may explain the increase in the expression of some genes, which are controlled by NF-κB, related to the antioxidant response (SOD3) [41] and DNA repair (XRCC4, XRCC5, H2AX, Ogg1, and Apex1) [40].

The panel of DNA repair-associated genes in the irradiated 3T3 fibroblasts was markedly activated, whereas, after the Prdx6 addition, the activation of the gene panel was significantly reduced (Figure 6), which may indicate a decrease in ROS-induced oxidative DNA damage in the presence of Prdx6. These results support the radioprotective efficacy of Prdx6.

Moreover, the anti-inflammatory effect of Prdx6 in irradiated 3T3 fibroblasts was demonstrated. Indeed, while irradiation induced the expression of toll-like receptors (TLR1, TLR2, and TLR4), which is consistent to previous data [42], the production of pro-inflammatory cytokines IL-6 and TNFα, cell senescence (assessed by SA-β-Gal staining), and Prdx6 almost completely removed the pro-inflammatory effects of X-ray irradiation.

One of the important regulators of cellular activity is a low-molecular-weight p21 protein, transcribed from the CDKN1A gene, which was first described as a cyclin-dependent kinase 1 (CDKN1) inhibitor. It plays an important role in cell cycle control [43]. p21 stops cell cycle progression during G1 and S-phases via the binding and inhibition of cyclin-CDKN1,2,4,6 complexes [44]. Indeed, we have shown that X-ray irradiation at a dose of 6 Gy significantly increased CDKN1 gene expression, p21 production, and p21 phosphorylation, while the addition of Prdx6 into the culture medium of the X-ray irradiated fibroblasts normalized the proliferation of the 3T3 cells.

In addition, we have shown that genes regulating the production of heat shock proteins HSP90 and HSP70 were activated in the irradiated cells, with an inducible form of the HSP90 protein, HSP90β, with the most noticeable activation. Since these proteins are markers of cellular stress, we may conclude that IR induces cellular stress. It should be noted that Prdx6 also acts as a radioprotector, reducing the cellular stress caused by irradiation.

Advantages of new radioprotector development are related not only to providing protection in "working spaces" or during incidents of radioactive contamination but also to the use of radiation therapy [45]. Radiation therapy is currently one of the main treatments for cancer; despite the many benefits of this treatment, such as non-invasiveness, preservation of organ integrity, and precision when targeting a tumor, it can lead to complications in the irradiated healthy tissue. Therefore, applying radioprotective means may alleviate radiation-induced complications. Although many studies have aimed to identify radioprotective agents [46], there is still a need for new effective radioprotectors. Previously, we demonstrated that the radioprotective effects of Prdx6 are based on its capability for ROS neutralization and, potentially, on its ability to activate signaling regulatory mechanisms for the restoration of unbalanced redox homeostasis [10]. The summary on the protective effects of exogenous Prdx6 in the irradiated cells is shown in Figure 8. This study additionally supports this conclusion, importantly, using the post-radiation administration of the recombinant antioxidant protein peroxiredoxin 6, which may be a promising radioprotector/ radiomitigator.

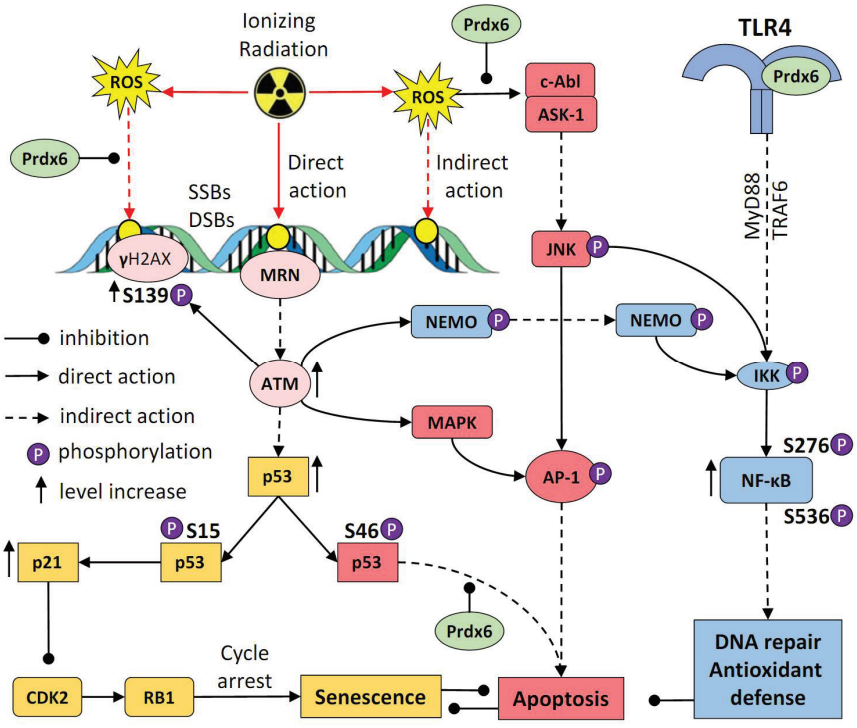


**Figure 8.** Schematic representation of the action of exogenous Prdx6 applied after exposure to X-rays. Ionizing radiation directly and indirectly (via ROS) causes single-stranded (SSBs) or double-stranded (DSBs) DNA breaks. The MRN complex (Mre11, Rad50, and Nbs1 proteins) recognizes DNA damage and activates ataxia telangiectasia-mutated (ATM) kinase. ATM phosphorylates histone H2AX at Ser139 (γH2AX), as well as checkpoint kinases CHK1 and CHK2, which phosphorylate p53. Phosphorylation of p53 at Ser15 leads to cell cycle arrest, while phosphorylation at Ser46 promotes apoptosis. In turn, p-p53 (ar Ser15) promotes the expression of p21 (cyclin-dependent kinase inhibitor p21 (CDKN1A)), which inhibits cyclin-dependent kinase 2 (CDK2), thereby inhibiting phosphorylation of retinoblastoma (Rb) protein and causing cell arrest. Exogenous Prdx6 prevents increase in the level of intracellular ROS by their elimination in the extracellular space, as well as directly inside the cell after Prdx6's penetration into cytoplasm [8]. Thus, the recombinant Prdx6 inhibits an increase of DNA damage and p21 activation, preventing the development of senescence. Prdx6 also prevents apoptosis by suppressing ROS-mediated activation of the ASK-1/JNK/AP-1 signaling pathway and an increase in the level of p-p53 (Ser46). An important role in the suppression of apoptosis is played by NF-κB, which is activated with the participation of NEMO (NF-κB essential modulator), and stimulation of the TLR4 receptor by exogenous Prdx6.

**Supplementary Materials:** The following are available online at https://www.mdpi.com/article/10.3390/antiox10121951/s1, Table S1: Oligonucleotides used for real-time PCR.

**Author Contributions:** Conceptualization, O.V.G. and E.G.N.; methodology, O.V.G., S.B.P., M.G.S., M.O.K.; formal analysis, O.V.G., M.G.S., E.K.M.; investigation, O.V.G., S.B.P., M.O.K., M.G.S., E.K.M., A.A.K., R.G.G., T.V.N.; data curation, O.V.G., S.M.L., M.O.K., M.G.S., E.K.M.; writing—original draft preparation, E.G.N., O.V.G., S.M.L.; writing—review and editing, E.G.N., S.M.L., O.V.G., M.G.S.; visualization, O.V.G., E.K.M.; supervision, O.V.G., E.G.N.; project administration, E.G.N., O.V.G., M.G.S., S.M.L.; funding acquisition, O.V.G., M.G.S. All authors have read and agreed to the published version of the manuscript.

**Funding:** This work was supported by Russian Foundation for Basic Research [grants 20-015-00216 and 19-04-00080]. The authors report no conflict of interest.

**Institutional Review Board Statement:** Not applicable.

**Informed Consent Statement:** Not applicable.

**Data Availability Statement:** Data is contained within the article or Supplementary Materials.

**Acknowledgments:** Part of the experiments was carried out using the technical base of Collective Use Centers of ICB RAS (X-ray system).

**Conflicts of Interest:** Authors report no conflict of interests.

## References

1. Cadet, J.; Douki, T.; Ravanat, J.-L. Oxidatively generated base damage to cellular DNA. *Free Radic. Biol. Med.* **2010**, *49*, 9–21. [CrossRef] [PubMed]
2. Gordeeva, A.E.; Sharapov, M.G.; Tikhonova, I.V.; Chemeris, N.K.; Fesenko, E.E.; Novoselov, V.I.; Temnov, A.A. Vascular pathology of ischemia/reperfusion injury of rat small intestine. *Cells Tissues Organs* **2017**, *203*, 353–364. [CrossRef] [PubMed]
3. Palutina, O.A.; Sharapov, M.G.; Temnov, A.A.; Novoselov, V.I. Nephroprotective Effect Exogenous Antioxidant Enzymes during Ischemia/Reperfusion-Induced Damage of Renal Tissue. *Bull. Exp. Biol. Med.* **2016**, *160*, 322–326. [CrossRef]
4. Karaduleva, E.V.; Mubarakshina, E.K.; Sharapov, M.G.; Volkova, A.E.; Pimenov, O.Y.; Ravin, V.K.; Kokoz, Y.M.; Novoselov, V.I. Cardioprotective effect of modified peroxiredoxins in retrograde perfusion of isolated rat heart under conditions of oxidative stress. *Bull. Exp. Biol. Med.* **2016**, *160*, 639–642. [CrossRef] [PubMed]
5. Novoselova, E.G.; Glushkova, O.V.; Parfenuyk, S.B.; Khrenov, M.O.; Lunin, S.M.; Novoselova, T.V.; Sharapov, M.G.; Shaev, I.A.; Novoselov, V.I. Protective effect of peroxiredoxin 6 against toxic effects of glucose and cytokines in pancreatic RIN-m5F βcells. *Biochemistry* **2019**, *84*, 637–643. [CrossRef]
6. Forshaw, T.E.; Holmila, R.; Nelson, K.J.; Lewis, J.E.; Kemp, M.L.; Tsang, A.W.; Poole, L.B.; Lowther, W.T.; Furdui, C.M. Peroxiredoxins in cancer and response to radiation therapies. *Antioxidants* **2019**, *8*, 11. [CrossRef]
7. Zhang, B.; Wang, Y.; Su, Y. Peroxiredoxins, a novel target in cancer radiotherapy. *Canc. Lett.* **2009**, *286*, 154–160. [CrossRef]
8. Sharapov, M.G.; Glushkova, O.V.; Parfenyuk, S.B.; Gudkov, S.V.; Lunin, S.M.; Novoselova, E.G. The role of TLR4/NF-κB signaling in the radioprotective effects of exogenous Prdx6. *Arch. Biochem. Biophys.* **2021**, *702*, 108830. [CrossRef]
9. Sharapov, M.G.; Gudkov, S.V.; Gordeeva, A.E.; Karp, O.E.; Ivanov, V.E.; Shelkovskaya, O.V.; Bruskov, V.I.; Novoselov, V.I.; Fesenko, E.E. Peroxiredoxin 6 is a natural radioprotector. *Dokl. Biochem. Biophys.* **2016**, *467*, 110–112. [CrossRef] [PubMed]
10. Sharapov, M.G.; Novoselov, V.I.; Fesenko, E.E.; Bruskov, V.I.; Gudkov, S.V. The role of peroxiredoxin 6 in neutralization of X-ray mediated oxidative stress: Effects of gene expression, preservation of radiosensitive tissues and postradiation survival of animals. *Free Radic. Res.* **2017**, *51*, 148–166. [CrossRef]
11. Sharapov, M.G.; Novoselov, V.I.; Gudkov, S.V. Radioprotective role of peroxiredoxin 6. *Antioxidants* **2019**, *8*, 15. [CrossRef]
12. Sharapov, M.G.; Gudkov, S.V.; Lankin, V.Z.; Novoselov, V.I. Role of Glutathione Peroxidases and Peroxiredoxins in Free Radical-Induced Pathologies. *Biochemistry* **2021**, *86*, 1418–1433. [CrossRef]
13. Turtoi, A.; Brown, I.; Oskamp, D.; Schneeweisset, F.H.A. Early gene expression in human lymphocytes after gamma-irradiation-a genetic pattern with potential for biodosimetry. *Int. J. Radiat. Biol.* **2008**, *84*, 375–387. [CrossRef] [PubMed]
14. Manning, G.; Kabacik, S.; Finnon, P.; Bouffler, S.; Badieet, C. High and low dose responses of transcriptional biomarkers in ex vivo X-irradiated human blood. *Int. J. Radiat. Biol.* **2013**, *89*, 512–522. [CrossRef]
15. Turtoi, A.; Brown, I.; Schlager, M.; Schneeweisset, F.H.A. Gene expression profile of human lymphocytes exposed to (211)At alpha particles. *Radiat. Res.* **2010**, *174*, 125–136. [CrossRef]
16. Van de Kamp, G.; Heemskerk, T.; Kanaar, R.; Essers, J. DNA Double Strand Break Repair Pathways in Response to Different Types of Ionizing Radiation. *Front. Genet.* **2021**, *12*, 738230. [CrossRef]
17. Bai, M.; Ma, X.; Li, X.; Wang, X.; Mei, Q.; Li, X.; Wu, Z.; Han, H. The accomplices of NF-κB lead to radioresistance. *Review Curr. Protein Pept. Sci.* **2015**, *16*, 279–294. [CrossRef] [PubMed]
18. Zhu, H.F.; Yan, P.W.; Wang, L.J.; Liu, Y.T.; Wen, J.; Zhang, Q.; Fan, Y.X.; Luo, Y.H. Protective properties of Huperzine A through activation Nrf2/ARE-mediated transcriptional response in X-rays radiation-induced NIH3T3 cells. *J. Cel.l Biochem.* **2018**, *119*, 8359–8367. [CrossRef]
19. Kuang, Y.; Kang, J.; Li, H.; Liu, B.; Zhao, X.; Li, L.; Jin, X.; Li, Q. Multiple functions of p21 in cancer radiotherapy. *J. Cancer. Res. Clin. Oncol.* **2021**, *147*, 987–1006. [CrossRef] [PubMed]
20. Zordoky, B.N.M.; El-Kadi, A.O.S. Role of NF-kappaB in the regulation of cytochrome P450 enzymes. *Curr. Drug. Metab.* **2009**, *10*, 164–178. [CrossRef] [PubMed]
21. Zaher, N.H.; Salem, A.A.M.; Ismail, A.F.M. Novel amino acid derivatives bearing thieno[2,3-d]pyrimidine moiety down regulate NF-κB in rats' liver injury induced by γ-irradiation. *J. Photochem. Photobiol. B* **2016**, *165*, 328–339. [CrossRef]
22. Chen, X.L.; Dodd, G.; Thomas, S.; Zhang, X.; Wasserman, M.A.; Rovin, B.H.; Kunsch, C. Activation of Nrf2/ARE pathway protects endothelial cells from oxidant injury and inhibits inflammatory gene expression. *Am. J. Physiol. Heart Circ. Physiol.* **2006**, *290*, H1862–H1870. [CrossRef]
23. Zeng, P.Z.; Zhao, Y.; Kanchana, K.; Zhang, Y.; Khan, Z.A.; Chakrabarti, S.; Wu, L.; Wang, J.; Liang, G. Curcumin protects hearts from FFA-induced injury by activating Nrf2 and inactivating NF-kB both in vitro and in vivo. *J. Mol. Cell. Cardiol.* **2015**, *79*, 1–12. [CrossRef]

24. Goncharov, R.G.; Rogov, K.A.; Temnov, A.A.; Novoselov, V.I.; Sharapov, M.G. Protective role of exogenous recombinant peroxiredoxin 6 under ischemia reperfusion injury of kidney. *Cell. Tissue Res.* **2019**, *378*, 319–332. [CrossRef] [PubMed]
25. Eccles, M.; Li, C.G. Senescence associated beta-galactosidase staining. *Bio-Protocol* **2012**, *2*, e247. [CrossRef]
26. Glushkova, O.V.; Khrenov, M.O.; Novoselova, T.V.; Lunin, S.M.; Parfenyuk, S.B.; Alekseev, S.I.; Fesenko, E.E.; Novoselova, E.G. The role of the NF-κB, SAPK/JNK, and TLR4 signalling pathways in the responses of RAW 264.7 cells to extremely low-intensity microwaves. *Int. J. Radiat. Biol.* **2015**, *91*, 321–328. [CrossRef] [PubMed]
27. Schmittgen, T.D.; Livak, K.J. Analyzing real-time PCR data by the comparative CT method. *Nat. Protoc.* **2008**, *3*, 1101–1108. [CrossRef]
28. Glushkova, O.V.; Parfenyuk, S.B.; Novoselova, T.V.; Khrenov, M.O.; Lunin, S.M.; Novoselova, E.G. The role of p38 and CK2 protein kinases in the response of RAW 264.7 macrophages to lipopolysaccharide. *Biochemistry* **2018**, *83*, 746–754. [CrossRef]
29. Liu, Y.; Tavana, O.; Gu, W. P53 modifications: Exquisite decorations of the powerful guardian. *J. Mol. Cell Biol.* **2019**, *11*, 564–577. [CrossRef]
30. Christmann, M.; Kaina, B. Transcriptional regulation of human DNA repair genes following genotoxic stress: Trigger mechanisms, inducible responses and genotoxic adaptation. *Nucleic Acids Res.* **2013**, *41*, 8403–8420. [CrossRef]
31. Chen, J.H.; Hales, C.N.; Ozanne, S.E. DNA damage, cellular senescence and organismal ageing: Causal or correlative? *Nucleic Acids Res.* **2007**, *35*, 7417–7428. [CrossRef] [PubMed]
32. Ye, L.F.; Chaudhary, K.R.; Zandkarimi, F.; Harken, A.D.; Kinslow, C.J.; Upadhyayula, P.S.; Dovas, A.; Higgins, D.M.; Tan, H.; Zhang, Y.; et al. Radiation-Induced Lipid Peroxidation Triggers Ferroptosis and Synergizes with Ferroptosis Inducers. *ACS Chem. Biol.* **2020**, *15*, 469–484. [CrossRef]
33. Bruskov, V.I.; Karp, O.E.; Garmash, S.A.; Shtarkman, I.N.; Chernikov, A.V.; Gudkov, S.V. Prolongation of oxidative stress by long-lived reactive protein species induced by X-ray radiation and their genotoxic action. *Free Radic. Res.* **2012**, *46*, 1280–1290. [CrossRef] [PubMed]
34. Azzam, E.I.; Jay-Gerin, J.P.; Pain, D. Ionizing radiation-induced metabolic oxidative stress and prolonged cell injury. *Cancer Lett.* **2012**, *327*, 48–60. [CrossRef]
35. Fisher, A.B. Peroxiredoxin 6: A bifunctional enzyme with glutathione peroxidase and phospholipase A2 activities. *Antioxid. Redox. Signal.* **2011**, *15*, 831–844. [CrossRef]
36. McKelvey, K.J.; Hudson, A.L.; Back, M.; Eade, T.; Diakos, C.I. Radiation, inflammation and the immune response in cancer. *Mammal. Genome* **2018**, *29*, 843–865. [CrossRef] [PubMed]
37. Pei, D.; Zhang, Y.; Zheng, J. Regulation of p53: A collaboration between Mdm2 and Mdmx. *Oncotarget* **2012**, *3*, 228–235. [CrossRef]
38. Ma, Q. Role of Nrf2 in oxidative stress and toxicity. *Annu. Rev. Pharmacol. Toxicol.* **2013**, *53*, 401–426. [CrossRef]
39. Ishii, T. Close teamwork between Nrf2 and peroxiredoxins 1 and 6 for the regulation of prostaglandin D2 and E2 production in macrophages in acute inflammation. *Free Radic. Biol. Med.* **2015**, *88*, 189–198. [CrossRef]
40. Hellweg, C.E. The Nuclear Factor κB pathway: A link to the immune system in the radiation response. *Cancer Lett.* **2015**, *368*, 275–289. [CrossRef] [PubMed]
41. Miao, L.; St. Clair, D.K. Regulation of superoxide dismutase genes: Implications in disease. *Free Radic. Biol. Med.* **2009**, *47*, 344–356. [CrossRef] [PubMed]
42. Liu, Z.; Lei, X.; Li, X.; Cai, J.M.; Gao, F.; Yang, Y.Y. Toll-like receptors and radiation protection. *Eur. Rev. Med. Pharmacol. Sci.* **2018**, *22*, 31–39. [CrossRef]
43. Harper, J.W.; Adami, G.R.; Wei, N.; Keyomarsi, K.; Elledge, S.J. The p21 Cdk-interacting protein Cip1 is a potent inhibitor of G1 cyclin-dependent kinases. *Cell* **1993**, *75*, 805–816. [CrossRef]
44. Georgakilas, A.G.; Martin, O.A.; Bonner, W.M. p21: A two-faced genome guardian trends. *Mol. Med.* **2017**, *23*, 310–319. [CrossRef] [PubMed]
45. Sheikholeslami, S.; Khodaverdian, S.; Dorri-Giv, M.; Mohammad Hosseini, S.; Souri, S.; Abedi-Firouzjah, R.; Zamani, H.; Dastranj, L.; Farhood, B. The radioprotective effects of alpha-lipoic acid on radiotherapy-induced toxicities: A systematic review. *Int. Immunopharm.* **2021**, *96*, 107741. [CrossRef]
46. El-Gazzar, M.G.; Zaher, N.H.; El-Hossary, E.M.; Ismail, A.F.M. Radio-protective effect of some new curcumin analogues. *J. Photochem. Photobiol. B* **2016**, *162*, 694–702. [CrossRef] [PubMed]

*antioxidants*

MDPI

*Article*

# New Properties of a Well-Known Antioxidant: Pleiotropic Effects of Human Lactoferrin in Mice Exposed to Gamma Irradiation in a Sublethal Dose

**Marina Yu. Kopaeva [1,*], Irina B. Alchinova [2], Anton B. Cherepov [1], Marina S. Demorzhi [2], Mikhail V. Nesterenko [3], Irina Yu. Zarayskaya [1] and Mikhail Yu. Karganov [2]**

[1] National Research Center "Kurchatov Institute", 1 Akademika Kurchatova Sq., 123182 Moscow, Russia
[2] Institute of General Pathology and Pathophysiology, 8 Baltiyskaya St., 125315 Moscow, Russia
[3] "Lactobio" LLC, 29 Prospekt Vernadskogo, 119331 Moscow, Russia
* Correspondence: m.kopaeva@mail.ru; Tel.: +7-9-166-345-141

**Abstract:** We studied the effects of human lactoferrin (hLf), a multifunctional protein from the transferrin family, on integral (survival, lifespan during the experiment, body weight, behavior, subfractional compositions of blood serum) and systemic (hemoglobin level, leukocyte number, differential leukocyte count, histological structure of the liver and spleen) parameters of the body in mice after acute gamma irradiation in a sublethal dose. The experiments were performed on male C57BL/6 mice. The mice in the experimental groups were exposed to whole-body gamma radiation in a dose of 7.5 Gy from a $^{60}$Co source. Immediately after irradiation and 24 h after it, some animals received an intraperitoneal injection of hLf (4 mg/mouse). Single or repeated administration of hLf had a positive pleiotropic effect on irradiated animals: animal survival increased from 28% to 78%, and the mean life expectancy during the experiment (30 days) increased from 16 to 26 days. A compensatory effect of hLf on radiation-induced body weight loss, changes in homeostasis parameters, and a protective effect on the structural organization of the spleen were demonstrated. These data indicate that Lf has potential as a means of early therapy after radiation exposure.

**Keywords:** human lactoferrin; acute gamma irradiation; C57Bl/6 mice; survival rate; open field test; spleen; serum homeostasis; leukocytes

**Citation:** Kopaeva, M.Y.; Alchinova, I.B.; Cherepov, A.B.; Demorzhi, M.S.; Nesterenko, M.V.; Zarayskaya, I.Y.; Karganov, M.Y. New Properties of a Well-Known Antioxidant: Pleiotropic Effects of Human Lactoferrin in Mice Exposed to Gamma Irradiation in a Sublethal Dose. *Antioxidants* **2022**, *11*, 1833. https://doi.org/10.3390/antiox11091833

Academic Editors: Elena Obrador Pla and Alegria Montoro

Received: 29 July 2022
Accepted: 15 September 2022
Published: 18 September 2022



## 1. Introduction

Ionizing radiation is a phenomenon that is present in our daily life, originating from both natural and artificial sources. The power of this radiation can be either within the natural background range or significantly exceed it. During radiation therapy, one of the leading therapeutic methods of treating many types of human cancer, as well as during radiodiagnosis, the patients can develop side effects, including immunosuppression, changes in blood composition, and mucosal lesions. Medical workers in radiological laboratories and X-ray rooms are occupationally exposed to radiation and are at risk of developing the same adverse effects. The interaction of pathogenetic and adaptive processes underlying these adverse effects and activated by radiation exposure occurs at all levels of biological organization—from molecules to the whole body. In this context, the search for effective therapeutic agents of pleiotropic action for the treatment of socially significant diseases associated with radiation exposure is an urgent problem.

According to existing ideas about the pathogenesis of radiation damage, a leading role in the mechanism of its development is played by oxidative stress [1,2]. Reactive oxygen species and free radicals can initiate long-lasting alternative processes in various organs and tissues. The destructive effect of free radicals can be prevented by antioxidants that reduce the damaging effect of ionizing radiation on the body. Their protective effect is related to the suppression of free radical oxidation and activation of the antioxidant systems

in the body [3]. One of these antioxidants, protein lactoferrin, inhibits the Fenton reaction through iron chelation [4,5].

Lactoferrin (Lf) is a multifunctional globular glycoprotein with a molecular weight of ~80 kDa, a member of the transferrin family. It is present in various mammalian secretory fluids, as well as in neutrophil granules [6,7]. Lf is involved in various physiological processes, including binding and transport of iron ions and immune and inflammatory reactions. This protein has multiple protective functions [8] and radioprotective properties [9]. The biological effects of Lf are mediated by specific surface receptors on target cells. Lf receptors were detected on B cells, T cells, monocytes [10,11], platelets [12], hepatocytes [13], fibroblasts [14], osteoblasts [15], and endothelial cells of brain vessels [16].

There are several options for drugs to reduce radiation damage. Nevertheless, current treatments, although beneficial, may have attendant side effects and long-term sequelae, usually more or less affecting the quality of patients' lives. Lf shows high bioavailability after oral, intravenous, intranasal, and intraperitoneal administration; high selectivity toward damaged cells; and a wide range of molecular targets controlling cell proliferation, survival and migration [17]. Moreover, Lf can prevent or inhibit the development of radiation damage by stimulation of the adaptive immune response [9].

Numerous tests in animals and humans have proven Lf safety and tolerability. No adverse effect was observed in both rats orally administered with Lf at 2000 mg/kg per 13 days [18] and in humans with 1.5–9 g of Lf per 15 days [19]. There were no changes attributable to administration of the Lf in clinical signs, body weight, food consumption, ophthalmological findings, blood chemistry, or gross pathological examination findings. No hematological, hepatic, or renal toxicities were reported. The lack of toxicity was observed in previous studies in healthy volunteers with doses at 15 g in a 24-h period [20], and no toxicities were found in mouse with doses at 1000 mg/kg administered twice daily for 8 days [21]. In addition to oral administration, several different other modes were tested in animal models and humans. No adverse effect was observed in mice intravenously administered with Lf at 250 μg/g [22]. Of note, Lf is classified as a "generally recognized as safe" (GRAS) substance by the USA Food and Drug Administration [23].

The therapeutic effect of the chronic administration of bovine Lf after whole-body exposure to X-rays was demonstrated; it manifested itself in increasing the survival rate of irradiated mice, stimulating hematopoiesis [4,24], and reducing damage to the small intestinal epithelium [25]. The use of Lf as a therapeutic agent to minimize radiation-induced damage remains rarely studied, and therefore, a comprehensive study of the effect of Lf on the dynamics of the state of the body is required.

Our aim was to study the effects of human Lf (hLf) on integral (survival, lifespan during the experiment, body weight, behavior, subfractional compositions of blood serum) and systemic (hemoglobin level, leukocyte number, differential leukocyte count, histological structure of the liver and spleen) indicators of the organism after acute gamma irradiation of mice in a sublethal dose. Lf was administered to animals once or twice, unlike most previous studies, where long-term repeated administration of Lf was used. The study included a wide range of methods at the body, organ, tissue, cellular, and molecular levels.

## 2. Materials and Methods

The study was conducted on 2–2.5-month-old mice ($n$ = 238) weighing 20–28 g (Pushchino nursery for laboratory animals, a branch of the M. M. Shemyakin and Yu. A. Ovchinnikov Institute of Bioorganic Chemistry, Russian Academy of Science). The animals were kept in standard laboratory cages, type 1285L (Techniplast, Buguggiate, Italy), five mice per cage, at controlled temperature and humidity, 12/12 h light–dark cycle with free access to food and water. All experimental procedures were carried out during the light hours between 9:00 and 18:00 h. All manipulations were carried out in accordance with Directive 2010/63/EU on the Protection of Animals Used for Scientific Purposes [26]; the study was approved by the Local Ethical Committee on Biomedical Research of the National Research Center "Kurchatov Institute" (Protocol No. 1, 13 February 2020) and

Ethical Committee of the Institute of General Pathology and Pathophysiology (Protocol No. 4, 7 October 2021).

We used hLf (Lactobio LLC, Moscow, Russia) isolated from female colostrum by preparative ion exchange chromatography [27] and additionally purified by affinity chromatography on heparin-sepharose [28]. HPLC by the method of Y. Zhang [29] showed that the purity of the resulting protein preparation was 97%.

The animals were exposed to gamma radiation from a $^{60}$Co source (GUT-200M apparatus; National Research Center "Kurchatov Institute", Moscow, Russia). The mice were weighed every three days throughout the experiment on electronic scales Adventurer Pro (Ohaus Corporation, Pine Brook, NJ, USA). The effect of hLf on animal behavior was evaluated using the open field test. Changes in physiological parameters were assessed by shifts in the subfractional composition of the blood plasma assessed by the dynamic light scattering method, total and differential leukocyte count, hemoglobin level, and histological examination of the liver and spleen at different terms after irradiation. Three independent experimental series were performed.

### 2.1. Experimental Groups and Treatments

The mice were randomly divided into seven groups: experimental (IR, $n$ = 50; IR+Lf, $n$ = 44; IR+Lf×2, $n$ = 45), active control (sham-irradiated: AC, $n$ = 28; AC+Lf, $n$ = 28; AC+Lf×2, $n$ = 27), and passive control (intact: PC, $n$ = 16). The mice in the experimental groups were exposed to whole-body gamma radiation in a dose of 7.5 Gy (at a dose rate of 0.6 Gy/min). Exposure to this sublethal dose induces serious changes in behavioral and physiological parameters in mice but allows us to keep alive a sufficient number of animals for analysis during a 30-day experiment [30,31].

Immediately after irradiation, the animals in groups IR+Lf, IR+Lf×2, AC+Lf, and AC+Lf×2 received intraperitoneal injection of hLf (4 mg/mouse in 0.3 mL of saline (0.9% NaCl, Dalkhimpharm, Khabarovsk, Russia)). In 24 h after irradiation, the mice were re-injected with hLf (groups IR+Lf×2, AC+Lf×2) or saline (groups IR+Lf, AC+Lf). The dose of Lf was chosen based on published data [4], results of our previous studies [32,33], and pilot experiments [34]. The animals in the IR and AC groups were twice injected with saline in the same way. The scheme of the experiment is shown in Figure 1.

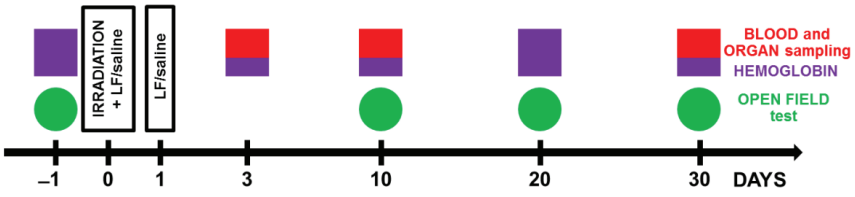


**Figure 1.** Experimental timeline. Animals from experimental groups were exposed to 7.5 Gy whole-body gamma irradiation. Some animals received intraperitoneal injections of Lf (4 mg/mouse) immediately and 24 h after irradiation. The open field test (OF) was performed prior to irradiation and on days 10, 20, and 30 after it. On days 3, 10, and 30 after irradiation, organs (liver, spleen) and whole blood were taken for analysis. The hemoglobin level and the number of leukocytes in the peripheral blood of animals were determined.

### 2.2. Analysis of Mouse Behavior in the Open Field Test

The open field test (OF) is a standard method for assessing spontaneous motor activity and behavior in rodents [35]. The OF was a round plastic arena (d = 120 cm, h = 45 cm) with a central part of 60 cm in diameter; the OF was illuminated to 115 lx. Testing was performed 1 day before and on days 10, 20, and 30 after irradiation (Figure 1). The testing process was described in detail in our previous report [33]. Each animal was placed in the OF center and allowed to explore the arena for 5 min. During testing, mouse behavior was recorded with a WV-CP500G video camera (Panasonic, Osaka, Japan) and an EthoVision

XT 8.5 video recording system (Noldus Information Technology, Netherlands); The videos were analyzed using EthoVision XT 8.5 software; the total distance traveled was measured and the time spent in the central zone was calculated and expressed as a percentage of the total time of the test. The number of rearings was determined.

### *2.3. Collection and Processing of Samples*

In the peripheral blood, hemoglobin level and leukocyte count were determined. Blood was collected from the caudal vein at different terms of the experiment. In 3, 10, or 30 days after irradiation, the animals were anesthetized with isoflurane (Baxter, Baxter Healthcare Corporation of Puerto Rico, Deerfield, IL, USA) and decapitated; the organs (liver, spleen) and whole blood were collected.

#### 2.3.1. Measurement of Hemoglobin Level

The hemoglobin level was measured using an Easy Touch GCHb automatic analyzer (Bioptik Technology, Inc., Jhunan, Taiwan) before irradiation and on days 10, 20, and 30 after it (Figure 1). To this end, a drop of blood was applied to an Easy Touch hemoglobin test strip.

#### 2.3.2. Leukocyte Counting

Leukocytes were counted in the Goryaev chamber according to the standard procedure on days 10, 20, and 30 after irradiation (Figure 1). A blood sample (2.5 μL) was diluted by 20 times with 3% acetic acid with methylene blue.

#### 2.3.3. Differential Leukocyte Counting

For determining the percentage of different types of leukocytes, blood smears were prepared according to the standard method, stained by the Pappenheim method (successive staining with May-Grünwald and Romanovsky-Giemsa dyes), washed, dried, and examined under a Zeiss Imager Z2 VivaTome microscope (Carl Zeiss, Jena, Germany) with oil immersion. In each smear, 200 cells were counted and classified as neutrophils, lymphocytes, monocytes, eosinophils, or basophils based on morphological criteria.

#### 2.3.4. Calculation of the Absolute Number of Leukocytes of Different Types

Based on the total number of leukocytes and differential blood count, the absolute numbers of neutrophils, lymphocytes, monocytes, eosinophils, and basophils for each animal were calculated.

#### 2.3.5. Dynamic Light Scattering Analysis of Blood Serum (DLS)

Blood serum was obtained from mouse whole blood on days 3 or 30 after irradiation (Figure 1) The samples were left for 2 h at 4 °C, centrifuged at 3000 rpm for 10 min, and the supernatant was collected and stored at −20 °C until analysis. Changes in the subfraction composition of blood serum were evaluated using an LKS-03 laser correlation spectrometer (INTOX, St. Petersburg, Russia). To this end, the samples were thawed at room temperature, diluted 1:10 with saline, and transferred to a cuvette of the spectrometer in the volume of 0.2 mL. The method is based on the analysis of light scattering spectra obtained on particles present in biological fluids when a laser beam with coherent monochromatic radiation passes through the sample [36]. Processing of the obtained spectra yields size distribution histograms of particles present in the fluid and contributing to the light scatter.

### *2.4. Histological Analysis*

The spleen and liver were isolated on days 3, 10, or 30 after irradiation and fixed in 4% neutral formalin (Figure 1). The preparations were processed routinely. The samples were embedded in paraffin, and tissue sections (thickness 5 μm) were sliced on a Leitz 1208 microtome (Leitz, Oberkochen, Germany). Dewaxed sections were routinely stained with hematoxylin and eosin by the Perls method [37] and by the van Gieson method (Van

Gieson; ErgoProdaction LLC, St. Petersburg, Russia) according to manufacturer's instructions. The stained sections were embedded in a mounting medium (DiaPath, Martinengo, Italy) and examined under a Zeiss Imager Z2 VivaTome light microscope (Carl Zeiss, Jena, Germany). At each of the above terms, organs of 7–10 mice in each group were examined.

### *2.5. Statistical Analysis*

The statistical analysis was performed using GraphPad Prizm 8.0.1 software (La Jolla, San Diego, CA, USA). The normality of data distribution was assessed using the Shapiro–Wilk or Kolmogorov–Smirnov tests (depending on the sample sizes). In the case of normal distribution of the studied parameters, One-Way ANOVA was applied, followed by Tukey's *post hoc* test or Šidák test for multiple comparisons. In cases where the hypothesis on the normal distribution of the test results cannot be accepted, a nonparametric one-way Kruskal–Wallis test was used for comparative analysis, followed by *post hoc* Dunn test for multiple comparisons. Animal survival was evaluated using the Kaplan–Meyer method (Gehan–Breslow–Wilcoxon test). The data are presented as the mean and standard error of the mean or as medians, quartiles, and minimum and maximum values. The differences were significant at $p < 0.05$.

## 3. Results

### *3.1. Effects of Lf on Survival Rate and Lifespan of Mice Exposed to Irradiation*

The effects of hLf on survival and mean lifespan (MLS) of mice ($n = 32$ in each experimental group) during the experiment were assessed daily over 30 days after irradiation. No animal deaths were recorded in the control groups throughout the experiment. In the IR group, the first deaths were recorded on day 5 and their number reached its maximum on days 7–14 after irradiation. By day 30, animal survival in this group was 28.1% (Figure 2a), and MLS was 16.0 ± 1.7 days (Figure 2b).

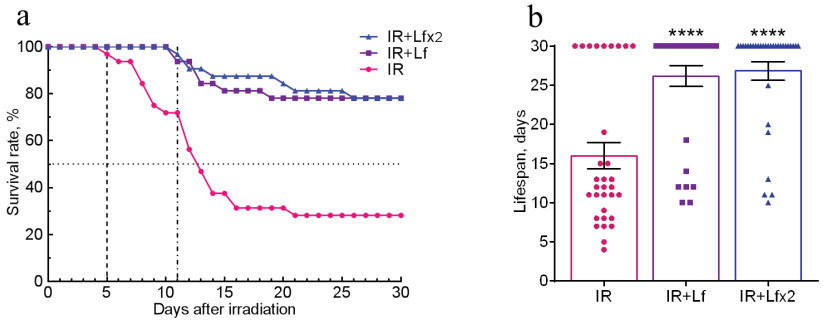


**Figure 2.** Effects of Lf on the survival rate (**a**) and lifespan (**b**) of mice after 7.5 Gy whole-body gamma irradiation. Lf (i.p.; 4 mg/mouse) was administered immediately after irradiation (IR+Lf and IR+Lf×2) and 24 h after it (IR+Lf×2). $n = 32$ in each group. The survival rates (%) and lifespan (days) during the 30-day period after irradiation are presented. **** $p < 0.0001$ in comparison with the IR group.

In the groups of IR+Lf and IR+Lf×2, the first death occurred on day 11 after irradiation (Figure 2a). It was found that administration of hLf increased survival rate to 78.1% in both groups of irradiated animals (Figure 2a), and MLS increased to 26.8 ± 1.2 (IR+Lf×2) and 26.2 ± 1.3 (IR+Lf) days (Figure 2b).

### *3.2. Effect of Lf on the Body Weight of Mice Exposed to Irradiation*

After irradiation, the body weight of the mice began to decrease, while in controls it gradually increased. In the control mice, hLf produced no appreciable effect on body weight gain; no differences by this parameter were found between the groups of active (AC, AC+Lf, AC+Lf×2) and passive control (PC) throughout the experiment. In all three

experimental groups, a decrease in body weight was observed on day 3 after irradiation, although in the IR+Lf×2 group, this decrease was less pronounced (Figure 3).

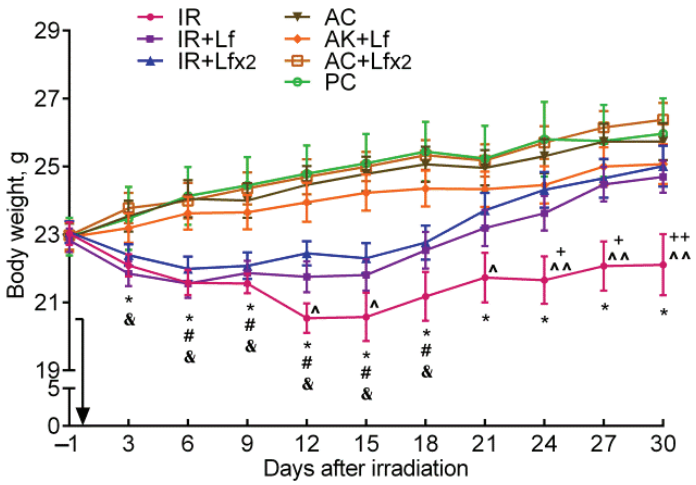


**Figure 3.** Effect of Lf on the body weight of mice after 7.5 Gy whole-body gamma irradiation. The arrow shows the day of irradiation. Lf (i.p.; 4 mg/mouse) was administered immediately after irradiation/sham-irradiation (IR+Lf, IR+Lf×2, AC+Lf, AC+Lf×2) and 24 h after it (IR+Lf×2, AC+Lf×2). $n$ = 32 (for IR, IR+Lf, and IR+Lf×2); $n$ = 17 (for AC, AC+Lf, and AC+Lf×2); $n$ = 10 (PC). Values are presented as mean ± SEM. * $p < 0.05$—IR vs. AC; $^{\#}$ $p < 0.05$—IR+Lf vs. AC+Lf; $^{\&}$ $p < 0.05$—IR+Lf×2 vs. AC+Lf×2; $^{+}$ $p < 0.05$, $^{++}$ $p < 0.01$—IR vs. IR+Lf; $^{\wedge}$ $p < 0.05$, $^{\wedge\wedge}$ $p < 0.01$—IR vs. IR+Lf×2 on the same day.

In the experimental groups, the dynamics of body weight were different. In animals in the IR group, the body weight decreased until day 12, remained approximately constant on days 12–15 and 21–30, and increased on days 15–21. The body weight in irradiated animals treated with hLf decreased until day 6, remained practically constant on days 6–15, and then gradually increased.

In the IR group, the body weight was significantly lower than in the AC group starting from day 3 and until the end of the experiment; it was also lower than in the IR+Lf group on days 24–30 and in the IR+Lf×2 group on days 12, 15, and 21–30 (Figure 3). The animals in all experimental groups significantly differed by this parameter from the corresponding controls on days 6–18. By day 30, the body weight in the IR group mice did not return to the initial level. On the contrary, the body weight of animals in the IR+Lf and IR+Lf×2 groups reached the baseline level by day 21 and did not significantly differ from the corresponding controls.

### *3.3. Effects of Lf on Mouse Behavior in Open Field Test after Whole-Body Gamma Irradiation*

The total distance traveled reflects motor activity [38], and the number of rearing is a measure of exploratory activity [39] of animals. All groups of mice showed similar motor activity and exploratory behavior before experimental exposures.

On days 10 and 20 after irradiation, the total distance traveled by the mice in the OF in the experimental groups was lower than in the corresponding controls (Figure 4a). On day 30, the irradiated mice did not differ from the control animals by this parameter, but significant differences were revealed between the groups of IR and IR+Lf and between the groups AC and AC+Lf (Figure 4a). The mice that received a single injection of hLf passed a longer distance in the OF during the final testing.

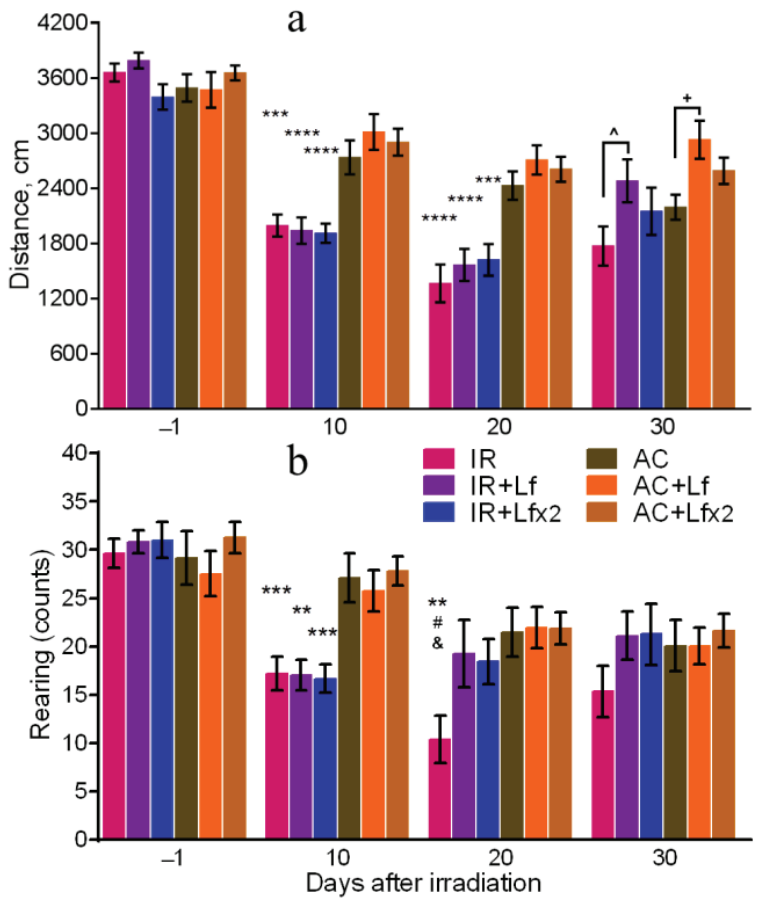


**Figure 4.** Effects of Lf on mouse behavior in the open field test after 7.5 Gy whole-body gamma irradiation. Lf (i.p.; 4 mg/mouse) was administered immediately after irradiation/sham-irradiation (IR+Lf, IR+Lf×2, AC+Lf, AC+Lf×2) and 24 h after it (IR+Lf×2, AC+Lf×2). Total distance traveled (**a**). Number of rearings (**b**). $n$ = 32, 20, 20 (day −1; for IR, IR+Lf, and IR+Lf×2, respectively); $n$ = 17 (for AC, AC+Lf, and AC+Lf×2). Values are presented as mean ± SEM. ** $p < 0.01$, *** $p < 0.001$, **** $p < 0.0001$ in comparison with the corresponding control (sham-irradiated) groups on the same day; $^{\#}$ $p < 0.05$ in comparison with the IR+Lf group, $^{\&}$ $p < 0.05$ in comparison with the IR+Lf×2 group on day 20. $^{\wedge}$ $p < 0.05$; $^{+}$ $p < 0.05$.

The irradiated mice demonstrated a lower number of rearings on day 10 after the exposure in comparison with the control animals (Figure 4b). On day 20, this parameter in the IR group was significantly lower than in the AC ($p < 0.01$), IR+Lf ($p < 0.05$), and IR+Lf×2 ($p < 0.05$) groups, while experimental groups treated with hLf did not differ by this parameter from the corresponding controls. On day 30, there were no significant differences in the number of rearings between the groups.

By day 10, the mice in the IR group spent significantly less time in the central zone than the control animals ($p < 0.01$) (Figure 5), while on days 20 and 30, this parameter in the IR group was below the control ($p < 0.001$ and $p < 0.05$) and the corresponding values in groups IR+Lf ($p < 0.001$ and $p < 0.001$) and IR+Lf×2 ($p < 0.01$ and $p < 0.05$). By the time spent in the central zone, both experimental groups treated with hLf did not differ from the control groups at all stages of testing.

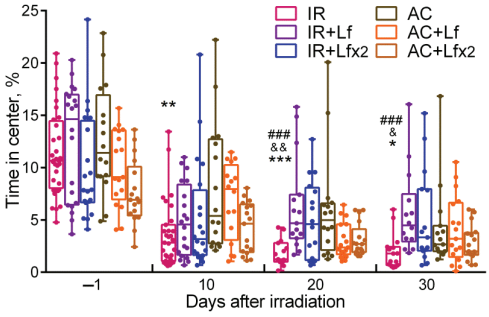


**Figure 5.** Effect of Lf on mouse behavior in the open field test after 7.5 Gy whole-body gamma irradiation. Lf (i.p.; 4 mg/mouse) was administered immediately after irradiation/sham-irradiation (IR+Lf, IR+Lf×2, AC+Lf, AC+Lf×2) and 24 h after it (IR+Lf×2, AC+Lf×2). Percent time spent in the center. Each dot represents a single animal. $n$ = 32, 20, 20 (day −1; for IR, IR+Lf, and IR+Lf×2, respectively); $n$ = 17 (for AC, AC+Lf, and AC+Lf×2). Data are presented as the median, quartiles, and min–max range. * $p < 0.05$, ** $p < 0.01$, *** $p < 0.001$ in comparison with the AC group; $^{\#\#\#}$ $p < 0.001$ in comparison with the IR+Lf group; $^{\&}$ $p < 0.05$; $^{\&\&}$ $p < 0.01$ in comparison with the IR+Lf×2 group on the same day.

### *3.4. Effects of Lf on Changes in Blood Parameters of Mice Exposed to Irradiation*

Blood samples were used to determine the following parameters: hemoglobin level (before and on days 3, 10, 20, and 30 after irradiation), total number of leukocytes (days 3, 10, and 30) and differential leukocyte count (days 3 and 30). The hematological parameters in the mice in the control groups (AC, AC+Lf, AC+Lf×2) did not differ from the reference values [24,40]. There were no differences in blood parameters between the active control groups (AC, AC+Lf, AC+Lf×2) during the experiment.

#### 3.4.1. Hemoglobin Level

Irradiation caused a significant decrease in hemoglobin levels. On days 10 and 20, mice of all experimental groups differed by this parameter from the corresponding controls (Figure 6a). By day 30, the hemoglobin concentration in irradiated animals almost returned to the initial levels.

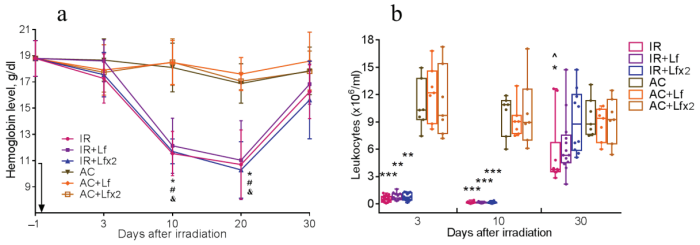


**Figure 6.** Dynamics of changes in the hemoglobin level (**a**) and the number of leukocytes (**b**) in the peripheral blood of mice after 7.5 Gy whole-body gamma irradiation. The arrow shows the day of irradiation. Lf (i.p.; 4 mg/mouse) was administered immediately after irradiation/sham-irradiation (IR+Lf, IR+Lf×2, AC+Lf, AC+Lf×2) and 24 h after it (IR+Lf×2, AC+Lf×2). (**a**) $n$ = 21, 15, 15 (day −1; for IR, IR+Lf, and IR+Lf×2, respectively); $n$ = 9 (for AC, AC+Lf, and AC+Lf×2). * $p < 0.05$—IR vs. AC; $^{\#}$ $p < 0.05$—IR+Lf vs. AC+Lf; $^{\&}$ $p < 0.05$—IR+Lf×2 vs. AC+Lf×2 on the same day. (**b**) Each dot represents a single animal. $n$ = 20, 15, 12 (day −1; for IR, IR+Lf, and IR+Lf×2, respectively); $n$ = 7 (for AC, AC+Lf, and AC+Lf×2). * $p < 0.05$, ** $p < 0.01$, *** $p < 0.001$ in comparison with the corresponding control (sham-irradiated) groups on the same day; $^{\wedge}$ $p < 0.05$ in comparison with group IR+Lf×2 on day 30.

3.4.2. Total Leukocyte Count

Irradiation caused a sharp decrease in the leukocyte count in all experimental groups. On days 3 and 10, the groups IR, IR+Lf, and IR+Lf×2 significantly differed from the corresponding controls by this parameter (Figure 6b).

On day 30, the leukocyte count in the experimental groups increased, while in the group IR it remained significantly lower than control ($p < 0.05$). On day 30 after irradiation, the mice in groups IR+Lf and IR+Lf×2 did not differ from the corresponding controls by this parameter. In addition, the number of leukocytes in the IR+Lf×2 group on day 30 was significantly higher than in the IR group ($p < 0.05$).

3.4.3. Differential Leukocyte Count

In the experimental groups, depletion of the lymphocyte reserve and an increase in the relative number of neutrophils were observed on day 3 after irradiation (Figure 7, left). The relative number of leukocytes in the IR+Lf×2 group was significantly higher than in the IR group ($p < 0.05$). The number of monocytes, eosinophils, and basophils in the irradiated mice did not differ from the control values.

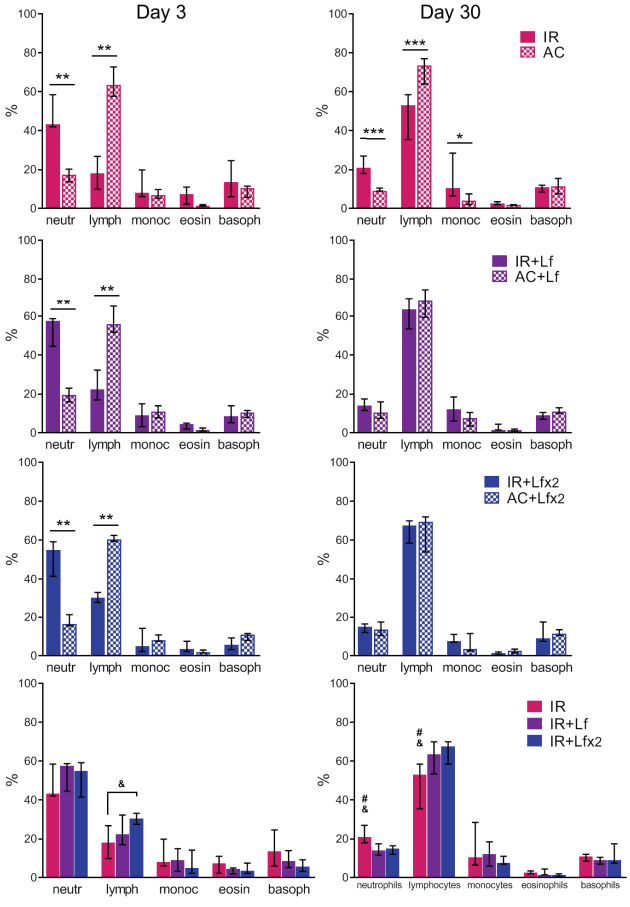


**Figure 7.** Effects of Lf on differential leukocyte count in the mice on days 3 (left) and 30 (right) after 7.5 Gy whole-body gamma irradiation. The relative content of blood cells (%). $n$ = 5–6 (day 3), $n$ = 7 (day 30) for each group. Data are presented as median ± interquartile range. * $p < 0.05$, ** $p < 0.01$, *** $p < 0.001$; $^{\#}$ $p < 0.05$ in comparison with the IR+Lf group; $^{\&}$ $p < 0.05$ in comparison with the IR+Lf×2 group.

In both experimental groups treated with hLf, the differential leukocyte count was restored by day 30 (Figure 7, right). The relative number of monocytes in the animals in the IR group on day 30 was higher than in the control ($p < 0.05$). In the IR group, a trend to normalization of the differential leukocyte count was observed, though the relative numbers of lymphocytes and neutrophils in this group significantly differed from the corresponding parameters in groups AC ($p < 0.001$), IR+Lf ($p < 0.05$) and IR+Lf×2 ($p < 0.05$) on day 30 after irradiation.

The absolute numbers of leukocytes of different types in the blood of mice on days 3 and 30 after irradiation are shown in Tables 1 and 2, respectively. A dose-dependent effect of hLf on the recovery of the lymphocyte and basophil number was revealed on day 30.

**Table 1.** Absolute number of leukocytes of different types in the blood of mice on day 3 after 7.5 Gy gamma irradiation ($\times 10^6$/mL), Mean ± SEM.

| Group | Day 3 | | | | |
|---|---|---|---|---|---|
| | **Neutrophils** | **Lymphocytes** | **Monocytes** | **Eosinophils** | **Basophils** |
| IR | 0.24 ± 0.02 * | 0.09 ± 0.02 * | 0.06 ± 0.02 * | 0.03 ± 0.01 * | 0.07 ± 0.02 * |
| IR+Lf | 0.41 ± 0.03 * | 0.19 ± 0.03 * | 0.07 ± 0.02 * | 0.03 ± 0.01 * | 0.07 ± 0.02 * |
| IR+Lf×2 | 0.39 ± 0.03 * | 0.23 ± 0.01 * | 0.06 ± 0.03 * | 0.03 ± 0.01 * | 0.05 ± 0.01 * |
| AC | 1.85 ± 0.20 | 7.02 ± 0.39 | 0.80 ± 0.11 | 0.17 ± 0.03 | 0.97 ± 0.15 |
| AC+Lf | 2.38 ± 0.21 | 7.07 ± 0.41 | 1.33 ± 0.20 | 0.21 ± 0.05 | 1.21 ± 0.05 |
| AC+Lf×2 | 2.01 ± 0.16 | 6.81 ± 0.11 | 1.00 ± 0.09 | 0.25 ± 0.04 | 1.12 ± 0.09 |

* $p < 0.01$ in comparison with the corresponding controls (Mann–Whitney U test).

**Table 2.** Absolute number of leukocytes of different types in the blood of mice on day 30 after 7.5 Gy gamma irradiation ($\times 10^6$/mL), Mean ± SEM.

| Group | Day 30 | | | | |
|---|---|---|---|---|---|
| | **Neutrophils** | **Lymphocytes** | **Monocytes** | **Eosinophils** | **Basophils** |
| IR | 1.22 ± 0.12 * | 2.54 ± 0.29 * | 0.91 ± 0.32 | 0.13 ± 0.02 | 0.69 ± 0.12 * |
| IR+Lf | 0.90 ± 0.10 | 4.05 ± 0.24 * | 0.84 ± 0.16 | 0.18 ± 0.04 | 0.56 ± 0.05 * |
| IR+Lf×2 | 1.34 ± 0.11 | 5.79 ± 0.36 | 0.87 ± 0.16 | 0.14 ± 0.03 | 1.00 ± 0.16 |
| AC | 0.97 ± 0.08 | 6.90 ± 0.23 | 0.43 ± 0.09 | 0.16 ± 0.01 | 1.07 ± 0.13 |
| AC+Lf | 1.03 ± 0.14 | 5.91 ± 0.27 | 0.70 ± 0.13 | 0.14 ± 0.02 | 1.00 ± 0.08 |
| AC+Lf×2 | 1.28 ± 0.17 | 6.06 ± 0.31 | 0.54 ± 0.16 | 0.22 ± 0.04 | 1.11 ± 0.05 |

* $p < 0.01$ in comparison with the corresponding controls (Mann–Whitney U test).

### *3.5. Effects of Lf on Changes in Subfraction Composition of the Blood Serum after Gamma Irradiation*

The dynamic light scattering (DLS) method based on the measurement of the spectral characteristics of light scattering allows for assessing particle size in biological fluids and their ratio [41]. The results of measurement are usually presented in the form of a histogram, where the abscissa corresponds to the size of particles (in nm) and the ordinate shows their contribution to the light scatter (in %).

In our experiment, the DLS spectra of mouse serum had a form of a three-modal distribution (Figures 8a, 9a and 10a). In these DLS spectra, three discrete zones were distinguished corresponding to small (<20.58 nm), medium (20.58–91.26 nm), and large (>91.26 nm) particles [30]; and the contribution of particles in each of these zones to the light scatter was estimated.

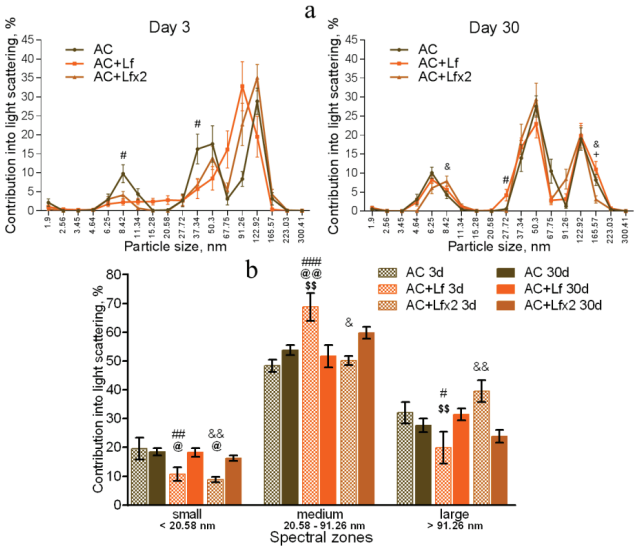


**Figure 8.** Changes in the DLS spectra of the blood serum from mice in the control groups on days 3 and 30 after sham-irradiation. $n$ = 5–6 (day 3), $n$ = 12–14 (day 30) for each group. Particle size distribution (**a**). $^{\#}$ $p < 0.05$—AC+Lf vs. AC, $^{\&}$ $p < 0.05$—AC+Lf×2 vs. AC, $^{+}$ $p < 0.05$—AC+Lf vs. AC+Lf×2. Particle distribution by spectral zones (**b**). $^{\#}$ $p < 0.05$, $^{\#\#}$ $p < 0.01$, $^{\#\#\#}$ $p < 0.001$, $^{\&}$ $p < 0.05$, $^{\&\&}$ $p < 0.01$ in comparison with the same group on day 30; $^{@}$ $p < 0.05$, $^{@@}$ $p < 0.01$ in comparison with the AC group on day 3; $^{\$\$}$ $p < 0.01$ in comparison with the AC+Lf×2 group on day 3.

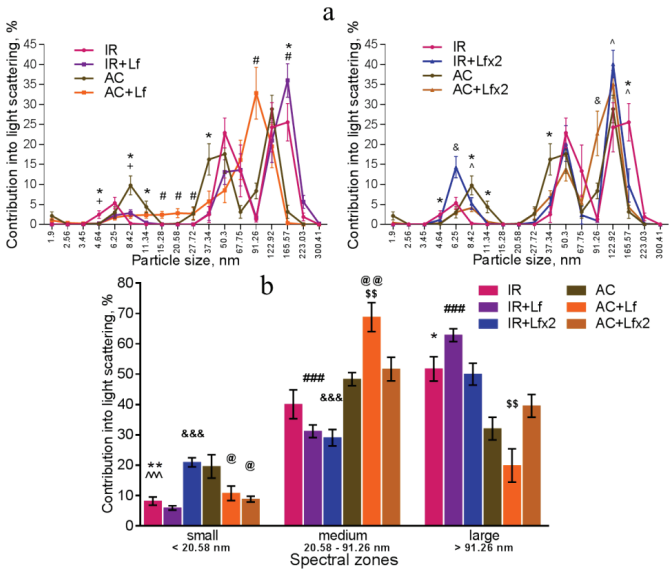


**Figure 9.** Changes in the DLS spectra of mouse blood serum on day 3 after 7.5 Gy whole-body gamma irradiation. Particle size distribution (**a**). Particles distribution by spectral zones (**b**). $n$ = 5–6 for each group. * $p < 0.05$, ** $p < 0.01$—IR vs. AC, $^{\#}$ $p < 0.05$, $^{\#\#\#}$ $p < 0.001$—IR+Lf vs. AC+Lf, $^{\&}$ $p < 0.05$, $^{\&\&\&}$ $p < 0.001$—IR+Lf×2 vs. AC+Lf×2, $^{+}$ $p < 0.05$—IR vs. IR+Lf, $^{\wedge}$ $p < 0.05$, $^{\wedge\wedge\wedge}$ $p < 0.001$—IR vs. IR+Lf×2, $^{@}$ $p < 0.05$, $^{@@}$ $p < 0.01$ in comparison with the AC group; $^{\$\$}$ $p < 0.01$ in comparison with the AC+Lf×2 group.

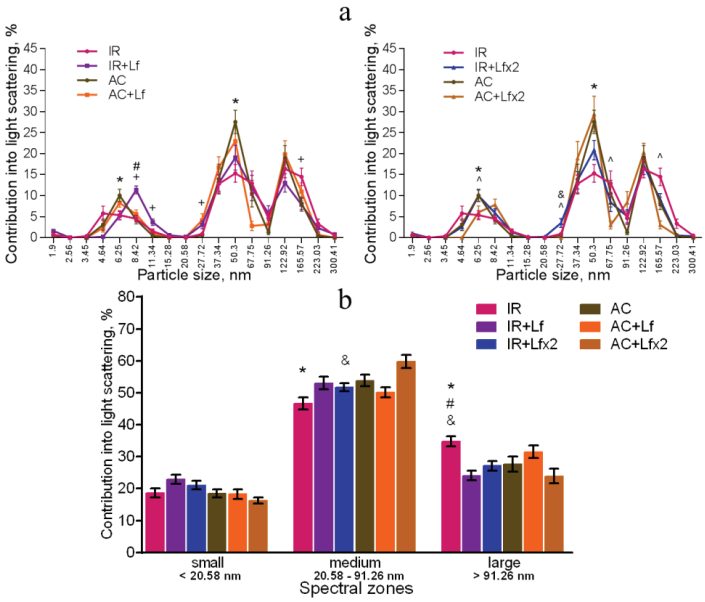


**Figure 10.** Effect of Lf on the changes in the DLS spectra of mouse blood serum on day 30 after 7.5 Gy gamma irradiation. Lf (i.p.; 4 mg/mouse) was administered immediately after irradiation/sham-irradiation (IR+Lf, IR+Lf×2, AC+Lf, AC+Lf×2) and 24 h after it (IR+Lf×2, AC+Lf×2). Particle size distribution (**a**). Particles distribution by spectral zones (**b**). $n$ = 9–15 for each group. * $p < 0.05$—IR vs. AC, $^{\#}$ $p < 0.05$—IR+Lf vs. AC+Lf, $^{\&}$ $p < 0.05$—IR+Lf×2 vs. AC+Lf×2, $^{+}$ $p < 0.05$—IR vs. IR+Lf, $^{\wedge}$ $p < 0.05$—IR vs. IR+Lf×2.

The DLS spectra of the serum from AC group mice remained constant throughout the experiment. On day 30, the distribution of serum particles did not differ from that on day 3 (Figure 8a,b). Single and repeated injections of hLf to the control animals (groups AC+Lf and AC+Lf×2) led to a significant decrease in the contribution of small particles to the light scatter on day 3 (Figure 8b); on day 30, this parameter returned to the level of the AC group.

In groups AC+Lf and AC+Lf×2, different dynamics of the distribution of medium and large particles was observed. A single injection of hLf increased the contribution of medium particles (67.75–91.26 nm) and decreased the contribution of large particles (122.92–165.57 nm) on day 3. In the AC+Lf group, only one peak corresponding to the large-molecular fraction was seen; the position of this peak was shifted towards medium particles (Figure 8a). The distribution of serum particles in this group was restored by day 30.

Repeated injections of hLf changed the effect of the first dose observed on day 3: contributions of medium and large particles in the group AC+Lf×2 did not differ from those in the AC group. On day 30, the contribution of large particles to the light scatter slightly decreased, and the contribution of medium particles increased, while both indicators did not differ from the corresponding indicators in the AC group. Thus, the DLS spectra of the serum in the control groups did not significantly differ from each other in all three spectral zones on day 30. In all three control groups, the maximum contribution to the light scatter on days 3 and 30 was made by medium particles (Figure 8b).

Irradiation induced significant changes in the DLS spectra. A common pattern of changes in the subfraction composition of the serum after irradiation was an increase in the contribution of large particles (>122.92 nm) [42]. This reaction was observed in all experimental groups on day 3 after irradiation (Figure 9a,b).

In the irradiated animals, a single injection of hLf was followed by an increase in the contribution of large particles (165.57–223.03 nm) and a decrease in the contribution of medium particles to the light scatter (Figure 9a left, b). Repeated injections of hLf led to a slight increase in the contribution of particles with a size of 122.92 nm and a significant increase in the contribution of small particles (6.25–8.42 nm) (Figure 9a right, b). In the sera of irradiated mice (groups IR, IR+Lf, IR+Lf×2) on day 3, the maximum contribution to the light scatter was made by large particles. Repeated injections of hLf (group IR+Lf×2) led to slight shifts towards the control DLS histograms, and a predominant peak corresponding to large particles (122.92 nm) appeared. The position of this peak and the contribution to the light scatter corresponded to the values in the control groups (Figure 9a right).

On day 30, the contribution of medium particles to the light scatter was significantly lower, and the contribution of large particles remained significantly higher in the IR group in comparison with the control (Figure 10a,b). In addition, the contribution of large particles in irradiated animals (IR group) was higher than in mice treated with hLf after irradiation (groups IR+Lf and IR+Lf×2). The position of the peak corresponding to small particles in the IR group was shifted to the left (4.64 nm) in comparison with the control (6.25 nm), and the contribution of medium particles (50.3 nm) to the light scatter in this experimental group was significantly lower than in the AC group (Figure 10a). Thus, the subfraction distribution of serum particles in irradiated animals (IR group) did not return to normal by the end of the experiment, which is consistent with previously published data [42].

On day 30, the DLS spectra of mouse sera in groups IR+Lf and IR+Lf×2 practically did not differ from those in the control groups (AC, AC+Lf, AC+Lf×2) in all three spectral zones by the position of peaks and their percentage contribution to the light scatter. At the same time, a decrease in the contribution of medium particles to the light scatter was found in the IR+Lf×2 group in comparison with the AC+Lf×2 group. The position of the small particle peak was slightly shifted towards medium particles (8.42 nm) in groups IR+Lf (Figure 10a left) and AC+Lf×2 (Figure 10a right).

### *3.6. Histological Analysis of Mouse Spleen and Liver after Total Gamma Irradiation*

Histological analysis of the spleen and liver was performed on days 3, 10, and 30 after irradiation. It is known that acute exposure to high doses of ionizing radiation causes significant morphological changes in these organs [43,44].

#### 3.6.1. Spleen

In animals in the control groups (AC, AC+Lf, AC+Lf×2), the spleen had smooth clear-cut contours at all studied terms (days 3, 10, and 30) (Figures 11 and 12). The main structural elements (white and red pulp, trabeculae) were clearly distinguished on sections. The lymphoid follicles in the white pulp were of medium size with clear boundaries and lighter germinal centers located in the central part. The vascular walls were not changed, moderate blood filling of the red pulp was observed. A small amount of hemosiderin was found in macrophages in the red pulp. The administration of hLf (groups AC+Lf, AC+Lf×2) did not induce histological changes in the organ.

Irradiation led to the accumulation of hemosiderin in the red pulp of the spleen in mice of all experimental groups (IR, IR+Lf, IR+Lf×2); the content of hemosiderin increased significantly from day 3 to day 10 and then decreased but remained above the control level on day 30 (Figure 11).

In mice in the group IR, the ratio of the white and red pulp changed as soon as on day 3 after irradiation; on day 10, reduction in follicles began, the boundaries of follicles disappeared (Figure 11). On day 30, the spleens of the IR group animals had no clear division in the white and red pulp, the follicles were reduced. Solitary giant cells of irregular shape morphologically similar to megakaryocytes were somewhere seen (Figure 12). The decrease in the total volume of the organ led to the appearance of folds on its surface. In both experimental groups, IR+Lf and IR+Lf×2, the structural organization of the spleen was preserved throughout the experiment (Figures 11 and 12).

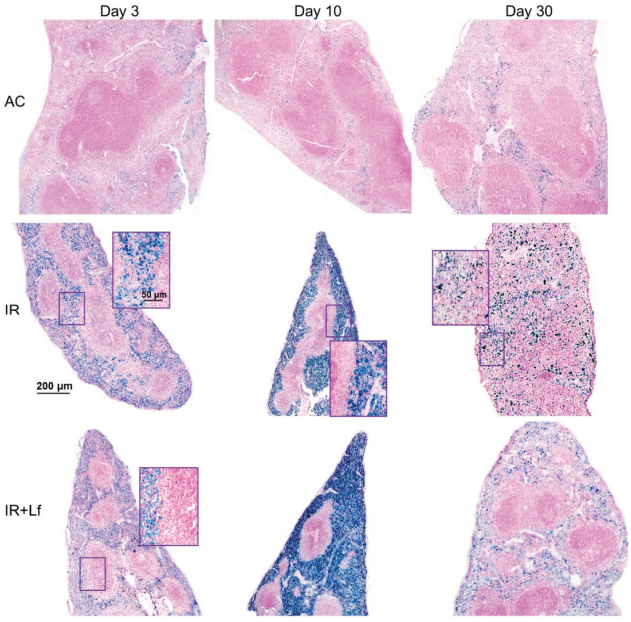


**Figure 11.** Protective effect of Lf on the structural organization of the spleen in the irradiated mice. Representative photomicrographs of spleen sections on days 3 (left column; $n$ = 5–6 for each group), 10 (middle column; $n$ = 5–6 for each group), and 30 (right column; $n$ = 7–10 for each group) days after 7.5 Gy whole-body gamma irradiation. Groups: AC (sham-irradiated), IR (irradiated), IR+Lf (Lf was administered immediately after irradiation; i.p.; 4 mg/mouse). Pearl's staining for iron (III). Scale bars = 200 μm and 50 μm.

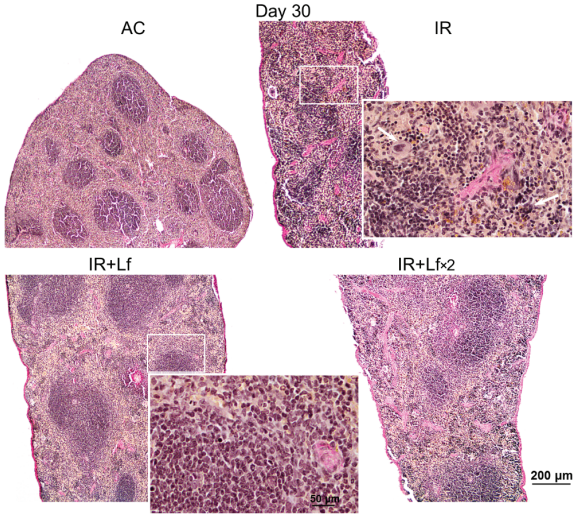


**Figure 12.** Protective effect of Lf on the structural organization of the spleen in the irradiated mice. Representative photomicrographs of spleen sections on day 30 after 7.5 Gy whole-body gamma irradiation. Groups: AC (sham-irradiated), IR (irradiated), IR+Lf (Lf was administered immediately after irradiation; i.p.; 4 mg/mouse), IR+Lf×2 (Lf was administered twice: immediately after irradiation and 24 h after it). Megakaryocytes (arrows). van Gieson staining. Scale bars = 200 μm and 50 μm.

3.6.2. Liver

In animals in the control groups (AC, AC+Lf, AC+Lf×2), the liver tissue had a cord structure, the cells had clear-cut boundaries at all terms of the experiment (days 3, 10, and 30). Hepatocytes had a polygonal shape, granular cytoplasm, and contained one or sometimes two round or elongated nuclei with clear-cut contours and chromatin lumps. The administration of hLf (groups AC+Lf, AC+Lf×2) did not change the liver structure.

Solitary clusters of mononuclear cells were observed in the liver parenchyma of the control mice (AC group). In the animals in groups AC+Lf and AC+Lf×2, these clusters were larger and more numerous as soon as day 3 (Figure 13 left); the same picture was also observed on day 10. On day 30, clusters of mononuclear cells in the animals of all the control groups (AC, AC+Lf, AC+Lf×2) had similar size (Figure 13 middle, right), but their number was higher in group AC+Lf×2.

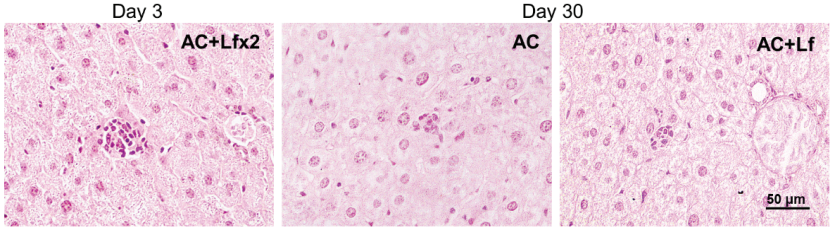


**Figure 13.** Solitary clusters of mononuclear cells in the liver parenchyma of control mice. Representative photomicrographs of liver sections on days 3 (left) and 30 (middle; right) after sham-irradiation. Groups: AC, AC+Lf, AC+Lf×2. Hematoxylin and Eosin staining. Scale bar = 50 µm.

Histological examination revealed degenerative changes of varying severity in the liver tissue of the IR group mice; they appeared as soon as day 3 after irradiation and persisted on days 10 and 30. Numerous abnormalities in the hepatocyte nuclei were revealed: vacuolization, pyknosis, chromatin condensation; appearance of trinuclear and an increase in the number of binuclear cells; vacuolar degeneration (Figure 14). The sinusoids were dilated, the central veins had increased diameter, the interlobular connective tissue was poorly developed. We also observed focal necrosis of hepatocytes and multiple mononuclear infiltrates in the periportal zone that developed against the background of circulatory disorders. The number of mitoses in hepatocytes was increased, spindle disturbances were somewhere seen. The maximum number of mitoses was observed on day 10 of the experiment. In the liver tissue, giant cells of irregular shape morphologically similar to megakaryocytes were somewhere seen (Figure 14b). The administration of hLf to the irradiated animals (groups IR+Lf and IR+Lf×2) had no effect on the severity of the above-mentioned reactive changes on days 3, 10, and 30.

Irradiation led to the disappearance of clusters of mononuclear cells in the liver parenchyma in animals of all the experimental groups (IR, IR+Lf, IR+Lf×2) on day 3 after the exposure. These structures started to recover on day 10 of the experiment (Figure 15 upper). By day 30, the number and size of these clusters were significantly higher in the irradiated mice treated with hLf (IR+Lf, IR+Lf×2) than in the IR group animals (Figure 15 bottom) and close to the corresponding control values (groups AC+Lf, AC+Lf×2, respectively).

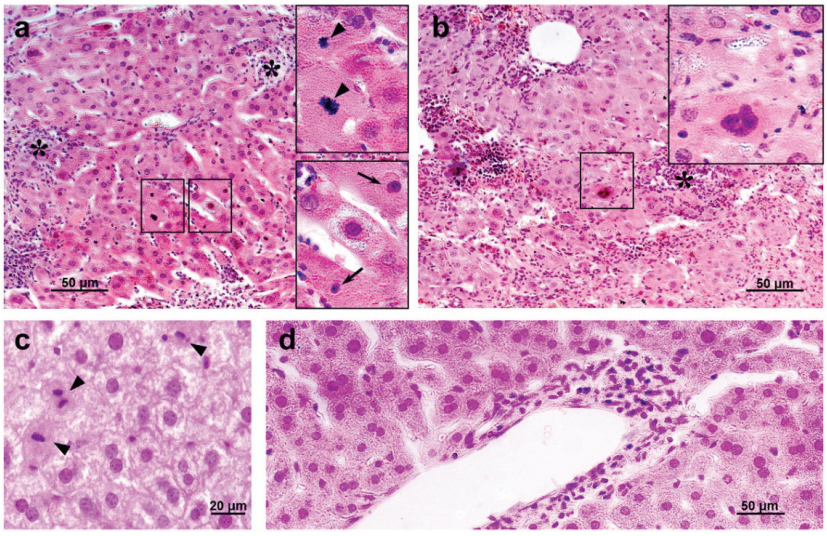


**Figure 14.** The histological changes in mouse liver after 7.5 Gy whole-body gamma irradiation: necrosis ((**a**,**b**), asterisks), pyknotic nuclei ((**a**), arrows), numerous mitoses ((**a**,**c**), arrow heads), vacuolar dystrophy of hepatocytes (**c**), mononuclear infiltration (**d**). Megakaryocyte (**b**). Representative photomicrographs of liver sections (groups: IR, IR+Lf, IR+Lf×2). Hematoxylin and Eosin staining. Scale bars = 50 μm and 20 μm.

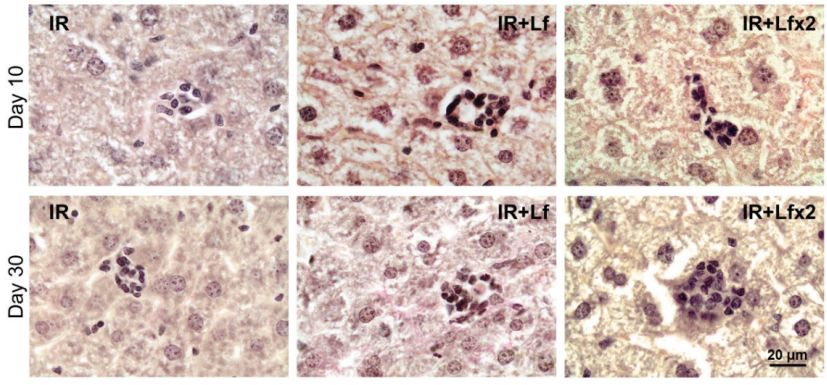


**Figure 15.** Lf promoted recovery of mononuclear cell clusters in the liver parenchyma of mice exposed to 7.5 Gy whole-body gamma irradiation. Representative photomicrographs of liver sections on days 10 (upper; $n$ = 5–6 for each group) and 30 (bottom; $n$ = 7–10 for each group) after irradiation. Groups: IR (irradiated), IR+Lf (Lf was administered immediately after irradiation; i.p.; 4 mg/mouse), IR+Lf×2 (Lf was administered twice: immediately after irradiation and 24 h after it). van Gieson staining. Scale bar = 20 μm.

## 4. Discussion

The exposure to high doses of ionizing radiation can induce significant body weight loss and lead to animal death. For instance, the body weight of mice exposed to whole-body gamma irradiation in a dose of 8 Gy decreased by 15% on day 14 [31], in a dose of 7.5 Gy—on day 9 [45]. It was shown that the mouse survival rate on day 30 was 20% [31,46] or 13% [47] after whole-body gamma irradiation in a dose of 8 Gy and 33% after X-ray

irradiation in a dose of 7 Gy [24], while the first deaths of animals were recorded on days 9, 5, 10, or 6, respectively.

In our study, a similar moderate body weight loss was observed in all experimental groups within the first 6 days after irradiation. In the IR group, the first wave of intensive animal deaths was observed on day 5; by day 9, 75% of mice remained alive (Figure 2a). A sharp decrease in mouse body weight in the IR group on days 9–12 was followed by a second wave of deaths on days 12–16 (survival rate 31%); after that, some more animals died. By day 30, the body weight in the IR group mice did not return to the initial level. Injections of hLf made it possible to prolong the lifespan of irradiated mice. The first death in both experimental groups treated with hLf occurred only on day 11. The weight loss in these groups continued up to day 6 and then the animals progressively gained weight from day 15 to the end of the experiment. By day 21, the body weight of animals in groups IR+Lf and IR+Lf×2 returned to the initial level and did not differ from the corresponding controls (Figure 3). It was shown that single and repeated administration of hLf increased the survival rate of irradiated mice from 28 to 78% during the experiment (Figure 2a) and had a compensatory effect on body weight loss in irradiated animals.

These findings agree with previous reports. On day 30 after whole-body X-ray irradiation in a dose of 6.8 Gy or 7 Gy, the survival rate of mice receiving a diet containing 0.1% bovine Lf for 7 days before and 30 days after irradiation was higher: 85 compared to 62% [4] or 50 compared to 33% [24], respectively. Bovine Lf intraperitoneally injected in mice (4 mg/animal) immediately after X-ray irradiation in a dose of 6.8 Gy increased the 30-day survival rate from 50 to 92% [4]. In guinea pigs subjected to whole-body gamma irradiation in a dose of 2.5 Gy, daily subcutaneous injections of Lf obtained by a biotechnological method from rabbit colostrum in doses of 65 or 300 μg/kg on days 1–14 after the exposure increased the 30-day survival rate from 54 to 86% or 100%, respectively [48]. It was reported that after X-ray irradiation in a dose of 7 Gy, the body weight of mice decreased until day 10 and then began to increase; in animals irradiated against the background of a diet containing 0.1% bovine Lf (7 days before and 30 days after), this indicator on days 20–30 was significantly higher [24]. One of the main causes of body weight loss in irradiated animals is radiation damage to the intestinal mucosa. In mice subjected to X-ray irradiation in a dose of 5 Gy, intraperitoneal injections of bovine Lf (2 or 4 mg/animal, 4 h before and once a day over 3 days after irradiation) alleviated damage to the small intestinal epithelium (assessed by the length of the intestinal villi and the ratio of villus length to crypt depth) [25].

X-ray irradiation in a dose of 10 Gy led to a decrease in motor activity and aggressive behavior in mice [49]. The suppression of motor and exploratory activity was observed in mice after gamma irradiation in a dose of 8 Gy, slow recovery of these parameters began only after 17 days [46]. Acute X-ray irradiation in a dose of 6 Gy reduced motor activity and coordination of movements and increased anxiety tested 72 h after the exposure [50].

Our findings obtained in behavioral experiments for the IR group are consistent with the results of the reports cited above. The administration of hLf had a compensatory effect on the radiation-induced decrease in the exploratory activity of mice (Figure 4b) and prevented a change in their behavior in terms of the time spent in the OF center (Figure 5). These data were obtained by us for the first time.

Changes in the composition of peripheral blood are one of the main criteria for assessing the effects of radiation on the body. Previous studies showed that mouse survival after sublethal irradiation depends on recovery of the hematopoiesis system [31,51]. It is also known that the decrease in leukocyte count correlates with the radiation dose [52].

Our experiments showed that irradiation caused a significant decrease in the hemoglobin level (Figure 6a) and leukocyte count (Figure 6b); the latter parameter did not return to normal by day 30. These findings are consistent with the reports of other researchers. After X-ray irradiation in doses of 6.8 and 7 Gy, the hemoglobin level in mice was significantly reduced on day 15 [4] and between days 7 and 29 [24], and after gamma irradiation in doses of 5 Gy—between days 7 and 14 [53]. The number of leukocytes in the

peripheral blood decreased significantly 3 days after whole-body gamma irradiation in a dose of 8 Gy and did not return to the normal range within 21 days [31]. After whole-body X-ray irradiation in a dose of 7 Gy, the leukocyte count rapidly decreased until day 14, then began to increase gradually but remained significantly below the control level on day 29 [24]. In our experiments, the animals of the experimental groups treated with hLf did not differ from the corresponding control groups by this parameter on day 30 after irradiation (Figure 6b). This is in line with the study of Feng et al., in which the number of peripheral blood leukocytes in animals treated with bovine Lf over 7 days before irradiation (7 Gy) and 30 days after it returned to normal by day 29 [24].

Each type of blood cell has its own relative radiosensitivity; and it is highest in lymphocytes [54]. The exposure to ionizing radiation in a high dose leads to the depletion in lymphocyte stores and an increase in the relative number of neutrophils [54]. This particular reaction was observed in all experimental groups on day 3 after irradiation (Figure 7, left; Table 1). Neither relative nor absolute numbers of different types of leukocytes in animals in the IR group recovered by day 30 (Figure 7, right, Table 2). This can indicate that a sufficient renewal of leukocytes after radiation damage was not achieved by this term. It was previously shown that the blood content of lymphocytes and neutrophils in mice was not restored on day 30 after whole-body gamma irradiation in a dose of 8 Gy [47].

In both experimental groups treated with hLf, the differential leukocyte count was restored by day 30 (Figure 13, right). Moreover, a dose-dependent effect of hLf on the recovery of the absolute number of lymphocytes and basophils was revealed on day 30 (Table 2). This is in line with previously published reports. It was shown that long-term administration of Lf (65 or 300 μg/kg, subcutaneously, daily from day 1 to day 14) obtained from rabbit colostrum promoted normalization of the cellular composition of the peripheral blood in guinea pigs after deep suppression of hematopoiesis induced by gamma irradiation in a dose of 2.5 Gy and increased the content of lymphocytes (day 12) and neutrophils (days 16 and 18) [48]. The data presented by us suggest that hLf had a compensatory effect on the radiation-induced decrease in the total number of leukocytes in the blood and changes in the differential leukocyte count in mice.

Irradiation induced significant shifts in the subfraction distribution of serum particles in mice (Figure 9), which is consistent with previously published data [42]. In our DLS study, we showed for the first time that administration of hLf promoted recovery of serum homeostasis parameters to their normal values by the end of the experiment (Figure 10).

It is known that acute exposure to high doses of ionizing radiation induces significant morphological changes in various organs [43,44]. In 3 and 6 weeks after single whole-body gamma irradiation in a dose of 7.5 Gy, fatty degeneration of hepatocytes, intensive fibrosis, increased number of cells with mitosis figures, increased number of apoptotic cells and cells with nuclear abnormalities, dilation of sinus vessels, focal necrosis of hepatocytes, and multiple mononuclear infiltrates in the liver parenchyma were observed [30,43]. In the spleen, the absence of clear-cut subdivision of the parenchyma into the white and red pulp, the absence of boundaries between the follicles, increased content of macrophages and leukocytes, and solitary megakaryocytes were observed in the same studies. The data obtained by us are consistent with these reports (Figures 11, 12 and 14). It should be noted that hLf had a protective effect on the structural organization of the spleen in irradiated animals (Figures 11 and 12).

In our study, hLf produced pleiotropic effects on mice subjected to gamma irradiation, which indicates that it affects several targets triggering various biochemical processes in the body of experimental animals. The mechanism underlying the effects of Lf in irradiated animals remains poorly understood. The positive effect of Lf can be related to its antioxidant properties [4,5]. The development of infectious diseases due to impaired immunity is a cause of postirradiation death. The radioprotective effect of Lf can be related to its immunomodulatory function [9]. It was shown that exogenous Lf suppresses the expression of some pro-inflammatory cytokines (tumor necrosis factor and interleukins −1β and −6) and activates the expression of anti-inflammatory factors (IL-4 and IL-10) [11,25].

In our study, hLf had a protective effect on the structural organization of the spleen, an immune system organ. It was previously shown that Lf alleviated damage to the small intestinal epithelium [25] and increased survival by stimulating recovery of the intestinal microflora and inhibiting the development and exacerbation of infectious diseases [4] in mice subjected to irradiation.

The degree of damage to the hematopoietic function positively correlates with the radiation dose [31]. The bone marrow, the primary hematopoietic tissue, is highly sensitive to irradiation. Even a low dose of ionizing radiation can disrupt the hematopoietic balance in the bone marrow, while the resulting anemia, bleeding, and infections have a serious impact on animal survival. Hematopoiesis is an intricate process regulated by numerous factors. Even though the bone marrow is the main organ of hematopoiesis, it can occur in many other tissues both during intrauterine development and after birth. In mice, the spleen remains a hematopoietic organ throughout their lives, although the intensity of splenic hematopoiesis is low. During adult life, the liver maintains hematopoietic stem cells, erythropoiesis and myelopoiesis also at a low level [55,56]. After birth, extramedullary hematopoiesis is observed in mammals (in particular, in rodents) when immune reactions occur at the periphery, as a normal reaction to infection and inflammation, as a response to bleeding, hemolysis, and radiation exposure. The liver and the spleen are the main organs that can become the sites of extramedullary hematopoiesis [57].

In contrast to rapid activation of erythropoiesis in the spleen in response to peripheral anemic stress, erythropoiesis in this organ after acute radiation stress can be restored only after recovery of the bone marrow. Within 6 days after acute whole-body gamma irradiation in a dose of 4 Gy, the basal level of erythropoiesis in the mouse spleen was absent despite rapid recovery of the bone marrow, while within 10 days, significant enlargement of the red pulp was noted and histological analysis confirmed extramedullary erythropoiesis in the spleen [58]. Extensive extramedullary hematopoiesis was observed in the mouse spleen on day 10 after gamma irradiation in a dose of 6 Gy [59]. In our experiment, the mice were exposed to whole-body gamma radiation in a higher dose (7.5 Gy). This can explain the increase in the number of leukocytes in the blood of animals in the experimental groups only on day 30 but not on day 10, as in the above-mentioned studies. To clarify the dynamics of recovery of animals by this parameter, the blood samples should be examined at intermediate terms between days 10 and 30 after irradiation. On day 30, megakaryocytes were identified in histological sections of the spleen (IR group) and liver (IR, IR+Lf, and IR+Lf×2 groups), which can be indicative of active extramedullary hematopoiesis in these organs [60]. It can also be assumed that solitary clusters of mononuclear cells in the liver parenchyma (Figure 15) represented the foci of extramedullary hematopoiesis that disappeared on day 3 and started to recover on day 10 after irradiation. Administration of hLf led to an increase in the number and size of these clusters.

In the normal liver, constantly changing metabolic and tissue remodeling activity combined with regular exposure to microbial products results in persistent regulated inflammation [61]. Activation of inflammatory processes is closely related to mechanisms that eliminate inflammation and promote tissue regeneration. In our experiments, the postirradiation death of lymphocytes led to the suppression of local immunity in the liver and the disappearance of mononuclear cell clusters in the liver parenchyma. The treatment with hLf stimulated local immunity by attracting immunocompetent cells to the liver tissue when their number in the circulation increased. It can be assumed that these clusters in the liver parenchyma consisted of immunocompetent cells.

The regenerative potential of the liver is determined by inflammatory mediators (e.g., IL-1α, TNFα, IL-6), growth factors (e.g., hepatocyte growth factor), and populations of immune cells located in the liver [62]. Kupffer cells play a central role in this regeneration through the release of IL-6 and TNFα, which promotes hepatocyte proliferation, while depletion of Kupffer cells prevents subsequent liver regeneration [63]. It is known that Lf can bind to macrophages and activate these cells [64,65]. In addition, in a mouse model of liver damage induced by acetaminophen (300 mg/kg, intraperitoneally), which directly

affects hepatocytes by inducing mitochondrial dysfunction, lipid peroxidation, oxidative stress, and DNA fragmentation, bovine Lf (50 mg/kg, intravenously) administered 1 and 4 h after acetaminophen injection prevented liver damage in animals [66]. Lf exhibited its hepatoprotective effect only in the presence of Kupffer cells. Researchers believe that Lf protects hepatocytes by stimulating production of protective mediators by Kupffer cells.

As noted above, Lf can perform many different functions depending on the cellular system it affects, due to the specificity of the receptors. It is known that exogenous Lf is mainly utilized in the liver [67,68]. Here, it can directly affect hepatocytes, endothelial cells, and Kupffer cells that express receptors to this protein (LRP1 and asialoglycoprotein receptor, intelectin-1, and CD14, respectively).

Of great interest is the ability of Lf to modulate a whole range of processes by changing the expression of genes encoding some regulatory and effector proteins [69,70]. In our previous studies, we found that in neuronal cultures under conditions of stimulation, Lf enhances the expression of transcription factor c-Fos, a marker of neuronal activity and long-term plasticity [71]. Lf binding to the surface of immune cells suggests that it can trigger cell reactions such as differentiation, activation, and proliferation [11]. It was shown that hLf accelerated differentiation of immature B and T cells and stimulated maturation of mouse splenic B cells [10,72]. Specific receptors nucleolin (expressed in B and T cells) and CD14 (expressed in monocytes) can be involved in triggering the cell response to stimulation by exogenous Lf. Since nucleolin is a multiligand protein acting as a shuttle between the cell surface and the nucleus [73,74], it can be expected that many biological functions of Lf are related to binding to this receptor.

## 5. Conclusions

The results of our study demonstrate positive pleiotropic effects of hLf on experimental animals subjected to sublethal irradiation that manifested in an increase in animal survival from 28% to 78%, a compensatory effect on radiation-induced body weight loss and the total number of leukocytes, changes in the differential leukocyte count, parameters of serum homeostasis, protective effect on the structural organization of the spleen, and normalization of the behavior of the irradiated mice. It should be noted that even a single injection of hLf immediately after irradiation was followed by the appearance of these positive effects. Our findings indicate the prospects for the development of radioprotective drugs based on this protein for the prevention and treatment of complications during occupational radiation exposure and for reducing side effects of radiation therapy.

**Author Contributions:** Conceptualization, M.Y.K. (Mikhail Yu. Karganov), I.Y.Z. and M.V.N.; methodology, M.Y.K. (Marina Yu. Kopaeva), I.B.A. and A.B.C.; investigation, M.Y.K. (Marina Yu. Kopaeva), A.B.C., I.B.A. and M.S.D.; formal analysis, visualization, writing—original draft, M.Y.K. (Marina Yu. Kopaeva); writing—review and editing, M.Y.K. (Mikhail Yu. Karganov), I.Y.Z. and A.B.C.; project administration, M.Y.K. (Mikhail Yu. Karganov) and I.Y.Z. All authors have read and agreed to the published version of the manuscript.

**Funding:** The work was carried out partially within the framework of the state task on the topic N°075-01248-22-00 "Fundamental interdisciplinary research in nano-, bio-, info- and cognitive technologies" and partially within the framework of the state task on the topic N°FGFU-2022-0010 "Assessment of the body's adaptive responses to the action of physicochemical and environmental factors" (dynamic light scattering analysis of blood serum; histological analysis).

**Institutional Review Board Statement:** The animal study protocol was approved by the Local Ethics Committee for Biomedical Research of the National Research Center "Kurchatov Institute" (protocol No. 1 of 13.02.2020) and the Ethics Committee of the Institute of General Pathology and Pathophysiology (protocol No. 4 of 07.10.2021).

**Informed Consent Statement:** Not applicable.

**Data Availability Statement:** Data are contained within the article.

**Acknowledgments:** This work was accomplished using the resource facilities at the National Research Center "Kurchatov Institute".

**Conflicts of Interest:** The authors declare no conflict of interest.

## References


1. Seed, T.M. Radiation protectants: Current status and future prospects. *Health Phys.* **2005**, *89*, 531–545. [CrossRef] [PubMed]
2. Reisz, J.A.; Bansal, N.; Qian, J.; Zhao, W.; Furdui, C.M. Effects of Ionizing Radiation on Biological Molecules—Mechanisms of Damage and Emerging Methods of Detection. *Antioxid. Redox Signal.* **2014**, *21*, 260–292. [CrossRef] [PubMed]
3. Weiss, J.F.; Landauer, M.R. Radioprotection by Antioxidantsa. *Ann. N. Y. Acad. Sci.* **2006**, *899*, 44–60. [CrossRef]
4. Nishimura, Y.; Homma-Takeda, S.; Kim, H.-S.; Kakuta, I. Radioprotection of Mice by Lactoferrin against Irradiation with Sublethal X-rays. *J. Radiat. Res.* **2014**, *55*, 277–282. [CrossRef]
5. Ogasawara, Y.; Imase, M.; Oda, H.; Wakabayashi, H.; Ishii, K. Lactoferrin Directly Scavenges Hydroxyl Radicals and Undergoes Oxidative Self-Degradation: A Possible Role in Protection against Oxidative DNA Damage. *Int. J. Mol. Sci.* **2014**, *15*, 1003–1013. [CrossRef]
6. Ward, P.P.; Conneely, O.M. Lactoferrin: Role in Iron Homeostasis and Host Defense against Microbial Infection. *BioMetals* **2004**, *17*, 203–208. [CrossRef]
7. Johnson, E.E.; Wessling-Resnick, M. Iron Metabolism and the Innate Immune Response to Infection. *Microbes Infect.* **2012**, *14*, 207–216. [CrossRef]
8. Orsi, N. The Antimicrobial Activity of Lactoferrin: Current Status and Perspectives. *BioMetals* **2004**, *17*, 189–196. [CrossRef]
9. García-Montoya, I.A.; Cendón, T.S.; Arévalo-Gallegos, S.; Rascón-Cruz, Q. Lactoferrin a Multiple Bioactive Protein: An Overview. *Biochim. Biophys. Acta BBA Gen. Subj.* **2012**, *1820*, 226–236. [CrossRef]
10. Suzuki, Y.A.; Lopez, V.; Lönnerdal, B. Lactoferrin: Mammalian Lactoferrin Receptors: Structure and Function. *Cell. Mol. Life Sci.* **2005**, *62*, 2560–2575. [CrossRef]
11. Legrand, D.; Elass, E.; Carpentier, M.; Mazurier, J. Interactions of Lactoferrin with Cells Involved in Immune FunctionThis Paper Is One of a Selection of Papers Published in This Special Issue, Entitled 7th International Conference on Lactoferrin: Structure, Function, and Applications, and Has Undergone the Journal's Usual Peer Review Process. *Biochem. Cell Biol.* **2006**, *84*, 282–290. [CrossRef]
12. Leveugle, B.; Mazurier, J.; Legrand, D.; Mazurier, C.; Montreuil, J.; Spik, G. Lactotransferrin Binding to Its Platelet Receptor Inhibits Platelet Aggregation. *Eur. J. Biochem.* **1993**, *213*, 1205–1211. [CrossRef] [PubMed]
13. Bennatt, D.J.; McAbee, D.D. Identification and Isolation of a 45-KDa Calcium-Dependent Lactoferrin Receptor from Rat Hepatocytes. *Biochemistry* **1997**, *36*, 8359–8366. [CrossRef]
14. Takayama, Y.; Takahashi, H.; Mizumachi, K.; Takezawa, T. Low Density Lipoprotein Receptor-Related Protein (LRP) Is Required for Lactoferrin-Enhanced Collagen Gel Contractile Activity of Human Fibroblasts. *J. Biol. Chem.* **2003**, *278*, 22112–22118. [CrossRef] [PubMed]
15. Grey, A.; Banovic, T.; Zhu, Q.; Watson, M.; Callon, K.; Palmano, K.; Ross, J.; Naot, D.; Reid, I.R.; Cornish, J. The Low-Density Lipoprotein Receptor-Related Protein 1 Is a Mitogenic Receptor for Lactoferrin in Osteoblastic Cells. *Mol. Endocrinol.* **2004**, *18*, 2268–2278. [CrossRef] [PubMed]
16. Fillebeen, C.; Descamps, L.; Dehouck, M.-P.; Fenart, L.; Benaïssa, M.; Spik, G.; Cecchelli, R.; Pierce, A. Receptor-Mediated Transcytosis of Lactoferrin through the Blood-Brain Barrier. *J. Biol. Chem.* **1999**, *274*, 7011–7017. [CrossRef]
17. Cutone, A.; Rosa, L.; Ianiro, G.; Lepanto, M.S.; Bonaccorsi di Patti, M.C.; Valenti, P.; Musci, G. Lactoferrin's Anti-Cancer Properties: Safety, Selectivity, and Wide Range of Action. *Biomolecules.* **2020**, *10*, 456. [CrossRef]
18. Yamauchi, K.; Toida, T.; Nishimura, S.; Nagano, E.; Kusuoka, O.; Teraguchi, S.; Hayasawa, H.; Shimamura, S.; Tomita, M. 13-Week oral repeated administration toxicity study of bovine lactoferrin in rats. *Food Chem. Toxicol.* **2000**, *38*, 503–512. [CrossRef]
19. Hayes, T.G.; Falchook, G.F.; Varadhachary, G.R.; Smith, D.P.; Davis, L.D.; Dhingra, H.M.; Hayes, B.P.; Varadhachary, A. Phase I trial of oral talactoferrin alfa in refractory solid tumors. *Investig. New Drugs.* **2006**, *24*, 233–240. [CrossRef]
20. Troost, F.J.; Saris, W.H.; Brummer, R.J. Recombinant human lactoferrin ingestion attenuates indomethacin-induced enteropathy in vivo in healthy volunteers. *Eur. J. Clin. Nutr.* **2003**, *57*, 1579–1585. [CrossRef]
21. Varadhachary, A.; Wolf, J.S.; Petrak, K.; O'Malley, B.W., Jr.; Spadaro, M.; Curcio, C.; Forni, G.; Pericle, F. Oral lactoferrin inhibits growth of established tumors and potentiates conventional chemotherapy. *Int. J. Cancer.* **2004**, *111*, 398–403. [CrossRef]
22. Yamaguchi, M.; Matsuura, M.; Kobayashi, K.; Sasaki, H.; Yajima, T.; Kuwata, T. Lactoferrin protects against development of hepatitis caused by sensitization of Kupffer cells by lipopolysaccharide. *Clin. Diagn. Lab. Immunol.* **2001**, *8*, 1234–1239. [CrossRef] [PubMed]
23. U.S. Food and Drug Administration. *GRN 000456 Cow's Milk-Derived Lactoferrin*; U.S. Food and Drug Administration's Office of Food Additive Safety: Silver Spring, MD, USA, 2016. Available online: https://www.fda.gov/media/153787/download (accessed on 9 September 2022).
24. Feng, L.; Li, J.; Qin, L.; Guo, D.; Ding, H.; Deng, D. Radioprotective Effect of Lactoferrin in Mice Exposed to Sublethal X-ray Irradiation. *Exp. Ther. Med.* **2018**, *16*, 3143–3148. [CrossRef] [PubMed]

25. Wei, Y.-L.; Xu, J.-Y.; Zhang, R.; Zhang, Z.; Zhao, L.; Qin, L.-Q. Effects of Lactoferrin on X-Ray-Induced Intestinal Injury in Balb/C Mice. *Appl. Radiat. Isot.* **2019**, *146*, 72–77. [CrossRef] [PubMed]
26. Caring for Animals Aiming for Better Science. Directive 2010/63/EU on the Protection of Animals Used for Scientific Purposes. Available online: https://ec.europa.eu/environment/chemicals/lab_animals/pdf/guidance/directive/en.pdf (accessed on 28 July 2022).
27. Faraji, N.; Zhang, Y.; Ray, A.K. Determination of Adsorption Isotherm Parameters for Minor Whey Proteins by Gradient Elution Preparative Liquid Chromatography. *J. Chromatogr. A* **2015**, *1412*, 67–74. [CrossRef] [PubMed]
28. Kumar, V.; Hassan, M.I.; Kashav, T.; Singh, T.P.; Yadav, S. Heparin-Binding Proteins of Human Seminal Plasma: Purification and Characterization. *Mol. Reprod. Dev.* **2008**, *75*, 1767–1774. [CrossRef] [PubMed]
29. Zhang, Y.; Lou, F.; Wu, W.; Dong, X.; Ren, J.; Shen, Q. Determination of Bovine Lactoferrin in Food by HPLC with a Heparin Affinity Column for Sample Preparation. *J. AOAC Int.* **2017**, *100*, 133–138. [CrossRef]
30. Alchinova, I.B.; Polyakova, M.V.; Yakovenko, E.N.; Medvedeva, Y.S.; Saburina, I.N.; Karganov, M.Y. Effect of Extracellular Vesicles Formed by Multipotent Mesenchymal Stromal Cells on Irradiated Animals. *Bul.l Exp. Biol. Med.* **2019**, *166*, 574–579. [CrossRef]
31. Liu, C.; Liu, J.; Hao, Y.; Gu, Y.; Yang, Z.; Li, H.; Li, R. 6,7,3′,4′-Tetrahydroxyisoflavone Improves the Survival of Whole-Body-Irradiated Mice via Restoration of Hematopoietic Function. *Int. J. Radiat. Biol.* **2017**, *93*, 793–802. [CrossRef]
32. Kopaeva, Y.; Cherepov, A.B.; Zarayskaya, I.Y.; Nesterenko, M.V. Transport of Human Lactoferrin into Mouse Brain: Administration Routes and Distribution. *Bull. Exp. Biol. Med.* **2019**, *167*, 561–567. [CrossRef]
33. Kopaeva, M.Y.; Cherepov, A.B.; Nesterenko, M.V.; Zarayskaya, I.Y. Pretreatment with Human Lactoferrin Had a Positive Effect on the Dynamics of Mouse Nigrostriatal System Recovery after Acute MPTP Exposure. *Biology* **2021**, *10*, 24. [CrossRef] [PubMed]
34. Kopaeva, M.Y.; Alchinova, I.B.; Nesterenko, M.V.; Cherepov, A.B.; Demorzhi, M.S.; Zarayskaya, I.Y.; Karganov, M.Y. Radioprotective effect of human lactoferrin against gamma-irradiation with sublethal dose. In *Proceedings of the RAD Conference Proceedings. 20–24 Aug. 2020, Herceg Novi, Montenegro*; RAD Centre: Nis, Serbia, 2020; Volume 4, pp. 45–49. [CrossRef]
35. Gould, T.D.; Dao, D.T.; Kovacsics, C.E. The Open Field Test. In *Mood and Anxiety Related Phenotypes in Mice*; Gould, T.D., Ed.; Neuromethods; Humana Press: Totowa, NJ, USA, 2009; Volume 42, pp. 1–20. ISBN 978-1-60761-302-2.
36. Karganov, M.; Alchinova, I.; Arkhipova, E.; Skalny, A.V. Laser Correlation Spectroscopy: Nutritional, Ecological and Toxic Aspects. In *Biophysics*; Misra, A.N., Ed.; InTech: London, UK, 2012; pp. 1–16. ISBN 978-953-51-0376-9.
37. Pearse, A.G.E. *Histochemistry, Theoretical and Applied*, 4th ed.; Churchill Livingstone: Edinburgh, UK; London, UK; New York, NY, USA, 1980; Volume 1.
38. Mandillo, S.; Tucci, V.; Hölter, S.M.; Meziane, H.; Al, M.; Kallnik, M.; Lad, H.V.; Nolan, P.M.; Ouagazzal, A.-M.; Coghill, E.L.; et al. Reliability, Robustness, and Reproducibility in Mouse Behavioral Phenotyping: A Cross-Laboratory Study. *Physiol. Genomics.* **2008**, *34*, 243–255. [CrossRef] [PubMed]
39. Carola, V.; D'Olimpio, F.; Brunamonti, E.; Mangia, F.; Renzi, P. Evaluation of the Elevated Plus-Maze and Open-Field Tests for the Assessment of Anxiety-Related Behaviour in Inbred Mice. *Behav. Brain Res.* **2002**, *134*, 49–57. [CrossRef]
40. Bella, L.M.; Fieri, I.; Tessaro, F.H.G.; Nolasco, E.L.; Nunes, F.P.B.; Ferreira, S.S.; Azevedo, C.B.; Martins, J.O. Vitamin D Modulates Hematological Parameters and Cell Migration into Peritoneal and Pulmonary Cavities in Alloxan-Diabetic Mice. *BioMed Res. Int.* **2017**, *2017*, 1–10. [CrossRef] [PubMed]
41. Kiselev, M.F.; Akleev, A.V.; Pashkov, I.A.; Klopov, N.V.; Noskin, V.A.; Noskin, L.A. Lazernaia korreliatsionnaia spektroskopiia plazmy krovi dlia diagnostiki postradiatsionnykh posledstviĭ [Laser correlation spectroscopy of blood plasma for diagnosis of postradiation sequels]. *Radiats Biol. Radioecol.* **1999**, *39*, 64–78. (In Russian) [PubMed]
42. Alchinova, I.B.; Arkhipova, E.N.; Medvedeva, Y.S.; Cherepov, A.B.; Karganov, M.Y. Dynamics of Changes in Physiological Parameters of Mice with Different Radiosensitivity after Acute γ-Irradiation. *Bull. Exp. Biol. Med.* **2014**, *157*, 190–193. [CrossRef]
43. Alchinova, I. The Complex of Tests for the Quantitative Evaluation of the Effects of Radiation on Laboratory Animals. *Am. J. Life Sci.* **2015**, *3*, 5. [CrossRef]
44. Wang, S.; Lee, K.; Hyun, J.; Lee, Y.; Kim, Y.; Jung, Y. Hedgehog Signaling Influences Gender-Specific Response of Liver to Radiation in Mice. *Hepatol. Int.* **2013**, *7*, 1065–1074. [CrossRef]
45. Zhou, X.; Wang, H.; Li, D.; Song, N.; Yang, F.; Xu, W. MST1/2 Inhibitor XMU-MP-1 Alleviates the Injury Induced by Ionizing Radiation in Haematopoietic and Intestinal System. *J. Cell. Mol. Med.* **2022**, *26*, 1621–1628. [CrossRef]
46. Der Meeren, A.V.; Lebaron-Jacobs, L. Behavioural Consequences of an 8 Gy Total Body Irradiation in Mice: Regulation by Interleukin-4. *Can. J. Physiol. Pharmacol.* **2001**, *79*, 140–143. [CrossRef]
47. Kumar, V.P.; Holmes-Hampton, G.P.; Biswas, S.; Stone, S.; Sharma, N.K.; Hritzo, B.; Guilfoyle, M.; Eichenbaum, G.; Guha, C.; Ghosh, S.P. Mitigation of Total Body Irradiation-Induced Mortality and Hematopoietic Injury of Mice by a Thrombopoietin Mimetic (JNJ-26366821). *Sci. Rep.* **2022**, *12*, 3485. [CrossRef] [PubMed]
48. Ivanov, A.A.; Ulanova, A.M.; Stavrakova, N.M.; Deshevoĭ, I.B.; Nasonova, T.A.; Koterov, A.N.; Gutsenko, K.K.; Mal'tsev, V.N. Antiradiation effects of Lactoferrin. *Radiatsionnaia Biol. Radioecol. Radiat. Biol. Radioecol.* **2009**, *49*, 456–461. (In Russian)
49. Maier, D.M.; Landauer, M.R.; Davis, H.D.; Walden, T.L. Effect of electron radiation on aggressive behavior, activity, and hemopoiesis in mice. *J Radiat Res.* **1989**, *30*, 255–265. [CrossRef] [PubMed]
50. Soares, F.A.; Dalla Corte, C.L.; Andrade, E.R.; Marina, R.; González, P.; Barrio, J.P. Purple grape juice as a protector against acute x-irradiation induced alterations on mobility, anxiety, and feeding behaviour in mice. *Nutr. Hosp.* **2014**, *29*, 812–821. [CrossRef] [PubMed]

51. Li, Z.-T.; Wang, L.-M.; Yi, L.-R.; Jia, C.; Bai, F.; Peng, R.-J.; Yu, Z.-Y.; Xiong, G.-L.; Xing, S.; Shan, Y.-J.; et al. Succinate Ester Derivative of δ-Tocopherol Enhances the Protective Effects against $^{60}$Co γ-Ray-Induced Hematopoietic Injury through Granulocyte Colony-Stimulating Factor Induction in Mice. *Sci. Rep.* **2017**, *7*, 40380. [CrossRef] [PubMed]
52. Erexson, G.L.; Kligerman, A.D.; Bryant, M.F.; Sontag, M.R.; Halperin, E.C. Induction of Micronuclei by X-Radiation in Human, Mouse and Rat Peripheral Blood Lymphocytes. *Mutat. Res. Mutagen. Relat. Subj.* **1991**, *253*, 193–198. [CrossRef]
53. Xue, J.; Du, R.; Ling, S.; Song, J.; Yuan, X.; Liu, C.; Sun, W.; Li, Y.; Zhong, G.; Wang, Y.; et al. Osteoblast Derived Exosomes Alleviate Radiation- Induced Hematopoietic Injury. *Front. Bioeng. Biotechnol.* **2022**, *10*, 850303. [CrossRef]
54. Christensen, D.M.; Iddins, C.J.; Sugarman, S.L. Ionizing Radiation Injuries and Illnesses. *Emerg. Med. Clin. North Am.* **2014**, *32*, 245–265. [CrossRef]
55. Wolber, F.M.; Leonard, E.; Michael, S.; Orschell-Traycoff, C.M.; Yoder, M.C.; Srour, E.F. Roles of Spleen and Liver in Development of the Murine Hematopoietic System. *Exp. Hematol.* **2002**, *30*, 1010–1019. [CrossRef]
56. Golden-Mason, L.; O'Farrelly, C. Having It All? Stem Cells, Haematopoiesis and Lymphopoiesis in Adult Human Liver. *Immunol. Cell Biol.* **2002**, *80*, 45–51. [CrossRef]
57. Kim, C. Homeostatic and Pathogenic Extramedullary Hematopoiesis. *J. Blood Med.* **2010**, *1*, 13–19. [CrossRef] [PubMed]
58. Peslak, S.A.; Wenger, J.; Bemis, J.C.; Kingsley, P.D.; Koniski, A.D.; McGrath, K.E.; Palis, J. EPO-Mediated Expansion of Late-Stage Erythroid Progenitors in the Bone Marrow Initiates Recovery from Sublethal Radiation Stress. *Blood* **2012**, *120*, 2501–2511. [CrossRef] [PubMed]
59. Masutani, M.; Nozaki, T.; Nakamoto, K.; Nakagama, H.; Suzuki, H.; Kusuoka, O.; Tsutsumi, M.; Sugimura, T. The Response of Parp Knockout Mice against DNA Damaging Agents. *Mutat. Res. Mutat. Res.* **2000**, *462*, 159–166. [CrossRef]
60. Volinsky, E.; Lazmi-Hailu, A.; Cohen, N.; Adani, B.; Faroja, M.; Grunewald, M.; Gorodetsky, R. Alleviation of Acute Radiation-Induced Bone Marrow Failure in Mice with Human Fetal Placental Stromal Cell Therapy. *Stem Cell Res. Ther.* **2020**, *11*, 337. [CrossRef] [PubMed]
61. Robinson, M.W.; Harmon, C.; O'Farrelly, C. Liver Immunology and Its Role in Inflammation and Homeostasis. *Cell. Mol. Immunol.* **2016**, *13*, 267–276. [CrossRef]
62. Michalopoulos, G.K.; Bhushan, B. Liver Regeneration: Biological and Pathological Mechanisms and Implications. *Nat. Rev. Gastroenterol. Hepatol.* **2021**, *18*, 40–55. [CrossRef]
63. Selzner, N.; Selzner, M.; Odermatt, B.; Tian, Y.; van Rooijen, N.; Clavien, P. ICAM-1 Triggers Liver Regeneration through Leukocyte Recruitment and Kupffer Cell–Dependent Release of TNF-α/IL-6 in Mice. *Gastroenterology* **2003**, *124*, 692–700. [CrossRef]
64. Birgens, H.S.; Hansen, N.E.; Karle, H.; Kristensen, L.Ø. Receptor Binding of Lactoferrin by Human Monocytes. *Br. J. Haematol.* **1983**, *54*, 383–391. [CrossRef]
65. Crouch, S.; Slater, K.; Fletcher, J. Regulation of Cytokine Release from Mononuclear Cells by the Iron- Binding Protein Lactoferrin. *Blood* **1992**, *80*, 235–240. [CrossRef]
66. Yin, H.; Cheng, L.; Holt, M.; Hail, N.; MacLaren, R.; Ju, C. Lactoferrin Protects against Acetaminophen-Induced Liver Injury in Mice. *Hepatology* **2010**, *51*, 1007–1016. [CrossRef]
67. Levay, P.F.; Viljoen, M. Lactoferrin: A general review. *Haematologica* **1995**, *80*, 252–267. [PubMed]
68. Adlerova, L.; Bartoskova, A.; Faldyna, M. Lactoferrin: A Review. *Vet. Med.* **2008**, *53*, 457–468. [CrossRef]
69. Chen, Y.; Zheng, Z.; Zhu, X.; Shi, Y.; Tian, D.; Zhao, F.; Liu, N.; Hüppi, P.S.; Troy, F.A.; Wang, B. Lactoferrin Promotes Early Neurodevelopment and Cognition in Postnatal Piglets by Upregulating the BDNF Signaling Pathway and Polysialylation. *Mol. Neurobiol.* **2015**, *52*, 256–269. [CrossRef] [PubMed]
70. Wang, B. Molecular Determinants of Milk Lactoferrin as a Bioactive Compound in Early Neurodevelopment and Cognition. *J. Pediatr.* **2016**, *173*, S29–S36. [CrossRef]
71. Kopaeva, M.Y.; Azieva, A.M.; Cherepov, A.B.; Nesterenko, M.V.; Zarayskaya, I.Y. Human lactoferrin enhances the expression of transcription factor c-Fos in neuronal cultures under stimulated conditions. *Nauchno-Prakt. Zhurnal Patogenez* **2021**, *19*, 74–78. [CrossRef]
72. Zimecki, M.; Mazurier, J. Human Lactoferrin Induces Phenotypic and Functional Changes in Murine Splenic B Cells. *Immunology* **1995**, *86*, 122–127.
73. Legrand, D.; Vigie, K.; Said, E.A.; Elass, E.; Masson, M.; Slomianny, M.-C.; Carpentier, M.; Briand, J.-P.; Mazurier, J.; Hovanessian, A.G. Surface Nucleolin Participates in Both the Binding and Endocytosis of Lactoferrin in Target Cells. *Eur. J. Biochem.* **2004**, *271*, 303–317. [CrossRef]
74. Jia, W.; Yao, Z.; Zhao, J.; Guan, Q.; Gao, L. New Perspectives of Physiological and Pathological Functions of Nucleolin (NCL). *Life Sci.* **2017**, *186*, 1–10. [CrossRef]

*antioxidants*

MDPI

*Article*

# Differential Radiomodulating Action of *Olea europaea* L. cv. Caiazzana Leaf Extract on Human Normal and Cancer Cells: A Joint Chemical and Radiobiological Approach

**Severina Pacifico [1,2,†], Pavel Bláha [2], Shadab Faramarzi [3], Francesca Fede [4], Katarina Michaličková [2,4], Simona Piccolella [1,2], Valerio Ricciardi [2] and Lorenzo Manti [2,4,*,†]**

[1] Dipartimento di Scienze e Tecnologie Ambientali Biologiche e Farmaceutiche, Università della Campania "Luigi Vanvitelli", 81100 Caserta, Italy
[2] Istituto Nazionale di Fisica Nucleare-Sezione di Napoli, 80126 Napoli, Italy
[3] Department of Plant Production and Genetics, Faculty of Agriculture, Razi University, Kermanshah 67149-67346, Iran
[4] Dipartimento di Fisica "E. Pancini", Università degli Studi di Napoli Federico II, 80126 Napoli, Italy
* Correspondence: lorenzo.manti@unina.it
† These authors contributed equally to this work.

**Abstract:** The identification of a natural compound with selectively differential radiomodulating activity would arguably represent a valuable asset in the striving quest for widening the therapeutic window in cancer radiotherapy (RT). To this end, we fully characterized the chemical profile of olive tree leaf polyphenols from the Caiazzana cultivar (OLC), autochthonous to the Campania region (Italy), by ultra-high-performance liquid chromatography–high-resolution mass spectrometry (UHPLC-HR-MS). Oleacein was the most abundant molecule in the OLC. Two normal and two cancer cells lines were X-ray-irradiated following 24-h treatment with the same concentration of the obtained crude extract and were assessed for their radioresponse in terms of micronucleus (MN) induction and, for one of the normal cell lines, of premature senescence (PS). Irradiation of pre-treated normal cells in the presence of the OLC reduced the frequency of radiation-induced MN and the onset of PS. Conversely, the genotoxic action of ionising radiation was exacerbated in cancer cells under the same experimental conditions. To our knowledge, this is the first report on the dual action of a polyphenol-rich olive leaf extract on radiation-induced damage. If further confirmed, these findings may be pre-clinically relevant and point to a substance that may potentially counteract cancer radioresistance while reducing RT-associated normal tissue toxicity.

**Keywords:** *Olea europaea* L. cv. Caiazzana; oleacein; ionising radiation; cancer; radiotherapy; normal tissue; radioprotection; radiosensitization; radiomodulation

**Citation:** Pacifico, S.; Bláha, P.; Faramarzi, S.; Fede, F.; Michaličková, K.; Piccolella, S.; Ricciardi, V.; Manti, L. Differential Radiomodulating Action of *Olea europaea* L. cv. Caiazzana Leaf Extract on Human Normal and Cancer Cells: A Joint Chemical and Radiobiological Approach. *Antioxidants* **2022**, *11*, 1603. https://doi.org/10.3390/antiox11081603

Academic Editors: Elena Obrador Pla and Alegria Montoro

Received: 5 July 2022
Accepted: 16 August 2022
Published: 19 August 2022



## 1. Introduction

External beam-based radiotherapy (RT) is one of the most effective strategies used to treat cancer by ionising radiation (IR). However, RT-associated acute and late-occurring normal tissue reactions may significantly affect a patient's life quality [1,2] and increase the risk of RT-induced secondary cancers [3,4], limiting de facto the curative dose that can be safely administered to the tumour [5]. Moreover, acquired [6,7] or intrinsic [8,9] cancer cell radioresistance correlates with failure in achieving tumour local control in RT, leading to poor prognosis, recurrence, and/or metastatization. Hence, although technological development and improvements in treatment planning systems have greatly increased accuracy in dose delivery to the tumour target and normal tissue sparing, late RT toxicity (e.g., fibrosis, cardiac events, cognitive impairment) remains a burden for adult cancer survivors and a long-term health hazard in paediatric patients [10]. In this context, the pursuit of radiomodulating agents is an actively sought strategy for widening the therapeutic index when administered in conjunction with IR as they can be a valuable aid if able

to increase normal tissue protection and/or IR tumouricidal effectiveness. In fact, the IR research program of the National Cancer Institute classified, according to administration timing, agents with IR-protective properties in three categories: (a) protection, (b) mitigation, and (c) therapeutic agents [11,12]. Analogously, many compounds that selectively modify cancer cell radioresponse have long been studied, such as halogenated pyrimidines and hypoxic cell sensitizers [13], in order to shift the tumour-control curve to lower doses without affecting the normal-tissue complication curve. This would result in an increase in tumour-control probability for a given level of adverse effects. However, currently available radioprotectors/radiosensitizers have several limitations, including high toxicity per se and costs. Moreover, for a radiomodulating compound to offer a practical gain in RT, it has to show a differential effect between normal tissues and tumours, as it would be of no avail to use a drug that increases the radiosensitivity of tumours and normal tissues alike, nor would it be therapeutically sound to mitigate radiation-induced damage in the two compartments to the same extent. The general failure of synthetic compounds to act as selective radioprotectors and the difficulty in finding effective radiosensitizers with low normal-tissue toxicity has driven researchers to focus on natural substances with radiomodulating potential and several botanicals, which could be less expensive than synthetic ones, have been screened for their radioprotective or radiosensitizing activity [14–16]. Plant-derived polyphenols in particular have gained considerable attention in the long-standing quest for intrinsically low-toxic radioprotecting/radiosensitizing drugs [12,17]. Free radical scavenging, anti-inflammation properties, facilitation of repair processes, and the regeneration of hematopoietic cells are the main mechanisms attributable to natural radioprotectors. In particular, since most of the IR damage arises from the interaction of IR-induced free radicals with biomolecules, natural substances, such as curcumin, chlorogenic acids, and different flavonoids could serve as radioprotectors, being able to combine with or prevent the formation of free radicals [18]. On the other hand, the anti-cancer activity of natural radiosensitizers has been correlated with their ability to inhibit the intracellular glutathione (GSH) redox buffering metabolism [19], to abrogate radiation-induced cell-cycle checkpoints that favour damage repair [20], to downregulate expression of genes implicated in cancer cell proliferation and resistance to radiation-induced apoptosis such as COX-2 [21], and to counteract tumour progression and migration by inhibiting pro-inflammation nuclear factor kappa B (NF-kB) transcription factor and disrupting a number of signalling pathways implicated in uncontrolled proliferation and enhanced angiogenesis, as reviewed in [16].

Moreover, the attractive double-edged potential of pure polyphenols or polyphenol-enriched extracts to act as both radiosensitizing and radioprotective agents would arguably hold pre-clinical significance and have a significant impact on the general prognosis of tumours refractory to radiation treatment [17,20,22]. *Olea europaea* L. leaf is a rich source of phenols and polyphenols, whose radioprotective potential was marginally investigated in pre-IR and post-IR treatments [23]. Anticlastogenic and antiradical activities of an olive leaf extract, constituted by 24.5% in oleuropein, 1.5% in hydroxytyrosol, and by almost 3% in flavone-7-glucosides and 1% in verbascoside, were found. On the other hand, a radiosensitizing action by pure oleuropein on cancer cell radioresponse was determined in nasopharyngeal carcinoma [24], highlighting the need of acquiring new insights in olive leaf radio-nutraceutical properties. Hence, taking into account the abundance and uniqueness of olive trees varieties in the Campania Region [25], we investigated the chemistry and radiobiology of the leaves of *O. europaea* cultivar "Caiazzana", autochthonous of the Campania region, whose name derives from Caiazzo, near Caserta [26]. To this purpose, an alcoholic olive leaf extract was prepared and chemically characterized by means of high-resolution tandem mass spectrometry; its antiradical capability was assessed through DPPH and ABTS tests. Furthermore, normal and cancer cell lines were exposed in vitro to graded doses of X-rays following treatment with, and in the presence of, a given concentration of the extract, whose effect on their radioresponse was evaluated in terms of the modulation of radiation-induced cyto-genotoxicity. Specifically, all cell lines were

assayed for the induction of DNA damage-associated micronuclei (MN) and one normal cell line for the onset of radiation-induced premature senescence (PS). At the investigated concentration, the extract consistently reduced MN frequency in normal cells but increased their occurrence in cancer cells after exposure to X-rays. Treatment with, and irradiation in the presence of, the extract also abated PS. To the best of our knowledge, this is the first time that the phytochemical profile and the radiomodulating activity of an olive leaf extract have been investigated, unveiling a specifically selective action that expressed itself, at the same extract concentration, as a concomitant mitigation or exacerbation of radiation-induced damage in normal and cancer cells, respectively.

## 2. Materials and Methods

### *2.1. Olive Leaf Collection and Extraction*

*O. europaea* L. cv. Caiazzana leaves were collected at the experimental site of CREA (Consiglio per la ricerca in agricoltura e l'analisi dell'economia agraria) in Casagiove (Caserta, Italy; 41°04′25.0″ N 14°18′59.4″ E, alt. 68 a.s.l) on 2 September 2020. Immediately after harvesting, they were transferred to the Food Chemistry Laboratory of University of Campania "Luigi Vanvitelli" and lyophilized by the FTS-System Flex-dryTM instrument (SP Scientific, Stone Ridge, NY, USA) for 48 h.

An aliquot of the plant matrix was pulverized by using a mortar and a pestle and then extracted through Ultrasound Assisted Maceration (UAM), using pure ethanol as extractant with a solid:liquid ratio equal to 1:10 (*w*:*v*). At the end each sonication cycle (3 in total; 30 min each), the sample was filtered and then dried by a rotary evaporator ((Heidolph Hei-VAP Advantage, Schwabach, Germany), obtaining a crude extract (OLC) with a yield of 27%.

### *2.2. Chemical Characterization: UV-Vis, HPLC-UV-DAD and UHPLC-ESI-TOF/MS*

OLC UV-Vis spectrum was recorded by double beam, dual chopper Cary 100 spectrophotometer (Agilent, Milano, Italia) in the range of 200–800 nm.

HPLC-UV-DAD analyses were carried out on a 1260 Infinity II LC System (Agilent, Santa Clara, CA, USA) equipped with an Agilent G711A quaternary pump and a WR G7115A diode array detector. The separation was achieved on Phenyl-Hexyl Column (150 × 2.0 mm i.d., 3.0 μm particle size, Phenomenex, Torrance, CA, USA), with a gradient of water (A) and acetonitrile (B), both with 0.1% formic acid. Starting with 95% A, a linear gradient was followed to 85% A in 10 min, which then decreased to 75.0% A at 25 min, to 60% A at 40 min, to 30% A at 50 min, and, finally, to 5% A at 60 min. The mobile phase composition was maintained at 5% A for another 2.0 min, then returned to the starting conditions and was allowed to re-equilibrate for 2 min. The flow rate was set at 0.3 mL $min^{-1}$, and the injection volume was 5.0 μL. UV detection was set at five different wavelengths (220, 280, 320, 340, and 360 nm).

UHPLC-HR-MS techniques were applied for a detailed profiling of OLC chemical constituents. To this purpose, a NEXERA UHPLC system (Shimadzu, Tokyo, Japan) was used with a Luna® Omega C-18 column (1.6 μm particle size, 50 × 2.1 mm, Phenomenex). The separation took advantage of a linear gradient of water (A) and acetonitrile (B), both with 0.1% formic acid, as follows: 0–5 min, 5→15% B; 5–12.5 min, 15→25% B; 12.5–20 min, 25→40% B; 20–25 min, 40→70% B; held at 75% B for other 2 min. The %B reached 95% for a column clean-up step and then returned to the starting conditions re-equilibrated for 1 min. The total analysis time was 27 min, the flow rate was 0.5 mL/min, and the injection volume was 2.0 μL. HR-MS and MS/MS spectra were recorded in negative electrospray ionization (ESI) mode, using the AB SCIEX Triple TOF® 4600 (AB Sciex, Concord, ON, Canada). The APCI probe was used for automated mass calibration in all scan functions using the Calibrant Delivery System (CDS). Non-targeted approach was developed, combining TOF-MS and MS/MS with Information Dependent Acquisition (IDA), consisting of a full scan TOF survey (accumulation time 250 ms, 100–1000 Da) and eight IDA MS/MS scans (accumulation time 100 ms, 80–800 Da). Other source and analyser parameters were the

following: curtain gas (CUR) 35 psi, nebulizer gas (GS 1) 60 psi, heated gas (GS 2) 60 psi, ion spray voltage (ISVF) 4.5 kV, interface heater temperature (TEM) 600 °C, declustering potential (DP) −70 V, collision Energy (CE) −35 V, collision energy spread (CES) 10 V. The instrument was controlled by Analyst® TF 1.7 software, while data processing was carried out using PeakView® software version 2.2.

### *2.3. Radical Scavenging Capacity: DPPH and ABTS Tests*

OLC was tested at 50, 25, 12.5, 6.25, and 3.125 μg/mL (final concentrations) vs. ABTS [2,2′-azinobis-(3-ethylbenzothiazolin-6-sulfonic acid)] radical cation and 2,2-diphenyl-1-picrylhydrazyl (DPPH) radical [27]. Trolox (4, 8, 16, 32 μM) was used as standard, and all recorded activities were compared to a blank sample, arranged in parallel. $ABTS^{\bullet+}$ was produced by mixing (2,2′-azinobis-(3-ethylbenzothiazolin-6-sulfonic acid); 7 mM) and potassium persulfate ($K_2S_2O_8$; 2.45 mM) in the dark for 12 h. $ABTS^{\bullet+}$ was thus diluted with PBS (pH 7.4) to reach an absorbance of 0.7 at 734 nm and was allowed to react with the OLC concentrations. After 6 min, the absorbance was measured using a Wallac Victor3 spectrophotometer in reference to a blank. $DPPH^{\bullet}$ methanol solution ($9.4 \times 10^{-5}$ M), reacting with OLC at different concentrations, served to assess $DPPH^{\bullet}$ scavenging activity. The mixtures were stirred for 15 min, and the absorption was read at 517 nm by Wallac Victor3 spectrophotometer in reference to a blank. The results were expressed in terms of the percentage reduction in the initial radicals' adsorption by tested samples. Trolox (4, 8, 16, 32 μM) was used as positive standard. All data were expressed as mean ± standard deviation (SD).

### *2.4. Fe (III) Reducing Power*

The ability of OLC (at 50, 25, 12.5, 6.25, and 3.125 μg/mL final concentrations) to reduce the $Fe^{3+}$ using a ferricyanide FRAP assay was evaluated according to PFRAP procedure [27]. The absorbance was measured at 700 nm. The increase in absorbance with reference to the blank was considered. Trolox (4, 8, 16, 32 μM) was used as positive standard. All data were expressed as mean ± standard deviation (SD).

### *2.5. Cell Cultures: Maintenance and Preparation*

All cell lines employed in this work are commercially available and were either purchased or received as a gift. Human Umbilical Vein Endothelial Cells (HUVECs) were purchased from Lonza Ltd. (Basel, Switzerland) as cryopreserved ampules of pooled cells from donors at passage 1. After thawing, they were grown in EGM-2 Bullet Kit™ and routinely sub-cultured at a density between 2000 and 4000 cells/$cm^2$ as per manufacturer's instructions. All experiments were performed with cells between passage 3 and 5. The spontaneously immortalized, non-transformed human mammary epithelial MCF-10A cells and the primary prostate adenocarcinoma DU145 cells were kindly donated by Dr. P. Chaudhary (CCRCB, Queens University, Belfast, UK). As described in detail by Debnath et al., two DMEM/F12-based media were necessary for MCF-10A cells: one for optimal growth, enriched with 5% horse serum, Endothelial Growth Factor (20 ng/mL), hydrocortisone (0.5 mg/mL), insulin (10 mg/mL), and cholera toxin (100 ng/mL); the other, devoid of all supplements but rich in horse serum (20%), to be used only for the quenching of trypsin during routine sub-cultivation and cell counting dilutions. DU145 cells were grown in RPMI medium, complemented with 10% foetal bovine serum (FBS) and 1% of L-glutamine (L-Gln). Finally, human pancreatic epithelioid carcinoma PANC-1 cells (a gift from Dr. A. Facoetti, CNAO, Pavia, Italy) were cultured in a high-glucose (4.5 g/l) DMEM medium and supplemented with FBS and L-Gln as mentioned above. Penicillin/streptomycin was added (1%) to media for all cell lines except HUVECs. Cell lines were grown in standard tissue culture flasks maintained at 37 °C in a humidified atmosphere (95% air, 5% $CO_2$).

To assess the radiomodulating properties of OLC, the water-soluble extract was added at a final concentration of 12.5 μL/mL to exponentially growing cells seeded at appropriate densities in T12.5 or T25 tissue culture flasks for senescence time-course experiments

(around $1.5 \times 10^4$ and $5 \times 10^4$ cells/flask, respectively) or in Nunc™ (Thermo Fisher Scientific, Waltham, MA, USA) slide flasks (around $2 \times 10^4$ cells/slide flask) for DNA damage evaluation by the CBMN assay. Cells were thus incubated for 24 h prior to exposure to radiation. Cells were irradiated in OLC-containing media. Immediately after irradiation, the medium was discarded, cells were rinsed thoroughly in Phosphate Buffer Saline (PBS) solution, and the samples were processed for evaluation of radiation-induced PS or MN formation, as detailed below. Non-OLC-treated cells were used as controls and subjected to the same experimental conditions.

### *2.6. Cell Irradiation*

In all experiments, cells were exposed to 1-mm Cu-filtered X-rays generated by a radiogen tube (STABILIPAN, Siemens, Berlin, Germany) at 250 kVp at a dose rate of about 1.36 Gy/min at the Radiation Biophysics Laboratory, Physics Department, University of Naples Federico II. Dose uniformity was within 5% in a 15-cm-long square field as ensured by regular dosimetry performed with an Accu-Pro™ Radcal® ionization chamber.

### *2.7. β-Galactosidase Assay for Quantification of Cellular Senescence in HUVECs*

The occurrence of radiation-induced PS was assessed by the detection of senescence-associated β-galactosidase activity at pH 6.0 using a commercially available kit (Sigma-Aldrich, Merck KGaA, Darmstadt, Germany). After irradiation, HUVECs were placed back into the incubator (after eventually removing the extract-containing medium, as mentioned in Section 2.3): those seeded in T12.5 flasks were assayed after 24 or 48 h, while those irradiated in T25 flasks were left to grow for one week and then trypsinized and re-seeded in T12.5 tissue culture flasks. When attached after a few hours, they were processed as their early time counterparts. For all time points, glutaraldehyde-fixed cells were incubated in the β-gal-specific solution at 37 °C in the absence of $CO_2$ overnight. Senescence-specific affinity for β-gal conferred a distinct greenish colour to cells when observed under bright field microscopy using a 10× magnification. The fraction of senescent cells was thus determined by the counting of random fields. Between 750 and 1000 cells were scored per time, dose, and treatment (OLC vs. non-OLC) conditions. The use of T12.5 flasks was the optimal compromise between having enough cells to analyze and economize the kit's reagents.

### *2.8. Determination of Radiation-Induced DNA Damage*

The genotoxic action of X-rays was evaluated by means of the Cytokines-Block MicroNucleus (CBMN) assay in all the cell lines. After irradiation, cells seeded onto slide flasks were treated for 24 h with 2.0 μg/mL of the actin-disrupting agent Cythocalasin B (CytB) that inhibits cytoplasmic furrow cleavage in dividing cells, thereby arresting them at the binucleated (BN) stage. In the CBMN assay, therefore, DNA damage manifests itself in the form of round DNA portions that failed to be incorporated in either of the daughter nuclei and is quantified by the occurrence of such micronuclei (MN) satisfying well-established morphological criteria in BN cells. After 24 h, cells were washed by PBS and then fixed by slowly adding a freshly prepared 4:1 Carnoy's solution (Methanol; Acetic acid) that had been kept at −20 °C for at least 20 min. Fixation was also performed at −20 °C for 20 min before removing the fixative and breaking apart the slide flasks. These were air-dried for 24 h and then stained by 12–14 μL of 250 ng/mL DAPI/Antifade. Scoring was performed by an epi-fluorescence Zeiss Axioplan 2 imaging microscope with a 40× magnification objective. The frequency of MN/cell was determined according to the formula:

$$\frac{MN_1 + 2 \times MN_2 + 3 \times MN_3 + 4 \times MN_4}{BN} \quad (1)$$

where $MN_n$ is the number of BN cells with n MN and BN is the total number of BN cells scored. BN cells carrying more than 5 MN were extremely rare and mostly accompanied by aberrant cell morphology and were hence not included in the analysis. Between 500 and

1500 BN cells were scored according to the radiation dose for statistical robustness. Statistical significance was determined at the 95% confidence level using a two-sample *t*-test using SYSTAT (version 13.1, USA).

## 3. Results

A crude extract, hereinafter referred to as OLC, from *O. europaea* L. cv. Caiazzana leaves, was metabolically profiled for its polyphenolic content by an array of techniques aimed at compound separation and structural characterization. The putative ability by the thus profiled polyphenol-rich OLC, to afford in vitro normal tissue radioprotection and to increase tumour cell radiosensitivity, was subsequently tested by measuring its modulation of X-ray-induced cytogenetic damage in four cell lines, namely two of cancer and two of non-cancer origin.

### *3.1. Chemical Profiling of Olive Tree Leaf Polyphenols*

The experimental workflow applied in order to investigate the radiomodulating activity of olive leaf polyphenols for their radionutraceutical exploitation cannot disregard a rational and systematic chemical approach. Thus, with the aim to maximize the recovery of polyphenol compounds, leaves from *O. europaea* L. cv. Caiazzana (Figure 1A) were pulverized and underwent Ultrasound-Assisted Maceration (UAM) in ethanol. The alcoholic extract obtained was firstly evaluated by Ultraviolet-Visible (UV-Vis) spectroscopy, highlighting that, beyond typical phenol secoiridoids' absorptions, bands relative to flavonoids, carotenoids (415 and 480 nm), and chlorophylls (670 nm) occurred. The High-Performance Liquid Chromatography–Ultraviolet (HPLC-UV) chromatograms, reported in Figure 1B, showed a main peak at 280 nm, whose Ultraviolet Diode Array Detection (UV-DAD) spectrum was in accordance with that of phenolic secoiridoids, with three main peaks detected at <210, 230, and 282 nm [28]. Furthermore, the HPLC-UV profile at 360 nm confirmed the presence of flavonoids, as this absorption could be due to B ring band I [29].

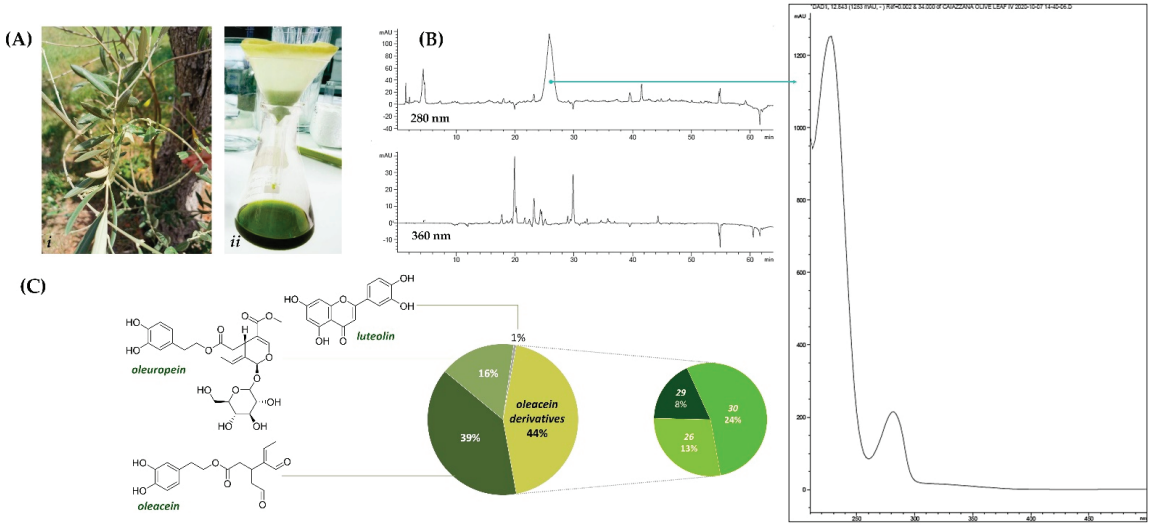


**Figure 1.** (**A**) Leaves of *O. europaea* cv. Caiazzana (i) and OLC extract therefrom (ii); (**B**) HPLC-UV chromatograms with the UV-DAD spectrum of a secoiridoid compound; (**C**) calculated amounts (%) of quantified compounds in OLC.

Based on this preliminary experimental evidence, a deep investigation of the chemical composition and relative content was carried out by means of Ultra High Performance Liquid Chromatography High Resolution Mass Spectrometry (UHPLC-HR-MS) techniques.

In Table 1, all TOF-MS and TOF-MS/MS data were listed, while the Total Ion Current (TIC) and base peak chromatogram (BPC) are depicted in Figure S1, whereas quantitation data are depicted in Figure 1C.

Beyond an hexitol (**1**), likely mannitol, previously detected in water-stressed *O. europaea* leaves [30], and 12-hydroxyjasmonate sulfate (**5**), also commonly associated to plant stress and defense responses [31], quinic acid (**2**) [32], hydroxytyrosol (**3**), and its hexoside (**4**), were putatively identified. TOF-MS/MS spectra of both compounds **3** and **4** showed the fragment ion at $m/z$ 123.046, likely formed by the loss of formaldehyde (Figure S2). Phenethyl primeveroside (**7**) and the ethyl-glucopyranosyloxy-oxopropylcyclohexaneacetic (**8**) were also identified [33]. Indeed, most of the OLC compounds consisted in phenolic secoiridoids. Oleuropein (**22**), which is one of the most representative constituents of olive tree organs and related products, by-products, and wastes [34], was detected at 10.183 min retention time. Although it was not the most abundant compound, it accounted for 16% of OLC metabolic composition (Figure 1C). The TOF-MS/MS experiment of oleuropein (**22**) allowed us to gain an insight into diagnostic fragment ions for its ready identification. In fact, the deprotonated molecular ion at $m/z$ 539.1784 underwent neutral loss of the dehydrated hydroxytyrosol to provide the ion at $m/z$ 403.1240 (elenolic acid glucoside). The latter, in turn, could lose the hexose unit to achieve the ion at $m/z$ 223.0605 (elenolic acid). Furthermore, the deprotonated molecular ion underwent sugar loss, providing the ion at $m/z$ 377.1237, which supplied the fragment at $m/z$ 307.0839 following the secoiridoid moiety cleavage. Other important peaks in the TOF-MS/MS spectrum were rationalized, and their chemical structures are reported in Figure 2A.

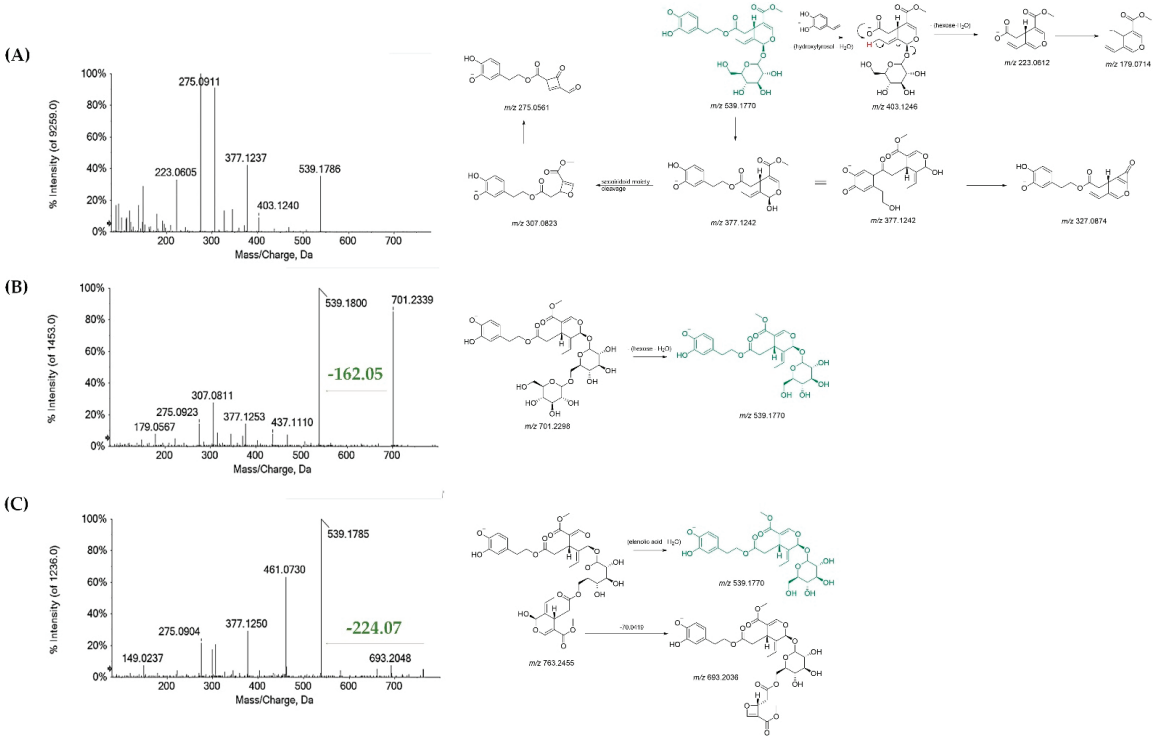


**Figure 2.** Tandem mass spectra and relative proposed comprehensive fragmentation pattern of (**A**) oleuropein (**22**); (**B**) oleuropein hexoside (**18**); (**C**) elenoyl oleuropein (**31**). Theoretical $m/z$ values are reported under each structure.

**Table 1.** TOF-MS and MS/MS data of compounds tentatively identified in OLC extract. (RDB = Ring and Double Bond. Base peaks are reported in bold).

| Peak n. | RT (min) | Tentative Assignment | Formula | [M-H]$^-$ calc. (*m*/*z*) | [M-H]$^-$ Found (*m*/*z*) | Error (ppm) | RDB | HR-MS/MS Fragment Ions (*m*/*z*) (Base Peaks in Bold) |
|---|---|---|---|---|---|---|---|---|
| **1** | 0.316 | Hexitol | $C_6H_{14}O_6$ | 181.0718 | 181.0719 | 0.8 | 0 | 181.0722; 163.0636; 136.8708; 119.0352; 113.0240; **101.0241**; 89.0245 |
| **2** | 0.326 | Quinic acid | $C_7H_{12}O_6$ | 191.0561 | 191.0565 | 2.0 | 2 | **191.0558**; 173.0447; 127.0403; 109.0293; 93.0348 |
| **3** | 1.651 | Hydroxytyrosol | $C_8H_{10}O_3$ | 153.0557 | 153.0557 | 0.0 | 4 | 153.0561; **123.0454** |
| **4** | 1.835 | Hydroxytyrosol hexoside | $C_{14}H_{20}O_8$ | 315.1085 | 315.1084 | −0.4 | 5 | 315.1081; 153.0556; **135.0454**; 123.0453; 119.0352; 119.0352; 113.0251; 101.0252; 89.0254 |
| **5** | 3.375 | 12-hydroxyjasmonate sulfate | $C_{12}H_{18}O_7S$ | 305.0700 | 305.0702 | 0.5 | 4 | 305.0705; 225.1135; 174.9560; 147.0816; 130.9665; **96.9606** |
| **6** | 4.509 | Unknown | $C_{16}H_{26}O_{10}$ | 377.1453 | 377.1454 | 0.2 | 4 | 377.1455; 197.0824; **153.0925** |
| **7** | 5.329 | Phenethyl primeveroside | $C_{19}H_{28}O_{10}$ | 415.1610 | 415.1609 | −0.2 | 6 | 191.0557; 179.0566; 161.0455; 149.0458; 131.0359; 119.0356; 113.0245; 101.0252; **89.0250** |
| **8** | 6.377 | 2-(2-ethyl-3-hydroxy-6-propionylcyclohexyl) acetic acid glucoside | $C_{19}H_{32}O_9$ | 403.1974 | 403.1977 | 0.9 | 4 | 403.1992; 241.1448; **223.1346**; 161.0463; 119.0355; 113.0252; 101.0253; 89.0247 |
| **9** | 6.482 | Luteolin di-hexoside | $C_{27}H_{30}O_6$ | 609.1461 | 609.1463 | 0.3 | 13 | 609.1486; **447.0949**; 285.0403 |
| **10** | 7.789 | Rutin | $C_{27}H_{30}O_6$ | 609.1461 | 609.1472 | 1.8 | 13 | **609.1482**; 301.0347; 300.0271; 271.0229 |
| **11** | 8.058 | Luteolin hexoside 1 | $C_{21}H_{20}O_{11}$ | 447.0933 | 447.0935 | 0.5 | 12 | 447.0945; **285.0405**;284.0329 |
| **12** | 8.063 | Verbascoside | $C_{29}H_{36}O_{15}$ | 623.1981 | 623.1983 | 0.2 | 12 | **623.1999**; 461.1665; 161.0243 |
| **13** | 8.958 | Oleacein | $C_{17}H_{20}O_6$ | 319.1187 | 319.1190<br>639.2455<br>[2M-H]$^-$ | 0.9 | 8 | 183.0670; 165.0561; 139.0772; 123.0454; 113.0251; **95.0512** |
| **14** | 9.194 | Quercetin deoxyhexoside | $C_{21}H_{20}O_{11}$ | 447.0933 | 447.0931 | −0.4 | 12 | 447.0950; 301.0359; **300.0279**; 271.0246; 255.0290; 178.9986; 151.0036 |
| **15** | 9.437 | Lipedoside A isomer 1 | $C_{29}H_{36}O_{14}$ | 607.2032 | 607.2029 | −0.5 | 12 | **607.2027**; 461.1684; 163.0400; 145.0296 |
| **16** | 9.450 | Apigenin hexosyldeoxyhexoside 1 | $C_{27}H_{30}O_{14}$ | 577.1563 | 577.1563 | 0 | 13 | **577.1575**; 269.0447; 268.0371 |
| **17** | 9.551 | Luteolin hexoside 2 | $C_{21}H_{20}O_{11}$ | 447.0933 | 447.0940 | 1.6 | 12 | **285.0403** |

**Table 1.** *Cont.*

| Peak n. | RT (min) | Tentative Assignment | Formula | [M-H]⁻ calc. (*m*/*z*) | [M-H]⁻ Found (*m*/*z*) | Error (ppm) | RDB | HR-MS/MS Fragment Ions (*m*/*z*) (Base Peaks in Bold) |
|---|---|---|---|---|---|---|---|---|
| **18** | 9.588 | Oleuropein hexoside | $C_{31}H_{42}O_{18}$ | 701.2298 | 701.2287 | −1.6 | 11 | 701.2339; **539.1800**; 469.1362; 437.1110; 377.1253; 307.0811; 275.0923; 179.0567 |
| **19** | 9.620 | Lucidumoside B | $C_{25}H_{34}O_{13}$ | 541.1927 | 541.1931 | 0.9 | 9 | 361.1293; **225.0770**; 193.0504; 181.0872; 149.0606; 121.0659; 89.0248 |
| **20** | 9.873 | Apigenin hexosyldeoxyhexoside 2 | $C_{27}H_{30}O_{14}$ | 577.1563 | 577.1577 | 2.5 | 13 | 577.1577; **269.0450** |
| **21** | 9.865 | Lipedoside A isomer 2 | $C_{29}H_{36}O_{14}$ | 607.2032 | 607.2044 | 1.9 | 12 | **607.2049**; 461.1679; 163.0404; 145.0295 |
| **22** | 10.183 | Oleuropein | $C_{25}H_{32}O_{13}$ | 539.1770 | 539.1784 | 2.6 | 10 | 539.1786; 403.1240; 377.1237; 345.0975; 327.0874; 307.0823; **275.0911**; 223.0605; 179.0564; 149.0247; 95.0509 |
| **23** | 10.343 | Luteolin hexoside 3 | $C_{21}H_{20}O_{11}$ | 447.0933 | 447.0930 | −0.6 | 12 | 447.0929; **285.0406** |
| **24** | 10.539 | Diosmin | $C_{28}H_{32}O_{15}$ | 607.1668 | 607.1679 | 1.7 | 13 | **607.1689**; 299.0552; 284.0311 |
| **25** | 12.136 | Luteolin | $C_{15}H_{10}O_6$ | 285.0405 | 285.0406 | 0.5 | 11 | **285.0413**; 217.0507; 199.0402; 175.0403; 151.0038; 133.0300; 107.0140 |
| **26** | 13.213 | Oleacein dimethyl acetal | $C_{19}H_{26}O_7$ | 365.1606 | 365.1603 | −0.8 | 7 | **229.1086**; 211.0976; 201.1133; 185.1185; 169.0868; 153.0922; 138.0687; 121.0665 |
| **27** | 14.273 | Apigenin | $C_{15}H_{10}O_5$ | 269.0455 | 269.0453 | −0.9 | 11 | **269.0453**; 225.0550; 201.0554; 183.0445; 181.0664; 159.0453; 151.0037; 149.0241; 117.0347; 107.0141 |
| **28** | 14.999 | Diosmetin | $C_{16}H_{12}O_6$ | 299.0561 | 299.0561 | 0.0 | 11 | 299.0559; **284.0321**; 256.0374 |
| **29** | 15.313 | Oleacein ethylmethyl acetal | $C_{20}H_{28}O_7$ | 379.1762 | 379.1769 | 1.8 | 7 | **243.1243**; 225.1138; 215.1285; 199.1338; 167.1075; 153.0921; 138.0690; 121.0659 |
| **30** | 17.198 | Oleacein diethyl acetal | $C_{21}H_{30}O_7$ | 393.1919 | 393.1925 | 1.6 | 7 | **257.1399**; 239.1289; 229.1446; 213.1497; 167.1080; 139.0766; 121.0664 |
| **31** | 17.671 | Oleuropein derivative | $C_{36}H_{44}O_{18}$ | 763.2455 | 763.2461 | 0.8 | 15 | 693.2048; **539.1785**; 461.0730; 377.1250; 307.0829; 275.0904; 149.0237 |
| **32** | 25.740 | Oleanolic acid | $C_{30}H_{48}O_3$ | 455.3531 | 455.3527 | −0.9 | 7 | **455.3531**; 407.3318; 405.3162; 373.2506; 345.2192 |

Other phenolic secoiridoids were a monohexosyl oleuropein (**18**), with the [M-H]-ion at *m*/*z* 701.2287 (Figure 2B) [35] and lucidumoside B (**19**). The latter, previously isolated in other plants belonging to the same family, e.g., *Ligustrum lucidum* [36], was closely related to oleuropein. Another oleuropein derivative was compound **31**, whose deprotonated molecular ion was detected at *m*/*z* 763.2461 (Figure 2C). A thorough and systematic study of its high-resolution MS/MS spectrum, compared to those of the secoiridoids discussed herein, allowed us to tentatively identify it as an interesting oleuropein derivative, never described before, and characterized by the presence of a second elenolate moiety, likely linked to the sugar residue at its hydroxymethyl function (Figure S3).

The most abundant OLC compound was oleacein (**13**), accounting for 39%. This compound, also known as hydroxyoleocanthal, is a di-aldehydic derivative of oleuropein aglycone, with antioxidant, anti-inflammatory, anti-proliferative, and antimicrobial activities [37]. The TOF-MS/MS spectrum of the compound highlighted a diagnostic loss of 136 Da due to 4-vinylbenzene-1,2-diol from the hydroxytyrosol moiety (Figure 3A). This spectrometric feature was also found in the TOF-MS/MS spectra of compounds **26**, **29,** and **30** (Figure 3, panels B–E). The first one is likely an oleacein dimethyl acetal, whereas compounds **29** and **30** were the ethylmethyl and the diethyl acetal derivatives. These compounds, accounting for 44% of OLC (Figure 1), were reported as possible artifacts in virgin olive oils due to the oleacein interaction with polar solvents used for oil extraction and LC analysis methods [38,39].

Other minor compounds in OLC were verbascoside (**12**) [40] and the *p*-coumaroyl phenylethanoid glycoside isomers (**15** and **21**). The TOF-MS/MS spectra of all these compounds shared the loss of the hydroxycinnamoyl moiety to achieve the deprotonated glycosylated hydroxytyrosol and the dehydrated hydroxycinnamate as a less abundant fragment ion (Figure S3). Finally, several glycosylated flavonoids (**9**–**11**, **14**, **16**, **17**, **20**, **23**, **24**) were tentatively identified. Briefly, compounds **9**, **11**, **17,** and **23** shared luteolin as aglycone, and they differed in the number and/or the identity and/or glycosylation site of saccharide moieties (Figure S4). TOF-MS/MS spectra of the identified apigenin glycosides at *m*/*z* 577.1575(7) (**16**, **20**), diosmin (**24**) and rutin (**10**) showed the loss of a dehydrated rutinose (−308.11 Da). Luteolin, apigenin, and diosmetin also occurred in free form (**25**, **27**, **28**) (Figure S5). In particular, among flavonoids, luteolin was the most abundant, although its content was about only 1% in OLC (Figure 1). Quercetin deoxyhexoside (**14**) was also tentatively identified (Figure S4). The presence of almost all glycosides in this plant organ was thoroughly documented, among which flavone 7-*O*-glycosides are the most cited, together with rutin, as reported by Quirantes-Piné et al. [32] and references therein.

The less polar compound, eluting at 25.740 min retention time, was identified as the pentacyclic triterpenoid oleanolic acid (**32**). In fact, the [M-H]-ion, detected at *m*/*z* 455.3549, underwent decarboxylation and subsequent reduction to achieve the ion at *m*/*z* 407.3324, which in turn could be reduced to give the ion at *m*/*z* 405.3152 or undergo methane loss to provide the ion at *m*/*z* 373.2535 (Figure S6). The identification was confirmed by comparison with a pure commercial standard. Oleanolic acid was previously found to enhance the radiosensitizing effect on tumour cells. It was observed that MN frequencies in the hypoxic cells treated with oleanolic acid were augmented after irradiation compared with the cells without oleanolic acid treatment. The effect of the pentacyclic triterpenoid was ascribed to the reduction in intracellular GSH content and HIF-1$\alpha$ expression [41].

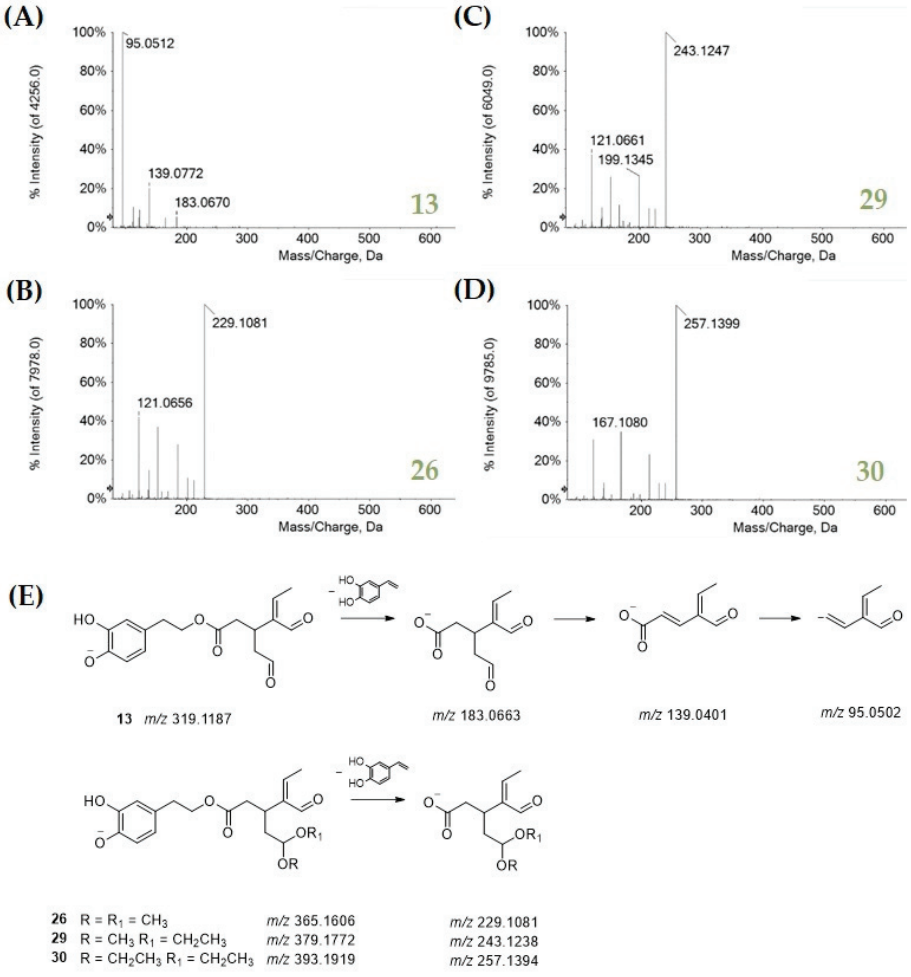


**Figure 3.** TOF-MS/MS spectra of (**A**) oleacein and its acetal derivatives **26** (**B**), **29** (**C**), and **30** (**D**). The proposed fragmentation pattern of all these compounds is in panel (**E**). Theoretical *m*/*z* values are reported under each structure.

### *3.2. OLC Antiradical and Reducing Activities*

OLC underwent antiradical screening using as probes the radicals $ABTS^{\bullet+}$ [2,2′-azinobis-(3-ethylbenzothiazoline-6-sulfonic acid)] and $DPPH^{\bullet}$ (2,2-Diphenyl-1-picrylhydrazyl). The $ID_{50}$ value, which is the dose of antioxidant species able to reduce by 50% the initial UV absorption of the radical probe, was calculated by plotting radical scavenging capability versus extract dose levels (Figure 4).

Data acquired allowed us to observe that OLC exerted a strongly dose-dependent radical scavenging capability. It was effective towards ABTS cation radical with an $ID_{50}$ value equal to 13.5 μg/mL, whereas it was able to scavenge by 50% DPPH when it was at 26 μg/mL. The activity was comparable to that exerted by Trolox in the analogue water soluble of vitamin E, commonly used as a pure reference compound in antioxidant assays. Moreover, OLC exhibited a strong reducing power. In fact, it was also able to effectively reduce ferric ions when the lowest concentration was tested. The activity gradually increased, reaching the plateau at 25 μg/mL. Data acquired were in line with previous findings by Lins et al. [42], although no details about the chemical composition

of the investigated extract were reported. The hydroxytyrosol moiety, which is shared by the largest part of the identified compounds, thanks to its electron donating capacity, reasonably allowed the scavenging effect, as well as the reducing power, to be exerted [25].

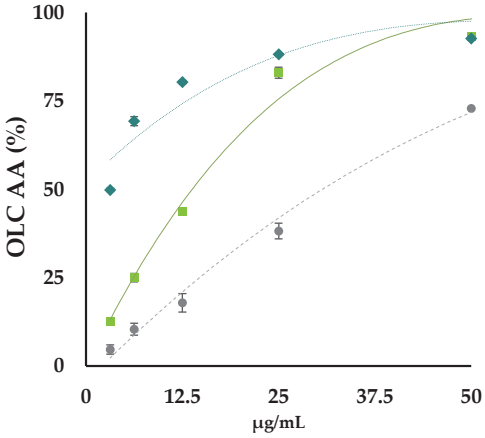


**Figure 4.** OLC antioxidant activity (AA%) vs. 2,2′-azino-bis(3-ethylbenzothiazoline)-6-sulfonic acid (ABTS) radical cation (♦), and vs. 2,2-diphenyl-1-picrylhydrazy (DPPH) radical (●). Fe (III) reducing power (RP) by PFRAP assay is also reported (■). Values reported are the mean ± SD of three independent measurements.

### *3.3. Selective OLC-Mediated Radiomodulating Effects in Normal and Cancer Cells*

Preliminary tests by MTT (3-[4,5-dimethylthiazol-2-yl]-2,5 diphenyl tetrazolium bromide) assay were conducted on HUVECs and allowed us to identify the optimal OLC concentration of 12.5 µg/mL and pre-treatment time (24 h), as defined by the absence of significant metabolic alterations and cytotoxicity in unirradiated samples (data not shown). HUVECs were chosen because they are a particularly sensitive primary cell line. Such experimental conditions were then applied to all investigated cell lines. Their appropriateness was confirmed by the lack of any detectable difference in terms of the induction of cytogenetic damage per se between unirradiated OLC-treated cells and unirradiated non-OLC-treated cells, as shown below.

A clear and consistent differential action was exhibited by the OLC on the cellular radioresponse of cancer and normal cells. The 24-h treatment period followed by exposure to graded doses of the X-rays of cells in the presence of the extract at the concentration of 12.5 µg/mL resulted in a significant reduction in radiation-induced damage in the two normal cell lines (HUVEC and MCF-10A) while exacerbating its occurrence in the two cancer cell lines (DU145 and PANC-1) used in this study compared to non-OLC-treated irradiated samples.

#### 3.3.1. OLC Decreases Radiation-Induced Premature Senescence (PS) in HUVECs

Pre-treatment with, and irradiation in the presence of, OLC resulted in a marked decrease in the onset of X-ray-induced PS in HUVECs, a widely used model system for endothelium dysfunction [43] associated with the pro-inflammatory response promoted by the secretome from ectopically senescing cells [44]. In fact, IR-induced PS is often associated with RT side effects such as tissue fibrosis, organ function disruption, and the elevation of secondary cancer risk as well as of cardiovascular disease incidence [45,46]. Figure 5 shows the occurrence of senescence, assessed by the histochemical staining of β-galactosidase (β-GAL) activity [47], both as an early (24 and 48 h) and as a delayed response (7 days) to the 0.5, 2, and 4 Gy of X-rays.

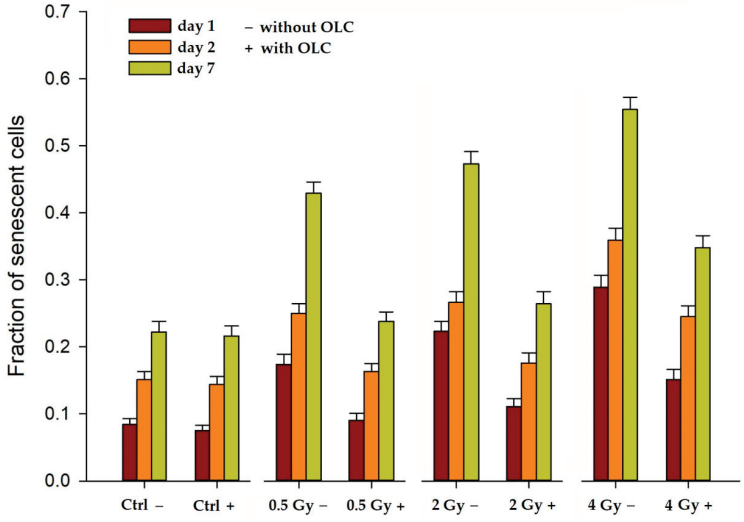


**Figure 5.** Time–course occurrence of X-ray-induced premature senescence (PS) in HUVECs in the presence (+ with OLC) and the absence of (− without OLC) of the extract. OLC mediates reduction of PS for all radiation doses at the three times assayed post-irradiation. Reported values refer to two separate experiments. Error bars refer to standard errors (SE) of the mean.

It can be seen that: (a) exposure to radiation alone (0.5 Gy−, 2 Gy− and 4 Gy− in Figure 5) causes cells to readily enter PS compared to the control unirradiated cells with no extracts, that is Ctrl −, which show physiological time-dependent senescence; (b) such a response occurs as early as 24 h after irradiation, persisting up to a week; (c) at each given time, the fraction of senescent cells increases with the X-ray dose. These data are in agreement with published results [48,49]. More interestingly, however, the OLC clearly appears to suppress the onset of PS at all times and for all doses investigated (Figure 5). In fact, among the OLC-treated irradiated HUVECs, the proportion of senescent cells also increases in time as a function of the radiation dose; however, it always stays significantly lower than that of their irradiated non-OLC-treated counterparts. Specifically, whereas, at 7 days post-irradiation, the level of PS reaches its maximum, ranging from 0.45 to about 0.55 in HUVECs exposed to 0.5 ÷ 4 Gy in the absence of the extract (Figure 5, green bars), the fraction of senescent cells among irradiated OLC-treated HUVECs never exceeds 0.4 at all times over the same dose interval. As mentioned above, treatment with the 12.5 μg/mL OLC alone (Ctrl +) did not exert any effect compared to the untreated unirradiated cells (Ctrl −), as shown by the almost identical levels of physiological senescence as time progressed.

### 3.3.2. OLC Mitigates Radiation-Induced DNA Damage in Normal Cell Lines

DNA damage elicited by X-ray irradiation was measured as the frequency of micronuclei (MN) in binucleated (BN) cells according to the well-established Cytokinesis-Block MicroNucleus (CBMN) assay [50]. MN represent portions of damaged DNA, either whole chromosomes or thereof acentric fragments, which fail to properly segregate in daughter nuclei and lag behind during cell division, hence the possibility to visualize them if cell division is arrested at the BN stage by means of cytochalasin B (CytB), an inhibitor of the actin polymerization required for the cytokinesis. Together with the analysis of radiation-induced structural chromosome aberrations (CA) that result from unrepaired double-strand breaks, the CBMN assay is one of the most reliable and widely used methods to quantify IR-associated genotoxicity given its relative simplicity and its sensitivity to reveal dose-dependent DNA breakage and/or chromosome loss following, as is the case for the CA [51,52], varying radiation exposure regimes [53,54]. The panel in Figure 6 shows typical images of BN cells, with or without MN, for the studied cell lines and the exper-

imental conditions (exposure in the presence or the absence of the OLC), for the highest dose used, that is 4 Gy of X-rays.

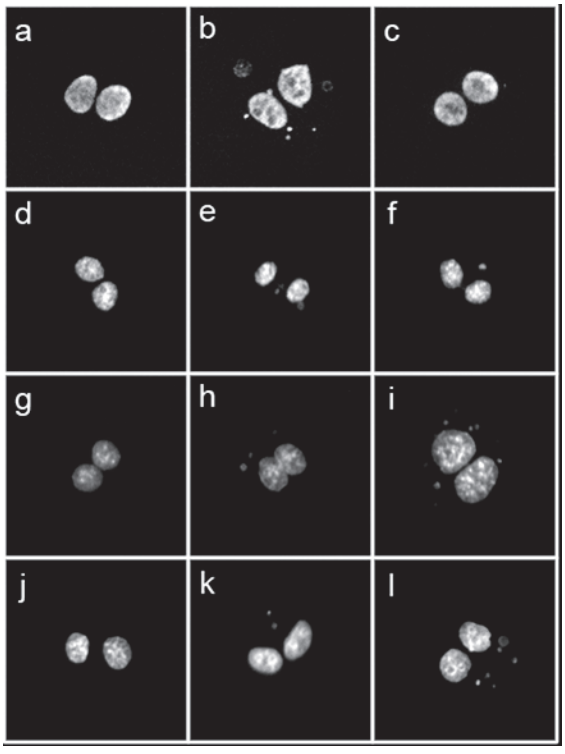


**Figure 6.** 10× magnification micrograph showing the typology of observed DNA damage per cell line and treatment conditions (no OLC vs. OLC): (**a**,**d**) unirradiated binucleated (BN) cells from normal MCF-10A and HUVEC cell lines, respectively; (**b**,**e**) BN MCF-10A and HUVECs irradiated with 4 Gy of X-rays in the absence of extract presenting multiple micronuclei (MN); (**c**,**f**) BN MCF-10A and HUVEC irradiated with the same dose but after OLC treatment and showing just one MN in each BN cell; (**g**,**j**) BN cells from cancer DU-145 and PANC-1 cell lines, respectively; (**h**,**k**) BN cells from DU-145 and PANC-1 respectively, irradiated with 4 Gy of X-rays without extract and showing only a couple of MN; (**i**,**l**) BN cells from DU-145 and PANC-1, 4Gy-irradiated in the presence of OLC showing a considerable amount of DNA damage in the form of several MN per BN cell.

When the CBMN was performed on the two normal cell lines employed in this study, that is HUVECs and MCF-10A, the presence of the OLC resulted in a significant attenuation of the measured MN frequency, as shown in Figure 7. At the used concentration, the OLC did not cause damage per se in unirradiated samples: for example, at 0 Gy the MN frequency in HUVECs was 0.028 in non OLC-treated samples compared to a value of 0.041 measured for OLC-treated cells ($p = 0.096$). On the other hand, although the absolute frequency of DNA damage recorded in HUVECs (Figure 7A) was smaller compared to that observed in MCF-10 (Figure 7B), the presence of OLC markedly reduced the MN frequency in both cell lines, such a sparing effect proportionally greater at 2 and 4 Gy in HUVECs compared to MCF-10A. In fact, in HUVECs at 4Gy OLC suppressed X-ray-induced MN formation by more than two thirds (Figure 6a). At the same dose, the protection afforded by OLC in MCF-10A was less but still statistically different (Figure 7B), with a yield of 0.945 MN/cell in the absence of OLC compared to a value of 0.831 MN/cell in OLC-treated MCF-10A cells ($p < 0.001$). At the lowest dose used, that is 0.5 Gy, the OLC was able to

almost exactly halve the damaged caused by radiation in both cells lines, reducing the MN frequency from 0.110 and 0.190 to 0.055 and 0.116 in HUVEC and MCF-10A, respectively. The overall lower MN frequency measured in HUVECs compared to epithelial MCF-10A cells could be due to their proneness to undergo PS as well as reflecting a sensitivity to apoptosis (the latter confirmed by frequent apoptotic bodies observed during microscopic scoring), both processes preventing a fraction of irradiated HUVECs to actively engage in the cell cycle and proceed through the first post-irradiation division, hence not reaching the BN stage. Exemplary images of undamaged MCF-10 and HUVEC BN cells (Figure 6a,d) can be compared to micronucleated BN cells for these cell lines, clearly showing more MN in MCF-10 cells and HUVECs following exposure to 4 Gy of X-rays in the absence of the extract (Figure 6b,e, respectively) compared to lesser damage expressed in BN cells following the same dose in the presence of the OLC (Figure 6c,f).

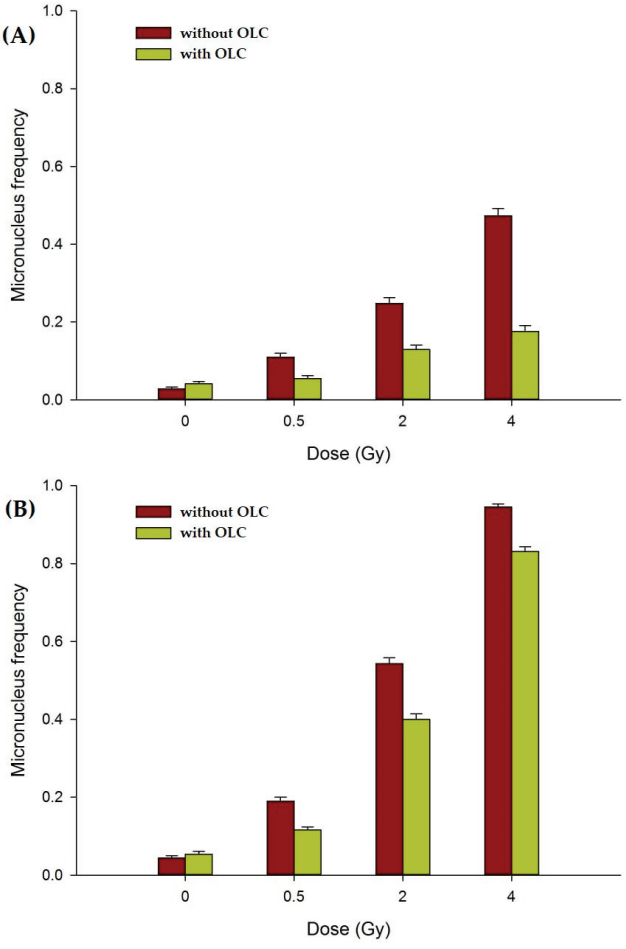


**Figure 7.** MN frequency in normal cell lines: (**A**) Dose-dependent MN induction in HUVECs; (**B**) Dose-dependent MN induction in MCF-10A cells. Irradiation in the presence of the OLC (green bars) yielded consistently less DNA damage compared to non OLC-treated samples (brown bars). MN frequency values are depicted as mean ± SE for at least two independent experiments per cell lines.

3.3.3. The OLC Presence Exacerbates Radiation-Induced DNA Damage in Cancer Cells

When prostate DU145 and pancreatic PANC-1 cancer cell lines were subjected to the same experimental conditions as those adopted for the non-cancer cell lines HUVEC and MCF-10A, that is 24-h treatment with, and irradiation in the presence of, 12.5 μg/mL OLC, the measured frequency of MN per BN cell was significantly higher than that observed in cancer cells irradiated without OLC (Figure 8). This clearly shows that OLC acts differently in terms of its ability to modulate X-ray-induced damage between cancer and normal cells.

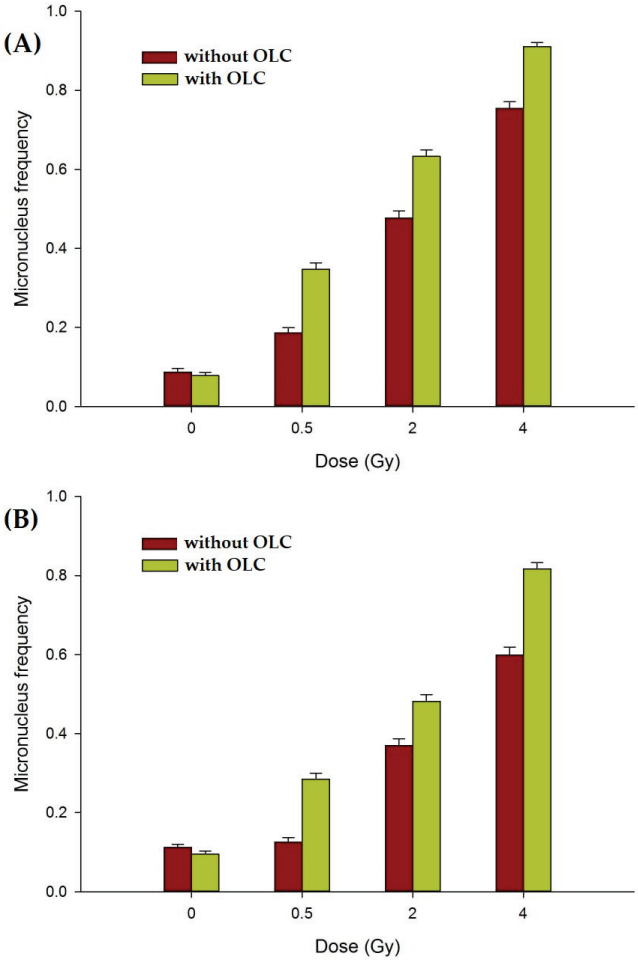


**Figure 8.** MN frequency in cancer cell lines: (**A**) Dose-dependent MN induction in prostate DU145 cancer cells; (**B**) dose-dependent MN induction in pancreatic PANC-1 cancer cells. Irradiation in the presence of the extract (green bars) causes more DNA damage compared to that measured in non OLC-treated samples (brown bars). Error bars represent SE from at least two independent experiments per cell line.

As also reported for normal cells (Section 3.3.2), the presence of OLC did not significantly add to the baseline MN level at 0 Gy. Such a baseline damage level was indeed slightly higher in DU145 and PANC-1 cells compared to normal HUVECs and MCF-10A cells, in keeping with the more pronounced genomic instability that characterizes cancer cells: an average of 0.10 MN per BN cell was found in unirradiated cancer cell samples, whether treated or untreated with OLC, compared to a baseline MN frequency of around

0.04 in non-cancer cells (Figure 7). Exposure to radiation led to an increase in such frequency in both cancer lines in a dose-dependent manner and to a greater extent in DU145 than in PANC-1 cells, in agreement with their greater radioresistance exhibited by pancreatic cancer [55]. Interestingly, in fact, not only does OLC enhance radiation damage in these cancer cells, but its radiosensitizing action is, on average, greater in the most radioresistant PANC-1 cells (Figure 7B): OLC leads to about a 1.8 to 1.2-fold increase in MN frequency in DU145 as X-ray doses increase from 0.5 to 4 Gy, whereas in PANC-1 cells such an enhancement factor ranges from 2.3 to 1.4 over the same dose interval. Thus, the presence of OLC in PANC-1 following 2 Gy of X-rays increases the mean frequency of MN per cell from 0.37 to almost 0.5. The capacity by OLC to exacerbate radiation-induced damage selectively in cancer cells can be appreciated by representative images of cancer cells exposed to 4 Gy (Figure 6), specifically showing an elevated mean number of MN in the extract-treated cells compared to those without in DU145 and PANC-1 cells (Figure 6i,l vs. Figure 6h,k, respectively).

## 4. Discussion

The chemical and metabolic profile of the crude leaf extract (OLC) of *O. europaea* L. cv. Caiazzana, an autochthonous cultivar from the Campania region (Italy) was investigated. The analysis confirmed the expected constitutive richness in oleuropein and its derivatives, mainly oleacein. The presence and content of the latter compound was related to olive tree genotypes, and, in olive drupes, levels were found to decrease during fruit maturation [56]. In leaves, it is reasonable to assume that there is a close connection to the harvest season and to the occurrence of oleuropein. Indeed, isotopic labelling of olive shoots showed its significant precursory role in the production of oleuropein and that this process was cultivar-, season-, and environment-dependent [57].

The putative radiomodulating properties of OLC were tested in vitro on a panel of cancer and normal cell lines. Our data seem to indicate that the same concentration of the investigated OLC exerts a differentially radioprotective action on normal cells while exhibiting radiosensitizing abilities in cancer cells over the X-ray dose range $0.5 \div 4$ Gy. While previous studies had demonstrated the ability of phenolic secoiridoids, such as oleuropein, either to grant protection from IR deleterious effects due to its antioxidant properties or to enhance IR-induced damage owing to its pro-oxidant properties [23,24], this is the first report of an oleuropein derivatives-rich extract able to discriminate between cancer and normal cell in terms of their radioresponse under the same experimental conditions. Indeed, the ability to differentially act on healthy and cancer cells is the all-important criterion for clinically useful radioprotectors and radiosensitizers.

Even in the most innovative and technologically advanced RT approaches, increasing the therapeutic ratio continues to be a crucial factor [58,59]. The radiosensitivity of normal tissue and organs still remains the main dose-limiting factor in curative RT because of severe sequelae [2]. In addition, acquired/intrinsic cancer radioresistance is the underlying cause of recurrence and metastasization [7]. In this context, natural compounds have gained attention since they may abate IR adverse effects and enhance tumour radioresponse; in particular, food-isolable nutraceuticals show anti-proliferative and pro-oxidant effects on tumours [60,61] and antioxidant and anti-inflammatory activity in normal cells [62]. Such a dual behaviour advocates their use in RT since radiotoxicity mainly relies on DNA-damaging IR-induced reactive oxygen species (ROS). Despite a wealth of information on the bioactivity and cellular as well as in vivo effects of plant-derived polyphenols, specifically of *O. europaea*, as recently summarized by Olivares-Vincente et al. [63], only a few studies have addressed the effects oleuropein and oleuropein-derived compounds on radiation-induced cyto-genotoxicity as expressed by cellular senescence and MN formation, and even fewer where olive leaf extracts were tested.

The radiobiological endpoints chosen to investigate the OLC-mediated radiomodulation, that is premature senescence (PS) and DNA damage in the form of micronuclei (MN), are of clinical relevance. The accumulation of radiation-induced prematurely senescing non-

cancer cells has been increasingly shown to impact normal tissue/organ homeostasis and function as well as promoting inflammatory responses. In fact, the endothelium integrity is of paramount importance as IR-induced inflammation may lead to RT-induced secondary cancers [4] and late cardiotoxicity [64]. At the same time, sublethally damaged normal cells pose a threat to genomic stability and contribute to elevate the risk of RT-induced secondary cancers. On the other hand, radiation-induced genotoxicity is the premise for cancer cell death and, ultimately, for successful RT outcome. Therefore, since in vitro MN induction is commonly considered as a reliable measure of IR effectiveness at damaging the DNA, its mitigation in normal cells is an indication of radioprotection whereas its elevation in cancer cells reflects radiosensitization.

The presence of OLC very effectively lowered the fraction of HUVECs undergoing PS as a result of X-ray exposure (Figure 5), and such a protecting effect was consistently shown at all doses and at each time point when cells were assayed. Recently, polyphenols have been considered to be of potential therapeutic importance for their ability to actually promote cancer cell senescence via several molecular targets, including oncogene regulation, the activation of DNA Damage Response (DDR), and other stress-related pathways [65]. However, equally compelling evidence exists in support of the anti-senescence action by polyphenols and their derivatives on several skin-derived cultured cells such as keratinocytes, melanocytes, and fibroblasts [66]; moreover, Menicacci et al. [67] showed that oleuropein aglycone from extra-virgin olive oil caused a significant reduction in β-gal positive cells and in the expression of the senescence-associated p16 in pre-senescent human lung (MRC-5) and neonatal dermal fibroblasts. Despite seemingly participating in the disruption of several pathways leading to PS, the main molecular anti-senescence mechanisms by polyphenols appear to hinge on their ability to counteract ROS production and pro-inflammatory responses [68]. A very recent work by Frediani et al. [69] showed that the deglycosylated product of oleuropein and hydroxytyrosol from olive fruit decreased the level of senescence elicited by very high doses of IR (6–8 Gy) suppressing the Senescence-Associated Secretory Phenotype. Our results therefore seem to confirm such findings proving that the OLC tested in this study can already exert an anti-senescence protective effect at doses as low as 0.5 Gy.

Our data showing an OLC-mediated reduction in radiation-induced genotoxicity, expressed in the form of MN scored in normal BN cells (Figure 6), are in keeping with similar findings that have been scantly reported over a long time on the radioprotection afforded by polyphenols to irradiated cellular DNA using the same endpoint. Thus, while, almost twenty years ago, Greenrod and Fenech [70] had assessed the impact of several wine-derived polyphenols on human lymphocytes irradiated in vitro by the CBMN assay reporting an anti-genotoxic action, Alcaraz et al. [71] very recently reported on the radioprotective effect by flavonoids in mice whole-body irradiated with 0.5 Gy of γ-radiation assessed by MN formation in polychromatic erythrocytes. More specifically, another recent work by Amani et al. [72] found that 100 mM of oleuropein afforded protection from apoptosis, clastogenicity, and genotoxicity, with the latter measured by MN occurrence, in human cultured lymphocytes exposed to a single dose of 2 Gy of γ-rays.

The effect of the same concentration of OLC granting DNA radioprotection in normal cells was instead reversed when cancer cells were treated with, and irradiated in the presence of, the extract: a significant radiosensitization manifested itself as an increase in the frequency of MN per BN cell following X-ray irradiation in two cancer cell lines, as shown in Figure 7. In a very recent review, Zhang et al. [73] analysed the most up-to-date data on the anti-cancer properties of oleuropein; however, apart from the already cited work by Xu and Xiao [24] on the radiosensitization of nasopharyngeal carcinoma, only one study on the effects of oleuropein can be found showing that it led to the suppression of ovarian cancer cell hypoxia-mediated radioresistance in a xenograft model [74]. Indeed, oleuropein alone, that is, without concomitant exposure to radiation, was tested on one of the two cancer cell lines used in this study, that is in prostate DU145 cancer cells, where it was shown to inhibit proliferation via an increase in ROS production [75].

There exists consensus around the notion that, at the heart of the double-edged geno-protective or geno-toxic potential of polyphenols, and therefore of oleuropein-based compounds, there ought to be an anti- or pro-oxidant activity that is very often concentration-dependent. As concentration increases, such extracts tend to switch from effective ROS scavengers to potent pro-oxidant agents. This view is reinforced by the few studies carried out in the presence of IR, which is a powerful source of ROS. However, to the best of our knowledge, this is the first report showing the ability by the same concentration of an extract from olive leaves to exert the radiomodulating ability differentially between normal and cancer cells. A similar result was recently published by Bektay et al. [76], who found that 0.25 mg/mL of olive leaf extracts selectively inhibited the cell viability of a rat liver cell line, sparing a healthy clone of rat liver cells. However, no radiation was used in this study. Our results may therefore have important implication in RT scenarios to widen the therapeutic window using a toxicity-free nutraceutical approach but warrant further in vitro and in vivo studies to elucidate the exact molecular mechanisms underlying the dual behaviour exhibited by the same concentration of the OLC tested in our study. One possibility for such selectivity may be related to the intracellular ROS (iROS) content, which tends to be physiologically different between normal and cancer cells, with the latter being able to generate more iROS and with the known ability of oleuropein to suppress the NF-kB signalling pathway involved in a variety of important cellular processes in many cancer cells. Inhibition of NF-kB activation results in an increase in TNF$\alpha$-induced ROS production, lipid peroxidation, and protein oxidation. Radiation would add to such a higher "background" oxidative stress in cancer cells. As suggested by Alcaraz et al. [71], under certain conditions depending, among other factors, on the number and positions of hydroxyl groups, polyphenolic compounds through the chelation of chromosome-associated metal ion $Cu^{2+}$ can switch from an anti-oxidant to a pro-oxidant activity, a mechanism already postulated to explain flavonoid-mediated DNA damage [77]. Thus, it is possible that, in normal cells, the additional level of ROS produced by radiation can be dealt with effectively by the anti-oxidant scavenging ability of the oleuropein-rich OLC at the concentration used in this study, whereas the peculiar redox status of cancer cells combined with the mentioned properties of oleuropein and the additional radiation-induced ROS could reverse the same amount of OLC to an effective pro-oxidant agent. Interestingly, none of the compounds tentatively identified in the OLC tested in this study appear to be associated with the modification of known target gene expression in pancreatic or prostate cancer cells, as reported in an extensive biodatabase (NaturaProDB) recently compiled by Theofylaktou et al. [78]. This therefore adds to the novelty of our findings and warrants further studies on the radiomodulating properties of the *Olea europaea* L. cv. Caiazzana leaf extract at both the genetic and epigenetic levels to elucidate its precise mode of action. Furthermore, preclinical and clinical studies will be needed to verify the efficacy of the OLC single radiomodulating dose. In this context, it has been shown that olive leaf phenolic extracts or their formulas increase the bioavailability of hydroxytyrosol and oleuropein in both mice and humans [79,80]. In fact, although conducted on a small number of volunteers, quantification studies of the bioavailability and metabolism of the two most attentive compounds of the olive leaf have shown that the formulation of the extract and the delivery method influence absorption and metabolism [80]. Indeed, any future study must strictly consider the chemical composition of OLC, which is particularly rich in oleacenin and its derivatives. Unfortunately, knowledge in this regard is extremely limited to date, with the exception of one study aimed at quantifying the distribution of oleacenin, administered in rats in a single dose (2.5 mL/300 g body weight) by gavage, in plasma and several organs, including stomach, small intestine, liver, heart, spleen, thyroid, lung, brain, kidney, and skin [81].

## 5. Conclusions

We have, for the first time, chemically and radiobiologically profiled the olive leaf Caiazzana (OLC) crude extract obtained from a cultivar (Caiazzana) autochthons to Regione

Campania, in Southern Italy. The metabolic analysis of its polyphenolic content showed that it is rich in oleacein and its esters, which, reasonably, through their hydroxytyrosol moiety, allowed OLC to exert an important antiradical and to reduce efficacy. Interestingly, the extract exhibited peculiar in vitro radiomodulating properties, being capable, for one identical concentration, to exert a differential action, exacerbating the DNA damage inflicted by graded doses of X-rays in the two tested cancer lines, whilst mitigating the cyto- and genotoxicity caused by such doses in the two normal cell lines. To our knowledge, this behavior is unique. In fact, it is well known that plant polyphenols may either act as radiosensitizers or radioprotectors; however, no study has thus far reported such a dual, cell-type-specific action using the same compound concentration. Such selectivity between tumour and non-cancer cells bears important implications, if further confirmed, for its potential usefulness to widen the radiotherapy therapeutic window. Finally, the sustainability of the extraction process from pruned leaves, normally regarded as waste, adds value to the possible societal impact of our findings.

**Supplementary Materials:** The following supporting information can be downloaded at: https://www.mdpi.com/article/10.3390/antiox11081603/s1, Figure S1: (a) Total Ion Current (TIC) and (b) Base Peak Chromatogram (BPC) of OLC extract. Red arrows denote the quantified compounds, considered the main responsible for the observed bioactivity; Figure S2: TOF-MS/MS spectra of (a) hydroxytyrosol and (b) hydroxytyrosol hexoside; (c) hypothesized fragmentation pathways; Figure S3: TOF-MS/MS spectra of compounds 12 (at $m/z$ 623.1981, calc. mass), 15 and 21 (at $m/z$ 607.2032, calc. mass). The hypothesized chemical structures of the detected ions are reported with theoretical $m/z$ values; Figure S4: TOF-MS/MS spectra of detected flavonoid glycosides. The aglycone structures are provided together with the glyconic moieties. Figure S5: TOF-MS spectra of flavones: (a) luteolin, (b) apigenin, and (c) diosmetin; Figure S6: Experimental evidence of the occurrence of oleanolic acid (XIC = eXtracted Ion Chromatogram).

**Author Contributions:** Conceptualization, L.M. and S.P. (Severina Pacifico); methodology, S.P. (Severina Pacifico), S.P. (Simona Piccolella), S.F. and L.M.; software, K.M., S.P. (Severina Pacifico), S.P. (Simona Piccolella) and V.R.; formal analysis, F.F., L.M., S.F., S.P. (Severina Pacifico) and S.P. (Simona Piccolella); investigation, L.M. and S.P. (Severina Pacifico); resources, L.M. and S.P. (Severina Pacifico); data curation, F.F., P.B., S.P. (Severina Pacifico) and S.P. (Simona Piccolella); writing—original draft preparation, L.M., S.P. (Severina Pacifico) and S.P. (Simona Piccolella); writing—review and editing, L.M. and S.P. (Severina Pacifico). All authors have read and agreed to the published version of the manuscript.

**Funding:** This research received no external funding.

**Institutional Review Board Statement:** Not applicable.

**Informed Consent Statement:** Not applicable.

**Data Availability Statement:** The data is contained within the article and Supplementary Materials.

**Acknowledgments:** The authors thank Milena Petriccione of the Research Centre for Olive, Fruit Trees and Citrus of Caserta (CRA-OFA), Council for Agricultural Research and Analysis of Agricultural Economics for allowing us to collect the investigated olive leaves cv. Caiazzana.

**Conflicts of Interest:** The authors declare no conflict of interest.

## References

1. Allali, S.; Kirova, Y. Radiodermatitis and Fibrosis in the Context of Breast Radiation Therapy: A Critical Review. *Cancers* **2021**, *13*, 5928. [CrossRef] [PubMed]
2. van der Laan, H.P.; Van den Bosch, L.; Schuit, E.; Steenbakkers, R.J.H.M.; van der Schaaf, A.; Langendijk, J.A. Impact of radiation-induced toxicities on quality of life of patients treated for head and neck cancer. *Radiother. Oncol.* **2021**, *160*, 47–53. [CrossRef] [PubMed]
3. Suit, H.; Goldberg, S.; Niemierko, A.; Ancukiewicz, M.; Hall, E.; Goitein, M.; Wong, W.; Paganetti, H. Secondary Carcinogenesis in Patients Treated with Radiation: A Review of Data on Radiation-Induced Cancers in Human, Non-human Primate, Canine and Rodent Subjects. *Radiat. Res.* **2007**, *167*, 12–42. [CrossRef] [PubMed]

4. Kamran, S.C.; Berrington de Gonzalez, A.; Ng, A.; Haas-Kogan, D.; Viswanathan, A.N. Therapeutic radiation and the potential risk of second malignancies. *Cancer* **2016**, *122*, 1809–1821. [CrossRef]
5. Barnett, G.C.; West, C.M.; Dunning, A.M.; Elliott, R.M.; Coles, C.E.; Pharoah, P.D.; Burnet, N.G. Normal tissue reactions to radiotherapy: Towards tailoring treatment dose by genotype. *Nat. Rev. Cancer.* **2009**, *9*, 134–142. [CrossRef] [PubMed]
6. Shimura, T.; Kakuda, S.; Ochiai, Y.; Nakagawa, H.; Kuwahara, Y.; Takai, Y.; Kobayashi, J.; Komatsu, K.; Fukumoto, M. Acquired radioresistance of human tumor cells by DNA-PK/AKT/GSK3beta-mediated cyclin D1 overexpression. *Oncogene* **2010**, *29*, 4826–4837. [CrossRef]
7. McCann, E.; O'Sullivan, J.; Marcone, S. Targeting cancer-cell mitochondria and metabolism to improve radiotherapy response. *Transl. Oncol.* **2021**, *14*, 100905. [CrossRef]
8. Wang, H.; Jiang, H.; Van De Gucht, M.; De Ridder, M. Hypoxic Radioresistance: Can ROS Be the Key to Overcome It? *Cancers* **2019**, *11*, 112. [CrossRef]
9. Arnold, C.R.; Mangesius, J.; Skvortsova, I.-I.; Ganswindt, U. The Role of Cancer Stem Cells in Radiation Resistance. *Front. Oncol.* **2020**, *10*, 164. [CrossRef]
10. De Ruysscher, D.; Niedermann, G.; Burnet, N.G.; Siva, S.; Lee, A.W.M.; Hegi-Johnson, F. Radiotherapy toxicity. *Nat. Rev. Dis. Primers* **2019**, *5*, 13. [CrossRef]
11. Mun, G.I.; Kim, S.; Choi, E.; Kim, C.S.; Lee, Y.S. Pharmacology of natural radioprotectors. *Arch. Pharm. Res.* **2018**, *41*, 1033–1050. [CrossRef] [PubMed]
12. Faramarzi, S.; Piccolella, S.; Manti, L.; Pacifico, S. Could polyphenols really be a good radioprotective strategy? *Molecules* **2021**, *26*, 4969. [CrossRef] [PubMed]
13. Zdrowowicz, M.; Spisz, P.; Hać, A.; Herman-Antosiewicz, A.; Rak, J. Influence of Hypoxia on Radiosensitization of Cancer Cells by 5-Bromo-20-deoxyuridine. *Int. J. Mol. Sci.* **2022**, *23*, 1429. [CrossRef] [PubMed]
14. Hazra, B.; Ghosh, S.; Kumar, A.; Pandey, B.N. The prospective role of plant products in radiotherapy of cancer: A current overview. *Front. Pharmacol.* **2012**, *2*, 94. [CrossRef] [PubMed]
15. Malik, A.; Sultana, M.; Qazi, A.; Qazi, M.H.; Parveen, G.; Waquar, S.; Ashraf, A.B.; Rasool, M. Role of Natural Radiosensitizers and Cancer Cell Radioresistance: An Update. *Anal. Cell. Pathol.* **2016**, *2016*, 6146595. [CrossRef] [PubMed]
16. Akter, R.; Najda, A.; Rahman, M.H.; Shah, M.; Wesołowska, S.; Hassan, S.S.u.; Mubin, S.; Bibi, P.; Saeeda, S. Potential Role of Natural Products to Combat Radiotherapy and Their Future Perspectives. *Molecules* **2021**, *26*, 5997. [CrossRef]
17. Piccolella, S.; Crescente, P.; Nocera, P.; Pacifico, F.; Manti, L.; Pacifico, S. Ultrasound-assisted aqueous extraction, LC-MS/MS analysis and radiomodulating capability of autochthonous Italian sweet cherry fruits. *Food Funct.* **2018**, *9*, 1840–1849. [CrossRef]
18. Calvaruso, M.; Pucci, G.; Musso, R.; Bravatà, V.; Cammarata, F.P.; Russo, G.; Forte, G.I.; Minafra, L. Nutraceutical Compounds as Sensitizers for Cancer Treatment in Radiation Therapy. *Int. J. Mol. Sci.* **2019**, *20*, 5267. [CrossRef]
19. Wang, J.; Yu, M.; Xiao, L.; Xu, S.; Yi, Q.; Jin, W. Radiosensitizing effect of oleanolic acid on tumor cells through the inhibition of GSH synthesis in vitro. *Oncol. Rep.* **2013**, *30*, 917–924. [CrossRef]
20. Sebastià, N.; Montoro, A.; Hervás, D.; Pantelias, G.; Hatzi, V.I.; Soriano, J.M.; Villaescusa, J.I.; Terzoudi, G.I. Curcumin and trans-resveratrol exert cell cycle-dependent radioprotective or radiosensitizing effects as elucidated by the PCC and G2-assay. *Mutat. Res.* **2014**, *766–767*, 49–55. [CrossRef]
21. Kefayat, A.; Ghahremani, F.; Safavi, A.; Hajiaghababa, A.; Moshtaghian, J. C-phycocyanin: A natural product with radiosensitizing property for enhancement of colon cancer radiation therapy efficacy through inhibition of COX-2 expression. *Sci. Rep.* **2019**, *9*, 19161. [CrossRef] [PubMed]
22. Ricciardi, V.; Portaccio, M.; Piccolella, S.; Manti, L.; Pacifico, S.; Lepore, M. Study of SH-SY5Y Cancer Cell Response to Treatment with Polyphenol Extracts Using FT-IR Spectroscopy. *Biosensors* **2017**, *7*, 57. [CrossRef]
23. Castillo, J.J.; Alcaraz, M.; Benavente-garcía, O. Antioxidant and radioprotective effects of olive leaf extract. In *Olives and Olive Oil in Health and Disease Prevention*, 1st ed.; Preedy, V., Watson, R., Eds.; Elsevier Inc.: Amsterdam, The Netherlands, 2010; Chapter 102; pp. 951–958.
24. Xu, T.; Xiao, D. Oleuropein enhances radiation sensitivity of nasopharyngeal carcinoma by downregulating PDRG1 through HIF1α-repressed microRNA-519d. *J. Exp. Clin. Cancer Res.* **2017**, *36*, 3. [CrossRef] [PubMed]
25. Scognamiglio, M.; D'Abrosca, B.; Pacifico, S.; Fiumano, V.; De Luca, P.; Monaco, P.; Fiorentino, A. Polyphenol characterization and antioxidant evaluation of *Olea europaea* varieties cultivated in Cilento National Park (Italy). *Food Res. Int.* **2012**, *46*, 294–303. [CrossRef]
26. Il Germoplasma Dell'olivo in Campania. Available online: http://agricoltura.regione.campania.it/pubblicazioni/pdf/germoplasma_olivo.pdf (accessed on 2 November 2021).
27. Formato, M.; Piccolella, S.; Zidorn, C.; Vastolo, A.; Calabrò, S.; Cutrignelli, M.I.; Pacifico, S. UHPLC-ESI-QqTOF Analysis and In Vitro Rumen Fermentation for Exploiting Fagus sylvatica Leaf in Ruminant Diet. *Molecules* **2022**, *27*, 2217. [CrossRef]
28. Longo, E.; Morozova, K.; Scampicchio, M. Effect of light irradiation on the antioxidant stability of oleuropein. *Food Chem.* **2017**, *237*, 91–97. [CrossRef]
29. Piccolella, S.; Crescente, G.; Volpe, M.G.; Paolucci, M.; Pacifico, S. UHPLC-HR-MS/MS-guided recovery of bioactive flavonol compounds from Greco di Tufo vine leaves. *Molecules* **2019**, *24*, 3630. [CrossRef]
30. Dichio, B.; Margiotta, G.; Xiloyannis, C.; Bufo, S.A.; Sofo, A.; Cataldi, T.R.I. Changes in water status and osmolyte contents in leaves and roots of olive plants (*Olea europaea* L.) subjected to water deficit. *Trees* **2009**, *23*, 247–256. [CrossRef]

31. Asteggiano, A.; Franceschi, P.; Zorzi, M.; Aigotti, R.; Dal Bello, F.; Baldassarre, F.; Lops, F.; Carlucci, A.; Medana, C.; Ciccarella, G. HPLC-HRMS Global Metabolomics Approach for the Diagnosis of "Olive Quick Decline Syndrome" Markers in Olive Trees Leaves. *Metabolites* **2021**, *11*, 40. [CrossRef]
32. Quirantes-Piné, R.; Lozano-Sánchez, J.; Herrero, M.; Ibáñez, E.; Segura-Carretero, A.; Fernández-Gutiérrez, A. HPLC–ESI–QTOF–MS as a Powerful Analytical Tool for Characterising Phenolic Compounds in Olive-leaf Extracts. *Phytochem. Anal.* **2013**, *24*, 213–223. [CrossRef]
33. Alañón, M.E.; Ivanović, M.; Gómez-Caravaca, A.M.; Arráez-Román, D.; Segura-Carretero, A. Choline chloride derivative-based deep eutectic liquids as novel green alternative solvents for extraction of phenolic compounds from olive leaf. *Arab. J. Chem.* **2020**, *13*, 1685–1701. [CrossRef]
34. Nediani, C.; Ruzzolini, J.; Romani, A.; Calorini, L. Oleuropein, a Bioactive Compound from *Olea europaea* L., as a Potential Preventive and Therapeutic Agent in Non-Communicable Diseases. *Antioxidants* **2019**, *8*, 578. [CrossRef]
35. Wang, X.F.; Li, C.; Shi, Y.P.; Di, D.L. Two new secoiridoid glycosides from the leaves of *Olea europaea* L. *J. Asian Nat. Prod. Res.* **2009**, *11*, 940–944. [CrossRef]
36. He, Z.D.; But, P.P.H.; Chan, T.W.D.; Dong, H.; Xu, H.X.; Lau, C.P.; Sun, H.D. Antioxidative Glucosides from the Fruits of *Ligustrum Lucidum*. *Chem Pahrm. Bull.* **2001**, *49*, 780–784. [CrossRef]
37. Naruszewicz, M.; Czerwiska, M.E.; Kiss, A.K. Oleacein. Translation from Mediterranean Diet to Potential Antiatherosclerotic Drug. *Curr. Pharm. Des.* **2015**, *21*, 1205–1212. [CrossRef]
38. Sanchez de Medina, V.; Luque de Castro, M.D.; Miho, H.; Melliou, E.; Magiatis, P.; Priego-Capote, F. Quantitative method for determination of oleocanthal and oleacein in virgin olive oils by liquid chromatography-tandem mass spectrometry. *Talanta* **2017**, *162*, 24–31. [CrossRef]
39. Celano, R.; Piccinelli, A.L.; Pugliese, A.; Carabetta, S.; di Sanzo, R.; Rastrelli, L.; Russo, M. Insights into the Analysis of Phenolic Secoiridoids in Extra Virgin Olive Oil. *J. Agric. Food Chem.* **2018**, *66*, 6053–6063. [CrossRef]
40. Cádiz-Gurrea, M.d.l.L.; Pinto, D.; Delerue-Matos, C.; Rodrigues, F. Olive Fruit and Leaf Wastes as Bioactive Ingredients for Cosmetics—A Preliminary Study. *Antioxidants* **2021**, *10*, 245. [CrossRef]
41. Qi, R.; Jin, W.; Wang, J.; Yi, Q.; Yu, M.; Xu, S.; Jin, W. Oleanolic acid enhances the radiosensitivity of tumor cells under mimetic hypoxia through the reduction in intracellular GSH content and HIF-1α expression. *Oncol. Rep.* **2014**, *31*, 2399–2406. [CrossRef]
42. Lins, P.G.; Marina Piccoli Pugine, S.; Scatolini, A.M.; de Melo, M.P. In vitro antioxidant activity of olive leaf extract (*Olea europaea* L.) and its protective effect on oxidative damage in human erythrocytes. *Heliyon* **2018**, *4*, e00805. [CrossRef]
43. Jimenez Trinidad, F.R.; Arrieta Ruiz, M.; Solanes Batlló, N.; Vea Badenes, À.; Bobi Gibert, J.; Valera Cañellas, A.; Roqué Moreno, M.; Freixa Rofastes, X.; Sabaté Tenas, M.; Dantas, A.P.; et al. Linking In Vitro Models of Endothelial Dysfunction with Cell Senescence. *Life* **2021**, *11*, 1323. [CrossRef]
44. Coppé, J.P.; Desprez, P.Y.; Krtolica, A.; Campisi, J. The senescence-associated secretory phenotype: The dark side of tumor suppression. *Annu. Rev. Pathol.* **2010**, *5*, 99–118. [CrossRef]
45. Nguyen, H.Q.; To, N.H.; Zadigue, P.; Kerbrat, S.; De La Taille, A.; Le Gouvello, S.; Belkacemi, Y. Ionizing radiation-induced cellular senescence promotes tissue fibrosis after radiotherapy. A review. *Crit. Rev. Oncol. Hematol.* **2018**, *129*, 13–26. [CrossRef]
46. Banerjee, P.; Kotla, S.; Reddy Velatooru, L.; Abe, R.J.; Davis, E.A.; Cooke, J.P.; Schadler, K.; Deswal, A.; Herrmann, J.; Lin, S.H.; et al. Senescence-Associated Secretory Phenotype as a Hinge Between Cardiovascular Diseases and Cancer. *Front. Cardiovasc. Med.* **2021**, *8*, 763930. [CrossRef]
47. Itahana, K.; Campisi, J.; Dimri, G.P. Methods to detect biomarkers of cellular senescence: The senescence-associated beta-galactosidase assay. *Methods Mol. Biol.* **2007**, *371*, 21–31. [CrossRef]
48. Wang, Y.; Boerma, M.; Zhou, D. Ionizing Radiation-Induced Endothelial Cell Senescence and Cardiovascular Diseases. *Radiat. Res.* **2016**, *186*, 153–261. [CrossRef]
49. Manti, L.; Perozziello, F.M.; Borghesi, M.; Candiano, G.; Chaudhary, P.; Cirrone, G.A.P.; Doria, D.; Gwynne, D.; Leanza, R.; Prise, K.M.; et al. The radiobiology of laser-driven particle beams: Focus on sub-lethal responses of normal human cells. *J. Instrum.* **2017**, *12*, C03084. [CrossRef]
50. Fenech, M. The in vitro micronucleus technique. *Mutat. Res.* **2000**, *455*, 81–95. [CrossRef]
51. Manti, L.; Durante, M.; Cirrone, G.A.P.; Grossi, G.; Lattuada, M.; Pugliese, M.; Sabini, M.G.; Scampoli, P.; Valastro, L.; Gialanella, G. Modelled microgravity does not modify the yield of chromosome aberrations induced by high-energy protons in human lymphocytes. *Int. J. Radiat. Biol.* **2005**, *81*, 147–155. [CrossRef]
52. Manti, L.; Durante, M.; Grossi, G.; Ortenzia, O.; Pugliese, M.; Scampoli, P.; Gialanella, G. Measurements of metaphase and interphase chromosome aberrations transmitted through early cell replication rounds in human lymphocytes exposed to low-LET protons and high-LET 12C ions. *Mutat. Res.* **2006**, *596*, 151–165. [CrossRef]
53. Manti, L.; Jamali, M.; Prise, K.M.; Michael, B.D.; Trott, K.R. Genomic instability in Chinese hamster cells after exposure to X rays or alpha particles of different mean linear energy transfer. *Radiat. Res.* **1997**, *147*, 22–28. [CrossRef]
54. Sannino, A.; Zeni, O.; Romeo, S.; Massa, R.; Gialanella, G.; Grossi, G.; Manti, L.; Vijayalaxmi Scarfì, M.R. Adaptive response in human blood lymphocytes exposed to non-ionizing radiofrequency fields: Resistance to ionizing radiation-induced damage. *J. Radiat. Res.* **2014**, *55*, 210–217. [CrossRef]

55. Seshacharyulu, P.; Baine, M.J.; Souchek, J.J.; Menning, M.; Kaur, S.; Yan, Y.; Ouellette, M.M.; Jain, M.; Lin, C.; Batra, S.K. Biological determinants of radioresistance and their remediation in pancreatic cancer. *Biochim. Biophys. Acta Rev. Cancer* **2017**, *1868*, 69–92. [CrossRef]
56. Sabetta, W.; Mascio, I.; Squeo, G.; Gadaleta, S.; Flamminii, F.; Conte, P.; Di Mattia, C.D.; Piga, A.; Caponio, F.; Montemurro, C. Bioactive Potential of Minor Italian Olive Genotypes from Apulia, Sardinia and Abruzzo. *Foods* **2021**, *10*, 1371. [CrossRef]
57. Ryan, D.; Antolovich, M.; Herlt, T.; Prenzler, P.D.; Lavee, S.; Robards, K. Identification of phenolic compounds in tissues of the novel olive cultivar hardy's mammoth. *J. Agric. Food Chem.* **2002**, *50*, 6716–6724. [CrossRef]
58. Bláha, P.; Feoli, C.; Agosteo, S.; Calvaruso, M.; Cammarata, F.P.; Catalano, R.; Ciocca, M.; Cirrone, G.A.P.; Conte, V.; Cuttone, G.; et al. The Proton-Boron Reaction Increases the Radiobiological Effectiveness of Clinical Low- and High-Energy Proton Beams: Novel Experimental Evidence and Perspectives. *Front. Oncol.* **2021**, *11*, 682647. [CrossRef]
59. Schillaci, F.; Anzalone, A.; Cirrone, G.A.P.; Carpinelli, M.; Cuttone, G.; Cutroneo, M.; De Martinis, C.; Giove, D.; Korn, G.; Maggiore, M.; et al. ELIMED, MEDical and multidisciplinary applications at ELI-Beamlines. *J. Phys. Conf. Ser.* **2014**, *508*, 012010. [CrossRef]
60. Cárdeno, A.; Sánchez-Hidalgo, M.; Rosillo, M.A.; Alarcón de la Lastra, C. Oleuropein, a secoiridoid derived from olive tree, inhibits the proliferation of human colorectal cancer cell through downregulation of HIF-1α. *Nutr. Cancer* **2013**, *65*, 147–156. [CrossRef]
61. Benot-Dominguez, R.; Tupone, M.G.; Castelli, V.; d'Angelo, M.; Benedetti, E.; Quintiliani, M.; Cinque, B.; Forte, I.M.; Cifone, M.G.; Ippoliti, R.; et al. Olive leaf extract impairs mitochondria by pro-oxidant activity in MDA-MB-231 and OVCAR-3 cancer cells. *Biomed. Pharmacother.* **2021**, *134*, 111139. [CrossRef]
62. Hahn, D.; Shin, S.H.; Bae, J.S. Natural Antioxidant and Anti-Inflammatory Compounds in Foodstuff or Medicinal Herbs Inducing Heme Oxygenase-1 Expression. *Antioxidants* **2020**, *9*, 1191. [CrossRef]
63. Olivares-Vicente, M.; Barrajon-Catalan, E.; Herranz-Lopez, M.; Segura-Carretero, A.; Joven, J.; Encinar, J.A.; Micol, V. Plant-Derived Polyphenols in Human Health: Biological Activity, Metabolites and Putative Molecular Targets. *Curr. Drug Metab.* **2018**, *19*, 351–369. [CrossRef]
64. Nabiałek-Trojanowska, I.; Lewicka, E.; Wrona, A.; Kaleta, A.M.; Lewicka-Potocka, Z.; Raczak, G.; Dziadziuszko, R. Cardiovascular complications after radiotherapy. *Cardiol. J.* **2020**, *27*, 836–847. [CrossRef]
65. Bian, Y.; Wei, J.; Zhao, C.; Li, G. Natural Polyphenols Targeting Senescence: A Novel Prevention and Therapy Strategy for Cancer. *Int. J. Mol. Sci.* **2020**, *21*, 684. [CrossRef]
66. Csekes, E.; Račková, L. Skin Aging, Cellular Senescence and Natural Polyphenols. *Int. J. Mol. Sci.* **2021**, *22*, 12641. [CrossRef]
67. Menicacci, B.; Cipriani, C.; Margheri, F.; Mocali, A.; Giovannelli, L. Modulation of the Senescence-Associated Inflammatory Phenotype in Human Fibroblasts by Olive Phenols. *Int. J. Mol. Sci.* **2017**, *18*, 2275. [CrossRef]
68. Gurău, F.; Baldoni, S.; Prattichizzo, F.; Espinosa, E.; Amenta, F.; Procopio, A.D.; Albertini, M.C.; Bonafè, M.; Olivieri, F. Anti-senescence compounds: A potential nutraceutical approach to healthy aging. *Ageing Res. Rev.* **2018**, *46*, 14–31. [CrossRef]
69. Frediani, E.; Scavone, F.; Laurenzana, A.; Chillà, A.; Tortora, K.; Cimmino, I.; Leri, M.; Bucciantini, M.; Mangoni, M.; Fibbi, G.; et al. Olive phenols preserve lamin B1 expression reducing cGAS/STING/NFκB-mediated SASP in ionizing radiation-induced senescence. *J. Cell. Mol. Med.* **2022**, *26*, 2337–2350. [CrossRef]
70. Greenrod, W.; Fenech, M. The principal phenolic and alcoholic components of wine protect human lymphocytes against hydrogen peroxide- and ionizing radiation-induced DNA damage in vitro. *Mutagenesis* **2003**, *18*, 119–126. [CrossRef]
71. Alcaraz, M.; Olivares, A.; Achel, D.G.; García-Gamuz, J.A.; Castillo, J.; Alcaraz-Saura, M. Genoprotective Effect of Some Flavonoids against Genotoxic Damage Induced by X-rays In Vivo: Relationship between Structure and Activity. *Antioxidants* **2021**, *11*, 94. [CrossRef]
72. Amani, F.; Allahbakhshian Farsani, M.; Gholami, M.; Aghamiri, S.M.R.; Bakhshandeh, M.; Hossein Mohammadi, M. The protective effect of oleuropein against radiation-induced cytotoxicity, apoptosis, and genetic damage in cultured human lymphocytes. *Int. J. Radiat. Biol.* **2021**, *97*, 179–193. [CrossRef]
73. Zheng, Y.; Liu, Z.; Yang, X.; Liu, L.; Ahn, K.S. An updated review on the potential antineoplastic actions of oleuropein. *Phytother. Res.* **2022**, *36*, 365–379. [CrossRef] [PubMed]
74. Xing, Y.; Cui, D.; Wang, S.; Wang, P.; Xing, X.; Li, H. Oleuropein represses the radiation resistance of ovarian cancer by inhibiting hypoxia and microRNA-299-targetted heparanase expression. *Food Funct.* **2017**, *8*, 2857–2864. [CrossRef] [PubMed]
75. Acquaviva, R.; Di Giacomo, C.; Sorrenti, V.; Galvano, F.; Santangelo, R.; Cardile, V.; Gangia, S.; D'Orazio, N.; Abraham, N.G.; Vanella, L. Antiproliferative effect of oleuropein in prostate cell lines. *Int. J. Oncol.* **2012**, *41*, 31–38. [CrossRef] [PubMed]
76. Bektay, M.Y.; Güler, E.M.; Gökçe, M.; Kızıltaş, M.V. Investigation of the Genotoxic, Cytotoxic, Apoptotic, and Oxidant Effects of Olive Leaf Extracts on Liver Cancer Cell Lines. *Turk. J. Pharm. Sci.* **2021**, *18*, 781–789. [CrossRef]
77. Cao, G.; Sofic, E.; Prior, R.L. Antioxidant and prooxidant behavior of flavonoids: Structure-activity relationships. *Free Radic. Biol. Med.* **1997**, *22*, 749–760. [CrossRef]
78. Theofylaktou, D.; Takan, I.; Karakülah, G.; Biz, G.M.; Zanni, V.; Pavlopoulou, A.; Georgakilas, A.G. Mining Natural Products with Anticancer Biological Activity through a Systems Biology Approach. *Oxid. Med. Cell Longev.* **2021**, *2021*, 9993518. [CrossRef]
79. Aponte, M.; Ungaro, F.; d'Angelo, I.; De Caro, C.; Russo, R.; Blaiotta, G.; Dal Piaz, F.; Calignano, A.; Miro, A. Improving in vivo conversion of oleuropein into hydroxytyrosol by oral granules containing probiotic *Lactobacillus plantarum* 299v and an *Olea europaea* standardized extract. *Int. J. Pharm.* **2018**, *543*, 73–82. [CrossRef]

80. de Bock, M.; Thorstensen, E.B.; Derraik, J.G.; Henderson, H.V.; Hofman, P.L.; Cutfield, W.S. Human absorption and metabolism of oleuropein and hydroxytyrosol ingested as olive (*Olea europaea* L.) leaf extract. *Mol. Nutr. Food Res.* **2013**, *57*, 2079–2085. [CrossRef]
81. López-Yerena, A.; Vallverdú-Queralt, A.; Lamuela-Raventós, R.M.; Escribano-Ferrer, E. LC-ESI-LTQ-Orbitrap-MS for profiling the distribution of oleacein and its metabolites in rat tissues. *Antioxidants* **2021**, *10*, 1083. [CrossRef]

antioxidants

MDPI

*Review*

# Auranofin and Pharmacologic Ascorbate as Radiomodulators in the Treatment of Pancreatic Cancer

**Garett J. Steers [1,2], Gloria Y. Chen [1,2], Brianne R. O'Leary [1,2], Juan Du [1,2], Hannah Van Beek [1] and Joseph J. Cullen [1,2,*]**

[1] Free Radical and Radiation Biology Program, Department of Radiation Oncology, The University of Iowa Carver College of Medicine, Iowa City, IA 52242, USA; garett-steers@uiowa.edu (G.J.S.); gloria-chen@uiowa.edu (G.Y.C.); brianne-oleary@uiowa.edu (B.R.O.); juan-du@uiowa.edu (J.D.); vanbeekhm@outlook.com (H.V.B.)

[2] Department of Surgery, The University of Iowa Carver College of Medicine, Iowa City, IA 52242, USA

* Correspondence: joseph-cullen@uiowa.edu; Tel.: +1-(319)-353-8297; Fax: +1-(319)-356-8378

**Abstract:** Pancreatic cancer accounts for nearly one fourth of all new cancers worldwide. Little progress in the development of novel or adjuvant therapies has been made over the past few decades and new approaches to the treatment of pancreatic cancer are desperately needed. Pharmacologic ascorbate (P-AscH$^-$, high-dose, intravenous vitamin C) is being investigated in clinical trials as an adjunct to standard-of-care chemoradiation treatments. In vitro, P-AscH$^-$ has been shown to sensitize cancer cells to ionizing radiation in a manner that is dependent on the generation of $H_2O_2$ while simultaneously protecting normal tissue from radiation damage. There is renewed interest in Auranofin (Au), an FDA-approved medication utilized in the treatment of rheumatoid arthritis, as an anti-cancer agent. Au inhibits the thioredoxin antioxidant system, thus increasing the overall peroxide burden on cancer cells. In support of current literature demonstrating Au's effectiveness in breast, colon, lung, and ovarian cancer, we offer additional data that demonstrate the effectiveness of Au alone and in combination with P-AscH$^-$ and ionizing radiation in pancreatic cancer treatment. Combining P-AscH$^-$ and Au in the treatment of pancreatic cancer may confer multiple mechanisms to increase $H_2O_2$-dependent toxicity amongst cancer cells and provide a promising translatable avenue by which to enhance radiation effectiveness and improve patient outcomes.

**Keywords:** pharmacologic ascorbate; vitamin C; pancreatic cancer; Auranofin; thioredoxin; thioredoxin reductase; peroxiredoxin

**Citation:** Steers, G.J.; Chen, G.Y.; O'Leary, B.R.; Du, J.; Van Beek, H.; Cullen, J.J. Auranofin and Pharmacologic Ascorbate as Radiomodulators in the Treatment of Pancreatic Cancer. *Antioxidants* **2022**, *11*, 971. https://doi.org/10.3390/antiox11050971

Academic Editors: Elena Obrador Pla and Alegria Montoro

Received: 6 April 2022
Accepted: 11 May 2022
Published: 14 May 2022



## 1. Pancreatic Cancer

Pancreatic ductal adenocarcinoma is one of the most common cancers worldwide and has remained a leading cause of cancer deaths. In the United States, the estimated incidence is 13.2 cases per 100,000 people, with a mortality rate of 11.1 per 100,000 people, making it the third leading cause of cancer deaths after lung and colorectal cancer [1,2]. Despite a small upward trend in 5-year survival rate since 1975, survival remains the lowest among all cancer types globally, with a current 5-year survival rate of 10.8% for all stages [2,3]. Similarly, the mortality rate for pancreatic cancer has not changed in nearly 50 years; by comparison, colorectal cancer, the second most common cause of cancer deaths, has seen a drop in mortality rate of nearly 60% over the same period [1]. This poor prognosis is attributed to the delayed diagnosis and poor response to therapy. As a result, incidence and mortality rates have increased throughout all regions of the world and are predicted to continue to rise [3].

Treatment of pancreatic cancer is complex and often requires a multi-disciplinary approach given its high mortality and morbidity. Primary factors affecting prognosis and survival are resectability and metastasis. The resectability of a tumor is based on its relation to nearby structures as well as the degree of lymphatic spread. Tumors that invade or

encase nearby vasculature, distort vascular anatomy, or invade other nearby organs such as the stomach are considered borderline resectable or locally advanced, indicating a need for neoadjuvant chemoradiotherapy prior to reevaluation for resection [4]. In a similar fashion, the degree of disease in the regional lymph nodes also guides the decision for resection. Distant lymph nodes outside of the field of resection are indicative of more distant, metastatic disease, where upfront resection is avoided. Only approximately 13% of patients are considered resectable at the time of their diagnosis; thus, neoadjuvant chemoradiotherapy is critical in managing more extensive disease with the goal of converting locally advanced, unresectable tumors to resectable [1,5]. Rates of survival for resected patients have increased to as high as 17.4% in 2011 from 1.5% in 1975, while the survival rate of non-resected patients has expectedly remained unchanged during this time, less than 1% [3,6].

For both resectable and unresectable tumors, chemotherapy is a vital component of pancreatic cancer treatment. Patients who undergo initial surgical resection without evidence of recurrence or metastatic disease postoperatively will still require systemic adjuvant treatment [4]. In several multi-center randomized controlled trials, FOLFIRNOX (a combination treatment of fluorouracil, leucovorin, oxaliplatin, and irinotecan) improved overall survival and progression-free survival compared to gemcitabine alone and is now considered standard of care for both neoadjuvant and adjuvant therapy [7,8]. Additional chemotherapy regimens such as gemcitabine plus nab-paclitaxel also offer survival benefit [9]. For locally advanced disease requiring neoadjuvant therapy prior to the consideration of resection, several adjuncts to chemotherapy are available, including radiation therapy, thermal and non-thermal ablation, and intra-arterial chemotherapy. These treatments have varying amounts of success but have been seen to improve overall prognosis [10].

Radiation Therapy as Adjunct Treatment for Pancreatic Cancer

Radiation is primarily known to cause direct DNA damage [11–14]. It also generates reactive oxygen species, which cause further damage at the DNA level with single- and double-stranded DNA breaks, as well as damage to proteins and lipids [15]. Radiotherapy is often used in conjunction with chemotherapy to increase radiation effectiveness. In pancreatic cancer, fluorouracil (5-FU) was classically utilized, while gemcitabine, capecitabine, and oral 5-FU derivatives such as Xeloda are commonly used today [4]. Neoadjuvant treatment with radiation aims to improve the likelihood of margin-negative resection or downsizing of tumors, although there is no standard practice [16]. In locally advanced and unresectable disease, radiation may assist in local control or prevent local progression or recurrence, despite no evidence of improved overall survival in the limited studies available. A phase III randomized controlled trial, LAP07, investigated locally advanced pancreatic cancer receiving chemoradiotherapy compared to chemotherapy alone. Although there was no survival benefit, there were some improvements in local tumor progression and time to re-initiation of therapy [10,16,17]. As adjuvant therapy, chemoradiation has varying results, with no significant benefit in overall survival, but it has shown some potential in certain patients, particularly those with positive margins [18]. Radiation therapy is also used as an aid in relieving pain, bleeding, or obstructive symptoms in palliative or metastatic disease. Advances such as intensity-modulated RT (IMRT) and stereotactic-body RT (SBRT) have enabled more dose escalation and reduced volumes to improve clinical outcomes [10]. These may be better tolerated by patients and investigations are underway to further assess their role in pancreatic cancer treatment [19–21].

The efficacy of radiotherapy has been restricted due to the toxic effects on patients' quality of life. Due to the location of the pancreas, many nearby organs, such as the small intestine and stomach, are directly within the radiation field. The standard dose is then limited to 50–54 Gy to maintain local control of the cancer without significant toxicity and side effects [10]. Common significant side effects include hematologic toxicities, GI symptoms such as nausea, diarrhea, and abdominal pain, and biliary obstruction. These side effects lead to decreased tolerance of radiation, poorer quality of life for patients, and a limited effect of the radiation itself [22]. Despite increasing the intensity of treatment by

altering radiation fractionation or with different concurrent chemotherapies, the majority of patients still experience local failure and succumb to their disease [23]. Thus, there are a significant number of pancreatic cancer patients who would benefit from improvements in the efficacy of standard-of-care chemoradiation therapy.

## 2. Pharmacologic Ascorbate

Vitamin C (ascorbic acid, ascorbate) at normal physiologic doses is typically considered a donor antioxidant. Ascorbic acid ($AscH_2$) readily oxidizes to ascorbate ($AscH^-$), which then undergoes two one-electron oxidations to form the ascorbate radical ($Asc^-$) [24]. The ascorbate radical is relatively unreactive and can combine with hydrogen ions to reform ascorbate, making ascorbate an effective antioxidant at physiologic levels [24]. However, at supraphysiologic levels, ascorbate exerts pro-oxidant effects. Intestinal absorption of ascorbate is tightly regulated by sodium-dependent vitamin C transporters in enterocytes, with average serum levels maintained around 40–80 μM [25–29]. Thus, supraphysiologic levels cannot be obtained by oral supplementation.

Intravenous administration of ascorbate circumvents this limitation. Pharmacologic ascorbate (P-$AscH^-$, high-dose intravenously administered ascorbate) produces much higher serum ascorbate levels, up to 20 mM [30]. At these supraphysiologic levels, ascorbate acts as a pro-oxidant, donating electrons to form high levels of extracellular hydrogen peroxide ($H_2O_2$) that readily crosses cell membranes [24,25,31]. Once $H_2O_2$ is intracellular, it reacts with redox-active metals to form the hydroxyl radical ($HO^{\cdot}$), a highly toxic radical that causes oxidative damage to proteins, lipids, and DNA [24,31–33]. Due to this pathway, P-$AscH^-$ has garnered significant interest as a potential cancer therapy.

### *2.1. Pharmacologic Ascorbate Use in Cancer*

The use of vitamin C for the treatment of cancer dates back to the 1970s, when Cameron et al. suggested that high-dose ascorbate could provide a survival benefit when used to treat a variety of cancers, including stomach, colon, rectal, breast, bladder, and pancreatic cancer [34–36]. In these studies, patients considered to have terminal disease were given intravenous ascorbic acid (typically 10 g/day) in addition to the standard of care at that time. They observed significantly increased survival times in the P-$AscH^-$ treated patients compared to the controls, results which would be demonstrated again in subsequent studies [35,36]. However, in the late 1970s and mid-1980s, two double-blinded, randomized controlled trials studying the use of ascorbate in the treatment of several solid organ tumors demonstrated no effect on patient survival [37,38]. These studies slowed the adoption of P-$AscH^-$ in cancer research and treatment. However, these studies differed significantly from those performed by Cameron in that patients received only oral ascorbate as opposed to high-dose ascorbate administered intravenously. As described above, oral supplementation of ascorbate fails to elevate serum levels above the normal physiologic threshold [25,27–29]. These findings in the late 1990s and early 2000s ignited a resurgence in interest around P-$AscH^-$ in the treatment of cancer.

Pharmacologic ascorbate has shown promise in the treatment of a variety of cancers over the last decade. In vitro and in vivo studies in pancreatic, breast, colorectal, ovarian, glioblastoma, and lung cancer have demonstrated that P-$AscH^-$ decreases cell viability, decreases tumor volume, and improves survival alone or in combination with other standard-of-care chemotherapy regimens [33,39–45]. The selectivity of ascorbate-induced cytotoxicity between normal cells and malignant cells may be due to lower levels of peroxide-reducing enzymes such as catalase, glutathione peroxidase, and peroxiredoxins, as well as higher endogenous levels of reactive oxygen species in cancer cells, leading to the less efficient degradation of $H_2O_2$ and increased susceptibility to P-$AscH^-$ [31,32,43,46,47].

Following these findings, numerous clinical trials have examined the effects of P-$AscH^-$ in combination with chemotherapy or chemoradiation therapy in the treatment of several cancer types. In 2012, Monti et al. published the results of their phase I clinical trial studying the effects of P-$AscH^-$ when combined with gemcitabine and erlotinib in

14 subjects with metastatic pancreatic cancer [48]. They observed no significant increase in side effects or toxicity with P-AscH$^-$ while also observing a decrease in tumor size in 8 of 9 patients. In 2013, Welsh et al. published similar findings from their phase I clinical trial observing the effects of P-AscH$^-$ in combination with gemcitabine in metastatic and node-positive pancreatic cancer [49]. Instead of treating patients with a set dose of P-AscH$^-$ (50 g, 75 g, or 100 g), as was done in Monti's study, patients were treated based upon their plasma ascorbate levels following the previous day's infusion. Welsh et al. demonstrated that plasma ascorbate concentrations of up to 30 mM could safely be achieved while also demonstrating a potential survival benefit, with mean progression-free survival (PFS) and mean overall survival (OS) of 26 weeks and 12 months, respectively, compared to a mean OS of 5–7 months for gemcitabine alone and 11 months for FOLFIRINOX at that time [7,50]. This was one of the first clinical trials that suggested that P-AscH$^-$ may offer a survival benefit to cancer patients.

Additional phase I and II clinical trials in pancreatic, lung, glioblastoma, and ovarian cancer have demonstrated similar results. Ma et al. observed that patients who received P-AscH$^-$ in combination with carboplatin and paclitaxel for stage III/IV ovarian cancer had significantly fewer grade 1 and 2 toxicities compared to patients who did not receive P-AscH$^-$, with no increase in grade 3 and 4 toxicities [45]. This study again showed a potential survival benefit, with a prolongation of the median time for disease progression. In a phase I trial observing P-AscH$^-$ effects in glioblastoma by Schoenfeld et al., patients receiving P-AscH$^-$ in combination with temozolomide and radiation demonstrated mean PFS of 13.3 months and mean OS of 21.5 months, respectively, compared to 7 months and 14 months historically [33]. Multiple ongoing phase I and II clinical studies utilizing P-AscH$^-$ in pancreatic, lung, breast, colorectal, bladder, prostate, glioblastoma, and myeloid malignancies will report their findings in the coming years. Recently published studies in pancreatic cancer, including an additional phase I clinical trial, have focused on the effects of P-AscH$^-$ when given in combination with radiation therapy.

### *2.2. Pharmacologic Ascorbate Increases Radiation Toxicity in Pancreatic Cancer While Protecting Normal Tissue*

While P-AscH$^-$ has shown efficacy when combined with standard-of-care chemotherapies in both in vivo experiments and clinical trials, it has also shown promise as a radiomodulator [41,44,51–55]. Du et al. demonstrated that the addition of P-AscH$^-$ to radiation significantly increased DNA damage and significantly decreased the clonogenic survival of multiple pancreatic cancer cell lines compared to radiation alone [52]. They also showed significantly decreased tumor volume and increased survival compared to radiation or P-AscH$^-$ alone in a xenograft model. Furthermore, mice that received radiation alone demonstrated a significant reduction in jejunal crypt cells that was partially reversed with the addition of P-AscH$^-$ treatment. These results suggested that P-AscH$^-$ may not only be an effective adjuvant to chemoradiotherapy but may also offer radioprotection to normal cells. Alexander et al. further demonstrated that P-AscH$^-$ significantly improves clonogenic survival, decreases DNA damage, and decreases collagen deposition in normal intestinal cells following radiation [53]. Normal tissue toxicity secondary to radiation damage can have devastating effects on patients. Complication rates are 50% when the nearby intestine receives a total of 60 Gy, making radiation therapy a relatively risky endeavor for pancreatic cancer patients [56]. In addition to its radiosensitization effects on cancer, P-AscH$^-$ may also offer normal tissue protection to ensure that more patients can tolerate full, uninterrupted radiation regimens.

### *2.3. Long-Term Survival following P-AscH$^-$ in Pancreatic Cancer*

P-AscH$^-$ has experienced a rebirth in the field of cancer therapy, with clinical trials underway in a variety of cancers [49,57]. The first phase I clinical trial to actively infuse P-AscH$^-$ during the "beam on" time of radiation for the treatment of locally advanced pancreatic cancer, "Gemcitabine, Ascorbate, Radiation therapy for pancreatic cancer, phase

I" (NCT01852890), was performed at the University of Iowa [53]. Pharmacologic ascorbate was administered concurrently with gemcitabine and radiation, where gemcitabine was administered weekly for 6 weeks and P-AscH$^-$ was administered at 50–100 g during each radiotherapy treatment, either 28 fractions at 50.4 Gy or 25 fractions at 50 Gy. Fourteen subjects completed the protocol therapy between 2014 and 2017. Three study participants are now more than 5 years out from the completion of their neoadjuvant therapies as of January 2022, with the longest surviving participant out nearly 8 years (90 months), resulting in significant increases in both median overall survival (Figure 1A) and median progression-free survival (Figure 1B). Median overall survival for the P-AscH$^-$/gemcitabine/radiation group is 22.8 months, with three long-term survivors (more than 5 years), compared to 12.7 months in the control group and 14 months historically for locally advanced pancreatic cancer [58]. Similarly, the median progression-free survival of 13.7 months in the P-AscH$^-$ treatment group is also significantly longer than 4.6 months in the control group and roughly 3.8 months historically for all stages of pancreatic cancer [59]. Three long-term survivors from the relatively small sample size of a phase I trial suggests the efficacy of P-AscH$^-$ as a chemotherapeutic agent and radiosensitizer. Currently, there are dozens of clinical trials using P-AscH$^-$ in a variety of cancers, including phase II trials in pancreatic cancer utilizing P-AscH$^-$ in combination with standard-of-care gemcitabine and nab-paclitaxel (NCT02905578) as well as more experimental regimens (NCT01905150).

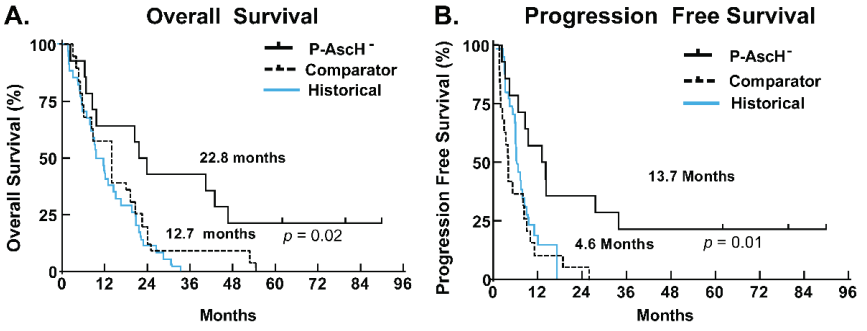


**Figure 1.** Survival analysis from phase I trial (NCT01852890). (**A**) Kaplan–Meier curve estimating median overall survival in subjects treated with P-AscH$^-$ plus gemcitabine and radiation therapy as of 25 January 2022 ($n$ = 14) was 22.8 months vs. 12.7 months in institutional controls treated with gemcitabine and radiation therapy ($n$ = 19, Log-Rank test $p$ = 0.02); (**B**) Kaplan–Meier curve demonstrating median progression-free survival in subjects treated with P-AscH$^-$ plus gemcitabine and radiation therapy as of 25 January 2022 ($n$ = 14) was 13.7 months vs. 4.6 months in institutional controls treated with gemcitabine and radiation therapy ($n$ = 19, Log-Rank test $p$ = 0.01). These data are updated from data previously published by Du et al. [60].

## 3. Pathways for Hydrogen Peroxide Removal

Cancer cells' decreased ability to neutralize the P-AscH$^-$-induced increase in $H_2O_2$ has been shown to be secondary to the decreased expression and activity of enzymes responsible for removing $H_2O_2$, including catalase, glutathione peroxidase (GPx), and peroxiredoxins (Prx) [46,47,61,62]. Catalase, predominantly located in peroxisomes, has been shown to be the principal enzyme in $H_2O_2$ removal, especially in the presence of high amounts of $H_2O_2$, where it is responsible for removing as much as 99% of $H_2O_2$ in erythrocytes [63,64]. GPx and peroxiredoxin are considered more important for the removal of lower levels of $H_2O_2$ due to their higher affinity [64]. The catalytic activity of GPx is dependent on a regenerating system in which NADPH is used as an electron donor [65]. Utilizing two glutathione (GSH) molecules, GPx generates $H_2O$ and glutathione disulfide (GSSG) that is reduced back to glutathione (GSH) by glutathione reductase (GR) using

NADPH. Any process that interferes with GPx activity, GR activity, GSSG recycling, or NADPH recycling can impair GPx turnover and reduce its effectiveness [66].

Another means by which to reduce $H_2O_2$-scavenging capacity is the targeting of the thioredoxin (Trx) redox buffer system. The thioredoxin system consists of thioredoxin and peroxiredoxin. Thioredoxin is a 12 kDa oxidoreductase necessary for a myriad of cellular processes, including deoxynucleoside triphosphate (dNTP) synthesis, transcriptional regulation, and antioxidant defense [67,68]. The disulfide exchange activity of thioredoxin is integral to the maintenance of peroxiredoxin. Peroxiredoxins are important $H_2O_2$ scavengers, with a reaction rate approaching diffusion-controlled limits ($10^{7–8}$ $M^{-1}$ $s^{-1}$) and comparable to catalase ($10^7$ $M^{-1}$ $s^{-1}$) and GPx ($10^8$ $M^{-1}$ $s^{-1}$) [64,69–71]. Thus, the presence of sufficient reduced thioredoxin ($Trx_{(SH)2}$) to maintain peroxiredoxin in the active (reduced) form is vital for cellular defense against $H_2O_2$. Following the two-electron reduction of a peroxiredoxin by reduced thioredoxin, thioredoxin disulfide ($Trx_{S\text{-}S}$) is recycled back to reduced thioredoxin by thioredoxin reductase (TrxR), a flavin-containing selenoprotein, using reducing equivalents from NADPH [72,73]. Previous studies have shown that inhibition of the thioredoxin/thioredoxin reductase complex reduces peroxiredoxin function [2].

Targeting these pathways offers another potential avenue for cancer treatment. By decreasing cancer cells' ability to degrade $H_2O_2$, oxidative stress within cancer cells may be further amplified, ultimately leading to enhanced cancer-specific cytotoxicity. A recent study examining the role of catalase in pancreatic cancer demonstrated that catalase knockout cells exhibited greater radiosensitization to P-$AscH^-$ and that cancer cells in long-term survivors may express lower levels of catalase than cancer cells in short-term survivors [60]. These results suggest that inhibiting a portion of the peroxide removal system—catalase, glutathione reductase, thioredoxin reductase, or peroxiredoxin—may enhance the effectiveness of treatments aimed at increasing oxidative stress within cancer cells.

## 4. Auranofin

Auranofin (Au) is a gold-triethylphosphine compound originally FDA-approved in 1985 for the treatment of rheumatoid arthritis [74,75]. Au is one of three disease-modifying antirheumatic drugs (DMARDs) that contain gold, though it is the only drug in this group that can be administered orally due to its lipophilic properties [74]. Au is believed to exert multiple anti-inflammatory effects by altering the production and secretion of pro-inflammatory cytokines and modulating intracellular signaling pathways such as activating mitogen-activated protein kinases (MAPK), all of which play a role in rheumatoid arthritis disease severity and progression [76–81]. The exact mechanisms behind these effects are not completely understood but do seem to involve enzyme inhibition and appear to be dependent on the gold atom situated between a sulfur atom and the triethylphopshine group [82–85]. Additionally, Au has shown effectiveness outside of its immune-modulating effects and has garnered interest for its antibacterial, antiviral, cytoprotective, and anticancer potential [86–91].

### *4.1. Auranofin Use in Cancer*

Over the past few decades, significant interest in the anticancer effects of Au has arisen. The key mechanism of action thought to be responsible for the anticancer effects of Au is thioredoxin reductase inhibition (Figure 2) [92,93]. Au serves as an electrophile and reacts with the selenocysteine residue in the active site of thioredoxin reductase by forming a covalent adduct and inactivating the enzyme [73]. Inhibition of thioredoxin reductase inhibits the flow of electrons from NADPH to peroxiredoxin by impairing the recycling of thioredoxin, leading to a subsequent reduction in peroxiredoxin activity and an increase in $H_2O_2$ [94]. Increasing $H_2O_2$ via this mechanism may lead to additional cancer-specific cytotoxicity, as discussed previously [31,95]. Several in vitro studies have demonstrated a synergistic induction of apoptosis when Au is given in combination with various chemotherapy agents in breast cancer cell models [96–98]. In one study, Lee et al. demonstrated that the combination of Au and mesupron, a urokinase-type plasminogen

activator inhibitor currently undergoing clinical trials in breast cancer, promoted the inhibition of breast cancer cell proliferation and induced cell cycle arrest and apoptosis, while also significantly increasing reactive oxygen species within cancer cells [97]. Similar studies in colon, ovarian, and lung cancer cell lines demonstrating synergistic increases in cancer cell death show that Au may be an effective anticancer agent when combined with other chemotherapy agents [99–101]. Based on these findings, a previous study hypothesized that Au may sensitize cancer cells to P-AscH$^-$ by impairing hydroperoxide removal [102]. To test this, pancreatic ductal adenocarcinoma cancer cells were treated with inhibitors of hydroperoxide metabolism. Data show that targeting of the thioredoxin system with Au inhibits thioredoxin reductase activity and sensitizes pancreatic cancer cells to P-AscH$^-$-generated $H_2O_2$. The combination of Au and P-AscH$^-$ also significantly increases the sensitivity of pancreatic cancer cells to ionizing radiation. Based on these results, repurposing Au in combination with P-AscH$^-$ as a chemotherapy and radiomodulatory regimen may provide a potentially promising and translatable new treatment for pancreatic cancer. For all experiments, Au was dissolved in PBS containing 1% EtOH.

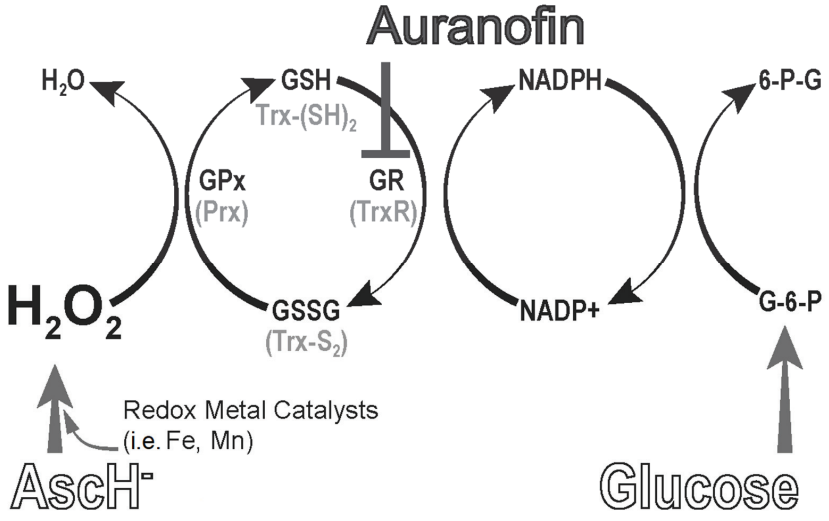


**Figure 2.** Thioredoxin and glutathione peroxidase (GPx) antioxidant enzyme systems and inhibitors. GSH = glutathione; GSSG = glutathione disulfide; GR = glutathione disulfide reductase; GPx = glutathione peroxidase; Trx-$(SH)_2$ = reduced thioredoxin; Trx-$S_2$ = oxidized thioredoxin; TrxR = thioredoxin reductase; Prx = peroxiredoxin; G-6-P = glucose-6-phosphate; 6-P-G = 6-phosphoglucono-δ-lactone. Inhibitors of the pathway are: Auranofin [103].

### *4.2. Au Inhibits Thioredoxin Reductase Activity in Pancreatic Cancer Cells*

To determine if Au inhibits thioredoxin reductase activity in pancreatic cancer cells, MIA PaCa-2 pancreatic cancer cells were treated with Au for 3 h and thioredoxin reductase activity was measured by spectrophotometrically following the reduction of 5,5-dithiobis-(2-nitrobenzoic acid) (DTNB) utilizing a thioredoxin reductase assay kit. Activity was normalized to the protein concentration determined by the Lowry protein assay. Au was shown to significantly decrease thioredoxin reductase activity in pancreatic cancer cells (Figure 3) [102].

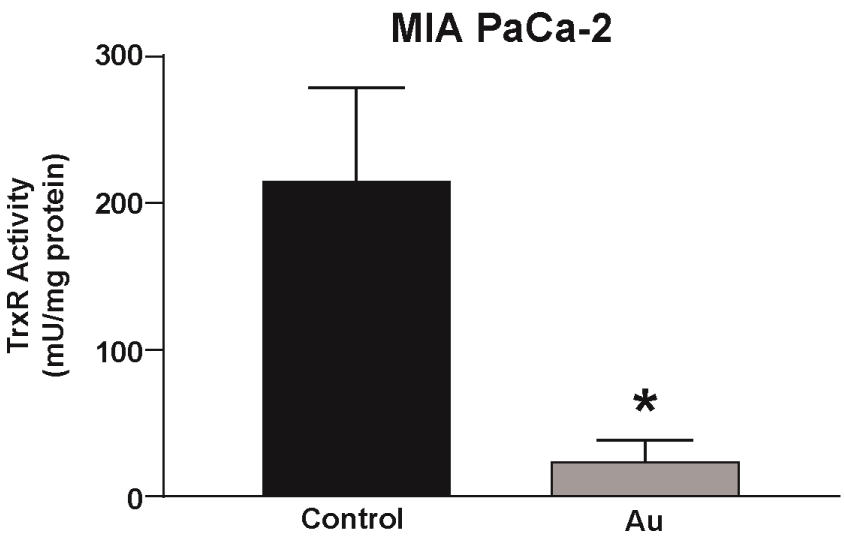


**Figure 3.** Au inhibits thioredoxin reductase activity in pancreatic cancer cells. MIA PaCa-2 cells were incubated with 1 μM Au for 3 h prior to measuring thioredoxin reductase activity. Au significantly reduced thioredoxin reductase activity compared to control. Data represent thioredoxin reductase activity in mU/mg protein ± SE (* $p < 0.05$; two-tailed unpaired Student's *t* test). Reprinted/adapted with permission from [102,103]. Copyright 2017 Elsevier.

### *4.3. Auranofin Sensitizes Pancreatic Cancer Cells to P-AscH⁻*

As described above, P-AscH⁻ is selectively cytotoxic to cancer cells due to the generation of high amounts of $H_2O_2$ [24,25,31]. Furthermore, the cytotoxic effects of P-AscH⁻ are enhanced in catalase knockout cell lines [60]. Based on these findings, it was hypothesized that inhibition of thioredoxin reductase by Au would disrupt the thioredoxin-dependent hydroperoxide scavenging system and sensitize pancreatic cancer cells to P-AscH⁻ treatment [102]. To test this, exponentially growing MIA PaCa-2 cells were treated with Au for 3 h prior to P-AscH⁻ treatment for 1 h. Stock solutions of L-ascorbic acid were prepared under argon and stored in screw-cap glass vials at 4 °C. The utilized dose of P-AscH⁻ has been previously demonstrated to result in 50% clonogenic survival ($ED_{50}$) of the MIA PaCa-2 cell line over many iterations of clonogenic survival analysis [43]. Following treatment, cells were detached, counted, and plated at designated densities, and allowed to grow for 10–14 days. Surviving fractions were calculated and normalized to control plates. Auranofin alone decreased clonogenic survival compared to the control, while the combination treatment of P-AscH⁻ with Au further decreased clonogenic survival compared to either treatment alone (Figure 4) [102].

Cancer cell killing by P-AscH⁻ has been shown to be dependent on extracellular $H_2O_2$ [33,41]. Thus, the overexpression of catalase or addition of bovine catalase in media was hypothesized to partially or completely rescue cancer cells from toxicity, mediated by the combination of P-AscH⁻ and Au. P-AscH⁻ was again dosed at the $ED_{50}$ of the cell line, as determined in previous experimentation [43]. P-AscH⁻ caused slightly more cell death in this set of experiments (~40% vs. ~60% in Figure 4), though this small difference is not uncommon [43]. The addition of bovine catalase to cell media prevented the synergistic effect of Au/P-AscH⁻ in pancreatic cancer cells (Figure 5) [102]. These findings support the hypothesis that $H_2O_2$ is responsible for the effects of P-AscH⁻ when cells are treated with Au and P-AscH⁻ in combination.

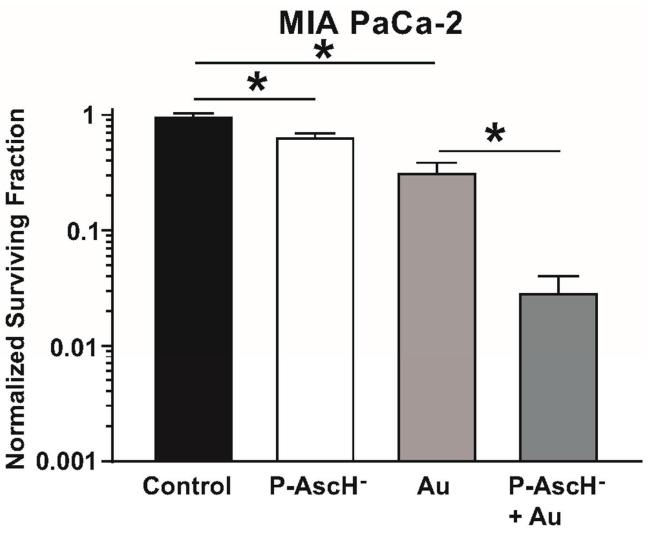


**Figure 4.** Au sensitizes pancreatic cancer cells to P-AscH$^-$. Clonogenic cell survival of MIA PaCa-2 cells incubated with Au (1 μM for 3 h) followed by 2 mM P-AscH$^-$ (1 h) was significantly decreased compared to control and to either treatment alone. Treatment with either Au or P-AscH$^-$ also decreased clonogenic survival compared to control. Data represent normalized surviving fractions compared to control ± SE (* $p < 0.01$; one-way ANOVA with Tukey's multiple comparisons). Reprinted/adapted with permission from [102,103]. Copyright 2017 Elsevier.

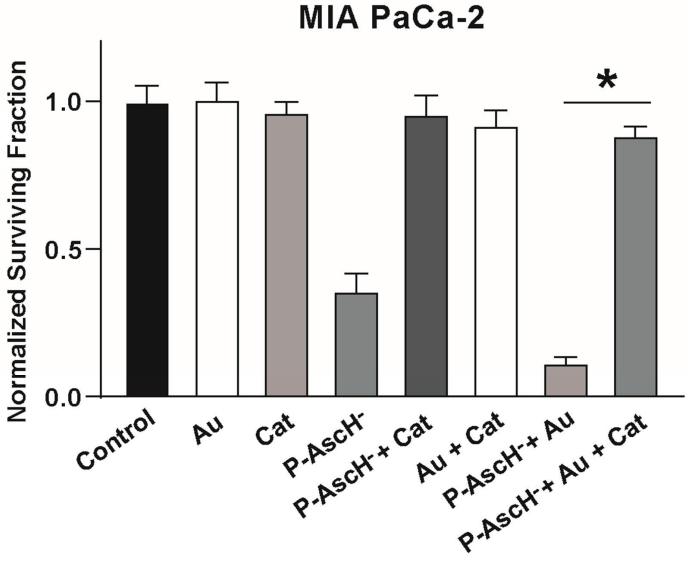


**Figure 5.** Catalase reverses killing induced by the combination of Au and P-AscH$^-$. MIA PaCa-2 cells were evaluated for clonogenic cell survival after treatment with either catalase (Cat, 100 U/mL, 1 h), Au (500 nM, 24 h), and/or P-AscH$^-$ (1 mM, 1 h). The combination of P-AscH$^-$ and Au significantly decreased clonogenic cell survival compared to P-AscH$^-$, and the addition of catalase completely reversed the decrease. Data represent normalized surviving fractions compared to controls ± SE (* $p < 0.05$; one-way ANOVA with Tukey's multiple comparisons). Reprinted/adapted with permission from [102,103]. Copyright 2017 Elsevier.

### *4.4. Au Combined with P-AscH⁻ Sensitizes Pancreatic Cancer Cells to Ionizing Radiation*

P-AscH⁻ has been shown to sensitize cancer cells to ionizing radiation in an $H_2O_2$-dependent manner in both in vitro and in vivo studies and has shown promise in recent phase I clinical trials [52,53]. To determine the radiosensitizing effects of Au and P-AscH⁻ in combination in pancreatic cancer cell lines, exponentially growing MIA PaCa-2 and AsPC-1 pancreatic cancer cells were radiated with 1–2 Gy ionizing radiation with or without treatment with Au for 24 h prior to treatment with P-AscH⁻ for 1 h. Cells were then detached, counted, and plated at designated densities and allowed to grow for 10–14 days and surviving fractions calculated as described previously [43]. The combination of Au and P-AscH⁻ caused significant cell death (~90%) when combined with radiation (Figure 6) [102]. These data suggest that combining Au with P-AscH⁻ has the possibility of increasing radiation-induced toxicity.

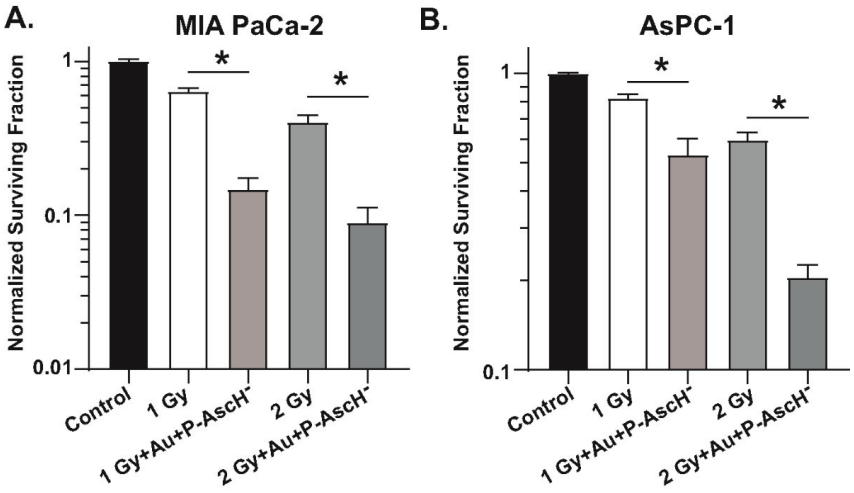


**Figure 6.** Au + P-AscH⁻ radiosensitizes pancreatic cancer cell lines. (**A**) MIA PaCa-2 and (**B**) AsPC-1 cells were evaluated for clonogenic survival after treatment with either irradiation alone (1–2 Gy) or in combination with Au (500 nM, 24 h), P-AscH⁻ (1–2 mM, 1 h), and irradiation (1–2 Gy). The combination of Auranofin and P-AscH⁻ significantly reduced clonogenic cell survival of MIA PaCa-2 and AsPC-1 cells at both 1 and 2 Gy. Data represent normalized surviving fractions compared to controls ± SE (* $p < 0.05$; two-tailed unpaired Student's $t$ test). Reprinted/adapted with permission from [102,103]. Copyright 2017 Elsevier.

### *4.5. Au and P-AscH⁻ Potential in Cancer Therapy*

These studies demonstrate that inhibition of the thioredoxin antioxidant system by the FDA-approved anti-rheumatic agent Au inhibits thioredoxin reductase activity and sensitizes pancreatic cancer cell lines to treatment with P-AscH⁻ in a manner that is dependent on $H_2O_2$. In addition, the combination of Au and P-AscH⁻ sensitizes pancreatic cancer cells to radiation therapy. The selective sensitivity imposed by thioredoxin reductase inhibition may be due to the impairment of $H_2O_2$ metabolism by peroxiredoxin, resulting in enhanced $H_2O_2$-mediated oxidative damage, leading to cell death from oxidative protein, lipid, and/or DNA damage. Alternatively, the unique role of the thioredoxin system in redox signaling may also explain the efficacy of Au. Due to the environment around the redox-active cysteines, peroxiredoxins are uniquely amenable to oxidation by $H_2O_2$ [104]. In fact, peroxiredoxins exhibit a reactivity toward $H_2O_2$ approximately six to eight orders of magnitude higher than other redox-regulated proteins [105]. This sensitivity allows peroxiredoxin to outcompete other thiols for $H_2O_2$ and serve as a medium through which oxidative equivalents can be transduced as a signal [106,107]. Indeed, peroxiredoxins

exhibit a significant influence over cell death signaling [108–110] through the oxidative modification of several targets, such as p38 [111], ERK [109], ASK1 [112,113], Akt [111,114], and STAT3 [115], among many others.

Studies have shown that peroxiredoxin hyper-oxidation sensitizes cells to cell death signaling induced by agents that produce $H_2O_2$ [111]. Other groups have shown that Auranofin-induced peroxiredoxin oxidation sensitizes triple-negative breast cancer and malignant B-cells to P-AscH$^-$ [116,117]. Peroxiredoxin hyper-oxidation induced by the combination of a decreased capacity to recycle reduced thioredoxin and enhanced $H_2O_2$ generated by P-AscH$^-$ may cause a synergistic enhancement of cell death signaling. Thus, the combination of Au and P-AscH$^-$ may serve as a highly effective means to exploit the signaling of the peroxiredoxin system to induce tumor cell-specific cell death. Future experiments can interrogate the role of peroxiredoxin signaling in cell death induced by Au/Asc by using cell lines depleted of select peroxiredoxins [106].

## 5. Conclusions

Pancreatic cancer continues to carry an extremely poor prognosis and remains the third-leading cause of cancer deaths, despite advances in chemotherapy and radiation protocols. Pharmacologic ascorbate has shown promise as an effective adjunct therapy, with phase I and phase II clinical trials suggesting a survival benefit compared to standard-of-care therapies. Ongoing clinical trials in multiple cancer types will help to further elucidate the efficacy and role of pharmacologic ascorbate in cancer therapy. The effects of P-AscH$^-$ on normal tissue have yet to be delineated. However, recent studies demonstrate radioprotective effects. This aspect of P-AscH$^-$ therapy could improve quality of life for patients and help patients tolerate higher doses of chemotherapy and/or radiation, providing additional incentive for its use. In line with previous studies' observations in other cancers, Au may also be useful as an adjunct therapy in the treatment of pancreatic cancer. Previous supporting data demonstrate that Au inhibits thioredoxin reductase and sensitizes pancreatic cancer cells to P-AscH$^-$ in a manner that is dependent on $H_2O_2$. The combination of these two clinically available agents and their roles as radiomodulators presents an exciting avenue to enhance tumor responses to chemoradiation therapies and should be explored in future experimentation by comparing Auranofin to other current standard-of-care regimens. Additionally, studying the Auranofin mechanism in cancer treatment could offer significant insight into other models and techniques for exploiting $H_2O_2$-induced cytotoxicity in cancer.

**Author Contributions:** Conceptualization, G.J.S., G.Y.C., B.R.O., J.D., H.V.B. and J.J.C.; methodology, G.J.S., G.Y.C., B.R.O., J.D. and J.J.C.; validation, G.J.S., G.Y.C., B.R.O., J.D. and J.J.C.; formal analysis, G.J.S., B.R.O. and J.D.; investigation, G.J.S., B.R.O. and J.D.; data curation, G.J.S., B.R.O., J.D. and H.V.B.; writing—original draft preparation, G.J.S., G.Y.C., B.R.O., J.D. and J.J.C.; writing—review and editing, G.J.S., G.Y.C., B.R.O., J.D. and J.J.C.; visualization, G.J.S.; supervision, J.J.C.; funding acquisition, J.J.C. All authors have read and agreed to the published version of the manuscript.

**Funding:** This research was supported by NIH grants P01 CA217797, T32 CA148062, and T32 CA78586.

**Conflicts of Interest:** The authors declare no conflict of interest.

## References

1. Siegel, R.L.; Miller, K.D.; Fuchs, H.E.; Jemal, A. Cancer statistics, 2022. *CA Cancer J. Clin.* **2022**, *72*, 7–33. [CrossRef] [PubMed]
2. Low, F.M.; Hampton, M.B.; Peskin, A.V.; Winterbourn, C.C. Peroxiredoxin 2 functions as a noncatalytic scavenger of low-level hydrogen peroxide in the erythrocyte. *Blood* **2007**, *109*, 2611–2617. [CrossRef] [PubMed]
3. Hu, J.X.; Zhao, C.F.; Chen, W.B.; Liu, Q.C.; Li, Q.W.; Lin, Y.Y.; Gao, F. Pancreatic cancer: A review of epidemiology, trend, and risk factors. *World J. Gastroenterol.* **2021**, *27*, 4298–4321. [CrossRef] [PubMed]
4. Network, N.C.C. NCCN Clinical Practice Guidelines in Oncology: Pancreatic Adenocarcinoma. 2022. Available online: https://www.nccn.org/ (accessed on 1 April 2022).
5. Li, D.; Xie, K.; Wolff, R.; Abbruzzese, J.L. Pancreatic cancer. *Lancet* **2004**, *363*, 1049–1057. [CrossRef]

6. Bengtsson, A.; Andersson, R.; Ansari, D. The actual 5-year survivors of pancreatic ductal adenocarcinoma based on real-world data. *Sci. Rep.* **2020**, *10*, 16425. [CrossRef]
7. Conroy, T.; Desseigne, F.; Ychou, M.; Bouche, O.; Guimbaud, R.; Becouarn, Y.; Adenis, A.; Raoul, J.L.; Gourgou-Bourgade, S.; de la Fouchardiere, C.; et al. FOLFIRINOX versus gemcitabine for metastatic pancreatic cancer. *N. Engl. J. Med.* **2011**, *364*, 1817–1825. [CrossRef]
8. Conroy, T.; Hammel, P.; Hebbar, M.; Ben Abdelghani, M.; Wei, A.C.; Raoul, J.L.; Chone, L.; Francois, E.; Artru, P.; Biagi, J.J.; et al. FOLFIRINOX or Gemcitabine as Adjuvant Therapy for Pancreatic Cancer. *N. Engl. J. Med.* **2018**, *379*, 2395–2406. [CrossRef]
9. Chin, V.; Nagrial, A.; Sjoquist, K.; O'Connor, C.A.; Chantrill, L.; Biankin, A.V.; Scholten, R.J.; Yip, D. Chemotherapy and radiotherapy for advanced pancreatic cancer. *Cochrane Database Syst. Rev.* **2018**, *3*, CD011044. [CrossRef]
10. Spiliopoulos, S.; Zurlo, M.T.; Casella, A.; Laera, L.; Surico, G.; Surgo, A.; Fiorentino, A.; de'Angelis, N.; Calbi, R.; Memeo, R.; et al. Current status of non-surgical treatment of locally advanced pancreatic cancer. *World J. Gastrointest. Oncol.* **2021**, *13*, 2064–2075. [CrossRef]
11. Goldstein, M.; Kastan, M.B. The DNA damage response: Implications for tumor responses to radiation and chemotherapy. *Annu. Rev. Med.* **2015**, *66*, 129–143. [CrossRef]
12. Powell, S.; McMillan, T.J. DNA damage and repair following treatment with ionizing radiation. *Radiother Oncol.* **1990**, *19*, 95–108. [CrossRef]
13. Sutherland, B.M.; Bennett, P.V.; Sidorkina, O.; Laval, J. Clustered DNA damages induced in isolated DNA and in human cells by low doses of ionizing radiation. *Proc. Natl. Acad. Sci. USA* **2000**, *97*, 103–108. [CrossRef] [PubMed]
14. Sutherland, B.M.; Bennett, P.V.; Sutherland, J.C.; Laval, J. Clustered DNA damages induced by x rays in human cells. *Radiat. Res.* **2002**, *157*, 611–616. [CrossRef]
15. Kobayashi, J.; Iwabuchi, K.; Miyagawa, K.; Sonoda, E.; Suzuki, K.; Takata, M.; Tauchi, H. Current topics in DNA double-strand break repair. *J. Radiat. Res.* **2008**, *49*, 93–103. [CrossRef]
16. Tempero, M.A.; Malafa, M.P.; Al-Hawary, M.; Asbun, H.; Bain, A.; Behrman, S.W.; Benson, A.B.; Binder, E.; Cardin, D.B.; Cha, C.; et al. Pancreatic Adenocarcinoma, Version 2.2017, NCCN Clinical Practice Guidelines in Oncology. *J. Natl. Compr. Cancer Netw.* **2017**, *15*, 1028–1061. [CrossRef]
17. Hammel, P.; Huguet, F.; van Laethem, J.L.; Goldstein, D.; Glimelius, B.; Artru, P.; Borbath, I.; Bouche, O.; Shannon, J.; Andre, T.; et al. Effect of Chemoradiotherapy vs Chemotherapy on Survival in Patients with Locally Advanced Pancreatic Cancer Controlled After 4 Months of Gemcitabine With or Without Erlotinib: The LAP07 Randomized Clinical Trial. *JAMA* **2016**, *315*, 1844–1853. [CrossRef]
18. Tempero, M.A.; Malafa, M.P.; Chiorean, E.G.; Czito, B.; Scaife, C.; Narang, A.K.; Fountzilas, C.; Wolpin, B.M.; Al-Hawary, M.; Asbun, H.; et al. NCCN Guidelines Insights: Pancreatic Adenocarcinoma, Version 1.2019: Featured Updates to the NCCN Guidelines. *J. Natl. Compr. Cancer Netw.* **2019**, *17*, 202–210. [CrossRef]
19. Abi Jaoude, J.; Thunshelle, C.P.; Kouzy, R.; Nguyen, N.D.; Lin, D.; Prakash, L.; Bumanlag, I.M.; Noticewala, S.S.; Niedzielski, J.S.; Beddar, S.; et al. Stereotactic Versus Conventional Radiation Therapy for Patients with Pancreatic Cancer in the Modern Era. *Adv. Radiat. Oncol.* **2021**, *6*, 100763. [CrossRef]
20. Ghaly, M.; Gogineni, E.; Herman, J.; Saif, M.W. New Potential Options for SBRT in Pancreatic Cancer. *Cancer Med. J.* **2021**, *4*, 41–50.
21. Pavic, M.; Niyazi, M.; Wilke, L.; Corradini, S.; Vornhulz, M.; Mansmann, U.; Al Tawil, A.; Fritsch, R.; Horner-Rieber, J.; Debus, J.; et al. MR-guided adaptive stereotactic body radiotherapy (SBRT) of primary tumor for pain control in metastatic pancreatic ductal adenocarcinoma (mPDAC): An open randomized, multicentric, parallel group clinical trial (MASPAC). *Radiat. Oncol.* **2022**, *17*, 18. [CrossRef]
22. Qing, S.; Gu, L.; Zhang, H. Phase I study of dose-escalated stereotactic body radiation therapy for locally advanced pancreatic head cancers: Initial clinical results. *Cancer Med.* **2021**, *10*, 6736–6743. [CrossRef] [PubMed]
23. Oberstein, P.E.; Olive, K.P. Pancreatic cancer: Why is it so hard to treat? *Therap. Adv. Gastroenterol.* **2013**, *6*, 321–337. [CrossRef] [PubMed]
24. Buettner, G.R. The pecking order of free radicals and antioxidants: Lipid peroxidation, alpha-tocopherol, and ascorbate. *Arch. Biochem. Biophys.* **1993**, *300*, 535–543. [CrossRef]
25. Padayatty, S.J.; Sun, H.; Wang, Y.; Riordan, H.D.; Hewitt, S.M.; Katz, A.; Wesley, R.A.; Levine, M. Vitamin C pharmacokinetics: Implications for oral and intravenous use. *Ann. Intern. Med.* **2004**, *140*, 533–537. [CrossRef] [PubMed]
26. Levine, M.; Wang, Y.; Padayatty, S.J.; Morrow, J. A new recommended dietary allowance of vitamin C for healthy young women. *Proc. Natl. Acad. Sci. USA* **2001**, *98*, 9842–9846. [CrossRef]
27. Vera, J.C.; Rivas, C.I.; Velasquez, F.V.; Zhang, R.H.; Concha, I.I.; Golde, D.W. Resolution of the facilitated transport of dehydroascorbic acid from its intracellular accumulation as ascorbic acid. *J. Biol. Chem.* **1995**, *270*, 23706–23712. [CrossRef] [PubMed]
28. Savini, I.; Rossi, A.; Pierro, C.; Avigliano, L.; Catani, M.V. SVCT1 and SVCT2: Key proteins for vitamin C uptake. *Amino. Acids.* **2008**, *34*, 347–355. [CrossRef]
29. Levine, M.; Conry-Cantilena, C.; Wang, Y.; Welch, R.W.; Washko, P.W.; Dhariwal, K.R.; Park, J.B.; Lazarev, A.; Graumlich, J.F.; King, J.; et al. Vitamin C pharmacokinetics in healthy volunteers: Evidence for a recommended dietary allowance. *Proc. Natl. Acad. Sci. USA* **1996**, *93*, 3704–3709. [CrossRef]

30. Verrax, J.; Calderon, P.B. Pharmacologic concentrations of ascorbate are achieved by parenteral administration and exhibit antitumoral effects. *Free Radic. Biol. Med.* **2009**, *47*, 32–40. [CrossRef]
31. Du, J.; Martin, S.M.; Levine, M.; Wagner, B.A.; Buettner, G.R.; Wang, S.H.; Taghiyev, A.F.; Du, C.; Knudson, C.M.; Cullen, J.J. Mechanisms of ascorbate-induced cytotoxicity in pancreatic cancer. *Clin. Cancer Res. Off. J. Am. Assoc. Cancer Res.* **2010**, *16*, 509–520. [CrossRef]
32. Chen, Q.; Espey, M.G.; Krishna, M.C.; Mitchell, J.B.; Corpe, C.P.; Buettner, G.R.; Shacter, E.; Levine, M. Pharmacologic ascorbic acid concentrations selectively kill cancer cells: Action as a pro-drug to deliver hydrogen peroxide to tissues. *Proc. Natl. Acad. Sci. USA* **2005**, *102*, 13604–13609. [CrossRef] [PubMed]
33. Schoenfeld, J.D.; Sibenaller, Z.A.; Mapuskar, K.A.; Wagner, B.A.; Cramer-Morales, K.L.; Furqan, M.; Sandhu, S.; Carlisle, T.L.; Smith, M.C.; Abu Hejleh, T.; et al. $O_2^-$ and $H_2O_2$-Mediated Disruption of Fe Metabolism Causes the Differential Susceptibility of NSCLC and GBM Cancer Cells to Pharmacological Ascorbate. *Cancer Cell* **2017**, *31*, 487–500. [CrossRef] [PubMed]
34. Cameron, E.; Campbell, A.; Jack, T. The orthomolecular treatment of cancer. III. Reticulum cell sarcoma: Double complete regression induced by high-dose ascorbic acid therapy. *Chem. Biol. Interact.* **1975**, *11*, 387–393. [CrossRef]
35. Cameron, E.; Pauling, L. Supplemental ascorbate in the supportive treatment of cancer: Prolongation of survival times in terminal human cancer. *Proc. Natl. Acad. Sci. USA* **1976**, *73*, 3685–3689. [CrossRef] [PubMed]
36. Cameron, E.; Pauling, L. Supplemental ascorbate in the supportive treatment of cancer: Reevaluation of prolongation of survival times in terminal human cancer. *Proc. Natl. Acad. Sci. USA* **1978**, *75*, 4538–4542. [CrossRef]
37. Creagan, E.T.; Moertel, C.G.; O'Fallon, J.R.; Schutt, A.J.; O'Connell, M.J.; Rubin, J.; Frytak, S. Failure of high-dose vitamin C (ascorbic acid) therapy to benefit patients with advanced cancer. A controlled trial. *N. Engl. J. Med.* **1979**, *301*, 687–690. [CrossRef] [PubMed]
38. Moertel, C.G.; Fleming, T.R.; Creagan, E.T.; Rubin, J.; O'Connell, M.J.; Ames, M.M. High-dose vitamin C versus placebo in the treatment of patients with advanced cancer who have had no prior chemotherapy. A randomized double-blind comparison. *N. Engl. J. Med.* **1985**, *312*, 137–141. [CrossRef]
39. Ghanem, A.; Melzer, A.M.; Zaal, E.; Neises, L.; Baltissen, D.; Matar, O.; Glennemeier-Marke, H.; Almouhanna, F.; Theobald, J.; Abu El Maaty, M.A.; et al. Ascorbate kills breast cancer cells by rewiring metabolism via redox imbalance and energy crisis. *Free Radic. Biol. Med.* **2021**, *163*, 196–209. [CrossRef]
40. Yun, J.; Mullarky, E.; Lu, C.; Bosch, K.N.; Kavalier, A.; Rivera, K.; Roper, J.; Chio, I.I.; Giannopoulou, E.G.; Rago, C.; et al. Vitamin C selectively kills KRAS and BRAF mutant colorectal cancer cells by targeting GAPDH. *Science* **2015**, *350*, 1391–1396. [CrossRef]
41. Chen, Q.; Espey, M.G.; Sun, A.Y.; Pooput, C.; Kirk, K.L.; Krishna, M.C.; Khosh, D.B.; Drisko, J.; Levine, M. Pharmacologic doses of ascorbate act as a prooxidant and decrease growth of aggressive tumor xenografts in mice. *Proc. Natl. Acad. Sci. USA* **2008**, *105*, 11105–11109. [CrossRef]
42. Cieslak, J.A.; Strother, R.K.; Rawal, M.; Du, J.; Doskey, C.M.; Schroeder, S.R.; Button, A.; Wagner, B.A.; Buettner, G.R.; Cullen, J.J. Manganoporphyrins and ascorbate enhance gemcitabine cytotoxicity in pancreatic cancer. *Free Radic. Biol. Med.* **2015**, *83*, 227–237. [CrossRef] [PubMed]
43. Doskey, C.M.; Buranasudja, V.; Wagner, B.A.; Wilkes, J.G.; Du, J.; Cullen, J.J.; Buettner, G.R. Tumor cells have decreased ability to metabolize $H_2O_2$: Implications for pharmacological ascorbate in cancer therapy. *Redox Biol.* **2016**, *10*, 274–284. [CrossRef] [PubMed]
44. Espey, M.G.; Chen, P.; Chalmers, B.; Drisko, J.; Sun, A.Y.; Levine, M.; Chen, Q. Pharmacologic ascorbate synergizes with gemcitabine in preclinical models of pancreatic cancer. *Free Radic. Biol. Med.* **2011**, *50*, 1610–1619. [CrossRef] [PubMed]
45. Ma, Y.; Chen, P.; Drisko, J.A.; Khabele, D.; Godwin, A.K.; Chen, Q. Pharmacological ascorbate induces 'BRCAness' and enhances the effects of Poly(ADP-Ribose) polymerase inhibitors against BRCA1/2 wild-type ovarian cancer. *Oncol. Lett.* **2020**, *19*, 2629–2638. [CrossRef]
46. Schafer, F.Q.; Buettner, G.R. Redox environment of the cell as viewed through the redox state of the glutathione disulfide/glutathione couple. *Free Radic. Biol. Med.* **2001**, *30*, 1191–1212. [CrossRef]
47. Liu, J.; Hinkhouse, M.M.; Sun, W.; Weydert, C.J.; Ritchie, J.M.; Oberley, L.W.; Cullen, J.J. Redox regulation of pancreatic cancer cell growth: Role of glutathione peroxidase in the suppression of the malignant phenotype. *Hum. Gene Ther.* **2004**, *15*, 239–250. [CrossRef]
48. Monti, D.A.; Mitchell, E.; Bazzan, A.J.; Littman, S.; Zabrecky, G.; Yeo, C.J.; Pillai, M.V.; Newberg, A.B.; Deshmukh, S.; Levine, M. Phase I evaluation of intravenous ascorbic acid in combination with gemcitabine and erlotinib in patients with metastatic pancreatic cancer. *PLoS ONE* **2012**, *7*, e29794. [CrossRef]
49. Welsh, J.L.; Wagner, B.A.; van't Erve, T.J.; Zehr, P.S.; Berg, D.J.; Halfdanarson, T.R.; Yee, N.S.; Bodeker, K.L.; Du, J.; Roberts, L.J., 2nd; et al. Pharmacological ascorbate with gemcitabine for the control of metastatic and node-positive pancreatic cancer (PACMAN): Results from a phase I clinical trial. *Cancer Chemother. Pharmacol.* **2013**, *71*, 765–775. [CrossRef]
50. Di Marco, M.; Di Cicilia, R.; Macchini, M.; Nobili, E.; Vecchiarelli, S.; Brandi, G.; Biasco, G. Metastatic pancreatic cancer: Is gemcitabine still the best standard treatment? (Review). *Oncol. Rep.* **2010**, *23*, 1183–1192. [CrossRef]
51. Polireddy, K.; Dong, R.; Reed, G.; Yu, J.; Chen, P.; Williamson, S.; Violet, P.C.; Pessetto, Z.; Godwin, A.K.; Fan, F.; et al. High Dose Parenteral Ascorbate Inhibited Pancreatic Cancer Growth and Metastasis: Mechanisms and a Phase I/IIa study. *Sci. Rep.* **2017**, *7*, 17188. [CrossRef]

52. Du, J.; Cieslak, J.A., 3rd; Welsh, J.L.; Sibenaller, Z.A.; Allen, B.G.; Wagner, B.A.; Kalen, A.L.; Doskey, C.M.; Strother, R.K.; Button, A.M.; et al. Pharmacological Ascorbate Radiosensitizes Pancreatic Cancer. *Cancer Res.* **2015**, *75*, 3314–3326. [CrossRef] [PubMed]
53. Alexander, M.S.; Wilkes, J.G.; Schroeder, S.R.; Buettner, G.R.; Wagner, B.A.; Du, J.; Gibson-Corley, K.; O'Leary, B.R.; Spitz, D.R.; Buatti, J.M.; et al. Pharmacologic Ascorbate Reduces Radiation-Induced Normal Tissue Toxicity and Enhances Tumor Radiosensitization in Pancreatic Cancer. *Cancer Res.* **2018**, *78*, 6838–6851. [CrossRef] [PubMed]
54. Chen, Q.; Espey, M.G.; Sun, A.Y.; Lee, J.H.; Krishna, M.C.; Shacter, E.; Choyke, P.L.; Pooput, C.; Kirk, K.L.; Buettner, G.R.; et al. Ascorbate in pharmacologic concentrations selectively generates ascorbate radical and hydrogen peroxide in extracellular fluid in vivo. *Proc. Natl. Acad. Sci. USA* **2007**, *104*, 8749–8754. [CrossRef] [PubMed]
55. Alexander, M.S.; O'Leary, B.R.; Wilkes, J.G.; Gibson, A.R.; Wagner, B.A.; Du, J.; Sarsour, E.; Hwang, R.F.; Buettner, G.R.; Cullen, J.J. Enhanced Pharmacological Ascorbate Oxidation Radiosensitizes Pancreatic Cancer. *Radiat. Res.* **2019**, *191*, 43–51. [CrossRef]
56. Perrakis, N.; Athanassiou, E.; Vamvakopoulou, D.; Kyriazi, M.; Kappos, H.; Vamvakopoulos, N.C.; Nomikos, I. Practical approaches to effective management of intestinal radiation injury: Benefit of resectional surgery. *World J. Gastroenterol.* **2011**, *17*, 4013–4016. [CrossRef]
57. Ngo, B.; Van Riper, J.M.; Cantley, L.C.; Yun, J. Targeting cancer vulnerabilities with high-dose vitamin C. *Nat. Rev. Cancer* **2019**, *19*, 271–282. [CrossRef]
58. Wang, H.; Liu, J.; Xia, G.; Lei, S.; Huang, X.; Huang, X. Survival of pancreatic cancer patients is negatively correlated with age at diagnosis: A population-based retrospective study. *Sci. Rep.* **2020**, *10*, 7048. [CrossRef]
59. Petrelli, F.; Coinu, A.; Borgonovo, K.; Cabiddu, M.; Barni, S. Progression-free survival as surrogate endpoint in advanced pancreatic cancer: Meta-analysis of 30 randomized first-line trials. *Hepatobiliary Pancreat. Dis. Int.* **2015**, *14*, 124–131. [CrossRef]
60. Du, J.; Carroll, R.S.; Steers, G.J.; Wagner, B.A.; O'Leary, B.R.; Jensen, C.S.; Buettner, G.R.; Cullen, J.J. Catalase Modulates the Radio-Sensitization of Pancreatic Cancer Cells by Pharmacological Ascorbate. *Antioxidants* **2021**, *10*, 614. [CrossRef]
61. Du, J.; Cullen, J.J.; Buettner, G.R. Ascorbic acid: Chemistry, biology and the treatment of cancer. *Biochim. Biophys. Acta* **2012**, *1826*, 443–457. [CrossRef]
62. Oberley, T.D.; Oberley, L.W. Antioxidant enzyme levels in cancer. *Histol. Histopathol.* **1997**, *12*, 525–535. [PubMed]
63. Sasaki, K.; Bannai, S.; Makino, N. Kinetics of hydrogen peroxide elimination by human umbilical vein endothelial cells in culture. *Biochim. Biophys. Acta* **1998**, *1380*, 275–288. [CrossRef]
64. Mueller, S.; Riedel, H.D.; Stremmel, W. Direct evidence for catalase as the predominant $H_2O_2$-removing enzyme in human erythrocytes. *Blood* **1997**, *90*, 4973–4978. [CrossRef] [PubMed]
65. Flohe, L. The glutathione peroxidase reaction: Molecular basis of the antioxidant function of selenium in mammals. *Curr. Top Cell Regul.* **1985**, *27*, 473–478. [CrossRef]
66. Schoenfeld, J.D.; Alexander, M.S.; Waldron, T.J.; Sibenaller, Z.A.; Spitz, D.R.; Buettner, G.R.; Allen, B.G.; Cullen, J.J. Pharmacological Ascorbate as a Means of Sensitizing Cancer Cells to Radio-Chemotherapy While Protecting Normal Tissue. *Semin. Radiat. Oncol.* **2019**, *29*, 25–32. [CrossRef]
67. Larsson, A. Enzymatic Synthesis of Deoxyribonucleotides. VII. Studies on the Hydrogen Transfer with Tritiated Water. *Biochemistry* **1965**, *4*, 1984–1993. [CrossRef]
68. Moore, E.C. A thioredoxin—thioredoxin reductase system from rat tumor. *Biochem. Biophys. Res. Commun.* **1967**, *29*, 264–268. [CrossRef]
69. Lu, J.; Holmgren, A. The thioredoxin antioxidant system. *Free Radic. Biol. Med.* **2014**, *66*, 75–87. [CrossRef]
70. Deisseroth, A.; Dounce, A.L. Catalase: Physical and chemical properties, mechanism of catalysis, and physiological role. *Physiol. Rev.* **1970**, *50*, 319–375. [CrossRef]
71. Ogusucu, R.; Rettori, D.; Munhoz, D.C.; Netto, L.E.; Augusto, O. Reactions of yeast thioredoxin peroxidases I and II with hydrogen peroxide and peroxynitrite: Rate constants by competitive kinetics. *Free Radic. Biol. Med.* **2007**, *42*, 326–334. [CrossRef]
72. Holmgren, A.; Lu, J. Thioredoxin and thioredoxin reductase: Current research with special reference to human disease. *Biochem. Biophys. Res. Commun.* **2010**, *396*, 120–124. [CrossRef] [PubMed]
73. Shoeib, T.; Atkinson, D.W.; Sharp, B.L. Structural analysis of the anti-arthritic drug Auranofin: Its complexes with cysteine, selenocysteine and their fragmentation products. *Inorg. Chim. Acta* **2010**, *363*, 184–192. [CrossRef]
74. Finkelstein, A.E.; Walz, D.T.; Batista, V.; Mizraji, M.; Roisman, F.; Misher, A. Auranofin. New oral gold compound for treatment of rheumatoid arthritis. *Ann. Rheum. Dis.* **1976**, *35*, 251–257. [CrossRef] [PubMed]
75. Champion, G.D.; Graham, G.G.; Ziegler, J.B. The gold complexes. *Baillieres Clin. Rheumatol.* **1990**, *4*, 491–534. [CrossRef]
76. Kim, N.H.; Lee, M.Y.; Park, S.J.; Choi, J.S.; Oh, M.K.; Kim, I.S. Auranofin blocks interleukin-6 signalling by inhibiting phosphorylation of JAK1 and STAT3. *Immunology* **2007**, *122*, 607–614. [CrossRef]
77. Stern, I.; Wataha, J.C.; Lewis, J.B.; Messer, R.L.; Lockwood, P.E.; Tseng, W.Y. Anti-rheumatic gold compounds as sublethal modulators of monocytic LPS-induced cytokine secretion. *Toxicol. Vitr.* **2005**, *19*, 365–371. [CrossRef]
78. Kim, N.H.; Oh, M.K.; Park, H.J.; Kim, I.S. Auranofin, a gold(I)-containing antirheumatic compound, activates Keap1/Nrf2 signaling via Rac1/iNOS signal and mitogen-activated protein kinase activation. *J. Pharmacol. Sci.* **2010**, *113*, 246–254. [CrossRef]
79. Han, S.; Kim, K.; Kim, H.; Kwon, J.; Lee, Y.H.; Lee, C.K.; Song, Y.; Lee, S.J.; Ha, N.; Kim, K. Auranofin inhibits overproduction of pro-inflammatory cytokines, cyclooxygenase expression and PGE2 production in macrophages. *Arch. Pharm. Res.* **2008**, *31*, 67–74. [CrossRef]

80. Han, S.; Kim, K.; Song, Y.; Kim, H.; Kwon, J.; Lee, Y.H.; Lee, C.K.; Lee, S.J.; Ha, N.; Kim, K. Auranofin, an immunosuppressive drug, inhibits MHC class I and MHC class II pathways of antigen presentation in dendritic cells. *Arch. Pharm. Res.* **2008**, *31*, 370–376. [CrossRef]
81. Park, S.J.; Kim, I.S. The role of p38 MAPK activation in auranofin-induced apoptosis of human promyelocytic leukaemia HL-60 cells. *Br. J. Pharmacol.* **2005**, *146*, 506–513. [CrossRef]
82. Honda, Z.; Iizasa, T.; Morita, Y.; Matsuta, K.; Nishida, Y.; Miyamoto, T. Differential inhibitory effects of auranofin on leukotriene B4 and leukotriene C4 formation by human polymorphonuclear leukocytes. *Biochem. Pharmacol.* **1987**, *36*, 1475–1481. [CrossRef]
83. Yamada, M.; Niki, H.; Yamashita, M.; Mue, S.; Ohuchi, K. Prostaglandin E2 production dependent upon cyclooxygenase-1 and cyclooxygenase-2 and its contradictory modulation by auranofin in rat peritoneal macrophages. *J. Pharmacol. Exp. Ther.* **1997**, *281*, 1005–1012. [PubMed]
84. Yamashita, M.; Niki, H.; Yamada, M.; Watanabe-Kobayashi, M.; Mue, S.; Ohuchi, K. Dual effects of auranofin on prostaglandin E2 production by rat peritoneal macrophages. *Eur. J. Pharmacol.* **1997**, *325*, 221–227. [CrossRef]
85. Walz, D.T.; DiMartino, M.J.; Griswold, D.E.; Intoccia, A.P.; Flanagan, T.L. Biologic actions and pharmacokinetic studies of auranofin. *Am. J. Med.* **1983**, *75*, 90–108. [CrossRef]
86. Sannella, A.R.; Casini, A.; Gabbiani, C.; Messori, L.; Bilia, A.R.; Vincieri, F.F.; Majori, G.; Severini, C. New uses for old drugs. Auranofin, a clinically established antiarthritic metallodrug, exhibits potent antimalarial effects in vitro: Mechanistic and pharmacological implications. *FEBS Lett.* **2008**, *582*, 844–847. [CrossRef] [PubMed]
87. Newman, Z.L.; Sirianni, N.; Mawhinney, C.; Lee, M.S.; Leppla, S.H.; Moayeri, M.; Johansen, L.M. Auranofin protects against anthrax lethal toxin-induced activation of the Nlrp1b inflammasome. *Antimicrob. Agents Chemother.* **2011**, *55*, 1028–1035. [CrossRef] [PubMed]
88. Hutton, M.L.; Pehlivanoglu, H.; Vidor, C.J.; James, M.L.; Thomson, M.J.; Lyras, D. Repurposing auranofin as a Clostridioides difficile therapeutic. *J. Antimicrob. Chemother.* **2020**, *75*, 409–417. [CrossRef]
89. Sharma, N.; Singh, A.; Sharma, R.; Kumar, A. Repurposing of Auranofin Against Bacterial Infections: An In silico and In vitro Study. *Curr. Comput. Aided Drug Des.* **2021**, *17*, 687–701. [CrossRef]
90. Lewis, M.G.; DaFonseca, S.; Chomont, N.; Palamara, A.T.; Tardugno, M.; Mai, A.; Collins, M.; Wagner, W.L.; Yalley-Ogunro, J.; Greenhouse, J.; et al. Gold drug auranofin restricts the viral reservoir in the monkey AIDS model and induces containment of viral load following ART suspension. *AIDS* **2011**, *25*, 1347–1356. [CrossRef]
91. Ashino, T.; Sugiuchi, J.; Uehara, J.; Naito-Yamamoto, Y.; Kenmotsu, S.; Iwakura, Y.; Shioda, S.; Numazawa, S.; Yoshida, T. Auranofin protects against cocaine-induced hepatic injury through induction of heme oxygenase-1. *J. Toxicol. Sci.* **2011**, *36*, 635–643. [CrossRef]
92. Gromer, S.; Arscott, L.D.; Williams, C.H., Jr.; Schirmer, R.H.; Becker, K. Human placenta thioredoxin reductase. Isolation of the selenoenzyme, steady state kinetics, and inhibition by therapeutic gold compounds. *J. Biol. Chem.* **1998**, *273*, 20096–20101. [CrossRef] [PubMed]
93. Saei, A.A.; Gullberg, H.; Sabatier, P.; Beusch, C.M.; Johansson, K.; Lundgren, B.; Arvidsson, P.I.; Arner, E.S.J.; Zubarev, R.A. Comprehensive chemical proteomics for target deconvolution of the redox active drug auranofin. *Redox Biol.* **2020**, *32*, 101491. [CrossRef] [PubMed]
94. Cox, A.G.; Brown, K.K.; Arner, E.S.; Hampton, M.B. The thioredoxin reductase inhibitor auranofin triggers apoptosis through a Bax/Bak-dependent process that involves peroxiredoxin 3 oxidation. *Biochem. Pharmacol.* **2008**, *76*, 1097–1109. [CrossRef] [PubMed]
95. Olney, K.E.; Du, J.; van't Erve, T.J.; Witmer, J.R.; Sibenaller, Z.A.; Wagner, B.A.; Buettner, G.R.; Cullen, J.J. Inhibitors of hydroperoxide metabolism enhance ascorbate-induced cytotoxicity. *Free Radic. Res.* **2013**, *47*, 154–163. [CrossRef]
96. Joo, M.K.; Shin, S.; Ye, D.J.; An, H.G.; Kwon, T.U.; Baek, H.S.; Kwon, Y.J.; Chun, Y.J. Combined treatment with auranofin and trametinib induces synergistic apoptosis in breast cancer cells. *J. Toxicol. Environ. Health A* **2021**, *84*, 84–94. [CrossRef]
97. Lee, J.E.; Kwon, Y.J.; Baek, H.S.; Ye, D.J.; Cho, E.; Choi, H.K.; Oh, K.S.; Chun, Y.J. Synergistic induction of apoptosis by combination treatment with mesupron and auranofin in human breast cancer cells. *Arch. Pharm. Res.* **2017**, *40*, 746–759. [CrossRef]
98. Ye, D.J.; Kwon, Y.J.; Baek, H.S.; Cho, E.; Kwon, T.U.; Chun, Y.J. Combination treatment with auranofin and nutlin-3a induces synergistic cytotoxicity in breast cancer cells. *J. Toxicol. Environ. Health A* **2019**, *82*, 626–637. [CrossRef]
99. Freire Boullosa, L.; Van Loenhout, J.; Flieswasser, T.; De Waele, J.; Hermans, C.; Lambrechts, H.; Cuypers, B.; Laukens, K.; Bartholomeus, E.; Siozopoulou, V.; et al. Auranofin reveals therapeutic anticancer potential by triggering distinct molecular cell death mechanisms and innate immunity in mutant p53 non-small cell lung cancer. *Redox Biol.* **2021**, *42*, 101949. [CrossRef]
100. Lin, Z.; Li, Q.; Zhao, Y.; Lin, Z.; Cheng, N.; Zhang, D.; Liu, G.; Lin, J.; Zhang, H.; Lin, D. Combination of Auranofin and ICG-001 Suppress the Proliferation and Metastasis of Colon Cancer. *Front. Oncol.* **2021**, *11*, 738085. [CrossRef]
101. Park, S.H.; Lee, J.H.; Berek, J.S.; Hu, M.C. Auranofin displays anticancer activity against ovarian cancer cells through FOXO3 activation independent of p53. *Int. J. Oncol.* **2014**, *45*, 1691–1698. [CrossRef]
102. O'Leary, B.; Du, J.; Heer, C.; Van Beek, H.; Spitz, D.R.; Cullen, J.J. Inhibition of Peroxide Removal Enhances Pharmacological Ascorbate and Ionizing Radiation-Induced Cytotoxicity of Pancreatic Ductal Adenocarcinoma. *Free Radical. Bio. Med.* **2017**, *112*, 97. [CrossRef]
103. Van Beek, H. Inhibition of Peroxide Removal Systems and Ascorbate-Induced Cytotoxicity in Pancreatic Cancer. Master's Thesis, University of Iowa, Iowa City, IA, USA, 2016. [CrossRef]

104. Day, A.M.; Brown, J.D.; Taylor, S.R.; Rand, J.D.; Morgan, B.A.; Veal, E.A. Inactivation of a peroxiredoxin by hydrogen peroxide is critical for thioredoxin-mediated repair of oxidized proteins and cell survival. *Mol. Cell* **2012**, *45*, 398–408. [CrossRef] [PubMed]
105. Nagy, P.; Karton, A.; Betz, A.; Peskin, A.V.; Pace, P.; O'Reilly, R.J.; Hampton, M.B.; Radom, L.; Winterbourn, C.C. Model for the exceptional reactivity of peroxiredoxins 2 and 3 with hydrogen peroxide: A kinetic and computational study. *J. Biol. Chem.* **2011**, *286*, 18048–18055. [CrossRef] [PubMed]
106. Stocker, S.; Maurer, M.; Ruppert, T.; Dick, T.P. A role for 2-Cys peroxiredoxins in facilitating cytosolic protein thiol oxidation. *Nat. Chem. Biol.* **2018**, *14*, 148–155. [CrossRef]
107. Stocker, S.; Van Laer, K.; Mijuskovic, A.; Dick, T.P. The Conundrum of Hydrogen Peroxide Signaling and the Emerging Role of Peroxiredoxins as Redox Relay Hubs. *Antioxid. Redox Signal.* **2018**, *28*, 558–573. [CrossRef]
108. Chang, T.S.; Cho, C.S.; Park, S.; Yu, S.; Kang, S.W.; Rhee, S.G. Peroxiredoxin III, a mitochondrion-specific peroxidase, regulates apoptotic signaling by mitochondria. *J. Biol. Chem.* **2004**, *279*, 41975–41984. [CrossRef]
109. Kang, S.W.; Chang, T.S.; Lee, T.H.; Kim, E.S.; Yu, D.Y.; Rhee, S.G. Cytosolic peroxiredoxin attenuates the activation of Jnk and p38 but potentiates that of Erk in Hela cells stimulated with tumor necrosis factor-alpha. *J. Biol. Chem.* **2004**, *279*, 2535–2543. [CrossRef]
110. Kim, H.; Lee, T.H.; Park, E.S.; Suh, J.M.; Park, S.J.; Chung, H.K.; Kwon, O.Y.; Kim, Y.K.; Ro, H.K.; Shong, M. Role of peroxiredoxins in regulating intracellular hydrogen peroxide and hydrogen peroxide-induced apoptosis in thyroid cells. *J. Biol. Chem.* **2000**, *275*, 18266–18270. [CrossRef]
111. Collins, J.A.; Wood, S.T.; Nelson, K.J.; Rowe, M.A.; Carlson, C.S.; Chubinskaya, S.; Poole, L.B.; Furdui, C.M.; Loeser, R.F. Oxidative Stress Promotes Peroxiredoxin Hyperoxidation and Attenuates Pro-survival Signaling in Aging Chondrocytes. *J. Biol. Chem.* **2016**, *291*, 6641–6654. [CrossRef]
112. Kim, S.Y.; Kim, T.J.; Lee, K.Y. A novel function of peroxiredoxin 1 (Prx-1) in apoptosis signal-regulating kinase 1 (ASK1)-mediated signaling pathway. *FEBS Lett.* **2008**, *582*, 1913–1918. [CrossRef]
113. Zhang, M.; Niu, W.; Zhang, J.; Ge, L.; Yang, J.; Sun, Z.; Tang, X. Peroxiredoxin 1 suppresses apoptosis via regulation of the apoptosis signal-regulating kinase 1 signaling pathway in human oral leukoplakia. *Oncol. Lett.* **2015**, *10*, 1841–1847. [CrossRef] [PubMed]
114. Hu, J.; Zhang, H.; Cao, M.; Wang, L.; Wu, S.; Fang, B. Auranofin Enhances Ibrutinib's Anticancer Activity in EGFR-Mutant Lung Adenocarcinoma. *Mol. Cancer Ther.* **2018**, *17*, 2156–2163. [CrossRef] [PubMed]
115. Sobotta, M.C.; Liou, W.; Stocker, S.; Talwar, D.; Oehler, M.; Ruppert, T.; Scharf, A.N.; Dick, T.P. Peroxiredoxin-2 and STAT3 form a redox relay for $H_2O_2$ signaling. *Nat. Chem. Biol.* **2015**, *11*, 64–70. [CrossRef] [PubMed]
116. Hatem, E.; Azzi, S.; El Banna, N.; He, T.; Heneman-Masurel, A.; Vernis, L.; Baille, D.; Masson, V.; Dingli, F.; Loew, D.; et al. Auranofin/Vitamin C: A Novel Drug Combination Targeting Triple-Negative Breast Cancer. *J. Natl. Cancer Inst.* **2019**, *111*, 597–608. [CrossRef]
117. Graczyk-Jarzynka, A.; Goral, A.; Muchowicz, A.; Zagozdzon, R.; Winiarska, M.; Bajor, M.; Trzeciecka, A.; Fidyt, K.; Krupka, J.A.; Cyran, J.; et al. Inhibition of thioredoxin-dependent $H_2O_2$ removal sensitizes malignant B-cells to pharmacological ascorbate. *Redox Biol.* **2019**, *21*, 101062. [CrossRef]

antioxidants

MDPI

*Article*

# Supplemental Ferulic Acid Inhibits Total Body Irradiation-Mediated Bone Marrow Damage, Bone Mass Loss, Stem Cell Senescence, and Hematopoietic Defect in Mice by Enhancing Antioxidant Defense Systems

**Sajeev Wagle [1,†], Hyun-Jaung Sim [1,2,†], Govinda Bhattarai [1], Ki-Choon Choi [3], Sung-Ho Kook [1,2,*], Jeong-Chae Lee [1,2,*] and Young-Mi Jeon [1,*]**

[1] Cluster for Craniofacial Development and Regeneration Research, Institute of Oral Bioscience, Jeonbuk National University School of Dentistry, Jeonju 54896, Korea; swagle@jbnu.ac.kr (S.W.); skynow@hanmail.net (H.-J.S.); govinda@jbnu.ac.kr (G.B.)
[2] Department of Bioactive Material Sciences and Research Center of Bioactive Materials, Jeonbuk National University, Jeonju 54896, Korea
[3] Grassland and Forages Research Center, National Institute of Animal Science, Cheonan 31002, Korea; choiwh@korea.kr
* Correspondence: kooksh@jbnu.ac.kr (S.-H.K.); leejc88@jbnu.ac.kr (J.-C.L.); young@jbnu.ac.kr (Y.-M.J.); Tel.: +82-63-270-3327 (S.-H.K.); +82-63-270-4049 (J.-C.L.); +82-63-250-2130 (Y.-M.J.); Fax: +82-63-270-4312 (S.-H.K.); +82-63-270-4004 (J.-C.L.); +82-63-270-4312 (Y.-M.J.)
† These authors contributed equally to this study.

**Citation:** Wagle, S.; Sim, H.-J.; Bhattarai, G.; Choi, K.-C.; Kook, S.-H.; Lee, J.-C.; Jeon, Y.-M. Supplemental Ferulic Acid Inhibits Total Body Irradiation-Mediated Bone Marrow Damage, Bone Mass Loss, Stem Cell Senescence, and Hematopoietic Defect in Mice by Enhancing Antioxidant Defense Systems. *Antioxidants* **2021**, *10*, 1209. https://doi.org/10.3390/antiox10081209

Academic Editors: Elena Obrador Pla and Alegria Montoro

Received: 25 June 2021
Accepted: 25 July 2021
Published: 28 July 2021



**Abstract:** While total body irradiation (TBI) is an everlasting curative therapy, the irradiation can cause long-term bone marrow (BM) injuries, along with senescence of hematopoietic stem cells (HSCs) and mesenchymal stem cells (MSCs) via reactive oxygen species (ROS)-induced oxidative damages. Thus, ameliorating or preventing ROS accumulation and oxidative stress is necessary for TBI-requiring clinical treatments. Here, we explored whether administration of ferulic acid, a dietary antioxidant, protects against TBI-mediated systemic damages, and examined the possible mechanisms therein. Sublethal TBI (5 Gy) decreased body growth, lifespan, and production of circulating blood cells in mice, together with ROS accumulation, and senescence induction of BM-conserved HSCs and MSCs. TBI also impaired BM microenvironment and bone mass accrual, which was accompanied by downregulated osteogenesis and by osteoclastogenic and adipogenic activation in BM. Long-term intraperitoneal injection of ferulic acid (50 mg/kg body weight, once per day for 37 consecutive days) protected mice from TBI-mediated mortality, stem cell senescence, and bone mass loss by restoring TBI-stimulated disorders in osteogenic, osteoclastic, and adipogenic activation in BM. In vitro experiments using BM stromal cells supported radioprotective effects of ferulic acid on TBI-mediated defects in proliferation and osteogenic differentiation. Overall, treatment with ferulic acid prevented TBI-mediated liver damage and enhanced endogenous antioxidant defense systems in the liver and BM. Collectively, these results support an efficient protection of TBI-mediated systemic defects by supplemental ferulic acid, indicating its clinical usefulness for TBI-required patients.

**Keywords:** ferulic acid; total body irradiation; bone marrow microenvironment; stem cell senescence; bone marrow injury; reactive oxygen species; antioxidant defense system

## 1. Introduction

Radiotherapy via localized or total body irradiation (TBI), in combination with surgical operation, is a common treatment for cancer patients. TBI in moderate or high doses is also applied in bone marrow transplantation therapy. However, TBI may impair the bone marrow (BM) microenvironment, hematopoietic development, and stem cell functions, eventually causing irrecoverable systemic damages [1,2]. TBI-mediated damages are closely

associated with abnormal accumulation of reactive oxygen species (ROS) in BM and BM-conserved stem cells, such as hematopoietic stem cells (HSCs) and mesenchymal stem cells (MSCs) [3–5]. Persistent and prolonged ROS generation induces stem cell senescence and self-renewal defect in BM, which contributes oxidative-stress-associated long-term BM injuries [3–5]. TBI-induced BM injury also disrupts bone mass accrual, and this disruption is associated with the high radiation-absorbing property of bone compared to surrounding soft tissues [6,7].

As TBI-induced adverse events are to be great challenges to cancer patients and in stem cell transplantation therapy, numerous studies have focused on the development of bioactive materials that effectively prevent TBI-mediated systemic impairments. In this regard, many reports indicate a clinical usefulness of naturally occurring hydroxycinnamates, a class of major phenolic compounds, in attenuating and/or protecting TBI-mediated oxidative damages [8,9]. Of the hydroxycinnamates, ferulic acid (4-hydroxy-3-methoxycinamic acid) is a dietary antioxidant that protects radiation-induced damages by tremendously ameliorating cellular ROS accumulation [10–12]. This protection is related to its chemical property possessing three distinctive structural motifs that participate in free radical scavenging [13]. A recent report also suggests that supplemental ferulic acid enhances the healing of irradiation-mediated bone defect by maintaining stemness of skeletal stem cells, as well as by activating mitogen-activated protein kinases in the cells [14]. In addition to radioprotection, ferulic acid is also known to exhibit various pharmacological and medicinal activities, including anti-aging, anti-inflammatory, anti-diabetic, anti-cancer, and neuroprotective roles [15].

Given that irradiation induces oxidative-stress-associated cellular DNA damage and senescence of HSCs [16,17], we suggest that cellular mechanisms by which ferulic acid exerts radioprotection are closely associated with its ability to scavenge ROS and to ameliorate TBI-mediated oxidative stress. However, the underlying mechanisms of how ferulic acid protects BM and BM-conserved HSCs against TBI-mediated damages still remain to be defined; the roles of ferulic acid on TBI-mediated impairments in MSC functions and bone mass accrual are not completely understood. Furthermore, the impacts of ferulic acid on TBI-mediated BM injuries, and oxidative systemic disorders by its long-term administration are not investigated. Here, we administered mice with ferulic acid intraperitoneally once per day for 37 consecutive days, from 7 days before and to 30 days after TBI. We explored whether the treatment with ferulic acid protects TBI-induced oxidative damages on HSCs, hematopoietic development, and maintenance of BM microenvironment together with the associated mechanisms. We also investigated how long-term administration of ferulic acid affects the functions of BM-conserved MSCs, bone mass accrual, and life span in TBI-exposed mice. The current findings not only demonstrate radioprotective potentials of ferulic acid in mice and the associated mechanisms, but also provide evidence that ferulic acid is a supplemental antioxidant that ameliorates or prevents TBI-mediated oxidative damages.

## 2. Material and Methods

### *2.1. Chemicals, Laboratory Equipment, and Mice*

Ferulic acid was purchased from Sigma-Aldrich Co. LLC (CAS:537-98-4; St. Louis, MI, USA), and 2′,7′-dichlorodihydrofluorescein-diacetate (DCF-DA) was from Abcam (Cambridge, UK). Fetal bovine serum (FBS) was purchased from HyClone Laboratories (Logan, UT, USA). Unless specified otherwise, other chemicals and laboratory consumables were purchased from Sigma-Aldrich Co. LLC and Falcon Labware (BD Biosciences, Franklin Lakes, NJ, USA), respectively. C57BL/6 mice (6 weeks old) were purchased from Damul Science (Daejeon, Republic of Korea) and equilibrated for 7 days before use. During the experimental period, all mice were housed at 22 ± 1 °C and 55 ± 5% humidity, along with 12 h light/dark autocycle, allowing *ad libitum* feeding in the Animal Center of School of Dentistry, Jeonbuk National University.

### *2.2. Ferulic Acid Administration and TBI*

Mice were divided into three groups: non-TBI mice (control group), TBI mice with vehicle injection (TBI group), and TBI mice administered with ferulic acid (FA+TBI group). FA+TBI group intraperitonially received ferulic acid (50 mg/kg body weight) once per day for 37 consecutive days, from 7 days before and 30 days after TBI, whereas TBI group was injected with phosphate-buffered saline (PBS; vehicle solution) for the same days. TBI and FA+TBI groups were exposed to 5 Gy TBI with γ-rays by regulating dosage time (0.66 Gy/min) that was based on the radioactive half-life of γ-rays on a rotating platform (Model 109-85 series- JL Shepherd & Associates, San Fernando, CA, USA).

### *2.3. Flowcytometry and Blood Cell Counting*

MSCs and HSCs were harvested from femoral and tibial bones of mice by flushing them with PBS using a 5 mL syringe after cutting the ends of the bones. After the removal of red blood cells (RBC), cells were analyzed by multicolor flow cytometry (BD Aria III, BD Biosciences, Franklin Lakes, NJ, USA), and the phenotypical identification of cell populations was performed using FlowJo software (FLOWJO, Ashland, OR, USA) at the Center for University-Wide Research Facilities of Jeonbuk National University. HSCs ($CD150^+CD48^-LSK$) and MSCs ($CD29^+CD105^+LSK$) were characterized with their specific lineage antibodies (antibodies were purchased from BD Biosciences, unless specified otherwise). Briefly, MSCs were characterized by PE-Cy7-conjugated lineage cocktail, APC-Cy7-conjugated anti-Sca-1 (eBioscience, Waltham, MA, USA), PE-conjugated anti-CD29, and APC-conjugated anti-CD105 antibodies, whereas HSCs were characterized by PE-Cy7-conjugated lineage cocktail, FITC- or PE-conjugated anti-Sca-1, APC-conjugated anti-c-Kit, APC-Cy7-conjugated anti-CD48 (eBioscience), and PerCP/Cy5.5-conjugated CD150 (eBioscience) antibodies. The lineage-marker-conjugated MSCs and HSCs were further stained with MitoSox$^{TM}$ Red (Invitrogen, Carlsbad, CA, USA) or Di-β-D-galactopyranoside ($C_{12}$FDG; Molecular probes, Eugene, OR, USA) to analyze levels of cellular ROS accumulation and senescence-associated β-galactosidase (SA-β-gal) activity. Peripheral blood samples were collected from mice via a tail vein cutting or a cardiac puncture into $K_2$EDTA-treated tubes (BD Biosciences) 2, 7, 30, and 60 days after TBI. Levels of circulating white blood cells (WBC), granulocytes, lymphocytes, platelets, and RBC were analyzed using an automated blood cell counter (Sysmex XE-2100; TOA Medical Electronics Co., Kobe, Japan).

### *2.4. Micro-Computed Tomography (μCT) Analysis*

The femurs were isolated from mice at 60 days post-TBI and scanned using a desktop scanner (1076 Skyscan Micro-CT; Skyscan, Kontich, Belgium), followed by analysis using CTAn software (Skyscan). The X-ray source was set at 75 KV and 100 μA, with a pixel size of 18 mm. The image slices were reconstructed using a cone-beam reconstruction software based on the Feldkamp algorithm (Dataviewer; Skyscan, Belgium). On the stacked reconstruction of μCT cross-section images, manual regions of interest (ROIs) were drawn. The volume of interest (VOI) consisted of a stack of ROIs drawn over 201 cross-sections, resulting in a height of 5 mm extending from the plate of distal femur to trabecular region. Based on the reconstructed three-dimensional (3D) μCT images, values of bone parameters, including bone volume (BV, $mm^3$), bone surface (BS, $mm^2$), bone specific surface (BS/BV, %), and bone volume percentage (BV/TV, %), were calculated. Bone mineral density (BMD, $g/cm^3$) was also determined by converting the attenuation data for VOI into Hounsfield units and BMD units using phantoms (SkyScan) that had a standard density corresponding to mouse bone.

### *2.5. Histological Analyses*

Femurs were isolated from mice 30 and 60 days after TBI and fixed with a 4% paraformaldehyde solution for 48 h, followed by decalcification in 10% EDTA at 4 °C for 4 weeks. The tissue, including the trabecular region, was dehydrated in series of alcohol, embedded in paraffin, and sectioned into 5.0 μm in thickness. For hematoxylin and

eosin (H & E) staining, tissue sections were treated with hematoxylin solution (Gill No. 3) before counterstaining with 0.25% eosin Y Stain (bioWORLD Life Sciences, Dublin, OH, USA). Parts of tissue sections were subjected to tartrate-resistant acid phosphatase (TRAP) staining using a leukocyte acid phosphatase kit (Cosmo Bio, Tokyo, Japan), followed by counterstaining with hematoxylin. The levels of osteoprotegerin (OPG; BS1862, Bioworld Technology, St. Louis Park, MN, USA), receptor activator of nuclear factor κB ligand (RANKL; ALX-804-243, Enzo Life Sciences, Inc., Farmingdale, NY, USA), osteocalcin (OCN; AB10911, Millipore corporation, Temecula, CA, YSA), runt-related transcription factor 2 (RUNX2; BS2831), cathepsin K (CTSK; SC-48353, Santa Cruz Biotechnology, Inc., Dallas, TX, USA), nuclear factor erythroid 2-related factor 2 (NRF2; BS1258), and adiponectin (ab22554, Abcam) were evaluated by immunohistochemistry (IHC). In IHC assay, tissue sections were stained with each primary antibody (1:200–400 dilutions) specific to the factors, and the expression patterns were determined using rabbit-anti- or mouse-anti-Vectastain ABC DAB-HRP kits (Vector Laboratories, Burlingame, CA, USA). All procedures for TRAP and IHC staining followed the manufacturer's instructions, and the stained sections were observed under a light microscope (EL-Einsatz 451888, Carl Zeiss, Ostalbkreis, Germany).

### *2.6. Isolation and Culture of BM Stromal Cells (BMSCs)*

Whole BM cells were isolated from femurs and tibias of mice at 30 and 60 days post-TBI. Cells were resuspended in alpha-minimum essential media (αMEM, Thermo Fisher Scientific, Waltham, MA, USA) and centrifuged at 2000× *g* for 3 min. The pellets were spread onto 60 mm culture plates and incubated in growth medium (αMEM supplemented with 2 mM glutamine, 100 IU/mL penicillin G, 100 μg/mL streptomycin, and 20% FBS). On the second day, nonadherent cells were removed and, after 12 days of additional incubation, the adherent cells were harvested to use as BMSCs.

### *2.7. Assay for BMSC Proliferation*

To evaluate a direct effect of ferulic acid on cell proliferation, BMSCs isolated from non-TBI control mice (7 weeks old) were seeded onto 96-multiwell culture plates ($2 \times 10^3$ cells/well) in growth medium supplemented without and with various concentrations (0–500 μM) of ferulic acid. After 48 h of incubation, the proliferation rate of BMSCs was assessed using Cell Counting Kit-8 (CCK-8; Dojindo Lab, Rockville, MD, USA) according to the manufacturer's instructions. In addition, BMSCs were isolated from mice 30 and 60 days after TBI and cultured in 96-multiwell culture plates ($2 \times 10^3$ cells/well) containing growth medium. After 1, 3, and 5 days of incubation, proliferation rate of the cells was determined by CCK-8 assay. Optical density specific to the CCK-8 dye was measured at 450 nm using a microplate reader (SPECTROstar® Nano, BMG LABTECH, Ortenberg, Germany).

### *2.8. Osteogenic and Adipogenic Differentiation Assays*

BMSCs ($5 \times 10^4$ cells/well) isolated from mice at 30 or 60 days post-TBI were divided into 48-well culture plates in an osteogenic medium (αMEM supplemented with 100 nM dexamethasone, 50 μM ascorbic acid, 10 mM β-glycerol phosphate, and 5% FBS). During incubation, the medium was newly replaced to the same osteogenic medium every 2 days. After 21 days of incubation, cells were stained with 2% Alizarin red S (ARS, pH 4.2) for 20 min and observed under a light microscope. The stained cells were also treated with 10% cetylpyridinium chloride dissolved in 10 mM sodium phosphate (pH 7.0), and absorbance of the dye was measured at 405 nm using a microplate reader (SPECTROstar® Nano). Parts of BMSCs ($5 \times 10^4$ cells/well) were seeded onto 48-well culture plates and incubated in an adipogenic medium (DMEM supplemented with 10 μg/mL insulin, 50 μM indomethacin, 1 μM dexamethasone, 500 μM 3-isobutyl-1-methylxanthine, and 5% FBS). After 21 days of incubation, cells were stained with 60% isopropanol containing 0.6% Oil red O (ORO), followed by capture of photographs. In addition, the ORO-stained cells were washed with water and treated with 100% isopropanol. The red-colored lipid droplets in these cells were

quantified by determining the absorbance of the dye at 510 nm using a microplate reader (SPECTROstar® Nano).

### *2.9. Quantitative Reverse Transcription-PCR (qRT-PCR) Assay*

Total RNA was extracted from BMSCs that were isolated from mice at 30 and 60 days post-TBI using a TRIzol reagent (Invitrogen). Total RNA samples (1 μg/sample) were applied for cDNA synthesis using AmpiGene cDNA synthesis Kit (Enzo Life Sciences, Inc.) following the manufacturer's instructions. The qRT-PCR was performed with Power SYBR Green PCR Master Mix (Applied Biosystems, Foster City, CA, USA) and ABI StepOnePlus Real-Time PCR System (Applied Biosystems). The thermocycling conditions were maintained at 95 °C for 10 min for pre-denaturation and amplified using three-step cycles of denaturation at 95 °C for 15 s, annealing at 60 °C for 30 s, and extension at 72 °C for 30 s for 40 cycles. Oligonucleotide primers specific to CCAA-enhancer-binding protein α (*C/EBPα*), peroxisome proliferator-activated receptor γ (*PPARγ*), and adiponectin (*apM1*) were designed as listed in Table S1, Supporting Information. The level of glyceraldehyde 3-phosphate dehydrogenase (*Gapdh*) was considered as the endogenous reference during the quantification.

### *2.10. Western Blot Analysis*

Whole BM cells were isolated from femurs and tibias of mice at 7 days post-TBI. After removal of RBC, BM cells were lysed in a cocktail buffer containing protease/phosphatase inhibitor (Cell Signaling Technology, Danvers, MA, USA). The protein extracts (20 μg/sample) were separated through sodium dodecyl sulfate-polyacrylamide gel electrophoresis on 10–12% gels and electroblotted onto polyvinylidene difluoride membranes. Blots were washed with a buffer containing 10 mM Tris-HCl (pH 7.6), 150 mM NaCl, and 0.05% Tween-20, and blocked in 5% skim milk for 1 h prior to incubation with primary antibodies specific to PPARγ (1:500; SC-390740, Santa Cruz Biotechnology), adiponectin (1:500; ab22554, Abcam), and β-actin (1:2500; Santa Cruz Biotechnology). Finally, immunoreactive bands on the membranes were visualized using Western pico-EPD blot detection kit (ELPIS-Biotech, Daejeon, Republic of Korea), followed by exposure to X-ray film (Eastman Kodak, Rochester, NY, USA).

### *2.11. Assays for Enzyme Activities in Blood Serum and Liver Tissue*

After 2 and 30 days of TBI, peripheral blood was isolated from mice by cardiac puncture and collected into serum separation tubes (BD Biosciences). Blood sera were obtained by centrifugating the tube at 10,000× *g* for 20 min, and then the activities of alanine amino transaminase (ALT) and aspartate aminotransferase (AST) were determined using specific assay kits (ADVIA 1650, Bayer, Japan). After collecting the blood sera, liver tissues were isolated from the mice and homogenized in 50 mM $KH_2PO_4$ solution for 5 min using a homogenizer (PRO Scientific Inc., Oxford, CT, USA), or in a 200-μL cold assay buffer provided by BioAssay Systems (Hayward, CA, USA). After centrifugation at 14,000× *g* for 10 min, the supernatants were collected, and activities of superoxide dismutase (SOD), catalase (CAT), and glutathione peroxidase (GPx) were determined. In these assays, SOD activity was measured using an assay kit (No. 706002, Cayman Chemical, Ann Arbor, MI, USA), while CAT and GPx activities were determined using an EnzyChrom™ CAT assay kit (ECAT-100; BioAssay Systems) and GPx assay kit (EGPX-100; BioAssay Systems), respectively, according to the manufacturer's instructions.

### *2.12. Statistical Analyses*

All results are expressed as the mean ± standard deviation (SD). One-way analysis of variance with post-hoc Tukey test was used for multiple comparisons using GraphPad Prism 8 (GraphPad Software Inc., San Diego, CA, USA). Two-tailed Student's *t*-test was used when the significance of differences between two sets of data was determined using GraphPad Prism 8. A value of $p < 0.05$ was considered statistically significant.

## 3. Results

### *3.1. Supplemental Ferulic Acid Inhibits TBI-Mediated Impairments in Growth and Survival and Ameliorates HSC Senescence and Hematopoietic Defects in TBI Mice*

A schematic diagram of the experimental designs, along with the chemical structure of ferulic acid, is shown in Figure 1A. All mice groups exhibited age-related growth during the experimental period, whereas the TBI group revealed significantly lower body weight from 30 or 45 days after TBI compared with the control or FA+TBI group (Figure 1B). No different body weights between control and FA+TBI groups were found throughout the periods. Compared with the FA+TBI group that showed 90% survival rate until 16 months, all mice in the TBI group died at the same month after TBI (Figure 1C). Survival rate of the FA+TBI group was similar to that of the control group, even at 20 months post-TBI (data not shown). As HSC senescence is a characteristic phenotype occurring under ionizing irradiation and contributes to hematopoietic disorders [16], we measured the SA-β-gal activity of HSCs (phenotypically defined by $CD150^{+}CD48^{-}$lineage-Sca-$1^{+}$c-$Kit^{-}$ cells) by determining the levels of $C_{12}$FDG-positive HSCs (%) 2 and 30 days after TBI. The TBI group exhibited 2.97- and 1.98-fold higher levels of $C_{12}$FDG-positive HSCs at 2 days post-TBI compared with control and FA+TBI groups, respectively (Figure 1D). The TBI group also showed higher SA-β-gal activity in HSCs than the control or FA+TBI group 30 days after TBI (Figure S1, Supporting Information). However, the number of BM-conserved HSCs in the TBI group was comparable to those of the control and FA+TBI groups, both 2 and 30 days after TBI (Figure S2, Supporting Information). We next determined levels of circulating blood cells in mice 2, 7, 30, and 60 days after TBI. Compared with the control group, numbers of circulating WBC, platelets, and RBCs, as well as percentage of granulocytes and lymphocytes in peripheral blood, were reduced in the TBI group in relation to the days after TBI (Figure 1E). TBI-mediated decreases in WBC, granulocytes, and lymphocytes were further visible at relatively early times compared with that in platelets and RBC. Treatment with ferulic acid blocked the TBI-induced reduction in circulating WBC and granulocytes, and these cells in the FA+TBI group were restored up to the levels of the control group 30 days after TBI. Furthermore, levels of lymphocytes, platelets, and RBC in FA+TBI mice were comparable with those in control mice throughout the days after TBI. These findings indicate that ferulic acid protects mice from TBI-induced defects in growth and survival, and this protection is, in part, associated with its potential to inhibit HSC senescence and acute hematopoietic defects.

### *3.2. Treatment with Ferulic Acid Inhibits ROS Accumulation and Senescence Induction in MSCs of TBI Mice*

While MSCs play critical roles in bone mass accrual, irradiation can induce senescence of these cells via ROS-activated signaling [17]. We determined mitochondrial ROS levels and SA-β-gal activity in MSCs (phenotypically defined by $Lin^{-}$, Sca-$1^{+}$, c-$Kit^{+}$, $CD105^{+}$, and $CD29^{+}$) of mice 2, 30, and 60 days after TBI. MSCs from the TBI group exhibited an obvious increase in mitochondrial ROS level compared with cells from control mice, and this increase was significantly diminished by intraperitoneal injection of ferulic acid (Figure 2A,B). Similar to HSCs, the TBI group revealed greater SA-β-gal activity in MSCs compared with cells from control mice, while the SA-β-gal activity in MSCs from FA+TBI mice was comparable with that of control mice every day post-TBI (Figure 2C,D). The number of MSCs in BM of TBI and FA+TBI groups was also similar to that of control mice 2, 7, and 30 days after TBI (data not shown). These findings support the antioxidant and antisenescence effects of ferulic acid on BM-conserved MSCs in TBI mice.

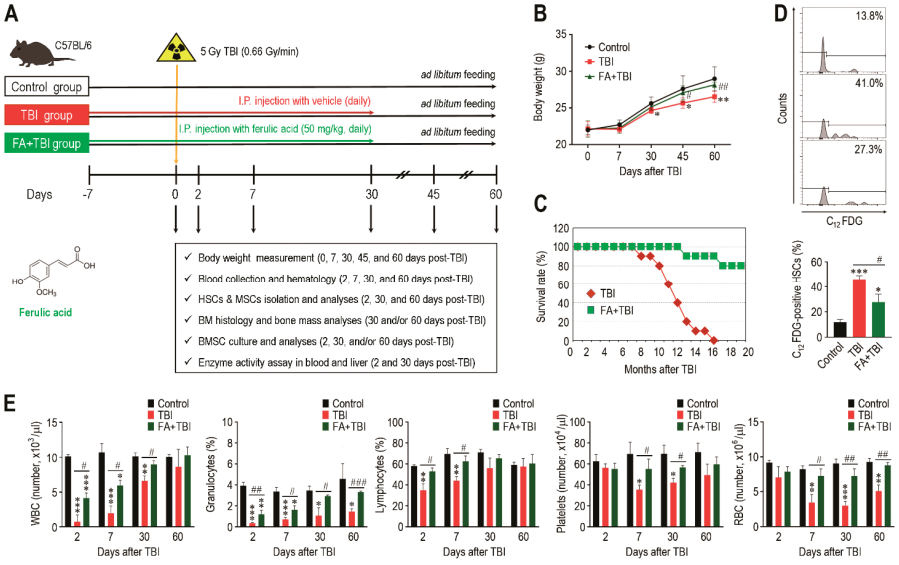


**Figure 1.** Supplemental ferulic acid diminishes HSC senescence in BM of TBI mice and restores TBI-mediated defects in body growth, survival, and production of circulating blood cells. (**A**) The experimental designs and chemical structure of ferulic acid. (**B**) Body weight (g) of mice groups were measured at the indicated days after TBI ($n$ = 10). (**C**) Survival rate of mice groups was monitored for the indicated months ($n$ = 10). (**D**) SA-β-gal activity in HSCs of mice groups was determined by measuring percentage of $C_{12}$FDG-positive HSCs at 2 days post-TBI via flow cytometric analysis ($n$ = 4). (**E**) Levels of circulating WBC, granulocytes, lymphocytes, platelets, and RBC in mice groups were measured using an automated complete blood cell counter at the indicated days after TBI ($n \geq 3$). All data are presented as the mean ± SD. * $p < 0.05$, ** $p < 0.01$, and *** $p < 0.001$ compared with control group; $^{\#}$ $p < 0.05$, $^{\#\#}$ $p < 0.01$, and $^{\#\#\#}$ $p < 0.001$ compared with TBI group.

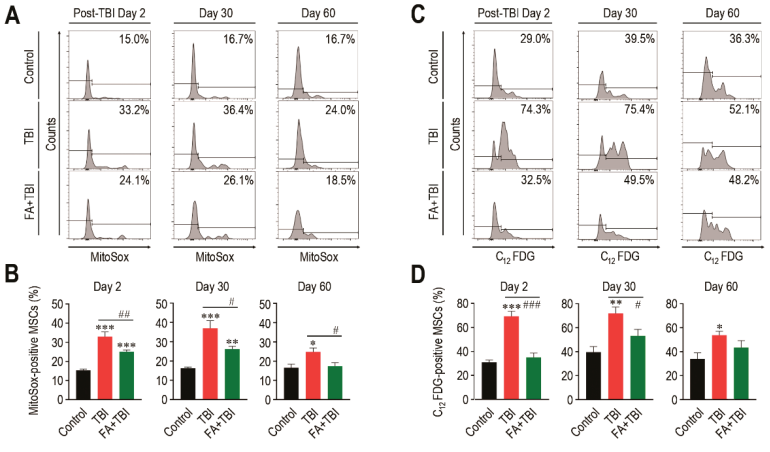


**Figure 2.** Supplemental ferulic acid inhibits TBI-mediated increases of ROS accumulation and senescence induction in BM-conserved MSCs. (**A**,**B**) Level of mitochondrial superoxide anions in BM MSCs from mice groups were assessed by flow cytometry using MitoSox$^{TM}$ Red reagent at the indicated days after TBI ($n$ = 4). (**C**,**D**) SA-β-gal activity in BM-conserved MSCs from mice groups was also measured by flow cytometry using $C_{12}$FDG at the same post-TBI days ($n$ = 4). All data are presented as the mean ± SD. * $p < 0.05$, ** $p < 0.01$, and *** $p < 0.001$ compared with control group; $^{\#}$ $p < 0.05$, $^{\#\#}$ $p < 0.01$, and $^{\#\#\#}$ $p < 0.001$ compared with TBI group.

### 3.3. Supplementation with Ferulic Acid Limits TBI-Induced Defect of BM Microenvironment

The BM microenvironment provides niches for retention and self-renewal of BM HSCs and MSCs, and its impairment is related to abnormal retention and senescence of these cells, along with bone mass loss [18]. We explored whether the TBI-induced stem cell senescence and body weight loss is associated with impaired BM microenvironments. The 2D μCT analysis 60 days after TBI showed greater bone mass in control and FA+TBI groups compared with the TBI group (Figure 3A). When values of bone parameters were evaluated, the TBI group revealed significantly lower values of BV ($p < 0.01$), BS ($p < 0.01$), BV/TV ($p < 0.01$), and BMD ($p < 0.05$) compared with the control group (Figure 3B). TBI-induced decreases in the bone values were restored in mice supplemented with ferulic acid up to the levels of control mice. Ferulic-acid-induced protection on TBI-mediated bone loss was supported by H&E staining, in which the TBI group showed relatively lower bone mass in the trabecular region at 60 days post-TBI than the control or FA+TBI group (Figure 3C).

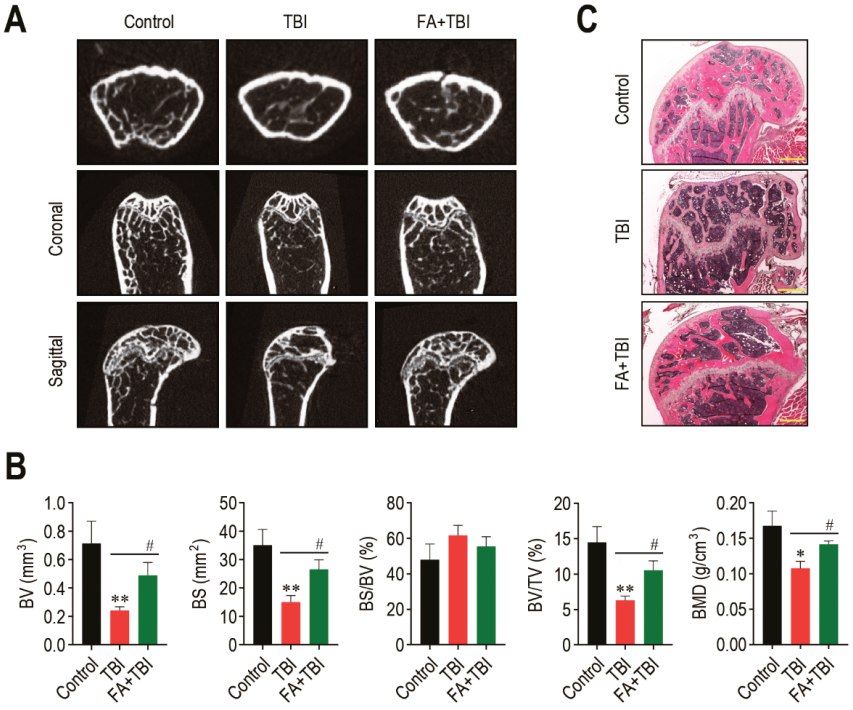


**Figure 3.** Administration of ferulic acid restores TBI-mediated impairments in BM microenvironment and bone mass accrual. (**A**) The 2D μCT images show femoral bones of mice groups 60 days after TBI. (**B**) Values of bone parameters, including BV ($mm^3$), BS ($mm^2$), BS/BV (%), BV/TV (%), and BMD ($g/cm^3$), in the trabecular region of the femoral bones were measured 60 days after TBI ($n = 4$). (**C**) Histological evaluation of bone mass accrual at the trabecular bones of mice groups was performed by H&E staining at 60 days post-TBI. A representative result from four different samples is shown. Scale bar = 500 μm. All data are presented as the mean ± SD. * $p < 0.05$ and ** $p < 0.01$ compared with control group; # $p < 0.05$ compared with TBI group.

### 3.4. Administration of Ferulic Acid Increases Osteogenic Marker Expression, but Inhibits Osteoclastic Activation in BM of TBI Mice

As a balanced activation between osteoblasts and osteoclasts is important in maintaining the BM microenvironment and bone mass accrual, we explored whether TBI-mediated BM impairment is directly associated with an alteration in osteoblastic and osteoclastic activation. Compared with the control group, the TBI group revealed significantly lower

levels of RUNX2 ($p < 0.05$) and OCN ($p < 0.01$) in BM 60 days after TBI (Figure 4). The TBI-mediated decreases in these factors were completely recovered up to the levels of the control group by treatment with ferulic acid. In contrast, the TBI group exhibited significantly higher levels ($p < 0.001$) of RANKL and CTSK in BM compared with control and FA+TBI groups (Figure 4B). TBI groups also exhibited a significantly lower level ($p < 0.05$) of OPG in BM compared with the control group, whereas this reduction was not affected by administration of ferulic acid (Figure 4C). Alternatively, the TBI group showed significantly higher numbers of TRAP-positive osteoclasts than did the control ($p < 0.01$) or FA+TBI group ($p < 0.05$) (Figure 4D). These results not only indicate a relationship between TBI-mediated BM injury and a preferable activation toward osteoclasts with reduced osteogenic activity, but also suggest that ferulic acid inhibits osteoclastic activation by decreasing the induction of RANKL and CTSK, rather than by increasing OPG in BM.

### *3.5. Ferulic Acid Inhibits TBI-Stimulated Adipogenic Differentiation in BM*

An adipogenic activation in BM is one of the important alterations after ionizing irradiation, and this contributes to deterioration in bone formation [19]. We assessed whether TBI actually stimulates adipogenic differentiation in BM, and whether this is also suppressed by supplementation with ferulic acid. To address this, we initially checked the presence of lipid spot formation in BM of mice and counted its numbers 60 days after TBI (Figure 5A). As shown in the images of H&E staining, the numbers of lipid spots in BM of the TBI group were significantly higher compared with that of the control ($p < 0.001$) or FA+TBI group ($p < 0.001$) at 60 days post-TBI. TBI-mediated increase in lipid accumulation was correlated with the expression levels of adipogenic markers, adiponectin and PPAR$\gamma$, in which supplemental ferulic acid significantly ($p < 0.05$) diminished expression of these markers in the BM (Figure 5B). To further evaluate the impacts of TBI or in combination with ferulic acid on adipogenesis in BM, we determined levels of *PPARγ*, *C/EBPα*, and *apM1* in BM cells of mice by qRT-PCR assay 30 and 60 days after TBI. The TBI group exhibited significantly higher levels ($p < 0.001$) of the adipogenic marker genes in BM cells compared with the control group 30 days after TBI (Figure 5C). TBI-mediated increases in *PPARγ*, *C/EBPα*, and *apM1* in BM cells were also found 60 days after TBI (Figure 5D). Treatment with ferulic acid diminished TBI-mediated upregulation of the adipogenic regulatory genes at both 30 and 60 days post-TBI, in which levels of *PPARγ* and *C/EBPα* in the FA+TBI group were comparable with those in control mice 60 days after TBI. These results indicate that, in addition to osteoclastic activation, TBI augments adipogenic activation in BM and BM-conserved cells, and this augmentation is attenuated by supplemental ferulic acid.

### *3.6. Ferulic Acid Treatment Stimulates Proliferation and Osteogenic Activation, but Inhibits Adipogenic Differentiation of BMSCs from TBI Mice*

We evaluated how a direct addition of ferulic acid affects proliferation of BMSCs from non-TBI control mice. When BMSCs were incubated in the presence of ferulic acid (0–500 μM) for 48 h, the cells exhibited a dose-dependent proliferation up to a ferulic acid concentration of 200 μM (Figure 6A). To further understand the impacts of supplemental ferulic acid on BMSC proliferation and their differentiation into osteoblastic or adipocytic lineage cells, BMSCs isolated from mice at various days post-TBI were incubated in growth or differentiating medium. When BMSCs from mice 30 (Figure 6B) and 60 days after TBI (Figure 6C) were incubated in growth medium for 1, 3, or 5 days, cells from all mice groups showed a time-dependent increase in optical density specific to CCK-8. However, BMSCs from the TBI group exhibited a significantly lower proliferation rate compared with the cells from the control or FA+TBI group at the same incubation times. No different values of optical density between the control and FA+TBI groups were found throughout the incubation. TBI-mice-derived BMSCs exerted relatively lower intensity specific to ARS compared with cells from the control or FA+TBI group, and this was further viable in the cells isolated 60 days rather than 30 days after TBI (Figure 6D). Determination of the mean optical density specific to the ARS dye also supported TBI-mediated decrease in mineralization of BMSCs, and its complete suppression by supplementation with ferulic

acid, both at 30 and 60 days post-TBI (Figure 6E). When BMSCs isolated from mice at 30 days post-TBI were incubated in adipogenic medium for 21 days, TBI-mice-derived cells showed greater levels of ORO-positive adipocytes along with higher ORO-specific optical density compared with cells from the control or FA+TBI group (Figure 6F). Western blot analysis also showed greater immunoreactive intensities of PPARγ and adiponectin in BMSCs from the TBI group compared with cells from the control or FA+TBI group 7 days after TBI (Figure 6G, left panel). TBI-mediated increase of PPARγ in BMSCs and its inhibition by ferulic acid were further supported by measuring the mean immunoreactive intensities of PPARγ and adiponectin at the same day post-TBI (Figure 6G, right panel).

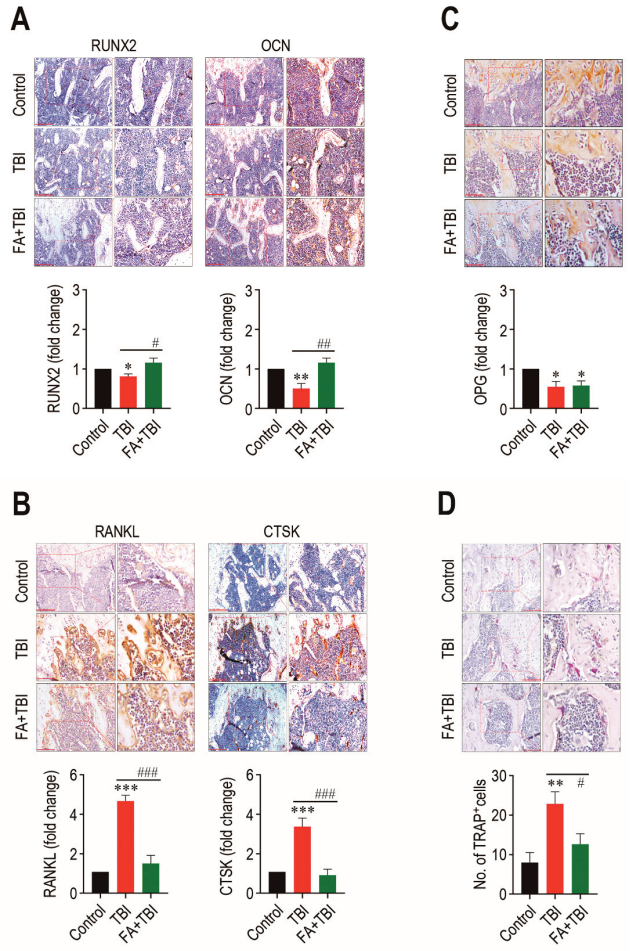


**Figure 4.** TBI causes an imbalanced activation between osteoblasts and osteoclasts, and this is completely prevented by long-term administration of ferulic acid. Levels of (**A**) RUNX2 and OCN, (**B**) RANKL and CTSK, and (**C**) OPG in BM of mice groups were evaluated by IHC assay at 60 days post-TBI. (**D**) Osteoclasts formed in BM of mice were determined by TRAP staining at the same day after TBI. The IHC images show representative results from four different mice. Scale bars in the images for RUNX2, OCN, and CTSK are 200 μm, while those for RANKL, OPG, and TRAP are 100 μm. All data are presented as the mean ± SD ($n$ = 4). * $p < 0.05$, ** $p < 0.01$, and *** $p < 0.001$ compared with control group; $^{\#}$ $p < 0.05$, $^{\#\#}$ $p < 0.01$, and $^{\#\#\#}$ $p < 0.001$ compared with TBI group.

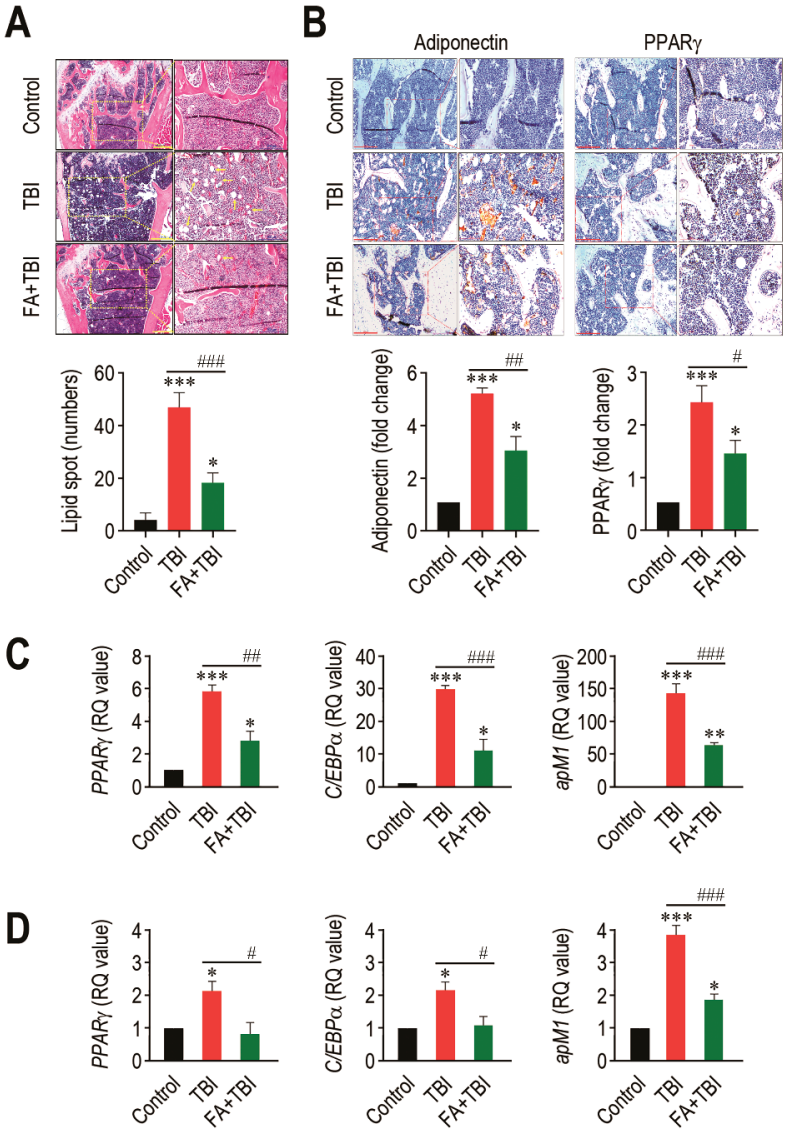


**Figure 5.** Long-term administration of ferulic acid inhibits TBI-mediated adipogenic activation in BM of mice. (**A**) Lipid accumulation in trabecular regions of mice groups was determined by H&E staining at 60 days post-TBI. Yellow arrows indicate the lipid spots formed in the bone. Scale bar = 500 μm. (**B**) Levels of adiponectin and PPARγ in BM of mice groups were measured by IHC assay at 60 days post-TBI. Scale bar = 200 μm. Number of lipid spots and relative intensity of adiponectin and PPARγ (fold change) in BM were calculated from four different samples. Expression levels of *PPARγ*, *C/EBPα*, and *apM1* in BM cells from mice groups were determined by qRT-PCR assay at (**C**) 30 and (**D**) 60 days post-TBI ($n$ = 4). All data are expressed as the mean ± SD. * $p < 0.05$, ** $p < 0.01$, and *** $p < 0.001$ compared with control group; $^{\#}$ $p < 0.05$, $^{\#\#}$ $p < 0.01$, and $^{\#\#\#}$ $p < 0.001$ compared with TBI group.

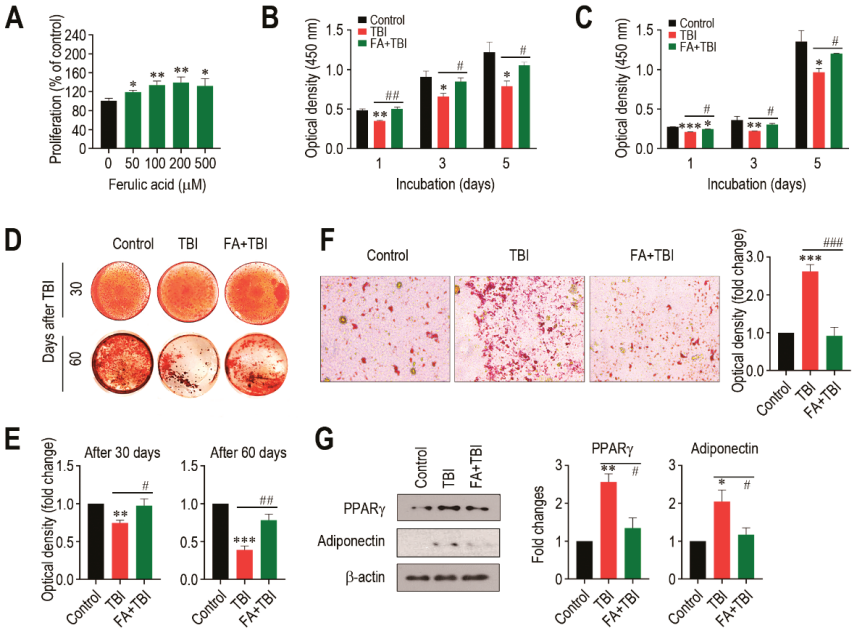


**Figure 6.** Supplemental ferulic acid restores proliferation and osteogenic differentiation of BMSCs and prevents adipogenic activation of the cells from TBI mice. (**A**) BMSCs isolated from non-TBI control mice were incubated in growth medium supplemented with ferulic acid (0–500 μm) for 48 h, and proliferation rate was determined by CCK-8 assay. BMSCs were isolated from mice exposed to TBI or in combination with ferulic acid at (**B**) 30 and (**C**) 60 days post-TBI, and the cells were incubated in growth medium for the indicated days, followed by CCK-8 assay. (**D**) BMSCs were isolated from mice groups at 30 and 60 days post-TBI and incubated in osteogenic medium. After 21 days of incubation, cellular mineralization of the cells was evaluated by ARS staining. (**E**) Mineralization of BMSCs from mice groups was also determined by measuring optical density specific to the ARS at 405 nm. (**F**) BMSCs were isolated from mice groups 30 days after TBI and incubated in adipogenic medium. The photographs showing ORO-positive adipocytes and optical density specific to the dye were obtained 21 days after incubation. (**G**) BM cells were isolated from mice groups 7 days after TBI and, after 48 h of incubation in adipogenic medium, protein levels of PPARγ and adiponectin in the cells were determined by immunoblot assay. The relative intensities specific to PPARγ and adiponectin were determined after normalizing the band to the relative intensity of β-actin. All data are presented as the mean ± SD ($n \geq 3$). * $p < 0.05$, ** $p < 0.01$, and *** $p < 0.001$ compared with control group; # $p < 0.05$, ## $p < 0.01$, and ### $p < 0.001$ compared with TBI group.

### *3.7. Supplementation with Ferulic Acid Inhibits TBI-Mediated Increases in AST and ALT Activities, but Enhances Cellular Antioxidant Defense Systems*

As TBI is known to acutely increase activities of AST and ALT, which are indicative of liver damage [9], we determined activities of the enzymes in blood serum 2 and 30 days after TBI. The TBI group showed significantly higher activity ($p < 0.05$) of AST at 2 days, but not at 30 days post-TBI compared with the control or FA+TBI group (Figure 7A). Similarly, ALT activity in the TBI group was significantly higher ($p < 0.05$) than that in the control or FA+TBI group at 2 days post-TBI (Figure 7B). Different to the liver-damage-indicative enzymes, the activities of liver-conserved antioxidant enzymes, such as SOD (Figure 7C), CAT (Figure 7D), and GPx (Figure 7E), in the TBI group were acutely diminished 2 days, but not 30 days, after TBI. Treatment with ferulic acid completely blocked TBI-mediated decreases in activities of the enzymes at 2 days post-TBI. In particular, the FA+TBI group revealed significantly higher SOD activity ($p < 0.01$) than the control or TBI group at 30 days post-TBI (Figure 7C). Furthermore, IHC assay revealed that the FA+TBI group expressed an approximately 2.5-fold higher level ($p < 0.01$) of NRF2 in BM at 60 days post-TBI compared with that in the control or TBI group (Figure 7F). These results suggest

that long-term supplementation with ferulic acid enhances antioxidant defense systems, specifically SOD activity and NRF2 induction, and this enhancement is closely associated with ferulic-acid-induced protection on TBI-mediated oxidative damages.

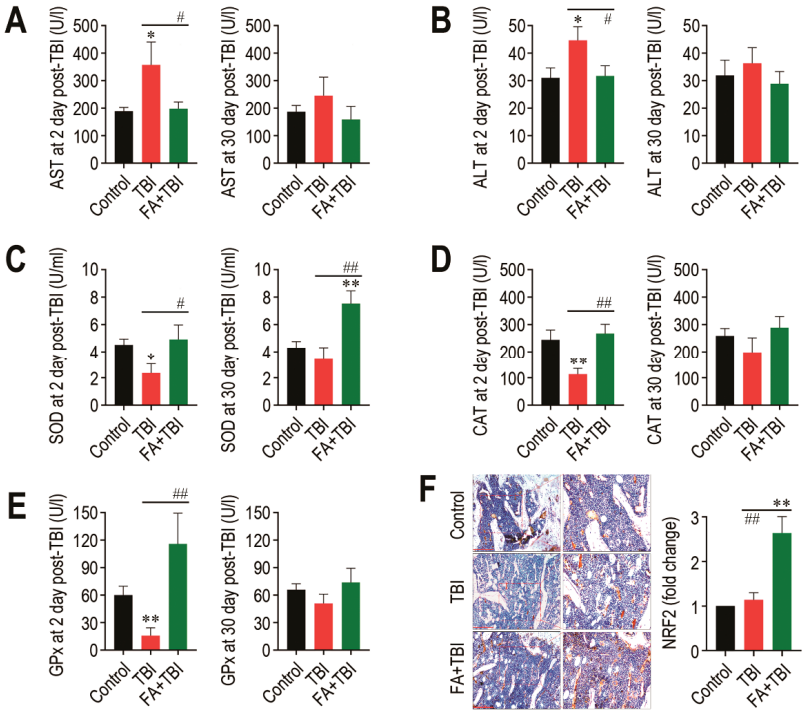


**Figure 7.** Long-term supplementation with ferulic acid prevents liver damage and increases the activities of liver-conserved antioxidant enzymes and the induction of NRF2 in BM of TBI mice. Levels of (**A**) AST and (**B**) ALT in blood serum of mice groups were determined 2 and 30 days after TBI. The activities of (**C**) SOD, (**D**) CAT, and (**E**) GPx in the liver from mice groups were determined 2 and 30 days after TBI. (**F**) Level of NRF2 in BM of mice groups was evaluated by IHC assay at 60 days post-TBI. Scale bar = 200 μm. All data are presented as the mean ± SD ($n$ = 4). * $p < 0.05$ and ** $p < 0.01$ compared with control group; $^{\#}$ $p < 0.05$ and $^{\#\#}$ $p < 0.01$ compared with TBI group.

## 4. Discussion

Although therapeutic radiation can cause severe damages to intact soft and hard tissues [20,21], TBI is required for cancer patients or in BM transplantation. Reduced bone mass accrual and BMD, increased ROS and oxidative stress, long-term residual BM injury, and stem cell senescence with the attendant hematopoietic defects are to be the hallmarks of TBI-mediated disorders [9,22–24]. Disruption of cellular redox balance and depletion of endogenous antioxidant defense systems are also the main events in TBI-mediated oxidative damages [9,25]. As cellular ROS accumulation and subsequent oxidative stress to cells and tissues are the key mediators in TBI-mediated impairments, supplemental antioxidants may ameliorate or recover TBI-mediated oxidative defects. Here, we highlight a long-lasting radioprotective potential of ferulic acid in mice exposed to a sub-lethal TBI. This study also provides the underlying mechanisms by which long-term administration of the antioxidant limits stem cell senescence and BM injuries, and encourages survival and bone mass accrual in TBI mice.

We previously found that, in addition to ferulic acid, dietary antioxidants, caffeic acid and coumaric acid prevent TBI-mediated damages of liver and spleen tissues and HSC

senescence, as well as restore activities of endogenous antioxidant enzymes [9]. Caffeic acid also exhibited an autonomous ameliorating effect on HSC-senescence-associated long-term BM injury and mortality in TBI mice, and induced in vitro anticancer activity, thereby indicating its clinical usefulness as a supplemental drug for cancer patients [24]. Different to the previous studies [9,24], this study administered mice with ferulic acid via intraperitoneal injection once per day for 37 consecutive days (7 days before and 30 days after TBI), and TBI-associated phenotypes in mice were analyzed at various time points after TBI. These experimental approaches allow the impacts of radioprotective antioxidant on TBI-mediated systemic damages to be defined in regard to its long-term administration, as well as to evaluate a time-dependent alteration of TBI-associated characteristic phenotypes. Our results support that intraperitoneal injection of ferulic acid inhibits TBI-mediated HSC senescence and acute reduction of circulating blood cells. As TBI-mediated defects in hematopoietic development may increase the risk of bleeding, infection, and mortality, our findings also indicate that long-term administration of ferulic acid protects mice against TBI-mediated mortality by restoring levels of circulating blood cells.

TBI-mediated defects in body growth and bone mass accrual can be associated with BM microenvironmental impairments that cause functional loss or dysregulated differentiation of BM-conserved stem cells. Indeed, exposure to TBI induced a long-term residual BM injury, depending on the exposed dose or time of TBI, and this negatively affected BM niches and bone homeostasis [16,24]. In addition to HSCs, TBI induced oxidative DNA damage of MSCs and defected their functionality [6,26,27]. TBI also impaired proliferation, differentiation, and chromosomal integrity in BMSCs [28]. Together, our results with previous reports suggest that the ferulic-acid-induced recovery of body growth and bone mass accrual in TBI mice is, in part, associated with its potential to limit ROS accumulation in MSCs and their senescence induction, as well as to maintain functionality of the cells.

The multipotency of MSCs are dysregulated after TBI, in which a preferable differentiation toward adipocytes, along with an imbalanced activation between osteogenic and osteoclastic differentiation, occurs in BM [7]. TBI diminishes proliferation of osteoblastic progenitor cells with cell cycle arrest, and decreases the production of bone-consisting components [29]. ROS accumulation and subsequent oxidative stress are also closely associated with osteoclastogenesis, skeletal aging, and bone diseases [30]. BM adipocytes account for approximately 10% of total body fat in healthy adults and play important roles in energy storage, endocrine function, and bone metabolism [31]. However, chemotherapy or irradiation can cause abnormal infiltration and accumulation of adipocytes in BM [7]. As proven by the decreased induction of RUNX2, OCN, and OPG, upregulated RANKL and CTSK induction, along with increased osteoclasts, and increases in lipid accumulation and adipogenic marker expression in BM of mice 60 days after TBI, the current findings suggest that TBI-mediated BM injury is closely associated with the dysregulated differentiation or functions of HSC- or MSC-derived progenitor cells in BM. Our findings also support that long-term administration of ferulic acid mostly suppresses TBI-mediated osteoclastic activation and restores osteoblastic activity in BM by activating osteogenic markers and by inhibiting directly osteoclastic activation, rather than by increasing OPG expression. Additionally, this study demonstrates that the inhibitory effect of ferulic acid on TBI-mediated adipogenic activation is also accompanied by its ability to diminish the expression of *PPARγ*, *C/EBPα*, and *apM1*, which are known to differentiate preadipocytes into adipocytes and to inhibit osteoblastic differentiation [32]. It was reported that ferulic acid attenuates adipocyte differentiation in 3T3-L1 cells via a positive regulation of heme oxygenase-1, a downstream effector of NRF2 [33]. Adipogenic activation in BM is also associated with a delayed engraftment of HSCs and hematopoietic defects [19]. Therefore, it is likely that supplemental ferulic acid inhibited TBI-stimulated adipogenesis in BM by activating NRF2-related antioxidant systems and by preventing senescence of HSCs and oxidative BM injury. All results from BMSC cultures also support that supplemental ferulic acid increases proliferation and differentiation of BMSCs into mineralized cells, but suppresses their differentiation into adipocytes.

Endogenous antioxidant defense systems maintain cellular redox balance and protect against acute or prolonged oxidative stress, and, thus, a defect in the systems facilitates ROS accumulation and systemic oxidative damages. Similar to the previous study [9], the present findings showed that TBI acutely induces liver injury and depletes the activities of SOD, CAT, and GPx, whereas these defects are recovered by supplemental ferulic acid. In particular, the activity of SOD, but not of CAT and GPx, in the FA+TBI group was greater than that in control mice, thereby indicating an enhancing effect of ferulic acid on SOD. Enzymes such as SOD, CAT, and GPx are the primary antioxidant defense systems that convert active oxygen molecules into nontoxic substances and/or remove directly reactive oxidants [34,35]. NRF2 is a sensitive sensor in response to cellular metabolic and stress states and plays a role as a key transcriptional regulator for antioxidant enzymes [36]. When exposed to oxidative stress, NRF2 is translocated into the nucleus and selectively activates gene transcription corresponding to various endogenous antioxidant enzymes, including CAT and SOD [37]. This indicates that upregulation of NRF2 ameliorates TBI-mediated DNA damages by enhancing the antioxidant defense system or by maintaining an intracellular redox balance [36,38,39]. Activation of NRF2 mitigated TBI-mediated hematopoietic death and augmented function and regeneration of HSCs, thereby increasing survival in TBI mice [40–42]. Taken as a whole, it is suggested that NRF2 is a potential therapeutic target to ameliorate or prevent TBI-mediated oxidative injuries, as well as to regulate self-renewal, proliferation, and differentiation of stem cells [43]. Overall, our current findings with previous reports [9,24] strongly suggest that the ferulic-acid-induced radioprotection is closely associated with the enhanced or maintained antioxidant defense systems that are followed by NRF2 upregulation.

## 5. Conclusions

In summary, small molecule antioxidants, such as dietary flavonoids and phenolic acids, may enhance HSC function and improve the efficacy of HSC transplantation therapy via the NRF2-related maintenance of BM and BM-conserved stem cells [42]. This study demonstrates that supplemental ferulic acid protects mice from TBI-mediated BM injuries and senescence of BM-conserved HSCs and MSCs by inhibiting ROS accumulation and osteoclastic and adipocytic activation in BM, as well as by recovering osteogenic activity and NRF2-associated antioxidant defense systems. This study also highlights that long-term administration of ferulic acid improves bone mass accrual and survival, and specifically accelerates SOD activity and NRF2 induction. The current findings indicate a preclinical potential of ferulic acid to prevent TBI-mediated oxidative disorders and to enhance therapeutic efficacy in BM transplantation. Overall, our results of this study imply that dietary phenolic antioxidants are attractive candidates as injectable materials for radioprotection.

**Supplementary Materials:** The following are available online at https://www.mdpi.com/article/10.3390/antiox10081209/s1, Figure S1: Flow cytometric analysis showing the mean percentage of $C_{12}$FDG-positive HSCs in BM of mice group at 30 days post-TBI. Figure S2: Flow cytometric analysis showing the mean number of HSCs in BM of mice groups at 2 and 30 days post-TBI. Table S1: Sequences of primers used to analyze the expression of adipogenesis-related genes.

**Author Contributions:** J.-C.L., S.-H.K., and Y.-M.J. conceived and designed the experiments; S.W., H.-J.S., G.B., and K.-C.C. performed the experiments; S.W. and H.-J.S. maintained, administered, and irradiated mice; S.W., G.B., J.-C.L., S.-H.K., and Y.-M.J. analyzed the data; H.-J.S., G.B., S.-H.K., Y.-M.J., and J.-C.L. contributed reagents/materials/analysis tools; S.W., S.-H.K., J.-C.L., and Y.-M.J. wrote and edited the manuscript. All authors have read and agreed to the published version of the manuscript.

**Funding:** This research was supported by Basic Science Research Program through the National Research Foundation (NRF) funded by the Ministry of Science, Information and Communications Technology and Future Planning (2018R1D1A1B07046563, 2020R1C1C1004968, 2021R1A2C2006032, and 2021R111A1A01044453), and by the RDA, Ministry of Agriculture and Forestry, Republic of Korea (PJ013394022021).

**Institutional Review Board Statement:** All procedures in this study were approved by the Animal Welfare Committee of Jeonbuk National University (Approval number: CBU 2014-00055).

**Informed Consent Statement:** Not applicable.

**Data Availability Statement:** Data is contained within the article and supplementary material.

**Conflicts of Interest:** The authors declare no conflict of interest.

## References


1. Mauch, P.; Constine, L.; Greenberger, J.; Knospe, W.; Sullivan, J.; Liesveld, J.L.; Deeg, H.J. Hematopoietic stem cell compartment: Acute and late effects of radiation therapy and chemotherapy. *Int. J. Radiat. Oncol. Biol. Phys.* **1995**, *31*, 1319–1339. [CrossRef]
2. Domen, J.; Gandy, K.L.; Weissman, I.L. Systemic overexpression of BCL-2 in the hematopoietic system protects transgenic mice from the consequences of lethal irradiation. *Blood* **1998**, *91*, 2272–2282. [CrossRef]
3. Balaban, R.S.; Nemoto, S.; Finkel, T. Mitochondria, oxidants, and aging. *Cell* **2005**, *120*, 483–495. [CrossRef] [PubMed]
4. Wang, Y.; Liu, L.; Pazhanisamy, S.K.; Li, H.; Meng, A.; Zhou, D. Total body irradiation causes residual bone marrow injury by induction of persistent oxidative stress in murine hematopoietic stem cells. *Free Radic. Biol. Med.* **2010**, *48*, 348–356. [CrossRef]
5. Shao, L.; Luo, Y.; Zhou, D. Hematopoietic stem cell injury induced by ionizing radiation. *Antioxid. Redox Signal.* **2014**, *20*, 1447–1462. [CrossRef]
6. Cao, X.; Wu, X.; Frassica, D.; Yu, B.; Pang, L.; Xian, L.; Frassica, F.J. Irradiation induces bone injury by damaging bone marrow microenvironment for stem cells. *Proc. Natl. Acad. Sci. USA* **2011**, *108*, 1609–1614. [CrossRef]
7. Costa, S.; Reagan, M.R. Therapeutic Irradiation: Consequences for bone and bone marrow adipose tissue. *Front. Endocrinol.* **2019**, *10*, 587. [CrossRef]
8. Zhang, R.; Kang, K.A.; Kang, S.S.; Park, J.W.; Hyun, J.W. Morin (2′,3,4′,5,7-pentahydroxyflabone) protected cells against radiation-induced oxidative stress. *Basic Clin. Pharmacol. Toxicol.* **2011**, *108*, 63–72. [CrossRef]
9. Kook, S.H.; Cheon, S.R.; Kim, J.H.; Choi, K.C.; Kim, M.K.; Lee, J.C. Dietary hydroxycinnamates prevent oxidative damages to liver, spleen, and bone marrow cells in irradiation-exposed mice. *Food Sci. Biotechnol.* **2017**, *26*, 279–285. [CrossRef]
10. Ma, Z.C.; Hong, Q.; Wang, Y.G.; Tan, H.L.; Xiao, C.R.; Liang, Q.D.; Gao, Y. Ferulic acid protects lymphocytes from radiation-predisposed oxidative stress through extracellular regulated kinase. *Int. J. Radiat. Biol.* **2011**, *87*, 130–140. [CrossRef] [PubMed]
11. Piazzon, A.; Vrhovsek, U.; Masuero, D.; Mattivi, F.; Mandoi, F.; Nardini, M. Antioxidant activity of phenolic acids and their metabolites: Synthesis and antioxidant properties of the sulfate derivatives of ferulic and caffeic acids and of the acyl glucuronide of ferulic acid. *J. Agric. Food Chem.* **2012**, *90*, 12312–12323. [CrossRef] [PubMed]
12. Das, U.; Manna, K.; Sinha, M.; Datta, S.; Da, D.K.; Chakraborty, A.; Ghosh, M.; Saha, K.D.; Dey, S. Role of ferulic acid in the amelioration of ionizing radiation induced inflammation: A murine model. *PLoS ONE* **2014**, *9*, e97599. [CrossRef]
13. Kanski, J.; Aksenova, M.; Stoyanova, A.; Butterfield, D.A. Ferulic acid antioxidant protection against hydroxyl and peroxyl radical oxidation in synaptosomal and neuronal cell culture systems in vitro: Structure-activity studies. *J. Nutr. Biochem.* **2002**, *13*, 273–281. [CrossRef]
14. Liang, J.W.; Li, P.L.; Wang, Q.; Liao, S.; Hu, W.; Zhao, Z.D.; Li, Z.L.; Yin, B.F.; Mao, N.; Ding, L.; et al. Ferulic acid promotes bone defect repair after radiation by maintaining the stemness of skeletal stem cells. *Stem Cells Transl. Med.* **2021**, 1–15. [CrossRef]
15. Srinivasan, M.; Sudheer, A.R.; Menon, V.P. Ferulic Acid: Therapeutic potential through its antioxidant property. *J. Clin. Biochem. Nutr.* **2007**, *40*, 92–100. [CrossRef] [PubMed]
16. Wang, Y.; Schulte, B.A.; LaRue, A.C.; Ogawa, M.; Zhou, D. Total body irradiation selectively induces murine hematopoietic stem cell senescence. *Blood* **2006**, *107*, 358–366. [CrossRef]
17. Bai, J.; Wang, Y.; Wang, J.; Zhai, J.; He, F.; Zhu, G. Irradiation-induced senescence of bone marrow mesenchymal stem cells aggravates osteogenic differentiation dysfunction via paracrine signaling. *Am. J. Physiol. Cell Physiol.* **2020**, *318*, C1005–C1017. [CrossRef]
18. Kiel, M.J.; Yilmaz, O.H.; Iwashita, T.; Yilmaz, O.H.; Terhorst, C.; Morrison, S.J. SLAM family receptors distinguish hematopoietic stem and progenitor cells and reveal endothelial niches for stem cells. *Cell* **2005**, *121*, 1109–1121. [CrossRef]
19. Naveiras, O.; Nardi, V.; Wenzel, P.L.; Fahey, F.; George, Q.; Cancer, D.F.; Medical, H. Bone marrow adipocytes as negative regulators of the hematopoietic microenvironment. *Nature* **2009**, *460*, 259–263. [CrossRef]
20. Schultze-Mosgau, S.; Lehner, B.; Rödel, F.; Wehrhan, F.; Amann, K.; Kopp, J.; Thorwarth, M.; Nkenke, E.; Grabenbauer, G. Expression of bone morphogenetic protein 2/4, transforming growth factor-beta1, and bone matrix protein expression in healing area between vascular tibia grafts and irradiated bone-experimental model of osteonecrosis. *Int. J. Radiat. Oncol. Biol. Phys.* **2005**, *61*, 1189–1196. [CrossRef]
21. King, A.D.; Griffith, J.F.; Abrigo, J.M.; Leung, S.F.; Yau, F.K.; Tse, G.M.; Ahuja, A.T. Osteoradionecrosis of the upper cervical spine: MR imaging following radiotherapy for nasopharyngeal carcinoma. *Eur. J. Radiol.* **2010**, *73*, 629–635. [CrossRef]
22. Rana, T.; Schultz, M.A.; Freeman, M.L.; Biswas, S. Loss of *Nrf2* accelerates ionizing radiation-induced bone loss by upregulating RANKL. *Free Radic. Biol. Med.* **2012**, *53*, 2298–2307. [CrossRef]
23. Shao, L.; Feng, W.; Li, H.; Gardner, D.; Luo, Y.; Wang, Y.; Liu, L.; Meng, A.; Sharpless, N.E.; Zhou, D. Total body irradiation causes long-term mouse BM injury via induction of HSC premature senescence in an Ink4a- and Arf-independent manner. *Blood* **2014**, *123*, 3105–3115. [CrossRef] [PubMed]

24. Sim, H.J.; Bhattarai, G.; Lee, J.; Lee, J.C.; Kook, S.H. The long-lasting radioprotective effect of caffeic acid in mice exposed to total body irradiation by modulating reactive oxygen species generation and hematopoietic stem cell senescence-accompanied long-term residual bone marrow injury. *Aging Dis.* **2019**, *10*, 1320–1327. [CrossRef]
25. Koc, M.; Taysi, S.; Buyukokuroglu, M.E.; Bakan, N. Melatonin protects rat liver against irradiation-induced oxidative injury. *J. Radiat. Res.* **2003**, *44*, 211–215. [CrossRef] [PubMed]
26. Islam, M.S.; Stemig, M.E.; Takahashi, Y.; Hui, S.K. Radiation response of mesenchymal stem cells derived from bone marrow and human pluripotent stem cells. *J. Radiat. Res.* **2015**, *56*, 269–277. [CrossRef]
27. Wang, Y.; Zhu, G.; Wang, J.; Chen, J. Irradiation alters the differentiation potential of bone marrow mesenchymal stem cells. *Mol. Med. Rep.* **2016**, *13*, 213–223. [CrossRef]
28. Lo, W.J.; Lin, C.L.; Chang, Y.C.; Bai, L.Y.; Lin, C.Y.; Liang, J.A.; Li, L.Y.; Chao, L.M.; Chiu, C.F.; Chen, C.M.; et al. Total body irradiation tremendously impair the proliferation, differentiation and chromosomal integrity of bone marrow-derived mesenchymal stromal stem cells. *Ann. Hematol.* **2018**, *97*, 697–707. [CrossRef]
29. Johnson, M.B.; Niknam-Bienia, S.; Soundararajan, V.; Pang, B.; Jung, E.; Gardner, D.J.; Xu, X.; Park, S.Y.; Wang, C.; Chen, X.; et al. Mesenchymal stromal cells isolated from irradiated human skin have diminished capacity for proliferation, differentiation, colony formation, and paracrine stimulation. *Stem Cells Trans. Med.* **2019**, *8*, 925–934. [CrossRef]
30. Callaway, D.A.; Jiang, J.X. Reactive oxygen species and oxidative stress in osteoclastogenesis, skeletal aging and bone diseases. *J. Bone Miner. Metab.* **2015**, *33*, 359–370. [CrossRef]
31. Herrmann, M. Marrow fat-secreted factors as biomarkers for osteoporosis. *Curr. Osteoporos. Rep.* **2019**, *17*, 429–437. [CrossRef]
32. Akune, T.; Ohba, S.; Kamekura, S.; Yamaguchi, M.; Chung, U.-I.; Kubota, N.; Terauchi, Y.; Harada, Y.; Azuma, Y.; Nakamura, K.; et al. PPARgamma insufficiency enhances osteogenesis through osteoblast formation from bone marrow progenitors. *J. Clin. Investig.* **2004**, *113*, 846–855. [CrossRef]
33. Koh, E.J.; Kim, K.J.; Seo, Y.J.; Choi, J.; Lee, B.Y. Modulation of HO-1 by ferulic acid attentuates adipocyte differentiation in 3T3-L1 cells. *Molecules* **2017**, *22*, 745. [CrossRef]
34. Yokozawa, T.; Chen, C.P.; Tanaka, T.; Kouno, I. Isolation from Wen-Pi-Tang of the active principles possessing antioxidation and radical-scavenging activities. *Phytomedicine* **1998**, *5*, 367–373. [CrossRef]
35. Grdina, D.J.; Murley, J.S.; Kataoka, Y.; Baker, K.L.; Kunnavakkam, R.; Coleman, M.C.; Spitz, D.R. Amifostien induces antioxidant enzymatic activities in normal tissues and a transplantable tumor that can affect radiation response. *Int. J. Radiat. Oncol. Biol. Phys.* **2009**, *73*, 886–896. [CrossRef]
36. Kim, S.B.; Pandita, R.K.; Eskiocak, U.; Ly, P.; Kaisani, A.; Kumar, R.; Cornelius, C.; Wright, W.E.; Pandita, T.K.; Shay, J.W. Targeting of Nrf2 induces DNA damage signaling and protects colonic epithelial cells from ionizing radiation. *Proc. Natl. Acad. Sci. USA* **2012**, *109*, E2949–E2955. [CrossRef]
37. Dong, J.; Sulik, K.K.; Chen, S. Nrf2-mediated transcriptional induction of antioxidant response in mouse embryos exposed to ethanol in vivo: Implications for the prevention of fetal alcohol spectrum disorders. *Antioxid. Redox Signal.* **2008**, *10*, 2023–2033. [CrossRef]
38. Frohlich, D.A.; McCabe, M.T.; Arnold, R.S.; Day, M.L. The role of Nrf2 in increased reactive oxygen species and DNA damage in prostate tumorigenesis. *Oncogene* **2008**, *27*, 4353–4362. [CrossRef]
39. Das, U.; Manna, K.; Khan, A.; Sinha, M.; Biswas, S.; Sengupta, A.; Chakraborty, A.; Dey, S. Ferulic acid (FA) abrogates γ-radiation induced oxidative stress and DNA damage by up-regulating nuclear translocation of Nrf2 and activation of NHEJ pathway. *Free Radic. Res.* **2017**, *51*, 47–63. [CrossRef] [PubMed]
40. Chute, J.P. NRF2 mitigates radiation-induced hematopoietic death. *J. Clin. Investig.* **2014**, *124*, 960–961. [CrossRef]
41. Kim, J.H.; Thimmulappa, R.K.; Kumar, V.; Cui, W.; Kumar, S.; Kombairaju, P.; Zhang., H.; Margolick, J.; Matsui, W.; Macvittie, T.; et al. NRF2-mediated Notch pathway activation enhances hematopoietic reconstitution following myelosuppressive radiation. *J. Clin. Investig.* **2014**, *124*, 730–741. [CrossRef] [PubMed]
42. Hu, L.; Zhang, Y.; Miao, W.; Cheng, T. Reactive oxygen species and Nrf2: Functional and transcriptional regulators of hematopoiesis. *Oxid. Med. Cell. Longev.* **2019**, *2019*, 5153268. [CrossRef]
43. Dai, X.; Yan, X.; Wintergerst, K.A.; Cai, L.; Keller, B.B.; Tan, Y. Nrf2: Redox and metabolic regulator of stem cell state and function. *Trends Mol. Med.* **2020**, *26*, 185–200. [CrossRef] [PubMed]

*antioxidants*

MDPI

*Article*

# *Limnospira indica* PCC 8005 Supplementation Prevents Pelvic Irradiation-Induced Dysbiosis but Not Acute Inflammation in Mice

**Charlotte Segers [1,2,†], Mohamed Mysara [1,‡], Amelie Coolkens [1,†], Shari Wouters [1,§], Sarah Baatout [1], Natalie Leys [1], Sarah Lebeer [2], Mieke Verslegers [1,‖] and Felice Mastroleo [1,*]**

[1] Interdisciplinary Biosciences Group, Belgian Nuclear Research Centre, SCK CEN, 2400 Mol, Belgium
[2] Department of Bioscience Engineering, University of Antwerp, 2020 Antwerp, Belgium
* Correspondence: felice.mastroleo@sckcen.be; Tel.: +32-14-33-23-88
† Current affiliation: NURA Research Group, Belgian Nuclear Research Centre, SCK CEN, 2400 Mol, Belgium.
‡ Current affiliation: Bioinformatics Group, Center for Informatics Science, Nile University, Giza 12677, Egypt.
§ Current affiliation: Faculty of Medicine and Health Sciences, University of Antwerp, 2610 Antwerp, Belgium.
‖ Current affiliation: Preclinical Sciences and Translational Safety, Janssen Research and Development, 2340 Beerse, Belgium.

**Abstract:** Pelvic irradiation-induced mucositis secondarily leads to dysbiosis, which seriously affects patients' quality of life after treatment. No safe and effective radioprotector or mitigator has yet been approved for clinical therapy. Here, we investigated the potential protective effects of fresh biomass of *Limnospira indica* PCC 8005 against ionizing irradiation-induced mucositis and dysbiosis in respect to benchmark probiotic *Lacticaseibacillus rhamnosus* GG ATCC 53103. For this, mice were supplemented daily before and after 12 Gy X-irradiation of the pelvis. Upon sacrifice, food supplements' efficacy was assessed for intestinal barrier protection, immunomodulation and changes in the microbiota composition. While both could not confer barrier protection or significant immunomodulatory effects, 16S microbial profiling revealed that *L. indica* PCC 8005 and *L. rhamnosus* GG could prevent pelvic irradiation-induced dysbiosis. Altogether, our data show that—besides benchmarked *L. rhamnosus* GG—*L. indica* PCC 8005 is an interesting candidate to further explore as a radiomitigator counteracting pelvic irradiation-induced dysbiosis in the presented in vivo irradiation–gut–microbiota platform.

**Keywords:** ionizing radiation; intestine; mucositis; microbiome; microbiota; dysbiosis; bacterial dietary supplement; radiomitigator

**Citation:** Segers, C.; Mysara, M.; Coolkens, A.; Wouters, S.; Baatout, S.; Leys, N.; Lebeer, S.; Verslegers, M.; Mastroleo, F. *Limnospira indica* PCC 8005 Supplementation Prevents Pelvic Irradiation-Induced Dysbiosis but Not Acute Inflammation in Mice. *Antioxidants* **2023**, *12*, 572. https://doi.org/10.3390/antiox12030572

Academic Editors: Elena Obrador Pla and Alegria Montoro

Received: 19 December 2022
Revised: 22 February 2023
Accepted: 23 February 2023
Published: 24 February 2023



## 1. Introduction

Radiotherapy is commonly used in the clinic to treat a wide variety of cancers. Despite technological improvements, the delivery of ionizing irradiation to a tumor unavoidably affects the surrounding healthy tissues, specifically the rapidly renewing and thus highly radio-sensitive intestine, which is situated within the treatment field for all intra-abdominal, retroperitoneal, as well as pelvic tumors [1,2]. As a consequence, patients often develop acute and chronic intestinal complications, with diarrhea being the most frequently reported symptom [1].

Previously, we reported that, secondarily to the induction of intestinal mucositis, acute pelvic irradiation affected the colonic microbial ecosystem in a mouse model [3]. So-called dysbiosis, defined by an altered composition of microbes having a cascading impact on the immune system and offering an advantage for emergence and outbreak of pathogens [4], may induce a chronic intestinal phenotype [5].

Accordingly, reconstitution or protection of the intestinal ecology following pelvic irradiation may be conferred by food supplements through immunomodulatory and barrier-protective mechanisms as well as intermicrobial interactions [2]. So far, the results of clinical

trials have not always been unambiguous, as reviewed earlier [2]. A crucial factor for success might be the appropriate choice of food supplement used.

One of the best-documented model probiotic strains, *Lacticaseibacillus rhamnosus* GG, was reported to exert TLR2/COX2-mediated protection of the intestinal barrier in mice following 12 Gy total body irradiation [6,7]. Additionally, other studies have shown its potential for use as adjunctive therapy in cases of diarrhea [8,9], cancer [10,11] and inflammatory bowel disease [12,13]. These promising results have prompted the initiation of a clinical trial currently exploring its radioprotective potential in patients receiving abdominopelvic irradiation (NCT01790035). Still, its safety, efficacy and mechanism(s) of action remain to be addressed.

Besides traditional probiotic strains, alternative food supplements are being explored for their radioprotective potential. Previously, we introduced anciently used *Limnospira indica* PCC 8005 (also known as *Arthrospira* sp. or its generic product name, Spirulina) [14] because of recent efforts showing beneficial effects of dried biomass and/or isolated bioactive compounds on the intestine's antioxidant status, immune system and/or bacterial communities [15–20]. In 2002, the edible character of *Limnospira* spp. was reviewed by the US Food and Drug Administration and received the GRAS (Generally Recognized as Safe) status. Although no (pre)clinical research investigating the potential of *Limnospira* spp. for reducing radiotherapy-induced intestinal toxicity has yet been conducted, its protective potential has been investigated in other organs. For instance, *Limnospira* sp. (1 g/kg for 15 days) was proposed to ensure nephroprotection in rats after 6.5 Gy total body irradiation by improving the overall lipid profile and reducing oxidative stress and apoptosis [21]. In mice exposed to 2.5 Gy total body irradiation, a crude ethanol precipitate of *Limnospira* sp. (three times 12 mg/kg) was reported to reduce bone marrow damage likely because of transient enhancement of radical-scavenging activity in irradiated cells [22]. The prophylactic and therapeutic potentials of extracted phycocyanin were evaluated in a mouse model exposed to thoracic irradiation in view of pulmonary fibrosis. Both strategies appeared capable of alleviating radiation-induced lung injury when evaluating histology as well as local and systemic inflammatory parameters [23].

To date, the radioprotective potential of unprocessed *L. indica* PCC 8005 on the intestinal ecosystem has not yet been explored in respect to *L. rhamnosus* GG. Therefore, we set out a comparative study in which mice were administered fresh, in-house prepared biomass of either *L. indica* PCC 8005, *L. rhamnosus* GG or saline before and after a single exposure of the pelvis to ionizing radiation.

## 2. Materials and Methods

### *2.1. Mice*

All animal experiments were approved by the SCK CEN animal welfare committee and were carried out in accordance with the Ethical Committee Animal Studies of Medanex Clinic (EC MxCl 2018-093), the Belgian laboratory animal legislation and the European Communities Council Directive of 22 September 2010 (2010/63/EU).

Five-week-old, male C57Bl/6JRj mice (Janvier, Bio Services, Uden, The Netherlands) were used, as they were described as one of the most recommended mouse strains for developing radiation countermeasures [24]. Moreover, given the higher incidence of pelvic cancers in males, as reported by the World Health Organization in 2020 (https://gco.iarc.fr/; accessed on 17 December 2022), male mice were chosen. Mice were housed individually in ventilated cages under standard laboratory conditions (12 h light/dark cycle) with ad libitum supply of regular chow and water and were acclimatized for two weeks prior to the start of the experiment.

Confounding factors were minimized across experimental cohorts by randomly assigning mice to a pre-specified number of groups using the *minDiff* package in RStudio (v.3.5.0).

### 2.2. Bacteria and Growth Conditions

*Limnospira indica* PCC 8005 morphotype P1 was obtained from the Pasteur Culture collection of Cyanobacteria (PCC) (Institut Pasteur, France). *L. indica* PCC 8005 cultures were grown axenically in Zarrouk medium (pH ~9.8) at a constant temperature of 30 °C while shaken at 120 rpm [25]. Cells were illuminated at a photon flux density of 45 µmol photons·$m^{-2}$·$s^{-1}$ (Osram, Belgium).

In parallel, *Lacticaseibacillus rhamnosus* GG ATCC 53103, a strain originally isolated from human fecal samples [26,27], was kindly gifted by professor Sarah Lebeer (University of Antwerp). This strain was grown statically in the dark at 37 °C in de Man, Rogosa and Sharpe (MRS) medium (Difco, Belgium) [28].

Fresh bacterial biomass of both species was prepared for supplementation as reported previously [14].

### 2.3. Experimental Setup

Mice were randomly distributed over 4 different groups ($n$ = 10 per group); mice receiving (1) sham-irradiation and daily saline (200 µL/mouse); (2) pelvic irradiation and daily saline (200 µL/mouse); (3) pelvic irradiation and daily *L. rhamnosus* GG (~7 × $10^8$ cells/mouse); and (4) pelvic irradiation and daily *L. indica* PCC 8005 (~3 × $10^7$ cells/mouse of 20 g) (Figure 1A). Bacterial suspensions were administered daily by oral gavage in a maximum volume of 10 µL/g body weight starting from seven days prior to pelvic irradiation until the day of sacrifice. The supplementation dose used for *L. rhamnosus* GG was associated with probiotic effects [29–31]. The amount of *L. indica* PCC 8005 administered to mice corresponded to a dosing regimen of 800 mg/kg, previously reported to have antioxidative effects in vivo [32–36]. During the entire experimental setup of maximum 14 days, mice were closely monitored for their overall health and body weight. Eventually, all mice were sacrificed at either post-irradiation day (PID) 1, 3 or 7.

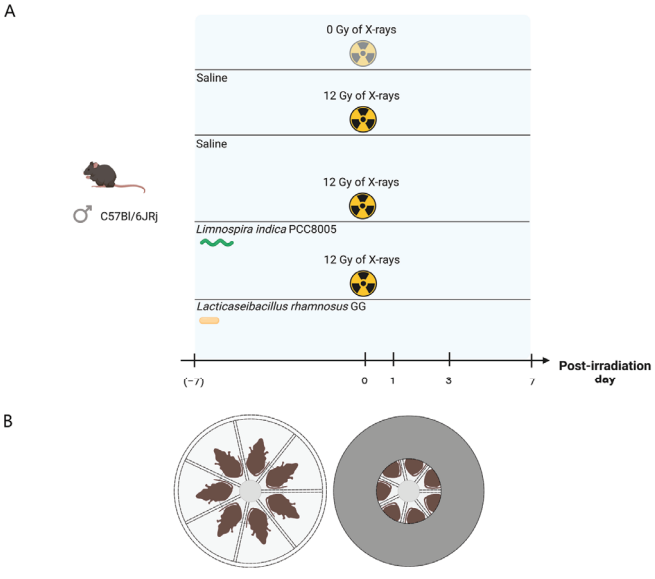


**Figure 1.** Experimental setup. (**A**) Experimental timeline for supplementation and pelvic irradiation of mice. Supplementation was carried out from seven days prior to pelvic irradiation until the day of sacrifice at either post-irradiation day 1, 3 or 7. Created with BioRender.com. (**B**) Disk-shaped plexiglas box used for local, pelvic irradiation of the mice. Individual animals were placed inside in a prone position (**left**). The entire box, except for the center (9 cm diameter), was shielded with lead (5 mm thick) (**right**). This figure was created with BioRender.com.

### *2.4. Irradiation Protocol*

Pelvic irradiation was performed as described earlier [3]. Briefly, eight-week-old mice were anesthetized and placed in a custom-made disk-shaped Plexiglas box, as illustrated in Figure 1B. The entire box, except for the center (9 cm diameter), was shielded with lead (5 mm thick), allowing local pelvic irradiation of the mice (0 Gy or 12 Gy of X-rays). Control (0 Gy) mice were also anesthetized but were not irradiated (i.e., sham-irradiation).

### *2.5. Ileal histology and Histochemistry*

We focused on distal ileum, which we previously reported to be more radiosensitive than proximal colon [3]. In detail, tissues were rinsed with ice-cold phosphate-buffered saline (GibcoTM, Thermo Fisher Scientific, Belgium) and fixed in 4% paraformaldehyde (Merck, Belgium). Histology and immunohistochemistry were performed on 5 µm paraffin-embedded tissues cut on a Thermo Scientific HM 340E Electronic Rotary Microtome perpendicular to the long axis of the intestine and mounted onto Superfrost$^{TM}$ microscope slides (Thermo Fisher Scientific, Merelbeke, Belgium).

For Terminal deoxynucleotidyl transferase-mediated dUTP nick end labeling (TUNEL), the In Situ Cell Death Detection Kit (#11684817910 Roche, Merck, Overijse, Belgium) was used according to the manufacturer's instructions. For visualization, the DAKO Envision+ HRP (DAB, Thermo Fisher Scientific, Belgium) system was used. Slides were imaged using a brightfield Nikon Ti-Eclipse microscope and a 20× objective. The number of positively stained cells were counted in 50 random crypts per mouse (blindly coded) and normalized to the total number of cells in the crypts. In parallel, general morphology of ileal samples was assessed on the same slides by quantifying villus length and crypt depth at 50 random places per mouse (blindly coded).

### *2.6. Ileal Myeloperoxidase Activity Assay*

To monitor the degree of acute inflammation, neutrophil myeloperoxidase activity was measured in ileal tissues as previously performed [3]. Data represent units per gram of tissue in which one unit equals the amount of myeloperoxidase necessary to degrade 1 µmol of hydrogen peroxide per minute at 25 °C.

### *2.7. Cytokine Analyses*

Total cell lysates from ileal samples were prepared in ice-cold lysis buffer (500 mM NaCl, 50 mM Tris pH 7.5, 2 mM EDTA, 1% Triton X-100, 0.5% sodium deoxycholic acid, 0.1% SDS, 1 mM protease inhibitor). Protein concentrations were determined by bicinchoninic acid assay (Sigma-Aldrich, Overijse, Belgium). Cell extracts were subjected to cytokine analyses using the MSD mouse pro-inflammatory V-plex assay containing antibodies for IL1β, IL10, IFNγ and TNFα. These assays were performed according to manufacturer's instructions using the MSD Quickplex SQ 120 instrument and MSD Discovery Workbench data analysis software v4.0 (Meso Scale Discovery$^{TM}$; MSD, Rockville, MD, USA).

### *2.8. Western Blot Analysis of Claudin 5*

Claudin 5 expression was reported to be positively correlated with barrier integrity [3]. Therefore, total cell lysates from ileal samples were prepared for Western blot analysis as previously performed [3].

### *2.9. Fecal DNA Extraction and 16S rRNA Gene Sequencing*

Fecal samples were longitudinally collected every other day, from arrival of mice onwards, to assess the impact of unprocessed *L. indica* PCC 8005 and *L. rhamnosus* GG on the microbiota. Total fecal DNA was extracted and quantified using the DNeasy PowerSoil Pro Kit (Qiagen, Venlo, The Netherlands) and the QuantiFluor dsDNA system (Promega, Leiden, The Netherlands) according to the manufacturer's instructions. High-throughput amplicon sequencing of the V3-V4 hypervariable region was conducted on BaseClear's Illu-

mina MiSeq (V3 chemistry) platform according to the manufacturer's guidelines. Positive and negative controls were included as recommended [37].

### *2.10. Sequencing Data Processing and Analyses*

16S rRNA gene sequencing data were processed and analyzed as previously described [3].

### *2.11. Statistical Analyses*

Data were processed, analyzed and visualized using RStudio software packages including *ggplot2* and *ggsci*. Outliers, as defined by the Tukey's fences criteria (i.e., values below Q1 − 1.5 * IQR or above Q3 + 1.5 × IQR), were excluded from further statistical analyses. Statistical significance was determined using linear (mixed) models using the *lme4* package in RStudio unless otherwise mentioned. Differences with $p < 0.05$ were considered statistically significant.

## 3. Results

### *3.1. L. indica PCC 8005 and L. rhamnosus GG Are Unsuccessful in Protecting the Ileal Barrier Damaged by Pelvic Irradiation*

First, daily monitoring of mice's body weights showed clear effects of pelvic irradiation (ß = −0.16819; $p = 0.001544$) (Figure 2). Specifically, significant irradiation-induced weight loss was noted at PID4 and PID5. However, supplements could not prevent and/or restore the temporal loss of body weight.

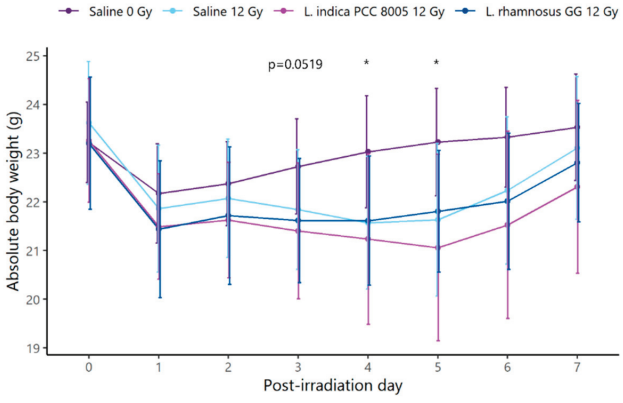


**Figure 2.** Curve of absolute body weight of all mice subdivided into four treatment groups: saline 0 Gy, saline 12 Gy, *L. indica* PCC 8005 12 Gy and *L. rhamnosus* GG 12 Gy. Data (in grams) are shown as means ± standard deviation, $n = 10$ per group. * $p < 0.05$ for pelvic irradiation-induced differences by linear modeling. Time-dependent differences in respect to the day of (sham-)irradiation (PID0) were not significant as assessed by linear mixed effects modeling.

Histopathology revealed a rapid, significant increase in the percentage of apoptotic nuclei in all ileal crypts of 12 Gy-exposed mice as compared to sham-irradiated mice (Figure 3A,B). However, both tested supplements appeared unsuccessful in preventing and/or reducing apoptosis induced by pelvic irradiation. A consequent decrease in villus length and crypt depth in response to radiation-induced apoptosis was not observed in our study following local acute pelvic irradiation (Figures 4 and S1). Hence, possible regenerative and/or healing effects of both supplements could not be identified following pelvic irradiation.

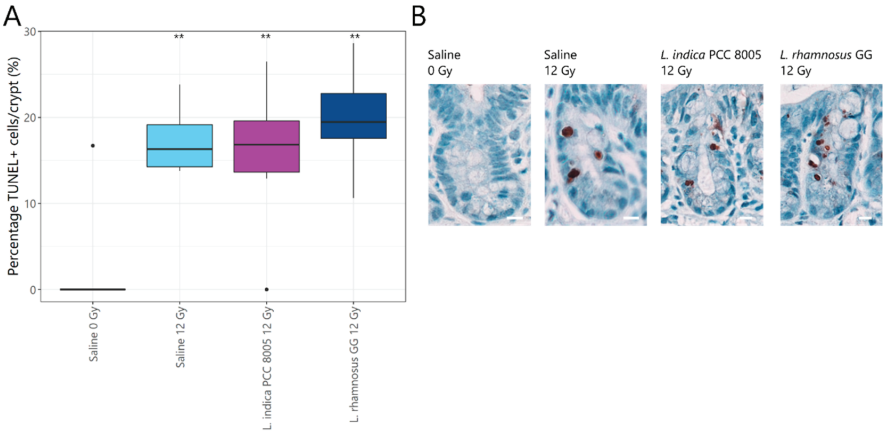


**Figure 3.** Crypt apoptosis one day following pelvic irradiation. (**A**) Boxplots showing the crypt apoptosis index representing the percentage of TUNEL+ cells per total number of ileal crypt cells one day following (sham-)irradiation. Outliers are depicted by dots, $n = 10$ per group, ** $p < 0.01$ for pelvic irradiation-induced differences in respect to sham-irradiation by Kruskal–Wallis test (Dunn's post hoc correction). (**B**) Representative images of TUNEL staining obtained at post-irradiation day 1. Brown nuclei are TUNEL+ cells and scale bar represents 10 µm.

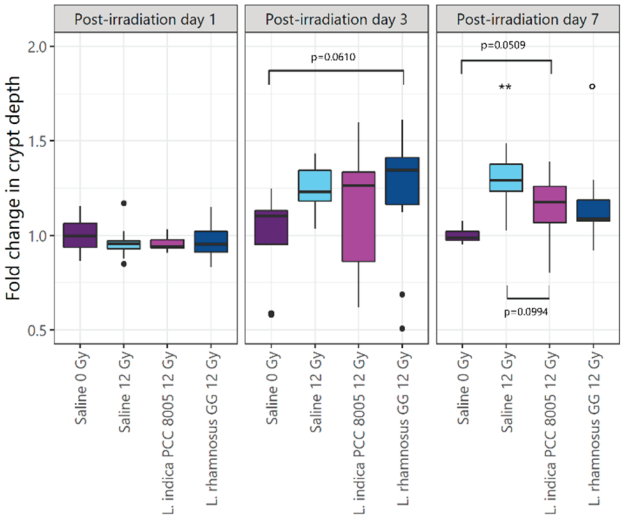


**Figure 4.** Boxplots showing the fold changes in mucosal crypt depth following pelvic (sham-)irradiation for all different experimental groups. Outliers are depicted by dots, $n = 10$ per group, ** $p < 0.01$ for pelvic irradiation-induced differences in respect to sham-irradiation, and $^{\circ}$ $p < 0.05$ for food supplement-dependent differences in respect to saline administration by linear modelling.

To assess the consequences of irradiation-induced epithelial apoptosis on mucosal integrity, claudin 5 tight junction expression was investigated by Western blot. Although completely restored at PID7, pelvic irradiation significantly reduced claudin 5 expression at PID3 (Figure 5A,B). Both tested supplements could not intervene in barrier impairment following pelvic irradiation.

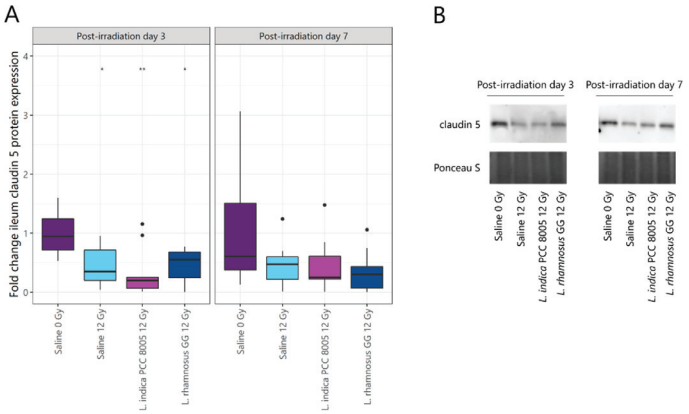


**Figure 5.** (**A**) Effects of pelvic irradiation on ileum claudin 5 protein expression. Outliers are depicted by dots, $n = 10$ per group. (**B**) Representative Western blot images of claudin 5 (23 kDa) and Ponceau S total protein staining, $n = 10$ per group, * $p < 0.05$ and ** $p < 0.01$ for pelvic irradiation-induced differences in respect to sham-irradiation by Kruskal–Wallis test (Dunn's post hoc correction).

### *3.2. L. rhamnosus GG and L. indica PCC 8005 Supplementation Are Not Able to Prevent Acute Ileal Inflammation Induced by Pelvic Irradiation*

Besides barrier protection, food supplements are being investigated in view of their capacity to modulate the immune response. Therefore, myeloperoxidase activity was measured to monitor mucosal neutrophil inflammation. Molecular analyses showed that pelvic irradiation acutely and temporally provoked an increase in myeloperoxidase activity, which was partly (37%) prevented by *L. rhamnosus* GG supplementation at PID1 (Figure 6).

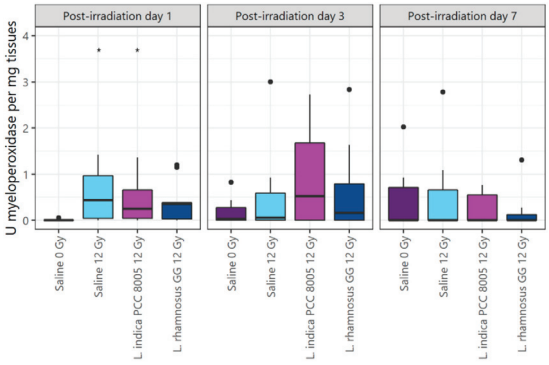


**Figure 6.** Ileal inflammatory myeloperoxidase activity following (sham-)irradiation. Outliers are depicted by dots, $n = 10$ per group, * $p < 0.05$ for pelvic irradiation-induced differences in respect to sham-irradiation by Kruskal–Wallis test (Dunn's post hoc correction).

In addition to myeloperoxidase activity, ileal levels of pro-inflammatory cytokines including IFNγ, IL1β, IL10 and TNFα were quantified. Despite a temporal decrease in IFNγ at PID1, pelvic irradiation significantly increased its levels from PID3 onwards (Figure 7A). This latter effect was partly reversed at PID3 and PID7 by *L. rhamnosus* GG supplementation, while IFNγ levels were only restored at PID7 with *L. indica* PCC 8005 supplementation. Both IL1β and IL10 were significantly increased three days following pelvic irradiation (Figure 7B, C). Although none of the tested supplements were capable of lowering these at PID3, IL10 levels partially recovered at PID7 following *L. rhamnosus* GG supplementation (Figure 7C). Finally, pelvic irradiation temporally provoked an increase in

TNFα at PID3 (Figure 7D). A modest increase in TNFα was already observed at PID1 for the *L. rhamnosus* GG supplemented group. No restoration of TNFα was observed for either of the tested supplements.

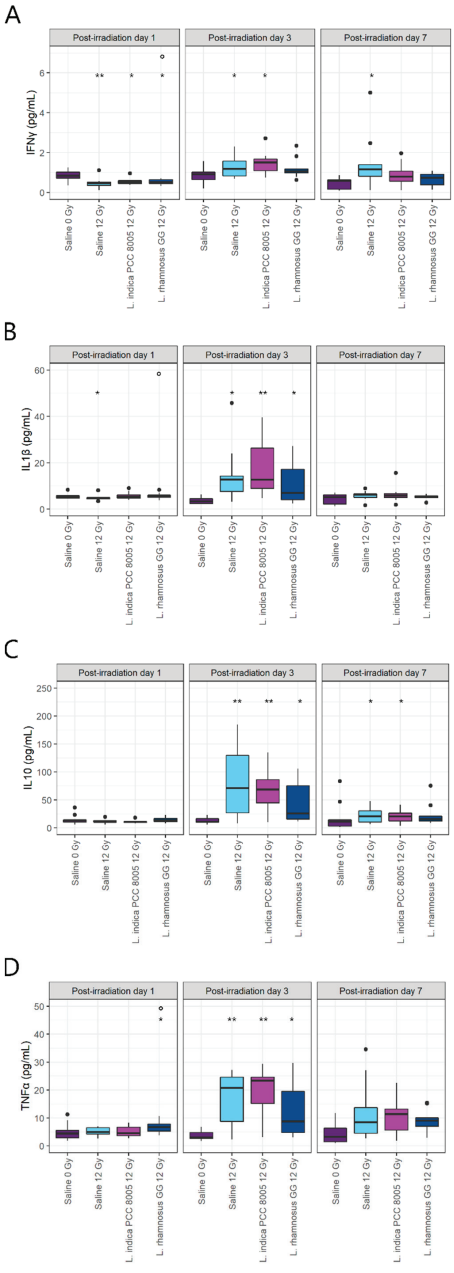


**Figure 7.** Ileal pro-inflammatory cytokine levels including (**A**) IFNγ, (**B**) IL1β, (**C**) IL10 and (**D**) TNFα following (sham-)irradiation. Outliers are depicted by dots, $n = 10$ per group, * $p < 0.05$ and ** $p < 0.01$ for pelvic irradiation-induced differences in respect to sham-irradiation, and ° $p < 0.05$ for supplementation-induced differences in respect to saline treatment by Kruskal–Wallis test (Dunn's post hoc correction).

### *3.3. L. indica PCC 8005 and L. rhamnosus GG Prevent Pelvic Irradiation-Induced Dysbiosis*

Next, to assess the impact of fresh *L. indica* PCC 8005 and *L. rhamnosus* GG on the irradiated microbiota, feces were collected before and after pelvic exposure for 16S microbial profiling. In this data set, the alpha rarefaction curve and the Good's estimator of coverage suggested that the 16S rRNA results from each library represented an adequate level of sequencing (Figure S2A,B) [38,39]. Following rarefaction, performed to a depth of ≥6117 reads representing the smallest sample depth, the obtained reads were linked to a total of 694 Operational Taxonomic Units (OTUs) (167 ± 16 OTUs on average per sample).

Changes in the microbial communities introduced by pelvic irradiation, and the different food supplements tested were evaluated using microbial alpha and beta diversity indices. At indicated sampling points, no irradiation- nor supplementation-induced effects on alpha diversity metrics were observed (Chao, Shannon, Shannon even indices; Figure 8, Figures S3 and S4). However, paired comparisons of alpha diversity metrics in respect to corresponding baseline (PID0) revealed a temporally increased richness at PID3 for mice supplemented with *L. rhamnosus* GG (Chao index; Figure 8).

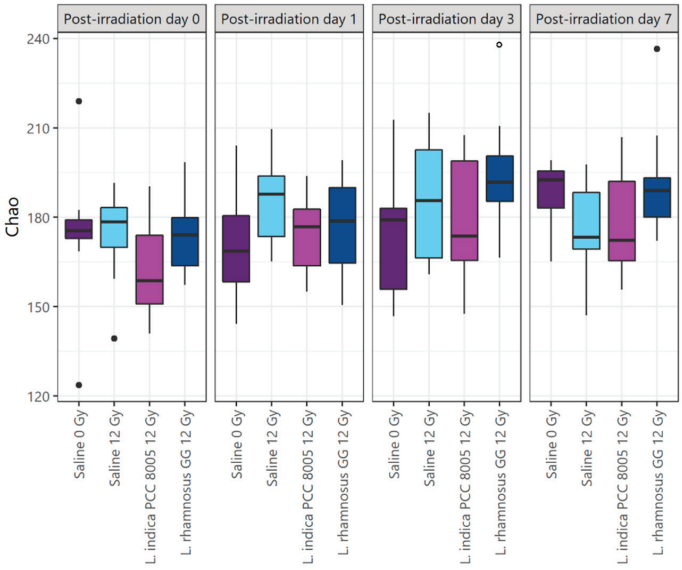


**Figure 8.** Changes in alpha diversity index Chao, considering solely richness, following (sham-)irradiation. Data are presented in boxplots and outliers are depicted by dots, $n = 10$ per group. Time-independent differences were assessed by Mann–Whitney's U test (Bonferroni's post hoc correction). Time-series, pairwise comparisons in respect to post-irradiation day 0 using ° $p < 0.05$ were performed by Wilcoxon's signed rank test (Bonferroni's *post-hoc* correction).

Microbiota community structures were further compared by a distance matrix based on unweighted (considering microbial membership) UniFrac beta diversity index with 1000 permutations. At baseline (at PID0), a significant shift of unweighted UniFrac beta diversity was noted when comparing both supplemented microbial communities to each other (Table S1 and Figure S5A). While differences were no longer detected at PID1 and PID3, shifts in microbial communities re-appeared at PID7 (Table S1 and Figure S5B–D).

To exclude the compositional differences present at PID0 introduced by the different supplementation regimens, analyses were performed in a paired manner, capturing the individual changes for each mouse over time. For saline-administered mice exposed to pelvic irradiation, analyses revealed a significant shift in unweighted UniFrac beta diversity at PID3 and PID7 in respect to its microbial community before pelvic irradiation (PID0) (Table 1 and Figure 9). When analyzing the other cohorts, including Saline 0 Gy, *L. indica*

PCC 8005 12 Gy and *L. rhamnosus* GG 12 Gy, no significant shifts could be detected over time (Table 1 and Figure 9).

**Table 1.** *p* values (** $p < 0.01$) of paired unweighted UniFrac beta diversity analyses by AMOVA. PID = post-irradiation day.

| | **Unweighted UniFrac Beta Diversity** |
|---|---|
| Saline 0 Gy | Overall *p* value: 0.453 |
| Saline 12 Gy | Overall *p* value: 0.006 **<br>*Post-hoc p* values:<br>• PID0 vs. PID1 $p = 0.658$<br>• PID0 vs. PID3 $p = 0.004$ **<br>• PID0 vs. PID7 $p = 0.001$ **<br>• PID1 vs. PID3 $p = 0.197$<br>• PID1 vs. PID7 $p = 0.006$ **<br>• PID3 vs. PID7 $p = 0.008$ ** |
| *L. indica* PCC 8005 12 Gy | Overall *p* value: 0.124 |
| *L. rhamnosus* GG 12 Gy | Overall *p* value: 0.422 |

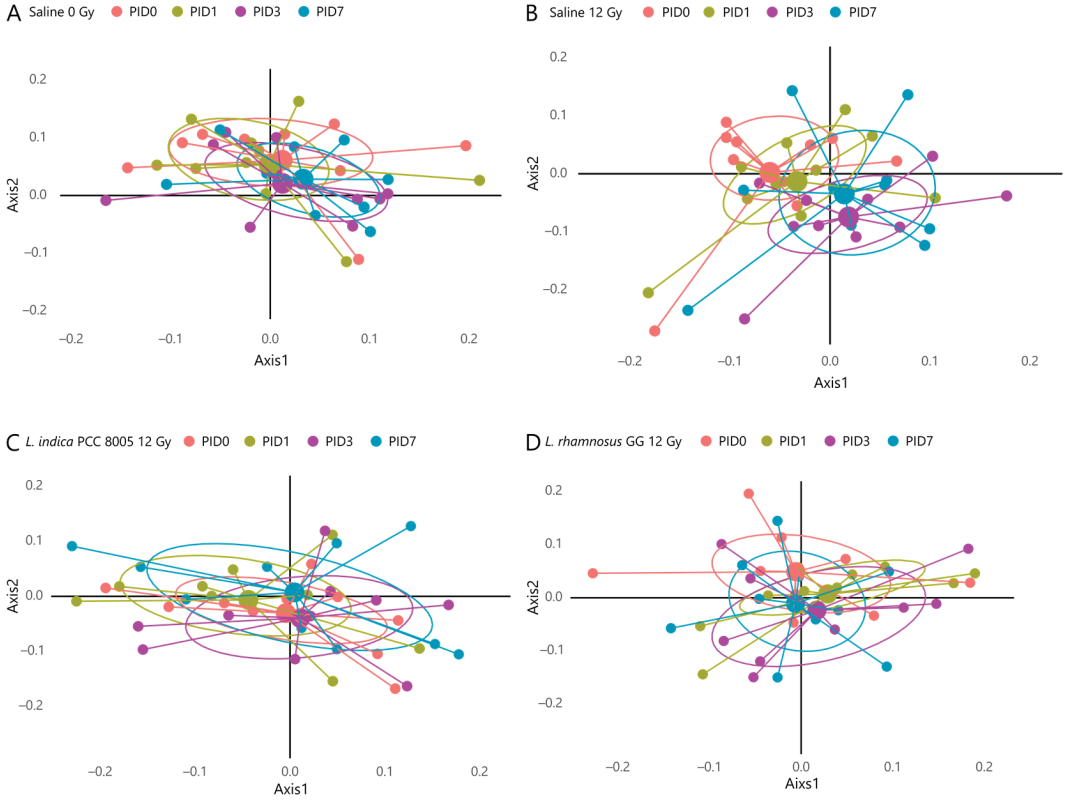


**Figure 9.** Unweighted UniFrac NMDS plots of (**A**) Saline 0 Gy-, (**B**) Saline 12 Gy-, (**C**) *L. indica* PCC 8005 12 Gy- and (**D**) *L. rhamnosus* GG 12 Gy-administered mice showing the beta diversity between samples, $n \geq 9$ per group. PID = post-irradiation day.

Next, to correlate specific OTUs with pelvic irradiation and/or supplementation, the composition of fecal microbiota was investigated in a paired manner using ANCOM and then further refined using oligotyping. A minor list of only three OTUs was identified for saline-administered, sham-irradiated mice (Table S2 and Figure S6), thus indicating a rather stable microbial community over time. In contrast, 13 OTUs were listed to be differentially affected in saline-administered, irradiated mice and belong to the *Porphyromonadaceae* and *Lachnospiraceae* families, including OTU135 (identified as *Alistipes putredinis*) (Table S3 and Figure S7). Furthermore, supplementation with either *L. indica* PCC 8005 or *L. rhamnosus* GG differentially impacted 7 and 11 OTUs, respectively (Tables 2 and 3 and Figures 10 and 11). Of interest, three significant OTUs were shared between the latter supplementation groups, including OTU14 (*Bacteroidales* spp.) and OTU59 (*Ruminococcaeae* spp.), as well as OTU290 (*Ruminococcaeae* spp.), which were introduced or reduced following pelvic irradiation, respectively. In particular, mice supplemented with *L. indica* PCC 8005 predominantly lost OTUs belonging to the *Porphyromonadaceae* and *Ruminococcaceae* family, while OTU7 (identified as *Akkermansia muciniphila*) was significantly increased in some mice (Table 2 and Figure 10). For mice supplemented with *L. rhamnosus* GG, members belonging to the *Porphyromonadaceae* family were elevated (Table 3 and Figure 11).

**Table 2.** Differential operational taxonomic units (OTUs) detected in *L. indica* PCC 8005-given mice following pelvic irradiation. PID = post-irradiation day.

| Taxonomic Classification (Following Ribosomal Database Project) | ANCOM Biomarkers' Effect Size and *W*-Statistic | Highest NCBI Blast Hit (% Identity) |
|---|---|---|
| *Akkermansia*_OTU7 | 1.03; *W* = 0.9 (PID7) | *Akkermansia muciniphila* (~100% identity) |
| *Bacteroidales*_OTU14 | 1.58; *W* = 0.9 (PID3) | |
| *Ruminococcus*_OTU59 | 1.57; *W*= 0.7 (PID3) | |
| *Porphyromonadaceae*_OTU2 | −1.21; *W* = 0.9 (PID7) | |
| *Ruminococcaceae*_OTU196 | −1.21; *W* = 0.9 (PID1) | |
| *Ruminococcaceae*_OTU267 | −1.10; *W* = 0.9 (PID3) | |
| *Ruminococcaceae*_OTU290 | −1.16; *W* = 0.9 (PID7) | |

**Table 3.** Differential operational taxonomic units (OTUs) detected in *L. rhamnosus* GG-given mice following pelvic irradiation. PID = post-irradiation day.

| Taxonomic Classification (Following Ribosomal Database Project) | ANCOM Biomarkers' Effect Size and *W*-Statistic | Highest NCBI Blast Hit (% Identity) |
|---|---|---|
| *Bacteroidales*_OTU14 | 1.14; *W* = 0.8 (PID3) | |
| *Porphyromonadaceae*_OTU20 | 1.27; *W* = 0.9 (PID7) | |
| *Porphyromonadaceae*_OTU40 | 1.41; *W* = 0.7 (PID7) | |
| *Ruminococcus*_OTU59 | 2.15; *W* = 0.8 (PID1);<br>1.43; *W* = 0.8 (PID3) | |
| *Ruminococcaceae*_OTU290 | 1.01; *W* = 0.9 (PID1) | |
| *Lachnospiraceae*_OTU445 | 1.09; *W*= 0.9 (PID7) | *Muricomes intestine* (>97% identity) |
| *Lachnospiraceae*_OTU16 | −1.31; *W* = 0.9 (PID7) | |
| *Firmicutes*_OTU228 | −1.06; *W* = 0.9 (PID1);<br>−1.17; *W* = 0.9 (PID7) | |
| *Firmicutes*_OTU236 | −1.20; *W* = 0.9 (PID1) | |
| *Lachnospiraceae*_OTU301 | −1.07; *W* = 0.9 (PID3) | |
| *Lachnospiraceae*_OTU351 | −1.17; *W* = 0.9 (PID7) | |

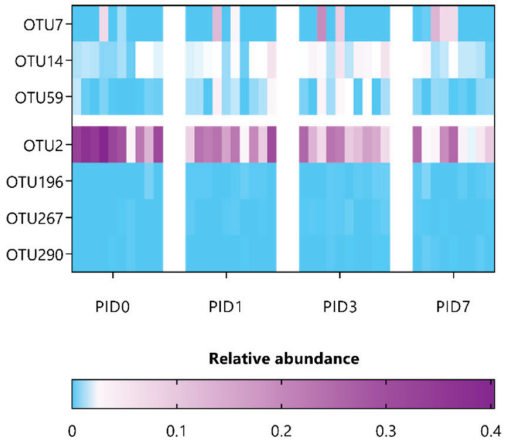


**Figure 10.** Heatmap representing the relative abundance of significant gut microbial dysbiosis markers detected in *L. indica* PCC 8005-given mice following sham-irradiation as listed in Table 2, $n$ = 10 per time point. OTU = operational taxonomic unit; PID = post-irradiation day.

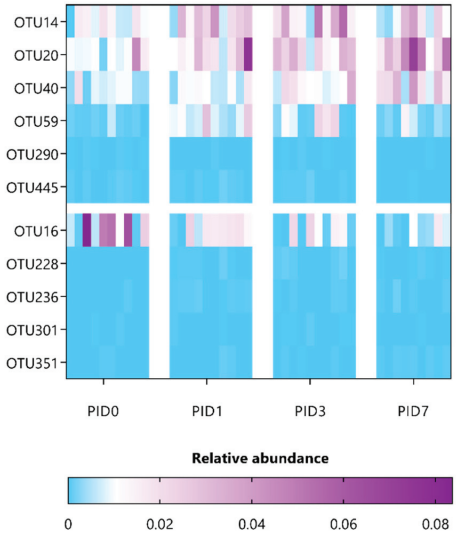


**Figure 11.** Heatmap representing the relative abundance of significant gut microbial dysbiosis markers detected *L. rhamnosus* GG-given mice following sham-irradiation as listed in Table 3, $n$ = 10 per time point. OTU = operational taxonomic unit; PID = post-irradiation day.

## 4. Discussion

Pelvic radiotherapy has commonly been associated with intestinal complications. Previously, we described the pathobiology of ileal mucositis in mice following pelvic irradiation [3]. Briefly, a primary damage response was rapidly initiated with apoptosis and inflammation, as shown by histology and myeloperoxidase activity, respectively. Amplification of these destructing signals impaired the barrier integrity, characterized by loss of tight junctions, which provides the opportunity for luminal bacteria to translocate into mesenteric lymph nodes. Hereafter, secondarily to these structural and functional changes, a dysbiotic microbial community developed, as summarized in Figure 12.

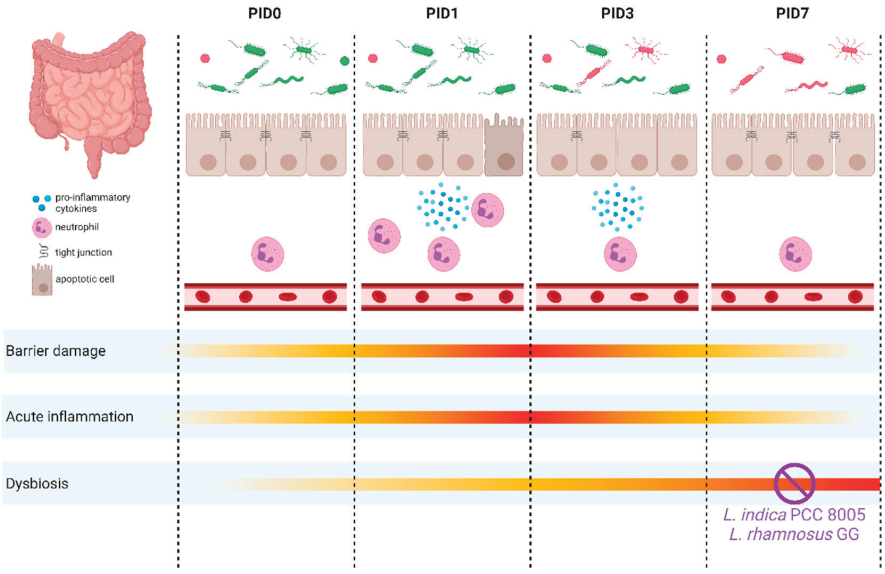


**Figure 12.** Graphical summary of the main results illustrating the impact of pelvic irradiation on the intestinal ecology based on the different parameters monitored in this study. Pelvic irradiation revealed morphological and inflammatory implications. Concurrent 16S microbial profiling showed a delayed impact of pelvic irradiation on the microbiota composition, which was prevented by both *L. indica* PCC 8005 and *L. rhamnosus* GG. This figure was created with BioRender.com and adapted from [3]. PID = post-irradiation day.

Among other—technical and biological—strategies, nutritional interventions including vitamins, prebiotics and probiotics have been explored to reconstitute and/or protect the intestinal ecology following pelvic irradiation, as reviewed earlier [2]. To exert beneficial effects, they are thought to intervene in barrier protection and immunomodulation as well as to interact with the microbial community. Unfortunately, (pre-)clinical evidence for the prevention and/or reduction of irradiation-induced intestinal toxicities has not always been unambiguous. The utmost challenge to be overcome concerns the inter-individual response attributed to the variability in patients' microbial profiles. Herein, the selection of an appropriate personalized therapy might provide a solution. Accordingly, apart from traditional probiotic strains including *L. rhamnosus* GG, alternative food supplements should be explored. Here, the radioprotective efficacy of fresh and unprocessed *L. indica* PCC 8005 biomass was studied in respect to benchmarked *L. rhamnosus* GG.

At first, both supplements were studied for their barrier-protective effects following pelvic irradiation, which was shown to drastically impair the barrier by increasing oxidative stress as well as epithelial cell death and permeability [3,40]. The research group of Stenson et al. showed that administration of *L. rhamnosus* GG steered the migration of mesenchymal stem cells to small intestinal crypts to support epithelial cell proliferation and re-enforce the small intestinal barrier following irradiation [6,7]. In contrast to these reports, *L. rhamnosus GG* appeared unsuccessful in preventing and/or restoring epithelial cells and/or tight junction proteins, likely due to the dramatic effects introduced by total body irradiation [6,7] as compared to acute local pelvic irradiation in our study. Additionally, *Limnospira* sp.-mediated activation of the antioxidant defense system, including glutathione-s-transferase, superoxide dismutase and catalase, is well-described for daily pure phycocyanin (50 mg/kg) supplementation [41,42]. However, significant interference in oxidative stress and subsequent cell death, or loss of epithelial tight junctions induced by pelvic irradiation, could not be observed in our study. This might be explained by the early

degradation of *L. indica* PCC 8005 biomass within the acid environment of the intestinal tract or the lower pigment content of the used biomass, both resulting in a lesser amount of antioxidant phycocyanin reaching the ileum.

Besides barrier protection, food supplements are commonly evaluated based on their immunomodulatory capacities. Our data indicate that *L. rhamnosus* GG appears to only be capable of partly reducing neutrophilic myeloperoxidase activity and IFNγ secretion, while elsewhere *L. rhamnosus* GG was shown to prevent epithelial barrier dysfunction induced by IFNγ in human intestinal enteroids and colonoids [43]. In contrast, *L. indica* PCC 8005 could not be linked with such acute anti-inflammatory effects in our experimental setup. Inconsistent outcomes have been reported for myeloperoxidase amelioration following *Limnospira* spp. supplementation in inflammatory mouse models [16,44].

Finally, with regard to the specific impact of food supplements *L. indica* PCC 8005 and *L. rhamnosus* GG on the host's microbiota, both seem to introduce supplement-specific changes in the microbial community. Here, we could report a temporally increased richness due to *L. rhamnosus* GG supplementation. Paired beta analysis—ruling out the inter-group variability at start—confirmed a delayed, yet significant, shift for saline-administered, irradiated mice, as reported earlier [3], which was impeded by both *L. indica* PCC 8005 and *L. rhamnosus* GG supplements. This indicates that a stable, yet different, microbiota is introduced by both supplementation regimens, which could not be disturbed by acute pelvic irradiation.

Then, unraveling relevant OTUs showed that *Alistipes putredinis* was increased by *L. indica* PCC 8005 supplementation in relative abundance following pelvic irradiation. Interestingly, *Alistipes* spp. were recently reviewed for their high relevance in dysbiosis and intestinal diseases, which can be either beneficial or harmful [45]. After daily supplementation, both *L. indica* PCC 8005 and *L. rhamnosus* GG do not seem to establish themselves in significant numbers in the murine gut. However, *L. rhamnosus* GG has been proven to survive intestinal passage [27,46,47], whereas no such evidence could be found for the highly digestible biomass of *Limnospira* spp. Nevertheless, changes in microbial members were noted for both, highlighting the non-necessity of bacterial supplements to colonize the gut in order to exert beneficial effects, as suggested by other researchers [46,48]. One possible explanation for these effects on the intestinal microbial community might be metabolic cross-feeding [49]. In *L. indica* PCC 8005-supplemented mice, an increased relative abundance of *Akkermansia muciniphila* was detected in some (30%) mice, in accordance with previous research [48,50]. Although the *Akkermansia* genus is widely studied for its promising next-generation probiotic potential, their broad effects on the host beyond their therapeutic niche require careful holistic investigations. For instance, better strain-level identification of human bacteria will help unravel some of this complexity [51]. Interestingly, *Limnospira* spp. are hypothesized to deliver a range of prebiotics including carbohydrates, polyphenols and polyunsaturated fatty acids, which may stimulate growth of beneficial bacteria exerting secondary health benefits such as antioxidative defense [18]. These data might suggest that longer and even combined supplementation of *L. indica* PCC 8005 and *L. rhamnosus* GG might be required to complete this path. To assess the consequences of both supplementation regimens, future research might focus on fecal metabolites to validate the mechanisms of cross-feeding between these taxa.

Despite their promising radiomitigating potential, supplementation of *L. indica* PCC 8005 or *L. rhamnosus* GG fresh biomass could not be associated with barrier protective or significant immunomodulatory effects. Stabilization of the microbial community members and thus prevention of pelvic irradiation-induced dysbiosis was observed for both of the supplementation regimens. The present study concludes that—besides benchmarked *L. rhamnosus* GG—*L. indica* PCC 8005 is an interesting candidate to further investigate how to counteract pelvic irradiation-induced dysbiosis.

**Supplementary Materials:** The following supporting information can be downloaded at: https://www.mdpi.com/article/10.3390/antiox12030572/s1, Figure S1: Boxplots showing the fold changes in mucosal parameter villus length following pelvic (sham-)irradiation for all different experimental

groups; Figure S2: An adequate depth of sequencing was reached to identify most diversity in the samples; Figure S3: Changes in alpha diversity index Shannon; Figure S4: Changes in alpha diversity index Shannon even, considering solely evenness, following (sham-)irradiation; Figure S5: Unweighted UniFrac NMDS plots; Figure S6: Heatmap representing the relative abundance of significant gut microbial dysbiosis markers detected in saline-given mice following sham-irradiation; Figure S7: Heatmap representing the relative abundance of significant gut microbial dysbiosis markers detected in saline-given mice following pelvic irradiation; Table S1: *p* values of conditional unweighted UniFrac beta diversity analyses by AMOVA; Table S2: Differential OTUs detected in saline-given mice following sham-irradiation; Table S3: Differential OTUs detected in saline-given mice following pelvic irradiation.

**Author Contributions:** C.S.: execution and design of experiments, data acquisition and interpretation, manuscript preparation; M.M.: 16s rRNA profiling and interpretation; A.C. and S.W.: execution of experiments; S.B.: supervision, financial support and lab management; N.L. and S.L.: supervision, financial support, microbiota expertise input and lab management; F.M. and M.V.: original concept, design of experiments, data interpretation and manuscript management; all authors: manuscript editing and revision. All authors have read and agreed to the published version of the manuscript.

**Funding:** C.S. was supported by the Belgian Nuclear Research Centre, SCK CEN, through a PhD Grant, in collaboration with the University of Antwerp.

**Institutional Review Board Statement:** The animal study protocol was approved by the Ethical Committee Animal Studies of Medanex Clinic (EC MxCl 2018-093) and by the SCK CEN animal welfare committee.

**Informed Consent Statement:** Not applicable.

**Data Availability Statement:** The data presented in this study are available on request from the corresponding author.

**Acknowledgments:** We are grateful to the members of the Interdisciplinary Biosciences group of SCK CEN, particularly M. Neefs, L. Daenen, B. Proesmans, J. Buset, R. Vermeesen, A. Janssen and L. Leysen, for their technical support.

**Conflicts of Interest:** The authors declare no conflict of interest.

## References

1. Hauer-Jensen, M.; Denham, J.W.; Andreyev, H.J.N. Radiation Enteropathy–Pathogenesis, Treatment and Prevention. *Nat. Rev. Gastroenterol. Hepatol.* **2014**, *11*, 470–479. [CrossRef] [PubMed]
2. Segers, C.; Verslegers, M.; Baatout, S.; Leys, N.; Lebeer, S.; Mastroleo, F. Food Supplements to Mitigate Detrimental Effects of Pelvic Radiotherapy. *Microorganisms* **2019**, *7*, 97. [CrossRef] [PubMed]
3. Segers, C.; Mysara, M.; Claesen, J.; Baatout, S.; Leys, N.; Lebeer, S.; Verslegers, M.; Mastroleo, F. Intestinal Mucositis Precedes Dysbiosis in a Mouse Model for Pelvic Irradiation. *ISME Commun.* **2021**, *1*, 1–10. [CrossRef] [PubMed]
4. Berg, G.; Rybakova, D.; Fischer, D.; Cernava, T.; Vergès, M.C.; Charles, T.; Chen, X.; Cocolin, L.; Eversole, K.; Corral, G.H.; et al. Microbiome Definition Re-Visited: Old Concepts and New Challenges. *Microbiome* **2020**, *8*, 1–22.
5. Gerassy-Vainberg, S.; Blatt, A.; Danin-Poleg, Y.; Gershovich, K.; Sabo, E.; Nevelsky, A.; Daniel, S.; Dahan, A.; Ziv, O.; Dheer, R.; et al. Radiation Induces Proinflammatory Dysbiosis: Transmission of Inflammatory Susceptibility by Host Cytokine Induction. *Gut* **2018**, *67*, 97–107. [CrossRef]
6. Ciorba, M.A.; Riehl, T.E.; Rao, M.S.; Moon, C.; Ee, X.; Nava, G.M.; Walker, M.R.; Marinshaw, J.M.; Stappenbeck, T.S.; Stenson, W.F. Lactobacillus Probiotic Protects Intestinal Epithelium from Radiation Injury in a TLR-2/Cyclo-Oxygenase-2-Dependent Manner. *Gut* **2012**, *61*, 829–838. [CrossRef]
7. Riehl, T.E.; Alvarado, D.; Ee, X.; Zuckerman, A.; Foster, L.; Kapoor, V.; Thotala, D.; Ciorba, M.A.; Stenson, W.F. *Lactobacillus Rhamnosus* GG Protects the Intestinal Epithelium from Radiation Injury through Release of Lipoteichoic Acid, Macrophage Activation and the Migration of Mesenchymal Stem Cells. *Gut* **2019**, *68*, 1003–1013. [CrossRef]
8. Baù, M.; Moretti, A.; Bertoni, E.; Vazzoler, V.; Luini, C.; Agosti, M.; Salvatore, S. Risk and Protective Factors for Gastrointestinal Symptoms Associated with Antibiotic Treatment in Children: A Population Study. *Pediatr. Gastroenterol. Hepatol. Nutr.* **2020**, *23*, 35–48. [CrossRef]
9. Esposito, C.; Roberti, A.; Turrà, F.; Cerulo, M.; Severino, G.; Settimi, A.; Escolino, M. Frequency of Antibiotic-Associated Diarrhea and Related Complications in Pediatric Patients Who Underwent Hypospadias Repair: A Comparative Study Using Probiotics vs Placebo. *Probiotics Antimicrob. Proteins* **2018**, *10*, 323–328. [CrossRef]

10. Gamallat, Y.; Meyiah, A.; Kuugbee, E.D.; Hago, A.M.; Chiwala, G.; Awadasseid, A.; Bamba, D.; Zhang, X.; Shang, X.; Luo, F.; et al. *Lactobacillus Rhamnosus* Induced Epithelial Cell Apoptosis, Ameliorates Inflammation and Prevents Colon Cancer Development in an Animal Model. *Biomed. Pharmacother.* **2016**, *83*, 536–541. [CrossRef]
11. Escamilla, J.; Lane, M.A.; Maitin, V. Cell-Free Supernatants from Probiotic Lactobacillus Casei and Lactobacillus Rhamnosus GG Decrease Colon Cancer Cell Invasion in Vitro. *Nutr. Cancer* **2012**, *64*, 871–878. [CrossRef]
12. Yoda, K.; Miyazawa, K.; Hosoda, M.; Hiramatsu, M.; Yan, F.; He, F. *Lactobacillus* GG-Fermented Milk Prevents DSS-Induced Colitis and Regulates Intestinal Epithelial Homeostasis through Activation of Epidermal Growth Factor Receptor. *Eur. J. Nutr.* **2014**, *53*, 105–115. [CrossRef]
13. Claes, I.J.J.; Lebeer, S.; Shen, C.; Verhoeven, T.L.A.; Dilissen, E.; De Hertogh, G.; Bullens, D.M.A.; Ceuppens, J.L.; Van Assche, G.; Vermeire, S.; et al. Impact of Lipoteichoic Acid Modification on the Performance of the Probiotic *Lactobacillus Rhamnosus* GG in Experimental Colitis. *Clin. Exp. Immunol.* **2010**, *162*, 306–314. [CrossRef] [PubMed]
14. Segers, C.; Mysara, M.; Coolkens, A.; Baatout, S.; Leys, N.; Lebeer, S.; Verslegers, M.; Mastroleo, F. Limnospira Indica PCC 8005 or Lacticaseibacillus Rhamnosus GG Dietary Supplementation Modulate the Gut Microbiome in Mice. *Appl. Microbiol.* **2022**, *2*, 636–650. [CrossRef]
15. Abdel-Daim, M.M.; Farouk, S.M.; Madkour, F.F.; Azab, S.S. Anti-Inflammatory and Immunomodulatory Effects of *Spirulina Platensis* in Comparison to *Dunaliella Salina* in Acetic Acid-Induced Rat Experimental Colitis. *Immunopharmacol. Immunotoxicol.* **2015**, *37*, 126–139. [CrossRef] [PubMed]
16. Morsy, M.A.; Gupta, S.; Nair, A.B.; Venugopala, K.N.; Greish, K.; El-Daly, M. Protective Effect of *Spirulina Platensis* Extract against Dextran-Sulfate-Sodium-Induced Ulcerative Colitis in Rats. *Nutrients* **2019**, *11*, 2309. [CrossRef] [PubMed]
17. Yu, T.; Wang, Y.; Chen, X.; Xiong, W.; Tang, Y.; Lin, L. *Spirulina Platensis* Alleviates Chronic Inflammation with Modulation of Gut Microbiota and Intestinal Permeability in Rats Fed a High-Fat Diet. *J. Cell. Mol. Med.* **2020**, *24*, 8603–8613. [CrossRef] [PubMed]
18. Hu, J.; Li, Y.; Pakpour, S.; Wang, S.; Pan, Z.; Liu, J.; Wei, Q.; She, J.; Cang, H.; Zhang, R.X. Dose Effects of Orally Administered Spirulina Suspension on Colonic Microbiota in Healthy Mice. *Front. Cell. Infect. Microbiol.* **2019**, *9*, 1–13. [CrossRef]
19. Najdenski, H.M.; Gigova, L.G.; Iliev, I.I.; Pilarski, P.S.; Lukavský, J.; Tsvetkova, I.V.; Ninova, M.S.; Kussovski, V.K. Antibacterial and Antifungal Activities of Selected Microalgae and Cyanobacteria. *Int. J. Food Sci. Technol.* **2013**, *48*, 1533–1540. [CrossRef]
20. Alwaleed, E.A.; El-Sheekh, M.; Abdel-Daim, M.M.; Saber, H. Effects of *Spirulina Platensis* and *Amphora Coffeaeformis* as Dietary Supplements on Blood Biochemical Parameters, Intestinal Microbial Population, and Productive Performance in Broiler Chickens. *Environ. Sci. Pollut. Res.* **2020**, *28*, 1801–1811. [CrossRef]
21. Aziz, M.M.; Eid, N.I.; Nada, A.S.; Amin, N.E.D.; Ain-Shoka, A.A. Possible Protective Effect of the Algae Spirulina against Nephrotoxicity Induced by Cyclosporine A and/or Gamma Radiation in Rats. *Environ. Sci. Pollut. Res.* **2018**, *25*, 9060–9070. [CrossRef]
22. Qishen, P.; Guo, B.J.; Kolman, A. Radioprotective Effect of Extract from *Spirulina Platensis* in Mouse Bone Marrow Cells Studied by Using the Micronucleus Test. *Toxicol. Lett.* **1989**, *48*, 165–169. [CrossRef] [PubMed]
23. Li, W.; Lu, L.; Liu, B.; Qin, S. Effects of Phycocyanin on Pulmonary and Gut Microbiota in a Radiation-Induced Pulmonary Fibrosis Model. *Biomed. Pharmacother.* **2020**, *132*, 110826. [CrossRef]
24. Williams, J.P.; Brown, S.L.; Georges, G.E.; Hauer-Jensen, M.; Hill, R.P.; Huser, A.K.; Kirsch, D.G.; Macvittie, T.J.; Mason, K.A.; Medhora, M.M.; et al. Animal Models for Medical Countermeasures to Radiation Exposure. *Radiat. Res.* **2010**, *173*, 557–578. [CrossRef] [PubMed]
25. Cogne, G.; Lehmann, B.; Dussap, C.-G.; Gros, J.-B. Uptake of Macrominerals and Trace Elements by the Cyanobacterium *Spirulina Platensis* (*Arthrospira Platensis* PCC 8005) under Photoautotrophic Conditions: Culture Medium Optimization. *Biotechnol. Bioeng.* **2003**, *81*, 588–593. [CrossRef] [PubMed]
26. Doron, S.; Snydman, D.R.; Gorbach, S.L. *Lactobacillus* GG: Bacteriology and Clinical Applications. *Gastroenterol. Clin. North Am.* **2005**, *34*, 483–498. [CrossRef]
27. Gorbach, S.L. The Discovery of *Lactobacillus* GG. *Nutr. Today* **1996**, *31*, 2S–4S. [CrossRef]
28. de Man, J.C.; Rogosa, M.; Sharpe, M.E. A Medium for the Cultivation of Lactobacilli. *J. Appl. Bacteriol.* **1960**, *23*, 130–135. [CrossRef]
29. Gamallat, Y.; Ren, X.; Walana, W.; Meyiah, A.; Xinxiu, R.; Zhu, Y.; Li, M.; Song, S.; Xie, L.; Jamalat, Y.; et al. Probiotic *Lactobacillus Rhamnosus* Modulates the Gut Microbiome Composition Attenuates Preneoplastic Colorectal Aberrant Crypt Foci. *J. Funct. Foods* **2019**, *53*, 146–156. [CrossRef]
30. Ki, Y.; Kim, W.; Cho, H.; Ahn, K.; Choi, Y.; Kim, D. The Effect of Probiotics for Preventing Radiation-Induced Morphological Changes in Intestinal Mucosa of Rats. *J. Korean Med. Sci.* **2014**, *29*, 1372–1378. [CrossRef]
31. Li, X.; Hu, D.; Tian, Y.; Song, Y.; Hou, Y.; Sun, L.; Zhang, Y.; Man, C.; Zhang, W.; Jiang, Y. Protective Effects of a Novel *Lactobacillus Rhamnosus* Strain with Probiotic Characteristics against Lipopolysaccharide-Induced Intestinal Inflammation in Vitro and in Vivo. *Food Funct.* **2020**, *11*, 5799–5814. [CrossRef]
32. Mittal, A.; Suresh Kumar, P.V.; Banerjee, S.; Rao, A.R.; Kumar, A. Modulatory Potential of *Spirulina Fusiformis* on Carcinogen Metabolizing Enzymes in Swiss Albino Mice. *Phyther. Res.* **1999**, *13*, 111–114. [CrossRef]
33. Chamorro-Cevallos, G.; Garduño-Siciliano, L.; Barrón, B.L.; Madrigal-Bujaidar, E.; Cruz-Vega, D.E.; Pages, N. Chemoprotective Effect of Spirulina (*Arthrospira*) against Cyclophosphamide-Induced Mutagenicity in Mice. *Food Chem. Toxicol.* **2008**, *46*, 567–574. [CrossRef]

34. El Bialy, B.E.; El-Boraey, N.G.; Hamouda, R.A.; Abdel-Daim, M.M. Comparative Protective Effects of Spirulina and Spirulina Supplemented with Thiamine against Sub-Acute Carbon Tetrachloride Toxicity in Rats. *Biomed. Pharmacol. J.* **2019**, *12*, 511–525. [CrossRef]
35. Sharma, M.K.; Sharma, A.; Kumar, A.; Kumar, M. *Spirulina Fusiformis* Provides Protection against Mercuric Chloride Induced Oxidative Stress in Swiss Albino Mice. *Food Chem. Toxicol.* **2007**, *45*, 2412–2419. [CrossRef]
36. Gutiérrez-Rebolledo, G.A.; Galar-Martínez, M.; García-Rodríguez, R.V.; Chamorro-Cevallos, G.A.; Hernández-Reyes, A.G.; Martínez-Galero, E. Antioxidant Effect of *Spirulina* (*Arthrospira*) *Maxima* on Chronic Inflammation Induced by Freund's Complete Adjuvant in Rats. *J. Med. Food* **2015**, *18*, 865–871. [CrossRef]
37. Hornung, B.V.H.; Zwittink, R.D.; Kuijper, E.J. Issues and Current Standards of Controls in Microbiome Research. *FEMS Microbiol. Ecol.* **2019**, *95*, 1–7. [CrossRef]
38. Chao, A.; Jost, L. Coverage-Based Rarefaction and Extrapolation: Standardizing Samples by Completeness Rather than Size. *Ecology* **2012**, *93*, 2533–2547. [CrossRef]
39. Edgar, R.C. UPARSE: Highly Accurate OTU Sequences from Microbial Amplicon Reads. *Nat. Methods* **2013**, *10*, 996–998. [CrossRef]
40. Banerjee, S.; Fu, Q.; Shah, S.K.; Melnyk, S.B.; Sterneck, E.; Hauer-Jensen, M.; Pawar, S.A. C/EBPδ Protects from Radiation-Induced Intestinal Injury and Sepsis by Suppression of Inflammatory and Nitrosative Stress. *Sci. Rep.* **2019**, *9*, 1–12. [CrossRef]
41. Hassaan, M.S.; Mohammady, E.Y.; Soaudy, M.R.; Sabae, S.A.; Mahmoud, A.M.A.; El-Haroun, E.R. Comparative Study on the Effect of Dietary β-Carotene and Phycocyanin Extracted from Spirulina Platensis on Immune-Oxidative Stress Biomarkers, Genes Expression and Intestinal Enzymes, Serum Biochemical in Nile Tilapia, Oreochromis Niloticus. *Fish Shellfish Immunol.* **2021**, *108*, 63–72. [CrossRef] [PubMed]
42. Lu, L.; Li, W.; Sun, C.; Kang, S.; Qin, S. Phycocyanin Ameliorates Radiation-Induced Acute Intestinal Toxicity by Regulating the Effect of the Gut Microbiota on the TLR4 / Myd88/NF- κ B Pathway. *J. Parenter. Enter. Nutr.* **2019**, *44*, 1308–1317. [CrossRef]
43. Han, X.; Lee, A.; Huang, S.; Gao, J.; Spence, J.R.; Owyang, C. Lactobacillus Rhamnosus GG Prevents Epithelial Barrier Dysfunction Induced by Interferon-Gamma and Fecal Supernatants from Irritable Bowel Syndrome Patients in Human Intestinal Enteroids and Colonoids. *Gut Microbes* **2019**, *10*, 59–76. [CrossRef]
44. de Oliveira Garcia, F.A.; Sales-Campos, H.; Yuen, V.G.; Machado, J.R.; de Barros Viana, G.S.; Oliveira, C.J.F.; McNeill, J.H. Arthrospira (Spirulina) Platensis Attenuates Dextran Sulfate Sodium-Induced Colitis in Mice by Suppressing Key Pro-Inflammatory Cytokines. *Korean J. Gastroenterol.* **2020**, *76*, 150–158. [CrossRef]
45. Parker, B.J.; Wearsch, P.A.; Veloo, A.C.M.; Rodriguez-Palacios, A. The Genus Alistipes: Gut Bacteria With Emerging Implications to Inflammation, Cancer, and Mental Health. *Front. Immunol.* **2020**, *11*, 1–15. [CrossRef]
46. Lebeer, S.; Claes, I.J.J.; Verhoeven, T.L.A.; Shen, C.; Lambrichts, I.; Ceuppens, J.L.; Vanderleyden, J.; De Keersmaecker, S.C.J. Impact of LuxS and Suppressor Mutations on the Gastrointestinal Transit of *Lactobacillus Rhamnosus* GG. *Appl. Environ. Microbiol.* **2008**, *74*, 4711–4718. [CrossRef]
47. Alander, M.; Satokari, R.; Korpela, R.; Saxelin, M.; Vilpponen-Salmela, T.; Mattila-Sandholm, T.; Von Wright, A. Persistence of Colonization of Human Colonic Mucosa by a Probiotic Strain, Lactobacillus Rhamnosus GG, after Oral Consumption. *VTT Publ.* **2001**, *65*, 79–82. [CrossRef]
48. Chandrarathna, H.P.S.U.; Liyanage, T.D.; Edirisinghe, S.L.; Dananjaya, S.H.S. Marine Microaglae, Spirulina Maxima-Derived Modified Pectin and Modified Pectin Nanoparticles Modulate the Gut Microbiota and Trigger Immune Responses in Mice. *Mar. Drugs* **2020**, *18*, 175. [CrossRef]
49. Lebeer, S.; Vanderleyden, J.; De Keersmaecker, S.C.J. Genes and Molecules of Lactobacilli Supporting Probiotic Action. *Microbiol. Mol. Biol. Rev.* **2008**, *72*, 728–764. [CrossRef]
50. Ma, H.; Xiong, H.; Zhu, X.; Ji, C.; Xue, J.; Li, R.; Ge, B.; Cui, H. Polysaccharide from Spirulina Platensis Ameliorates Diphenoxylate-Induced Constipation Symptoms in Mice. *Int. J. Biol. Macromol.* **2019**, *133*, 1090–1101. [CrossRef]
51. Cirstea, M.; Radisavljevic, N.; Finlay, B.B. Good Bug, Bad Bug: Breaking through Microbial Stereotypes. *Cell Host Microbe* **2018**, *23*, 10–13. [CrossRef] [PubMed]

*antioxidants*

MDPI

*Article*

# A Study on the Planarian Model Confirms the Antioxidant Properties of Tameron against X-ray- and Menadione-Induced Oxidative Stress

**Elena Tsarkova [1,2], Kristina Filippova [1,2], Vera Afanasyeva [1,2], Olga Ermakova [1,2], Anastasia Kolotova [1], Artem Blagodatski [1] and Artem Ermakov [1,2,*]**

[1] Institute of Theoretical and Experimental Biophysics of the Russian Academy of Sciences, 142290 Pushchino, Moscow Region, Russia
[2] ANO Engineering Physics Institute, Bolshoi Udarny Pereulok, 142210 Serpukhov, Moscow Region, Russia
* Correspondence: ao_ermakovy@rambler.ru

**Abstract:** Ionizing radiation and radiation-related oxidative stress are two important factors responsible for the death of actively proliferating cells, thus drastically reducing the regeneration capacity of living organisms. Planarian flatworms are freshwater invertebrates that are rich in stem cells called neoblasts and, therefore, present a well-established model for studies on regeneration and the testing of novel antioxidant and radioprotective substances. In this work, we tested an antiviral and antioxidant drug Tameron (Monosodium α-Luminol or 5-amino-2,3-dihydro-1,4-phthalazinedione sodium salt) for its ability to reduce the harm of X-ray- and chemically induced oxidative stress on a planarian model. Our study has revealed the ability of Tameron to effectively protect planarians from oxidative stress while enhancing their regenerative capacity by modulating the expression of neoblast marker genes and NRF-2-controlled oxidative stress response genes.

**Keywords:** planarians; Tameron; antioxidant; regeneration; radioprotection

**Citation:** Tsarkova, E.; Filippova, K.; Afanasyeva, V.; Ermakova, O.; Kolotova, A.; Blagodatski, A.; Ermakov, A. A Study on the Planarian Model Confirms the Antioxidant Properties of Tameron against X-ray- and Menadione-Induced Oxidative Stress. *Antioxidants* **2023**, *12*, 953. https://doi.org/10.3390/antiox12040953

Academic Editors: Elena Obrador Pla and Alegria Montoro

Received: 13 March 2023
Revised: 5 April 2023
Accepted: 14 April 2023
Published: 18 April 2023



## 1. Introduction

Antioxidants are compounds that reduce damage to molecules, organs, tissues, and the cells of a living organism caused by exposure to reactive oxygen species (ROS). Their effects are mostly based on boosting natural antioxidant cell defenses and ROS inactivation [1]. Antioxidants are highly important components of various therapeutic agents for oxidative stress is a common cause of many chronic and aging-related diseases [2]. A large number of antioxidants are also known as radioprotective substances, which can reduce the negative effects of ionizing radiation by neutralizing ROS that emerge as a result of X-ray interaction with water and biological molecules [3]. It is an established fact that the main damaging effect of ionizing radiation on living organisms is caused by the formation of different forms of free radicals [4]. On account of the presence of unpaired electrons, ROS possess a high level of redox activity, which causes oxidative damage in biological molecules such as nucleic acids, proteins, and membrane lipids [5].

The search for novel antioxidant and radioprotective substances for medical purposes is a task of high importance, despite the progress that has already been made. Radioprotectors are highly desired agents for radiation therapy [6–9]. Antioxidants may find their use in future therapies for aging and aging-related conditions, such as inflammaging, one of the crucial hallmarks of aging [10]. Amongst the different drug development strategies, repositioning existing drugs against new diseases is a promising approach as they have already passed preclinical and clinical tests and are well studied in terms of safety and side effects [11].

Tameron (Monosodium α-Luminol or 5-amino-2,3-dihydro-1,4-phthalazinedione sodium salt) is a novel generic drug also known as Galavit (GVT) or MP1032. This compound has

already found its use as an antiviral and immunomodulatory agent utilized for the treatment of various conditions. It was applied as a neuroprotector against Gulf War disease, improving cognition, mood, and neurogenesis and alleviating neuro- and systemic inflammation [12]. It was also used against different viral infections, such as T cell-tropic, cytopathic retrovirus ts1 infection on a mouse model, protecting thymic epithelial cell cytoarchitecture and allowing thymocyte survival [13,14]. Its action mechanism involved the stabilization of the Nrf2 transcription factor, a known anti-inflammatory and antioxidant protein [15]. It was also tested on a mouse model and human peripheral blood mononuclear cells as an immunomodulatory agent for preventing cytokine storm, a devastating condition of the COVID-19 disease [16].

Given the effective results that were achieved by Tameron as an antiviral, immunomodulatory, and anti-inflammatory agent with an antioxidant mechanism of action, we decided to further explore its role as a potential antioxidant and radioprotective agent. For our tests, we have chosen planarians as a model.

Planarians are model animals with an extremely high regeneration ability because their bodies are extremely rich in neoblast stem cells (up to 30%) [17]. Neoblasts are totipotent stem cells that are capable of differentiating into all types of cells of the adult animal, including germline cells [18]. These cells give the planarian body an almost unlimited regenerative potential allowing it to replace missing body parts or even regenerate a whole worm from a small body fragment [19]. These features make planarians an excellent object for studies of regenerative processes, stem cell proliferation, testing of pharmacological substances, and aging in vivo [20]. In particular, the *Schmidtea mediterranea* planarian has many advantages over vertebrate models: the animals are cheap and easy to handle, their asexual strain is immortal and fast-reproducing, their genome is sequenced, and they are available in large amounts.

Planarian neoblasts, like any fast-proliferating cells, are extremely sensitive to ionizing radiation [21]. Doses of more than 15 Gy lead to complete neoblast death and termination of regenerative processes [22], which is followed by typical abdominal curling of the animals and further dying within several weeks after irradiation [23]. Smaller radiation doses kill only some parts of neoblasts, while the remaining parts are able to restore the stem cell population, providing the ability for normal regeneration [24]. Irradiation of planarians with sublethal X-ray doses, preserving a part of neoblasts with a potential for further regeneration, is the basis of our experimental model. The effect of potential radioprotectors can be easily quantified by measuring the regeneration rate of the blastema, the amount of surviving neoblasts, and the expression of neoblast marker genes as well as the activity of ROS generation in the planarian body. The same principles are applicable not only to ionizing radiation studies but also to studies of chemically induced oxidative stress. Our model has been previously proven to be robust and effective for testing new radioprotectors and antioxidants in the example of a classical antioxidant, N-acetylcysteine [25]. In the present work, we have tested the antioxidant, radioprotective, and pro-regenerative properties of Tameron on models of X-ray- and chemically induced oxidative stress in the *Schmidtea mediterranea* planarian.

## 2. Materials and Methods

### *2.1. Animals*

An asexual strain of *Schmidtea mediterranea* flatworm (*Turbellaria, Platyhelminthes*) was cultured at room temperature, in darkened glass bowls containing a mixture of distilled and tap $H_2O$ at 1:2 vol. Animals were nourished twice a week with mosquitoes larvae (*Chironomidae*). Before the trials, planarians were starved for one week to exclude the possible interference of food components with the effects of X-ray treatment [26]. Then, animals with similar body lengths (about 8 mm) were chosen for the experiment. The planarians were decapitated, with the removal of circa 1/5 of the total body length containing the cephalic ganglion using a Carl Zeiss Stemi 2000 dissecting microscope with a thin eye scalpel. Before decapitation, the planarians were immobilized by placing them on a cooling

table for 3–4 min. The number of animals included in each experimental group was the same (35 animals).

### *2.2. Computer-Assisted Morphometry In Vivo*

The blastema regeneration rate was quantified using computer morphometry [27]. Seventy-two hours after decapitation, the planarians were photographed using a Carl Zeiss Stemi 2000 microscope equipped with a Carl Zeiss AxioCam camera (Figure S1). To calculate the blastema regeneration speed, the regeneration index $R = s/S$ was used, where $s$ is the blastema area and $S$—total body area. $S$ and $s$ values were determined using the Plana 4.0 software (author's development). Thirty-five animals were used in each experimental or control group. The results demonstrated here are the mean values of three independent trials.

### *2.3. Whole-Mount Immunocytochemical Study of Planarian Stem Cell Mitotic Activity*

Animals with a body length of about 4 mm were chosen for this study. The number of mitotic cells was calculated a week after decapitation. Animals were treated with a 7% solution of N-acetylcysteine for 5 min and fixed in 4% formaldehyde and 0.3% Triton X100 in PBS for 20 min. Staining for mitotic cells was conducted according to Newmark and Alvarado [28]. Briefly, we labeled a mitotic cell marker—phosphorylated histone H3—with a primary antibody (Santa Cruz, Dallas, TX, USA) at 1/1000 dilution and a CF488A-conjugated secondary antibody (Biotium, Fremont, CA, USA) in 1/1000 dilution. After washing them in PBS three times, the whole-mount specimens were placed in Vectashield Antifade Mounting Medium (Vector Labs, Burlingame, CA, USA) and analyzed using a Leica TCS SP5 confocal laser scanning microscope. The mitotic cell number and the mitotic index (amount of mitotic cells per 1 $mm^2$ of planarian body) were then measured and calculated as described before [29,30]. The specificity of immunocytochemical staining was approved using a non-immune serum.

### *2.4. Experimental Testing Substances*

Menadione (Sigma, Saint Louis, MO, USA) was diluted in DMSO to a stock concentration of $10^{-3}$ M and then diluted further to a working concentration of $10^{-6}$ M. The stock solution of Tameron (5-amino-2,3-dihydro-1,4-phthalazinedione sodium salt, ANO Engineering Physics Institute, Serpukhov, Russia) (Figure S2) was prepared by diluting it in milliQ water to $10^{-2}$ M, further diluting it to $10^{-4}$–$10^{-5}$ M working concentrations.

### *2.5. Planarian X-ray Irradiation*

The animals were irradiated using an X-ray device, RUT-12 (15 mA, 200 kV). For treatment, worms were placed into Petri dishes on filter paper moistened with water. In studies involving Tameron as an antioxidant or radioprotective agent, it was added 12 h before irradiation. The radiation doses were 10 and 15 Gy at a power of 2 Gy per min.

### *2.6. RT-PCR for Gene Expression Analysis*

The state of the neoblast population was characterized by the expression of 13 neoblast marker genes (Supplementary Table S1) [31,32] and 23 oxidative stress response genes controlled by the NRF2 transcription factor (Supplementary Table S2) [33]. mRNA was isolated from five planarians with a magnetic beads isolation kit (Sileks, Moscow, Russia). The concentration of isolated mRNA was measured with Qubit RNA High Sensitivity (HS) Assay Kits (Thermo, Carlsbad, CA, USA) on the Qubit 4 device (Thermo, Carlsbad, CA, USA) and diluted to 10 ng/reaction for the reverse transcription reaction. Reverse transcription was carried out with a Sileks (Moscow, Russia) kit, using oligo dT primer. The outcoming cDNA served as a template for real-time PCR. The reaction was performed using a reaction mixture with SybrGreen (Evrogen, Moscow, Russia), on a QuantStudio 5 thermocycler (Thermo FS, Waltham, MA, USA). The level of gene transcription was normalized by two housekeeping genes Smed-ef1 (GenBank accession number AY067688)

and Smed_01699 (GenBank accession number JX010505). A sample without the stage of reverse transcription served as a control for genomic DNA contamination and was amplified with genome-specific primers. Gene-specific primers were selected using the Primer Express program (Applied Biosystems, Waltham, MA, USA). The expression data were analyzed using the online service http://www.qiagen.com (accessed on 25 September 2022), the mayday-2.14 program (Center for Bioinformatics, Tübingen, Germany), and the Genesis program [34]. Only those results, of which changes in the gene expression level were observed at $p < 0.05$, were taken into account.

### *2.7. Cellular Antioxidant Activity (CAA) Assay in Planarians*

ROS activity in the animal body after irradiation was identified using H2DCFDA (2,7-dichloro-dihydrofluorescein-diacetate-acetyl) or CellROX® Green Reagent. This dye is a well-known fluorescent intracellular sensor of reactive oxygen species [35]. Planarians were put in a solution of 10 μM H2DCFDA (Biotium, Fremont, CA, USA) and incubated for 1 h in darkness. Next, the animals were treated with Tameron, washed twice with water, and irradiated using an X-ray device or incubated in menadione solution. The positive control group was obtained by pre-incubation of animals for 30 min in 100 μM $H_2O_2$ (Sigma, Saint Louis, MO, USA) or CellROX® Green Reagent (C10444, Thermo, Carlsbad, CA, USA). Then, the planarians were anesthetized for 5–10 min in a 0.1% solution of chloretone (Sigma, Saint Louis, MO, USA) [36] and photographed with an Axio Scope A1 fluorescence microscope (Carl Zeiss, Jena, Germany) (Ex/Em = 492–495/517–527 nm). In the images obtained using the ImageJ program (National Institute of Health, Bethesda, MD, USA), the total fluorescence intensity of the animal body was evaluated. The measurement results were averaged over 15 animals.

### *2.8. Tameron-Mediated H2DCFDA Oxidation In Vitro*

To study the possible catalysis of H2DCFDA-$H_2O_2$ oxidation by Tameron, we performed an in vitro study. Stock solution of H2DCFDA (2.5 mM) was prepared in DMSO. Tameron stock solution was prepared as described before. Stock solutions were further diluted in TE buffer (pH = 7.5). Experiment was performed on 5 groups of samples: 25 μM H2DCFDA, 25 μM H2DCFDA + 1 mM $H_2O_2$, 25 μM H2DCFDA + 1 mM $H_2O_2$ + $10^{-3}$ M Tameron, 25 μM H2DCFDA + 1 mM $H_2O_2$ + $10^{-4}$ M Tameron, and 25 μM H2DCFDA + 1 mM $H_2O_2$ + $10^{-5}$ M Tameron. The solutions were incubated for 30 min in the dark; then, fluorescence was measured with Qubit4 (Thermo FS, Waltham, MA, USA) fluorimeter in the channel Ex 430–495 nm, Em 510–580 nm. Every measurement was performed in 3 repeats.

### *2.9. Statistical Data Analysis*

The data obtained were treated statistically by the Sigma-Plot 9.11 program (Systat Software Inc., Erkrath, Germany) using one-way ANOVA analyses of variance.

### *2.10. Ethical Standards*

All procedures performed in this study involving animals were performed in accordance with the ethical standards of the institution at which the studies were conducted.

## 3. Results

### *3.1. Tameron Acts as Radioprotector, Boosting the Planarian Regeneration*

Tameron has shown pro-regenerative properties in the model of regenerating planarian blastema. On the third and fourth days after decapitation, it enhanced the regeneration rate by a statistically significant difference compared to control animals. After irradiation with doses of 10 and 15 Gy, the regeneration capacity of planarians was reduced by 34.9% to 52.1% of normal value ($p < 0.001$), respectively, on the third day after irradiation, and by 34.8% и 49.8% ($p < 0.001$) on the fourth day. Tameron ($10^{-4}$ M) was able to significantly increase the regeneration speed on the third day of regeneration by 25.2% for the 10 Gy dose,

and by 56.6% for the 15 Gy dose ($p < 0.001$) (Figure 1). On the fourth day, after 10 and 15 Gy doses, the blastema area of Tameron-treated animals was 14% and 40.8% bigger, respectively, than the untreated control ($p < 0.001$). Tameron itself enhanced the blastema growth on the third and fourth days by 15.9% and 12%, respectively, in non-irradiated animals.

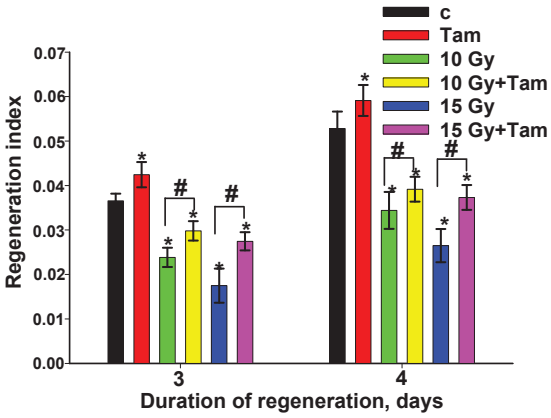


**Figure 1.** Radioprotective effects of Tameron on regenerating planarians in non-irradiated animals and after X-ray irradiation with 10 and 15 Gy. c—non-irradiated control, Tam—Tameron ($10^{-4}$ M). * $p < 0.001$ (difference from control), # $p < 0.001$ (difference from irradiated group without Tameron treatment). Data are presented as mean ± SD.

### *3.2. Tameron Increases the Survival of Mitotic-Active Planarian Neoblasts after X-ray Irradiation*

It is known that planarian regeneration depends on neoblasts, which are capable of proliferating and differentiating into all types of planarian cells [18]. Being completely eliminated at doses higher than 30 Gy, they retain some viability and mitotic activity at sublethal doses of 10–15 Gy, which we have used in our work [25]. We could observe that sublethal X-ray doses drastically reduce the mitotic index (number of mitotic cells per 1 $mm^2$) in planarians, but the presence of Tameron in a concentration of $10^{-4}$ M saves the phenotype, retaining 3 to 5 times more neoblasts on the first day after irradiation. On the third day, the results are less distinguishable, although we can still see a significant increase in the mitotic index after Tameron treatment at 15 Gy. The most pronounced effect could be observed at 15 Gy after 7 days, where the mitotic index of untreated planarians was close to zero, while in the Tameron-treated group, it was restored to 65.9% of the non-irradiated control group (Figures 2 and S3).

### *3.3. Tameron Saves the Expression of Neoblast Marker Genes after Sublethal Doses of X-ray Irradiation*

To monitor the influence of Tameron on planarian regeneration activity more precisely, we have measured the expression of a panel of neoblast marker genes [32] by means of RT-qPCR. On the first day after irradiation, we could observe a clear downregulation of most neoblast markers (Figure 3). Treatment with Tameron, on the contrary, significantly upregulates all of the observed genes. The presence of Tameron partially ameliorates the effect of irradiation. On the first day, it boosts the expression level of part of the marker genes at 10 Gy while reducing the downregulation of the rest. At 15 Gy, the downregulation of all the genes is less pronounced after Tameron treatment. On the tenth day, the expression of most markers is still reduced at 10, and especially at 15 Gy; in the presence of Tameron, the expression of markers remains reduced at 10 Gy, but it is restored to control levels or even slightly higher at 15 Gy. In general, we can observe a protective effect of Tameron on the neoblast pool and stem cell proliferation, especially after higher doses of radiation.

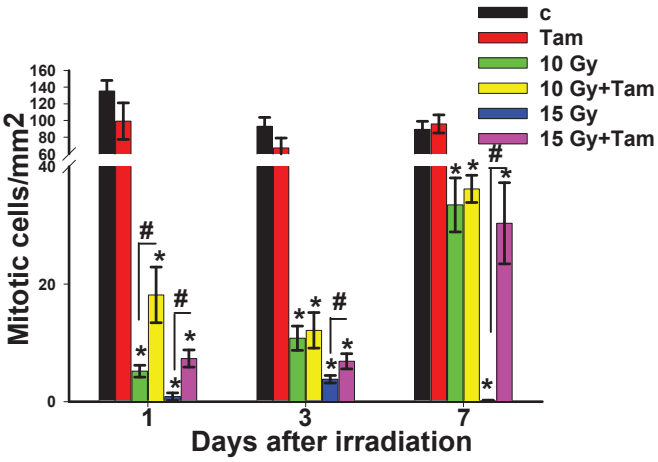


**Figure 2.** Tameron protects proliferating planarian neoblasts from elimination after X-ray irradiation at sublethal doses of 10 and 15 Gy. c—non-irradiated control, Tam—Tameron ($10^{-4}$ M). * $p < 0.001$ (difference from control), # $p < 0.001$ (difference from irradiated group without Tameron treatment). Data are presented as mean ± SD.

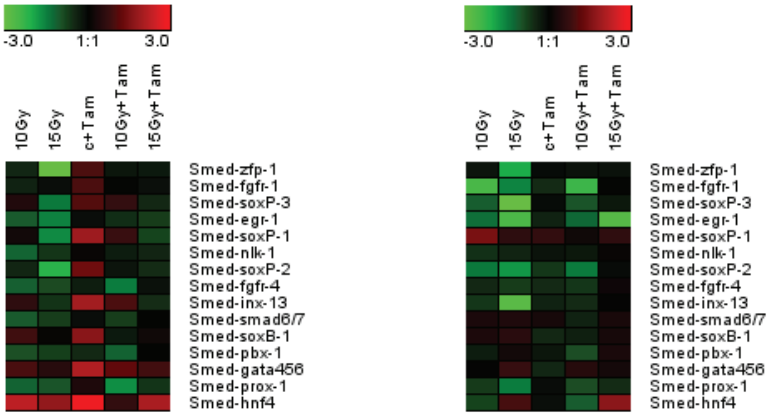


**Figure 3.** Tameron stimulates expression of neoblast marker genes. The figure shows a heatmap reflecting changes in expression of a test panel of neoblast marker genes in planarians after irradiation and/or treatment with Tameron (Tam) ($10^{-4}$ M) compared to unirradiated and untreated animals. The scale of intensity of the standardized expression values extends from −3 (green: low expression) to +3 (red: high expression). The 1:1 intensity value (black) represents the non-treated control. The measurements were made on the first and on the tenth day after irradiation.

### *3.4. Tameron Modulates the Expression of Oxidative Stress Response Genes*

To monitor the antioxidant activity of Tameron in terms of influence on the expression pattern of genes responsible for planarian redox metabolism, we have analyzed a test panel of antioxidant-related genes by RT-qPCR (Figure 4). These genes are known to be controlled by the transcription factor NRF2 which is a therapeutic target of Tameron [14]. The expression was measured after 24, 48, and 72 h after 10 Gy irradiation in the presence and absence of Tameron and compared to unirradiated and untreated control. After 24 h, the expression of most analyzed genes was reduced compared to the control, but Tameron

treatment upregulated or restored to normal levels a significant part of them. After 48 h, the expression of most of the analyzed genes was elevated in the 10 Gy-irradiated sample but slightly downregulated or brought to normal levels in Tameron-treated samples. These results may reflect the fact that Tameron leads to earlier induction of antioxidant genes, providing a prompter response to damage caused by ionizing radiation. After 72 h, expression of most antioxidant genes was brought to normal level or slightly downregulated in the 10 Gy-irradiated sample. In the Tameron-treated sample, we still observed the upregulation of six genes while other genes were downregulated, which reflects the continuation of the modulatory activity of Tameron on antioxidant genes.

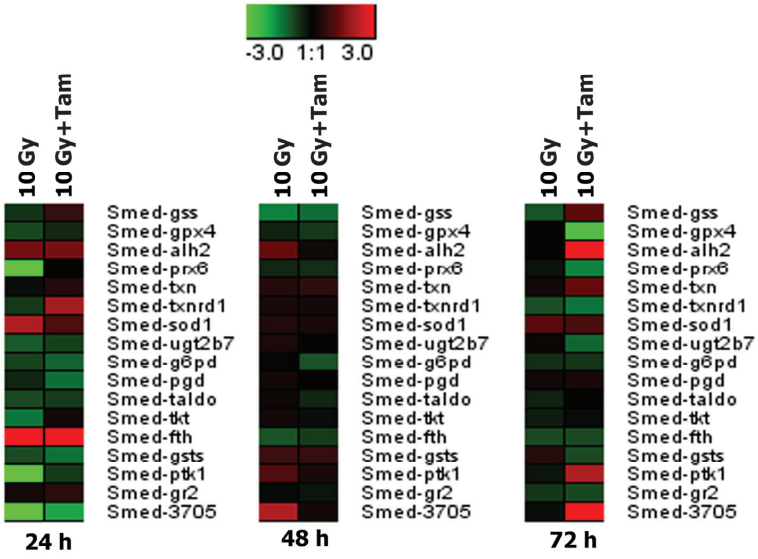


**Figure 4.** Tameron modulates expression of oxidative stress response genes. The figure shows a heatmap reflecting changes in expression of a test panel of NRF-2-controlled antioxidant defense genes in planarians after irradiation and/or treatment with Tameron (Tam) ($10^{-4}$ M) compared to unirradiated and untreated animals. The scale of intensity of the standardized expression values extends from −3 (green: low expression) to +3 (red: high expression). The 1:1 intensity value (black) represents the non-treated control.

### *3.5. Tameron Boosts Planarian Regeneration after Menadione-Mediated Inhibition*

Menadione [37] is a prooxidant drug that is used in a classical model of oxidative stress induction in biological systems [38]. We have used it in our planarian regeneration test system in concentrations of $10^{-6}$ M to evaluate the antioxidant properties of Tameron. Menadione on its own significantly inhibited the planarian regeneration for 21.8%, while Tameron boosted the regeneration activity for 16.3% ($10^{-4}$ M) and for 11.5% ($10^{-5}$ M) (Figure 5). When Tameron was added to the menadione-treated animals in concentrations of $10^{-4}$ and $10^{-5}$ M, it significantly upregulated the regeneration speed, restoring it almost to normal values (Figure 5).

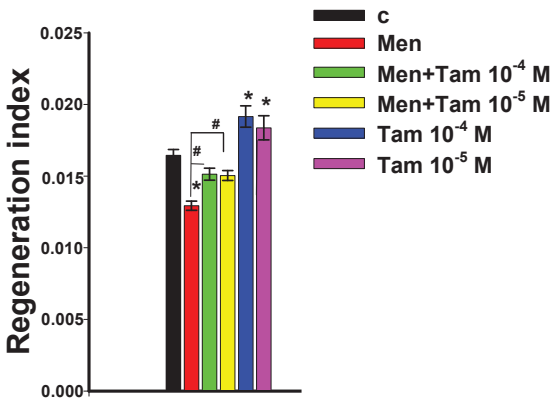


**Figure 5.** Antioxidant effects of Tameron on regenerating planarians in non-treated animals and after menadione-induced oxidative stress. c—non-irradiated control, Tam—Tameron, Men—menadione. * $p < 0.001$ (difference from control), # $p < 0.001$ (difference from irradiated group without Tameron treatment). Data are presented as mean ± SD.

### *3.6. Tameron Modulates the Expression of Neoblast Marker Genes after Menadione-Induced Oxidative Stress in Intact and Regenerating Planarians*

To further explore the pro-regenerative properties of Tameron, we tested its influence on the expression of neoblast marker genes in intact (Figure 6a) and regenerating (Figure 6b) planarians.

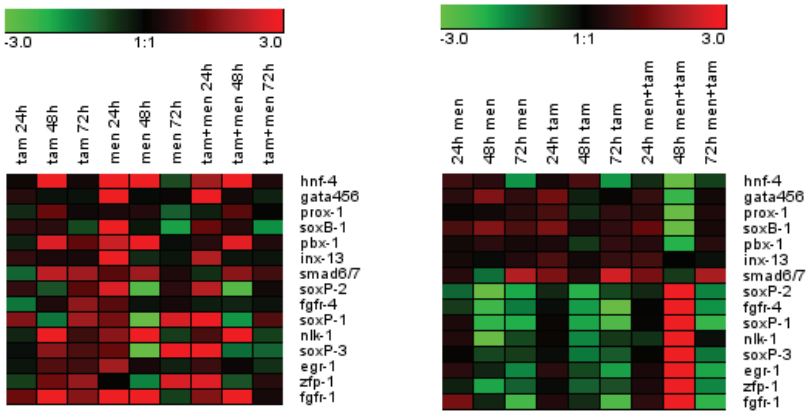


(**a**) (**b**)

**Figure 6.** Tameron effect on expression of neoblast marker genes in intact (**a**) and regenerating (**b**) planarians. The figure shows heatmaps reflecting changes in expression of a test panel of neoblast marker genes in planarians after menadione-induced oxidative stress and/or treatment with Tameron compared to untreated animals. The scale of intensity of the standardized expression values extends from −3 (green: low expression) to +3 (red: high expression). The 1:1 intensity value (black) represents the non-treated control. A non-treated control group was taken as a control. Menadione (Men) was used at working concentration of $10^{-6}$ M, Tameron (Tam)—$10^{-4}$ M. The measurements were made on the 24th, 48th, and 72nd h after treatment.

For intact animals (Figure 6a), Tameron treatment upregulates the expression of most genes from our panel (10 of 15) after 48 h—the highest upregulation was observed in the case of *smed-hnf-4* (22 times), *smed-nlk-1* (15 times), *smed-fgfr-1* (7 times), *smed-pbx-1*

(7 times), and *smed-smad6/7* (10 times). After 72 h, 7 of 10 genes kept elevated levels of transcription. In the menadione-treated group, an upregulation boost could be observed already after 24 h of incubation for almost all tested genes, then followed by transcriptional downregulation of most genes after 48 h. Most pronounced downregulation was seen in the case of *smed-soxP-1*, *smed-soxP-2,* and *smed-soxP-3*. After 72 h, *smed-soxP-3* and *smed-soxP-1* were upregulated again, 101 and 106 times, respectively, compared to the second day of incubation. For planarians treated with the Tameron-menadione combination, upregulation of most genes after 24 h was observed as well. So, the transcription of *smed-hnf-4* was increased 11 times, *smed-pbx-1* 4 times, *smed-nlk-1* 4 times, and *smed-fgfr-4* times.

For regenerating planarians (Figure 6b), incubation with menadione gives only a modest stimulation of most test panel genes expression in 24 h, while *smed-soxP-2* and *smed-fgfr-4* are downregulated. On the second day, the expression of most genes is downregulated—for example, *smed-nlk-1*–15 times, *smed-soxP-1*, and *smed-soxP-2*–6 times. On the third day, the picture remains practically the same, except for 5 times downregulation of *smed-hnf-4* and 11 times upregulation of *smed-smad6/7*. After Tameron treatment of regenerating planarians, the picture is quite similar to that of menadione—the same genes were up- and downregulated on the second and third day of the experiment. The situation changed after combined menadione-Tameron treatment. On the second day of incubation, half of the genes in the panel were drastically upregulated: *smed-soxP-2*—3452 times, *smed-fgfr-4*–в—1942 times, *smed-soxP-1*—2004 times, *smed-nlk-1*—568 times, *smed-soxP-3*—1228 times, *smed-egr-1*—3219 times, *smed-zfp-1*—3121 times, and *smed-fgfr-1*—9630 times. Some of the genes were downregulated: *smed-prox-1* went down 48 times, and *smed-soxB-1* went down 23 times. However, on the third day, the upregulated half went down strongly, while the expression level of other genes returned to normal values.

### *3.7. Tameron Modulates the Expression of Oxidative Stress Response Genes after Menadione-Induced Oxidative Stress in Intact and Regenerating Planarians*

On the first day after Tameron treatment of intact planarians (Figure 7a), we observed a pronounced downregulation of almost all genes of the panel, with the exception of *smed-GCL,* which went down during the following two days. On the second day, the previously downregulated *smed-gpx4, smed-alh1, smed-alh2, smed-prx6, smed-txn, smed-txnrd1, smed-sod1, smed-cat, smed-ugt2b7 smed-pgd, smed-taldo, smed-tkt,* and *smed-fth smed-9751* became activated. *Smed-txnrd1* expression was boosted 86 times, while all the others were upregulated 3–16 times. At the same time, the expression of *smed-GR* и *smed-G6PD* went down. On the third day, only the *smed-GR* gene was upregulated. A similar picture was observed in the group of animals incubated with Tameron and menadione: most parts of the genes downregulated on the first day were upregulated on the second day, and then the expression levels returned to normal values. A pronounced expression downregulation could be observed for the *smed-gpx4, smed-alh1*, and *smed-9751* genes. After treatment with menadione only, the same genes from the previous group were upregulated, but with several exceptions. The most pronounced upregulation was observed for the gene *smed-txnrd1* (22 times). On the third day, upregulation was observed for the *smed-pgd* and *smed-gr* genes.

In regenerating animals (Figure 7b), we could observe a significant upregulation of almost all oxidative stress response genes from the tested panel after menadione treatment on the first day of incubation. The only exception is the *Smed-gr2* gene—its activity was close to the control in all of the experimental groups. The biggest difference from the control was detected for the *Smed-tkt* and *Smed-txnrd1* genes (18 times upregulation). On the second day, the expression of *Smed-alh1*, *Smed-alh2*, *Smed-txnrd1*, *Smed-cat*, and *Smed-ptk1* genes remained elevated, while other genes became downregulated. The largest degree of downregulation could be observed for the *Smed-fth* gene (55 times). On the third day of incubation, the expression of the upregulated genes went down as well: 12 times for *Smed-alh1*, 8 times for *Smed-alh2*, 155 times for *Smed-txnrd1*, 29 times for *Smed-cat*, and 8 times for *Smed-ptk1*.

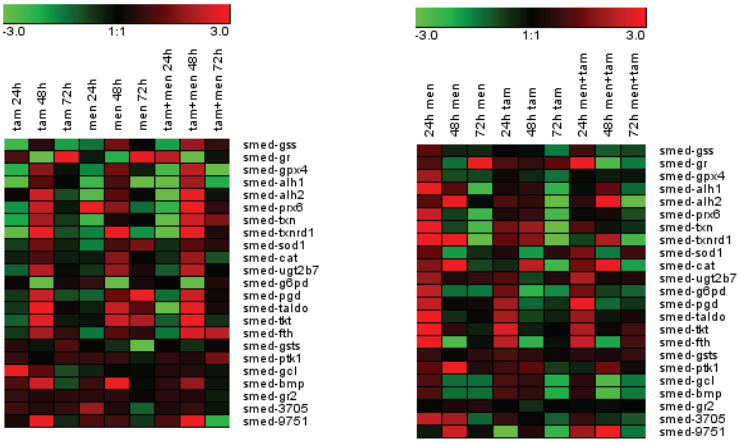


**Figure 7.** Tameron's effect on expression of oxidative stress response genes in intact (**a**) and regenerating (**b**) planarians. The figure shows heatmaps reflecting changes in expression of a test panel of neoblast marker genes in planarians after menadione-induced oxidative stress and/or treatment with Tameron compared to untreated animals. The scale of intensity of the standardized expression values extends from −3 (green: low expression) to +3 (red: high expression). The 1:1 intensity value (black) represents the non-treated control. A non-treated control group was taken as a control. Menadione (Men) was used at working concentration of $10^{-6}$ M, Tameron (Tam)—$10^{-4}$ M. The measurements were made on the 24th, 48th, and 72nd h after treatment.

On the first day, after Tameron treatment, almost half of the panel was also upregulated. The highest overexpression was detected for the following genes: *Smed-tkt*, *Smed-fth*, *Smed-taldo*, and *Smed-pgd*; however, on the second day, their expression was downregulated by 7, 22, 7, and 9 times, respectively. The activity of catalase *Smed-cat* was elevated 7 times on the second day. On the third day of incubation with Tameron, the expression of the entire panel was inhibited. The activity of *Smed-txn* went down 46 times, *Smed-txnrd1*—61 times, and *Smed-alh2*—158 times.

After incubation of regenerating planarians with the Tameron-menadione combination, we observed upregulation of most genes on the first day; the most pronounced stimulation was detected for the *Smed-gr* gene (110 times) and *Smed-pgd* (7 times). On the second day, the expression of the following genes was further elevated: *Smed-cat* (3 times) and *Smed-alh2* (5 times). The *Smed-alh1* and *Smed-txnrd1* genes, which were downregulated on the first day, were upregulated on the second day. On the second day, the expression of the remaining genes was significantly reduced, particularly *Smed-gr*—691 times and *Smed-fth*—19 times. On the third day, the *Smed-alh2*, *Smed-cat*, and *Smed-txnrd1* were strongly downregulated, 392, 27, and 22 times, respectively. The expression of the remaining genes was insignificantly higher or lower than the control.

### *3.8. Tameron Is an Effective ROS Scavenger in the CAA Assay*

To prove whether Tameron could quench ROS in situ, we performed a cellular antioxidant activity (CAA) assay with the reagent 2′,7′-Dichlorofluorescin diacetate (H2DCFDA), which is oxidized in the presence of ROS into a fluorescent dichlorofluorescein (DCF)—fluorescent intensity reflects ROS concentration in the cells of the studied specimen. Surprisingly, Tameron did not lower the DCF fluorescence, but, vice versa, enhanced it by itself, when combined with 10 and 15 Gy irradiation, which by itself predictably enhanced the fluorescence (Figure 8a). Menadione treatment boosted the fluorescence by itself, while the menadione-Tameron combination enhanced it even further on the first and second days and did not differ significantly from Tameron alone (Figure 8b). To clarify this paradoxical

result, we incubated the dye H2DCFDA with $H_2O_2$ alone and with a combination of $H_2O_2$ and three gradually decreasing concentrations of Tameron, presuming that Tameron could directly catalyze the H2DCFDA oxidation, and thus produced an artifact in our experimental system rather than reflecting an increase in the ROS amount. Indeed, Tameron strongly boosted the oxidation of H2DCFDA in vitro, and this effect was concentration-dependent (Figure 8c). When we substituted H2DCFDA CellROX® Green Reagent, we found out that Tameron did not promote CellROX® Green Reagent fluorescence in an in vitro experiment. Using this reagent on ROS, we were able to detect the activity of Tameron as a free radical scavenger. As shown in Figure 8d, in the presence of exposure to ionizing radiation at doses of 5 and 10 Gy, the drug effectively reduced the amount of ROS almost to control values. Similarly, menadione increased the fluorescence intensity of CellROX® by more than 2.5 times, and, in the presence of Tameron, the fluorescence intensity of the planarian body was comparable to that of the control group (Figure 8e). This indicates the effective scavenging of ROS by Tameron.

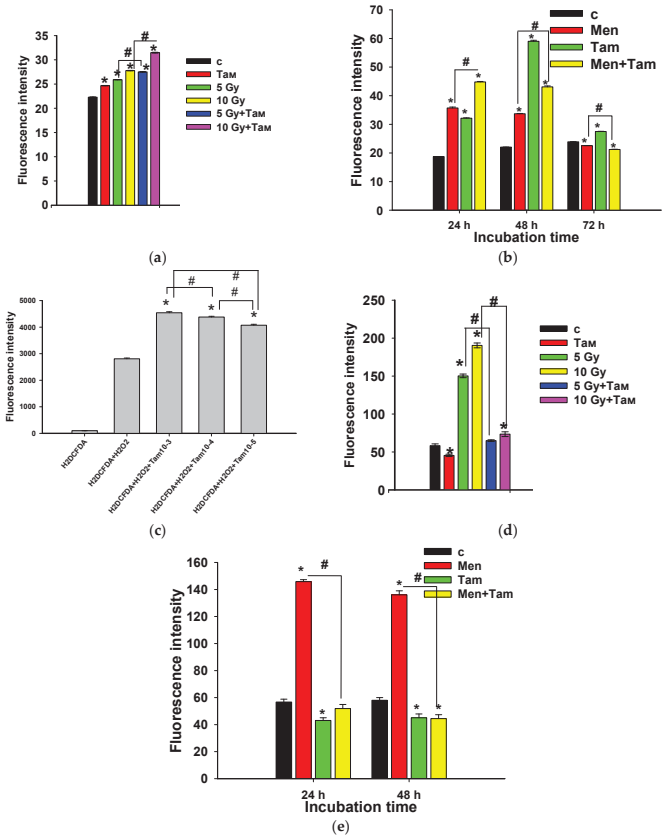


**Figure 8.** Tameron-mediated catalysis of H2DCFDA oxidation in vivo and in vitro. (**a**) Effect of Tameron (Tam) on DCF fluorescence in intact and 5 and 10 Gy-irradiated worms. (**b**) Effect of Tameron, menadione (Men), and Tameron-menadione combination on DCF fluorescence in planarians after 24, 48, and 72 h. (**c**) Tameron catalyzes H2DCFDA oxidation by $H_2O_2$ in a concentration-dependent manner. (**d**) The effect of Tameron as a ROS scavenger in planarian bodies after X-ray exposure, revealed with CellROX® Green dye. (**e**) Effect of Tameron as a ROS scavenger in planarian bodies after menadione exposure, revealed using CellROX® Green dye. c—non-treated control, Tam—Tameron, Men—menadione. * $p < 0.001$ (difference from control), # $p < 0.001$ (difference from group without Tameron treatment). Data are presented as mean ± sem.

## 4. Discussion

Taking into account the chemical properties of Tameron, it is believed to scavenge abundant inflammation-induced ROS. During this process, Tameron is oxidized, generating a photon emission that can be detected by sensitive photon-counting devices—for example, by the ultra-weak photon emission (UPE) method [39]. Tameron has been described as an antiviral agent [16], boosting the cellular antioxidant stress defenses after viral infection by activation and stabilization of the redox-sensitive NF-E2-related transcription factor 2 (Nrf2) [13,15], which can ameliorate the devastating impact of immune reactions on viruses, including cytokine storm [40–42]. Similar effects were observed for Tameron on a model of Gulf War illness—a neurological condition induced by chemical damage to brain tissue [12].

Stabilization and activation of Nrf2 have previously been demonstrated to be a protective mechanism utilized by the endothelial cells against stress-induced oxidative damage [43], as well as in cadmium-induced oxidative stress [44]. In cells under the influence of oxidative stress, Nrf2 undergoes upregulation and translocation to the nucleus, where it upregulates the expression of genes related to GSH synthesis [45,46].

To prove whether Tameron is a potent antioxidant and radioprotector, we tested its action on our highly robust and reliable planarian model [25] for both X-ray- and chemically induced oxidative stress. In our study, we conducted a series of experiments to monitor the action of Tameron on intact and regenerating worms on multiple levels. These experiments are as follows: first, the measurements of the blastema regeneration rate; second, the calculations of the number of surviving neoblasts and an evaluation of their mitotic activity; third, the monitoring of the expression of the neoblast marker gene panel; fourth, the monitoring of the expression of antioxidant gene panel; and fifth, the estimation of ROS generation rate by the planarian tissue.

The experiments on the regeneration rate of X-ray-irradiated planarians and the neoblast mitotic activity have, indeed, confirmed that Tameron acts as a potent radioprotector. The studies on neoblast marker genes expression showed their clear upregulation after Tameron treatment on top of X-ray irradiation, giving clues to the mechanisms of the pro-regenerative and stem cell-protective activity of Tameron. The effect of Tameron on neoblast marker genes after chemically induced oxidative stress by menadione is more complex. We can still see that Tameron modulates the expression of neoblast marker genes when compared to untreated controls, thus influencing regenerative activity. In general, irradiation significantly lowers the expression levels of neoblast markers, which is most likely an outcome of neoblast death and results in the drastic collapse of the regeneration process. The presence of Tameron saves the expression of neoblast markers at levels comparable to unirradiated controls; this observed effect is a consequence of Tameron's protective action. The drug protects planarian neoblasts and the regenerative potential of the animals. Moreover, Tameron itself is capable of stimulating the neoblast marker expression and thereby stimulating the regenerative process itself.

Concerning the NRF2-controlled genes responsible for oxidative stress response genes, the X-ray irradiation did not lead, in general, to a significant induction of their expression. Still, we have to point out that we have observed an increase in the expression of the *alh* gene responsible for the oxidation of aldehyde and ketone groups which are formed in lipids as a result of ionizing radiation [47]. The presence of Tameron also increased the expression of this gene after irradiation, while the expression of glutathioneperoxidase was significantly reduced three days after irradiation, which may indicate that Tameron is capable of efficiently degrading the peroxide compounds by itself, thereby reducing the levels of oxidative stress.

In cases of menadione-induced oxidative stress, Tameron also boosts the regenerative activity of planarians, demonstrating its antioxidant potential. On the level of antioxidant response genes, it has a complex influence in cases of X-ray irradiation, strongly upregulating some of them. In the case of menadione-induced oxidative stress, Tameron also produces a complex pattern of changes in the antioxidant response gene expression panel, upregulating some of them, which may be crucial for combating oxidative stress. As we

have shown, menadione in intact planarians significantly stimulated the level of expression of neoblast marker genes. It is likely that oxidative stress caused by the presence of menadione is a trigger mechanism for activating the regenerative activity of stem cells. It was previously demonstrated that one of the triggers for the activation of neoblast proliferation and regeneration is ROS activity in the area of damage to the animal body [48]. Obviously, in regenerating animals, the mechanism of neoblast activation has already been launched, and an additional stimulus in the form of ROS from menadione leads, on the contrary, to a decrease in the expression of neoblast gene markers, which is obviously a consequence of the suppression of the regenerative process by menadione in planarians. At the same time, as we have already said, Tameron by itself activates the regeneration of planarians, which manifests itself at elevated levels of expression of neoblast markers (an active proliferative process is underway) in intact animals, while in regenerating animals, the inhibitory effect of menadione is neutralized by Tameron, which can be traced by the expression of neoblast markers—for example, after 24 h of regeneration, it is mostly similar to the control values.

Oxidative stress caused by menadione significantly increased the transcription of genes controlled by NRF2 in planarians. In intact planarians, most of the studied genes were actively transcribed after 48 h, and in regenerating ones after 24 h of incubation. These differences in dynamics are probably related to the physiological status of the animals—as we said above, regenerating planarians already have an increased level of ROS and, accordingly, menadione enhances this effect immediately after being added. In intact animals, the level of ROS increases after the addition of menadione, and this, accordingly, causes additional activation of the antioxidant defense system as early as 24 h of incubation. Tameron, being an NRF2 stabilizer, activates the antioxidant defense system itself (as can be seen from the level of gene expression that is observed in intact animals at 48 h of incubation and in regenerating animals at 24 h) due to this factor. Moreover, the differences in dynamics are, again, associated with the physiological state of the animals and the initial level of ROS. Furthermore, the effect of the combination of Tameron and menadione on the level of expression of antioxidant defense genes controlled by NRF2 follows the same dynamics, as is observed when these substances are exposed separately from each other. Additionally, since both of these substances activate antioxidant defense systems in almost the same way in dynamics and patterns, their combined effects are also similar on the level of gene transcription.

Experiments on direct measurement of ROS using the H2DCFDA oxidation to DCF did not provide reliable results in our hands. As previously reported [49], DCF can actually produce $O_2^{\bullet -}$ and $H_2O_2$ via the reaction of DCF radical with oxygen, thus artificially elevating the very ROS that it is attempting to quantify. That was proven in our assay, creating an artifact, and making it unable to precisely quantify the ROS amount after X-ray- and menadione-induced oxidative stress and Tameron treatment. Indeed, Tameron enhances the oxidation of H2DCFDA and, accordingly, fluorescence is evidence of this. Obviously, Tameron is involved in the redox process, and this gives an inverse relationship in terms of the level of H2DCFDA fluorescence. While neutralizing free radicals, Tameron increases the intensity of H2DCFDA fluorescence. In the case of using CellROX® Green, we, indeed, observed the effect of Tameron as a free radical scavenger, as this reagent does not get oxidized by Tameron. This should be taken into account when using the antioxidant properties of other substances—the absence of ROS scavenging effect may be an artifact due to the chemical interaction of the dye and the substance studied.

## 5. Conclusions

In general, Tameron has shown itself to be a potent novel radioprotector and antioxidant, robustly enhancing the regeneration rate in planarians damaged by X-ray- or menadione-induced oxidative stress and protecting mitotic activity of neoblasts while modulating the expression patterns of neoblast markers and oxidative stress response genes.

**Supplementary Materials:** The following supporting information can be downloaded at: https://www.mdpi.com/article/10.3390/antiox12040953/s1, Figure S1: The representative photographs of regenerating planarians for blasthema growth rate analysis by means of computer morphometry; Figure S2: Structural chemical formula of Tameron (5-amino-2,3-dihydro-1,4-phthalazinedione sodium salt); Figure S3: Mitotic cells in planarian bodies (whole-mount Immunocytochemistry) 7 days after 15 Gy irradiation; Table S1: Selected gene groups for RT-PCR analysis of neoblast marker genes. Table S2: Selected gene groups for RT-PCR analysis of oxidative stress response genes.

**Author Contributions:** Conceptualization, A.E. and A.B.; methodology, E.T., K.F., V.A. and O.E.; validation, K.F., V.A. and E.T.; formal analysis, O.E.; investigation, E.T., K.F., V.A., O.E. and A.K.; resources, A.E.; data curation, O.E. and A.E.; writing—original draft preparation, A.B.; writing—review and editing, A.E.; visualization, V.A., K.F. and E.T.; supervision, A.B.; project administration, A.E. All authors have read and agreed to the published version of the manuscript.

**Funding:** This research received no external funding.

**Institutional Review Board Statement:** The animal study protocol was approved by the Ethics Committee of the Institute of Theoretical and Experimental Biophysics of the Russian Academy of Sciences (protocol No 154-21, date of approval 14 October 2021).

**Informed Consent Statement:** Not applicable.

**Data Availability Statement:** The data are contained within this article.

**Conflicts of Interest:** The authors declare no conflict of interest.

## References

1. Sindhi, V.; Gupta, V.; Sharma, K.; Bhatnagar, S.; Kumari, R.; Dhaka, N. Potential applications of antioxidants—A review. *J. Pharm. Res.* **2013**, *7*, 828–835. [CrossRef]
2. Forman, H.J.; Zhang, H. Targeting oxidative stress in disease: Promise and limitations of antioxidant therapy. *Nat. Rev. Drug Discov.* **2021**, *20*, 689–709. [CrossRef] [PubMed]
3. Kamran, M.Z.; Ranjan, A.; Kaur, N.; Sur, S.; Tandon, V. Radioprotective Agents: Strategies and Translational Advances. *Med. Res. Rev.* **2016**, *36*, 461–493. [CrossRef] [PubMed]
4. Azzam, E.I.; Jay-Gerin, J.P.; Pain, D. Ionizing radiation-induced metabolic oxidative stress and prolonged cell injury. *Cancer Lett.* **2012**, *327*, 48–60. [CrossRef]
5. Reisz, J.A.; Bansal, N.; Qian, J.; Zhao, W.; Furdui, C.M. Effects of ionizing radiation on biological molecules–mechanisms of damage and emerging methods of detection. *Antioxid. Redox Signal.* **2014**, *21*, 260–292. [CrossRef]
6. Kouvaris, J.R.; Kouloulias, V.E.; Vlahos, L.J. Amifostine: The first selective-target and broad-spectrum radioprotector. *Oncologist* **2007**, *12*, 738–747. [CrossRef]
7. Singh, V.K.; Seed, T.M. The efficacy and safety of amifostine for the acute radiation syndrome. *Expert Opin. Drug Saf.* **2019**, *18*, 1077–1090. [CrossRef]
8. Du, J.; Zhang, P.; Cheng, Y.; Liu, R.; Liu, H.; Gao, F.; Shi, C.; Liu, C. General principles of developing novel radioprotective agents for nuclear emergency. *Radiat. Med. Prot.* **2020**, *1*, 120–126. [CrossRef]
9. Rosen, E.M.; Day, R.; Singh, V.K. New approaches to radiation protection. *Front. Oncol.* **2014**, *4*, 381. [CrossRef]
10. Labarrere, C.A.; Kassab, G.S. Glutathione: A Samsonian life-sustaining small molecule that protects against oxidative stress, ageing and damaging inflammation. *Front. Nutr.* **2022**, *9*, 1007816. [CrossRef]
11. Xue, H.; Li, J.; Xie, H.; Wang, Y. Review of Drug Repositioning Approaches and Resources. *Int. J. Biol. Sci.* **2018**, *14*, 1232–1244. [CrossRef] [PubMed]
12. Shetty, A.K.; Attaluri, S.; Kodali, M.; Shuai, B.; Shetty, G.A.; Upadhya, D.; Hattiangady, B.; Madhu, L.N.; Upadhya, R.; Bates, A.; et al. Monosodium luminol reinstates redox homeostasis, improves cognition, mood and neurogenesis, and alleviates neuro- and systemic inflammation in a model of Gulf War Illness. *Redox Biol.* **2020**, *28*, 101389. [CrossRef] [PubMed]
13. Scofield, V.L.; Yan, M.; Kuang, X.; Kim, S.J.; Crunk, D.; Wong, P.K. The drug monosodium luminol (GVT) preserves thymic epithelial cell cytoarchitecture and allows thymocyte survival in mice infected with the T cell-tropic, cytopathic retrovirus ts1. *Immunol. Lett.* **2009**, *122*, 159–169. [CrossRef]
14. Jiang, Y.; Scofield, V.L.; Yan, M.; Qiang, W.; Liu, N.; Reid, A.J.; Lynn, W.S.; Wong, P.K. Retrovirus-induced oxidative stress with neuroimmunodegeneration is suppressed by antioxidant treatment with a refined monosodium alpha-luminol (Galavit). *J. Virol.* **2006**, *80*, 4557–4569. [CrossRef] [PubMed]
15. Reddy, P.V.; Lungu, G.; Kuang, X.; Stoica, G.; Wong, P.K. Neuroprotective effects of the drug GVT (monosodium luminol) are mediated by the stabilization of Nrf2 in astrocytes. *Neurochem. Int.* **2010**, *56*, 780–788. [CrossRef]

16. Schumann, S.; Kaiser, A.; Nicoletti, F. Immune-Modulating Drug MP1032 with SARS-CoV-2 Antiviral Activity In Vitro: A potential Multi-Target Approach for Prevention and Early Intervention Treatment of COVID-19. *Int. J. Mol. Sci.* **2020**, *21*, 8803. [CrossRef]
17. Rink, J.C. Stem cell systems and regeneration in planaria. *Dev. Genes Evol.* **2013**, *223*, 67–84. [CrossRef]
18. Reddien, P.W.; Sánchez Alvarado, A. Fundamentals of planarian regeneration. *Annu. Rev. Cell Dev. Biol.* **2004**, *20*, 725–757. [CrossRef]
19. Roberts-Galbraith, R.H.; Newmark, P.A. On the organ trail: Insights into organ regeneration in the planarian. *Curr. Opin. Genet. Dev.* **2015**, *32*, 37–46. [CrossRef]
20. Pagán, O.R. Planaria: An animal model that integrates development, regeneration and pharmacology. *Int. J. Dev. Biol.* **2017**, *61*, 519–529. [CrossRef]
21. Pellettieri, J.; Sánchez Alvarado, A. Cell turnover and adult tissue homeostasis: From humans to planarians. *Annu. Rev. Genet.* **2007**, *41*, 83–105. [CrossRef] [PubMed]
22. Salvetti, A.; Rossi, L.; Bonuccelli, L.; Lena, A.; Pugliesi, C.; Rainaldi, G.; Evangelista, M.; Gremigni, V. Adult stem cell plasticity: Neoblast repopulation in non-lethally irradiated planarians. *Dev. Biol.* **2009**, *328*, 305–314. [CrossRef] [PubMed]
23. Reddien, P.W.; Oviedo, N.J.; Jennings, J.R.; Jenkin, J.C.; Sánchez Alvarado, A. SMEDWI-2 is a PIWI-like protein that regulates planarian stem cells. *Science* **2005**, *310*, 1327–1330. [CrossRef] [PubMed]
24. Rossi, L.; Cassella, L.; Iacopetti, P.; Ghezzani, C.; Tana, L.; Gimenez, G.; Ghigo, E.; Salvetti, A. Insight into stem cell regulation from sub-lethally irradiated worms. *Gene* **2018**, *662*, 37–45. [CrossRef]
25. Ermakov, A.M.; Kamenskikh, K.A.; Ermakova, O.N.; Blagodatsky, A.S.; Popov, A.L.; Ivanov, V.K. Planarians as an In Vivo Experimental Model for the Study of New Radioprotective Substances. *Antioxidants* **2021**, *10*, 1763. [CrossRef]
26. Goupil, L.S.; Ivry, S.L.; Hsieh, I.; Suzuki, B.M.; Craik, C.S.; O'Donoghue, A.J.; McKerrow, J.H. Cysteine and Aspartyl Proteases Contribute to Protein Digestion in the Gut of Freshwater Planaria. *PLoS Negl. Trop. Dis.* **2016**, *10*, e0004893. [CrossRef]
27. Ermakov, A.M.; Ermakova, O.N.; Maevskiĭ, E.I. A role of some intracellular signaling cascades in planarian regeneration activated under irradiation with low-temperature argon plasma. *Biofizika* **2014**, *59*, 552–557. [CrossRef]
28. Newmark, P.A.; Sánchez Alvarado, A. Bromodeoxyuridine specifically labels the regenerative stem cells of planarians. *Dev. Biol.* **2000**, *220*, 142–153. [CrossRef]
29. Ermakova, O.N.; Ermakov, A.M.; Tiras Kh, P.; Lednev, V.V. Melatonin effect on the regeneration of the flatworm Girardia tigrina. *Ontogenez* **2009**, *40*, 466–469. [CrossRef]
30. Ermakov, A.; Popov, A.; Ermakova, O.; Ivanova, O.; Baranchikov, A.; Kamenskikh, K.; Shekunova, T.; Shcherbakov, A.; Popova, N.; Ivanov, V. The first inorganic mitogens: Cerium oxide and cerium fluoride nanoparticles stimulate planarian regeneration via neoblastic activation. *Mater. Sci. Eng. C Mater. Biol. Appl.* **2019**, *104*, 109924. [CrossRef]
31. Ermakov, A.M.; Ermakova, O.N.; Afanasyeva, V.A.; Popov, A.L. Dose-Dependent Effects of Cold Atmospheric Argon Plasma on the Mesenchymal Stem and Osteosarcoma Cells In Vitro. *Int. J. Mol. Sci.* **2021**, *22*, 6797. [CrossRef]
32. van Wolfswinkel, J.C.; Wagner, D.E.; Reddien, P.W. Single-cell analysis reveals functionally distinct classes within the planarian stem cell compartment. *Cell Stem Cell* **2014**, *15*, 326–339. [CrossRef] [PubMed]
33. Kobayashi, M.; Yamamoto, M. Molecular mechanisms activating the Nrf2-Keap1 pathway of antioxidant gene regulation. *Antioxid. Redox Signal.* **2005**, *7*, 385–394. [CrossRef] [PubMed]
34. Sturn, A.; Quackenbush, J.; Trajanoski, Z. Genesis: Cluster analysis of microarray data. *Bioinformatics* **2002**, *18*, 207–208. [CrossRef] [PubMed]
35. Lee, J.G.; Noh, W.J.; Kim, H.; Lee, M.Y. Generation of reactive oxygen species contributes to the development of carbon black cytotoxicity to vascular cells. *Toxicol. Res.* **2011**, *27*, 161–166. [CrossRef] [PubMed]
36. Guedelhoefer, O.C.T.; Sánchez Alvarado, A. Amputation induces stem cell mobilization to sites of injury during planarian regeneration. *Development* **2012**, *139*, 3510–3520. [CrossRef] [PubMed]
37. Hassan, G.S. Menadione. *Profiles Drug Subst. Excip. Relat. Methodol.* **2013**, *38*, 227–313. [CrossRef]
38. Abe, K.; Saito, H. Menadione toxicity in cultured rat cortical astrocytes. *Jpn. J. Pharmacol.* **1996**, *72*, 299–306. [CrossRef]
39. Cifra, M.; Pospíšil, P. Ultra-weak photon emission from biological samples: Definition, mechanisms, properties, detection and applications. *J. Photochem. Photobiol. B Biol.* **2014**, *139*, 2–10. [CrossRef]
40. Liu, Z.; Deng, P.; Liu, S.; Bian, Y. Is Nuclear Factor Erythroid 2-Related Factor 2 a Target for the Intervention of Cytokine Storms? *Antioxidants* **2023**, *12*, 172. [CrossRef]
41. Qiang, W.; Cahill, J.M.; Liu, J.; Kuang, X.; Liu, N.; Scofield, V.L.; Voorhees, J.R.; Reid, A.J.; Yan, M.; Lynn, W.S.; et al. Activation of transcription factor Nrf-2 and its downstream targets in response to moloney murine leukemia virus ts1-induced thiol depletion and oxidative stress in astrocytes. *J. Virol.* **2004**, *78*, 11926–11938. [CrossRef] [PubMed]
42. Qiang, W.; Kuang, X.; Liu, J.; Liu, N.; Scofield, V.L.; Reid, A.J.; Jiang, Y.; Stoica, G.; Lynn, W.S.; Wong, P.K. Astrocytes survive chronic infection and cytopathic effects of the ts1 mutant of the retrovirus Moloney murine leukemia virus by upregulation of antioxidant defenses. *J. Virol.* **2006**, *80*, 3273–3284. [CrossRef] [PubMed]
43. Warabi, E.; Takabe, W.; Minami, T.; Inoue, K.; Itoh, K.; Yamamoto, M.; Ishii, T.; Kodama, T.; Noguchi, N. Shear stress stabilizes NF-E2-related factor 2 and induces antioxidant genes in endothelial cells: Role of reactive oxygen/nitrogen species. *Free Radic. Biol. Med.* **2007**, *42*, 260–269. [CrossRef] [PubMed]

44. He, X.; Chen, M.G.; Ma, Q. Activation of Nrf2 in defense against cadmium-induced oxidative stress. *Chem. Res. Toxicol.* **2008**, *21*, 1375–1383. [CrossRef] [PubMed]
45. Itoh, K.; Wakabayashi, N.; Katoh, Y.; Ishii, T.; Igarashi, K.; Engel, J.D.; Yamamoto, M. Keap1 represses nuclear activation of antioxidant responsive elements by Nrf2 through binding to the amino-terminal Neh2 domain. *Genes Dev.* **1999**, *13*, 76–86. [CrossRef] [PubMed]
46. Lee, J.M.; Calkins, M.J.; Chan, K.; Kan, Y.W.; Johnson, J.A. Identification of the NF-E2-related factor-2-dependent genes conferring protection against oxidative stress in primary cortical astrocytes using oligonucleotide microarray analysis. *J. Biol. Chem.* **2003**, *278*, 12029–12038. [CrossRef] [PubMed]
47. Deger, Y.; Dede, S.; Belge, A.; Mert, N.; Kahraman, T.; Alkan, M. Effects of X-ray radiation on lipid peroxidation and antioxidant systems in rabbits treated with antioxidant compounds. *Biol. Trace Elem. Res.* **2003**, *94*, 149–156. [CrossRef]
48. Pirotte, N.; Stevens, A.-S.; Fraguas, S.; Plusquin, M.; Van Roten, A.; Van Belleghem, F.; Paesen, R.; Ameloot, M.; Cebrià, F.; Artois, T.; et al. Reactive Oxygen Species in Planarian Regeneration: An Upstream Necessity for Correct Patterning and Brain Formation. *Oxidative Med. Cell. Longev.* **2015**, *2015*, 392476. [CrossRef]
49. Dikalov, S.I.; Harrison, D.G. Methods for detection of mitochondrial and cellular reactive oxygen species. *Antioxid. Redox Signal.* **2014**, *20*, 372–382. [CrossRef]

antioxidants

MDPI

*Article*

# Antioxidant Potential of Resveratrol as the Result of Radiation Exposition

**Natalia Rosiak [1], Judyta Cielecka-Piontek [1], Robert Skibiński [2], Kornelia Lewandowska [3], Waldemar Bednarski [3] and Przemysław Zalewski [1,*]**

[1] Department of Pharmacognosy, Poznan University of Medical Sciences, Rokietnicka 3, 60-806 Poznań, Poland
[2] Department of Medicinal Chemistry, Faculty of Pharmacy, Medical University of Lublin, Jaczewskiego 4, 20-090 Lublin, Poland
[3] Institute of Molecular Physics, Polish Academy of Sciences, Smoluchowskiego 17, 60-179 Poznań, Poland
* Correspondence: pzalewski@ump.edu.pl

**Abstract:** The purpose of this study was to determine the effect of electron beam irradiation (EBI) at a dose of 25 kGy on the stability and antioxidant properties of resveratrol (RSV), a nutraceutical with clinically proven activity. The electron paramagnetic resonance (EPR) method was used to evaluate the concentration of free radicals after irradiation. Minor changes in chemical structure due to free radicals induced by EBI were confirmed by FTIR spectroscopy. HPLC and HPLC-MS analysis ruled out the appearance of degradation products after irradiation. In addition, HPLC analysis confirmed the absence of trans- to cis-resveratrol conversion. Changes in the antioxidant potential of RSV after irradiation were studied using DPPH, ABTS, CUPRAC, and FRAP techniques. It was confirmed that EBI favorably affected the antioxidant properties of tests based on the HAT mechanism (increase in DPPH and CUPRAC tests).

**Keywords:** stilbenoid; electron paramagnetic resonance (EPR); FT-IR; electron beam radiation

**Citation:** Rosiak, N.; Cielecka-Piontek, J.; Skibiński, R.; Lewandowska, K.; Bednarski, W.; Zalewski, P. Antioxidant Potential of Resveratrol as the Result of Radiation Exposition. *Antioxidants* **2022**, *11*, 2097. https://doi.org/10.3390/antiox11112097

Academic Editors: Elena Obrador Pla and Alegria Montoro

Received: 8 September 2022
Accepted: 21 October 2022
Published: 24 October 2022



## 1. Introduction

Resveratrol (RSV), a natural compound, is a clinically proven nutraceutical [1–3]. It is found in many plants, including red grapes, mulberries, and peanuts. RSV's valuable biological properties are due to its significant antioxidant potential [4]. The antioxidant potential of plant-derived structures (mainly flavonoids), including resveratrol, is important from the point of view of the possibility of neutralizing free radical forms that are formed during pathological processes (their excessive accumulation in the human body occurs in the process of treatment, whether during the use of pharmacotherapy or radiotherapy, and ultimately contributes to damage to macromolecules in the human body). Naturally occurring pathological processes that induce free radicals formation include neoplastic, neurodegenerative diseases (e.g., Alzheimer's [5], Parkinson's [6], Huntington's [7]) or degenerative changes that occur with age (when intrinsic antioxidant mechanisms are less efficient). In addition, the antioxidant activity of resveratrol has been shown to protect tissues such as the liver and kidney from a various types of oxidative stress-induced damage [8]. Singh et al. described that the efficacy, safety, and pharmacokinetics of resveratrol have been documented in more than 244 clinical trials (data for the 2019 year) [2]. For example, resveratrol intake has been proven in clinical trials to have a positive effect on the treatment of Alzheimer's disease (reduction of matrix metalloproteinase 9) [9,10], diabetes (lowering blood glucose levels, increasing insulin sensitivity) [11–13], non-alcoholic fatty liver disease [2,14] or cardiovascular disease (affects multiple molecular targets that are associated with cardioprotective effects) [15,16].

Electron radiation is widely used in many fields of knowledge. Of particular importance is the use of this technology to ensure the microbiological safety of food and

drugs. One of the most important advantages of this method is that it is carried out at low temperature, which is especially important for heat-sensitive products.

The literature reports on the chemical instability of many compounds of natural and synthetic origin after exposure to ionizing radiation [17–20]. There is also evidence that many substances are resistant to ionizing radiation [21–24]. Therefore, ionizing radiation can be used to obtain sterile forms of drugs (25 kGy) or to achieve adequate microbiological purity (15 kGy). The specified doses of ionizing radiation are justified by ISO 11137 standard, which defines them as the minimum necessary to achieve the specified microbiological purity/sterility requirement [25]. Many brands of nutraceuticals containing resveratrol are available, so it is important to check the stability and antioxidative potential of RSV after exposure to ionizing radiation [3,26].

The purpose of our study was to evaluate the radiostability of resveratrol following exposure to ionizing radiation (25 kGy) and to assess its antioxidant properties after exposure to electron beam irradiation.

## 2. Materials and Methods

### *2.1. Materials*

Pure resveratrol (99%), potassium bromide (KBr), 2,2-Diphenyl-1-picrylhydrazyl (DPPH), Iron (III) chloride hexahydrate, 2,4,6-Tri(2-pyridyl)-s-triazine (TPTZ), ascorbic acid and neocuproine were supplied by Sigma Aldrich (St. Louis, MO, USA). Ammonium acetate ($NH_4Ac$) and methanol were supplied by Chempur (Piekary Śląskie, Poland). Cupric chloride dihydrate, acetic acid (99.5%), ethanol (96%), sodium acetate trihydrate, and glacial acetic acid were supplied by POCH (Gliwice, Poland). Acetonitrile of an HPLC grade was supplied by Romil (Waterbeach, Cambridgeshire, UK). Direct-Q 3 UV system delivered ultrapure water. (Millipore, Molsheim, France, model Exil SA 67120).

### *2.2. Irradiation*

Resveratrol was irradiated with an electron beam (NIIEFA, St. Petersburg, Russia) with a dose of 25 kGy on behalf of the Radiation Sterilization Plant of Medical Devices and Allografts. Parameters: set dose 25 kGy, transporter 0.620 $m \cdot min^{-1}$, set current 500 mA, energy 10 MeV, calibration factor 15.5, sampling 0.3 s.

### *2.3. Electron Paramagnetic Resonance (EPR) Spectroscopy*

Free radicals detection was carried out at room temperature using a multi-frequency (S, X and Q-band) ELEXSYS 500 spectrometer (Bruker, Billerica, MA, USA). EPR spectra of resveratrol powder were recorded at X-band, using low microwave power (2 mW) to avoid line saturation. Due to the low signal-to-noise ratio for the samples, each spectrum was accumulated ten times. Free radicals concentration was determined by comparing the double integrated EPR spectra of resveratrol with a spin number standard ($Al_2O_3:Cr^{3+}$).

A sample and $Al_2O_3:Cr^{3+}$ crystal with a known number of paramagnetic complexes ($Cr^{3+}$ ions) were placed into the resonance cavity. EPR lines of $Al_2O_3:Cr^{3+}$ were recorded below 2000 Gs, and above 4000 Gs. The ratio of the numbers obtained after the double integration of the standard line (EPR spectra were recorded as the first derivative of microwave absorption) and the tested sample allowed us to obtain the number of radicals in resveratrol. Before each line integration, the background of the spectrum was subtracted to obtain thee correct values. Both the integration and background correction of the spectra were carried out on the basic BRUKER Xepr 2.4b.28 program (Bruker, Billerica, MA, USA) used for recording and pre-processing of EPR spectra. Due to the low signal-to-noise ratio for radicals, we adjusted the spectra into single lines [27].

### *2.4. Fourier Transform Infrared Spectroscopy (FTIR)*

The FTIR analysis of non-irradiated (0 kGy) and irradiated (25 kGy) resveratrol samples were performed. Absorption spectra were obtained under room temperature conditions on a Bruker Equinox 55 spectrometer (Bruker Optics, Ettlingen, Germany).

Analyses were carried out in a KBr pellet (1 mg resveratrol sample and 200 mg KBr; diameter: 13 mm; pressure: 10 ton·cm$^{-2}$). The spectra were recorded in the wavelength region of 400–4000 cm$^{-1}$ with 400 scans and a 4 cm$^{-1}$ resolution. In all analyses, the pure KBr pellet was a blank sample. The obtained data were analyzed using the Origin 2021b software (OriginLab Corporation, Northampton, MA, USA).

### *2.5. Computation*

The density functional theory (DFT) was used to optimize the molecular geometry of resveratrol. The geometries were fully optimized with B3LYP/6-311G (d,p) using Gaussian 09 software (Wallingford, CT, USA) [28]. GaussView program was used to visually inspect the normal modes [29].

### *2.6. HPLC and HPLC-MS Analysis*

The Shimadzu Prominence-i LC-2030C HPLC instrument equipped with DAD detector was used in the study. The software was LabSolution DB/CS (version 6.50, Shimadzu, Kyoto, Japan). Solutions of irradiated and non-irradiated resveratrol were prepared in acetonitrile at a concentration of 0.4 mg·mL$^{-1}$. Solutions thus obtained were filtered through 0.45 µm syringe filters into 1.5 mL vials. Samples were measured on a Kinetex, C18, 100A, 100 × 2.1 mm column (Phenomenex, Torrance, CA, USA) with a particle sizes of 5 µm. The mobile phase was acetonitrile and 0.1% acetic acid (20:80 *v*/*v*) filtered through a 0.22 µm nylon membrane and ultrasonically degassed before use. The mobile phase flow rate was 1.0 mL·min$^{-1}$. The injection volume was 10 µL. Chromatograms were monitored at $\lambda_{max}$ = 306 nm using the UV detector. Separation was performed at 40 °C, and the analysis time was 5 min per sample.

The Agilent high-resolution mass spectrometer (Q-TOF LC-MS system model) with electrospray ion source (ESI) and Infinity 1290 UHPLC liquid chromatography system consisting of a binary pump (G4220A), autosampler (G4226A), thermostat (G1330B), and DAD (G4212A) (Agilent Technologies, Santa Clara, CA, USA) were used. The MassHunter software was used for system control and data analysis. A Hibar RP-18e (2.1 × 50 mm, dp = 2 µm) column (Merck, Darmstadt, Germany) was used and isocratic elution by acetonitrile:water with 0.1% formic acid (10:90 *v*/*v*) was performed for 0.5 min. In the next step, a gradient elution was carried out to a composition ratio (60:40) within 9 min. The flow rate was 0.3 mL·min$^{-1}$, and thermostating at 35 °C was used. The main parameters were set as follows: MS: ESI—negative polarity, source temp 325 °C, drying gas 10 L·min$^{-1}$, nebulizer pressure 40 psig, capillary voltage 3500 V, fragmentor voltage 175 V, skimmer voltage 65 V, octopol RF 750 V. For spectral data recording, auto MS/MS mode was used with the range to mass: 90–1050 *m*/*z* and acquisition rate: 2 spectra·s$^{-1}$.

### *2.7. Antioxidant Assay*

Antioxidant activity was carried out using four methods: DPPH, ABTS, CUPRAC, and FRAP. The concentration ranges of resveratrol and vitamin C that were prepared for the study are shown in Table 1.

**Table 1.** Ranges of resveratrol and ascorbic acid concentrations used in studies of antioxidant properties.

| Method | Solution of Resveratrol | Solution of Ascorbic Acid |
|---|---|---|
| DPPH assay | 0.4–0.025 mg·mL$^{-1}$ | 100−10 µg·mL$^{-1}$ |
| ABTS assay | 0.2–0.005 mg·mL$^{-1}$ | 100−10 µg·mL$^{-1}$ |
| CUPRAC assay | 0.4–0.025 mg·mL$^{-1}$ | 125−8 µg·mL$^{-1}$ |
| FRAP assay | 0.2–0.025 mg·mL$^{-1}$ | 300−100 µg·mL$^{-1}$ |

In a 96-well plate, the working solution and sample solution were added (6 replicates for each concentration). The plate was then wrapped with aluminum foil, shaken, and incubated at room temperature (DPPH/ABTS/CUPRAC) or 37 °C (FRAP). Color changes

were read using a Multiskan GO UV reader (Thermo-Scientific, Waltham, MA, USA). The measurements were taken in duplicate. Ascorbic acid was used as a standard.

The most important parameters of each method are shown in Table 2.

**Table 2.** The most important parameters of DPPH, ABTS, CUPRAC, and FRAP activity.

| Method | Sample Solution + Working Solution | Incubation | Measured |
|---|---|---|---|
| DPPH | 25 µL + 175 µL | 30 min reaction, 5 min: 600 rpm, 25 °C | 517 nm |
| ABTS | 10 µL + 200 µL | 10 min reaction, 10 min: 600 rpm, 25 °C | 734 nm |
| CUPRAC | 50 µL + 150 µL | 30 min reaction, 5 min: 600 rpm, 25 °C | 450 nm |
| FRAP | 25 µL + 175 µL | 30 min reaction, 30 min: 100 rpm, 37 °C | 593 nm |

DPPH determination was performed according to the procedure given by Kikowska et al. [30]. A solution of the radical was prepared by dissolving 3.9 mg of DPPH in 50.0 mL of methanol. The solution was shaken in the dark for about 2 h. ABTS assay was performed according to the procedure outlined by Chanaj-Kaczmarek et al. [31]. Preparation of solutions for the assays: 7.0 mM ABTS in water and 2.45 mM aqueous potassium persulfate (1:1 $v/v$) were mixed. The solution was shaken in the dark for about 24 h. It was then diluted with deionized water until the absorbance reached ~0.77 (measured at 734 nm). CUPRAC assay was performed according to the procedure outlined by Özyürek et al. [32]. Preparation of CUPRAC solution: mixed neocuproine solution ($7.5 \times 10^{-3}$ M), 10.0 mM copper (II) chloride solution, ammonium acetate buffer (pH 7.0) (1:1:1 $v/v$). FRAP assay was performed according to the procedure outlined by Benzie et al. [33]. Preparation of test solutions: 25.0 mL of acetate buffer (pH = 3.6), 2.4 mL of TPTZ solution and 2.5 mL of 20 mM aqueous $FeCl_3 \cdot 6\ H_2O$ solution were mixed.

The degree of radical scavenging for DPPH and ABTS effects by the sample was calculated using the following formula:

$$\text{the degree of radical scavenging } (\%) = \frac{A_0 - A_i}{A_0} \cdot 100\%, \quad (1)$$

where $A_0$ is the absorbance of the control and $A_i$ is the absorbance of the sample.

The results of DPPH and ABTS effects are presented as a plot of %inhibition versus concentration. The results of CUPRAC and FRAP effects are presented as a plot of absorbance versus concentration.

The $IC_{50}$ or $IC_{0.5}$ value was determined from linear (Equation (2)) or polynomial (Equation (3)) regression analysis.

$$y = ax + b \quad (2)$$

where $x$ is the final concentrations of the sample, $y$ is the inhibition ratios, and $a$ and $b$ are the coefficients.

$$y = ax^2 + bx + c \quad (3)$$

where $x$ is the final concentrations of the sample, $y$ is inhibition ratios, and $a$, $b$, $c$ are the coefficients.

$X$ (final sample concentration) for $IC_{50}$ was calculated when $Y$ in the regression equation was substituted with 50. For $IC_{0.5}$, $Y$ was substituted with 0.5.

## 3. Results

Evaluation of the radiostability of resveratrol in the solid state 50 h and 597 h (EPR) after exposure to electron beam irradiation (dose of 25 kGy) was carried out by using methods such as EPR, FTIR, HPLC, and HPLC-MS. Changes in the antioxidant properties of irradiated resveratrol were checked (50 h after exposition)) by DPPH, ABTS, CUPRAC, and FRAP assay.

### *3.1. Electron Paramagnetic Resonance (EPR)*

The EPR technique was used to evaluate changes of free radicals in solid-state resveratrol samples after irradiation (dose 25 kGy). Figure 1a shows the concentration of free radicals vs. time after irradiation calculated from EPR spectra for radiation dose 25 kGy. EPR spectra of non-irradiated and irradiated resveratrol recorded 50 and 597 h after irradiation are presented in Figure 1b. The EPR spectrum for the non-irradiated sample does not show any line from free radicals. In contrast, the irradiated sample exhibits a partial decrease of spectral intensity with respect to the time after irradiation. The decrease in free radical concentration vs. time for the irradiated sample can be described by the following equation [27]:

$$C_{tot}(t) = C_s + C_u e^{-\frac{t}{T}} \quad (4)$$

where $C_{tot}(t)$ is the total concentration of free radicals determined at any time $t$ after irradiation, $C_s$ is the concentration of stable radicals, $C_u$ is the concentration of unstable free radicals, t is time after irradiation, $T$ is the mean lifetime of unstable radicals. After fitting the Equation (4) to the experimental points, the following values were obtained: $C_s = 0.14 \pm 0.01$ ppm, $C_u = 0.10 \pm 0.01$ ppm, and $T = 202 \pm 84$ h.

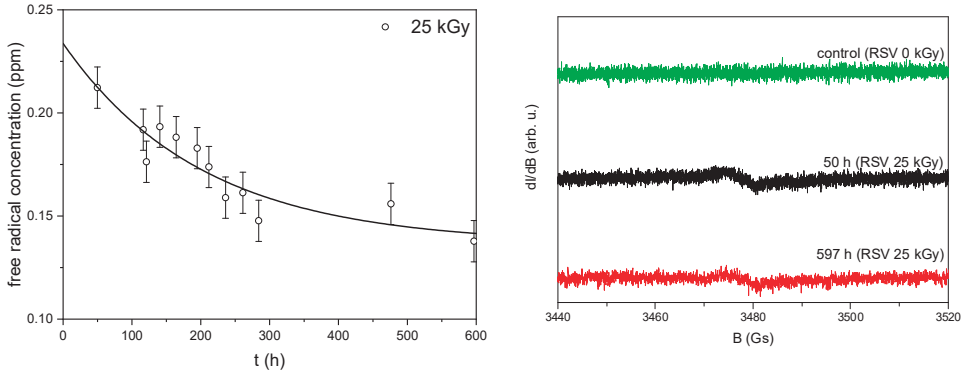


**Figure 1.** (**a**) Concentration of free radical vs. time after irradiation (25 kGy). The solid line is the approximation of Equation (4) to the experimental points; (**b**) EPR spectra of non-irradiated (green) and irradiated resveratrol recorded 50 h (black) and 597 h (red) after 25 kGy dose irradiation.

### *3.2. Fourier Transform Infrared Spectroscopy (FTIR) Analysis*

The assignment of resveratrol bands was made on the DFT study (Figure S1 and Table S1). All characteristic bands of RSV 0 kGy were observed after irradiation with a dose of 25 kGy (RSV 25 kGy, Figure 2a). However, the intensity of the band at about 1465 $cm^{-1}$ (C-C stretching vibrations, C-O-H bending vibration and C-H rocking vibration in the hydroxyphenyl group) increased (Figure 2b). This may indicate minor oxidative damage to RSV molecules at the hydroxyphenyl group caused by free radicals, the presence of which was confirmed by EPR.

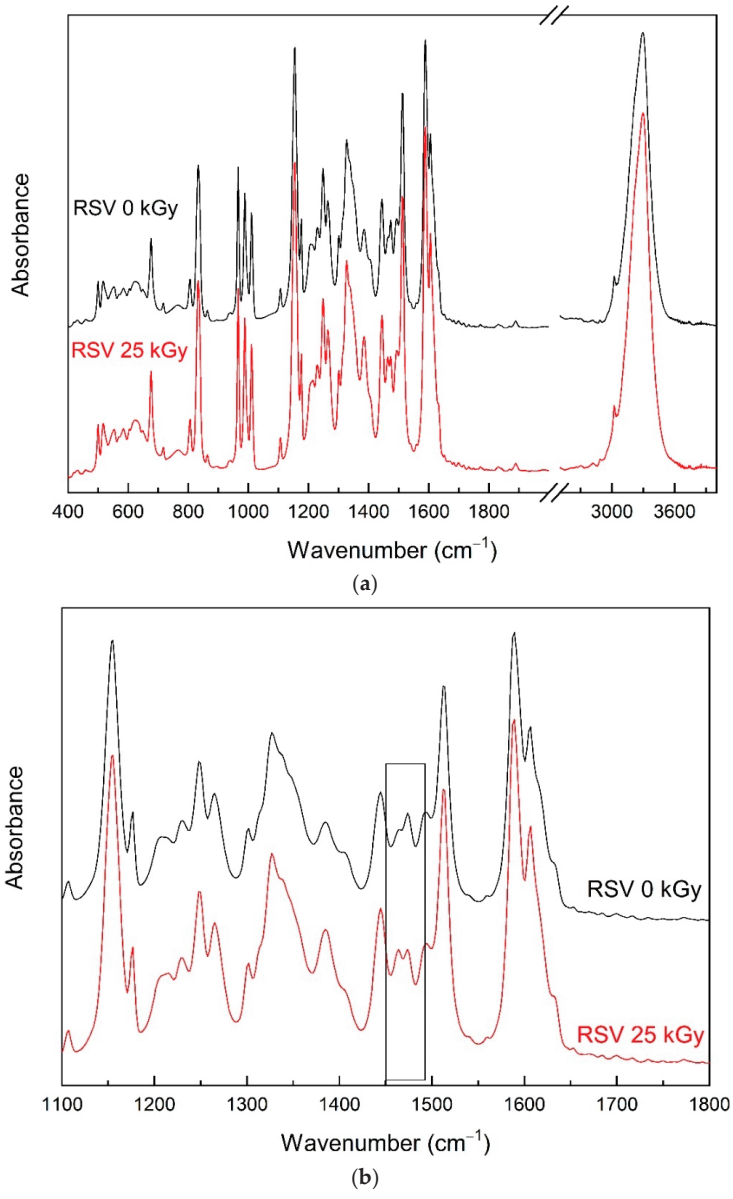


**Figure 2.** IR absorption spectra of non-irradiated (standard—black) and irradiated (red) resveratrol at room temperature: (**a**) range from 400 to 4000 cm$^{-1}$; (**b**) range from 1100 to 1800 cm$^{-1}$.

### *3.3. HPLC and HPLC-MS Analysis*

HPLC and LC-MS confirmed that EBI did not cause conversion from trans- to cis-resveratrol. In addition, no degradation product was confirmed. It is likely that the changes caused by oxidative stress (sugessted in Section 3.2—FTIR analysis) were so small that they could not be recorded by these testing methods.

### *3.4. Antioxidant Properties*

Antioxidant properties of non-irradiated (RSV 0 kGy) and irradiated RSV (25 kGy) was tested using DPPH, ABTS, CUPRAC, and FRAP. The bar graphs (Figure 3) show the $IC_{50}$ values for the DPPH and ABTS assay and the $IC_{0.5}$ values for the CUPRAC and FRAP assay. Resveratrol (0 kGy) shows the best antioxidant properties for tests that rely on the SET mechanism (SET—transfer reaction of a single electron): ABTS (2 µg/mL) and FRAP (5.1 µg/mL). This is also indicated by theoretical calculations by Leopoldini et al. [34]. After irradiation of resveratrol with a dose of 25 kGy, we observe a slight decrease of antioxidant properties in ABTS and FRAP assays, and an increase of antioxidant properties in DPPH and CUPRAC assay, which are based on the HAT (HAT—hydrogen atom transfer) mechanism (Figure 3).

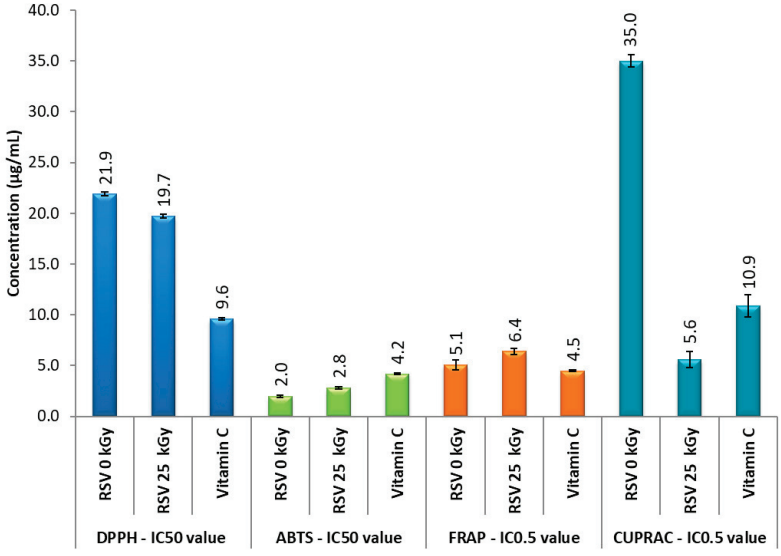


**Figure 3.** Summary of the results of antioxidant tests. Legend: X-axis—$IC_{50}$ (DPPH and ABTS assay) or $IC_{0.5}$ value (CUPRAC and FRAP assay), Y-axis—concentration of the sample, RSV 0 kGy—non-irradiated resveratrol, RSV 25 kGy—irradiated resveratrol.

The changes in antioxidant activity of irradiated RSV may be attributed to the free radicals generated by electron beam radiation, which may cause oxidative damage to the RSV's molecules. FT-IR analysis suggests that the changes involve the site in the structure of resveratrol that is most antioxidant active (position of OH groups in the para position) [35].

## 4. Discussion

The use of electron beam irradiation (EBI) has become an object of interest in the pharmaceutical and food industries due to the great potential of EBI bacteriocide and the fact that it causes less material degradation than other approaches. Nevertheless, it is confirmed that ionizing radiation (β-particles (electrons), γ-radiation, X-rays) may affect the biological properties of substances. The literature indicates the formation of degradation products [17–19], deterioration of antioxidant properties [36–41], improvement of antioxidant properties [42–47], and increase in anti-inflammatory properties [48] of substances exposed to radiation. Since the gas pedal accelerates the electron beam to near the speed of light (~99.999%c), the radiation transmits very high energy, affecting all material components in proportion to their electron contribution. During absorption of ionizing radiation, radicals are formed in the system, which, due to their reactive nature and short

duration, cause complex reactions in the material. As a result, they can lead to changes in the structure, which can have a significant impact on the physicochemical properties of the material under study.

Our research aimed to assess the radiostability of RSV, especially in the context of changes in its antioxidant properties after exposure to ionizing radiation. The studies conducted so far have focused on assessing the effects of the preventive action of resveratrol in living cells. Resveratrol, as with many other polyphenols, is a fundamental component of many nutraceuticals. Ensuring that the manufacturing process does not affect the properties of the product is essential to guarantee its effectiveness. To the best of our knowledge, no work has been published to date on the physicochemical and biological changes of resveratrol after exposure to electron beam irradiation (EBI). On the other hand, the assessment of after irradiation changes in resveratrol is important for the sake of ensuring the quality of resveratrol, when radiation sterilization is used as a compound stabilization technique. In our research, we used a dose of 25 kGy recommended by the pharmacopeia as appropriate to achieve microbiological stabilization and is large enough to exclude any changes in RSV during irradiation in living cells. The RSV post-sterilization changes were evaluated in the solid (EPR and FTIR) and after dissolving in water (HPLC, HPLC-MS).

EPR studies have shown that RSV is very resistant to the formation of radical damage caused by irradiation. The radiation dose of 25 kGy leads to the formation of only a small number of radical defects (not more than $0.24 \pm 0.02$ ppm), characterized by the EPR line with the spectroscopic splitting factor $g = 2.0051 \pm 0.0005$ and linewidth $\Delta Bpp = 5.9 \pm 0.5$ Gs. Most of the radicals, probably those close to the surface, are unstable and they decay when exposed to air particles. While the analysis of the bands of the infrared absorption spectrum of RSV carried out on the basis of a comparison with the theoretical spectrum (obtained as a result of calculations with the use of DFT) confirmed little changes in the hydroxyphenyl group. Bearing in mind that resveratrol requires dissolution in order to deliver it to the body, and the fact that in a dissolved form it is transported in body fluids, its stability in solutions was analyzed. HPLC-MS analysis of the chromatograms excludes the appearance of RSV impurities as radiolysis products. Moreover, the quantitative analysis of the peaks derived from the *trans* RSV isomer excludes its conversion to the cis form as a result of radiation transformation. It is likely that the changes in RSV's structure (confirmed by FTIR analysis) caused by oxidative stress were so small that they could not be recorded by HPLC methods.

It is known that the antioxidant activity of polyphenols is closely related to their structure [35]. Therefore, the next stage of the study was to check the effect of EBI on the antioxidant properties of resveratrol.

RSV 0 kGy has a very different scavenging efficiency on DPPH and ABTS free radicals. It caused by different mechanisms. In the DPPH experiment, the hydrogen supply capacity of a compound determines the scavenging effect of free radicals (HAT mechanism), while ABTS experiment is determined by SET mechanism (single electron transfer) [35]. It is well known that phenolic groups stabilize a radical formed on phenolic carbon with their resonance structure. Due to the deprotonation of the hydroxyl groups present in resveratrol, we distinguish 3 acid dissociation constants: $pKa_1 = 8.8$ (4-OH), $pKa_2 = 9.8$ (3-OH or 5-OH), $pKa_3 = 11.4$ (3-OH or 5-OH). According to the calculations by López et al. the para-4-hydroxy group is more acidic than the two meta-hydroxy groups [49]. Papuc et al. report that the OH group in the para position is the most antioxidant active site in RSV [35]. Test with CUPRAC reagent is carried out at pH = 7.0, which is close to the pH of physiological fluids. For this reason, this method is considered to be more advantageous compared to the FRAP test, which is carried out under alkaline conditions (pH = 3.6).

After irradiation of resveratrol with a dose of 25 kGy, we observed a slight decrease of antioxidant properties in the ABTS and FRAP assays and an increase of antioxidant properties in DPPH assay (a change of 2.2 μg/mL) and CUPRAC assay (a change of 29.4 μg/mL) (Figure 3). The changes in antioxidant activity of RSV 25 kGy may be probably attributed to the oxidative damage of RSV's molecules, caused by the presence of free radicals. Their presence in the RSV 25 kGy sample was confirmed by EPR analysis. In addition,

the FT-IR analysis suggests the changes in RSV's structure concern in the most antioxidant active site of RSV: OH group in the para position. The antioxidant property study conducted clearly indicate that EBI enhanced the action of the HAT mechanism in the DPPH and CUPRAC test.

The obtained results of maintaining or improving the antioxidant properties of counseling resveratrol correspond with the results of other research groups [42–47]. It was confirmed that it is possible to increase the antioxidant potential of biologically active compounds as a result of their exposure to ionizing radiation. For example, Shah et al. [50] reported that after irradiation the DPPH scavenging ability of oat β-glucan increase with irradiation dose (0 kGy: 6%, 6 kGy: 14%, 10 kGy: 19% inhibition). Also, research by Khan et al. showed increased activity for β-D-glucan extracted from *Agaricus bisporus*. The doses of γ radiation they administered were 0–50 kGy, for which the inhibition activity was, respectively, 34.63–49.36% [51]. An increase in DPPH radical scavenging activity with an increase in the irradiation dose was also observed for bean starches [51], soybean [52], and green tea leaf extracts [53]. Slightly increased antioxidant activity was observed for 10–20 kGy of γ irradiation in the case of extracts from *Antrodia camphorata mycelia* [54]. Interesting results were obtained by Ahn et al. for irradiated phytic acid. Non-irradiated phytic acid did not show scavenging ability, whereas phytic acid irradiated at 20 kGy, showed significantly higher DPPH radical scavenging capacity than ascorbic acid at the 800 μM level [55]. On the other hand, there are reports indicating no change or deterioration of antioxidant properties after irradiation [36–41]. For example, Lampart-Szapa et al. reported that increased irradiation doses decreased the antioxidant effect of most lupin extracts [40]. Al-Kuraieef et al. also observed this effect in the case of the methanolic extract of thyme [39]. Other studies conducted for the cinnamon compound in the dose range of 5–25 kGy did not show any effect on the antioxidant activity [36].

## 5. Conclusions

Analysis of the structure of resveratrol exposed to electron beam radiation (25 kGy) allows us to indicate minor oxidative damage to resveratrol molecules. Importantly, these changes improved antioxidant properties of resveratrol based on the HAT mechanism. This knowledge can be helpful in the production of nutraceuticals containing resveratrol in their formulation.

**Supplementary Materials:** The following supporting information can be downloaded at: https://www.mdpi.com/article/10.3390/antiox11112097/s1, Figure S1. Calculation (black-DFT) and experimental (red) IR absorption spectra of resveratrol at room temperature; Table S1. Selected characteristic vibronic features of resveratrol theory with application of 6–31 G (d,p) basis and experiment bands of resveratrol. s-stretching, b-bending, r-rocking, oop-outside of the plane.

**Author Contributions:** Conceptualization, P.Z. and J.C.-P.; methodology, N.R., P.Z., R.S., K.L., W.B. and J.C.-P.; software N.R., P.Z., R.S., K.L. and W.B.; validation, N.R., P.Z., R.S., K.L. and W.B.; formal analysis, N.R., P.Z., R.S., K.L. and W.B.; investigation, N.R., P.Z., R.S., K.L. and W.B.; resources, N.R., P.Z., R.S., K.L. and W.B.; data curation, N.R., P.Z., R.S., K.L. and W.B.; writing—original draft preparation, N.R., P.Z., K.L., W.B. and J.C.-P.; writing—review and editing, J.C.-P.; visualization, N.R., P.Z., R.S., K.L. and W.B.; supervision, P.Z. and J.C.-P. project administration, P.Z. and J.C.-P.; funding acquisition, P.Z. and J.C.-P. All authors have read and agreed to the published version of the manuscript.

**Funding:** This work was supported by the grant OPUS from the National Science Centre Poland UMO-2020/37/B/NZ7/03975.

**Institutional Review Board Statement:** Not applicable.

**Informed Consent Statement:** Not applicable.

**Data Availability Statement:** The data are contained within the article and Supplementary Materials.

**Conflicts of Interest:** The authors declare no conflict of interest.

## References


1. Berman, A.Y.; Motechin, R.A.; Wiesenfeld, M.Y.; Holz, M.K. The therapeutic potential of resveratrol: A review of clinical trials. *NPJ Precis. Oncol.* **2017**, *1*, 35. [CrossRef] [PubMed]
2. Singh, A.P.; Singh, R.; Verma, S.S.; Rai, V.; Kaschula, C.H.; Maiti, P.; Gupta, S.C. Health benefits of resveratrol: Evidence from clinical studies. *Med. Res. Rev.* **2019**, *39*, 1851–1891. [CrossRef] [PubMed]
3. Rossi, D.; Guerrini, A.; Bruni, R.; Brognara, E.; Borgatti, M.; Gambari, R.; Maietti, S.; Sacchetti, G. Trans-resveratrol in nutraceuticals: Issues in retail quality and effectiveness. *Molecules* **2012**, *17*, 12393–12405. [CrossRef]
4. Zhang, L.-X.; Li, C.-X.; Kakar, M.U.; Khan, M.S.; Wu, P.-F.; Amir, R.M.; Dai, D.-F.; Naveed, M.; Li, Q.-Y.; Saeed, M. Resveratrol (RV): A pharmacological review and call for further research. *Biomed. Pharmacother.* **2021**, *143*, 112164. [PubMed]
5. Pan, X.; Zhu, Y.; Lin, N.; Zhang, J.; Ye, Q.; Huang, H.; Chen, X. Microglial phagocytosis induced by fibrillar β-amyloid is attenuated by oligomeric β-amyloid: Implications for Alzheimer's disease. *Mol. Neurodegener.* **2011**, *6*, 45. [CrossRef]
6. Sevcsik, E.; Trexler, A.J.; Dunn, J.M.; Rhoades, E. Allostery in a Disordered Protein: Oxidative Modifications to α-Synuclein Act Distally To Regulate Membrane Binding. *J. Am. Chem. Soc.* **2011**, *133*, 7152–7158. [CrossRef]
7. Zhao, W.; Varghese, M.; Yemul, S.; Pan, Y.; Cheng, A.; Marano, P.; Hassan, S.; Vempati, P.; Chen, F.; Qian, X.; et al. Peroxisome proliferator activator receptor gamma coactivator-1alpha (PGC-1α) improves motor performance and survival in a mouse model of amyotrophic lateral sclerosis. *Mol. Neurodegener.* **2011**, *6*, 51. [CrossRef]
8. Schmatz, R.; Perreira, L.B.; Stefanello, N.; Mazzanti, C.; Spanevello, R.; Gutierres, J.; Bagatini, M.; Martins, C.C.; Abdalla, F.H.; Daci da Silva Serres, J.; et al. Effects of resveratrol on biomarkers of oxidative stress and on the activity of delta aminolevulinic acid dehydratase in liver and kidney of streptozotocin-induced diabetic rats. *Biochimie* **2012**, *94*, 374–383. [CrossRef]
9. Moussa, C.; Hebron, M.; Huang, X.; Ahn, J.; Rissman, R.A.; Aisen, P.S.; Turner, R.S. Resveratrol regulates neuro-inflammation and induces adaptive immunity in Alzheimer's disease. *J. Neuroinflamm.* **2017**, *14*, 1. [CrossRef]
10. Turner, R.S.; Thomas, R.G.; Craft, S.; Van Dyck, C.H.; Mintzer, J.; Reynolds, B.A.; Brewer, J.B.; Rissman, R.A.; Raman, R.; Aisen, P.S. A randomized, double-blind, placebo-controlled trial of resveratrol for Alzheimer disease. *Neurology* **2015**, *85*, 1383–1391. [CrossRef]
11. Brasnyó, P.; Molnár, G.A.; Mohás, M.; Markó, L.; Laczy, B.; Cseh, J.; Mikolás, E.; Szijártó, I.A.; Mérei, A.; Halmai, R. Resveratrol improves insulin sensitivity, reduces oxidative stress and activates the Akt pathway in type 2 diabetic patients. *Br. J. Nutr.* **2011**, *106*, 383–389. [CrossRef] [PubMed]
12. Thazhath, S.S.; Wu, T.; Bound, M.J.; Checklin, H.L.; Standfield, S.; Jones, K.L.; Horowitz, M.; Rayner, C.K. Administration of resveratrol for 5 wk has no effect on glucagon-like peptide 1 secretion, gastric emptying, or glycemic control in type 2 diabetes: A randomized controlled trial. *Am. J. Clin. Nutr.* **2016**, *103*, 66–70. [CrossRef] [PubMed]
13. Bhatt, J.K.; Thomas, S.; Nanjan, M.J. Resveratrol supplementation improves glycemic control in type 2 diabetes mellitus. *Nutr. Res.* **2012**, *32*, 537–541. [CrossRef] [PubMed]
14. Izzo, C.; Annunziata, M.; Melara, G.; Sciorio, R.; Dallio, M.; Masarone, M.; Federico, A.; Persico, M. The role of resveratrol in liver disease: A comprehensive review from in vitro to clinical trials. *Nutrients* **2021**, *13*, 933. [CrossRef]
15. Agarwal, B.; Campen, M.J.; Channell, M.M.; Wherry, S.J.; Varamini, B.; Davis, J.G.; Baur, J.A.; Smoliga, J.M. Resveratrol for primary prevention of atherosclerosis: Clinical trial evidence for improved gene expression in vascular endothelium. *Int. J. Cardiol.* **2013**, *166*, 246–248. [CrossRef]
16. Magyar, K.; Halmosi, R.; Palfi, A.; Feher, G.; Czopf, L.; Fulop, A.; Battyany, I.; Sumegi, B.; Toth, K.; Szabados, E. Cardioprotection by resveratrol: A human clinical trial in patients with stable coronary artery disease. *Clin. Hemorheol. Microcirc.* **2012**, *50*, 179–187. [CrossRef]
17. Ogrodowczyk, M.; Dettlaff, K.; Bednarski, W.; Ćwiertnia, B.; Stawny, M.; Spólnik, G.; Adamski, J.; Danikiewicz, W. Radiodegradation of nadolol in the solid state and identification of its radiolysis products by UHPLC–MS method. *Chem. Pap.* **2018**, *72*, 349–357. [CrossRef]
18. Zalewski, P.; Rosiak, N.; Kilińska, K.; Skibiński, R.; Szymanowska, D.; Tykarska, E.; Piekara-Sady, L.; Lewandowska, K.; Miklaszewski, A.; Piontek, J. The radiolytic studies of panipenem in the solid state. *Acta Pol. Pharm. Drug Res.* **2020**, *77*, 241–250. [CrossRef]
19. Ogrodowczyk, M.; Dettlaff, K.; Kachlicki, P.; Marciniec, B. Identification of Radiodegradation Products of Acebutolol and Alprenolol by HPLC/MS/MS. *J. AOAC Int.* **2015**, *98*, 46–50. [CrossRef]
20. Zhuan, R.; Wang, J. Degradation of sulfamethoxazole by ionizing radiation: Kinetics and implications of additives. *Sci. Total Environ.* **2019**, *668*, 67–73. [CrossRef]
21. Zalewski, P.; Skibiński, R.; Szymanowska-Powałowska, D.; Piotrowska, H.; Kozak, M.; Pietralik, Z.; Bednarski, W.; Cielecka-Piontek, J. The radiolytic studies of cefpirome sulfate in the solid state. *J. Pharm. Biomed. Anal.* **2016**, *118*, 410–416. [CrossRef] [PubMed]
22. Janiaczyk, M.; Jelińska, A.; Woźniak-Braszak, A.; Bilski, P.; Popielarz-Brzezińska, M.; Wachowiak, M.; Baranowski, M.; Tomczak, S.; Ogrodowczyk, M. Electron Beam Radiation as a Safe Method for the Sterilization of Aceclofenac and Diclofenac—The Usefulness of EPR and 1H-NMR Methods in Determination of Molecular Structure and Dynamics. *Pharmaceutics* **2022**, *14*, 1331. [CrossRef] [PubMed]

23. Kilińska, K.; Cielecka-Piontek, J.; Skibiński, R.; Szymanowska, D.; Miklaszewski, A.; Lewandowska, K.; Bednarski, W.; Mizera, M.; Tykarska, E.; Zalewski, P. The Radiation Sterilization of Ertapenem Sodium in the Solid State. *Molecules* **2019**, *24*, 2944. [CrossRef] [PubMed]
24. Kilińska, K.; Cielecka-Piontek, J.; Skibiński, R.; Szymanowska, D.; Miklaszewski, A.; Bednarski, W.; Tykarska, E.; Stasiłowicz, A.; Zalewski, P. The Radiostability of Meropenem Trihydrate in Solid State. *Molecules* **2018**, *23*, 2738. [CrossRef] [PubMed]
25. *ISO 11137-2:2013*; Sterilization of Health Care Products—Radiation—Part 2: Establishing the Sterilization Dose. International Organization for Standardization: Geneva, Switzerland, 2013.
26. Tomé-Carneiro, J.; Gonzálvez, M.; Larrosa, M.; Yáñez-Gascón, M.J.; García-Almagro, F.J.; Ruiz-Ros, J.A.; García-Conesa, M.T.; Tomás-Barberán, F.A.; Espín, J.C. One-year consumption of a grape nutraceutical containing resveratrol improves the inflammatory and fibrinolytic status of patients in primary prevention of cardiovascular disease. *Am. J. Cardiol.* **2012**, *110*, 356–363. [CrossRef]
27. Mai, V.C.; Bednarski, W.; Borowiak-Sobkowiak, B.; Wilkaniec, B.; Samardakiewicz, S.; Morkunas, I. Oxidative stress in pea seedling leaves in response to Acyrthosiphon pisum infestation. *Phytochemistry* **2013**, *93*, 49–62. [CrossRef]
28. Frisch, M.J.; Trucks, G.W.; Schlegel, H.B.; Scuseria, G.E.; Robb, M.A.; Cheeseman, J.R.; Scalmani, G.; Barone, V.; Petersson, G.A.; Nakatsuji, H.; et al. *Gaussian 09, Revision C. 01*; Gaussian, Inc.: Wallingford, CT, USA, 2016.
29. Dennington, R.; Keith, T.; Millam, J. *GaussView*, version 5; Semichem Inc.: Shawnee Mission, KS, USA, 2009.
30. Kikowska, M.A.; Chmielewska, M.; Włodarczyk, A.; Studzińska-Sroka, E.; Żuchowski, J.; Stochmal, A.; Kotwicka, M.; Thiem, B. Effect of pentacyclic triterpenoids-rich callus extract of *Chaenomeles japonica* (Thunb.) Lindl. ex spach on viability, morphology, and proliferation of normal human skin fibroblasts. *Molecules* **2018**, *23*, 3009. [CrossRef]
31. Chanaj-Kaczmarek, J.; Wysocki, M.; Karachitos, A.; Wojcińska, M.; Bartosz, G.; Matławska, I.; Kmita, H. Effects of plant extract antioxidative phenolic compounds on energetic status and viability of Saccharomyces cerevisiae cells undergoing oxidative stress. *J. Funct. Foods* **2015**, *16*, 364–377. [CrossRef]
32. Özyürek, M.; Güçlü, K.; Apak, R. The main and modified CUPRAC methods of antioxidant measurement. *TrAC Trends Anal. Chem.* **2011**, *30*, 652–664. [CrossRef]
33. Benzie, I.F.; Devaki, M. The ferric reducing/antioxidant power (FRAP) assay for non-enzymatic antioxidant capacity: Concepts, procedures, limitations and applications. In *Measurement of Antioxidant Activity & Capacity: Recent Trends and Applications*; Wiley: New York, NY, USA, 2018; Chapter 5; pp. 77–106.
34. Leopoldini, M.; Marino, T.; Russo, N.; Toscano, M. Antioxidant properties of phenolic compounds: H-atom versus electron transfer mechanism. *J. Phys. Chem. A* **2004**, *108*, 4916–4922. [CrossRef]
35. Hussein, M.A. A convenient mechanism for the free radical scavenging activity of resveratrol. *Int. J. Phytomed.* **2011**, *3*, 459.
36. Kitazuru, E.R.; Moreira, A.V.B.; Mancini-Filho, J.; Delincée, H.; Villavicencio, A.L.C.H. Effects of irradiation on natural antioxidants of cinnamon (*Cinnamomum zeylanicum* N.). *Radiat. Phys. Chem.* **2004**, *71*, 39–41. [CrossRef]
37. Byun, M.W.; Son, J.H.; Yook, H.S.; Jo, C.; Kim, D.H. Effect of gamma irradiation on the physiological activity of Korean soybean fermented foods, *Chungkookjang* and *Doenjang*. *Radiat. Phys. Chem.* **2002**, *64*, 245–248. [CrossRef]
38. Byun, M.W.; Yook, H.S.; Kim, K.S.; Chung, C.K. Effects of gamma irradiation on physiological effectiveness of Korean medicinal herbs. *Radiat. Phys. Chem.* **1999**, *54*, 291–300. [CrossRef]
39. Al-Kuraieef, A.N.; Alshawi, A.H. The effect of gamma irradiation on the essential oils and antioxidants in dried thyme. *Int. J. Food Stud.* **2020**, *9*, 203–212. [CrossRef]
40. Lampart-Szczapa, E.; Korczak, J.; Nogala-Kalucka, M.; Zawirska-Wojtasiak, R. Antioxidant properties of lupin seed products. *Food Chem.* **2003**, *83*, 279–285. [CrossRef]
41. Ahn, H.J.; Kim, J.H.; Kim, J.K.; Kim, D.H.; Yook, H.S.; Byun, M.W. Combined effects of irradiation and modified atmosphere packaging on minimally processed Chinese cabbage (*Brassica rapa* L.). *Food Chem.* **2005**, *89*, 589–597. [CrossRef]
42. Rajurkar, N.S.; Gaikwad, K.N. Effect of gamma irradiation on antioxidant activity of *Amoora rohitaka*. *J. Radioanal. Nucl. Chem.* **2012**, *293*, 409–413. [CrossRef]
43. Hussein, S.Z.; Yusoff, K.M.; Makpol, S.; Yusof, Y.A.M. Antioxidant Capacities and Total Phenolic Contents Increase with Gamma Irradiation in Two Types of Malaysian Honey. *Molecules* **2011**, *16*, 6378–6395. [CrossRef]
44. Khalil, M.I.; Sulaiman, S.A.; Alam, N.; Moniruzzaman, M.; Bai'e, S.; Man, C.N.; Jamalullail, S.M.S.; Gan, S.H. Gamma irradiation increases the antioxidant properties of tualang honey stored under different conditions. *Molecules* **2012**, *17*, 674–687. [CrossRef]
45. Jung, H.J.; Park, H.R.; Jung, U.; Jo, S.K. Radiolysis study of genistein in methanolic solution. *Radiat. Phys. Chem.* **2009**, *78*, 386–393. [CrossRef]
46. Choi, J.I.; Kim, J.K.; Srinivasan, P.; Kim, J.H.; Park, H.J.; Byun, M.W.; Lee, J.W. Comparison of gamma ray and electron beam irradiation on extraction yield, morphological and antioxidant properties of polysaccharides from tamarind seed. *Radiat. Phys. Chem.* **2009**, *78*, 605–609. [CrossRef]
47. Lee, H.J.; Yoon, M.; Sung, N.Y.; Choi, J. il Spirogyra varians mutant generated by high dose gamma-irradiation shows increased antioxidant properties. *Radiat. Phys. Chem.* **2012**, *81*, 1017–1019. [CrossRef]
48. Byun, E.-B.; Sung, N.-Y.; Park, J.-N.; Yang, M.-S.; Park, S.-H.; Byun, E.-H. Gamma-irradiated resveratrol negatively regulates LPS-induced MAPK and NF-κB signaling through TLR4 in macrophages. *Int. Immunopharmacol.* **2015**, *25*, 249–259. [CrossRef]
49. López-Nicolás, J.M.; García-Carmona, F. Aggregation state and p K a values of (E)-resveratrol as determined by fluorescence spectroscopy and UV-visible absorption. *J. Agric. Food Chem.* **2008**, *56*, 7600–7605. [CrossRef] [PubMed]

50. Shah, A.; Masoodi, F.A.; Gani, A.; Ashwar, B.A. Effect of γ-irradiation on antioxidant and antiproliferative properties of oat β-glucan. *Radiat. Phys. Chem.* **2015**, *117*, 120–127. [CrossRef]
51. Khan, A.A.; Gani, A.; Shah, A.; Masoodi, F.A.; Hussain, P.R.; Wani, I.A.; Khanday, F.A. Effect of γ-irradiation on structural, functional and antioxidant properties of β-glucan extracted from button mushroom (*Agaricus bisporus*). *Innov. Food Sci. Emerg. Technol.* **2015**, *31*, 123–130. [CrossRef]
52. Variyar, P.S.; Limaye, A.; Sharma, A. Radiation-induced enhancement of antioxidant contents of soybean (*Glycine max Merrill*). *J. Agric. Food Chem.* **2004**, *52*, 3385–3388. [CrossRef]
53. Jo, C.; Son, J.H.; Lee, H.J.; Byun, M.W. Irradiation application for color removal and purification of green tea leaves extract. *Radiat. Phys. Chem.* **2003**, *66*, 179–184. [CrossRef]
54. Huang, S.J.; Mau, J.L. Antioxidant properties of methanolic extracts from *Antrodia camphorata* with various doses of γ-irradiation. *Food Chem.* **2007**, *105*, 1702–1710. [CrossRef]
55. Ahn, H.J.; Kim, J.H.; Jo, C.; Kim, M.J.; Byun, M.W. Comparison of irradiated phytic acid and other antioxidants for antioxidant activity. *Food Chem.* **2004**, *88*, 173–178. [CrossRef]

*antioxidants*

MDPI

*Review*

# Combination Therapy of Radiation and Hyperthermia, Focusing on the Synergistic Anti-Cancer Effects and Research Trends

**Seeun Kwon †, Sumin Jung † and Seung Ho Baek ***

College of Korean Medicine, Dongguk University, 32 Dongguk-ro, Ilsandong-gu, Goyang-si 10326, Republic of Korea
* Correspondence: baekone99@gmail.com
† These authors contributed equally to this work.

**Abstract:** Despite significant therapeutic advances, the toxicity of conventional therapies remains a major obstacle to their application. Radiation therapy (RT) is an important component of cancer treatment. Therapeutic hyperthermia (HT) can be defined as the local heating of a tumor to 40–44 °C. Both RT and HT have the advantage of being able to induce and regulate oxidative stress. Here, we discuss the effects and mechanisms of RT and HT based on experimental research investigations and summarize the results by separating them into three phases. Phase (1): RT + HT is effective and does not provide clear mechanisms; phase (2): RT + HT induces apoptosis via oxygenation, DNA damage, and cell cycle arrest; phase (3): RT + HT improves immunological responses and activates immune cells. Overall, RT + HT is an effective cancer modality complementary to conventional therapy and stimulates the immune response, which has the potential to improve cancer treatments, including immunotherapy, in the future.

**Keywords:** radiation; hyperthermia; cancer; combination therapy; synergistic effect; oxygenation; hypoxia; immune response

**Citation:** Kwon, S.; Jung, S.; Baek, S.H. Combination Therapy of Radiation and Hyperthermia, Focusing on the Synergistic Anti-Cancer Effects and Research Trends. *Antioxidants* **2023**, *12*, 924. https://doi.org/10.3390/antiox12040924

Academic Editors: Elena Obrador Pla and Alegria Montoro

Received: 28 February 2023
Revised: 3 April 2023
Accepted: 12 April 2023
Published: 13 April 2023



## 1. Introduction

Due to the life expectancy of humans increasing, cancer has become a widespread disease affecting many individuals' lives. According to statistics from the American Cancer Society, 1,918,030 new cancer cases and 609,360 cancer-related deaths had been reported in the United States by 2022 [1]. Between the mid-1970s and 2011–2017, the five-year relative survival rate for all types of cancers increased from 49% to 68%. Despite significant therapeutic advances, the toxicity of conventional therapies poses a considerable barrier to their practical application [2].

Therapeutic hyperthermia (HT) can be defined as the local heating of a tumor to 40–44 °C, whereas normal tissues are rarely affected by temperatures below 45 °C [3]. During hyperthermia therapy, the temperature of the affected area is raised to around 40–45 °C (104–113 °F) using different methods, such as microwave, radiofrequency, ultrasound, or infrared radiation. Exposing the body or a specific area of the body to high temperatures is conducted to kill cancer cells or make them more sensitive to other cancer treatments, such as chemotherapy or radiation therapy. Because of its greater perfusion and heat transfer ability, normal tissue can resist heat shock better than cancer cells. In addition, HT does not raise the expression of the apoptosis-signaling p53 protein in normal tissue. HT is known to increase the production of reactive oxygen species (ROS), thereby inducing ROS-dependent cellular damage and cancer cell apoptosis [4]. In addition, targeted HT can increase tumor perfusion and blood flow in a temperature- and time-dependent way [5]. Changes in tumor blood flow may enhance vascular permeability, increase oxygenation, decrease interstitial fluid pressure, and help restore physiological pH to normal levels. HT modulates the tumor microenvironment to enhance radiation efficiency [6]. However,

because of its toxicity, HT may only be administered to patients in good general health. It is generally considered safe and well-tolerated, but, as with any cancer treatment, it can have side effects. High temperature HT over 45 °C may result in diarrhea, nausea, and vomiting [7]. Heating devices, including ultrasonic, radiofrequency, and microwave devices, must restrict electromagnetic radiation dispersion. HT alone may not be sufficient to destroy tumors when combined with other therapies [8].

Radiation therapy (RT), also known as radiotherapy, remains essential to cancer treatment. Approximately 50% of patients undergo RT [9]. High-energy radiation destroys cancer cells or slows down their growth. The radiation can be delivered externally, using a machine that directs high-energy beams of radiation at the cancer, or internally, by placing radioactive material directly into or near the tumor. As with any cancer treatment, RT can have side effects, which vary depending on the area of the body being treated and the dose of radiation being used. Patients receiving RT have been reported to experience increased discomfort, anxiety, and depression [10]. The primary goal of RT is to inhibit the proliferation of cancer cells. RT is well known to induce oxidative stress, resulting in DNA damage and cell death. RT also influences the tumor microenvironment [11]. Endothelial cells are damaged by radiation, which causes inflammation. Some processes occurring in the tumor microenvironment may paradoxically contribute to the activation of immunosuppression and the induction of radioresistance [12].

Both RT and HT have advantages and disadvantages. According to clinical research, they can be used together to compensate for each other's shortcomings [13]. When combined, they exert their greatest impact and function in a synergistic manner. In practice, combination therapy may produce a greater rate of cell death at lower HT temperatures, as well as a considerable increase in the local control of cancer, tumor therapeutic signals, and survival rates [7]. Both RT and HT have benefits over anti-cancer medications because they can reach the local target effectively [14]. Accordingly, it is necessary to actively conduct experimental investigations on the efficacy of these two treatments. Based on this, it would be beneficial to devise and use a novel therapeutic strategy in clinical practice. The current research on RT + HT focuses primarily on its clinical efficacy and experimental research on RT + HT is limited. This study reviews research involving the effect of RT + HT in cancer, including experimental approaches of in vitro and in vivo methods and clinical studies. Here, we discuss the effects and mechanisms of RT and HT based on experimental research, as well as prospects for future research.

## 2. Anti-Cancer Effects of RT + HT Treatment

HT acts as a radiosensitizer and makes tumor cells more susceptible to irradiation [15]. When combined with RT, HT can lead to increased cell death in cancer cells, help to shrink the tumor, and improve survival rates [16]. The results are presented in chronological order.

In 1982, Brewer et al. suggested that consecutive RT with HT was an effective therapy for canine fibrosarcoma [17]. Oral fibrosarcomas were heated to 50 °C for 30 s, and nasomaxillary fibrosarcomas were heated to 43 °C for 30 min after RT (32–48 Gy in total). One year after treatment, five of the nine dogs were disease-free.

Campos et al. observed that the body weight gain and survival rate of subcutaneous sarcoma 180-bearing C3H mice were dramatically enhanced by the combination of RT and HT [18]. The percentage of mice with cancer that survived 90 days following therapy with RT, HT, and RT plus HT was 3.33, 16.67, and 76.67, respectively.

TCD50, which measures the number of infectious viruses or bacteria in a sample, was reduced by RT with HT in the FM3A cells of C3H/He mice, as observed by Yamashita [19]. The TCD50 value for RT was 6024 rad, and RT and HT was 5108 rad.

In a study conducted by Dewhirst et al., 43 dogs with primary canine malignant melanomas were treated with either RT alone or RT (8 × 4.6 Gy) combined with HT (43 °C, 20 min) [20]. An increase in temperature led to an increase in the frequency of complete remissions (CR). For tumors treated with RT alone, the CR rate was 21% (3/14). The CR rate increased to 76% (16/21) with HT addition.

Legorreta et al. reported that two months of treatment with a combination of RT (14 × 3.5 Gy) and HT (44 °C, 30 min) successfully controlled a large infiltrating mast cell sarcoma in a dog [21]. The previously untreatable tumor experienced rapid and successful necrosis with combination therapy.

Morphological and morphometric studies on necrosis were conducted by Patrcio et al. to evaluate the therapeutic benefits of HT (43.5 °C, 30 min) combined with RT (2 × 8.5 Gy) [22]. Two tumors were injected into the right lower leg of male BALB/C mice: undifferentiated carcinoma of the mouse breast (Tx) and sarcoma 37 (S37). The level of necrosis induced by the combination treatment was much higher than that induced by a single treatment.

In 1990, Fujiwara et al. designed a study to assess the effects of RT (5 or 10 Gy), HT (46 °C, 60 min), and RT with HT on the morphological changes and vascular permeability of the rabbit VX-2 tumors [23]. At each time point, tumors treated with RT (10 Gy) and HT demonstrated a greater effect on tumor volume and necrosis than those treated with HT or RT alone. When HT was administered following RT (10 Gy), there was a considerable decrease in the tumor volume, and, after 21 days, the tumor appeared to have disappeared.

Ruifrok et al. devised an experiment to investigate the interactions between interstitial RT and interstitial HT (44 °C, 30 min) [24]. Rhabdomyosarcoma type R1 was transplanted into the left flank of the inbred Wag/Rij female rats. The total radiation dose was between 20 and 115 Gy, administered at a rate of 47 cGy/h. After RT and HT, the tumor volume decreased more rapidly than that after RT alone. In addition, a higher cure rate was observed with a lower dose of RT + HT. When treated with RT alone, 80 Gy resulted in several cures, and 115 Gy resulted in a 100% cure rate. In RT + HT cases, tumors treated with 30 Gy produced several cures, and 80 Gy resulted in a 100% cure rate. The cancer cure rate indicates treatment efficacy. The number of animals without tumor growth after treatment is divided by the total number of animals treated.

The thermal enhancement ratio and therapeutic gain factor were determined by Sougawa et al. for combined RT (7.2 Gy/min) and HT treatments of FSa-II tumors in C3Hf/Sed mice [25]. In addition to RT, HT prolonged the tumor growth time. Step-down heating, first at 45.5 °C for 10 min, followed by 41.5 °C for 60 min, resulted in a larger tumor prolongation delay than single heating (45.5 °C, 10 min). Moreover, these treatments alone did not cause any visible thermal injury to the foot, but they reduced the threshold dose shown in the RT dose–response curves for the foot responses.

Nishimura et al. investigated the effect of the timing and sequence of HT (43.5 °C, 45 min) on fractionated RT (5.5–5.6 Gy/min, 86.2–101.7 Gy for five days) of FSa-II tumors in C3Hf/Sed mice [26]. They examined whether HT should be used as an independent agent or used as a RT sensitizer. Regarding the tumor growth time and TCD50 assays, RT combined with HT had a therapeutic advantage over RT alone. The advantage was most evident when HT was combined with RT simultaneously.

Clamping is a method that cuts off the blood supply to a tumor to create complete hypoxia [27]. In 2001, Uma Devi et al. reported that RT (10 Gy) and HT (43 °C, 30 min) affected clamping-induced ischemia and reperfusion in B16F1-melanoma-bearing C57BL mice. Clamping alone or in conjunction with RT had no noticeable effect on apoptosis. HT under clamping induced a greater than 50% increase in apoptotic cells relative to the control and lowered the microvascular density (MVD) to one-third of the control level. Combining clamping with RT and HT increased the number of apoptotic cells to >70% and decreased MVD to one-sixth of the control level. The combination of RT and HT may be advantageous for the treatment of tumors with ischemia-induced acute hypoxia.

In 2002, Ressel et al. found that a combination of RT (5 × 2 Gy), HT (41.8 °C, 60 min), and cisplatin was significantly effective in the treatment of human head and neck squamous cell carcinoma transplanted into mice [28]. RT with HT was more successful than RT or HT alone in terms of the tumor volume and CR. In the RT group (5 × 2 Gy), the number of CR cases (2/15 mice) was the lowest. The combination of HT (41.8 °C) increased the CR rate (5/15 mice).

Rao et al. examined the response of S180, which was developed intradermally in inbred BALB/c mice after treating solid tumors with bleomycin (BLM), RT (10 Gy), and HT (43 °C, 30 min) [29]. The combination of BLM and HT further enhanced the frequency of micronuclei (MN) in the bimodality groups. At 24 h post-treatment, MN counts in the trimodality group (BLM + RT + HT) did not differ significantly from those of the bimodality treatments. However, trimodality-treated tumors exhibited severe tumor necrosis, indicating increased cell loss and immediate tumor regression.

In 2010, Kalthur et al. treated B16F1 melanoma cells grown in adult C57BL mice with Withaferin A (WA) and HT (43 °C, 30 min) to determine whether the RT response was enhanced [30]. Acute RT (30 Gy) and HT increased tumor growth delay compared with RT (40 Gy) alone. Acute RT and HT and WA and RT induced a partial response (PR) of 50% and 62.5%, respectively, indicating a decrease in tumor size of over 30%. However, RT alone did not produce a PR.

Franken applied the linear quadratic model to assess the efficiency of HT (41 °C or 43 °C, 1 h) with low RT (0.5 Gy) doses against high doses (15–30 Gy) [31]. Human SIHA, SW-1573, and RKO cells, as well as rodent V79, R1, and RUC cells, were used. The linear parameter α and quadratic parameter β determine the effectiveness of radiation at low or high doses. An increase in parameter α compared with parameter β indicates that RT and HT are more effective than RT alone. The differences between the values of α and β were larger at 43 °C than at 41 °C.

In 2015, according to Alya et al., partial body HT (PBH) (43 °C, 1 h) prior to γ-radiation (9 Gy) was advantageous in 396 Wistar rats [32]. This helped to restore normal cells following radiation treatment. Gamma-treated rats of both sexes had a lifespan and mortality prolonged by PBH treatment. In addition, PBH improved the recovery of the bone marrow in the femurs and tibias. PBH-treated males had a survival rate of approximately 35% by day 30, whereas all nine Gy-irradiated males died within 16 days.

Borasi et al. theoretically suggested that patients with glioblastoma multiforme (GBM) could be effectively treated with the rapid HT of a focused ultrasound (FUS) device combined with external beam radiation, which exhibits a low level of tumor cell survival and a long offset time [33].

Masunaga et al. discovered the effect of tirapazamine, metformin, or mild-temperature HT (40 °C, 60 min) on RT (2.5 Gy/min)-treated EL4 tumor total cells and quiescent tumor cells [34]. Mild-temperature HT (MTH) after radiation decreased the surviving fraction and increased the frequency of micronuclei and apoptosis compared to radiation alone. Under HT conditions, quiescent cells exhibited comparatively higher micronucleus and apoptosis frequencies than the total cell population.

Marloes et al. evaluated the radiosensitization effect of HT combined with molecular targeting agents, such as PARP1-i, DNA-PKcs-i, and HSP90-i, in cervical cancer cell lines [35]. The non-homologous end-joining or alternative non-homologous end-joining pathway is blocked when HT is coupled with DNA-PKcs-I and PARP1-i, resulting in a more effective radio enhancement.

Rajaee et al. investigated the effects of RT (6 Gy), HT (43 °C, 30 min), and the combination of RT and HT on human prostate carcinoma in cell line DU145 in both monolayer and spheroidal cultures [36]. In both monolayer and spheroid cultures, RT and HT, rather than RT alone, decreased the survival rate as the RT dose increased. RT and HT decreased the survival fraction in both monolayer and spheroid cultures, with greater effects in monolayer cultures.

McDonald et al. used modulated electro-HT (mEHT) (42 °C, 30 min) to evaluate the synergistic effect of RT (5 Gy) on Gs-9L rat gliosarcoma cells, Madin–Darby canine kidney (MDCK) cells, and MCF-7 cells [37]. When RT was combined with mEHT, the percentage of 9 L gliosarcoma cells decreased more than when treated with RT alone, and mEHT enhanced the mortality of 9 L gliosarcoma cells while preserving the survival of non-cancerous cells. On MCF7 or MDCK cells, however, mEHT had no synergistic effects with RT.

Prasad et al. evaluated the increase in the RT dose with HT [38]. The human lung cancer cell lines A549 and NCI-H1299 were used in vitro, and BALB/c nude mice were used in vivo. Adding HT (42 °C) to RT (2.75 Gy/min) increased the cell death and radiosensitivity of the NCI-H1299 and A549 cells. The equivalent RT dose with RT alone was a total of 60 Gy, whereas HT increased the effect of 60 Gy RT to 70.3 Gy for 40.5 °C, 86.3 Gy for 41.6 °C, and 93.6 Gy for 42.4 °C. Compared to RT or HT alone, RT (2 × 5 Gy) plus HT (42 °C, 30 min) significantly decreased the tumor volume and increased the apoptotic cells in an in vivo study.

In 2020, Brüningk et al. examined the response of tumor spheroids created from two human cancer cell lines (HCT116 and CAL27) to single and combination treatments with RT (2 × 5 and 5 × 2 Gy) and HT (47 °C) [39]. Tumor spheroids are three-dimensional structures composed of cancer cells that imitate the shape and organization of normal tissue [40]. Spheroids are frequently utilized in in vitro research to simulate the formation and activity of tumors as they reflect the complexity and variety of actual tumors more accurately than typical two-dimensional cell cultures [41]. The combination of RT and HT shared the same properties with either RT or HT alone, delaying spheroid growth with increasing RT or HT doses [39]. However, RT combined with HT induced the acceleration of spheroid growth compared to treatment with the relevant RT dose. Considering the finding that the size of the spheroid remained less than that of the control within 21 days, it could be inferred that the additional thermal dose further delayed growth when HT was combined with greater RT doses.

Hu et al. reported that non-invasive FUS-induced cavitation sensitized cancer cells to RT and HT [42]. Head and neck cancer (FaDu), glioblastoma (T98G), and prostate cancer (PC-3) cells were subjected to FUS followed by RT (10 Gy) or HT (45 °C, 30 min). FUS-Cav greatly enhanced the susceptibility of cancer cells to RT and HT by reducing long-term clonogenic survival, short-term cell metabolic activity, cell invasion, and activation of sonoporation.

Elming et al. found that combining HT (41.5 °C, 60 min) with low RT was as effective as high RT in inducing the control of C3H mammary carcinomas in CDF1 mice [43]. In addition, researchers have discovered that a shorter gap between RT and HT induces local tumor control. Only RT and cancer with low LET 240 kV resulted in TCD50 to 53 Gy, and 6 MV X-rays resulted in TCD50 to 55 Gy. RT followed by HT resulted in a TCD50 of 44 Gy and 46 Gy, respectively. Table 1 provides a summary of the studies on the effects and mechanisms of HT and RT.

**Table 1.** Effect of RT + HT on tumor cells (unknown mechanism).

| RT | HT | Cell Line and Observation Model | Classification of the Molecular Mechanism | Ref. |
|---|---|---|---|---|
| 32–48 Gy | 50 °C, 30 s<br>43 °C, 30 min | Oral or external nasal fibrosarcoma, ten dogs/in vivo | Necrosis | [17] |
| - | - | Murine sarcoma, sarcoma 180, C3H mice/in vivo | | [18] |
| 51.08 Gy | 43 °C, 10 min | Murine mammary carcinoma, FM3A, C3H mice/in vivo | | [19] |
| 36.8 Gy<br>(8 × 4.6 Gy) | 43 °C, 20 min | Primary malignant melanoma, 43 dogs/in vivo | | [20] |
| 45.5 Gy<br>(13 × 3.5 Gy) | 44 °C, 30 min | Mast cell sarcoma, a dog/in vivo | Necrosis | [21] |
| 17 Gy<br>(2 × 8.5 Gy) | 43.5 °C, 30 min | Breast carcinoma, Tx; the sarcoma 37, S37, BALB/C male mice/in vivo | Necrosis | [22] |
| 10 Gy | 46 °C, 60 min | Shope-virus-induced skin papilloma, VX-2, rabbits/in vivo | Necrosis | [23] |

**Table 1.** *Cont.*

| RT | HT | Cell Line and Observation Model | Classification of the Molecular Mechanism | Ref. |
|---|---|---|---|---|
| 30 Gy | 44 °C, 30 min | Rhabdomyosarcoma, R-1, Wag/Rij female rats/in vivo | | [24] |
| 7.2 Gy/min (total dose not reported) | 45.5 °C, 10 min; followed by 41.5 °C, 60 min | Murine fibrosarcoma, FSa-II, C3Hf/Sed mice/in vivo | | [25] |
| 5.5–5.6 Gy/min (86.2–101.7 Gy for five days) | 43.5 °C, 45 min | Murine fibrosarcoma, FSa-II, C3Hf/Sed mice/in vivo | | [26] |
| 10 Gy | 43 °C, 30 min | Murine melanoma, B16F1, C57BL mice/in vivo | Apoptosis | [27] |
| 10 Gy (5 × 2 Gy) | 41.8 °C, 60 min | Human-derived head and neck squamous cell carcinoma, athymic nude mice/in vivo | | [28] |
| 10 Gy | 43 °C, 30 min | Murine sarcoma, Sarcoma 180 (S180), Balb/c mice/in vivo | Necrosis | [29] |
| 30 Gy | 43 °C, 30 min | Murine melanoma, B16F1, C57BL mice/in vivo | | [30] |
| 0.5 Gy/min (total dose not reported) | 41 and 43 °C, 30 min | Human origin cervical carcinoma, SIHA; non-small-cell squamous lung carcinoma, SW-1573; colon cancer, RKO; rodents cell line V79, R1 and RUC/in vitro | | [31] |
| 9 Gy | 43 °C, 60 min | 396 Wistar rats / in vivo | | [32] |
| 36 Gy | 43 °C, 60 min | Human glioblastoma, U-87MG/in vitro | | [33] |
| 2.5 Gy/min (total dose not reported) | 40 °C, 60 min | Lymphoma, EL4, C57BL/6J mouse/in vitro | Apoptosis | [34] |
| 2 Gy | 42 °C, 60 min | Cervical cancer, SiHa and HeLa/in vitro | | [35] |
| 6 Gy | 43 °C, 60 and 90 min | Human prostate cancer stem cells (CSCs), DU145/in vitro | | [36] |
| 5 Gy | 42 °C, 30 min | Rat gliosarcoma, Gs-9L; non-cancerous tissue of canine kidney, MDCK; human-derived breast cancer, MCF-7/in vitro | Apoptosis | [37] |
| 10 Gy (2 × 5 Gy) | 42 °C, 30 min | Lung cancer, A549 and NCI-H1299, BALB/c nude mice/in vitro, in vivo | Apoptosis | [38] |
| 2 and 5 Gy | 47 °C, 0–780 CEM43 | Human colon cancer, HCT116; oral squamous carcinoma, CAL27/in vitro | Apoptosis, Necrosis | [39] |
| 10 Gy | 45 °C, 30 min | Human head and neck cancer, FaDu; human glioblastoma, T98G; human prostate cancer, PC-3/in vitro | | [42] |
| 44 and 46 Gy | 41.5 °C, 60 min | Mammary carcinoma cell line, C3H, CDF1 mice/in vivo | | [43] |

## 3. Physiological Changes Induced by RT + HT

### *3.1. Oxygenation*

Rapid and uncontrolled tumor growth restricts the availability of oxygen, leading to hypoxia [44]. The expressions of pro-angiogenic factors, such as vascular endothelial growth factor (VEGF), platelet-derived growth factor (PDGF), and hypoxia-inducible factor 1α (HIF-1α), are induced by hypoxia. HIF-1α activates the expression of pro-angiogenic factors, leading to hypoxia-induced angiogenesis to provide sufficient oxygen, blood supply, and nutrients for tumor growth. Hypoxia causes a disorganized distribution of the tumor vasculature, which increases the distance between capillaries, resulting in chronic hypoxia and necrosis. This can render tumors resistant to certain types of cancer treatments.

HT combined with RT can help overcome hypoxia in tumors by increasing blood flow to the tumor cells [45]. By increasing the oxygen supply, the activation of HIF-1α is not stimulated to suppress the growth of cancer. Additionally, the heat generated by HT can directly damage tumor cells, making them more vulnerable to the effects of radiation therapy. HT enhances the effect of RT by increasing the oxygen supply to target tumors, namely reoxygenation.

In 1994, Nishimura and Urano observed that HT (43.5 °C, 45 min) prior to RT (5.5–5.6 Gy/min) sensitized the normal tissue response to RT, regardless of whether RT is administered in a single dose or in fractionated doses, with no thermal radiosensitization [46]. Isotransplants of FSa-II and Mca were irradiated under hypoxia or air, and the TCD50 (50% tumor control dose) was assessed. The increasing disparity between the TCD50 values of hypoxia and air without HT shows that considerable reoxygenation occurred during fractionated irradiation. Following fractionated irradiation, the TCD50 (with heat in the air) was less than that of TCD50 (RT alone in the air), indicating that HT did not affect tumor reoxygenation.

Vujaskovic et al. investigated physiological changes induced by RT and HT in spontaneous canine soft tissue sarcomas [47] and effects of local heat on oxygenation, extracellular pH (pHe), and blood flow in spontaneous canine soft tissue sarcomas. Overall, tumor oxygenation improved, tumor perfusion increased reliably with thermal dose (most significant at T50 < 44 °C), and pHe levels decreased at higher T50 values. In addition, the effects of HT on physiological tumor parameters are biphasic. While perfusion and oxygenation are often increased at lower temperatures, vascular damage is prone to occur at higher temperatures, which leads to greater hypoxia.

In 2001, Ressel et al. studied the effects of different treatment modalities on oxygenation [48]. Head and neck squamous cell carcinoma xenografts obtained from humans were treated with various treatment methods and combinations thereof (RT with 5 × 2 or 10 × 2 Gy; HT at 41 °C or 41.8 °C; chemotherapy with ifosfamide or cisplatin). The median value of pO2 increased within the treatment time in all groups except the control group, and the proportion of pO2 below 10 mmHg reduced consistently. The groups with trimodality had the largest difference between the median pO2 values and the fraction of pO2 measurements below 10 mmHg and had the highest rate of CR at day 60.

Thrall et al. reported changes in tumor oxygenation under a fractionated course of combined treatments of RT (25 × 2.25 Gy) and HT (43 °C) using seven canine soft tissue sarcomas [49]. HT improved oxygenation in tumors that had low pretreatment oxygenation and remained throughout the course of fractionated irradiation. This may contribute to the increase in the cell killing effect of RT.

In 2018, Jabbari et al. studied the synergistic effect of HT combined with RT and calcium carbonate nanoparticles (CCNPs) on the proliferation of the human breast cancer cell line, MCF-7 cells [50].

Kim et al. reported that MTH suppresses the RT-induced upregulation of HIF-1 and its target genes by enhancing oxygenation in FSa-II fibrosarcoma tumors in vivo [51]. RT (15 Gy) led to a significant decrease in blood perfusion, an increase in hypoxia, and an upregulation of HIF-1α and VEGF, which promoted revascularization and recurrence. However, MTH (41 °C, 30 min) increased blood perfusion and tumor oxygenation, thereby inhibiting RT-induced HIF-1 and VEGF in tumors, which may result in the increased death of tumor cells and a delay in tumor growth.

Sadeghi et al. revealed that radiation effectiveness is enhanced by the HT-triggered release of the hypoxic cell radiosensitizer pimonidazole (PMZ) from temperature-sensitive liposomes (TSL) [52]. The effectiveness of TSL-PMZ in combination with RT and HT was evaluated in vitro to assess cell survival and DNA damage. Upon heating (42 °C, 5 min), the TSL-PMZ rapidly released substantial levels of PMZ, and the combination of PMZ-loaded TSLs with HT enhanced the effectiveness of RT under hypoxic conditions.

RT and HT can also affect ATP production by damaging cellular DNA, which can disrupt the normal metabolic processes that generate ATP. This can cause cells to have

less energy available for repair and make them more vulnerable to RT. In 1987, Sijens et al. investigated the response of murine mammary carcinoma NU-82 cells to RT and HT [53]. The ATP/Pi ratio was found to decrease, particularly at higher temperatures. The changes in phosphodiesters seemed to be correlated linearly with the decrease in ATP, especially when treated with RT (20 Gy) plus HT (44 °C, 15 min). Moreover, heavier doses not only temporarily induce decreases in tumor perfusion but also result in necrosis, as opposed to lower doses.

### *3.2. DNA Damage*

Radiation causes the generation of highly reactive free radicals and lethal DNA lesions. Heat stimulates radiation-induced DNA damage by generating more oxidative stress, thus directly damaging tumor cells [54]. These synergistic effects increase the susceptibility of tumor cells to cell death. Several studies have reported that proteins or genes such as RBL1 [55], p53 [56], Rad51 [57], and BRCA2 [58] are involved in DNA repair. Mutations or loss of function of these proteins or genes have been implicated in cancer, and RT + HT has shown an inhibitory effect on cancer proliferation by regulating these factors.

As the tumor suppressor gene *p53* plays a crucial role in cell cycle arrest, apoptosis, and DNA repair inhibition, its mutation might result in ineffective cancer treatment [59]. A study in 2005 showed that the hyperthermic augmentation of tumor growth suppression by irradiation is dependent on the *p53* gene state, using two types of cancer cell lines with different *p53* gene statuses (wtp53, mp53), treated with a combination of X-ray irradiation (2 Gy) and HT (42 °C, 20 min) [59]. Cell growth inhibition was assessed via the Bax and Caspase-3 pathways and the activation of Caspase-3 by PARP and Caspase-3 fragmentation. The hyperthermic augmentation of radiation-induced tumor growth suppression may result in *p53*-dependent apoptosis due to heat-induced inactivation of the cell survival system via control of the cell cycle or promotion of DNA repair.

In 2007, Masunaga et al. demonstrated that MTH inhibits the repair of radiation-induced damage, as measured by the micronuclei (MN) frequency of the total cell and quiescent cell (Q cell) populations in SCC VII tumors in vivo, under high-dose-rate (HDR) or low-dose-rate irradiation immediately followed by MTH (40 °C, 9 h) or the administration of caffeine or wortmannin [60]. MTH effectively reduced the loss in sensitivity in both the total and Q cell populations, thereby reducing the irradiation dose rate. In 2019, they investigated the effects of *p53* status on tumor cells [61]. Human head and neck squamous cell carcinoma cells transfected with mutant TP53 (SAS/mp53) or with neovector (SAS/neo) were injected into nude mice, received HDR immediately, followed by localized MHT (40 °C, 2 h) or caffeine or wortmannin administration. Contrary to the slight recovery of the total or Q tumor cells within SAS/mp3 tumors, SAS/neo tumor cells showed much less sensitivity due to the *p53* recovery from radiation-induced damage. Through two studies, it was concluded that MTH effectively suppressed recovery from radiation-induced damage, as well as wortmannin treatment combined with irradiation.

In 2013, Genet et al. suggested that HT inactivates homologous recombination repair and sensitizes cells to ionizing radiation in a time- and temperature-dependent manner using AG1521 human fibroblast cells and a series of DNA-repair-deficient Chinese hamster cells [62]. At and above 42.5 °C, significant changes in cellular toxicity due to HT were identified. Dissociation and subsequent reformation of Rad51 proteins at DNA double-strand break (DSB) sites in response to HT, which were identified as the major DNA repair proteins, are crucial in HT-induced radiosensitization.

Bergs et al. investigated the effects of HT on genotoxicity and radiosensitization by exposing SW1573 and RKO cells to HT (41 °C, 60 min) prior to irradiation (4 Gy) [63]. Exposure to HT radiosensitized RKO cells by inducing BRCA2 degradation and chromosomal translocation. Chromosomal translocations suggest the genotoxic effects of combined exposure of RT and HT. This was discovered quickly after combined exposure for 1 h but not detectable at 24 h after treatment.

Oorschot et al. suggested that HT and DNA-PKcs inhibitors pre-treatment can inhibit DNA-DSB repair and enhance RT-induced cancer cell cytotoxicity [64]. DSB can repair non-homologous end-joining or recombination. This may affect the efficacy of RT. In this study, suppression of DNA-DSB repair by HT (42 °C, 1 h) and the DNA-PKcs inhibitor NU7441 radiosensitizes human cervical and breast cancer cells and primary human breast cancer sphere cells (BCSCs).

In 2019, Son et al. demonstrated that irradiation (3 Gy) combined with HT (44 °C, 60 min) inhibited the progression of lung cancer via elevated NR4A3 and KLF11 expression, which is critical for enhancing the effectiveness of combined treatment [65]. A549 lung cancer cells exhibited increased levels of NR4A3 and KLF11 after combination therapy, which also induced apoptosis and inhibited cell proliferation by elevating intracellular ROS levels.

Singh et al. observed that, when RT and HT (42 °C, 30 min) were combined, there was additional DNA damage, and no repair was identified 30 min post-irradiation, which may be due to the HT-dependent suppression of DNA repair post-irradiation, as described by previous researchers [66].

Khurshed et al. demonstrated that the addition of HT (42 °C, 60 min) enhanced the efficiency of multimodal therapy with RT, cisplatin, and PARPi in *IDH1*$^{MUT}$, *IDH1*$^{WT}$ HCT116 colon cancer cells, and Hyperthermia1080 chondrosarcoma cancer cells [67]. Isocitrate dehydrogenase 1 (IDH1) is a homodimeric enzyme that catalyzes the conversion of isocitrate to α-ketoglutarate (αKG) via the reduction of NADP+ to NADPH. Mutations in *IDH1* lead to neomorphic IDH activity that converts αKG into the oncometabolite *D*-2 hydroxyglutarate (*D*-2HG), which suppresses the homologous recombination repair system and decreases intracellular reducing power (NADPH), resulting in improved cellular sensitivity to multimodal therapies and tumor progression. The combination of RT and HT resulted in an increase in DSBs and cell death by up to 10-fold in *IDH1*$^{MUT}$ cancer cells compared to *IDH1*$^{WT}$.

### *3.3. Cell Cycle Arrest*

Cell cycle arrest is an essential process as it prevents damaged cells from entering mitosis and helps them secure time for investigating their own DNA repair systems [68]. Defects in the G2/M arrest checkpoint allow damaged cells to initiate mitosis and undergo apoptosis, which may enhance the effectiveness of anti-cancer treatments by enhancing their cytotoxicity. HT can induce G2/M phase arrest via the ATM pathway [69]. Radiation also damages DNA and induces cell cycle arrest [70].

In 2002, Yuguchi et al. compared the antiproliferative effects of HT, RT, and combination therapy for esophageal cancer in humans, primarily using cell cycle analysis [71]. It is reported that HT (43.5 °C, 60 min) delayed the progression of cell cycles from the G0/G1 phase to the S-G2/M phase, and RT (5 × 2 Gy) accelerated the inhibition of DNA synthesis. This may result in a strong inhibitory effect on tumors and a high rate of apoptosis, leading to an accumulation of cells in the G2/M phase. The combined treatment enhanced the synergistic effects by inducing apoptosis.

### *3.4. Apoptosis*

Apoptosis is triggered by a variety of cellular stressors, including intrinsic stressors (e.g., genomic damage) and extrinsic stressors (e.g., binding to death receptors, heat, radiation, and hypoxia) [72]. Cancer proliferation is enhanced by the loss of balance between pro- and anti-apoptotic proteins, death receptor activation, and the AKT pathway. Several studies have shown that RT + HT can trigger apoptosis by modulating these elements.

#### 3.4.1. Intrinsic Apoptosis

Intrinsic apoptosis is a highly regulated and programmed cellular process that is essential for maintaining tissue homeostasis and eliminating damaged or abnormal cells. A variety of intracellular signals, such as DNA damage, oxidative stress, and the presence

of misfolded proteins, activate the intrinsic pathway of apoptosis. The key regulators of intrinsic apoptosis are the Bcl-2 family of proteins, which are classified as either pro-apoptotic or anti-apoptotic based on their function. Pro-apoptotic Bcl-2 proteins, such as Bax and Bak, promote the release of cytochrome C from the mitochondria, which then activates cleavage of caspase enzymes to induce the morphological changes associated with apoptosis (cell shrinkage and fragmentation) [73]. Cancer cells can evade apoptosis by various mechanisms, such as mutations in the Bcl-2 family of proteins, which alter their function and promote cell survival [74]. HT studies demonstrated an induction of the intrinsic apoptosis pathway of cancer cells [75]. HT can also sensitize cancer cells to achieve higher cytotoxicity by RT. Here, we describe studies on this.

Bax plays an essential role in the intrinsic apoptotic pathway. Cancer cells evade apoptosis by upregulating Bcl-2 anti-apoptotic proteins or downregulating pro-apoptotic proteins [76]. Direct activation of the Bax protein stimulates mitochondrial membrane permeabilization and the release of the apoptotic factor cytochrome C, leading to cell death [77].

Liang et al. examined alterations in apoptotic gene expression in human colon cancer cells (HT29) under different treatment modalities and combinations thereof (RT with 10 Gy; HT at 43 °C) [78]. All treatment modalities decreased the expression of p53 and Bcl-2 while increasing the expression of Bax. It was concluded that HT improves the efficacy of RT and chemotherapy against cancers by altering the expression of apoptotic genes.

In 2019, Talaat et al. showed the effectiveness of moderate HT in conjunction with RT for the treatment of hepatocellular carcinoma [79]. In the 40 °C/4 Gy/48 h group, a smaller proportion of viable cells and a high percentage of apoptotic (31%) and necrotic (63%) cells were observed, along with an increase in the expression of pro-apoptotic *Bax* and *FasL* genes, moderate expression of anti-apoptotic *Bcl-2* and *GRP78* genes, and a significant decrease in pro-angiogenic mediators VEGF and PDGF.

#### 3.4.2. Extrinsic Apoptosis and Other Pathways

The extrinsic apoptosis pathway plays a critical role in the immune surveillance of cancer cells. Cancer cells evade extrinsic apoptosis by various mechanisms, such as downregulating death receptors or blocking the downstream signaling cascade, such asAKT pathways. Therapeutic strategies targeting the extrinsic pathway of apoptosis have shown promise in treating cancer, particularly in combination with other therapies. Resistance to extrinsic apoptosis remains a significant challenge in cancer therapy. Applying HT and RT together induces apoptosis (both intrinsic and extrinsic) of cancer cells [79], showing a promising effect as an effective therapeutic strategy.

In 2021, Singh et al. demonstrated that the combination of HT and proton beam radiation (PBRT) might greatly accelerate chordoma cell death by activating the death receptor pathway and apoptosis, which holds promise for the treatment of metastatic chordoma [80]. HT followed by PBRT enhanced cell killing in human chordoma cell lines (U-CH2, Mug–Chor1), exhibiting an RT-dose-dependent decrease in brachyury expression, which could be an indication of chordoma aggression levels and enhanced HSP-70 expression. Overexpression of the brachyury gene is reported to be the most selectively critical gene in chordoma and is targeted as a potential mediator for cancer therapy [81].

AKT is a protein kinase that plays a key role in the PI3K/AKT signaling pathway in the regulation of cell growth, survival, and differentiation. It has been shown that the PI3K/AKT signaling pathway is frequently implicated in the pathogenesis of many cancers and has been validated as a promising therapeutic target [82]. RT and HT have been suggested to inhibit the AKT signaling pathway.

Man et al. showed that HT improves glioma stem-like cell (GSC) radiosensitivity by inhibiting AKT proliferative and pro-survival signaling by identifying the survival kinase AKT as a crucial sensitization factor for GSCs [83]. GSCs treated with HT (42.4 °C, 60 min) prior to irradiation exhibited a decrease in the activation of AKT and proliferation, in con-

trast to increased AKT activation in GSCs when treated with RT alone. Radiosensitization induced by HT further increased the pharmacological suppression of PI3K.

We have summarized the studies on the effects and mechanisms of RT + HT, including hypoxia, DNA damage, cell cycle, and induction and regulation of apoptosis, in Table 2.

**Table 2.** Oxygenation, DNA damage and cell cycle arrest, induction, and regulation of apoptosis.

| RT | HT | Cell Line and Observation Model | Classification of the Molecular Mechanism | Molecular Mechanism | Ref. |
|---|---|---|---|---|---|
| 20 Gy | 44 °C, 15 min | Murine mammary carcinoma, NU-82, DBA-2 mouse/in vivo | Necrosis/ ATP depletion | Pi ↑, ATP and phosphodiesters ↓ | [53] |
| 102.8 Gy (FSa-II); 40.4 Gy (MCa) | 43.5 °C, 45 min | Spontaneous murine fibrosarcoma, FSa-II; mammary carcinoma, MCa, C3Hf/Sed mice/in vivo | Oxygenation | - | [46] |
| 56.25 Gy (25 × 2.25 Gy) | 44 °C | Spontaneous canine soft tissue sarcomas, 13 dogs/in vivo | Oxygenation | pO2 ↑, tumor perfusion ↑, hypoxic fraction ↓, pHe ↓ | [47] |
| 10 Gy (5 × 2 Gy) | 41.8 °C, 60 min | Human-derived head and neck squamous carcinoma, athymic nude (nu-nu) mice/in vivo | Oxygenation | pO2 ↑ | [48] |
| 10 Gy (5 × 2 Gy) | 43.5 °C, 60 min | Human esophageal carcinoma SGF-3, −4, −5, −7, −8, and −9/in vitro | Cell cycle arrest | Chromosomal aberrations, G2/M phase accumulation | [71] |
| 2 Gy | 42 °C, 20 min | Cancer cell lines carrying a different p53 gene status (wt p53 and m p53)/in vitro | Apoptosis/ DNA damage | p53–dependent apoptosis, Bax and Caspase-3 pathways | [59] |
| 56.25 Gy (25 × 2.25 Gy) | 43 °C, CEM43°CT90 = 10 and 40 min | Canine soft tissue sarcomas/in vitro | Oxygenation | - | [49] |
| 10 Gy | 43 °C, 60 min | Human colon cancer, HT29, nude mice/in vivo | Apoptosis/ Bax | p53 and Bcl-2 ↓, Bax ↑ | [78] |
| 2.75 Gy/min (total dose not reported) | 40 °C, 9 h | Squamous cell carcinoma, SCC VII, C3H/He mice/in vivo | DNA damage | Change in MN frequency | [60] |
| 1 Gy | 42.5 °C, 60 min | Chinese hamster ovary cells, CHO WT (CHO 10B2); normal human fibroblast cell line, AG1521; DNA repair deficient CHO mutants, V3 (DNA-PKcs), irs1SF (XRCC3), KO40 (FancG), 51D1 (Rad51D), and xrs5 (Ku80); V79 mutants irs1 (XRCC2) and irs3 (Rad51C)/in vitro | DNA damage | Chromosomal aberrations, Rad51 activity at DSBs | [62] |
| 2 Gy | 42.4 °C, 60 min | GSC, patient specimens 3691 and 387, athymic nude mice/in vitro, in vivo | Apoptosis/ AKT | DNA repair ↓, AKT Signaling ↓ | [83] |
| 4 Gy | 41 °C, 60 min | Human lung carcinoma, SW-1573; human colorectal carcinoma, RKO/in vitro | Apoptosis/ DNA damage | Chromosomal aberrations and translocation, BRCA2 degradation, homologous recombination pathway ↓ | [63] |
| 4 Gy | 42 °C, 60 min | Human cervical cancer, HeLa and SiHa; human breast cancer, MCF7, and T47D; primary human breast cancer, BCSC, athymic mice/in vivo (SiHa), in vitro | Apoptosis/ DNA damage | DNA-DSB repair ↓, G2/M phase arrest, Caspase-3 activity ↑ | [64] |

**Table 2.** *Cont.*

| RT | HT | Cell Line and Observation Model | Classification of the Molecular Mechanism | Molecular Mechanism | Ref. |
|---|---|---|---|---|---|
| 2 Gy | 41 °C, 60 min | Human breast adenocarcinoma, MCF-7/in vitro | Apoptosis/ Oxygenation | ROS ↑, Caspase-3 and –9 ↑ | [50] |
| 15 Gy | 41 °C, 30 min | Fibrosarcoma, FSa-II, C3H mice/in vivo | Apoptosis/ Oxygenation | HIF-1a and VEGF ↓ | [51] |
| 4 Gy | 40 °C, 48 h | Liver cancer, HepG2/in vitro | Apoptosis, Necrosis/ Bax | Bax and FasL ↑, VEGF and PDGF ↓ | [79] |
| 8.5, 14, and 21 Gy (LDR); 4, 8.5, 14.5, 20, and 24 Gy (HDR) | 40 °C, 2 h | Human head and neck squamous cell carcinoma, SAS, nude mice/in vivo | Apoptosis/ DNA damage | Tumor sensitivity ↓, p53-dependent recovery | [61] |
| 4 Gy | 42 °C, 5 min | Human hypopharyngeal carcinoma, FaDu/in vitro | Oxygenation | histone γH2AX phosphorylation ↑ | [52] |
| 3 Gy | 44 °C, 60 min | Human non-small-cell lung cancer, A549 and NCI-H292/in vitro, in vivo | Apoptosis/ DNA damage, HSP70 | KLF11 and NR4A3↑, intracellular ROS ↑ | [65] |
| 2 Gy | 42 °C, 30 min | DNA extracts/in vitro | DNA damage | - | [66] |
| - | - | Human chordoma, U-CH2 and Mug-chor1/in vitro | Apoptosis/ gene expression, HSP70 | Brachyury ↓, death receptor activation | [80] |
| 2 Gy | 42 °C, 60 min | Colon cancer, $IDH1^{MUT}$ and $IDH1^{WT}$ HCT116; chondrosarcoma, Hyperthermia1080 cells/in vitro | DNA damage | NADPH↓, homologous recombination repair ↓ | [67] |

## 4. Immune Response

### *4.1. Cytokines and Antibodies*

HT can cause cancer cells to release antigens, which are molecules that help the immune system recognize and target cancer cells more effectively [84]. When combined with RT, HT can enhance immunological responses against cancer by triggering the release of antigens and cytokines (e.g., HSP70 and HMGB1), increasing the activity and number of immune cells, such as natural killer (NK) cells, dendritic cells, and T cells [85]. HSPs can efficiently enhance the immune response [86]. HSP70, a molecular chaperone protein, binds and delivers tumor antigens to antigen-presenting cells when released. Tumor antigens are subsequently presented by dendritic cells (DCs), which stimulate the CD8+ T cell response [87]. In addition, HSP promotes the release of inflammatory cytokines by DCs. Studies focusing on immune responses caused by HT and RT, especially the ones aiming to determine the role of cytokines, were completed in cell models.

In 2009, Schildkopf et al. examined which form of cell death was induced by treating the human colorectal cancer cell line HCT15 with HT (41.5 °C, 60 min) and X-irradiation (5 Gy) [88]. Although the proportion of apoptotic cells did not change, necrosis was the predominant form of cell death following combination treatment. Radioresponsive G2 cell cycle arrest and the release of the danger signal HMGB1 were observed, implying that the combination of RT and HT may contribute to inflammation and immunological activation. In 2010, the same group additionally experimented with human colorectal adenocarcinoma cells with different radiosensitivities using HT (41.5 °C, 60 min) and X-ray irradiation (5 or 10 Gy) [89]. Combinatorial treatment may induce anti-tumor immunity due to the induction of inflammatory necrotic cells and HMGB1 release.

Again, in 2011, Schildkopf et al. demonstrated that RT with HT stimulates the HSP70-dependent maturation of dendritic cells and the release of pro-inflammatory cytokines (IL-8 and IL-12) by dendritic cells and macrophages, in vitro and in vivo, using HCT15 and

SW480 [90]. The same HT condition was used, being combined with 2, 5, or 10 Gy X-rays. Combination therapy could boost the expression of surface HSP70, as well as significantly upregulate the co-stimulatory protein CD80 and chemokine receptor CCR7 on DC in a manner dependent on extracellular HSP70.

Wang et al. investigated the effects of magnetic induction HT (MIH) on a 4T1 mouse model of metastatic breast cancer [91]. When treated with MIH and RT (6-MV X-rays), there was a substantial decrease in tumor volume and lung metastasis, improvement in survival and Bax expression, and greater CD4 + T cell percentage and CD4 + /CD8+ cell ratio than with RT or MIH alone. MIH promotes the anti-tumor effect of RT via Bax-mediated cell death, enhances the immunity of cells undergoing RT, and suppresses the increase in matrix metalloproteinase-9 (MMP-9) expression induced by RT.

In 2016, Werthmöller et al. discovered that HT (41.5 °C, 60 min) combined with RT (2 Gy) stimulates the immunogenic potential more than RT alone, which may result in anti-tumor immunity [92]. To test immunity, radioresistant melanoma B16-F10 cells were derived from C57/BL6 mice. The combination of RT and HT enhanced apoptosis, necrosis, the release of HMGB1 and Hsp70, and the infiltration of CD8 + T cells, DCs, and NK cells.

Mahmood et al. discovered that HT (42.5 °C, 30 min) combined with RT (8 Gy) is efficient in reducing tumor volume and increased cytotoxic CD8a + T cells in C57BL/6 mice injected with Panc02 cells [93]. In addition, they discovered that the combination of RT, HT, and immunotherapy increased the number of CD4 + T cells.

### *4.2. NK Cells*

RT and HT can stimulate the immune system, including NK cell activation [94]. RT simultaneously causes the release of cytokines, attracts NK cells, and induces NK cells to kill cancer cells [95]. NK cells kill infected or cancerous cells by rupturing the membrane of the target cell and releasing cytokines that activate other immune cells [96]. Because of the release of cytotoxic granules by NK cells, cancer cells undergo apoptosis.

In 2016, Hietanen et al. studied NK cell cytotoxicity and its recovery after HT (31–45 °C, 0–180 min) or HT with RT [97]. From 31 °C to 37 °C, cytotoxicity remained unchanged but decreased as the temperature rose; at 43 °C, cytotoxicity was almost zero. HT (42 °C, 30 min) with RT (20 Gy) reduced cytotoxicity more than HT alone. The ratio of normal to tumor cells killed increased as the temperature increased. NK cell cytotoxicity was unaffected by the sequence or time interval. In 2018, they discovered that HT with RT decreased the ATP levels in NK cells, which determined the probability of cell death [98]. As HT duration increased, the ATP level of NK cells was decreased by RT after HT compared to that after RT. IL-2 restored cell viability and cytotoxicity after exposure to RT and HT.

Finkel et al. discovered immunogenic potential, especially the function of NK cells, in B16 melanoma cells treated with RT (15 Gy) and HT (41.5 °C, 60 min) [99]. RT plus HT enhances apoptosis, necrosis, HMGB1 release, and NK cell count in vitro. HT and RT substantially increased the number of infiltrating B cells (CD3-CD19+), NK cells (CD3-NK1.1+, CD27 + CD11b−), and T cell (CD3+) subpopulations (CD8 + CD4−, CD8 + CD4+) in vivo. A prolonged reduction in NK cells two days after HT and RT enhanced tumor growth. In contrast, the depletion of a single NK cell prior to RT and HT dramatically slowed tumor growth.

### *4.3. Immune Checkpoint Molecules (ICMs)*

ICMs regulate the immune responses in cancer cells. Checkpoint inhibitors bind to ICMs to prevent cancer cells from evading the immune system, thereby allowing the immune system to recognize and eliminate them [100]. HT enhances ICMs expression, thereby making cancer cells more accessible to the immune system and more susceptible to immune attack [101]. Radiation treatment can damage the DNA of cancer cells, prompting them to produce more molecules that bind to ICMs and activate the immune system [102].

In 2020, Hader et al. discovered that cell death and immune-modulatory capabilities increased with increasing HT or HT (39, 41, and 44 °C, 60 min) + RT with normofractiona-

tion (2 Gy) or hypofractionation (5 Gy) in MCF-7 and MDA-MB-231 human breast cancer cells [103]. HT was performed using either warm water (CH) or microwave heating (MH). The combination of HT with RT enhanced apoptosis and necrosis, and the expression of ICMs, especially hypofractionation (5 Gy), was more effective. RT with HT by MH was more effective in cell death at 41 and 44 °C in MCF-7 cells and at 39, 41, and 44 °C in MDA-MB-231 cells. The expression of immune suppressive ICMs (PD-L1, PD-L2, and HVEM), immune stimulatory ICMs (CD137-L, Ox40-L, CD27-L, and ICOS-L), and EGFR in breast cancer cells was enhanced by RT with HT, consequently enhancing anti-tumor responses. In 2021, they discovered that immunosuppressive ICMs were affected at all temperatures in murine B16 melanoma cells but not at temperatures above 44 °C in human cell lines [104]. HT by 2.45 GHz at 44 °C and RT (5 Gy) produced the highest rate of cell death regardless of HT duration.

In 2022, Sengedorj et al. discovered that cell death and immune phenotype of human MDA-MB-231 and MCF-7 breast cancer cells were not affected by the sequence of radiation and HT but rather by the combination of RT (5 Gy) [105]. Following RT and HT, apoptosis was the main method of cell death in MCF-7 cells, while both apoptosis and necrosis were observed in MDA-MB-231 cells. RT and HT increased the ICM expression (PD-L1, PD-L2, and HVEM) compared with RT alone.

Inhibitory ICMs (PD-L1, PD-L2, and HVEM) were considerably enhanced in MCF-7 breast cancer cells following 120 h of RT with HT (39, 41, 44 °C) treatment. MDA-MB-231 breast cancer cells increased PD-L1 expression early (24, 48 h) after exposure to RT and HT at 44 °C. RT with HT of 41 or 44 °C increased PD-L2 expression at all time points, although HVEM expression was only slightly influenced at earlier time points. In addition, OX40-L, an immunostimulatory ICM, was considerably increased, especially 120 h after RT and HT.

Stoll et al. showed the effect of RT, HT, and the combination of the two (RHT) on cell death mechanisms, the expression of ICM, and the release of the danger signal HSP70 in two human glioblastoma cell lines (U87 and U251) [101]. Particularly in U251 cells, combination therapy induced a significant increase in both apoptosis and necrosis. Moreover, it increased the release of HSP70, mainly after HT (44 °C) only or in combination with RT. A significant increase in immune suppressive (PD-L1, PD-L2, HVEM) and immune stimulatory (ICOS-L, CD137-L, and Ox40-L) ICM was found mostly in U87 cells, particularly after RHT at 41 °C.

Kim et al. studied C3H mice with FSa-II fibrosarcoma subjected to RT (15 Gy) and mild-HT (41.0 °C, 30 min) [106]. The combination of RT and HT disrupted the expression of HIF-1, VEGF, and PD-L1 and dramatically inhibited tumor growth. We have summarized the research on the effects and mechanisms of HT and RT on the immune response in Table 3.

**Table 3.** RT + HT induces the immune response in tumor cells.

| RT | HT | Cell Line and Observation Model | Classification of the Molecular Mechanism | Molecular Mechanism | Ref. |
|---|---|---|---|---|---|
| 5 Gy | 41.5 °C, 60 min | Human colorectal adenocarcinoma, HCT15/in vitro | Necrosis/ Immune response | HMGB1 release, G2/M phase arrest | [88] |
| 5 or 10 Gy | 41.5 °C, 60 min | Human colorectal adenocarcinoma, SW480, and HCT 15/in vitro | Necrosis/ Immune response | HMGB1 release, G2/M phase arrest | [89] |
| 2, 5, and 10 Gy | 41.5 °C, 60 min | Human colorectal tumor, HCT15, and SW480; mouse colon carcinoma tumor, CT26.WT (CRL-2638)/ in vitro, in vivo | Immune response, HSP70 | CD80 and CCR7 ↑, phagocytosis of macrophages and DCs ↑, IL-8, and IL-12 ↑ | [90] |

**Table 3.** *Cont.*

| RT | HT | Cell Line and Observation Model | Classification of the Molecular Mechanism | Molecular Mechanism | Ref. |
|---|---|---|---|---|---|
| 20 Gy (2 × 10 Gy) | 45 °C, 3 min | Human murine breast cancer, 4T1, BALB/C mice/in vivo | Apoptosis/ Immune response | CD4+ T cell and CD4+/CD8+ cell ratio ↑, TNF-α, IFN-γ, and IL-2 ↑, Bax ↑, MMP-9 ↓ | [91] |
| 2 Gy | 41.5 °C, 60 min | Mouse melanoma, B16-F10, C57/BL6 mice/ in vitro, in vivo | Apoptosis, Necrosis/ Immune response, HSP70 | HMGB1 ↑, infiltration of CD8 + T cells, DCs, and NK cells ↑ | [92] |
| 20 Gy | 42 °C, 30 min | Erythroleukemia, K-562/in vitro | Immune response | NK cytotoxicity ↓ | [97] |
| 15 Gy | 41.5 °C, 60 min | Mouse melanoma, B16-F10, C57BL/6 mice/ in vivo, in vitro | Apoptosis, Necrosis/ Immune response | HMGB1 release, NK cell, B cell, and T cell count ↑ | [99] |
| 20 Gy | 42 °C, 0–180 min | NK cell; Erythroleukemia, K-562/in vitro | Immune response | ATP level of NK cell ↓ | [98] |
| 8 Gy | 42.5 °C, 30 min | Murine syngeneic Panc02, Panc02, C57BL/6 mice/in vivo | Immune response | CD8a+ and CD4+ T cells ↑ | [93] |
| 10 Gy (5 × 2 and 2 × 5 Gy) | 39, 41, 44 °C, 60 min | Human breast cancer, MCF-7, and MDA-MB-231/in vitro | Apoptosis, Necrosis/ ICM, HSP70 | PD-L1, PD-L2, HVEM ↑, CD137-L, OX40-L, CD27-L, ICOS-L ↑, EGFR ↑ | [103] |
| 10 Gy (5 × 2 and 2 × 5 Gy) | 39, 41, 44 °C, 60 min | Murine melanoma, B16; human breast cancer, MCF-7, and MDA-MB-231/in vitro | Apoptosis, Necrosis/ ICM | PD-L1, PD-L2, HVEM, and Gal-9 ↑ | [104] |
| 10 Gy (5 × 2 Gy) | 41 and 44 °C, 1 h | Human glioblastoma, U87 and U251/in vitro | Apoptosis, Necrosis/ ICM, HSP70 | PD-L1, PD-L2, HVEM ↑, ICOS-L, CD137-L, and Ox40-L ICMs ↑ | [101] |
| 10 Gy (2 × 5 Gy) | 39, 41, 44 °C, 60 min | Human MCF-7 and MDA-MB-231 breast cancer cells/in vitro | Apoptosis, Necrosis/ICMs | PD-L1, PD-L2, and HVEM ↑ | [105] |
| 15 Gy | 41.0 °C, 30 min | Fibrosarcoma, FSa-II, C3H mice/in vitro | Apoptosis/ ICM, Hypoxia | PD-L1 ↓, VEGF ↓, HIF-1α ↓ | [106] |

## 5. Discussion

We reviewed 61 experimental studies of combined RT and HT therapy. According to the research era and subject matter, these studies can be separated into three distinct phases as follows:

In phase 1, neither the type nor the mechanism of cell death was identified; only the involvement of hypoxia was revealed.

In phase 2, researchers focused on hypoxia-induced DNA damage and cell cycle arrest.

In phase 3, research was conducted to uncover the mechanism of apoptosis and optimize the RT + HT technique.

In the following discussion, the characteristics of each phase of research are reviewed, and, based on this, the experimental research results of RT + HT are described, along with the research trends of RT + HT and future application approaches.

### *5.1. Discovery of Effects by the Combination of RT + HT (Phase 1)*

Through in vivo studies, researchers initially discovered the effects of the combination therapy of RT and HT on tumors. A series of studies focused on cell death, tumor volume, or growth rate but did not explain the mechanism in detail. There were seventeen papers studied in vivo: dog, three; rabbit, one; rat, two; mouse, eleven. Researchers have experimented with various tumor types, including oral or external nasal fibrosarcoma (one), murine sarcoma (two), murine mammary carcinoma (three), primary malignant melanoma

(one), mast cell sarcoma (one), skin papilloma (one), rhabdomyosarcoma (one), murine fibrosarcoma (two), murine melanoma (two), human-derived head and neck squamous cell carcinoma (one), and lung cancer (one). A study in 2015 experimented with a non-tumor model [32].

In 2006, the first in vitro study was initiated, which investigated the best exposure period and dose of RT with HT on human cancer cells. Since then, in vitro studies have been more frequent than in vivo studies, as discussed in ten and three papers, respectively. Since this effect has been demonstrated by in vivo studies, several in vitro studies have been carried out to maximize the effect of combined therapy. One of nine studies focused on the best exposure time and dose of HT or RT [38], four studies focused on combination with other therapies [31,34,35,42], two studies focused on spheroidal culture [36,39], and two studies focused on the effect [33,37]. Researchers have attempted to add a variety of medications, design a new research model using the latest technology (e.g., 3D tumor spheroids), and modify the concentration of the current treatment. In other words, optimization was sought to enhance the efficacy, followed by studies to minimize toxicity.

### *5.2. Exploration of the Physiological Changes Following the Demonstration of Effects (Phase 2)*

Twenty-four studies were included in this classification. These studies focused on hypoxia (eight), DNA damage (nine), cell cycle arrest (three), induction and regulation of apoptosis (four; Bax (two), Brachyury (one), AKT (one)). Proteins and transcription factors associated with apoptosis, such as Bax and AKT, were also identified. Recent studies have appeared to be more interested in apoptosis than necrosis, as opposed to earlier investigations that revealed necrosis. Additionally, it is noticeable that there have been several studies that have concentrated on identifying optimal conditions to avoid necrosis.

RT and HT can directly damage cancer cells and cause DNA damage, which disrupts ATP production and renders cells more vulnerable. We reviewed eight studies that demonstrated the effects of combined therapy with oxygenation. A study in 1987 demonstrated that combination therapy decreased the ATP/Pi ratio [53]. Four studies showed that combination therapy promoted reoxygenation but did not specify the type of cell death that occurred. One study reported a decrease in TCD50 (50% tumor control dose) [46], one an increase in tumor perfusion [47], one an increase in pO2 [48], and another without any mechanism [49]. Three papers discussed the molecular mechanisms in greater depth. One study reported an increase in ROS production and the expression of Caspase-3 and -9 [50], while another reported the suppression of RT-induced upregulation of HIF-1$\alpha$, VEGF, and CA9 [51]. These two studies demonstrated the occurrence of apoptosis. Another study showed that the addition of radiosensitizers enhances cell death and DNA damage [52], in addition to two additional interventions other than RT and HT, such as CCNPs [50] and TSL-PMZ [52].

HT can hinder recovery from radiation-induced damage and normal cell function. This can lead to the accumulation of DNA damage, resulting in cell cycle arrest in the G2/M phase and increased radiosensitivity. In addition, RT can directly cause DNA damage, which can trigger checkpoint pathways that halt the cell cycle. DNA damage and cell cycle arrest are discussed in sections 9 and 1, respectively. Five of nine mentioned apoptosis as the type of cell death, two mentioned necrosis, and the rest did not. In 2002, a study showed chromosomal and DNA abnormalities, cell cycle delay by HT, and inhibition of DNA synthesis by RT [71]. Researchers have demonstrated p53-dependent inhibition of tumor growth via Bax and apoptosis-related proteins (e.g., PARP, Caspase-3) [59,61]. According to a 2007 study, HT effectively suppressed the loss in sensitivity, as indicated by the MN frequency [60]. Three studies indicated that HT impairs homologous recombination repair. One study addressed the dissociation and reformation of Rad51 proteins as crucial in radiosensitization by HT [62], while another reported chromosomal abnormalities and transient BRCA2 degradation [63]. Another study found that mutations in IDH1 lead to the accumulation of the oncometabolite *D*-2HG, which suppresses homologous recombination repair and lowers NADPH [67]. According to a study in 2016, inhibition of DSB repair

promotes cell cytotoxicity, cell cycle arrest, and Caspase-3 activation [64]. A study in 2019 found that the upregulation of KLF11 and NR4A3 is associated with the induction of apoptosis and ROS generation and is critical for slowing the progression of lung cancer [65]. Overall, hypoxia and reoxygenation induced by RT + HT can trigger structural damage and DNA lesions, leading to cell cycle arrest or cell death. When HT is paired with RT, it exacerbates radiation-induced oxidative stress and suppresses the recovery of radiation-induced DNA damage. HT can improve the efficacy of tumor treatment.

An imbalance between pro- and anti-apoptotic proteins usually causes apoptosis in cancer cells. The pro-apoptotic gene, Bax, is involved in the intrinsic apoptotic pathway. All four studies referenced apoptosis and one study published in 2019 indicated necrosis at the same time. Two studies demonstrated changes in the expression of apoptosis-related genes, including p53, Bcl-2, and Bax [78,79]. One study demonstrated the suppression of pro-angiogenic factors, such as VEGF and PDGF [79]. The PI3K-AKT pathway is often aberrantly regulated in cancer cells. AKT is a protein kinase that plays a key role in regulating cell growth, survival, and differentiation. HT and RT may suppress the AKT signaling pathway, rendering cells more vulnerable to harm and causing DNA damage. Research published in 2015 showed that HT improves radiosensitivity by reversing the stimulation of AKT signaling and its downstream gene expression produced by RT, which is further enhanced by the suppression of PI3K [83]. A study in 2021 revealed an increase in HSP-70 expression, downregulation of the brachyury gene, and activation of the death receptor and apoptotic pathway [80].

### *5.3. Immune Response (Phase 3)*

By combining RT and HT therapy, we identified 14 papers that applied the mechanisms of the anti-tumor immune response. The detailed mechanisms studied were HMBG1 (two studies), pro-inflammatory cytokine (one), CD8 + T cells (three), NK cells (three), and ICMs (five).

Recently, immunotherapy has been suggested as a new anti-tumor therapeutic target. Immunotherapy offers several advantages over conventional cancer therapy. It provides a targeted approach, can have long-lasting outcomes, and can enhance patients' quality of life [107].

Recent research has indicated that RT with HT improves the immune response compared to RT alone. By heating the tumor, tumor cells can be forced to release antigens, thereby stimulating an immune response. Two studies referred to necrosis as the prevalent form of cell death and discussed the release of the danger signal HMGB1 and its contribution to immune activation [88,89]. HT and RT induce immune responses dependent on HSP70, including the upregulation of dendritic cell markers (CD80 and CCR7) and secretion of pro-inflammatory cytokines (IL-8 and IL-12) [92].

RT combined with HT can also increase the activity of immune cells, such as CD8+ T cells, CD4+ T cells, dendritic cells, and NK cells, resulting in tumor death. CD8+ and CD4+ T cells play a vital role in the killing of tumor cells, both in terms of their direct anti-tumor activity and their support for the immune response. Three papers studied T cells, one study focused on the CD4+ T cell percentage and CD4+/CD8+ cell ratio [91], one on the infiltration of CD8 + T cells [92], and one on cytotoxic CD8a+ T cells [93].

By combining RT with HT, NK cell activation, a defense mechanism against cancer cells, is significantly enhanced. NK cells target cancer cells to suppress proliferation by producing cytokines and inducing apoptosis. Three papers studied NK cells: one focused on NK cell cytotoxicity [97], one on NK cell count [99], and one on the ATP level of NK cells [98]. In addition, one study found that NK cells have a dual- and time-dependent effect on the efficiency of the anti-tumor immune response [99].

ICMs have recently become the subject of many studies on immune responses. ICMs, which are present on the surface of cancer cells, impair the ability of cancer cells to avoid the immune system. ICMs include immunostimulatory ICMs (CD137-L, Ox40-L, CD27-L, and ICOS-L) and immunosuppressive ICMs (PD-L1, PD-L2, and HVEM). The combination

of RT and HT can enhance the expression of ICMs and the production of immune cells that are capable of targeting cancer cells [101,103–106]. The interaction between RT with HT and ICMs is complicated; thus, new research has been conducted from 2020 to the present that looks at altering the time, sequence, cell line, and frequency [104,105]. Table 4 shows a summary of the studies on the combination therapy of RT + HT, published from 1984 to the present, by theme and period.

**Table 4.** Number of theses by period.

| Theme (Table No.) | Period 1 (1984 ~2001) | Period 2 (2002 ~2010) | Period 3 (2011 ~2022) | Total |
|---|---|---|---|---|
| Unknown mechanism (Table 1) | 11 | 3 | 11 | 25 |
| Hypoxia; DNA damage and Cell cycle arrest; Induction and regulation of apoptosis (Table 2) | 4 | 5 | 13 | 22 |
| Immune response (Table 3) | 0 | 2 | 12 | 14 |
| Total | 15 | 10 | 36 | 61 |

Overall, the combination therapy of RT and HT has a synergistic effect on cancer cells, rendering them more susceptible to cell death and ultimately improving treatment outcomes. Initial research was primarily concerned with identifying whether the two treatments have synergistic effects that enhance radiosensitivity. They did not reveal the exact mechanism but only mentioned the involvement of hypoxia. Based on the success of combination therapy established in earlier trials, the discovery of precise mechanisms began in phase 2. The goal of the studies in phase 3 has been to investigate the conditions for optimizing therapeutic efficacy and uncover mechanisms more precisely. Several studies in the third period have suggested that this mechanism is closely linked to the regulation of the immune response.

## 6. Conclusions

Cancer poses a threat to human health and wellbeing. Despite the biphasic nature of HT, it has a synergistic effect when paired with RT, making it a viable option for treating cancer. Table 4 summarizes the efficacy of RT + HT combination treatment and the trend of RT + HT research. RT was performed mostly within the range of 2–10 Gy with certain exception studies, which used up to 100 Gy. HT was relatively more consistent; 41–44 °C for a period not exceeding 60 min was the standard condition. Certain studies used lower (39–40 °C) or higher temperatures (45–47 °C) and a longer time period (90 min). Several limitations remain of such combination therapy. The purpose of introducing HT in combination with RT is mainly to sensitize tumor cells to RT without affecting the normal tissues. This is supported by extensive evidence. However, RT itself is not applied tumor-specifically; thus, we cannot rule out the effect on normal tissues. Further detailed investigation is necessary to clearly determine how RT and HT simultaneously affect non-malignant cells. Such efforts will increase the potential application of the RT + HT combined therapy to the clinical field. Recently, conventional cancer therapies, such as chemotherapy, RT, and surgical resection, have been gradually replaced by more advanced immunotherapy. The combination of RT and HT activates the immune system. This may be the most fundamental therapeutic strategy for the future. Although further studies are required, RT and HT may provide an important advancement to immunotherapy since they can impact the immune system of an individual. When the safety profile of RT and HT combination therapy is fully demonstrated, its potential will expand considering the recent cancer therapy trend involving the immune system. Overall, RT and HT are effective cancer treatments that complement conventional treatments while enhancing immunotherapy, which has the potential to improve cancer treatment outcomes in the future.

**Author Contributions:** Conceptualization, S.H.B.; investigation, S.J. and S.K.; data curation, S.H.B.; writing—original draft preparation, S.J. and S.K.; writing—review and editing, S.J., S.K. and S.H.B.; supervision, S.H.B.; funding acquisition, S.H.B. All authors have read and agreed to the published version of the manuscript.

**Funding:** This work was supported by National Research Foundation of Korea (NRF) grant funded by the Korean government (MSIP) (NRF- 2020R1I1A3063625).

**Conflicts of Interest:** The authors declare no conflict of interest.

## References

1. Siegel, R.L.; Miller, K.D.; Fuchs, H.E.; Jemal, A. Cancer statistics, 2022. *CA Cancer J. Clin.* **2022**, *72*, 7–33. [CrossRef] [PubMed]
2. Beyer, A.M.; Bonini, M.G.; Moslehi, J. Cancer therapy-induced cardiovascular toxicity: Old/new problems and old drugs. *Am. J. Physiol. Heart Circ. Physiol.* **2019**, *317*, H164–H167. [CrossRef] [PubMed]
3. Ahmed, K.; Zaidi, S.F. Treating cancer with heat: Hyperthermia as promising strategy to enhance apoptosis. *J. Pak. Med. Assoc.* **2013**, *63*, 504–508. [PubMed]
4. Ba, M.; Long, H.; Wang, S.; Wu, Y.; Zhang, B.; Yan, Z.; Yu, F.; Cui, S. Hyperthermia enhances radiosensitivity of colorectal cancer cells through ROS inducing autophagic cell death. *J. Cell. Biochem.* **2018**, *119*, 3763–3774. [CrossRef] [PubMed]
5. Dunne, M.; Regenold, M.; Allen, C. Hyperthermia can alter tumor physiology and improve chemo- and radio-therapy efficacy. *Adv. Drug Deliv. Rev.* **2020**, *163–164*, 98–124. [CrossRef] [PubMed]
6. Datta, N.R.; Puric, E.; Klingbiel, D.; Gomez, S.; Bodis, S. Hyperthermia and Radiation Therapy in Locoregional Recurrent Breast Cancers: A Systematic Review and Meta-analysis. *Int. J. Radiat. Oncol. Biol. Phys.* **2016**, *94*, 1073–1087. [CrossRef]
7. Habash, R.W. Therapeutic hyperthermia. *Handb. Clin. Neurol.* **2018**, *157*, 853–868.
8. Yi, G.Y.; Kim, M.J.; Kim, H.I.; Park, J.; Baek, S.H. Hyperthermia Treatment as a Promising Anti-Cancer Strategy: Therapeutic Targets, Perspective Mechanisms and Synergistic Combinations in Experimental Approaches. *Antioxidants* **2022**, *11*, 625. [CrossRef]
9. Baskar, R.; Lee, K.A.; Yeo, R.; Yeoh, K.-W. Cancer and Radiation Therapy: Current Advances and Future Directions. *Int. J. Med. Sci.* **2012**, *9*, 193–199. [CrossRef]
10. Di Lalla, V.; Chaput, G.; Williams, T.; Sultanem, K. Radiotherapy Side Effects: Integrating a Survivorship Clinical Lens to Better Serve Patients. *Curr. Oncol.* **2020**, *27*, 107–112. [CrossRef]
11. Wang, J.; Han, Y.; Li, Y.; Zhang, F.; Cai, M.; Zhang, X.; Chen, J.; Ji, C.; Ma, J.; Xu, F. Targeting Tumor Physical Microenvironment for Improved Radiotherapy. *Small Methods* **2022**, *6*, e2200570. [CrossRef] [PubMed]
12. Jarosz-Biej, M.; Smolarczyk, R.; Cichon, T.; Kulach, N. Tumor Microenvironment as A "Game Changer" in Cancer Radiotherapy. *Int. J. Mol. Sci.* **2019**, *20*, 3212. [CrossRef] [PubMed]
13. Huilgol, N.G.; Gupta, S.; Sridhar, C.R. Hyperthermia with radiation in the treatment of locally advanced head and neck cancer: A report of randomized trial. *J. Cancer Res. Ther.* **2010**, *6*, 492–496. [CrossRef] [PubMed]
14. Toraya-Brown, S.; Fiering, S. Local tumour hyperthermia as immunotherapy for metastatic cancer. *Int. J. Hyperth.* **2014**, *30*, 531–539. [CrossRef] [PubMed]
15. Besse, H.C.; Bos, C.; Zandvliet, M.M.J.M.; van der Wurff-Jacobs, K.; Moonen, C.T.W.; Deckers, R. Triggered radiosensitizer delivery using thermosensitive liposomes and hyperthermia improves efficacy of radiotherapy: An in vitro proof of concept study. *PLoS ONE* **2018**, *13*, e0204063. [CrossRef]
16. Le Guevelou, J.; Chirila, M.E.; Achard, V.; Guillemin, P.C.; Lorton, O.; Uiterwijk, J.W.E.; Dipasquale, G.; Salomir, R.; Zilli, T. Combined hyperthermia and radiotherapy for prostate cancer: A systematic review. *Int. J. Hyperth.* **2022**, *39*, 547–556. [CrossRef]
17. Brewer, W.G.; Turrel, J.M. Radiotherapy and hyperthermia in the treatment of fibrosarcomas in the dog. *J. Am. Veter Med. Assoc.* **1982**, *181*, 146–150.
18. Campos, S.N.; Górriz, F.J.M.; Ferrer, R.B.; Vitoria, A.H.; Ramírez, A.C.; Grasa, F.F.; Garrido, J.M.R. Evolution of weight and survival of C3H mice with solid, subcutaneous sarcoma 180, treated with radiotherapy, hyperthermia and a combination of hyperthermia and radiotherapy. *Rev. Esp. Oncol.* **1983**, *30*, 379–398.
19. Yamashita, M. Radiosensitizing effect of combined radiotherapy, hyperthermia and misonidazole on C3H mouse FM3A tumor. *Nihon Igaku Hoshasen Gakkai Zasshi* **1984**, *44*, 1181–1188.
20. Dewhirst, M.W.; Sim, D.A.; Forsyth, K.; Grochowski, K.J.; Wilson, S.; Bicknell, E. Local control and distant metastases in primary canine malignant melanomas treated with hyperthermia and/or radiotherapy. *Int. J. Hyperth.* **1985**, *1*, 219–234. [CrossRef]
21. Legorreta, R.A.; Denman, D.L.; Kelley, M.C.; Lewis, G.C. Use of hyperthermia and radiotherapy in treatment of a large mast cell sarcoma in a dog. *J. Am. Veter Med. Assoc.* **1988**, *193*, 1545–1548.
22. Patrício, M.B.; Vilhena, M.; Soares, J. Morphologic and morphometric studies on tumor necrosis produced by radiotherapy, and hyperthermia singly and in combination. *J. Surg. Oncol.* **1989**, *42*, 5–10. [CrossRef] [PubMed]
23. Fujiwara, K.; Watanabe, T. Effects of Hyperthermia, Radiotherapy and Thermoradiotherapy on Tumor Microvascular Permeability. *Acta Pathol. Jpn.* **1990**, *40*, 79–84. [CrossRef] [PubMed]
24. Ruifrok, A.C.; Levendag, P.C.; Lakeman, R.F.; Deurloo, I.K.; Visser, A.G. Combined treatment with interstitial hyperthermia and interstitial radiotherapy in an animal tumor model. *Int. J. Radiat Oncol. Biol. Phys.* **1991**, *20*, 1281–1286. [CrossRef] [PubMed]

25. Sougawa, M.; Urano, M. Significance of additive heat effect in the therapeutic gain factor in combined hyperthermia and radiotherapy: Murine tumor response and foot reaction. *Int. J. Radiat. Oncol. Biol. Phys.* **1991**, *21*, 1561–1568. [CrossRef]
26. Nishimura, Y.; Urano, M. Timing and sequence of hyperthermia in fractionated radiotherapy of a murine fibrosarcoma. *Int. J. Radiat. Oncol. Biol. Phys.* **1993**, *27*, 605–611. [CrossRef]
27. Devi, P.U.; Guruprasad, K. Influence of clamping-induced ischemia and reperfusion on the response of a mouse melanoma to radiation and hyperthermia. *Int. J. Hyperth.* **2001**, *17*, 357–367. [CrossRef]
28. Ressel, A.; Schmitt, O.; Weiss, C.; Feyerabend, T. Therapeutic outcome and side-effects after radiotherapy, chemotherapy and/or hyperthermia treatment of head and neck tumour xenografts. *Eur. J. Cancer* **2002**, *38*, 594–601. [CrossRef]
29. Rao, B.S.S.; Devi, P.U. Response of S 180 murine tumor to bleomycin in combination with radiation and hyperthermia using micronucleus assay: A multimodality approach for therapeutic augmentation. *Indian J. Exp. Biol.* **2005**, *43*, 596–600.
30. Kalthur, G.; Pathirissery, U.D. Enhancement of the Response of B16F1 Melanoma to Fractionated Radiotherapy and Prolongation of Survival by Withaferin A and/or Hyperthermia. *Integr. Cancer Ther.* **2010**, *9*, 370–377. [CrossRef]
31. Franken, N.A.P.; Barendsen, G.W. Enhancement of radiation effectiveness by hyperthermia and incorporation of halogenated pyrimidines at low radiation doses as compared with high doses: Implications for mechanisms. *Int. J. Radiat. Biol.* **2014**, *90*, 313–317. [CrossRef] [PubMed]
32. Alya, G.; Ekhtiar, A.; Saour, G. Effects of lethal dose of gamma-radiation and partial body hyperthermia on Wistar rats. *Int. J. Hyperth.* **2015**, *31*, 460–463. [CrossRef] [PubMed]
33. Borasi, G.; Nahum, A.; Paulides, M.M.; Powathil, G.; Russo, G.; Fariselli, L.; Lamia, D.; Cirincione, R.; Forte, G.I.; Borrazzo, C.; et al. Fast and high temperature hyperthermia coupled with radiotherapy as a possible new treatment for glioblastoma. *J. Ther. Ultrasound* **2016**, *4*, 32. [CrossRef] [PubMed]
34. Masunaga, S.-I.; Tano, K.; Sanada, Y.; Sakurai, Y.; Tanaka, H.; Suzuki, M.; Kondo, N.; Watanabe, T.; Takata, T.; Maruhashi, A.; et al. Effect of Tirapazamine, Metformin or Mild Hyperthermia on Recovery from Radiation-Induced Damage in Pimonidazole-Unlabeled Quiescent Tumor Cells. *World J. Oncol.* **2017**, *8*, 137–146. [CrossRef]
35. IJff, M.; van Oorschot, B.; Oei, A.L.; Krawczyk, P.M.; Rodermond, H.M.; Stalpers, L.J.A.; Kok, H.P.; Crezee, J.; Franken, N.A.P. Enhancement of Radiation Effectiveness in Cervical Cancer Cells by Combining Ionizing Radiation with Hyperthermia and Molecular Targeting Agents. *Int. J. Mol. Sci.* **2018**, *19*, 2420. [CrossRef]
36. Rajaee, Z.; Khoei, S.; Mahdavi, S.R.; Ebrahimi, M.; Shirvalilou, S.; Mahdavian, A. Evaluation of the effect of hyperthermia and electron radiation on prostate cancer stem cells. *Radiat. Environ. Biophys.* **2018**, *57*, 133–142. [CrossRef] [PubMed]
37. McDonald, M.; Corde, S.; Lerch, M.; Rosenfeld, A.; Jackson, M.; Tehei, M. First in vitro evidence of modulated electro-hyperthermia treatment performance in combination with megavoltage radiation by clonogenic assay. *Sci. Rep.* **2018**, *8*, 16608. [CrossRef] [PubMed]
38. Prasad, B.; Kim, S.; Cho, W.; Kim, J.K.; Kim, Y.A.; Kim, S.; Wu, H.G. Quantitative Estimation of the Equivalent Radiation Dose Escalation using Radiofrequency Hyperthermia in Mouse Xenograft Models of Human Lung Cancer. *Sci. Rep.* **2019**, *9*, 3942. [CrossRef] [PubMed]
39. Brüningk, S.C.; Rivens, I.; Box, C.; Oelfke, U.; ter Haar, G. 3D tumour spheroids for the prediction of the effects of radiation and hyperthermia treatments. *Sci. Rep.* **2020**, *10*, 1653. [CrossRef] [PubMed]
40. Gunti, S.; Hoke, A.T.K.; Vu, K.; London, N.R., Jr. Organoid and Spheroid Tumor Models: Techniques and Applications. *Cancers* **2021**, *13*, 874. [CrossRef]
41. Ishiguro, T.; Ohata, H.; Sato, A.; Yamawaki, K.; Enomoto, T.; Okamoto, K. Tumor-derived spheroids: Relevance to cancer stem cells and clinical applications. *Cancer Sci.* **2017**, *108*, 283–289. [CrossRef] [PubMed]
42. Hu, S.; Zhang, X.; Unger, M.; Patties, I.; Melzer, A.; Landgraf, L. Focused Ultrasound-Induced Cavitation Sensitizes Cancer Cells to Radiation Therapy and Hyperthermia. *Cells* **2020**, *9*, 2595. [CrossRef] [PubMed]
43. Elming, P.B.; Sorensen, B.S.; Spejlborg, H.; Overgaard, J.; Horsman, M.R. Does the combination of hyperthermia with low LET (linear energy transfer) radiation induce anti-tumor effects equivalent to those seen with high LET radiation alone? *Int. J. Hyperth.* **2021**, *38*, 105–110. [CrossRef] [PubMed]
44. Jing, X.; Yang, F.; Shao, C.; Wei, K.; Xie, M.; Shen, H.; Shu, Y. Role of hypoxia in cancer therapy by regulating the tumor microenvironment. *Mol. Cancer* **2019**, *18*, 157. [CrossRef] [PubMed]
45. Elming, P.B.; Sørensen, B.S.; Oei, A.L.; Franken, N.A.P.; Crezee, J.; Overgaard, J.; Horsman, M.R. Hyperthermia: The Optimal Treatment to Overcome Radiation Resistant Hypoxia. *Cancers* **2019**, *11*, 60. [CrossRef]
46. Nishimura, Y.; Urano, M. The effect of hyperthermia on reoxygenation during the fractionated radiotherapy of two murine tumors, FSa-II and MCa. *Int. J. Radiat. Oncol. Biol. Phys.* **1994**, *29*, 141–148. [CrossRef]
47. Vujaskovic, Z.; Poulson, J.M.; Gaskin, A.A.; Thrall, D.E.; Page, R.L.; Charles, H.C.; MacFall, J.R.; Brizel, D.M.; Meyer, R.E.; Prescott, D.M.; et al. Temperature-dependent changes in physiologic parameters of spontaneous canine soft tissue sarcomas after combined radiotherapy and hyperthermia treatment. *Int. J. Radiat. Oncol. Biol. Phys.* **2000**, *46*, 179–185. [CrossRef]
48. Ressel, A.; Weiss, C.; Feyerabend, T. Tumor oxygenation after radiotherapy, chemotherapy, and/or hyperthermia predicts tumor free survival. *Int. J. Radiat. Oncol. Biol. Phys.* **2001**, *49*, 1119–1125. [CrossRef]
49. Thrall, D.E.; LaRue, S.M.; Pruitt, A.F.; Case, B.; Dewhirst, M.W. Changes in tumour oxygenation during fractionated hyperthermia and radiation therapy in spontaneous canine sarcomas. *Int. J. Hyperth.* **2006**, *22*, 365–373. [CrossRef] [PubMed]

50. Jabbari, N.; Zarei, L.; Galeh, H.E.G.; Motlagh, B.M. Assessment of synergistic effect of combining hyperthermia with irradiation and calcium carbonate nanoparticles on proliferation of human breast adenocarcinoma cell line (MCF-7 cells). *Artif. Cells Nanomed. Biotechnol.* **2018**, *46*, 364–372. [CrossRef]
51. Kim, W.; Kim, M.-S.; Kim, H.-J.; Lee, E.; Jeong, J.-H.; Park, I.; Jeong, Y.K.; Jang, W.I. Role of HIF-1α in response of tumors to a combination of hyperthermia and radiation in vivo. *Int. J. Hyperth.* **2018**, *34*, 276–283. [CrossRef] [PubMed]
52. Sadeghi, N.; Kok, R.J.; Bos, C.; Zandvliet, M.; Geerts, W.J.C.; Storm, G.; Moonen, C.T.W.; Lammers, T.; Deckers, R. Hyperthermia-triggered release of hypoxic cell radiosensitizers from temperature-sensitive liposomes improves radiotherapy efficacy in vitro. *Nanotechnology* **2019**, *30*, 264001. [CrossRef] [PubMed]
53. Sijens, P.E.; Bovée, W.M.; Seijkens, D.; Koole, P.; Los, G.; Van Rijssel, R.H. Murine mammary tumor response to hyperthermia and radiotherapy evaluated by in vivo 31P-nuclear magnetic resonance spectroscopy. *Cancer Res.* **1987**, *47 Pt 1*, 6467–6473. [PubMed]
54. Multhoff, G.; Habl, G.; Combs, S.E. Rationale of hyperthermia for radio(chemo)therapy and immune responses in patients with bladder cancer: Biological concepts, clinical data, interdisciplinary treatment decisions and biological tumour imaging. *Int. J. Hyperth.* **2016**, *32*, 455–463. [CrossRef] [PubMed]
55. Ni, L.-P.; Sun, H.-T.; Wang, P.; Wang, J.; Zhou, J.-H.; Cao, R.-Q.; Yue, L.; Chen, Y.-G.; Shen, F.-R. Hyperthermia enhances the efficacy of chemotherapeutic drugs in heat-sensitive cells through interfering with DNA damage repair. *Ann. Transl. Med.* **2022**, *10*, 463. [CrossRef] [PubMed]
56. Guan, J.; Stavridi, E.; Leeper, D.B.; Iliakis, G. Effects of hyperthermia on p53 protein expression and activity. *J. Cell. Physiol.* **2002**, *190*, 365–374. [CrossRef]
57. Li, X.; Heyer, W.-D. Homologous recombination in DNA repair and DNA damage tolerance. *Cell Res.* **2008**, *18*, 99–113. [CrossRef]
58. Yoshida, K.; Miki, Y. Role of BRCA1 and BRCA2 as regulators of DNA repair, transcription, and cell cycle in response to DNA damage. *Cancer Sci.* **2004**, *95*, 866–871. [CrossRef]
59. Ohnishi, T. The role of the p53 molecule in cancer therapies with radiation and/or hyperthermia. *J. Cancer Res. Ther.* **2005**, *1*, 147–150. [CrossRef]
60. Masunaga, S.-I.; Nagata, K.; Suzuki, M.; Kashino, G.; Kinashi, Y.; Ono, K. Inhibition of repair of radiation-induced damage by mild temperature hyperthermia, referring to the effect on quiescent cell populations. *Radiat. Med.* **2007**, *25*, 417–425. [CrossRef]
61. Masunaga, S.-I.; Tano, K.; Sanada, Y.; Suzuki, M.; Takahashi, A.; Ohnishi, K.; Ono, K. Effects of p53 Status of Tumor Cells and Combined Treatment with Mild Hyperthermia, Wortmannin or Caffeine on Recovery from Radiation-Induced Damage. *World J. Oncol.* **2019**, *10*, 132–141. [CrossRef] [PubMed]
62. Genet, S.C.; Fujii, Y.; Maeda, J.; Kaneko, M.; Genet, M.D.; Miyagawa, K.; Kato, T.A. Hyperthermia inhibits homologous recombination repair and sensitizes cells to ionizing radiation in a time- and temperature-dependent manner. *J. Cell. Physiol.* **2013**, *228*, 1473–1481. [CrossRef] [PubMed]
63. Bergs, J.; Oei, A.L.; Cate, R.T.; Rodermond, H.M.; Stalpers, L.J.; Barendsen, G.W.; Franken, N.A. Dynamics of chromosomal aberrations, induction of apoptosis, BRCA2 degradation and sensitization to radiation by hyperthermia. *Int. J. Mol. Med.* **2016**, *38*, 243–250. [CrossRef] [PubMed]
64. van Oorschot, B.; Granata, G.; Di Franco, S.; Ten Cate, R.; Rodermond, H.M.; Todaro, M.; Medema, J.P.; Franken, N.A. Targeting DNA double strand break repair with hyperthermia and DNA-PKcs inhibition to enhance the effect of radiation treatment. *Oncotarget* **2016**, *7*, 65504–65513. [CrossRef]
65. Son, B.; Jeon, J.; Lee, S.; Kim, H.; Kang, H.; Youn, H.; Jo, S.; Youn, B. Radiotherapy in combination with hyperthermia suppresses lung cancer progression via increased NR4A3 and KLF11 expression. *Int. J. Radiat. Biol.* **2019**, *95*, 1696–1707. [CrossRef] [PubMed]
66. Singh, V.; Johansson, P.; Torchinsky, D.; Lin, Y.-L.; Öz, R.; Ebenstein, Y.; Hammarsten, O.; Westerlund, F. Quantifying DNA damage induced by ionizing radiation and hyperthermia using single DNA molecule imaging. *Transl. Oncol.* **2020**, *13*, 100822. [CrossRef]
67. Khurshed, M.; Prades-Sagarra, E.; Saleh, S.; Sminia, P.; Wilmink, J.W.; Molenaar, R.J.; Crezee, H.; van Noorden, C.J.F. Hyperthermia as a Potential Cornerstone of Effective Multimodality Treatment with Radiotherapy, Cisplatin and PARP Inhibitor in *IDH1*-Mutated Cancer Cells. *Cancers* **2022**, *14*, 6228. [CrossRef]
68. Lee, Y.S.; Ahmed, M.B.; Alghamdi, A.A.A.; Islam, S.U.; Ahsan, H. The Complex Roles of DNA Repair Pathways, Inhibitors, Hyperthermia, and Contact Inhibition in Cell Cycle Halts. *Mini Rev. Med. Chem.* **2022**, *23*, 514–529. [CrossRef]
69. Zhao, Y.Y.; Wu, Q.; Wu, Z.B.; Zhang, J.J.; Zhu, L.C.; Yang, Y.; Ma, S.L.; Zhang, S.R. Microwave hyperthermia promotes caspase-3-dependent apoptosis and induces G2/M checkpoint arrest via the ATM pathway in non-small cell lung cancer cells. *Int. J. Oncol.* **2018**, *53*, 539–550. [CrossRef]
70. Teyssier, F.; Bay, J.O.; Dionet, C.; Verrelle, P. Cell cycle regulation after exposure to ionizing radiation. *Bull. Cancer* **1999**, *86*, 345–357.
71. Yuguchi, T.; Saito, M.; Yokoyama, Y.; Saito, T.; Nagata, T.; Sakamoto, T.; Tsukada, K. Combined use of hyperthermia and irradiation cause antiproliferative activity and cell death to human esophageal cell carcinoma cells–mainly cell cycle examination. *Hum. Cell* **2002**, *15*, 33–42. [CrossRef] [PubMed]
72. Pistritto, G.; Trisciuoglio, D.; Ceci, C.; Garufi, A.; D'Orazi, G. Apoptosis as anticancer mechanism: Function and dysfunction of its modulators and targeted therapeutic strategies. *Aging* **2016**, *8*, 603–619. [CrossRef] [PubMed]
73. Shamas-Din, A.; Kale, J.; Leber, B.; Andrews, D.W. Mechanisms of Action of Bcl-2 Family Proteins. *Cold Spring Harb. Perspect. Biol.* **2013**, *5*, a008714. [CrossRef] [PubMed]

74. Plati, J.; Bucur, O.; Khosravi-Far, R. Dysregulation of apoptotic signaling in cancer: Molecular mechanisms and therapeutic opportunities. *J. Cell. Biochem.* **2008**, *104*, 1124–1149. [CrossRef] [PubMed]
75. Luo, Z.; Zheng, K.; Fan, Q.; Jiang, X.; Xiong, D. Hyperthermia exposure induces apoptosis and inhibits proliferation in HCT116 cells by upregulating miR-34a and causing transcriptional activation of p53. *Exp. Ther. Med.* **2017**, *14*, 5379–5386. [CrossRef] [PubMed]
76. Lopez, A.; Reyna, D.E.; Gitego, N.; Kopp, F.; Zhou, H.; Miranda-Roman, M.A.; Nordstrøm, L.U.; Narayanagari, S.-R.; Chi, P.; Vilar, E.; et al. Co-targeting of BAX and BCL-XL proteins broadly overcomes resistance to apoptosis in cancer. *Nat. Commun.* **2022**, *13*, 1199. [CrossRef] [PubMed]
77. Liu, Z.; Ding, Y.; Ye, N.; Wild, C.; Chen, H.; Zhou, J. Direct Activation of Bax Protein for Cancer Therapy. *Med. Res. Rev.* **2016**, *36*, 313–341. [CrossRef]
78. Liang, H. Change in expression of apoptosis genes after hyperthermia, chemotherapy and radiotherapy in human colon cancer transplanted into nude mice. *World J. Gastroenterol.* **2007**, *13*, 4365–4371. [CrossRef]
79. Talaat, R.M.; Abo-Zeid, T.M.; Abo-Elfadl, M.T.; El Maadawy, E.; Hassanin, M.M. Combined Hyperthermia and Radiation Therapy for Treatment of Hepatocellular Carcinoma. *Asian Pac. J. Cancer Prev.* **2019**, *20*, 2303–2310. [CrossRef]
80. Singh, P.; Eley, J.; Saeed, A.; Bhandary, B.; Mahmood, N.; Chen, M.; Dukic, T.; Mossahebi, S.; Rodrigues, D.B.; Mahmood, J.; et al. Effect of hyperthermia and proton beam radiation as a novel approach in chordoma cells death and its clinical implication to treat chordoma. *Int. J. Radiat. Biol.* **2021**, *97*, 1675–1686. [CrossRef]
81. Sharifnia, T.; Wawer, M.J.; Chen, T.; Huang, Q.-Y.; Weir, B.A.; Sizemore, A.; Lawlor, M.A.; Goodale, A.; Cowley, G.S.; Vazquez, F.; et al. Small-molecule targeting of brachyury transcription factor addiction in chordoma. *Nat. Med.* **2019**, *25*, 292–300. [CrossRef] [PubMed]
82. Shariati, M.; Meric-Bernstam, F. Targeting AKT for cancer therapy. *Expert Opin. Investig. Drugs* **2019**, *28*, 977–988. [CrossRef]
83. Man, J.; Shoemake, J.D.; Ma, T.; Rizzo, A.E.; Godley, A.R.; Wu, Q.; Mohammadi, A.M.; Bao, S.; Rich, J.N.; Yu, J.S. Hyperthermia Sensitizes Glioma Stem-like Cells to Radiation by Inhibiting AKT Signaling. *Cancer Res.* **2015**, *75*, 1760–1769. [CrossRef] [PubMed]
84. Skitzki, J.J.; Repasky, E.A.; Evans, S.S. Hyperthermia as an immunotherapy strategy for cancer. *Curr. Opin. Investig. Drugs* **2009**, *10*, 550–558. [PubMed]
85. Wan Mohd Zawawi, W.F.A.; Hibma, M.H.; Salim, M.I.; Jemon, K. Hyperthermia by near infrared radiation induced immune cells activation and infiltration in breast tumor. *Sci. Rep.* **2021**, *11*, 10278. [CrossRef] [PubMed]
86. Khandia, R.; Munjal, A.; Iqbal, H.M.N.; Dhama, K. Heat Shock Proteins: Therapeutic Perspectives in Inflammatory Disorders. *Recent Patents Inflamm. Allergy Drug Discov.* **2017**, *10*, 94–104. [CrossRef] [PubMed]
87. Gardner, A.; Ruffell, B. Dendritic Cells and Cancer Immunity. *Trends Immunol.* **2016**, *37*, 855–865. [CrossRef]
88. Schildkopf, P.; Holmer, R.; Sieber, R.; Ott, O.J.; Janko, C.; Mantel, F.; Frey, B.; Fietkau, R.; Gaipl, U.S. Hyperthermia in combination with X-irradiation induces inflammatory forms of cell death. *Autoimmunity* **2009**, *42*, 311–313. [CrossRef] [PubMed]
89. Schildkopf, P.; Frey, B.; Mantel, F.; Ott, O.J.; Weiss, E.-M.; Sieber, R.; Janko, C.; Sauer, R.; Fietkau, R.; Gaipl, U.S. Application of hyperthermia in addition to ionizing irradiation fosters necrotic cell death and HMGB1 release of colorectal tumor cells. *Biochem. Biophys. Res. Commun.* **2010**, *391*, 1014–1020. [CrossRef] [PubMed]
90. Schildkopf, P.; Frey, B.; Ott, O.J.; Rubner, Y.; Multhoff, G.; Sauer, R.; Fietkau, R.; Gaipl, U.S. Radiation combined with hyperthermia induces HSP70-dependent maturation of dendritic cells and release of pro-inflammatory cytokines by dendritic cells and macrophages. *Radiother. Oncol.* **2011**, *101*, 109–115. [CrossRef]
91. Wang, H.; Li, X.; Xi, X.; Hu, B.; Zhao, L.; Liao, Y.; Tang, J. Effects of magnetic induction hyperthermia and radiotherapy alone or combined on a murine 4T1 metastatic breast cancer model. *Int. J. Hyperth.* **2011**, *27*, 563–572. [CrossRef] [PubMed]
92. Werthmöller, N.; Frey, B.; Rückert, M.; Lotter, M.; Fietkau, R.; Gaipl, U.S. Combination of ionising radiation with hyperthermia increases the immunogenic potential of B16-F10 melanoma cells in vitro and in vivo. *Int. J. Hyperth.* **2016**, *32*, 23–30. [CrossRef] [PubMed]
93. Mahmood, J.; Alexander, A.A.; Samanta, S.; Kamlapurkar, S.; Singh, P.; Saeed, A.; Carrier, F.; Cao, X.; Shukla, H.D.; Vujaskovic, Z. A Combination of Radiotherapy, Hyperthermia, and Immunotherapy Inhibits Pancreatic Tumor Growth and Prolongs the Survival of Mice. *Cancers* **2020**, *12*, 1015. [CrossRef] [PubMed]
94. Dayanc, B.E.; Beachy, S.H.; Ostberg, J.R.; Repasky, E.A. Dissecting the role of hyperthermia in natural killer cell mediated anti-tumor responses. *Int. J. Hyperth.* **2008**, *24*, 41–56. [CrossRef]
95. Walle, T.; Kraske, J.A.; Liao, B.; Lenoir, B.; Timke, C.; von Bohlen Und Halbach, E.; Tran, F.; Griebel, P.; Albrecht, D.; Ahmed, A.; et al. Radiotherapy orchestrates natural killer cell dependent antitumor immune responses through CXCL8. *Sci. Adv.* **2022**, *8*, eabh4050. [CrossRef] [PubMed]
96. Sordo-Bahamonde, C.; Lorenzo-Herrero, S.; Payer, A.R.; Gonzalez, S.; López-Soto, A. Mechanisms of Apoptosis Resistance to NK Cell-Mediated Cytotoxicity in Cancer. *Int. J. Mol. Sci.* **2020**, *21*, 3726. [CrossRef] [PubMed]
97. Hietanen, T.; Kapanen, M.; Kellokumpu-Lehtinen, P.-L. Restoring Natural Killer Cell Cytotoxicity After Hyperthermia Alone or Combined with Radiotherapy. *Anticancer. Res.* **2016**, *36*, 555–563. [PubMed]
98. Hietanen, T.; Kapanen, M.; Kellokumpu-Lehtinen, P.L. Natural Killer Cell Viability After Hyperthermia Alone or Combined with Radiotherapy with or without Cytokines. *Anticancer Res.* **2018**, *38*, 655–663. [PubMed]

99. Finkel, P.; Frey, B.; Mayer, F.; Bösl, K.; Werthmöller, N.; Mackensen, A.; Gaipl, U.S.; Ullrich, E. The dual role of NK cells in antitumor reactions triggered by ionizing radiation in combination with hyperthermia. *Oncoimmunology* **2016**, *5*, e1101206. [CrossRef]
100. Li, B.; Chan, H.L.; Chen, P. Immune Checkpoint Inhibitors: Basics and Challenges. *Curr. Med. Chem.* **2019**, *26*, 3009–3025. [CrossRef]
101. Stoll, E.; Hader, M.; Rückert, M.; Weissmann, T.; Lettmaier, S.; Putz, F.; Hecht, M.; Fietkau, R.; Rosin, A.; Frey, B.; et al. Detailed in vitro analyses of the impact of multimodal cancer therapy with hyperthermia and radiotherapy on the immune phenotype of human glioblastoma cells. *Int. J. Hyperth.* **2022**, *39*, 796–805. [CrossRef] [PubMed]
102. Rogers, S.J.; Puric, E.; Eberle, B.; Datta, N.R.; Bodis, S.B. Radiotherapy for Melanoma: More than DNA Damage. *Dermatol. Res. Pract.* **2019**, *2019*, 9435389. [CrossRef] [PubMed]
103. Hader, M.; Savcigil, D.P.; Rosin, A.; Ponfick, P.; Gekle, S.; Wadepohl, M.; Bekeschus, S.; Fietkau, R.; Frey, B.; Schlücker, E.; et al. Differences of the Immune Phenotype of Breast Cancer Cells after Ex Vivo Hyperthermia by Warm-Water or Microwave Radiation in a Closed-Loop System Alone or in Combination with Radiotherapy. *Cancers* **2020**, *12*, 1082. [CrossRef] [PubMed]
104. Hader, M.; Streit, S.; Rosin, A.; Gerdes, T.; Wadepohl, M.; Bekeschus, S.; Fietkau, R.; Frey, B.; Schlücker, E.; Gekle, S.; et al. In Vitro Examinations of Cell Death Induction and the Immune Phenotype of Cancer Cells Following Radiative-Based Hyperthermia with 915 MHz in Combination with Radiotherapy. *Cells* **2021**, *10*, 1436. [CrossRef]
105. Sengedorj, A.; Hader, M.; Heger, L.; Frey, B.; Dudziak, D.; Fietkau, R.; Ott, O.J.; Scheidegger, S.; Barba, S.M.; Gaipl, U.S.; et al. The Effect of Hyperthermia and Radiotherapy Sequence on Cancer Cell Death and the Immune Phenotype of Breast Cancer Cells. *Cancers* **2022**, *14*, 2050. [CrossRef]
106. Kim, H.; Kim, D.; Kim, W.; Kim, E.; Jang, W.I.; Kim, M.-S. The Efficacy of Radiation is Enhanced by Metformin and Hyperthermia Alone or Combined Against FSaII Fibrosarcoma in C3H Mice. *Radiat. Res.* **2022**, *198*, 190–199. [CrossRef]
107. Zhang, Y.; Zhang, Z. The history and advances in cancer immunotherapy: Understanding the characteristics of tumor-infiltrating immune cells and their therapeutic implications. *Cell. Mol. Immunol.* **2020**, *17*, 807–821. [CrossRef]

antioxidants

*Article*

# Planarians as an In Vivo Experimental Model for the Study of New Radioprotective Substances

**Artem M. Ermakov [1], Kristina A. Kamenskikh [1], Olga N. Ermakova [1], Artem S. Blagodatsky [1], Anton L. Popov [1] and Vladimir K. Ivanov [2,*]**

[1] Institute of Theoretical and Experimental Biophysics, Russian Academy of Sciences, 142290 Pushchino, Russia; ermakovam@iteb.ru (A.M.E.); kamenskikhka@iteb.ru (K.A.K.); ermakovaon@iteb.ru (O.N.E.); blagodatskyas@iteb.ru (A.S.B.); popoval@iteb.ru (A.L.P.)
[2] Kurnakov Institute of General and Inorganic Chemistry, Russian Academy of Sciences, 119991 Moscow, Russia
* Correspondence: van@igic.ras.ru

**Abstract:** Ionising radiation causes the death of the most actively dividing cells, thus leading to depletion of the stem cell pool. Planarians are invertebrate flatworms that are unique in that their stem cells, called neoblasts, constantly replace old, damaged, or dying cells. Amenability to efficient RNAi treatments, the rapid development of clear phenotypes, and sensitivity to ionising radiation, combined with new genomic technologies, make planarians an outstanding tool for the discovery of potential radioprotective agents. In this work, using the well-known antioxidant N-acetylcysteine, planarians are, for the first time, shown to be an excellent model system for the fast and effective screening of novel radioprotective and radio-sensitising substances. In addition, a panel of measurable parameters that can be used for the study of radioprotective effects on this model is suggested.

**Keywords:** planarians; model animal; irradiation; regeneration; radioprotection

**Citation:** Ermakov, A.M.; Kamenskikh, K.A.; Ermakova, O.N.; Blagodatsky, A.S.; Popov, A.L.; Ivanov, V.K. Planarians as an In Vivo Experimental Model for the Study of New Radioprotective Substances. *Antioxidants* **2021**, *10*, 1763. https://doi.org/10.3390/antiox10111763

Academic Editors: Elena Obrador Pla and Alegria Montoro

Received: 28 September 2021
Accepted: 30 October 2021
Published: 4 November 2021



## 1. Introduction

Radioprotectors are the substances that guard the body from damage to its molecules, organs, tissues, and cells in case of exposure to ionising radiation [1]. Their effect is based mainly on enhancing antioxidant cell defences by inactivating reactive oxygen species (ROS) and free radicals which emerge from water radiolysis [2]. Today, a large number of radioprotective substances are known that can reduce the negative effects of ionising radiation [3]. One of the most well-known antioxidant radioprotective agents is N-acetyl-L-cysteine (NAC), which belongs to the thiol compounds family [4]. It is commonly accepted that the effect of ionising radiation on biological objects leads to the formation of various forms of free radicals with different lifetimes [5]. Due to the presence of a large number of unpaired electrons, ROS have a high level of redox activity, which leads to oxidative damage in components of the cell [6]. The presence of a reduced thiol group in NAC can effectively neutralise free radicals and ROS generated by ionising radiation exposure [7–9]. There is also evidence that exogenous NAC can be a source of cysteine (Cys), which can be used for enhanced biosynthesis of intracellular glutathione (GSH), which also acts as a low molecular weight antioxidant [10]. Today, NAC is widely used as a reference compound in assessing the antioxidant properties of test substances in various oxidative stress models [11–14].

Despite significant progress in the development of radioprotective substances for military purposes, there is still a need for the development of radioprotectors and radiomitigators for medical applications, in particular for radiation therapy [15–18]. Using various approaches and molecular systems, it is also possible to enhance the effect of ionising radiation on tumour tissue by changing its radiosensitivity [19]. However, using

common laboratory animals such as rats and mice, the search for such compounds is time-consuming and quite expensive. Thus, the development of new experimental models that are both relevant for biomedical purposes and capable of providing rapid screening with low cost is an urgent task. Planarians are model organisms that have a unique ability to regenerate due to the presence of neoblasts in their tissues [20]. Planarian neoblasts are totipotent stem cells that divide and differentiate into all types of cells in the adult body, including germline cells. The content of neoblasts in the planarian body reaches about 30% of the total cell number [21]. These cells endow the planarian body with an unlimited regenerative potential after damage or during organ self-renewal [22]. Moreover, planarian regeneration is possible, even from very small fragments, where at least one stem cell has been preserved [23]. The abovementioned features of planarians have made them a classic biological model for research into the regulation of stem cell proliferation and differentiation in vivo, restoration of differentiated tissue, and ageing [24]. In particular, the *Schmidtea mediterranea* planarian has a series of advantages over vertebrates as a model for biomedical research: the animals are cheap and easy to handle, they have a short life cycle, and they are available in large quantities.

It has previously been shown that neoblasts, like human stem cells, are sensitive to ionising radiation [25]. Irradiation of planarians in a dose of more than 15 Gy leads to the death of neoblasts, the inability to regenerate, and the termination of homeostatic tissue recovery [26]. The loss of neoblasts is accompanied by the characteristic abdominal curling of animals and further death within four weeks after irradiation [27]. Smaller doses of ionising radiation lead to the partial death of neoblasts, but the remaining part is able to restore the worm's body and provide the ability for normal regeneration [28].

The effect of a sublethal irradiation dose on planarians, which preserves part of the neoblast and provides further regenerative potential, is the basis of the experimental model proposed here for studying potential radioprotective agents. Radioactivity is known to have pronounced and measurable effects on planarians, which can easily be tracked and quantified, such as on blastema regeneration rate, the number of surviving neoblasts and their transcriptional activity, the amount of DNA damage, and ROS generation. The current study has used a well-known antioxidant with proven radioprotective activity (N-acetylcysteine) in order to develop an experimental model of planarian radiosensitivity, select optimal irradiation doses and patterns, determine the timing of the effective assessment and establish a panel of trackable characteristics that can be used for analysing the radioprotective effect of a chemical substance on the planarian model.

## 2. Materials and Methods

### *2.1. Animals*

The study featured an asexual laboratory strain of a freshwater flatworm *Schmidtea mediterranea* (*Turbellaria, Platyhelminthes*). The animals were kept at room temperature, in darkened glass aquariums containing a mixture of tap and distilled water at a 2:1 vol., which is the optimal ratio for keeping freshwater flatworms in lab conditions. Planarians were fed twice a week with mosquito larvae (*Chironomidae)*. Before the experiment, flatworms were starved for one week. This fasting stage is necessary to exclude the possible influence of nutritional components on the effect of X-ray radiation. This technique is generally accepted in planarian experiments [29].

For the experiments, the animals with nearly equal body lengths (about 8 mm) were selected. The anterior part of the planarian body (approximately 1/5 of the total length) containing the cephalic ganglion was cut off (decapitated) using a Carl Zeiss Stemi 2000 dissecting microscope, with a thin eye scalpel. Prior to decapitation, the planarians were placed on a cooling table for several minutes. The number of animals in each experimental group was the same (35 animals).

### 2.2. Computer-Assisted Morphometry In Vivo

The growth of regenerating blastema was studied using computer morphometry [30]. 72 h after decapitation, the images of control and experimental animals were taken using a Carl Zeiss Stemi 2000 microscope equipped with a Carl Zeiss AxioCam camera. To assess the blastema growth rate, the regeneration index R = s/S was used. The values of the blastema area (s) and total body area (S) were calculated using the Plana 4.0 software. 30 animals were used in each experimental or control group. Each experiment was repeated in triplicate. The relative change was calculated as follows:

$$\Delta R = \frac{(R_E - R_c) \pm (\delta_E - \delta_c)}{R_c} \times 100\% \quad (1)$$

Here, $R_E$ is the index of regeneration ($R$) in the experimental group of flatworms; $R_C$ is the index of regeneration ($R$) in the control group of flatworms; $\Delta R$ is the difference (%) between $R_E$ and $R_C$; $\delta_E$ and $\delta_C$ are standard errors of measurement in the experimental and control groups, respectively. The results presented here are mean values from three independent experiments.

### 2.3. Whole-Mount Immunocytochemical Study of Planarian Stem Cell Mitotic Activity

For this study, planarians with a body length of about 4 mm were selected. The number of mitotic cells in the regenerating worms was determined after seven days. Planarians were treated with 7% N-acetylcysteine solution for 5 min and fixed in PBS containing 4% formaldehyde and 0.3% Triton X100 for 20 min. Planarian staining for detecting mitotic cells was performed according to the protocol provided by Newmark and Alvarado [31]. To label mitotic cells, we used a primary antibody for phosphorylated histone H3 (Santa Cruz, Dallas, TX, USA), 1/1000 dilution. A secondary antibody conjugated to a fluorescent label CF488A (Biotium, Fremont, CA, USA) was used in 1/1000 dilution. Phosphorylated H3 histone has long been used as a classical marker of mitotic cells in studies of the planarian neoblast mitotic activity [32–34].

After washing in PBS, the whole-mount preparations were placed in Vectashield Antifade Mounting Medium (Vector Labs, Burlingame, CA, USA) and analysed using a Leica TCS SP5 confocal laser scanning microscope. The mitotic cell number and the planarian body area were measured using the Carl Zeiss Axio Image software. The number of mitotic cells per 1 $mm^2$ of planarian body (the mitotic index) was then calculated. The results obtained were analysed statistically. The average values of the mitotic indices (i.e., the relationship of the total number of mitotic cells to the body area of each animal) were obtained using 10 animals per experimental group, in three experimental repetitions [35,36]. The specificity of immunocytochemical staining was confirmed using a non-immune serum. All controls were negative and demonstrated the absence of specific and non-specific fluorescent staining in planarian tissues.

### 2.4. Experimental Testing Substance

N-acetylcysteine (NAC) (Sigma, Burlington, MA, USA) at final concentrations of 10 and 15 mM was used as a test radioprotective agent. A stock solution of NAC (1 M, pH = 7) was prepared using distilled water. NAC was added to planarians 12 h before irradiation.

### 2.5. Planarian X-ray Irradiation

The planarians were irradiated using an X-ray machine, RUT-12 (15 mA, 200 kV). For irradiation, animals were placed in Petri dishes on filter paper moistened with water. The radiation doses were 1, 5, 10, 15, and 30 Gy at a power of 2 Gy per min.

### 2.6. RAPD PCR for Genotoxicity Analysis

Non-regenerating planarians were incubated with NAC, irradiated, and then genotoxicity analysis was performed using an approved protocol. A detailed description of the

procedure was reported elsewhere [36]. For each primer, genomic template stability (GTS) was calculated:

$$GTS\ (\%) = (1 - a/n) \cdot 100\% \quad (2)$$

where $a$ is the number of polymorphic bands detected in each treated sample and $n$ is the number of total bands in the control. Polymorphism observed in a RAPD profile included the disappearance of a normal band or the appearance of a band in comparison with the control profile [37]. The sensitivity of the GTS parameter was calculated as a percentage of the control.

### *2.7. RT-PCR for Gene Expression Analysis*

The level of elimination and restoration of the stem cell population was determined by changing the expression of 24 neoblast marker genes [38,39]. For this, mRNA was isolated from five planarians in the experimental and control groups by means of a set with magnetic particles, according to the attached protocol (Sileks, Moscow, Russia). Reverse transcription was performed with a Sileks (Russia) kit, using oligo dT primer, according to the attached protocol. The resulting cDNA served as a template for real-time PCR. The reaction was carried out using a reaction mixture with SybrGreen (Eurogen, Russia), on a CFX-96 thermocycler (BioRad, Philadelphia, PA, USA). The level of gene transcription was normalised by the average transcription levels of housekeeping genes *Smed-ef1* (GenBank accession number AY067688) and *Smed_01699* (GenBank accession number JX010505). Genomic DNA contamination was determined by the sample without the stage of reverse transcription based on genome-specific primers. Gene-specific primers were selected using the Primer Express program (Applied Biosystems, Waltham, MA, USA).

The expression data were analysed using the online service http://www.qiagen.com (accessed on 25 September 2020), the mayday-2.14 program (Center for Bioinformatics, Tübingen, Germany), and the Genesis program [40]. Only those results were taken into account for which changes in the level of gene expression were observed at $p < 0.05$.

### *2.8. ROS Measurement in the Planarian Body*

ROS levels in the planarian body after irradiation were identified using H2DCFDA (2,7-dichloro-dihydrofluorescein-diacetate-acetyl). This dye is a well-known fluorescent intracellular sensor of active oxygen species [41]. Animals were placed in a solution of 10 μM -$H_2$DCFDA (Biotium, USA) and incubated for 60 min in the dark. Next, the planarians were incubated with NAC, washed twice with water, and irradiated using an X-ray machine. The positive control group was obtained by pre-incubation of animals for 30 min in 100 μM $H_2O_2$ (Sigma, USA). Then, the planarians were anesthetised for 5–10 min in a 0.1% solution of chloroethane (Sigma, USA) [42] and photographed with an Axio Scope A1 fluorescence microscope (Carl Zeiss) (Ex/Em = 492–495/517–527 nm). In the images obtained using the ImageJ program (National Institute of Health, Bethesda, MD, USA), the total fluorescence intensity of the animal body was estimated. The measurement results were averaged over 15 animals.

### *2.9. Statistical Data Analysis*

The data obtained were treated statistically by the Sigma-Plot 9.11 program (Systat Software Inc., Erkrath, Germany) using one–way ANOVA analyses of variance.

### *2.10. Ethical Standards*

All procedures performed in this study involving animals were performed in accordance with the ethical standards of the institution at which the studies were conducted.

## 3. Results and Discussion

### *3.1. Working Dose Selection*

Firstly, to select the dose range for further experiments, irradiation was carried out on decapitated regenerating planarians with a series of gradually increasing doses and the

regeneration rate, mitotic activity, and DNA damage were monitored. Dose-dependent effects on the growth process of the planarian head blastema under X-ray irradiation were found (Figure 1). The inhibition of blastema growth was observed after 5, 10, 15, and 30 Gy irradiation doses. The blastema size after 5 Gy irradiation was 32% less than in the unirradiated control group. An increase of irradiation dose to 10, 15, and 30 Gy led to the inhibition of blastema regeneration in a dose-dependent manner by 45, 63, and 83%, respectively.

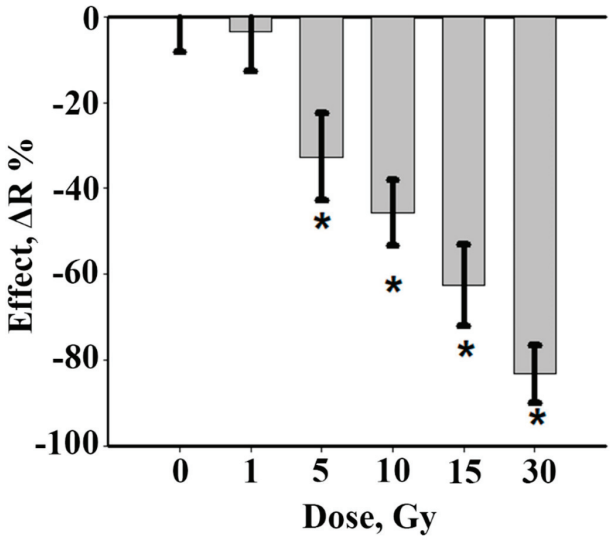


**Figure 1.** Inhibition of planarian head blastema growth on the 3rd day after X-ray irradiation (1–30 Gy). Data are shown as mean values ± standard error, $n = 90$, * $p < 0.001$.

An assessment of stem cell mitotic activity on the third day after irradiation revealed a complete absence of mitotic cells after 15 and 30 Gy irradiation. At lower irradiation doses (1, 5, or 10 Gy), the mitotic activity of the neoblasts was still present in the planarian body.

To evaluate the DNA damage caused by irradiation, the randomly amplified polymorphic DNA (RAPD)-PCR technique was used. RAPD is a PCR-based method that amplifies random DNA fragments through the use of single, short primers of arbitrary nucleotide sequence, under low annealing conditions. This method is widely used to determine genetic polymorphism in populations and DNA damage from genotoxic chemical or physical factors [37]. The genomic template stability (GTS) parameter reflects the difference between the control and the treated samples: a larger GTS value means greater similarity, i.e., less damage caused to the DNA by irradiation [37].

After 10 and 15 Gy irradiation, significant changes were observed in genomic template stability (GTS). In particular, GTS after 10 Gy irradiation dropped down to 71%, whereas after irradiation at a dose of 15 Gy, it made up 60%.

On the basis of the abovementioned observations, the working doses were selected for experiments on radioprotection. A dose of 5 Gy irradiation did not cause notable changes in the blastema growth rate, but a 30 Gy irradiation dose led to a significant slowdown in regeneration, up to complete inhibition. Only medium irradiation doses (10 and 15 Gy) yielded a significant slowdown in head regeneration, a decrease in the mitotic activity of stem cells, and damage in the DNA of treated planarians. Based on the results, only two irradiation doses were selected—10 and 15 Gy—for further studies of radioprotective action.

### 3.2. Blastema Growth Rate in Irradiated Planarians Was Increased by NAC

Next, NAC was introduced to test its radioprotective properties on regenerating planarians after irradiation. The first and most straightforward parameter to control was regenerating blastema growth rate. Pre-incubation of planarians in NAC solution in two different concentrations (10 and 15 mM) before X-ray irradiation led to an increase in blastema growth rate by the third day of regeneration (Figure 2). Statistically significant effects of NAC radioprotection were observed on days 3–7. Thus, NAC significantly improved the dynamics of regeneration and had a radioprotective effect on the planarian model.

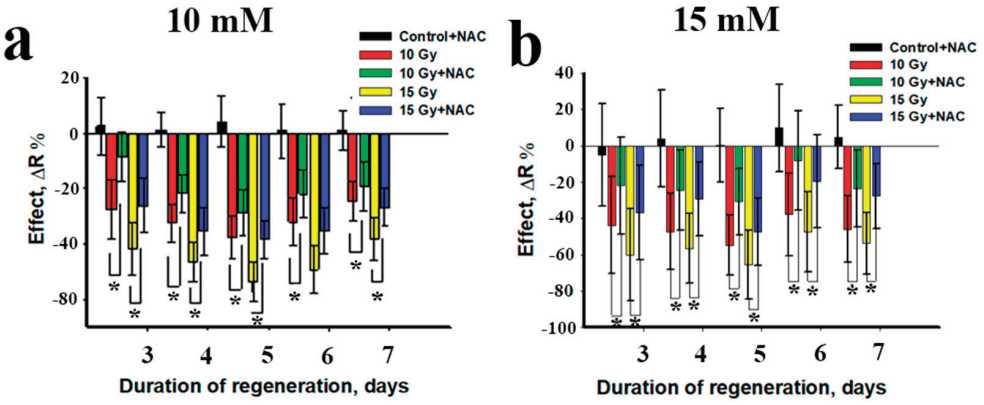


**Figure 2.** The radioprotective effect of NAC under X-ray exposure. (**a**) Radioprotective effect of N-acetylcysteine (10 mM) under 10 and 15 Gy irradiation; (**b**) radioprotective effect of N-acetylcysteine (15 mM) under 10 and 15 Gy irradiation, * $p < 0.001$ via ANOVA.

### 3.3. Neoblast Survival and Mitotic Activity Was Increased by NAC

To reveal the physiological mechanisms of NAC protective action, an analysis was made of the activity of the neoblasts after exposure to X-ray radiation (Figure 3). It was found that the recovery of regeneration potential directly correlated with the number of neoblasts in the planarian body after irradiation. An analysis of mitotic activity showed that there were no mitotic cells in the planarian body after irradiation at a dose of 15 Gy on day 7. When using NAC as a radioprotector (10 mM), the planarians retained about 10% of mitotically active neoblasts (Figure 3a,b). On the tenth day after irradiation (15 Gy), mitotic cells were observed mainly in the head while with NAC as a radioprotector they were found not only in the head, but also in the pharyngeal and caudal parts of the body (Figure 3c). It is known that doses up to 15 Gy are sublethal for planarians, and doses above 20–30 Gy are lethal. At lethal doses, the few surviving neoblasts completely lose their proliferation ability [43,44]. Note, radiation-induced death of planarian stem cells is probably due to the same mechanisms (DNA damage, repair, apoptosis) that have been described for mammalian stem cells [45,46]. At sublethal doses of radiation which were used in our study, the surviving neoblasts were still able to give rise to new clonal populations [47], but this process is quite slow. Therefore, when the decapitation is done immediately after irradiation, the deficiency of stem cells significantly reduces the regeneration rate of planaria and the blastema growth rate. The presence of NAC radioprotector in the planaria irradiated with sublethal doses preserves higher content of neoblasts which are able for further proliferation.

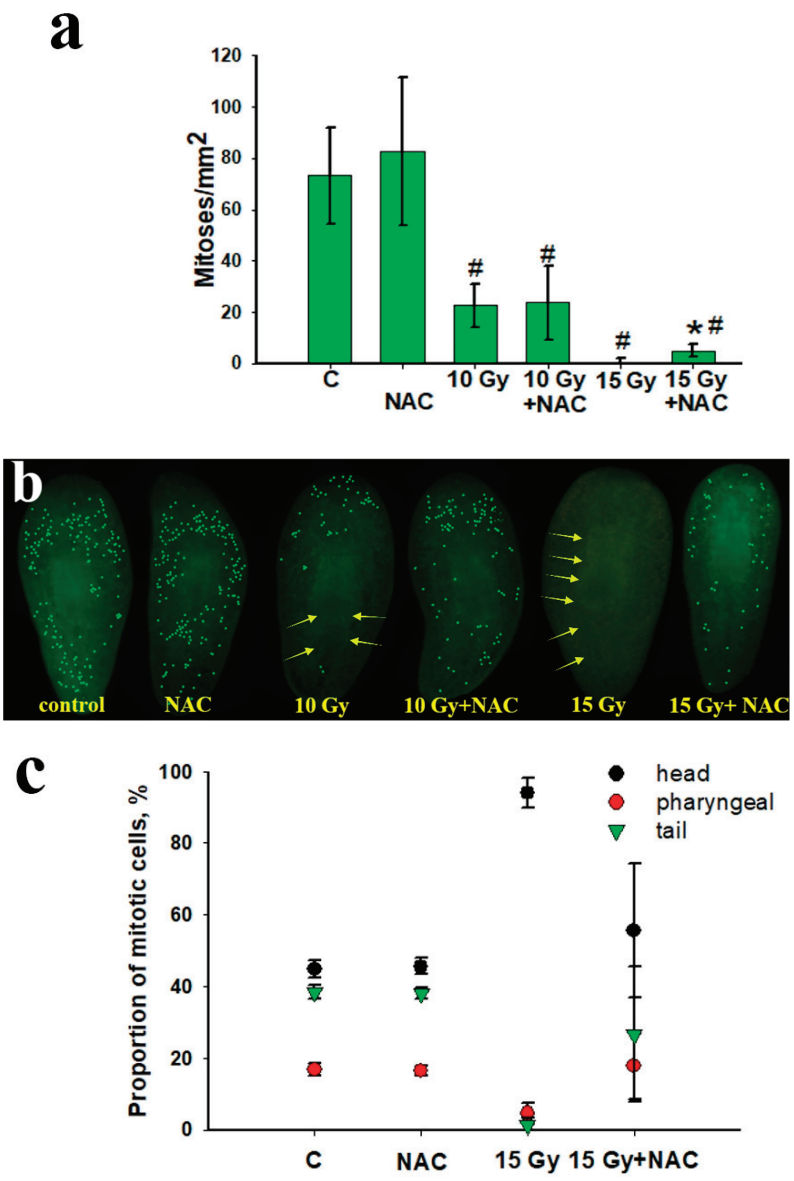


**Figure 3.** Number of mitotic cells in the planarian body 7 days after X-ray irradiation (10 and 15 Gy) with NAC (10 mM). (**a**,**b**) Determination of the total number of mitotic cells in the planarian body stained by immunohistochemistry; (**c**) distribution of mitotic cells in the planarian body 10 days after irradiation at a dose of 15 Gy. # $p < 0.001$ (from control), * $p < 0.001$ (from 15 Gy). Arrows indicate the absence of mitotic cells after X-ray irradiation.

### *3.4. NAC Increased the Neoblast Markers Expression and Reduced DNA Damage*

Gene expression analysis of planarian neoblast markers showed that, on the third and sixth day after X-ray irradiation, the concentration of the studied mRNAs significantly decreased in treated animals (Figure 4). The expression of the *Smed-soxP-1*, *Smed-fgfr-4*, *Smed-gata456*, and *Smed-hnf-4* genes was higher with NAC after a 15 Gy irradiation dose when compared to the control group [39].

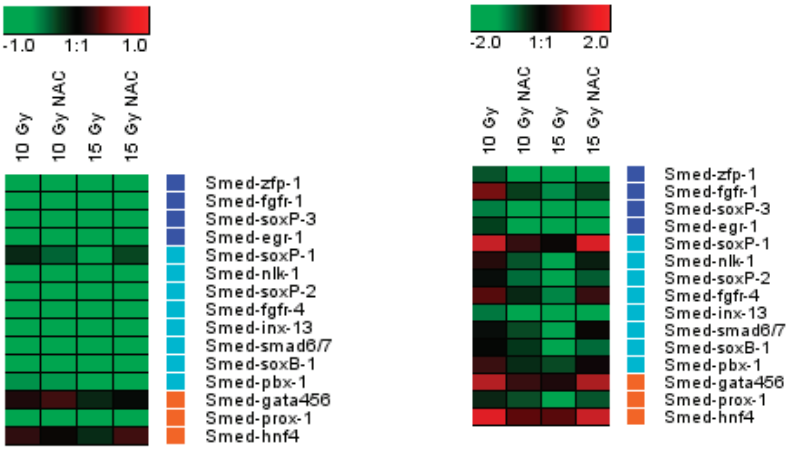


(**a**) (**b**)

**Figure 4.** Gene expression of three classes of neoblast markers in regenerating planarians treated with NAC (10 mM) for 3 h (**a**) and 6 h (**b**) after irradiation. The intensity scale of the standardised expression values range from −3 (green: low expression) to +3 (red: high expression), with a 1:1 intensity value (black) representing the control (unirradiated).

Similar results were obtained for the stability of planarian genomic DNA after X-ray irradiation. The damaging effect of radiation on the genomic DNA was least pronounced after treatment of the animals with NAC, which reduced the degree of change and increased genomic stability (Figure 5).

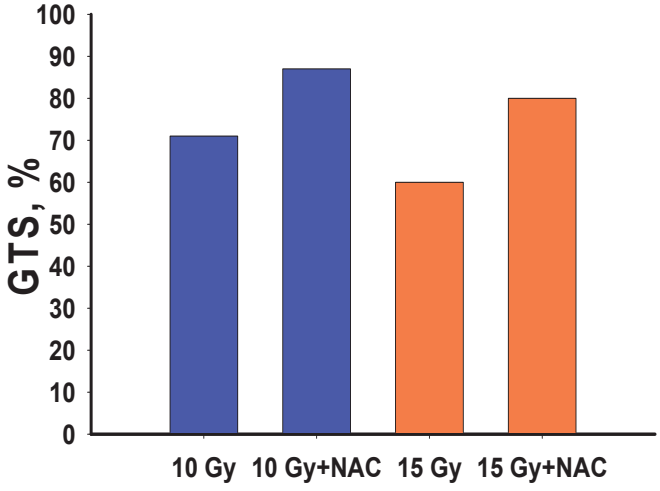


**Figure 5.** Genomic template stability (GTS) of planarians after X-ray irradiation (DNA was isolated 2 h after irradiation). GTS—genomic stability coefficient.

### *3.5. The Amount of ROS Generated after Irradiation Was Reduced by NAC*

Another parameter critical to control after irradiation is reactive oxygen species (ROS) generation. Results of ROS measurement in a planarian body after X-ray irradiation are shown in Figure 6. X-ray irradiation led to the formation of free radicals in a dose-

dependent manner, therefore the minimum autofluorescence intensity of the planarian body was observed in the control group. Irradiation led to a significant increase in the amount of ROS, which led to an increase in fluorescence intensity. It is also worth noting that neoblasts are mainly located in the parenchyma zone, which actively fluoresces after irradiation. Such colocalization of high ROS levels and neoblasts in the planarian body after irradiation confirms oxidative damage to stem cells, which affects their proliferation and migration. Pre-incubation of planarians with N-acetylcysteine (10 mM) resulted in a significant decrease in the level of dye fluorescence after irradiation of animals in various doses (5, 10, and 15 Gy). These results confirm directly that NAC acts as an antioxidant, effectively inactivating ROS under X-ray irradiation.

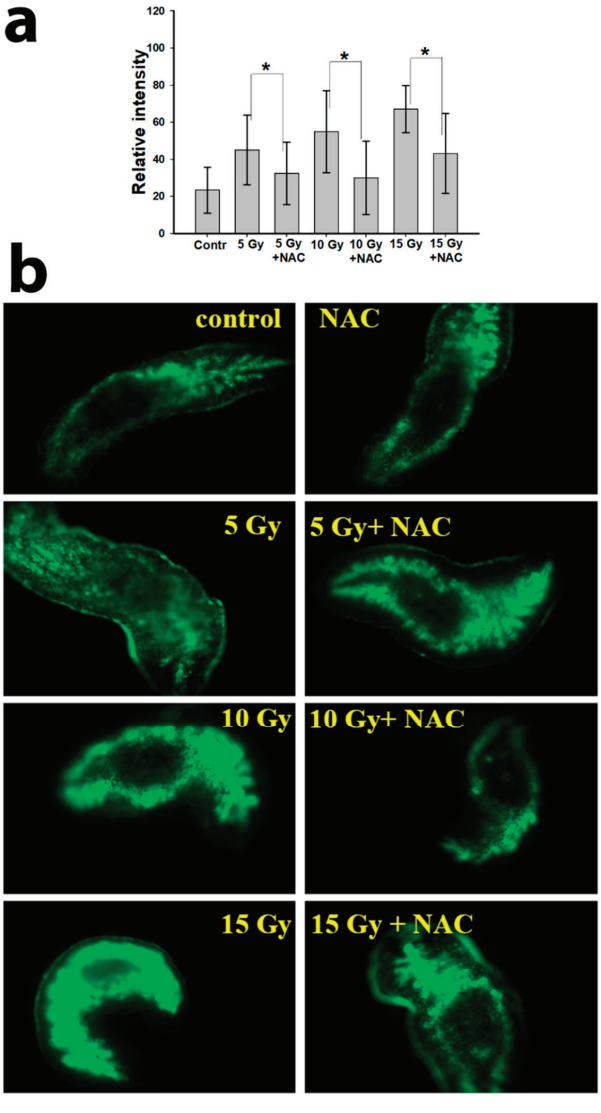


**Figure 6.** Inhibition of ROS formation by N-acetylcysteine, measured by H2DCFDA fluorescence. Quantitative determination of the fluorescence intensity in the body of planarians (**a**); fluorescence micrographs of planarians after irradiation (**b**). Standard deviation * $p < 0.001$.

## 4. Conclusions

In this study, a series of experiments was conducted proving that planarians provide a simple and suitable model for studying radioactive damage and the radioprotective effects of chemical substances. Using a well-known radioprotector, N-acetylcysteine, as a model substance, it has been shown that planarians possess a set of easily measurable characteristics which can be used to quantify radiation damage and the radioprotective effect. These are: (i) the growth rate of regenerating blastema, (ii) the number of surviving neoblasts and their mitotic activity, (iii) the expression of neoblast marker genes, (iv) the amount of DNA damage, and (v) the rate of ROS generation by the planarian tissue.

The first parameter can be used to directly evaluate the efficacy of radioprotection. This criterion is unique for planarians as model animals; it is simple but requires a microscope and software. The next two parameters investigate stem cell biology in greater depth and reflect the stage of neoblasts—the cells which are responsible for planarian regeneration. Monitoring the status of neoblasts is important, for radiation mostly damages fast dividing cells and neoblasts can serve as a perfect model thereof. The fourth parameter enables the measurement of the impact of radiation and the efficacy of radioprotectors on genotoxicity. Finally, the last of these parameters assess the molecular mechanisms of ionising radiation damage. Taken together, this set of simple and robust parameters makes it possible to screen and characterise potential radioprotectors in an inexpensive and robust manner. There are many new potential radioprotective substances among natural products [48], therefore the screening system described here has great potential. The search for radiosensitisers is also a task of high importance, for they enable radiation harm to cancer cells to be increased without affecting normal cells [49]. The model system described in the current study is also applicable for the screening of radiosensitisers.

In general, the observed effects of radiation-induced suppression of planarian regeneration are associated with partial or complete elimination of the neoblast population after X-ray radiation exposure. The results reported here show that the remaining pool of neoblasts after irradiation gives rise to a new population of stem cells and thus ensures the regeneration of the planarian body. The molecular mechanisms of neoblast proliferation, migration, and differentiation have been extensively studied using modern methods, including RNA interference (RNAi) for gene-specific knockdown [50]. This makes it possible to clearly monitor the influence of external factors and stimuli, including ionising radiation or a model drug action, on the planarian's vital processes. The radioprotective effect of N-acetylcysteine is based on the suppression of ROS formation during irradiation, which enables the saving of a fairly large number of neoblasts in the body of the planarian. Obviously, the survival of stem cells when using a radioprotector is associated not only with direct antioxidant protection, but also with the effect on the DNA repair rate. The results have demonstrated the possibility of using planarians as a convenient model for studying the radioprotective properties of various substances.

**Author Contributions:** A.M.E.—study concept and design, performance of experiments, data interpretation, writing of manuscript; K.A.K.—performance of experiments, data interpretation; O.N.E.—performance of experiments, data interpretation; A.S.B.—performance of experiments, data interpretation; A.L.P.—performance of experiments, data interpretation, writing of manuscript, conception of the structure of the article, provision of overall scientific advice, and manuscript revision; V.K.I.—supervision, writing, review, and editing. All authors have read and agreed to the published version of the manuscript.

**Funding:** This work was supported by the Russian Foundation for Basic Research grants No. 18-34-00820 mol_a and No. 18-15-00447 a.

**Institutional Review Board Statement:** Not applicable.

**Informed Consent Statement:** Not applicable.

**Data Availability Statement:** The data presented in this study are available in article.

**Conflicts of Interest:** The authors declare no conflict of interest.

## References


1. Singh, V.K.; Hauer-Jensen, M. γ-Tocotrienol as a Promising Countermeasure for Acute Radiation Syndrome: Current Status. *Int. J. Mol. Sci.* **2016**, *17*, 663. [CrossRef]
2. Mishra, K.; Alsbeih, G. Appraisal of biochemical classes of radioprotectors: Evidence, current status and guidelines for future development. *3 Biotech* **2017**, *7*, 292. [CrossRef] [PubMed]
3. Kamran, M.Z.; Ranjan, A.; Kaur, N.; Sur, S.; Tandon, V. Radioprotective Agents: Strategies and Translational Advances. *Med. Res. Rev.* **2016**, *36*, 461–493. [CrossRef] [PubMed]
4. Samuni, Y.; Goldstein, S.; Dean, O.M.; Berk, M. The chemistry and biological activities of N-acetylcysteine. *Biochim. Biophys. Acta* **2013**, *1830*, 4117–4129. [CrossRef]
5. Azzam, E.I.; Jay-Gerin, J.-P.; Pain, D. Ionizing radiation-induced metabolic oxidative stress and prolonged cell injury. *Cancer Lett.* **2012**, *327*, 48–60. [CrossRef]
6. Reisz, J.A.; Bansal, N.; Qian, J.; Zhao, W.; Furdui, C.M. Effects of ionizing radiation on biological molecules–mechanisms of damage and emerging methods of detection. *Antioxid. Redox Signal.* **2014**, *21*, 260–292. [CrossRef] [PubMed]
7. Benrahmoune, M.; Thérond, P.; Abedinzadeh, Z. The reaction of superoxide radical with N-acetylcysteine. *Free Radic. Biol. Med.* **2000**, *29*, 775–782. [CrossRef]
8. Winterbourn, C.C.; Metodiewa, D. Reactivity of biologically important thiol compounds with superoxide and hydrogen peroxide. *Free Radic. Biol. Med.* **1999**, *27*, 322–328. [CrossRef]
9. Gao, X.; Lampraki, E.M.; Al-Khalidi, S.; Qureshi, M.A.; Desai, R.; Wilson, J.B. N-acetylcysteine (NAC) ameliorates Epstein-Barr virus latent membrane protein 1 induced chronic inflammation. *PLoS ONE* **2017**, *12*, e0189167.
10. Ono, K.; Jung, M.; Zhang, T.; Tsutsuki, H.; Sezaki, H.; Ihara, H.; Wei, F.Y.; Tomizawa, K.; Akaike, T.; Sawa, T. Synthesis of l-cysteine derivatives containing stable sulfur isotopes and application of this synthesis to reactive sulfur metabolome. *Free Radic. Biol. Med.* **2017**, *106*, 69–79. [CrossRef] [PubMed]
11. Aldini, G.; Altomare, A.; Baron, G.; Vistoli, G.; Carini, M.; Borsani, L.; Sergio, F. N-Acetylcysteine as an antioxidant and disulphide breaking agent: The reasons why. *Free Radic. Res.* **2018**, *52*, 751–762. [CrossRef]
12. Chouchani, E.T.; Kazak, L.; Jedrychowski, M.P.; Lu, G.Z.; Erickson, B.K.; Szpyt, J.; Pierce, K.A.; Laznik-Bogoslavski, D.; Vetrivelan, R.; Clish, C.B.; et al. Mitochondrial ROS regulate thermogenic energy expenditure and sulfenylation of UCP1. *Nature* **2016**, *532*, 112. [CrossRef] [PubMed]
13. Park, E.J.; Min, K.J.; Lee, T.J.; Yoo, Y.H.; Kim, Y.S.; Kwon, T.K. β-Lapachone induces programmed necrosis through the RIP1-PARP-AIF-dependent pathway in human hepatocellular carcinoma SK-Hep1 cells. *Cell Death Dis.* **2014**, *5*, e1230. [CrossRef]
14. Wang, C.; Wong, W.-F. Observational wear leveling: An efficient algorithm for flash memory management. In *Proceedings of the 49th Annual Design Automation Conference*; ACM: San Francisco, CA, USA, 2012; pp. 235–242.
15. Kouvaris, J.R.; Kouloulias, V.E.; Vlahos, L.J. Amifostine: The first selective-target and broad-spectrum radioprotector. *Oncologist* **2007**, *12*, 738–747. [CrossRef] [PubMed]
16. Singh, V.K.; Seed, T.M. The efficacy and safety of amifostine for the acute radiation syndrome. *Expert Opin. Drug Saf.* **2019**, *18*, 1077–1090. [CrossRef] [PubMed]
17. Du, J.; Zhang, P.; Cheng, Y.; Liu, R.; Liu, H.; Gao, F.; Shi, C.; Liu, C. General principles of developing novel radioprotective agents for nuclear emergency. *Radiat. Med. Prot.* **2020**, *1*, 120–126. [CrossRef]
18. Rosen, E.M.; Day, R.; Singh, V.K. New approaches to radiation protection. *Front. Oncol.* **2015**, *4*, 381. [CrossRef] [PubMed]
19. Liu, Y.; Zhang, P.; Li, F.; Jin, X.; Li, J.; Chen, W.; Li, Q. Metal-based NanoEnhancers for Future Radiotherapy: Radiosensitizing and Synergistic Effects on Tumor Cells. *Theranostics* **2018**, *8*, 1824–1849. [CrossRef]
20. Rink, J.C. Stem cell systems and regeneration in planaria. *Dev. Genes Evol.* **2013**, *223*, 67–84. [CrossRef]
21. Reddien, P.W.; Sanchez Alvarado, A. Fundamentals of planarian regeneration. *Annu. Rev. Cell Dev. Biol.* **2004**, *20*, 725–757. [CrossRef] [PubMed]
22. Roberts-Galbraith, R.H.; Newmark, P.A. On the organ trail: Insights into organ regeneration in the freshwater flatworms. *Curr. Opin. Genet. Dev.* **2015**, *32*, 37–46. [CrossRef] [PubMed]
23. Gentile, L.; Cebrià, F.; Bartscherer, K. The planarian flatworm: An in vivo model for stem cell biology and nervous system regeneration. *Dis. Model. Mech.* **2011**, *4*, 12–19. [CrossRef] [PubMed]
24. Pagan, O.R. Planaria: An animal model that integrates development, regeneration and pharmacology. *Int. J. Dev. Biol.* **2017**, *61*, 519–529. [CrossRef]
25. Pellettieri, J.; Alvarado, S.A. Cell turnover and adult tissue homeostasis: From humans to planarians. *Annu. Rev. Genet.* **2007**, *41*, 83–105. [CrossRef] [PubMed]
26. Salvetti, A.; Rossi, L.; Bonuccelli, L.; Lena, A.; Pugliesi, C.; Rainaldi, G.; Evangelista, M.; Gremigni, V. Adult stem cell plasticity: Neoblast repopulation in non-lethally irradiated planarians. *Dev. Biol.* **2009**, *328*, 305–314. [CrossRef]
27. Reddien, P.W.; Oviedo, N.J.; Jennings, J.R.; Jenkin, J.C.; Alvarado, S.A. SMEDWI-2 is a PIWI-like protein that regulates planarian stem cells. *Science* **2005**, *310*, 1327–1330. [CrossRef] [PubMed]
28. Rossi, L.; Cassella, L.; Iacopetti, P.; Ghezzani, C.; Tana, L.; Gimenez, G.; Ghigo, E.; Salvetti, A. Insight into stem cell regulation from sub-lethally irradiated worms. *Gene* **2018**, *662*, 37–45. [CrossRef] [PubMed]
29. Goupil, L.S.; Ivry, S.L.; Hsieh, I.; Suzuki, B.M.; Craik, C.S.; O'Donoghue, A.J.; McKerrow, J.H. Cysteine and Aspartyl Proteases Contribute to Protein Digestion in the Gut of Freshwater Planaria. *PLoS Negl. Trop. Dis.* **2016**, *10*, e0004893. [CrossRef]

30. Ermakov, A.M.; Ermakova, O.N.; Mayevsky, E.I. The role of some intracellular signaling cascades in the activation of planarian regeneration upon irradiation with low-temperature argon plasma. *Biophysics* **2014**, *59*, 552–557. [CrossRef]
31. Newmark, P.A.; Sanchez Alvarado, A. Bromodeoxyuridine specifically labels the regenerative stem cells of planarians. *Dev. Biol.* **2000**, *220*, 142–153. [CrossRef] [PubMed]
32. Wenemoser, D.; Reddien, P.W. Planarian regeneration involves distinct stem cell responses to wounds and tissue absence. *Dev. Biol.* **2010**, *344*, 979–991. [CrossRef] [PubMed]
33. Hijioka, M.; Ikemoto, Y.; Fukao, K.; Inoue, T.; Kobayakawa, T.; Nishimura, K.; Takata, K.; Agata, K.; Kitamura, Y. MEK/ERK Signaling Regulates Reconstitution of the Dopaminergic Nerve Circuit in the Planarian *Dugesia japonica*. *Neurochem. Res.* **2021**. [CrossRef] [PubMed]
34. Hubert, A.; Henderson, J.M.; Cowles, M.W.; Ross, K.G.; Hagen, M.; Anderson, C.; Szeterlak, C.J.; Zayas, R.M. A functional genomics screen identifies an Importin-α homolog as a regulator of stem cell function and tissue patterning during planarian regeneration. *BMC Genom.* **2015**, *16*, 769. [CrossRef]
35. Ermakova, O.N.; Ermakov, A.M.; Tiras, H.P.; Lednev, V.V. The effect of melatonin on the regeneration of planaria Girardia tigrine. *Ontogenesis* **2009**, *6*, 466–469.
36. Ermakov, A.; Popov, A.; Ermakova, O.; Ivanova, O.; Baranchikov, A.; Kamenskikh, K.; Scherbakov, A.; Popova, N.; Ivanov, V. The first inorganic mitogens: Cerium oxide and cerium fluoride nanoparticles stimulate planarian regeneration via neoblastic activation. *Mater. Sci. Eng. C* **2019**, *104*, 109924. [CrossRef] [PubMed]
37. Zhang, H.C.; Shi, C.Y.; Yang, H.H.; Chen, G.W.; Liu, D. Z: Genotoxicity evaluation of ionic liquid 1-octyl-3-methylimidazolium bromide in freshwater planarian *Dugesia japonica* using RAPD assay. *Ecotoxicol. Environ. Saf.* **2016**, *134*, 17–22. [CrossRef]
38. Ermakov, A.M.; Ermakova, O.N.; Afanasyeva, V.A.; Popov, A.L. Dose-Dependent Effects of Cold Atmospheric Argon Plasma on the Mesenchymal Stem and Osteosarcoma Cells In Vitro. *Int. J. Mol. Sci.* **2021**, *22*, 6797. [CrossRef]
39. van Wolfswinkel, J.C.; Wagner, D.E.; Reddien, P.W. Single-Cell Analysis Reveals Functionally Distinct Classes within the Planarian Stem Cell Compartment. *Cell Stem Cell* **2014**, *15*, 326–339. [CrossRef]
40. Sturn, A.; Quackenbush, J.; Trajanoski, Z. Genesis: Cluster analysis of microarray data. *Bioinformatics* **2002**, *18*, 207–208. [CrossRef] [PubMed]
41. Lee, J.G.; Noh, W.J.; Kim, H.; Lee, M.-Y. Generation of Reactive Oxygen Species Contributes to the Development of Carbon Black Cytotoxicity to Vascular Cells. *Toxicol Res.* **2011**, *27*, 161–166. [CrossRef]
42. Guedelhoefer, O.C.; Alvarado, S. Amputation induces stem cell mobilization to sites of injury during planarian regeneration. *Development* **2012**, *139*, 3510–3520. [CrossRef]
43. Hayashi, T.; Asami, M.; Higuchi, S.; Shibata, N.; Agata, K. Isolation of planarian X-ray-sensitive stem cells by fluorescence-activated cell sorting. *Dev. Growth Differ.* **2006**, *48*, 371–380. [CrossRef]
44. Isolani, M.E.; Abril, J.F.; Saló, E.; Deri, P.; Bianucci, A.M.; Batistoni, R. Planarians as a Model to Assess In Vivo the Role of Matrix Metalloproteinase Genes during Homeostasis and Regeneration. *PLoS ONE* **2013**, *8*, e55649. [CrossRef] [PubMed]
45. Fabbrizi, M.R.; Warshowsky, K.E.; Zobel, C.L.; Hallahan, D.E.; Sharma, G.G. Molecular and epigenetic regulatory mechanisms of normal stem cell radiosensitivity. *Cell Death Discov.* **2018**, *4*, 117. [CrossRef]
46. Sahu, S.; Sridhar, D.; Abnave, P.; Kosaka, N.; Dattani, A.; Thompson, J.M.; Hill, M.A.; Aboobaker, A. Ongoing repair of migration-coupled DNA damage allows planarian adult stem cells to reach wound sites. *eLife* **2021**, *10*, e63779. [CrossRef] [PubMed]
47. Shiroor, D.A.; Bohr, T.E.; Adler, C.E. Injury delays stem cell apoptosis after radiation in planarians. *Curr. Biol.* **2020**, *30*, 2166–2174. [CrossRef] [PubMed]
48. Juan, J.Y.; Zhu, J.Q.; Zhao, C.Z.; Kang, Q.; Zhang, X.; Suo, K.; Cao, N.; Hao, L.; Lu, J. Potential of natural products as radioprotectors and radiosensitizers: Opportunities and challenges. *Food Funct.* **2021**, *12*, 5204–5218.
49. Tiwari, P.; Mishra, K.P. Flavonoids sensitize tumor cells to radiation: Molecular mechanisms and relevance to cancer radiotherapy. *Int. J. Radiat. Biol.* **2020**, *96*, 360–369. [CrossRef] [PubMed]
50. Shibata, N.; Rouhana, L.; Agata, K. Cellular and molecular dissection of pluripotent adult somatic stem cells in planarians. *Dev. Growth Differ.* **2010**, *52*, 27–41. [CrossRef]

*antioxidants*

MDPI

*Article*

# Radiation Type- and Dose-Specific Transcriptional Responses across Healthy and Diseased Mammalian Tissues

**Eftychia Sagkrioti [1,2], Gökay Mehmet Biz [3,†], Işıl Takan [4,5,†], Seyedehsadaf Asfa [4,5], Zacharenia Nikitaki [1], Vassiliki Zanni [1], Rumeysa Hanife Kars [6], Christine E. Hellweg [7], Edouard I. Azzam [8], Stella Logotheti [1], Athanasia Pavlopoulou [4,5] and Alexandros G. Georgakilas [1,*]**

[1] DNA Damage Laboratory, Physics Department, School of Applied Mathematical and Physical Sciences, National Technical University of Athens (NTUA), Zografou, 15780 Athens, Greece
[2] Biology Department, National and Kapodistrian University of Athens (NKUA), 15784 Athens, Greece
[3] Department of Technical Programs, Izmir Vocational School, Dokuz Eylül University, Buca, Izmir 35380, Turkey
[4] Izmir Biomedicine and Genome Center (IBG), Balcova, Izmir 35340, Turkey
[5] Izmir International Biomedicine and Genome Institute, Dokuz Eylül University, Balcova, Izmir 35340, Turkey
[6] Department of Biomedical Engineering, Istanbul Medipol University, Istanbul 34810, Turkey
[7] German Aerospace Center (DLR), Institute of Aerospace Medicine, Radiation Biology, Linder Höhe, D-51147 Köln, Germany
[8] Canadian Nuclear Laboratories, Chalk River, ON K0J 1J0, Canada
* Correspondence: alexg@mail.ntua.gr; Tel.: +30-210-7724453
† These authors have contributed equally to this work.

**Abstract:** Ionizing radiation (IR) is a genuine genotoxic agent and a major modality in cancer treatment. IR disrupts DNA sequences and exerts mutagenic and/or cytotoxic properties that not only alter critical cellular functions but also impact tissues proximal and distal to the irradiated site. Unveiling the molecular events governing the diverse effects of IR at the cellular and organismal levels is relevant for both radiotherapy and radiation protection. Herein, we address changes in the expression of mammalian genes induced after the exposure of a wide range of tissues to various radiation types with distinct biophysical characteristics. First, we constructed a publicly available database, termed RadBioBase, which will be updated at regular intervals. RadBioBase includes comprehensive transcriptomes of mammalian cells across healthy and diseased tissues that respond to a range of radiation types and doses. Pertinent information was derived from a hybrid analysis based on stringent literature mining and transcriptomic studies. An integrative bioinformatics methodology, including functional enrichment analysis and machine learning techniques, was employed to unveil the characteristic biological pathways related to specific radiation types and their association with various diseases. We found that the effects of high linear energy transfer (LET) radiation on cell transcriptomes significantly differ from those caused by low LET and are consistent with immunomodulation, inflammation, oxidative stress responses and cell death. The transcriptome changes also depend on the dose since low doses up to 0.5 Gy are related with cytokine cascades, while higher doses with ROS metabolism. We additionally identified distinct gene signatures for different types of radiation. Overall, our data suggest that different radiation types and doses can trigger distinct trajectories of cell-intrinsic and cell-extrinsic pathways that hold promise to be manipulated toward improving radiotherapy efficiency and reducing systemic radiotoxicities.

**Keywords:** radiation response; bioinformatics; oxidative stress; transcriptomics; radiobiology database; gene signature

**Citation:** Sagkrioti, E.; Biz, G.M.; Takan, I.; Asfa, S.; Nikitaki, Z.; Zanni, V.; Kars, R.H.; Hellweg, C.E.; Azzam, E.I.; Logotheti, S.; et al. Radiation Type- and Dose-Specific Transcriptional Responses across Healthy and Diseased Mammalian Tissues. *Antioxidants* **2022**, *11*, 2286. https://doi.org/10.3390/antiox11112286

Academic Editors: Elena Obrador Pla and Alegria Montoro

Received: 17 August 2022
Accepted: 15 November 2022
Published: 18 November 2022

**Publisher's Note:** MDPI stays neutral with regard to jurisdictional claims in published maps and institutional affiliations.



## 1. Introduction

Radiation therapy has witnessed unprecedented advances during the last decades, asserting its place as a major part of everyday clinical practice [1]. It contributes to ~40%

of curative cancer treatments [2], alone or in combination with chemotherapy [3], and tends to be less morbid than surgery [4]. In addition to its direct cytotoxic effects on the targeted tumors, irradiation often triggers indirect localized and systemic responses. These responses are not only occasionally linked with early or late adverse side effects proximal or distal to the treatment site but can also be beneficial for patient outcomes. Intriguingly, recent studies show that radiotherapy induces *bona fide* immunogenic cell death and engages tumor-targeting immune responses in support of enhancing treatment efficacy. Local irradiation reshapes the tumor microenvironment (TME) by promoting prooxidant and proinflammatory reactions, which may trigger adaptive immune responses [1]. Stressed and dying irradiated cells release numerous bioactive molecules, for example, major histocompatibility complex, cell-adhesion molecules, and proinflammatory cytokines and their receptors, as well as molecules with damage-associated molecular patterns (DAMPs), small metabolites, nucleic acids and lipids. These tumor-associated antigens interact with the immune system to induce immunogenic cell death [5,6] since they are taken up by the dendritic cells and stimulate downstream effector T cells, which subsequently recognize and lyse tumor cells both locally and at distant sites [7]. In several clinical cases, tumors distal to the targeted site regressed in response to irradiation-induced immunogenicity, a phenomenon termed as an abscopal effect [7]. In this respect, the irradiated cells act as in situ vaccines against tumors, sensitizing the immune system to detect cancer cells even long after the completion of radiation treatment. Hence, systemic effects of radiotherapy may act as a "blessing in disguise" due to their potential to ally with the immune system and increase responses that control the growth of micrometastases and malignant tissues at distant sites. However, the effects may also be a "curse" resulting in the suppression of antitumor immunity by mechanisms involving regulatory T cells [8].

The newly-discovered immunomodulatory properties of radiation have been linked with its ability to primarily activate the DNA damage response and repair (DDR/R) machinery. DDR/R is a highly conserved and complex network of signal transduction pathways that preserves the genetic information by repairing a variety of DNA lesions, such as nucleotide alterations, bulky adducts, single-strand breaks (SSBs) and double-strand breaks (DSBs). These pathways can be lesion-specific, for example, non-homologous end joining (NHEJ) and homologous recombination (HR) repair for DSBs; single-strand break repair (SSBR) for nicked DNA strands; mismatch repair (MMR) for errors that occurred during replication; base excision repair (BER) for oxidative base modifications; and nucleotide excision repair (NER) for helix-distorting lesions [9]. The stimulation of different components of DDR/R, either endogenously or from external sources, such as exposure to ionizing radiation (IR), alerts host immunity at the systemic level and vice versa [10], thereby accounting for the intriguing immunogenic properties of irradiated cells. These novel concepts have rejuvenated clinical interest to exploit this dynamic and bidirectional crosstalk between DDR/R and immune response (ImmR) signaling and manipulate it towards personalized radiotherapeutic solutions.

There are several types of therapeutic modalities, classified according to radiation quality associated mainly with the linear energy transfer (LET), a parameter accounting for the amount of energy deposited per unit length of the irradiating particle's path. Low-LET radiation entails the more frequently used $\gamma$- and X-rays, while high-LET refers to protons, carbon ions and $\alpha$-particles that capitalize on the physical and radiobiological properties of charged particles for an improved dose distribution and increased cell killing efficacy. Carbon ions kill cells twice or three times more effectively than protons and conventional radiation modalities [11]. In general, high-LET types induce more DSBs per dose unit, and more complex and dense lesions than low-LET types because they deposit large amounts of energy within a small distance [12]. The type of initial DNA damage largely determines the repair pathway that is subsequently activated. For example, heavy ions preferentially shift towards DSB repair pathways, such as HR and NHEJ, when compared with sparsely ionizing irradiation [1]. Given that a different type of DNA damage can trigger different DDR components, which in turn are associated with the release of

immunostimulatory neoantigens as "danger signals" (i.e., DAMPs), it is reasonable to envisage that each of these irradiation types governs distinct trajectories of DNA damage type—DDR pathway—immunogenic responses, which, however, to date, have not been identified [1]. In this regard, understanding the major differences of low- and high-LET treatment options is a current challenge of radiotherapy, not only for minimizing side effects, but also for making the most of each modality toward stimulating tumor-targeting adaptive immunity post-irradiation.

The effects of the various radiation types are mediated, at least partly, through changes in the transcriptomes of the irradiated cells. In general, different types of radiation trigger distinct gene transcription programs associated with divergent cellular responses both in cancer and normal cells. Although radiation type-specific transcriptional changes have been examined sporadically [13–18], to our knowledge, there is no systematic effort to characterize the effects of several high-LET or low-LET radiation types and doses of radiation in normal or diseased tissues, which would set a basis to untangle their side effects from their beneficial cytotoxic and immunogenic properties. Simultaneous screening of the transcriptomes across irradiated cancer and normal tissues would require large-scale experiments for each radiation type and/or dose. Furthermore, due to the genetic heterogeneity of cells in irradiated tissues, which is a major parameter of the efficacy of radiotherapy, extensive testing on a large variety of tissue contexts is required, transforming this effort to a "Herculean task".

As a "*deus ex machina*", computational approaches have entered the stage of radiobiology to accelerate and complement these efforts. In the present work, we constructed a publicly available, user-friendly database, termed RadBioBase version 1 (http://radbiodb.physics.ntua.gr/), which includes a collection of up-to-date existing data on mammalian genes differentially expressed after exposure to different types (X-rays, γ-rays, protons, carbon ions and α-particles) and doses of radiation in a variety of cell types. This database is a comprehensive tool for correlations of radiation type and/or dose with corresponding transcriptional responses across a variety of tissues. Following an integrated bioinformatics approach that included gene-centric, pathway-oriented and machine learning analyses, we consolidated the IR-induced differential gene expression to biological pathways and human diseases. In addition, we identified gene signatures for different radiation types. Our analyses provide insights into the links between the IR-induced damage and the signal propagation of stress to distant sites, and hold promise for a deeper understanding of the association between DDR and the immune system to a wider context, in a coordinated multiscale manner, which could be translated to more efficient and safer radiotherapy schemes.

## 2. Materials and Methods

### *2.1. Data Hybrid Collection and Transcriptomic Analyses*

A broad collection of genes was initially obtained by rigorous text mining of the bibliographic database MEDLINE/PubMed 2.0 (https://pubmed.ncbi.nlm.nih.gov/, accessed on 15 March 2021), with the use of keywords related to X-ray, γ-ray, proton, carbon ion and α-particle irradiation, i.e., ((gamma radiation) OR (gamma rays) OR (γ rays)) AND gene expression; ((proton(Title/Abstract)) AND (radiation(Title/Abstract))) AND (gene expression(Title/Abstract)); ((carbon(Title/Abstract)) AND (radiation(Title/Abstract))) AND (gene expression(Title/Abstract)) from 1 January 2006 to 30 August 2021. The articles were independently retrieved from the literature by three of the authors (E.S, R.H.K. and A.P.). Relevant data were extracted from the articles and recorded into an Excel worksheet.

For the articles to be considered eligible for inclusion in our study, they had to report the following information: (i) tissue/cell line, (ii) cell type (cancer or normal), (iii) model organism, (iv) type of irradiation, (v) irradiation exposure time, (vi) dose amount, (vii) availability of data regarding genes differentially expressed between irradiated and non-irradiated (control) cells/tissues, or sufficient data to calculate differential gene expression. To minimize investigator biases, compliance of the screened articles with the study eligibility criteria was assessed, independently, by three researchers, E.S, R.H.K. and A.P.

and validated by the supervising researcher (A.G.G.). In this way, a total of 39 studies were selected. Gene symbols were assigned to the extracted human, mouse and rat genes according to the HUGO Gene Nomenclature Committee (HGNC) (https://www.genenames.org/, accessed on 20 November 2021).

In cases where differential gene expression data were not provided in the corresponding articles, we searched for the original gene expression data files deposited in NCBI GEO (Gene Expression Omnibus) DataSets [19] according to the selection criteria: (i) gene expression data derived from irradiated and non-irradiated (control) tissue/cell samples, and (ii) inclusion of >5000 genes in the dataset. The following microarray transcriptome datasets were obtained where their respective GEO series and PubMed references are shown in brackets: X-rays (GSE107685 [20], GSE113611 [21], GSE107443 [22], GSE90909 [23], GSE85323 [24], GSE59861 [25], GSE6262 [26]); α particles (GSE12435 [27], GSE21059 [28], GSE18760 [29]); carbon ions (GSE6630 [30]); protons (GSE20629 [31]). The GEO2R interactive web server [19] was employed to detect genes differentially expressed at different conditions.

The differentially expressed genes (DEGs) with an absolute log2 fold-change (FC) greater than 1.5 ($|\log2FC \geq 1.5|$), or FC > 1.5 and FC < 0.67, and FDR-adjusted *p*-value (q-value) less than 0.05 or *p*-value < 0.001 (for transcriptomic data) and *p*-value < 0.05 (for the text mining data) were retained.

### *2.2. Functional Enrichment Analysis*

Venn diagrams were constructed using the online tool Draw Venn Diagram (https://bioinformatics.psb.ugent.be/webtools/Venn/, accessed on 20 January 2022) to identify common up and downregulated genes across radiation types, as well as of low- versus high-LET radiation (only for entries where the corresponding LET was provided in the original paper) and deregulated genes of lower versus higher doses in the range of clinical interest (0.3–0.5 Gy vs. 0.6–2.0 Gy). Furthermore, overrepresented biological pathways, along with the corresponding disease pathways, were identified in different sets of genes, related to every type of irradiation, as well as for low and high LET, and low and high clinical doses. Functional enrichment analysis was conducted with WebGestalt (WEB-based GEne SeT AnaLysis Toolkit) 2019, an online tool used for the identification of statistically significant enriched terms in the given gene sets compared to selected reference sets [32]. The WebGestalt parameters chosen were "Organism of Interest": Homo sapiens, "Method of Interest": Over-Representation Analysis (ORA), "Functional database": geneontology/Biological Process noRedundant and pathway/Wikipathway for biological paths, or disease/Disgenet for diseases, "Select gene ID type": gene symbol, "Select Reference set": genome; the default advanced parameters were chosen, and only pathways with false discovery rate (FDR)-corrected *p*-value less than 0.05 were considered in the analysis. Affinity propagation was used for clustering the terms (i.e., biological process and disease) by selecting a subset of representative terms.

### *2.3. Database Construction*

API-based Directus (https://docs.directus.io/, accessed on 10 April 2022), an open-source data platform, was used for content management, and MySQL (https://dev.mysql.com/, accessed on 10 April 2022), an open-access database management system, was used to store the data on the backend side. Data stored in excel format were imported to the MySQL database using Node.js.

On the front end, the popular VueJS framework, which provides officially maintained support packages for building web UIs, was used to create easily accessible content interfaces. Axios library (https://axios-http.com/, accessed on 12 April 2022), a promise-based HTTP client for the browser and Node.js, was used to obtain the data provided by Directus content management API services. Tailwind CSS framework (https://tailwindcss.com/, accessed on 12 April 2022) was utilized for the styles of the website interface.

### *2.4. Machine Learning Approach*

Random Forest is a bagging ensemble algorithm, which uses multiple different algorithms to generate a consensus output. It accepts as input a random sample generated from a given dataset with replacement, and then this sample is fed into the tree classifiers. At the end, the class of the sample is determined by voting with the principle of majority rule. During data classification, it can also provide the importance score of each variable (e.g., gene) and evaluate its role in the classification. There are many popular methods for gene selection, including deep gene selection [33], WERFE [34], Based Bayes error Filter [35], etc. The basic principle of all of these methods is to firstly rank the genes on the basis of certain evaluation criteria, and then select an optimal subset of genes. However, these methods cannot capture the relationship between the selected genes and the precision of the classification. Su and colleagues developed an algorithm based on recursive feature elimination (RFE), by taking into account the impact of both the gene numbers and prediction performance [36].

RFE is a greedy algorithm that creates gene sets recursively and then determines an optimal subset from those sets. The goal of RFE is to obtain the smallest possible sets of variables in an iterative way. RFE discards those genes of least importance in an iterative way and performs classification based on the new subsets of genes. All the gene subsets are evaluated based on their classification performance.

In our study, in order to prioritize the genes in the groups (a) irradiated *versus* non-irradiated, and (b) cancer *versus* normal, we first applied the RFE algorithm in Random Forest. All the methods were implemented by using the Python 3.9.7 *scikit-learn* module (https://pypi.org/project/scikit-learn/, accessed on 16 February 2022). To this end, we randomly divided our datasets into 75% training data and 25% testing data for all the models used for classification; the random state was set to 42. We first fit the model, then removed the less relevant genes (listed in the RadBioBase) and calculated the classification performance metric. After that, we removed the least important genes, fitted the model again and calculated the performance. This process was repeated until there were no genes left. The final set of genes was the set that maximized the performance. However, the gene subset selected in this study was the one with the highest accuracy since accuracy is the most common evaluation metric adopted for assessing the robustness and efficiency of algorithms. The final gene subsets of high *versus* low LET demonstrated classification accuracies of 95.54%, respectively.

Finally, to enhance the robustness of our results, robust rank aggregation (RRA) [37] was applied to the output of the previous steps so as to obtain the top-ranking genes. The RRA method uses a noise-robust probabilistic model to aggregate ranked lists, such as lists of genes, and to calculate the statistical significance ($p$-values) for all ranked elements. RRA was performed in the R programming environment (version 4.1.3) (https://www.r-project.org/, accessed on 10 March 2022).

### *2.5. Functional Network*

The STRING database (version 11.5) (https://string-db.org/, accessed on 15 May 2022) [38] was used to investigate and visualize both known and predicted associations among the protein products of the genes under study.

## 3. Results and Discussion

### *3.1. Development of RadBioBase*

For database construction, we performed text mining in PubMed, using appropriate keywords across studies that experimentally address the overall effect of five high- and low-LET radiation types of interest in a broad range of mammalian cell types, including human, mouse and rat study model systems. The database includes 7436 entries, with a total of 3730 unique genes derived from 14 tissues/cell lines [20–31,39–65]. For each entry, the following information was provided:

- Differential expression of genes: The expression status of the corresponding genes (i.e., up or downregulated in irradiated compared to non-irradiated tissue/cell control groups). In this version of the database, the canonical, full-length transcripts for each gene were used.
- Biological characteristics: Cell type (cancer or normal), organism and tissue/cell line.
- Type of irradiation: X-rays, γ-rays, protons, carbon ions or α-particles.
- Post-irradiation time when provided in the original study.
- Physical characteristics: LET (keV/μm), beam energy (MeV or kV for X-rays), dose (Gy) and average dose rate (Gy/min or Gy/h). In the cases where the LET of particles was not included in the original paper, it was calculated with the Stopping and Range of Ions in Matter (SRIM/TRIM) software, using as entrance parameters the type of ion, the target density and the energy of the irradiation beam when provided. For tissue targets not included in the compound dictionary of SRIM, the elemental compositions and mass densities were obtained from the bibliography [66–68]. Notably, the SRIM-calculated LET values were calculated only when provided in the relative studies, for the entrance point (highest energy values) of the beam instead of the Bragg peak, and thus were much smaller than the expected LET values for the Bragg peak region. According to the different energies in the various studies, LET values for protons were calculated as such: energies 100 MeV—-> 0.76 keV/μm, 250 MeV—-> 0.34 keV/μm, 190.6 MeV—-> 0.5 keV/μm, 230 MeV—-> 0.38 keV/μm, 4.5 MeV—-> 9.54 keV/μm (Table S1). Moreover, those α-particle energies not provided in the original paper were calculated empirically with the help of LET-energy curves [69].
- Comparison with low-LET irradiation: X-rays, γ-rays or electrons, depending on the information given in the original paper.
- DNA damage (in clusters per Gy per Gbp): DSBs and total clusters of DNA damage were calculated using the Monte Carlo Damage Simulation (MCDS) software [70,71] for each radiation type (Table S1). For each MCDS input file, the parameters were set as CELL: DNA = 1 ndia = 5 cdia = 10, SIMCON: nocs = 10,000 seed = 987,654,321, and the oxygen concentration was set to 20%, while X-ray and γ-ray radiation was simulated by a 10 keV electron beam. The inclusion of the "complex damages" is based on the well-documented importance of clustered DNA damages in defying biological responses and can provide the first hints for possible connections of the quality and quantity of DNA damage with specific gene expression [72]. PubMed ID of the corresponding article.
- Type of validation: depending on the method used in the original studies for data validation, we defined values as (a) microarrays, (b) RNA-Seq, (c) qPCR, (d) microarrays and qPCR, and (e) RNA-Seq and qPCR.

The above data are available through RadBioBase (http://radbiodb.physics.ntua.gr/). RadBioBase has a user-friendly interface and can be searched by using several options, such as (a) differentially expressed genes (b) gene expression status (up or downregulated), (c) type of radiation, (d) cell type (normal or cancer), (e) radiation dose, (f) radiation exposure time, (g) as well as a combination of the above options (Figure 1). The search results are displayed in a new window, in a tabular format, and can be downloaded to a CSV file. RadBioBase v1 is maintained by the National Technical University of Athens, Greece, and will be updated at regular intervals.

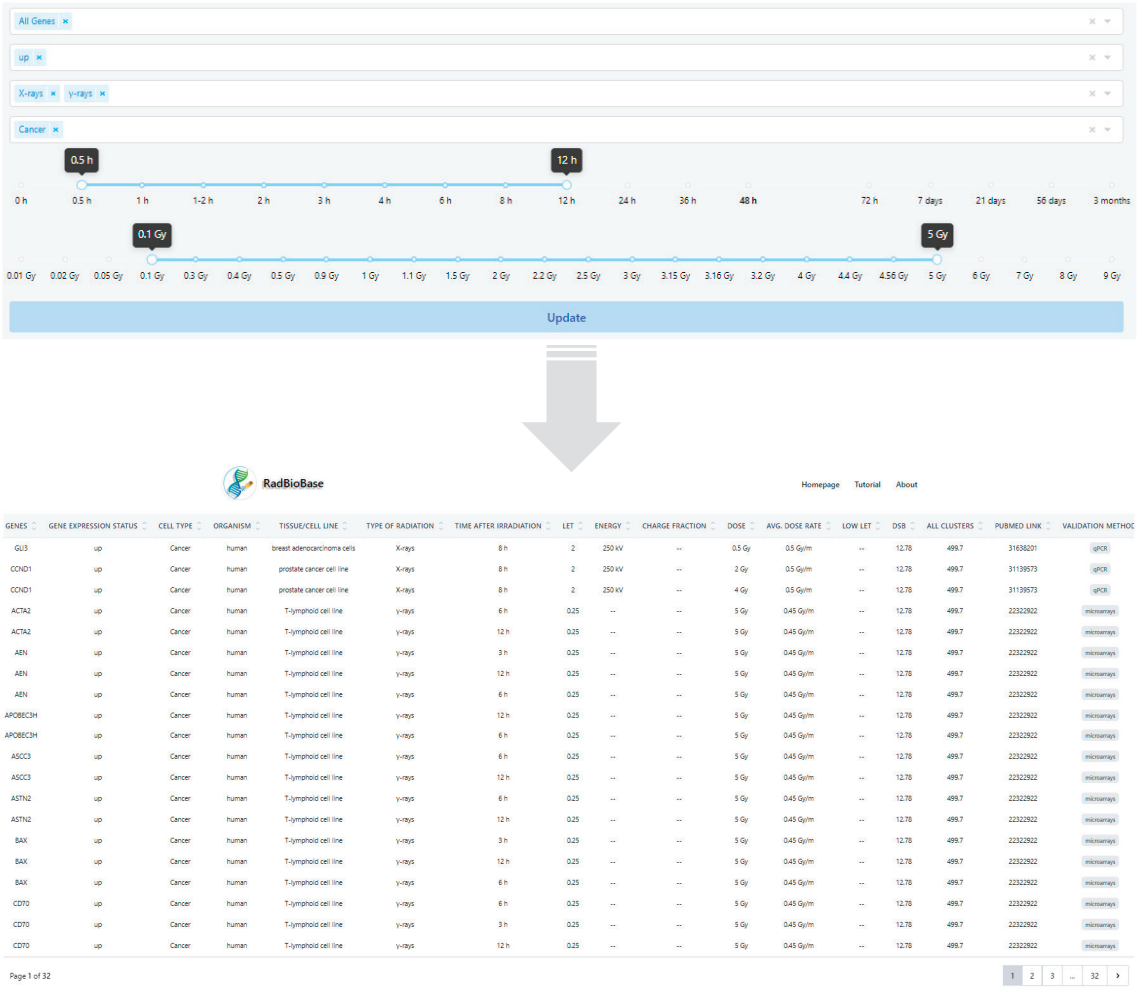


**Figure 1.** Example output page of RadBioBase. The database was searched using the "X-rays & γ-rays", "Cancer" and "up" options, by selecting the time and dose ranges 0.5–12 h and 0.1–5 Gy, respectively.

### *3.2. Commonalities among Radiation Types across a Number of Mammalian Tissues*

Using RadBioBase, we performed a comparison among all different types of irradiation (X-rays, γ-rays, protons, carbon ions and α-particles), to unveil basic commonalities across all therapeutic modalities and mammalian tissue types. One important consideration regarding this database is that, since its generation is based on publicly available data, it is inevitably more representative for the types of tissues and irradiation most frequently used across the corresponding studies. To collectively describe the content of this database, we estimated the number of entries for tissue type, radiation type, organism type and normal versus cancer cell type (Figure 2A–D). Overall, the database includes 14 types of cells/tissues (Figure 2A). The highest number of entries are assigned to blood, breast and lung tissue, possibly reflecting the types of cancers where irradiation represents a frequent standard of care treatment. Similarly, 50% of the entries correspond to X-rays, which have been in research and clinical use for longer periods than the more recent radiation types (Figure 2B). Moreover, 74% of the entries represent normal and 26% cancer cells (Figure 2C).

The percentages of entries in human versus rodent cells are similar, leading to a ratio of 1.06 (Figure 2D). This information facilitates the design of downstream analyses, interpretations of the results and inferences about disease pathways, especially in cases where the data are combined to generate universal signatures.

As shown in Figure 2E, among all up and downregulated genes (included in the current version of RadBioBase), we identified five genes that are commonly activated in all radiation groups (*GDF15*, *GADD45A*, *SESN1*, *CDKN1A* and *TP53INP1*). These genes are downstream effectors/targets of p53, a major tumor suppressor gene that encodes a transcription factor with a central role in preserving cell homeostasis and is one of the most important targets for translational cancer research. The physiologically low levels of mature p53 increase upon cellular stresses and, together with post-translational modifications, lead to the formation of oligomers that bind to specific p53 responsive elements on target gene promoters. Upon limited DNA damage, p53 induces cell cycle arrest and DNA repair genes, whereas upon extended and severe damage, it induces genes mediating senescence or cell death so as to isolate damaged cells from the intact cellular population [73]. The p53 pathways control five different kinds of cell death: (i) apoptosis, (ii) ferroptosis, (iii) TNF ligand- or (iv) FAS ligand-mediated necroptosis and (v) cellular senescence followed by the secretion of cytokines that attract immune system cells [74]. Our results are consistent with studies suggesting that the p53 pathway is a universally-induced sensitizer of cells to any type of irradiation [74]. They also suggest that p53-targeting molecules hold potential to be combined with any type of radiotherapeutic modality to increase treatment efficacy across a number of tissues.

As shown in Figure 2E, the number of non-overlapping genes for each radiation type tends to be higher than the genes that are in common in two or more radiation types. The fact that transcriptional responses tend to be radiation type-specific strongly indicates that along with the p53 cascades, each radiation modality can activate distinct biological pathways to exert its effects on cells. In an analogous manner, radiation-specific transcripts might be associated with different disease pathways, which can be predictors of specific side effects. To shed light on these aspects, we performed a detailed analysis of the overrepresented biological and disease pathways related to each type of radiation separately, along with the corresponding genes.

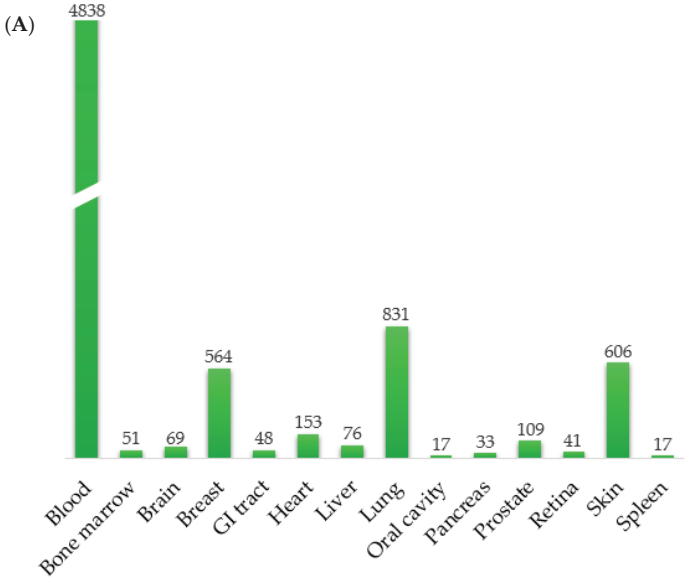


**Figure 2.** *Cont.*

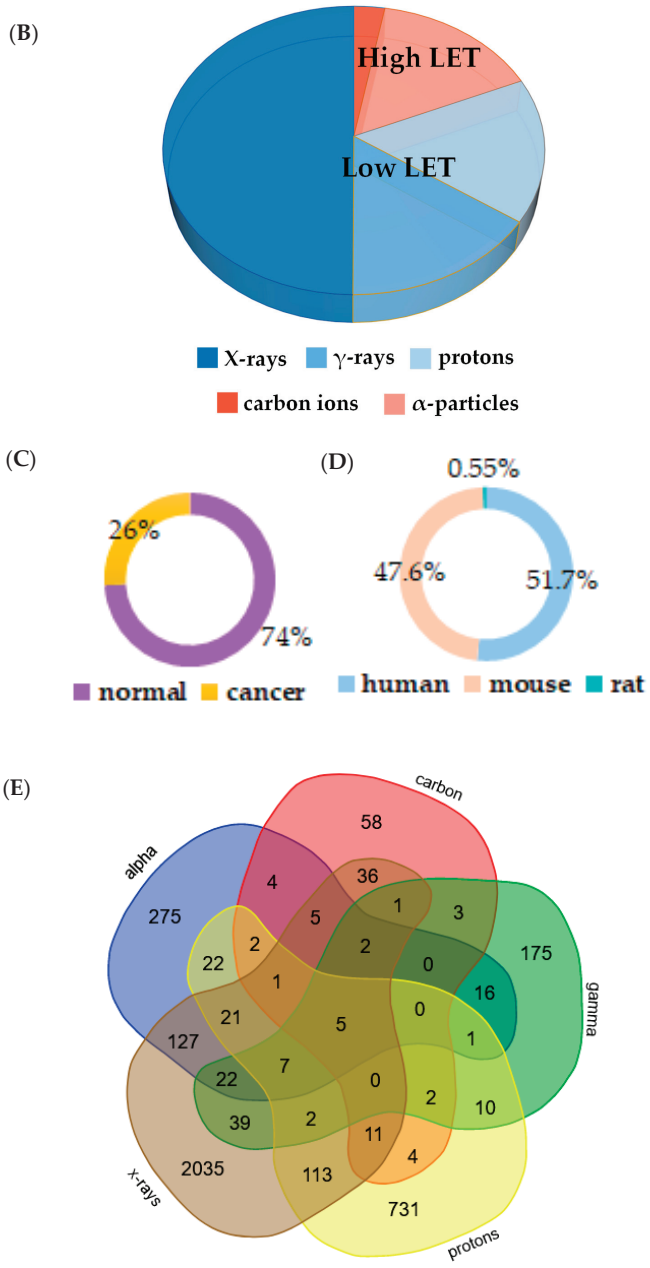


**Figure 2.** A description of the contents of the database and commonalities among the several radiation types. Database statistics. (**A**) Number of entries corresponding to tissues and cell lines are shown on top of the bars; the height of the bars is proportional to the number of entries. Percentage of entries related to (**B**) radiation types, (**C**) cancer and normal, (**D**) human and rodent tissues/cells across different types of radiation. (**E**) Venn diagram illustrating the overlapping of differentially expressed genes (both up and downregulated) between all radiation groups. The five common genes in all radiation groups are *GDF15*, *GADD45A*, *SESN1*, *CDKN1A* and *TP53INP1*.3.3. Each radiation type is linked to distinct biological functions.

We found that each radiation type, in general, exhibits a unique set of biological processes, beyond the expected pathways of response to stress and cell death. In particular, X-rays are related to metabolic processes, including the "fatty acid metabolic process", "small molecule catabolic process" and "sulfur compound metabolic process" (Figure 3A and Table S2). This is consistent with several studies showing that IR can cause metabolic changes, oxidative stress and cell death [75,76] and that sulfur-related enzymes play a major role in the radiation-induced oxidative stress response and detoxification [77]. Upon irradiation, where the levels of oxygen-free radicals are increased, sulfur-related metabolism acts as an antioxidative stress defense pathway. These processes are particularly prominent in the liver since its function is critical in the protection against induced stress, rendering the liver extremely sensitive to radiation. X-ray irradiation was also found to be associated with fatty acid (FA) metabolism. Interestingly, recent studies suggest that FA metabolism represents the link between X-ray irradiation and ferroptosis, a novel type of programmed cell death that depends on iron and is characterized by the accumulation of lipid peroxides [78]. This FA-related type of cell death is genetically and biochemically distinct from other forms of regulated cell death. In agreement, ferroptosis-inducing agents can sensitize cancer cells to X-ray irradiation [79], while pro-ferroptotic FA metabolism renders cancer cells immunogenic [80]. In light of these data, it would be interesting to investigate whether X-rays initiate an FA metabolism–ferroptosis axis, which subsequently modulates the immunogenic properties of irradiated cells towards enhancing therapeutic responses to immunotherapy.

Additionally, we found associations of X-ray-induced transcriptomes with zinc and copper homeostasis (Figure 3A and Table S2). On the one hand, zinc homeostasis is indirectly related to post-irradiation effects through increases in oxidative stress [81–83]. Zinc exhibits protective effects against irradiation by activating antioxidant enzymes, which in turn reduce reactive oxygen species (ROS) levels and oxidative stress [81,83,84]. In addition, zinc acts as an intracellular signaling molecule, activating apoptotic pathways, immunodeficiency and inflammation suppression [81,83,85]. On the other hand, copper ions contribute to radiation- and stress-resistance [86], tumor growth, inflammation and angiogenesis [87–90].

Among higher LET radiation types, protons are strongly related to apoptosis and oxidative stress (Figure 3B and Table S2), while carbon ion and alpha particles with enhanced proinflammatory signaling. However, while carbon ions exhibit overrepresented interleukin-18 (IL-18) signaling pathways (Figure 3B and Table S2), α-particles appear to be linked with photodynamic therapy (PDT)-induced NF-κB survival signaling (Figure 3B and Table S2). IL-18 is a proinflammatory cytokine of the interleukin-1 family, expressed in several cell types, including, but not limited to, macrophages, dendritic cells and epithelial cells. It is also involved in the regulation of immunomodulatory cytokine networks that mediate host defense, inflammation and tissue regeneration [91]. Regarding the transcription factor NF-κB, it integrates several stress signals and can regulate DNA transcription, cell survival, as well as immune system and inflammatory responses in a pleiotropic manner. NF-κB pathways are triggered by PDT and regulate the interplay between the immune system and an anti-cell death response through the release of cytokines and chemokines and the control of apoptosis or necrosis [92]. Intriguingly, IL-18 can also activate NF-κB; therefore, it is possible that the effects of carbon ions and alpha particles revolve around a complex inflammatory and immunomodulatory network, where NF-κB occupies a central hub position suggested also by Hellweg (2015) [93]. Taking into account that higher LET radiation can cause a higher level of DSBs and DNA damage clusters [94], it would be interesting to further investigate if these pathways may stand at the crossroads of high LET-specific DNA damage and the immune response [95,96].

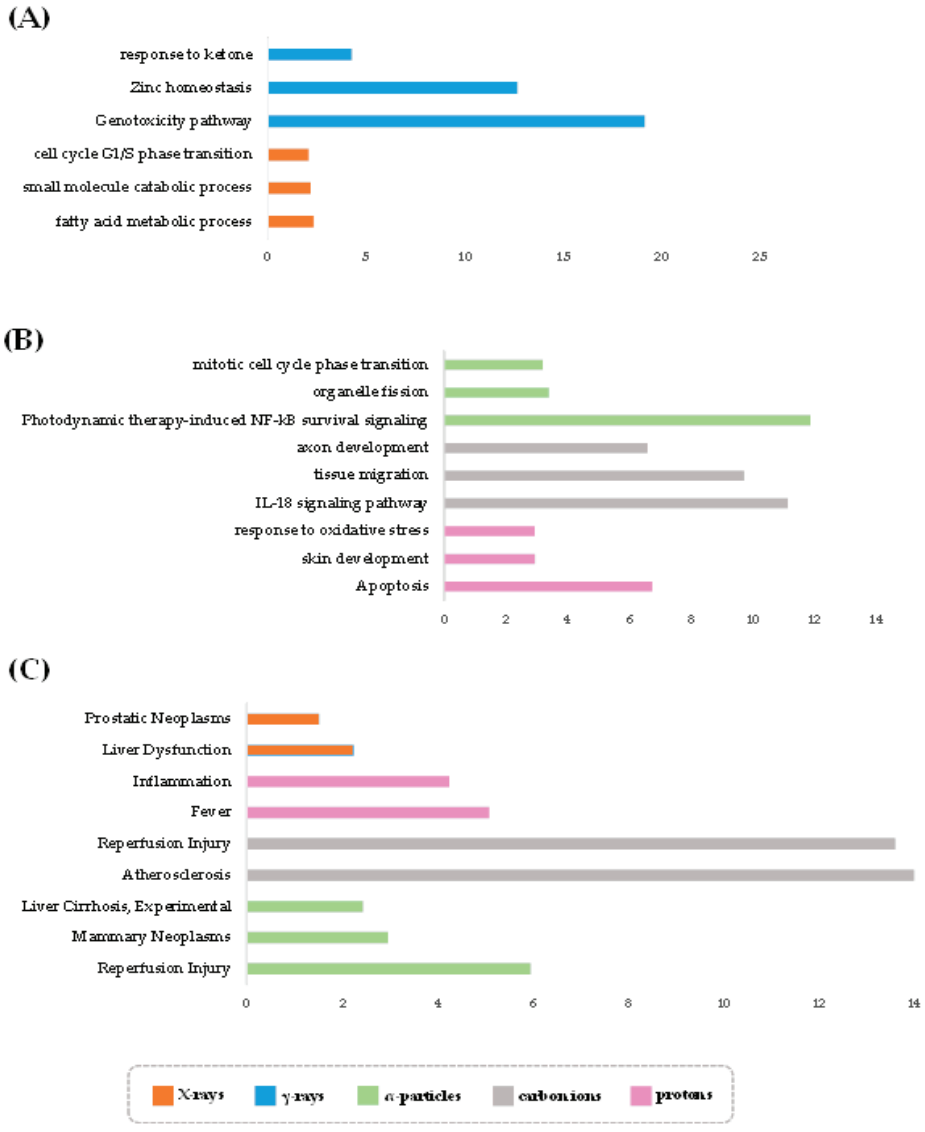


**Figure 3.** Gene set enrichment analysis. Overrepresented biological pathways (affinity propagation) for the DEGs in different types of radiation. (**A**) Low-LET radiation (X- and γ-rays) and (**B**) higher LET radiation (protons, carbon ions, α-particles). (**C**) Overrepresented disease pathways (affinity propagation) for all DEGs genes in different radiation types. The *x*-axis corresponds to the enrichment ratio, i.e., the ratio of the number of observed genes to the number of expected genes from each category in the input gene list.

We also observed that carbon ions activate transcripts involved in axon guidance and cell migration [96]. This finding is consistent with studies suggesting that cell migration and apoptosis in normal and tumorigenic tissues is regulated by many axon guidance molecules [97]. Notably, tumor-intrinsic activation of genes indispensable for neuronal development and neurological function is a nearly universal phenomenon in cancer, which, depending on the cancer type, can have either a negative or a positive effect in disease

initiation and progression [98,99]. To date, it remains a *terra incognita* as to whether some radiotherapeutic modalities also trigger this phenomenon. Another hypothesis is that the axon guidance processes identified in Figure 3B reflect associations between IL-18 and neuroinflammation and neurodegeneration (which are conditions further related to high-LET irradiation [100]). IL-18 is constitutively expressed in resident cells of the central nervous system (CNS), supporting a local IL-18-dependent immune response that can influence neural tissue homeostasis [101,102]. Investigating how carbon ion beams, compared to other radiation types, may activate neuronal pathways, and how this reflects to the tissue microenvironment and the crosstalk of the irradiated cells with surrounding neuronal and immune cells, remains a subject of fruitful research. Dissecting the connection between therapeutic radiation and the co-option of neuronal programs in the irradiated cells could provide invaluable insights for increasing the therapeutic efficacy of radiation and ameliorating any side effects on healthy tissues.

### *3.3. Radiation Type-Specific Disease Pathways Inferred from Transcriptomes of Irradiated Cells*

An analogous analysis of the overrepresented human disease pathways that are associated with irradiation-responsive transcripts indicated relatively distinct disease profiles across radiation types (Figure 3C and Table S3). In detail, liver dysfunction pathways are dominant upon X-ray irradiation (Figure 3C and Table S3), perhaps as a sequalae of the critical function of this organ in the protection against induced stress, hence indicating a sensitivity of the liver upon radiotherapy. Another vital organ that might be affected is the heart since carbon ion irradiation was found to be associated with atherosclerotic disease (Figure 3C and Table S3), in agreement with clinical reports that patients who have undergone radiotherapy are at increased risk for cardiovascular diseases (CVDs) [103]. Since IL-18 participates in atherogenesis [104], the increased incidence of CVDs might reflect the activation of IL-18 signaling pathways that are associated with this radiation type. These findings suggest that increased monitoring, further investigation and timely treatment might be required in order to prevent these unwanted effects. Proton-based therapy appears to be related with inflammation and fever (Figure 3C and Table S3), two mild side effects that are amenable to clinical management. Energetic carbon and alpha particles are associated with reperfusion injury (Figure 3C and Table S3), a type of ROS-induced tissue damage occurring when blood supply returns to tissue after a period of ischemia or hypoxia. Interestingly, single-dose radiotherapy coupled with early tumor ischemia/reperfusion can lead to tumor lethality via the inactivation of homologous recombination [105]. Hence, occurrence of this side effect in patients undergoing radiotherapy might be an indicator of selective tumor radiosensitization and increased therapeutic efficiency. In conclusion, our analysis reveals radiation type-specific side effects and possible comorbidities that call for increased surveillance for relevant patient complaints after radiation treatment.

### *3.4. Machine Learning-Generated Gene Signatures of Cell Sensitivity to High- Versus Low-LET Radiation Types*

One issue in the clinic is the selection of individual patients for high- or low-LET radiation treatment, which is in turn dependent on the radiobiological properties of the tumor [106]. In this regard, transcriptomics data of irradiated cells can infer radiosensitivity predictors, whereby differentially expressed genes are ranked on the basis of certain evaluation criteria, and then an optimal subset of genes is selected [107]. Although insightful, previously described methods may pose limitations in gene selection, as the produced gene signatures may not accurately capture the relationship between the selected genes and the precision of the classification. To bypass these limitations, we applied machine learning, a robust computational method that holds promise to reduce the complexity of whole genome gene expression patterns and produce manageable signatures of response while simultaneously taking into account several important selection criteria [108]. We used a recently-developed algorithm based on recursive feature elimination (RFE), which creates gene sets recursively and then determines an optimal subset, aiming to obtain

the smallest possible sets of variables in an iterative way while discarding those genes of least importance [36]. To verify the ability of the algorithm to generate gene signatures linked to the features of interest, we initially ran a control test in DEGs of cancer versus normal tissues that are included in the RadBioBase. The algorithm predicted correctly a number of markers of tumor initiation and progression, such as CD44 [109], MMP9 [110], CDC20 [111], FOS [112] and WNT5A [113] (Figure S1). Several of these genes are also associated with sensitivity to radiation, as confirmed by further comparisons versus our previously published comprehensive lists of molecular determinants of radiation response in cancer tissues [114]. Having assured the accuracy of the algorithm in our datasets, we proceeded to generate a gene signature (Figure 4A) for high- *versus* low-LET radiations, using clinically relevant criteria such as post-irradiation time and dose on the data of RadBioBase. The five types of radiation were grouped into two groups because the larger the dataset, the more information the machine learning algorithm can capture, thereby enhancing its predictive performance. This led to the identification of a 22-gene signature that is characteristic for the response to high-LET as opposed to low-LET irradiation. GSEA analysis showed that the most significantly enriched (FDR < 0.05) processes of those genes are cell cycle, cell division and inflammation.

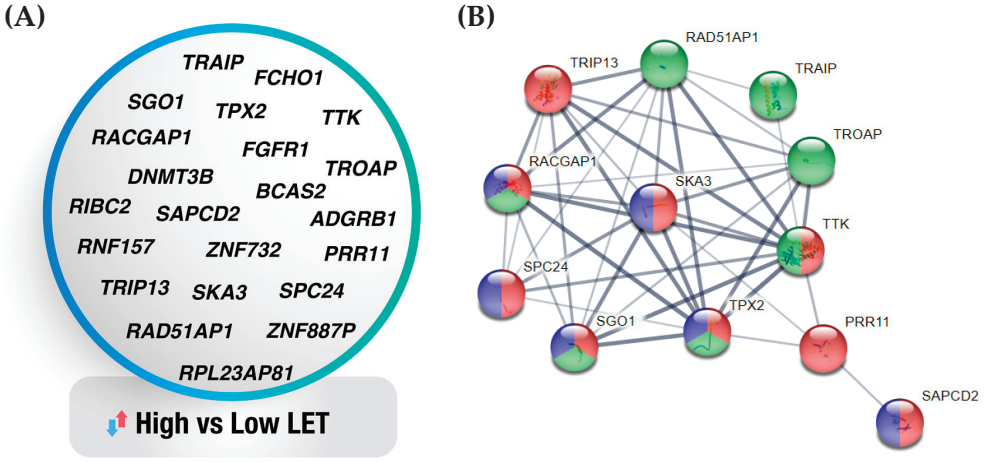


**Figure 4.** Gene signature of high- *versus* low-LET radiation types. (**A**) Twenty-two-gene signature characteristic of response to high-LET vs. low-LET irradiation. (**B**) Network depicting the associations (edges) of twelve signature genes/gene products (nodes) in cell cycle (red), cell division (blue) and inflammation (green).

A further STRING analysis of this signature revealed that twelve of those genes/proteins appear to interact (Figure 4B) and mediate cell cycle, cell division and/or inflammation (Figure 4B, genes with red, blue and green color-coding), thereby accurately reflecting the main processes known to be induced by LET. Among these genes, we were able to identify several recently-characterized effectors of radiosensitivity, such as RAD51-associated protein 1 (RAD51AP1), which plays an integral role in homologous recombination by activating RAD51 recombinase, and its knockout is shown to induce radiosensitivity [115]; TTK protein kinase, the inhibition of which radiosensitizes basal-like breast cancer cells through impaired homologous recombination [116]; the DNA methyltransferase 3B (DNMT3B), an epigenetic modifier that protects centromere integrity by restricting R-loop-mediated DNA damage [117], and its silencing can restore the p53/p21 signaling pathway via DNA demethylation [118]; and TRAIP, a novel RAP80-interacting protein that is necessary for translocation of RAP80 to DNA lesions and promotes homologous recombination in response to DNA damage [119]. This signature also revealed novel genes that are associated with the response to radiation, for example, the Spindle And Kinetochore Associated

Complex Subunit 3 (SKA3) and the Rac GTPase Activating Protein 1 (RACGAP1). Future clinical validation of this signature in tissues from patients that have undergone high-LET radiation therapy can define indicators of responsiveness in this therapeutic modality towards improving patient selection.

### *3.5. Low-Dose Irradiation Is Associated with Cytokine Cascades, While High with ROS Metabolism*

Thus far, the implementation of new technologies in radiotherapeutic treatment has been largely empirical and driven by the belief that increasing doses will increase cure [1]. Consequently, in a large number of studies, high doses have been preferentially used to address the effects of irradiation on tissues. However, increased doses pose clinical risks for acute and/or chronic toxicities, without substantially enhancing the therapeutic benefits. Moreover, there is emerging evidence that low doses can be beneficial against several pathological entities. For example, in cancer, low-dose irradiation reverses resistance to immunotherapy by reprogramming the TME of immune-cold tumors [120], while in COVID-19-induced pneumonia, it induces antiinflammatory responses [121]. To further explore whether low doses could have therapeutic potential, we mined the RadBioBase database for differences in transcriptomes induced at different doses. The database contains entries from 37 studies using doses over 5 Gy, 2 studies using less than 0.5 Gy and 3 studies using both. For our analysis, we particularly considered the entries with a value of 0.3–0.5 Gy as "low" and those with a value of 0.6–2.0 Gy as "high" since these correspond to the clinically relevant low/high dose ranges. A GSEA analysis for the 445 genes found commonly deregulated at the 0.3–0.5 Gy range, underscored a profound overrepresentation of cytokine and inflammatory response pathways, implying that low doses are capable of inducing inflammation-related cascades. This is distinct from effects at high doses, where the 668 genes commonly responding to the 0.6–2.0 Gy range are associated with ROS metabolism (Figure 5 and Table S4). Following a gene-centric approach, we found many up or/and downregulated cytokines and interleukins, as well as other inflammation-related genes, deregulated at "low" doses. These include, but are not limited to, the upregulation of antiinflammatory genes *IL4* and *TNFA1P3*, and downregulation of the proinflammatory genes *IL12B* and *CDK5R2*. Nevertheless, genes that can exert both anti and proinflammatory activity depending on cell content, for example, *IL1A*, *IL1B*, *IL6* and *CXCL3*, appear to be upregulated at low doses in the original dataset, implying a complex cytokine profile at this range. The transcription of cytokines and other secreted molecules mediating intercellular communication (e.g., *CCL3*, *CCL4*, *CXCL2*, *IL22*, *TNF*, *IL18R1*, *IL7R* and *IL13RA2*, *IL13* and *IL10)* were also deregulated at high doses. Hence, low doses alter the transcription of secreted factors, but the composition of these factors is distinct compared to that of the high dose. In support, it was recently shown that high and low doses of irradiation induce different secretome profiles [122]. Given that our analyses are inevitably based on a relatively small number of available studies at low doses, further comprehensive characterization of the secretomes of low-dose irradiated cells is required to confirm these findings and decipher the inflammatory molecules with *bona fide* effects from those related to toxicities and radioresistance [123]. Considering that different doses/types induce different kinds of DNA damage, future high-throughput identification and functional characterization of the secretomes of cells irradiated with several types and/or doses holds promise to unveil links between intrinsic cell damage and the effects on adjacent and remote tissues, which can be translated into improved clinical patient management.

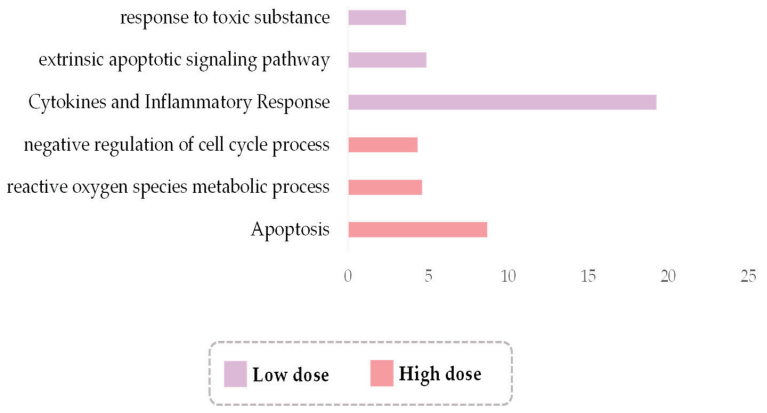


**Figure 5.** Overrepresented biological pathways (affinity propagation) for all 445 DEGs in low-dose (0.3–0.5 Gy) radiation group and all 668 DEGs in high-dose (0.6–2.0 Gy) radiation group considering all types of irradiation. The *x*-axis corresponds to the enrichment ratio.

## 4. Conclusions

The effects of irradiation are cell-intrinsic and cell-extrinsic, with the ability to reprogram the microenvironment both proximal and distal to the irradiated sites. Each irradiation type is suspected to cause different initial DNA lesions and activate distinct DDR/R components, inducing cell–cell interactions that ultimately lead to distinct immunogenic effects on cancer cells and on remote normal tissues. Predicting and characterizing the track of localized and systemic effects for each radiation type and dose can help fine-tune radiotherapy used alone or in combination with chemo- or immunotherapies, in a way that is less empirically-based and more guided by solid clinical and radiobiological data. To this end, comprehensive comparisons of changes in gene expression across normal and cancer cells for the several types and/or doses of radiation have a high clinical value for informing and improving decisions for radiotherapy. To address these novel challenges, we developed a database, termed RadBioBase, that can provide systemic insights into the attributes of irradiation relative to gene transcription in mammalian tissues. Further extending and updating this database to include additional tissue types in the future is anticipated to provide a cornerstone for the in silico prediction of the beneficial and toxic effects of radiation locally and systemically, which can be translated to more efficient and safer radiotherapy schemes. On the one hand, analyses of transcriptome changes in cancer cells can reveal novel pathways that enhance the response to radiation and/or awaken the immune system against the tumor cells. On the other hand, analyses of normal tissues can indicate genes associated with radiation type-specific side effects.

Notably, our database is designed to provide correlations between irradiation and the full-length transcripts of genes. At this point, it should be mentioned that several genes can synthesize isoforms or mutant forms with distinct or even opposing functions. Members of the TP53 family constitute such representative cases. For example, while wild-type TP53 induces radiosensitivity, expression of its missense mutants correlates with radioresistance [124]. Similarly, TP73, a sibling of TP53, synthesizes not only full-length TAp73 isoforms, which sensitize cells to irradiation, but also N-terminal truncated isoforms that are generated via aberrant splicing or alternative promoter usage at the 5'end and act as dominant negative inhibitors of their TAp73 counterparts, favoring resistance to radiation [125,126]. In cases of such genes, where their various protein products exert divergent effects on DDR and radiosensitivity, our database detects general associations with irradiation, without deciphering among the functionally divergent isoforms. The involvement of alternative forms or gain-of-function mutants needs to be subsequently

addressed in a more detailed, gene-centric manner, using complementary targeted next generation sequencing approaches.

Last but not least, the COVID-19 pandemic has changed our world by accelerating new digital and virtual reality megatrends in healthcare and setting in motion a dynamic that is expected to last and reform society and science at several levels. These changes are now more than ever before extrapolated to radiotherapy, a field that has historically evolved by taking advantage of contemporary technological trends. An important lesson taught is that central databases that share and disseminate information can improve global digital healthcare at several levels [127]. In line with this trend, our initiative to collect and systemically organize all available molecular information on the responses of mammalian tissues to irradiation can become a useful means for driving radiation oncology towards a new exciting digital health era.

**Supplementary Materials:** The following supporting information can be downloaded at: https://www.mdpi.com/article/10.3390/antiox11112286/s1, Figure S1: Markers of tumor initiation and progression; Table S1: MCDS simulation results for double-strand breaks (DSBs) and total clusters of DNA damage (DSBs and non-DSB oxidative lesions) per Gy per Gbp for radiation types used in this work; Table S2: Overrepresented biological pathways of the X-ray, γ-ray, protons, carbon ions and α-particle types of radiation and the corresponding retrieved genes; Table S3: Overrepresented disease pathways of the X-ray, protons, carbon ions and α-particle types of radiation and the corresponding genes; Table S4: Overrepresented pathways and related genes of the high (0.6–2.0 Gy) and low (0.3–0.5 Gy) radiation doses for all types of irradiation; Figure S1: Gene signature of cancer *versus* normal cells/tissues. Those genes implicated in radioresistance are underlined.

**Author Contributions:** Conceptualization, A.G.G.; methodology, E.S., S.A., S.L. and A.P.; software, S.A., G.M.B. and I.T.; validation, E.S., R.H.K., V.Z. and Z.N.; formal analysis, E.S., S.A., G.M.B., I.T., R.H.K. and A.P.; investigation, A.G.G., E.S., S.L. and A.P.; data curation, E.S., S.A., G.M.B., I.T., C.E.H., E.I.A. and A.P.; writing—original draft preparation, A.G.G., E.S., S.L. and A.P.; writing—review and editing, all authors; project administration, A.G.G. All authors have read and agreed to the published version of the manuscript.

**Funding:** AGG was funded from the project 21GRD02 BIOSPHERE, which has received funding from the European Partnership on Metrology, co-financed by the European Union's Horizon Europe Research and Innovation Programme and by the Participating States. Funder ID: 10.13039/100019599. Grant number: 21GRD02 BIOSPHERE.

**Institutional Review Board Statement:** Not applicable.

**Informed Consent Statement:** Not applicable.

**Data Availability Statement:** All data and analysis methodologies are contained in the manuscript. Any additional data requests can be addressed to the corresponding author.

**Acknowledgments:** The authors thank Konstantinos Anagnostopoulos (NTUA) for his help with the online version of the database.

**Conflicts of Interest:** The authors declare no conflict of interest.

## References

1. Schaue, D.; McBride, W.H. Opportunities and challenges of radiotherapy for treating cancer. *Nat. Rev. Clin. Oncol.* **2015**, *12*, 527–540. [CrossRef] [PubMed]
2. Baskar, R.; Lee, K.A.; Yeo, R.; Yeoh, K.W. Cancer and radiation therapy: Current advances and future directions. *Int. J. Med. Sci.* **2012**, *9*, 193–199. [CrossRef] [PubMed]
3. Delaney, G.; Jacob, S.; Featherstone, C.; Barton, M. The role of radiotherapy in cancer treatment: Estimating optimal utilization from a review of evidence-based clinical guidelines. *Cancer* **2005**, *104*, 1129–1137. [CrossRef] [PubMed]
4. Hong, A.M.; Stretch, J.R.; Thompson, J.F. Treatment of primary merkel cell carcinoma: Radiotherapy can be an effective, less morbid alternative to surgery. *Eur. J. Surg. Oncol.* **2021**, *47*, 483–485. [CrossRef] [PubMed]
5. Kroemer, G.; Galassi, C.; Zitvogel, L.; Galluzzi, L. Immunogenic cell stress and death. *Nat. Immunol.* **2022**, *23*, 487–500. [CrossRef] [PubMed]

6. Kroemer, G.; Galluzzi, L.; Kepp, O.; Zitvogel, L. Immunogenic cell death in cancer therapy. *Annu. Rev. Immunol.* **2013**, *31*, 51–72. [CrossRef]
7. Golden, E.B.; Apetoh, L. Radiotherapy and immunogenic cell death. *Semin. Radiat. Oncol.* **2015**, *25*, 11–17. [CrossRef]
8. Muroyama, Y.; Nirschl, T.R.; Kochel, C.M.; Lopez-Bujanda, Z.; Theodros, D.; Mao, W.; Carrera-Haro, M.A.; Ghasemzadeh, A.; Marciscano, A.E.; Velarde, E.; et al. Stereotactic radiotherapy increases functionally suppressive regulatory t cells in the tumor microenvironment. *Cancer Immunol. Res.* **2017**, *5*, 992–1004. [CrossRef]
9. Nakad, R.; Schumacher, B. DNA damage response and immune defense: Links and mechanisms. *Front. Genet.* **2016**, *7*, 147. [CrossRef]
10. Pateras, I.S.; Havaki, S.; Nikitopoulou, X.; Vougas, K.; Townsend, P.A.; Panayiotidis, M.I.; Georgakilas, A.G.; Gorgoulis, V.G. The DNA damage response and immune signaling alliance: Is it good or bad? Nature decides when and where. *Pharmacol. Ther.* **2015**, *154*, 36–56. [CrossRef]
11. Mohamad, O.; Sishc, B.J.; Saha, J.; Pompos, A.; Rahimi, A.; Story, M.D.; Davis, A.J.; Kim, D.W.N. Carbon ion radiotherapy: A review of clinical experiences and preclinical research, with an emphasis on DNA damage/repair. *Cancers* **2017**, *9*, 66. [CrossRef] [PubMed]
12. Nikitaki, Z.; Velalopoulou, A.; Zanni, V.; Tremi, I.; Havaki, S.; Kokkoris, M.; Gorgoulis, V.G.; Koumenis, C.; Georgakilas, A.G. Key biological mechanisms involved in high-let radiation therapies with a focus on DNA damage and repair. *Expert. Rev. Mol. Med.* **2022**, *24*, e15. [CrossRef] [PubMed]
13. Ding, L.H.; Park, S.; Peyton, M.; Girard, L.; Xie, Y.; Minna, J.D.; Story, M.D. Distinct transcriptome profiles identified in normal human bronchial epithelial cells after exposure to gamma-rays and different elemental particles of high z and energy. *BMC Genom.* **2013**, *14*, 372. [CrossRef] [PubMed]
14. Macaeva, E.; Tabury, K.; Michaux, A.; Janssen, A.; Averbeck, N.; Moreels, M.; De Vos, W.H.; Baatout, S.; Quintens, R. High-let carbon and iron ions elicit a prolonged and amplified p53 signaling and inflammatory response compared to low-let X-rays in human peripheral blood mononuclear cells. *Front. Oncol.* **2021**, *11*, 768493. [CrossRef]
15. Michalettou, T.D.; Michalopoulos, I.; Costes, S.V.; Hellweg, C.E.; Hada, M.; Georgakilas, A.G. A meta-analysis of the effects of high-let ionizing radiations in human gene expression. *Life* **2021**, *11*, 115. [CrossRef]
16. Nielsen, S.; Bassler, N.; Grzanka, L.; Laursen, L.; Swakon, J.; Olko, P.; Andreassen, C.N.; Alsner, J.; Singers Sorensen, B. Comparison of coding transcriptomes in fibroblasts irradiated with low and high let proton beams and cobalt-60 photons. *Int. J. Radiat. Oncol. Biol. Phys.* **2019**, *103*, 1203–1211. [CrossRef]
17. Niemantsverdriet, M.; van Goethem, M.J.; Bron, R.; Hogewerf, W.; Brandenburg, S.; Langendijk, J.A.; van Luijk, P.; Coppes, R.P. High and low let radiation differentially induce normal tissue damage signals. *Int. J. Radiat. Oncol. Biol. Phys.* **2012**, *83*, 1291–1297. [CrossRef]
18. Sertorio, M.; Nowrouzi, A.; Akbarpour, M.; Chetal, K.; Salomonis, N.; Brons, S.; Mascia, A.; Ionascu, D.; McCauley, S.; Kupneski, T.; et al. Differential transcriptome response to proton versus X-ray radiation reveals novel candidate targets for combinatorial pt therapy in lymphoma. *Radiother. Oncol.* **2021**, *155*, 293–303. [CrossRef]
19. Barrett, T.; Wilhite, S.E.; Ledoux, P.; Evangelista, C.; Kim, I.F.; Tomashevsky, M.; Marshall, K.A.; Phillippy, K.H.; Sherman, P.M.; Holko, M.; et al. Ncbi geo: Archive for functional genomics data sets–update. *Nucleic Acids Res.* **2013**, *41*, D991–D995. [CrossRef]
20. Becker, B.V.; Majewski, M.; Abend, M.; Palnek, A.; Nestler, K.; Port, M.; Ullmann, R. Gene expression changes in human ipsc-derived cardiomyocytes after X-ray irradiation. *Int. J. Radiat. Biol.* **2018**, *94*, 1095–1103. [CrossRef]
21. Mukherjee, S.; Grilj, V.; Broustas, C.G.; Ghandhi, S.A.; Harken, A.D.; Garty, G.; Amundson, S.A. Human transcriptomic response to mixed neutron-photon exposures relevant to an improvised nuclear device. *Radiat. Res.* **2019**, *192*, 189–199. [CrossRef] [PubMed]
22. Fujinaga, H.; Sakai, Y.; Yamashita, T.; Arai, K.; Terashima, T.; Komura, T.; Seki, A.; Kawaguchi, K.; Nasti, A.; Yoshida, K.; et al. Biological characteristics of gene expression features in pancreatic cancer cells induced by proton and X-ray irradiation. *Int. J. Radiat. Biol.* **2019**, *95*, 571–579. [CrossRef] [PubMed]
23. Broustas, C.G.; Xu, Y.; Harken, A.D.; Chowdhury, M.; Garty, G.; Amundson, S.A. Impact of neutron exposure on global gene expression in a human peripheral blood model. *Radiat. Res.* **2017**, *187*, 433–440. [CrossRef] [PubMed]
24. Broustas, C.G.; Xu, Y.; Harken, A.D.; Garty, G.; Amundson, S.A. Comparison of gene expression response to neutron and X-ray irradiation using mouse blood. *BMC Genom.* **2017**, *18*, 2. [CrossRef] [PubMed]
25. Hou, J.; Wang, F.; Kong, P.; Yu, P.K.N.; Wang, H.; Han, W. Gene profiling characteristics of radioadaptive response in ag01522 normal human fibroblasts. *PLoS ONE* **2015**, *10*, e0123316. [CrossRef] [PubMed]
26. Paul, S.; Smilenov, L.B.; Elliston, C.D.; Amundson, S.A. Radiation dose-rate effects on gene expression in a mouse biodosimetry model. *Radiat. Res.* **2015**, *184*, 24–32. [CrossRef]
27. Ghandhi, S.A.; Yaghoubian, B.; Amundson, S.A. Global gene expression analyses of bystander and alpha particle irradiated normal human lung fibroblasts: Synchronous and differential responses. *BMC Med. Genom.* **2008**, *1*, 63. [CrossRef]
28. Ghandhi, S.A.; Sinha, A.; Markatou, M.; Amundson, S.A. Time-series clustering of gene expression in irradiated and bystander fibroblasts: An application of fbpa clustering. *BMC Genom.* **2011**, *12*, 2. [CrossRef]
29. Ghandhi, S.A.; Ming, L.; Ivanov, V.N.; Hei, T.K.; Amundson, S.A. Regulation of early signaling and gene expression in the alpha-particle and bystander response of imr-90 human fibroblasts. *BMC Med. Genom.* **2010**, *3*, 31. [CrossRef]

30. Matsumoto, Y.; Iwakawa, M.; Furusawa, Y.; Ishikawa, K.; Aoki, M.; Imadome, K.; Matsumoto, I.; Tsujii, H.; Ando, K.; Imai, T. Gene expression analysis in human malignant melanoma cell lines exposed to carbon beams. *Int. J. Radiat. Biol.* **2008**, *84*, 299–314. [CrossRef]
31. Mezentsev, A.; Amundson, S.A. Global gene expression responses to low- or high-dose radiation in a human three-dimensional tissue model. *Radiat. Res.* **2011**, *175*, 677–688. [CrossRef] [PubMed]
32. Liao, Y.; Wang, J.; Jaehnig, E.J.; Shi, Z.; Zhang, B. Webgestalt 2019: Gene set analysis toolkit with revamped uis and apis. *Nucleic Acids Res.* **2019**, *47*, W199–W205. [CrossRef] [PubMed]
33. Alanni, R.; Hou, J.; Azzawi, H.; Xiang, Y. Deep gene selection method to select genes from microarray datasets for cancer classification. *BMC Bioinform.* **2019**, *20*, 608. [CrossRef] [PubMed]
34. Chen, Q.; Meng, Z.; Su, R. Werfe: A gene selection algorithm based on recursive feature elimination and ensemble strategy. *Front. Bioeng. Biotechnol.* **2020**, *8*, 496. [CrossRef]
35. Zhang, J.G.; Deng, H.W. Gene selection for classification of microarray data based on the bayes error. *BMC Bioinform.* **2007**, *8*, 370. [CrossRef]
36. Su, R.; Liu, X.; Wei, L. Mine-rfe: Determine the optimal subset from rfe by minimizing the subset-accuracy-defined energy. *Brief. Bioinform.* **2020**, *21*, 687–698. [CrossRef]
37. Kolde, R.; Laur, S.; Adler, P.; Vilo, J. Robust rank aggregation for gene list integration and meta-analysis. *Bioinformatics* **2012**, *28*, 573–580. [CrossRef]
38. Szklarczyk, D.; Gable, A.L.; Nastou, K.C.; Lyon, D.; Kirsch, R.; Pyysalo, S.; Doncheva, N.T.; Legeay, M.; Fang, T.; Bork, P.; et al. The string database in 2021: Customizable protein-protein networks, and functional characterization of user-uploaded gene/measurement sets. *Nucleic Acids Res.* **2021**, *49*, D605–D612. [CrossRef]
39. Baluchamy, S.; Zhang, Y.; Ravichandran, P.; Ramesh, V.; Sodipe, A.; Hall, J.C.; Jejelowo, O.; Gridley, D.S.; Wu, H.; Ramesh, G.T. Expression profile of DNA damage signaling genes in 2 gy proton exposed mouse brain. *Mol. Cell. Biochem.* **2010**, *341*, 207–215. [CrossRef]
40. Baluchamy, S.; Zhang, Y.; Ravichandran, P.; Ramesh, V.; Sodipe, A.; Hall, J.C.; Jejelowo, O.; Gridley, D.S.; Wu, H.; Ramesh, G.T. Differential oxidative stress gene expression profile in mouse brain after proton exposure. *Vitr. Cell. Dev. Biology. Anim.* **2010**, *46*, 718–725. [CrossRef]
41. Bravatà, V.; Cammarata, F.P.; Minafra, L.; Pisciotta, P.; Scazzone, C.; Manti, L.; Savoca, G.; Petringa, G.; Cirrone, G.A.P.; Cuttone, G.; et al. Proton-irradiated breast cells: Molecular points of view. *J. Radiat. Res.* **2019**, *60*, 451–465. [CrossRef] [PubMed]
42. Bravatà, V.; Minafra, L.; Cammarata, F.P.; Pisciotta, P.; Lamia, D.B.; Marchese, V.; Petringa, G.; Manti, L.; Cirrone, G.A.P.; Gilardi, M.C.; et al. Gene expression profiling of breast cancer cell lines treated with proton and electron radiations. *Br. J. Radiol.* **2018**, *91*, 20170934. [CrossRef] [PubMed]
43. Cammarata, F.P.; Forte, G.I.; Broggi, G.; Bravata, V.; Minafra, L.; Pisciotta, P.; Calvaruso, M.; Tringali, R.; Tomasello, B.; Torrisi, F.; et al. Molecular investigation on a triple negative breast cancer xenograft model exposed to proton beams. *Int. J. Mol. Sci.* **2020**, *21*, 6337. [CrossRef] [PubMed]
44. Chauhan, V.; Howland, M. Genomic profiling of a human leukemic monocytic cell-line (thp-1) exposed to alpha particle radiation. *Sci. World J.* **2012**, *2012*, 205038. [CrossRef]
45. Chauhan, V.; Howland, M.; Greene, H.B.; Wilkins, R.C. Transcriptional and secretomic profiling of epidermal cells exposed to alpha particle radiation. *Open Biochem. J.* **2012**, *6*, 103–115. [CrossRef] [PubMed]
46. Chauhan, V.; Howland, M. Gene expression responses in human lung fibroblasts exposed to alpha particle radiation. *Toxicol. Vitr.* **2014**, *28*, 1222–1229. [CrossRef] [PubMed]
47. Chauhan, V.; Howland, M.; Mendenhall, A.; O'Hara, S.; Stocki, T.J.; McNamee, J.P.; Wilkins, R.C. Effects of alpha particle radiation on gene expression in human pulmonary epithelial cells. *Int. J. Hyg. Environ. Health* **2012**, *215*, 522–535. [CrossRef]
48. Chauhan, V.; Howland, M.; Wilkins, R. Identification of gene-based responses in human blood cells exposed to alpha particle radiation. *BMC Med. Genom.* **2014**, *7*, 43. [CrossRef]
49. Fushimi, K.; Uzawa, K.; Ishigami, T.; Yamamoto, N.; Kawata, T.; Shibahara, T.; Ito, H.; Mizoe, J.e.; Tsujii, H.; Tanzawa, H. Susceptible genes and molecular pathways related to heavy ion irradiation in oral squamous cell carcinoma cells. *Radiother. Oncol.* **2008**, *89*, 237–244. [CrossRef]
50. Gridley, D.S.; Freeman, T.L.; Makinde, A.Y.; Wroe, A.J.; Luo-Owen, X.; Tian, J.; Mao, X.W.; Rightnar, S.; Kennedy, A.R.; Slater, J.M.; et al. Comparison of proton and electron radiation effects on biological responses in liver, spleen and blood. *Int. J. Radiat. Biol.* **2011**, *87*, 1173–1181. [CrossRef]
51. Gridley, D.S.; Pecaut, M.J.; Rizvi, A.; Coutrakon, G.B.; Luo-Owen, X.; Makinde, A.Y.; Slater, J.M. Low-dose, low-dose-rate proton radiation modulates cd4(+) t cell gene expression. *Int. J. Radiat. Biol.* **2009**, *85*, 250–261. [CrossRef] [PubMed]
52. Konings, K.; Belmans, N.; Vermeesen, R.; Baselet, B.; Lamers, G.; Janssen, A.; Isebaert, S.; Baatout, S.; Haustermans, K.; Moreels, M. Targeting the Hedgehog pathway in combination with X-ray or carbon ion radiation decreases migration of MCF-7 breast cancer cells. *Int. J. Oncol.* **2019**, *55*, 1339–1348. [CrossRef] [PubMed]
53. Konings, K.; Vandevoorde, C.; Belmans, N.; Vermeesen, R.; Baselet, B.; Walleghem, M.V.; Janssen, A.; Isebaert, S.; Baatout, S.; Haustermans, K.; et al. The combination of particle irradiation with the hedgehog inhibitor gant61 differently modulates the radiosensitivity and migration of cancer cells compared to X-ray irradiation. *Front. Oncol.* **2019**, *9*, 391. [CrossRef]

54. Leduc, A.; Chaouni, S.; Pouzoulet, F.; De Marzi, L.; Megnin-Chanet, F.; Corre, E.; Stefan, D.; Habrand, J.L.; Sichel, F.; Laurent, C. Differential normal skin transcriptomic response in total body irradiated mice exposed to scattered versus scanned proton beams. *Sci. Rep.* **2021**, *11*, 5876. [CrossRef]
55. Lindgren, T.; Stigbrand, T.; Riklund, K.; Johansson, L.; Eriksson, D. Gene expression profiling in molt-4 cells during gamma-radiation-induced apoptosis. *Tumour Biol.* **2012**, *33*, 689–700. [CrossRef] [PubMed]
56. Liu, F.; Wang, Z.; Li, W.; Wei, Y. Transcriptional response of murine bone marrow cells to total-body carbon-ion irradiation. *Mutat. Res. Genet. Toxicol. Environ. Mutagen.* **2019**, *839*, 49–58. [CrossRef]
57. Liu, Q.J.; Zhang, D.Q.; Zhang, Q.Z.; Feng, J.B.; Lu, X.; Wang, X.R.; Li, K.P.; Chen, D.Q.; Mu, X.F.; Li, S.; et al. Dose-effect of ionizing radiation-induced pig3 gene expression alteration in human lymphoblastoid ahh-1 cells and human peripheral blood lymphocytes. *Int. J. Radiat. Biol.* **2015**, *91*, 71–80. [CrossRef]
58. Mao, X.W.; Green, L.M.; Mekonnen, T.; Lindsey, N.; Gridley, D.S. Gene expression analysis of oxidative stress and apoptosis in proton-irradiated rat retina. *Vivo.* **2021**, *24*, 425–430.
59. Purgason, A.; Zhang, Y.; Hamilton, S.R.; Gridley, D.S.; Sodipe, A.; Jejelowo, O.; Ramesh, G.T.; Moreno-Villanueva, M.; Wu, H. Apoptosis and expression of apoptosis-related genes in mouse intestinal tissue after whole-body proton exposure. *Mol. Cell. Biochem.* **2018**, *442*, 155–168. [CrossRef]
60. Rizvi, A.; Pecaut, M.J.; Gridley, D.S. Low-dose gamma-rays and simulated solar particle event protons modify splenocyte gene and cytokine expression patterns. *J. Radiat. Res.* **2011**, *52*, 701–711. [CrossRef]
61. Song, L.H.; Yan, H.L.; Cai, D.L. Gene expression profiles in the liver of mice irradiated with (60)co gamma rays and treated with soybean isoflavone. *Eur. J. Nutr.* **2006**, *45*, 406–417. [CrossRef] [PubMed]
62. Suetens, A.; Moreels, M.; Quintens, R.; Chiriotti, S.; Tabury, K.; Michaux, A.; Grégoire, V.; Baatout, S. Carbon ion irradiation of the human prostate cancer cell line pc3: A whole genome microarray study. *Int. J. Oncol.* **2014**, *44*, 1056–1072. [CrossRef] [PubMed]
63. Tian, J.; Tian, S.; Gridley, D.S. Comparison of acute proton, photon, and low-dose priming effects on genes associated with extracellular matrix and adhesion molecules in the lungs. *Fibrogenesis Tissue Repair* **2013**, *6*, 4. [CrossRef]
64. Uehara, Y.; Ito, Y.; Taki, K.; Nenoi, M.; Ichinohe, K.; Nakamura, S.; Tanaka, S.; Oghiso, Y.; Tanaka, K.; Matsumoto, T.; et al. Gene expression profiles in mouse liver after long-term low-dose-rate irradiation with gamma rays. *Radiat. Res.* **2010**, *174*, 611–617. [CrossRef] [PubMed]
65. Nielsen, S.; Bassler, N.; Grzanka, L.; Swakon, J.; Olko, P.; Andreassen, C.N.; Overgaard, J.; Alsner, J.; Sorensen, B.S. Differential gene expression in primary fibroblasts induced by proton and cobalt-60 beam irradiation. *Acta Oncol.* **2017**, *56*, 1406–1412. [CrossRef] [PubMed]
66. Nsarsam, D.; Mohammed Saied, D.; Nasir Aklo, K. Theoretical study of energy loss of proton in human tissues. *Al-Qadisiyah J. Pure Sci.* **2013**, *18*, 23–31.
67. Raheem, Z.J.; Saied, B.M. Energy loss of carbon ion in lung tissue. *AIP Conf. Proc.* **2019**, *2190*, 020021.
68. Usta, M.; Tufan, M.Ç. Stopping power and range calculations in human tissues by using the hartree-fock-roothaan wave functions. *RaPC* **2017**, *140*, 43–50. [CrossRef]
69. Nikitaki, Z.; Choulilitsa, E.; Kalospyros, S.A.; Kaisaridi, S.; Terzoudi, G.I.; Kokkoris, M.; Georgakilas, A.G. Construction and evaluation of an α-particle-irradiation exposure apparatus. *Int. J. Radiat. Biol.* **2021**, *97*, 1404–1416. [CrossRef]
70. Semenenko, V.A.; Stewart, R.D. Fast monte carlo simulation of DNA damage formed by electrons and light ions. *Phys. Med. Biol.* **2006**, *51*, 1693–1706. [CrossRef]
71. Stewart, R.D.; Yu, V.K.; Georgakilas, A.G.; Koumenis, C.; Park, J.H.; Carlson, D.J. Effects of radiation quality and oxygen on clustered DNA lesions and cell death. *Radiat. Res.* **2011**, *176*, 587–602. [CrossRef] [PubMed]
72. Pavlopoulou, A.; Asfa, S.; Gioukakis, E.; Mavragani, I.V.; Nikitaki, Z.; Takan, I.; Pouget, J.P.; Harrison, L.; Georgakilas, A.G. In silico investigation of the biological implications of complex DNA damage with emphasis in cancer radiotherapy through a systems biology approach. *Molecules* **2021**, *26*, 7602. [CrossRef]
73. Prasanna, P.G.; Citrin, D.E.; Hildesheim, J.; Ahmed, M.M.; Venkatachalam, S.; Riscuta, G.; Xi, D.; Zheng, G.; Deursen, J.V.; Goronzy, J.; et al. Therapy-induced senescence: Opportunities to improve anticancer therapy. *J. Natl. Cancer Inst.* **2021**, *113*, 1285–1298. [CrossRef] [PubMed]
74. Levine, A.J. Targeting the p53 protein for cancer therapies: The translational impact of p53 research. *Cancer Res.* **2022**, *82*, 362–364. [CrossRef]
75. Azzam, E.I.; Jay-Gerin, J.P.; Pain, D. Ionizing radiation-induced metabolic oxidative stress and prolonged cell injury. *Cancer Lett.* **2012**, *327*, 48–60. [CrossRef] [PubMed]
76. Maier, P.; Hartmann, L.; Wenz, F.; Herskind, C. Cellular pathways in response to ionizing radiation and their targetability for tumor radiosensitization. *Int. J. Mol. Sci.* **2016**, *17*, 102. [CrossRef] [PubMed]
77. Nakajima, T. Roles of sulfur metabolism and rhodanese in detoxification and anti-oxidative stress functions in the liver: Responses to radiation exposure. *Med. Sci. Monit.* **2015**, *21*, 1721. [CrossRef]
78. Yuan, Z.H.; Liu, T.; Wang, H.; Xue, L.X.; Wang, J.J. Fatty acids metabolism: The bridge between ferroptosis and ionizing radiation. *Front. Cell Dev. Biol.* **2021**, *9*, 675617. [CrossRef]
79. Shibata, Y.; Yasui, H.; Higashikawa, K.; Miyamoto, N.; Kuge, Y. Erastin, a ferroptosis-inducing agent, sensitized cancer cells to X-ray irradiation via glutathione starvation in vitro and in vivo. *PLoS ONE* **2019**, *14*, e0225931. [CrossRef]

80. Liao, P.; Wang, W.; Wang, W.; Kryczek, I.; Li, X.; Bian, Y.; Sell, A.; Wei, S.; Grove, S.; Johnson, J.K.; et al. Cd8(+) t cells and fatty acids orchestrate tumor ferroptosis and immunity via acsl4. *Cancer Cell* **2022**, *40*, 365–378 e366. [CrossRef]
81. Olechnowicz, J.; Tinkov, A.; Skalny, A.; Suliburska, J. Zinc status is associated with inflammation, oxidative stress, lipid, and glucose metabolism. *J. Physiol. Sci.* **2018**, *68*, 19–31. [CrossRef] [PubMed]
82. Stork, C.J.; Martorano, L.M.; Li, Y.V. Uvb radiation induces an increase in intracellular zinc in human epidermal keratinocytes. *Int. J. Mol. Med.* **2010**, *26*, 463–469. [PubMed]
83. Wiseman, D.A.; Wells, S.M.; Hubbard, M.; Welker, J.E.; Black, S.M. Alterations in zinc homeostasis underlie endothelial cell death induced by oxidative stress from acute exposure to hydrogen peroxide. *Am. J. Physiol.—Lung Cell. Mol. Physiol.* **2007**, *292*, 165–177. [CrossRef]
84. Matsubara, J.; Shida, T.; Ishioka, K.; Egawa, S.; Inada, T.; Machida, K. Protective effect of zinc against lethality in irradiated mice. *Environ. Res.* **1986**, *41*, 558–567. [CrossRef]
85. Fukada, T.; Yamasaki, S.; Nishida, K.; Murakami, M.; Hirano, T. Zinc homeostasis and signaling in health and diseases. *J. Biol. Inorg. Chem.* **2011**, *16*, 1123–1134. [CrossRef] [PubMed]
86. Chan, R.K.; Ibrahim, S.I.; Verna, N.; Carroll, M.; Moore, F.D.; Hechtman, H.B. Ischaemia–reperfusion is an event triggered by immune complexes and complement. *Br. J. Surg.* **2003**, *90*, 1470–1478. [CrossRef]
87. Brewer, G.J. Anticopper therapy against cancer and diseases of inflammation and fibrosis. *Drug Discov. Today* **2005**, *10*, 1103–1109. [CrossRef]
88. Goodman, V.L.; Brewer, G.J.; Merajver, S.D. Copper deficiency as an anti-cancer strategy. *Endocr.-Relat. Cancer* **2004**, *11*, 255–263. [CrossRef]
89. Lowndes, S.A.; Harris, A.L. The role of copper in tumour angiogenesis. *J. Mammary Gland. Biol. Neoplasia* **2005**, *10*, 299–310. [CrossRef]
90. Wang, F.; Jiao, P.; Qi, M.; Frezza, M.; Dou, Q.P.; Yan, B. Turning tumor-promoting copper into an anti-cancer weapon via high-throughput chemistry. *Curr. Med. Chem.* **2010**, *17*, 2685. [CrossRef]
91. Rex, D.A.B.; Agarwal, N.; Prasad, T.S.K.; Kandasamy, R.K.; Subbannayya, Y.; Pinto, S.M. A comprehensive pathway map of il-18-mediated signalling. *J. Cell Commun. Signal.* **2020**, *14*, 257–266. [CrossRef] [PubMed]
92. Piette, J. Signalling pathway activation by photodynamic therapy: Nf-κb at the crossroad between oncology and immunology. *Photochem. Photobiol. Sci.* **2015**, *14*, 1510–1517. [CrossRef] [PubMed]
93. Hellweg, C.E. The nuclear factor kappab pathway: A link to the immune system in the radiation response. *Cancer Lett.* **2015**, *368*, 275–289. [CrossRef] [PubMed]
94. Buonanno, M.; de Toledo, S.M.; Pain, D.; Azzam, E.I. Long-term consequences of radiation-induced bystander effects depend on radiation quality and dose and correlate with oxidative stress. *Radiat. Res.* **2011**, *175*, 405–415. [CrossRef] [PubMed]
95. Bednarski, J.J.; Sleckman, B.P. At the intersection of DNA damage and immune responses. *Nat. Rev. Immunol.* **2019**, *19*, 231–242. [CrossRef]
96. Cancer Stat Facts: Leukemia—Acute Myeloid Leukemia (aml). Available online: https://seer.cancer.gov/statfacts/html/amyl.html (accessed on 7 June 2021).
97. Chedotal, A.; Kerjan, G.; Moreau-Fauvarque, C. The brain within the tumor: New roles for axon guidance molecules in cancers. *Cell Death Differ.* **2005**, *12*, 1044–1056. [CrossRef]
98. Logotheti, S.; Marquardt, S.; Richter, C.; Sophie Hain, R.; Murr, N.; Takan, I.; Pavlopoulou, A.; Putzer, B.M. Neural networks recapitulation by cancer cells promotes disease progression: A novel role of p73 isoforms in cancer-neuronal crosstalk. *Cancers* **2020**, *12*, 3789. [CrossRef]
99. Yilmaz, H.; Toy, H.I.; Marquardt, S.; Karakulah, G.; Kucuk, C.; Kontou, P.I.; Logotheti, S.; Pavlopoulou, A. In silico methods for the identification of diagnostic and favorable prognostic markers in acute myeloid leukemia. *Int. J. Mol. Sci.* **2021**, *22*, 9601. [CrossRef]
100. Rola, R.; Sarkissian, V.; Obenaus, A.; Nelson, G.A.; Otsuka, S.; Limoli, C.L.; Fike, J.R. High-let radiation induces inflammation and persistent changes in markers of hippocampal neurogenesis. *Radiat. Res.* **2005**, *164*, 556–560. [CrossRef]
101. Alboni, S.; Cervia, D.; Sugama, S.; Conti, B. Interleukin 18 in the cns. *J. Neuroinflammation* **2010**, *7*, 1–12. [CrossRef]
102. Felderhoff-Mueser, U.; Schmidt, O.I.; Oberholzer, A.; Bührer, C.; Stahel, P.F. Il-18: A key player in neuroinflammation and neurodegeneration? *Trends Neurosci.* **2005**, *28*, 487–493. [CrossRef] [PubMed]
103. Min, S.S.; Wierzbicki, A.S. Radiotherapy, chemotherapy and atherosclerosis. *Curr. Opin. Cardiol.* **2017**, *32*, 441–447. [CrossRef] [PubMed]
104. Wang, J.; Sun, C.; Gerdes, N.; Liu, C.; Liao, M.; Liu, J.; Shi, M.A.; He, A.; Zhou, Y.; Sukhova, G.K.; et al. Interleukin 18 function in atherosclerosis is mediated by the interleukin 18 receptor and the na-cl co-transporter. *Nat. Med.* **2015**, *21*, 820–826. [CrossRef] [PubMed]
105. Bodo, S.; Campagne, C.; Thin, T.H.; Higginson, D.S.; Vargas, H.A.; Hua, G.; Fuller, J.D.; Ackerstaff, E.; Russell, J.; Zhang, Z.; et al. Single-dose radiotherapy disables tumor cell homologous recombination via ischemia/reperfusion injury. *J. Clin. Investig.* **2019**, *129*, 786–801. [CrossRef]
106. Wambersie, A.; Hendry, J.; Gueulette, J.; Gahbauer, R.; Potter, R.; Gregoire, V. Radiobiological rationale and patient selection for high-let radiation in cancer therapy. *Radiother. Oncol.* **2004**, *73* (Suppl. S2), S1–S14. [CrossRef]

107. Dressman, H.K.; Muramoto, G.G.; Chao, N.J.; Meadows, S.; Marshall, D.; Ginsburg, G.S.; Nevins, J.R.; Chute, J.P. Gene expression signatures that predict radiation exposure in mice and humans. *PLoS Med.* **2007**, *4*, e106. [CrossRef]
108. Tran, K.A.; Kondrashova, O.; Bradley, A.; Williams, E.D.; Pearson, J.V.; Waddell, N. Deep learning in cancer diagnosis, prognosis and treatment selection. *Genome Med.* **2021**, *13*, 152. [CrossRef]
109. Hiraga, T.; Ito, S.; Nakamura, H. Cancer stem-like cell marker cd44 promotes bone metastases by enhancing tumorigenicity, cell motility, and hyaluronan production. *Cancer Res.* **2013**, *73*, 4112–4122. [CrossRef]
110. Owyong, M.; Chou, J.; van den Bijgaart, R.J.; Kong, N.; Efe, G.; Maynard, C.; Talmi-Frank, D.; Solomonov, I.; Koopman, C.; Hadler-Olsen, E.; et al. Mmp9 modulates the metastatic cascade and immune landscape for breast cancer anti-metastatic therapy. *Life Sci. Alliance* **2019**, *2*, e201800226. [CrossRef]
111. Wang, L.; Zhang, J.; Wan, L.; Zhou, X.; Wang, Z.; Wei, W. Targeting cdc20 as a novel cancer therapeutic strategy. *Pharmacol. Ther.* **2015**, *151*, 141–151. [CrossRef]
112. Mahner, S.; Baasch, C.; Schwarz, J.; Hein, S.; Wolber, L.; Janicke, F.; Milde-Langosch, K. C-fos expression is a molecular predictor of progression and survival in epithelial ovarian carcinoma. *Br. J. Cancer* **2008**, *99*, 1269–1275. [CrossRef] [PubMed]
113. Asem, M.S.; Buechler, S.; Wates, R.B.; Miller, D.L.; Stack, M.S. Wnt5a signaling in cancer. *Cancers* **2016**, *8*, 79. [CrossRef] [PubMed]
114. Toy, H.I.; Karakulah, G.; Kontou, P.I.; Alotaibi, H.; Georgakilas, A.G.; Pavlopoulou, A. Investigating molecular determinants of cancer cell resistance to ionizing radiation through an integrative bioinformatics approach. *Front. Cell Dev. Biol.* **2021**, *9*, 620248. [CrossRef] [PubMed]
115. Bridges, A.E.; Ramachandran, S.; Pathania, R.; Parwal, U.; Lester, A.; Rajpurohit, P.; Morera, D.S.; Patel, N.; Singh, N.; Korkaya, H.; et al. Rad51ap1 deficiency reduces tumor growth by targeting stem cell self-renewal. *Cancer Res.* **2020**, *80*, 3855–3866. [CrossRef] [PubMed]
116. Chandler, B.C.; Moubadder, L.; Ritter, C.L.; Liu, M.; Cameron, M.; Wilder-Romans, K.; Zhang, A.; Pesch, A.M.; Michmerhuizen, A.R.; Hirsh, N.; et al. Ttk inhibition radiosensitizes basal-like breast cancer through impaired homologous recombination. *J. Clin. Investig.* **2020**, *130*, 958–973. [CrossRef]
117. Shih, H.T.; Chen, W.Y.; Wang, H.Y.; Chao, T.; Huang, H.D.; Chou, C.H.; Chang, Z.F. Dnmt3b protects centromere integrity by restricting r-loop-mediated DNA damage. *Cell Death Dis.* **2022**, *13*, 546. [CrossRef]
118. Wu, C.; Guo, E.; Ming, J.; Sun, W.; Nie, X.; Sun, L.; Peng, S.; Luo, M.; Liu, D.; Zhang, L.; et al. Radiation-induced dnmt3b promotes radioresistance in nasopharyngeal carcinoma through methylation of p53 and p21. *Mol. Ther. Oncolytics* **2020**, *17*, 306–319. [CrossRef]
119. Soo Lee, N.; Jin Chung, H.; Kim, H.J.; Yun Lee, S.; Ji, J.H.; Seo, Y.; Hun Han, S.; Choi, M.; Yun, M.; Lee, S.G.; et al. Traip/rnf206 is required for recruitment of rap80 to sites of DNA damage. *Nat. Commun.* **2016**, *7*, 10463. [CrossRef]
120. Herrera, F.G.; Ronet, C.; Ochoa de Olza, M.; Barras, D.; Crespo, I.; Andreatta, M.; Corria-Osorio, J.; Spill, A.; Benedetti, F.; Genolet, R.; et al. Low-dose radiotherapy reverses tumor immune desertification and resistance to immunotherapy. *Cancer Discov.* **2022**, *12*, 108–133. [CrossRef]
121. Algara, M.; Arenas, M.; Marin, J.; Vallverdu, I.; Fernandez-Leton, P.; Villar, J.; Fabrer, G.; Rubio, C.; Montero, A. Low dose anti-inflammatory radiotherapy for the treatment of pneumonia by covid-19: A proposal for a multi-centric prospective trial. *Clin. Transl. Radiat. Oncol.* **2020**, *24*, 29–33. [CrossRef]
122. Zhang, Q.; Matzke, M.; Schepmoes, A.A.; Moore, R.J.; Webb-Robertson, B.J.; Hu, Z.; Monroe, M.E.; Qian, W.J.; Smith, R.D.; Morgan, W.F. High and low doses of ionizing radiation induce different secretome profiles in a human skin model. *PLoS ONE* **2014**, *9*, e92332. [CrossRef] [PubMed]
123. Multhoff, G.; Radons, J. Radiation, inflammation, and immune responses in cancer. *Front. Oncol.* **2012**, *2*, 58. [CrossRef] [PubMed]
124. Casey, D.L.; Pitter, K.L.; Wexler, L.H.; Slotkin, E.K.; Gupta, G.P.; Wolden, S.L. Tp53 mutations increase radioresistance in rhabdomyosarcoma and ewing sarcoma. *Br. J. Cancer* **2021**, *125*, 576–581. [CrossRef] [PubMed]
125. Logotheti, S.; Pavlopoulou, A.; Galtsidis, S.; Vojtesek, B.; Zoumpourlis, V. Functions, divergence and clinical value of tap73 isoforms in cancer. *Cancer Metastasis Rev.* **2013**, *32*, 511–534. [CrossRef] [PubMed]
126. Logotheti, S.; Pavlopoulou, A.; Marquardt, S.; Takan, I.; Georgakilas, A.G.; Stiewe, T. P73 isoforms meet evolution of metastasis. *Cancer Metastasis Rev.* **2022**. [CrossRef]
127. Aznar, M.C.; Bacchus, C.; Coppes, R.P.; Deutsch, E.; Georg, D.; Haustermans, K.; Hoskin, P.; Krause, M.; Lartigau, E.F.; Lock, S.; et al. Radiation oncology in the new virtual and digital era. *Radiother. Oncol.* **2021**, *154*, A1–A4. [CrossRef]

*antioxidants*

MDPI

*Article*

# Serum Proteomic and Oxidative Modification Profiling in Mice Exposed to Total Body X-Irradiation

**Masaru Yamaguchi [1,†], Yota Tatara [2,†], Eka Djatnika Nugraha [3], Yoshiaki Sato [1], Tomisato Miura [4], Masahiro Hosoda [1,4], Mukh Syaifudin [5], Shinji Tokonami [4] and Ikuo Kashiwakura [1,*]**

[1] Hirosaki University Graduate School of Health Sciences, 66-1 Hon-cho, Hirosaki 036-8564, Aomori, Japan
[2] Hirosaki University Graduate School of Medicine, 5 Zaifu-cho, Hirosaki 036-8562, Aomori, Japan
[3] The Research Center for Safety, Metrology, and Nuclear Quality Technology (PRTKMMN), Research Organization for Nuclear Energy, National Research and Innovation Agency of Indonesia (BRIN), JI. Lebak Bulus Raya No. 49, Jakarta Selatan 12440, DKI Jakarta, Indonesia
[4] Institute of Radiation Emergency Medicine, Hirosaki University, 66-1 Hon-cho, Hirosaki 036-8564, Aomori, Japan
[5] Research Center for Radioisotope, Radiopharmaceutical and Biodosimetry Technology, Research Organization for Nuclear Energy, National Research and Innovation Agency, Kw. Puspiptek, Setu, Tangerang Selatan 15312, Banten, Indonesia
* Correspondence: ikashi@hirosaki-u.ac.jp
† These authors contributed equally to this work.

**Abstract:** The details of the dose-dependent response of serum proteins exposed to ionizing radiation, especially the oxidative modification response in amino acid sequences of albumin, the most abundant protein, are unknown. Thus, a proteomic analysis of the serum components from mice exposed to total body X-irradiation (TBI) ranging from 0.5 Gy to 3.0 Gy was conducted using LC-MS/MS. The analysis of oxidative modification sequences of albumin (mOMSA) in TBI mouse serum revealed significant moderate or strong correlations between the X-irradiation exposure dose and modification of 11 mOMSAs (especially the 97th, 267th and 499th lysine residues, 159th methionine residue and 287th tyrosine residues). In the case of X-irradiation of serum alone, significant correlations were also found in the 14 mOMSAs. In addition, a dose-dependent variation in six proteins (Angiotensinogen, Odorant-binding protein 1a, Serine protease inhibitor A3K, Serum paraoxonase/arylesterase 1, Prothrombin and Epidermal growth factor receptor) was detected in the serum of mice exposed to TBI. These findings suggest the possibility that the protein variation and serum albumin oxidative modification responses found in exposed individuals are important indicators for considering the effects of radiation on living organisms, along with DNA damage, and suggests their possible application as biomarkers of radiation dose estimation.

**Keywords:** total body irradiation; proteomic analysis; oxidative modification profiling; serum albumin; amino acid sequences; radiation biomarker

**Citation:** Yamaguchi, M.; Tatara, Y.; Nugraha, E.D.; Sato, Y.; Miura, T.; Hosoda, M.; Syaifudin, M.; Tokonami, S.; Kashiwakura, I. Serum Proteomic and Oxidative Modification Profiling in Mice Exposed to Total Body X-Irradiation. *Antioxidants* **2022**, *11*, 1710. https://doi.org/10.3390/antiox11091710

Academic Editors: Elena Obrador Pla and Alegria Montoro

Received: 22 July 2022
Accepted: 27 August 2022
Published: 30 August 2022



## 1. Introduction

Very recently we reported on a proteomic analysis and oxidative modification profiling of serum collected from residents of a newly discovered high-level natural background radiation area (HBRA, annual effective dose of approximately 50 mSv $y^{-1}$) and normal-level background radiation area (NBRA, 1.22 mSv $y^{-1}$) in Mamuju, Indonesia [1]. A proteomic analysis showed that the apolipoprotein B-100 and hemoglobin subunit α1 expression of residents in the HBRA was significantly lower than that of residents in the NBRA. In addition, a total of 270 oxidation-mediated modification sites were identified in the amino acid sequence of human serum albumin (HSA) by liquid chromatography-tandem mass spectrometry (LC-MS/MS). Among these, four specific amino acid sequences of HSA showed a dose-dependent oxidative modifications. Notably, the 162nd and 356th tyrosine

residues and 111th and 470th methionine residues were found. None of these findings have been reported in humans exposed to chronic low-dose radiation. This can be used as a biomarker not only for the assessment of the presence or absence of radiation exposure but also for dose prediction of chronic radiation exposure in living organisms. These results suggest that traces of radiation exposure are recorded in serum albumin and that there is a possibility of a new methodology that can evaluate biological responses below 100 mSv.

Regarding the health effects of chronic low-dose radiation exposure, epidemiological studies of human populations, such as occupational studies of nuclear workers, are not as clear regarding whether low-dose-rate exposure results in lower risks than seen among Japanese atom bomb survivors who were acutely exposed to radiation [2]. In addition, the UNSCEAR report showed that epidemiological studies in several regions of the world (Ramsar, Yangjiang, Kerala and Guarapari) reported no correlation between radiation exposure and cancer rate or mortality in areas with high natural background radiation [3], indicating that the effect of low dose rates on health and the cancer risk after exposure to ionizing radiation is still unclear. Tang et al. also reported that the mechanisms of low-dose ionizing radiation ($\leq$100 mSv) or low-dose-rate ionizing radiation (<6 mSv/h)—induced health effects are poorly understood [4]. Issues related to the health effects of low doses require further research in the future.

The annual effective dose shown in the previous report was estimated as the accumulation of the dose from external exposure (environmental gamma radiation) and internal exposure (mainly through breathing of indoor radon) based on our previous reports. This radioactivity was mainly derived from uranium ($^{238}$U), thorium ($^{232}$Th), radon ($^{222}$Rn), thoron ($^{220}$Rn) and their progeny contained in soil [5,6]. However, do the proteomic changes observed in residents living under chronic long-term low-dose radiation exposure also occur with a single acute high-dose radiation exposure, such as a radiation exposure accident? Furthermore, the details of whether there is a dose-dependent response are unknown. In particular, prodromal symptoms seen in patients within 1 to 2 days after acute radiation exposure of $\geq$1 Gy may include symptoms such as loss of appetite, nausea, vomiting (>2 Gy), and diarrhea, making it easy to confirm the biological response to radiation exposure [7]. As pointed out by Shin et al., the effects of low-dose radiation, which many experimental studies consider to be defined as <0.5 Gy, are subtle, and the absence of reliable biological markers has been an obstacle [8,9]. With the rapid progress of analytical techniques in recent years, an increasing number of studies have reported on the search of the proteome of exposed individuals [9–12], and it is expected to be utilized as a biomarker for dose estimation in triage in the event of nuclear or radiological disasters [13–15]. However, the details of the relationship between the radiation dose and oxidative modification of serum albumin are unknown. Furthermore, considering its application to radiation accidents and nuclear disasters, it is necessary to verify it in animal experimental models, as it cannot be verified in humans.

In the present study, we analyzed the proteome and oxidative modification profile by LC-MS/MS using mouse serum after 24 h of single total body X-irradiation (0.5–3 Gy), assuming a nuclear disaster/radiation accident.

## 2. Materials and Methods

### *2.1. Animal Experiments*

Seven-week-old female C57BL/6JJcl mice were delivered from the breeding facilities of CLEA Japan (Tokyo, Japan). All mice were housed in a conventional clean room at an ambient temperature of 23 °C with 50% relative humidity, and a 12-h light/dark cycle. The mice had ad libitum access to sterilized standard laboratory mouse chow (CLEA Rodent Diet CE-2, CLEA, Tokyo, Japan) and drinking water. After obtaining approval from the animal experiment committee (approval number: G17001), all experiments were conducted according to the legal regulations in Japan and the Guidelines for Animal Experiments, and all efforts were made to minimize the number of animals used and their suffering in this study. After a week of acclimatization, 8-week-old mice were randomly divided into

4 groups with more than 8 mice per group and subjected to varying TBI doses of 0, 0.5, 1 or 3 Gy from X-rays (150 kVp, 20 mA, 0.5-mm aluminum and 0.3-mm copper filters) at a dose rate of 1.0 Gy/min using an MBR-1520R X-ray generator (Hitachi Medical, Tokyo, Japan) with a distance of 450 mm between the focus and the target. The air kerma was monitored with a thimble ionization chamber, which integrated the radiation dose and blocked X-rays when it reached a present dose value. Peripheral blood was harvested by capillary tube 24 h after TBI from the orbital venous plexus of mice after they were anesthetized using isoflurane (Powerful Isoful; Zoetis, London, UK). Samples were placed at room temperature for at least 30 min to allow blood clotting. Serum was collected by centrifugation at 1200× *g* for 10 min and stored at −80 °C until use. In addition, serum collected from non-irradiated mice was subjected to varying TBI doses of 0, 0.5, 1 or 3 Gy from X-rays; incubated at 37 °C for 24 h; and stored at −80 °C until use.

### *2.2. Liquid Chromatography-Tandem Mass Spectrometry (LC-MS/MS) and High-Resolution Multiple Reaction Monitoring (MRM-HR)*

The measurement was performed according to a previous report [1]. Briefly, serum proteins were precipitated with acetone and the precipitates were dissolved and denatured with 50% trifluoroethanol. The proteins were reduced and alkylated before trypsinization. Tryptic peptides were analyzed using a TripleTOF6600 mass spectrometer (AB Sciex). A non-labeled quantitative method (SWATH) was used for a serum proteome analysis. The peak areas of peptides were normalized to the sum of the total peak area sum of all measured peptides. The principal component analysis (PCA) and orthogonal partial least square-discriminant analysis (OPLS-DA) were performed using the Simca software program (Infocom Corp, Tokyo, Japan).

The high-resolution multiple reaction monitoring (MRM-HR) method was used to profile oxidative modification of serum albumin. On the basis of the information-dependent acquisition results (data not shown), an assay for MRM-HR experiments was developed using the Skyline software program (MacCoss Lab, University of Washington, Seattle, Washington, DC, USA). The transitions of MRM-HR are shown in Supplementary Table S1. All peak pickings were manually checked after automated matching. The peak areas obtained were normalized by calculating the relative abundance of each modified peptide using the corresponding non-modified peptide.

### *2.3. Statistical Analysis*

We used the Origin Pro 2020b software program (Northampton, MA, USA) for Windows to perform the linear and polynomial correlation analysis. Furthermore, the data were analyzed with a one-way ANOVA and Tukey-Kramer or Bonferroni/Dunn multiple comparison tests. Statistical significance in the analysis was all tested using a two-sided $p$ value of 0.05. The oxidation modification patterns of amino acids were drawn using BKChem, a freely available chemical drawing program.

## 3. Results

### *3.1. Multivariate Analysis of Serum Proteome of Mice with Different Irradiation Doses*

Eight-week-old female C57BL/6JJcl mice were subjected to varying TBI doses of 0.5, 1 or 3 Gy from X-rays, and peripheral blood was harvested 24 h after TBI for serum collection (in vivo model). Regarding animal conditions after 24 h of TBI, as shown in Figure 1A, the body weights of TBI (1 Gy and 3 Gy) mice were significantly decreased in comparison to those of the non-irradiated mice. However, haematocrit values, which indicate the ratio of the total volume of red blood cells to the total blood, did not differ to a statistically significant extent among all groups. To elucidate the effects of each irradiation exposure, LC-MS/MS was used to examine the expression of proteins in the serum in each treatment. Finally, 161 types of protein were identified. The full dataset from all serum samples was subjected to PCA to obtain an overview of the data. The first and second principal component scores were 16.8% and 8.81%, respectively, as shown in Figure 1B

(the ellipse represents a 95% tolerance region for the scores based on Hotelling's T2). There was no evidence of separation among the four classes along the first and second principal components. There were no major outliers. The score scatter plots of the OPLS-DA model in Figure 1C demonstrated satisfactory separation between non-irradiated mice and mice exposed to TBI (0.5 Gy, 1 Gy, or 3 Gy) using one predictive component and one orthogonal component. The above groups were completely separated along the first predictive component. These results indicate that the serum proteome profile can be used to distinguish mice with TBI doses of 0.5 Gy, 1 Gy or 3 Gy from X-rays from non-irradiated mice.

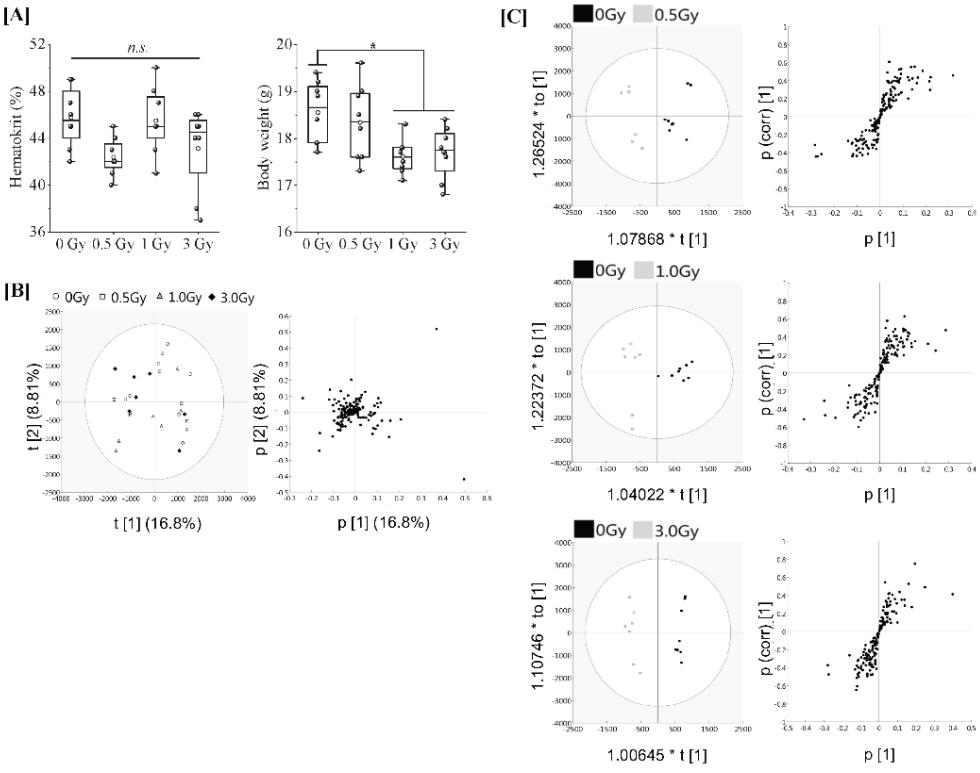


**Figure 1. Proteomic analysis of serum from mice exposed to single TBI in in vivo model.** **[A]** Eight-week-old female C57BL/6JJcl mice were randomly divided into 4 groups with more than 8 mice per group and subjected to varying TBI doses of 0, 0.5, 1 or 3 Gy of X-rays at a dose rate of 1.0 Gy/min. Peripheral blood was harvested 24 h after TBI from the orbital venous plexus of mice and placed at room temperature for at least 30 min to allow blood clotting for serum collection (in vivo model). Body weight changes and haematocrit values at the time of serum collection. Statistically significant differences were evaluated by a one-way ANOVA and the multiple comparison tests; $p < 0.05$ (*). **[B]** PCA score scatter plot of the serum proteome. Each dose treatment group of the samples are represented as shown in the (**left**) figure, respectively. Uncharacterized samples are plotted at the center, and those with features are plotted at a distance from the center (right) figure. Similar features are plotted at close positions. **[C]** The OPLS-DA model to discriminate the serum proteome of each irradiated mouse. The score scatter plot and S-plot are represented. The ellipse in the score scatter plot indicates the Hotelling T2 (0.95) range for each model.

The resultant S-plots using the OPLS-DA model revealed a significant increase in serine protease inhibitor A3K (Serpin A3K) in TBI (1Gy and 3Gy) mice (Table 1) and a further weak dose-dependent correlation was observed when the proteins expressed in non-TBI and TBI mice were compared (Supplemental Figure S1). Angiotensinogen (Serpin A8) and Odorant-binding protein 1a (Odorant-binding protein 1A) were decreased in TBI (0.5 Gy) mice and TBI (1 Gy) mice, respectively. Further serum paraoxonase/arylesterase 1 (PON1), prothrombin, and epidermal growth factor receptor (EGFR) were identified by TBI (3Gy) in addition to Serpin A3K (Table 1). At this time, only PON1 was decreasing.

**Table 1.** Proteins that varied significantly according to the dose of X-irradiation.

| Radiation Dose (Gy) | Protein Name | Protein Short Name | UniProt ID | FC [1] | Probability [2] |
|---|---|---|---|---|---|
| 0 vs. 0.5 | Angiotensinogen | Serpin A8 | P11859 | 0.37 | 0.037 |
| 0 vs. 1.0 | Odorant-binding protein 1a | Odorant-binding protein 1A | Q9D3H2 | 0.54 | 0.026 |
| 0 vs. 3.0 | Serine protease inhibitor A3K | Serpin A3K | P07759 | 1.84 | 0.026 |
| | Serum paraoxonase/arylesterase 1 | PON1 | P52430 | 0.38 | 0.00076 |
| | Prothrombin | - | P19221 | 2.04 | 0.0057 |
| | Epidermal growth factor receptor | FGFR | Q01279 | 1.96 | 0.022 |
| | Serine protease inhibitor A3K | Serpin A3K | P07759 | 2.54 | 0.046 |

[1] FC, Fold change in comparison to non-irradiated samples. [2] Probability represents the $p$ value determined by a $t$-test.

### *3.2. Oxidative Modification of Serum Albumin (OMSA) under Acute Single Radiation Exposure*

Next, we analyzed the oxidative modification of the chemical and spatial structure of albumin that occurred because of acute single radiation exposure. The amino acid sequence of mouse albumin and the identified modifications are shown in Figure 2. The albumin structural region was also totally glycated and oxidatively modified. In addition, nitration of the tyrosine residue and oxidation of the arginine residue, proline residue, methionine residue, and lysine residue were observed. The sequence information for 48 mouse OMSA (mOMSAs) is listed in Supplemental Table 1. For MRM-HR profiling of mOMSA, peptides containing each oxidatively modified amino acid residue were standardized against the peak area value of the corresponding unmodified peptide and analyzed for correlation with the radiation exposure dose as a relative peak area ratio. The fitting of quadratic equations was investigated for each mOMSA; in fact, most human genes show quadratic dose response to radiation [16,17]. In the in vivo model, eleven sequences showed significant dose-dependent correlations ($r$ value) of >0.5 by linear or curve fitting. Especially, significant moderate or strong correlations were found between the individual acute high radiation exposure dose and five mOMSAs: mOMSA3 (Linear $r = -0.51$, $p < 0.01$, Polynomial $r = -0.65$, $p < 0.001$), mOMSA9 (Linear $r = 0.53$, $p < 0.01$, Polynomial $r = 0.54$, $p < 0.01$), mOMSA14 (Linear $r = 0.6$, $p < 0.001$, Polynomial $r = 0.63$, $p < 0.001$), mOMSA20 (Linear $r = 0.55$, $p < 0.001$, Polynomial $r = 0.60$, $p < 0.01$), and mOMSA41 (Linear $r = 0.5$, $p < 0.01$, Polynomial $r = 0.5$, $p < 0.05$) (Figure 3). Furthermore, serum samples collected from non-irradiated mice were subjected to varying TBI doses of 0, 0.5, 1, or 3 Gy of X-rays and incubated at 37 °C for 24 h as an in vitro model (Figure 4A). Fourteen sequences showed significant dose-dependent correlations ($r$ value) of >0.5 by linear or curve fitting. Especially, significant moderate or strong correlations were found between the individual acute high radiation exposure dose and seven mOMSAs: mOMSA9 (Linear $r = -0.7$, $p < 0.00001$, Polynomial $r = -0.74$, $p < 0.001$), mOMSA13 (Linear $r = -0.5$, $p < 0.01$, Polynomial $r = -0.55$, $p < 0.01$), mOMSA16 (Linear $r = 0.5$, $p < 0.01$, Polynomial $r = 0.5$, $p < 0.05$), mOMSA23 (Linear $r = -0.62$, $p < 0.001$, Polynomial $r = -0.65$, $p < 0.001$), mOMSA25 (Linear $r = -0.56$, $p < 0.001$, Polynomial $r = -0.66$, $p < 0.001$), mOMSA33 (Linear $r = 0.7$, $p < 0.00001$,

Polynomial $r = 0.7$, $p < 0.0001$), and mOMSA36 (Linear $r = -0.55$, $p < 0.001$, Polynomial $r = -0.63$, $p < 0.001$) (Figure 4B).


**Figure 2. Oxidative modification of SA obtained from single TBI exposure.** Identified MSA sequences and their oxidative modification by LS-MS/MS. The modification sites are marked as follows: pink, aminoadipic acid; light blue, oxidation; blue, dioxidation; yellow, γ-glutamyl semialdehyde; purple, allysine; and grey, nitrotyrosine. Glycated or glycosylated amino acids are indicated with asterisks. The peptides targeted by an MRM-HR are underlined.

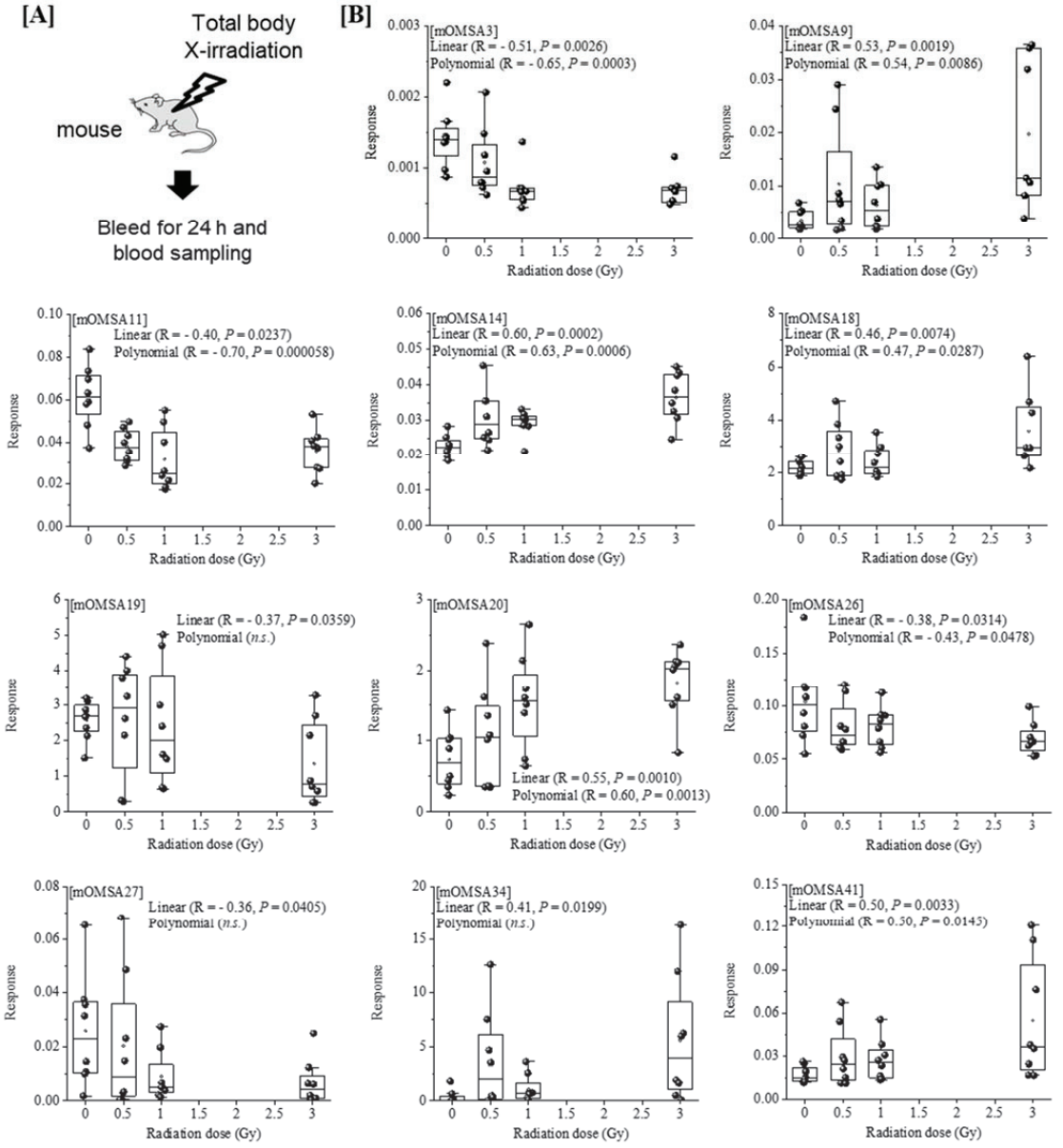


**Figure 3. Correlation between the oxidative modification sequence of MSA with single TBI and the radiation dose in vivo model.** [**A**] Eight-week-old female C57BL/6JJcl mice were exposed to varying TBI doses of 0, 0.5, 1 or 3 Gy of X-rays. Peripheral blood was harvested 24 h after TBI from the orbital venous plexus of mice (in vivo model). [**B**] Eleven sequences that showed significant dose-dependent correlations by linear or curve fitting are shown. Five sequences (mOMSA3, mOMSA9, mOMSA14, mOMSA20 and mOMSA41) showed a correlation coefficient (*r* value) of >0.5. *p* values of <0.05 were considered statistically significant.

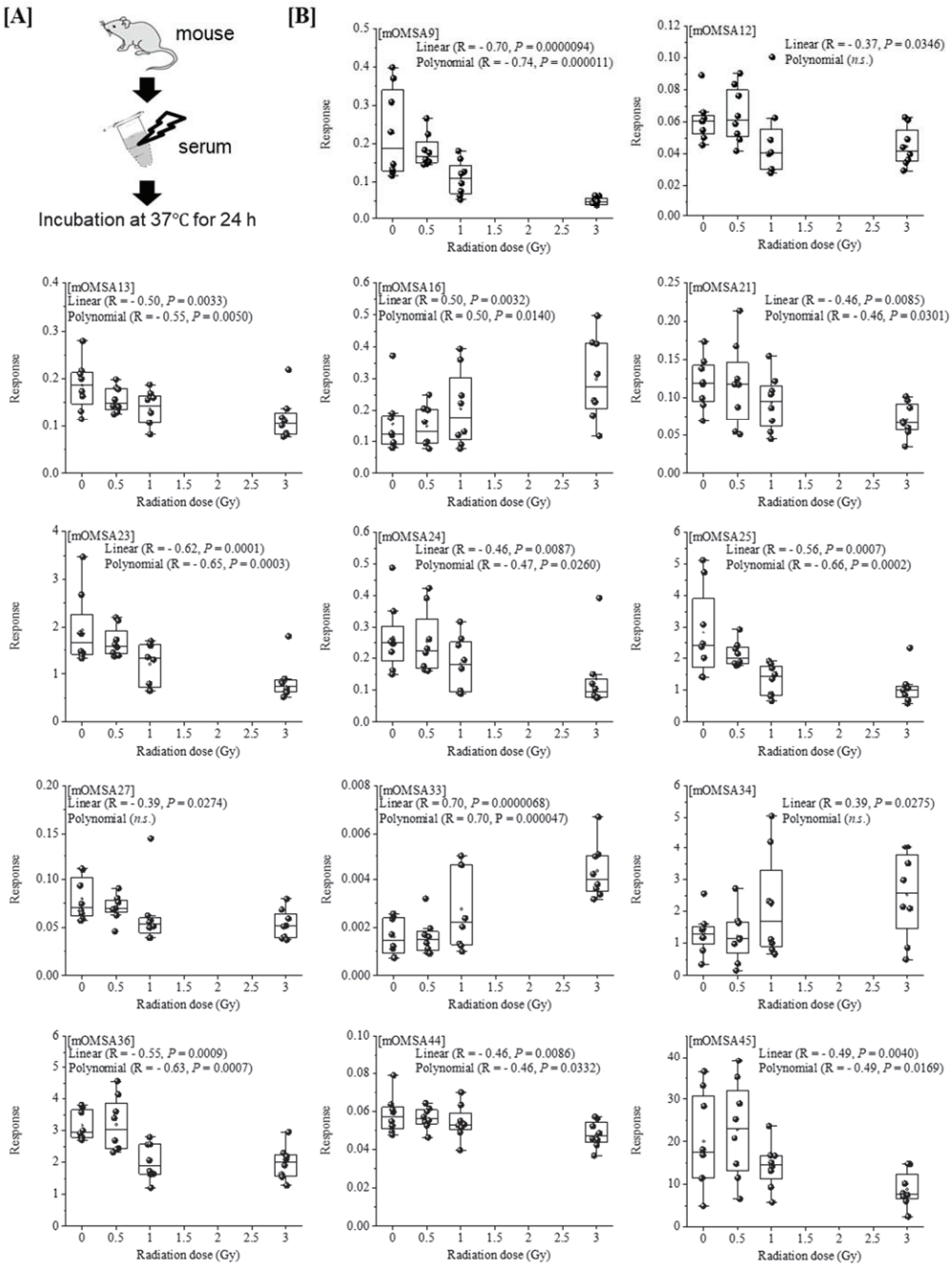


**Figure 4. Correlation between oxidative modification sequence of MSA irradiated in vitro.** **[A]** Serum samples collected from non-irradiated mice were subjecting to varying TBI doses of 0, 0.5, 1, or 3 Gy of X-rays and incubated at 37 °C for 24 h (in vitro model). **[B]** Fourteen sequences that showed significant dose-dependent correlations by linear or curve fitting are shown. Seven sequences (mOMSA9, mOMSA13, mOMSA16, mOMSA23, mOMSA25, mOMSA33 and mOMSA36) showed a correlation coefficient (*r* value) of >0.5. *p* values of <0.05 were considered statistically significant.

Based on the results of our previous report [1], the oxidative modification sites of MSA obtained in this study were compared with the results of humans with chronic low-dose radiation exposure (Figure 5). Among the identified amino acid sequences of mouse albumin, lysine, methionine and tyrosine underwent dose-dependent oxidative modification. In particular, half of the oxidative modifications occurred at lysine, unlike in the case of human albumin (Table below in Figure 5). These results indicate that the profile of OMSA induced by radiation exposure is quite different between mice and humans.

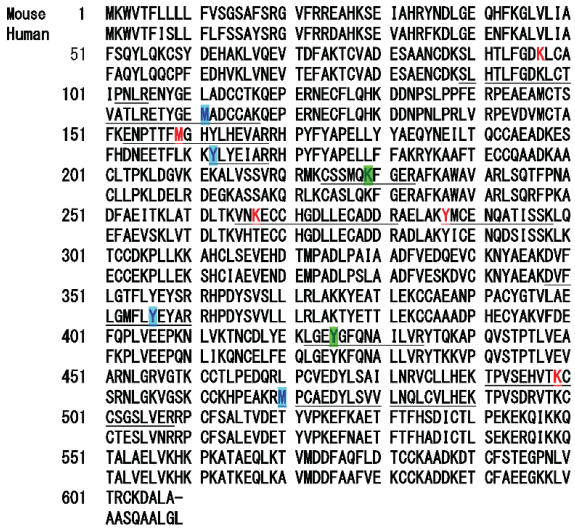


| Radiation exposure | mOMSAs that correlated with increasing radiation doses |
|---|---|
| Chronic low-dose radiation exposure in human | **M-111**, **Y-162**, **Y-356**, **M-470** |
| Acute single radiation exposure in mouse: *in vivo* | **K-97**, **M-159**, **K-267**, **Y-287**, **K-499** |
| Acute single radiation exposure in mouse serum: *in vitro* | **K-229**, **Y-425** |

**Figure 5. Comparison of oxidative modification sequences of human and mouse serum albumin.** Based on the results of our previous report [1], the oxidative modification sites of the serum albumin obtained in this study were compared. Among the identified amino acid sequences of mouse albumin, lysine, methionine and tyrosine underwent dose-dependent oxidative modification. Oxidation-modified amino acids in chronic low-dose radiation exposure in humans, acute single radiation exposure in mice (in vivo), and acute single radiation exposure in mouse serum (in vitro).

## 4. Discussion

In the present study, a proteomic analysis of serum components from mice exposed to 0.5 to 3.0 Gy single TBI revealed significant, dose-dependent variation in six proteins (Table 1). Among these proteins, Serpin A8, Odorant-binding protein 1A, and PON1 were decreased, while other proteins were increased. In particular, the expression of Serpin A3K was found to increase in a dose-dependent manner (Supplemental Figure S1). Serpin A3K is a member of the serine protease inhibitor family and is also known as kallikrein-binding protein, with anti-inflammatory and anti-angiogenic activities [18]. This is a new finding, as no previous reports have shown an association between radiation and the expression of Serpin A3K. Similarly, Serpin A8, which is involved in blood pressure [19], and Odorant-binding protein 1A, which is involved in the sense of smell [20], have never been reported to be related to radiation, and this point was clarified for the first time in this study. Numerous reports on the association with radiation have been made for

EGFR, which is a receptor of tyrosine kinase involved in cell survival/growth signaling that is overexpressed in several cancers [21,22]. In particular, EGFR is expressed in more than 90% of squamous cell carcinomas of the head and neck and is one of the most important therapeutic targets [23]. Following radiation, the activation of EGFR has been reported, leading to downstream signaling that contributes to cancer cell survival [24]. Further, EGFR has been shown to be involved in mediating DNA repair after irradiation, leading to the repair of damaged DNA [25]. There are also several reports on PON1 and prothrombin. Paraoxonase (PON-1) is an antioxidant enzyme that belongs to a family of calcium-dependent esterases that includes PON-1, PON-2 and PON-3 [26]. Serhatlioglu et al. examined the levels of malondialdehyde (an end-product of lipid peroxidation) and PON-1 activity/phenotypes in people, radiology workers, who were exposed to ionizing radiation for different time periods and doses [27]. They showed that PON-1 activity was reduced by 25–35% in subjects exposed to high-dose radiation (>3.5 mSv $y^{-1}$) and in people with long−term exposure (>5 years) to radiation in comparison to the controls. Moustafa et al. evaluated the role of various enzymes in irradiated rats (6 Gy), demonstrating that the PON activity was significantly declined ($p < 0.05$) in comparison to the control group in both serum and the liver [26]. Similarly in this study, the PON1 value was reduced to 38% (Table 1). In addition, prothrombin, a glycoprotein (carbohydrate-protein compound) occurring in blood plasma and an essential component of the blood-clotting mechanism, is transformed into thrombin by a clotting factor known as factor X or prothrombinase [28]. Rithidech et al. reported an increase in prothrombin precursors in the plasma of irradiated (3 Gy) mice on day 2, suggesting an association with radiation [29]. As shown above, significant fluctuations in six serum proteins were observed 24 h after TBI (0.5–3.0 Gy) mice, suggesting that these molecules may be an effective biomarker in this exposure dose range.

In our previous study, we developed an MRM-HR method targeting the 38 patterns of hOMSA using LS-MS/MS and performed the assay on serum samples collected from the residents of a newly discovered HBRA (annual effective dose approximately 50 mSv $y^{-1}$) [1]. As a result, we reported a dose-dependent oxidative change in a specific sequence of human serum albumin. Dose-dependent oxidative modification of mouse serum albumin was observed in single total-body-irradiated mice as well as in the residents with chronic low-dose radiation exposure. In this study, four sequences (mOMSA9, mOMSA14, mOMSA20, and mOSMA41) in the in vivo model and two sequences (mOMSA16 and mOMSA33) in the in vitro model showed positive dose-dependent correlations, but one sequence (mOMSA3) in the in vivo model and five sequences (mOMSA9, mOMSA13, mOMSA23, mOMSA25, and mOMSA36) in the in vitro model showed negative dose-dependent correlations (r value) of >0.5 with $p$ values of <0.05 by linear and curve fitting, suggesting that the correlation between the oxidative modification of MSA and the response to radiation differed between the in vivo and in vitro models (Figures 3 and 4). It is well known that proteins circulating in the blood are one of the main targets of reactive oxygen species (ROS) produced by the interaction of ionizing radiation and water molecules. In addition, two prime suspects in the intracellular generation of ROS are also the membrane-bound NADPH oxidase complex and the mitochondrial electron-transport chain (ETC) in vivo model. Differences in the sources of ROS production in both models may contribute to the responsiveness to radiation exposure. Under the action of ROS, proteins undergo oxidative modification, leading to disruption of their structures and functions. Oxidatively damaged proteins accumulate during the course of ageing and under various pathological conditions [30]. In particular, serum albumin, which is present in mouse blood at a concentration of approximately 27 mg/mL, is the most abundant protein, accounting for approximately 54% of the plasma protein weight [31], and since it is exposed to various active chemical species at high frequency, it provides information on oxidative stress in systemic circulation. Of these amino acid residues, the amino acid lysine in proteins is subject to the largest variety of physiological post-translational modifications and is also among the most frequently carbonylated amino acids [32] (Figure 6). In this study as well, lysine carbonylation accounted for half of the identified serum albumin oxidation-modified

sequence OMSA (Figure 5). Peroxynitrite ($ONOO^-$) binds to the phenolic ring of tyrosine residues to produce nitrotyrosine. In addition, the methyl thioether group of methionine changes to a sulfoxide structure in response to increased levels of intracellular oxidative stress (Figure 6). Oxidative modification of serum albumin was also observed in mice after a single exposure to TBI, as it was in humans with chronic low-dose radiation exposure. Interestingly, mOMSA14, an oxidation-mediated modification site of the 159th methionine residue in the mouse albumin amino acid sequence, and an oxidation-mediated modification site of the 162nd tyrosine residue in the human albumin amino acid sequence, is located in domain IB of the albumin molecule (Figure 5). Although the profile of oxidative modification of albumin as a whole differs between humans and mice, it is noteworthy that the amino acid residues Met-159 in MSA and Tyr-162 in HSA, which correlate with exposure, are both located in domain IB of albumin [33]. The common oxidative modification response of domain IB of serum albumin to radiation suggests a possible link between the steric structure of the protein and the biological response to radiation and can be used as a biomarker of both acute and chronic radiation exposure for living organisms. Persistent non-physiological protein modifications, such as non-reparable oxidative protein carbonylation, are irreversible and mostly deleterious to protein activity, and expectedly to their interactions with partner molecules. However, the functional changes of oxidatively modified albumin, the subsequent effects on individual health conditions, diseases, and longevity, as well as the relationship with radiation damage, are issues to be addressed in the future.

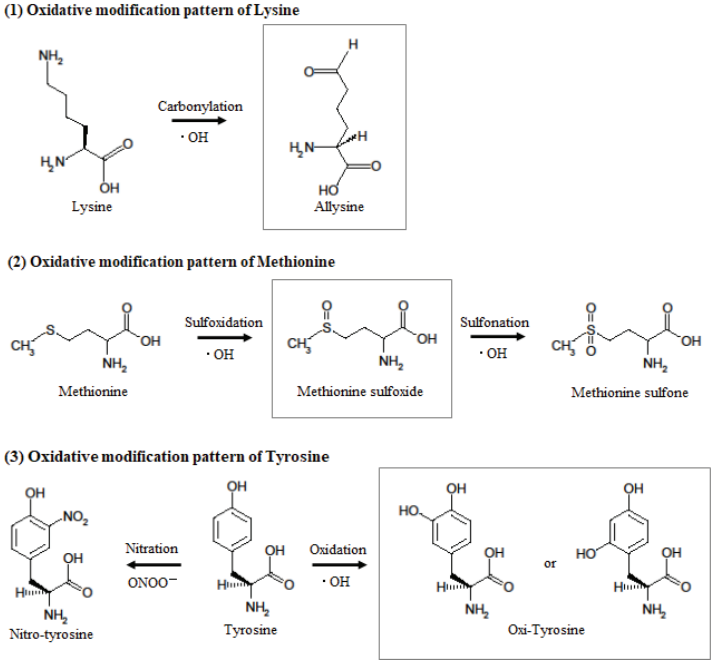


**Figure 6. Hypothesized mechanism of oxidative modification of mouse serum albumin after single TBI.** When tyrosine reacts with peroxynitrite or hydroxyl radicals, it becomes nitrotyrosine or hydroxytyrosine, but the aromatic substituent pattern cannot be identified by mass spectrometry. When methionine reacts with hydroxyl radicals, it becomes methionine sulfoxide and then methionine sulfone. When lysine reacts with hydroxyl radicals, it becomes allysine.

Regarding the biological effects of ionizing radiation, initially, it was dominated by target theory, which quantifies the damage caused by traversal of cellular targets such as

DNA by ionizing tracks [34,35]. Genomic DNA is the primary target, and double-strand breaks (DSBs) were found to be the most important radiation-induced DNA damage. DSBs differ from base excision repair in SSBs in that their repair pathway is more complex and requires more proteins. Later, the importance of "non-target" or "bystander" effects became recognized with the discovery that mutagenesis, death and/or altered behavior sometimes occur in cells that were not themselves traversed by any radiation tracks but which merely interacted with traversed cells [35,36]. A variety of short- and long-range cell-to-cell propagating signals have been reported, including small molecules capable of moving through gap junctions (e.g., lipid peroxide products, nucleotides), diffusible long-range signals such as proinflammatory cytokines (e.g., tumor necrosis factor-α) [37], and potentially micro RNAs [35] and exosomes [38]. Thus, various proteins are involved in radiation-induced damage and repair. On the other hand, the results of this study demonstrated the occurrence of dose-dependent protein oxidative modification by single TBI, revealing molecular damage to important proteins in targeting theory and non-targeted effects. Radman et al. reported that the first bottleneck in cell recovery from radiation damage is functional (proteome) rather than informational (DNA) [39,40]. They also indicated that although proteins and DNA are equally important for long-term survival, residual proteome activity after radiation stress can repair inactive damaged DNA and make it fit again for transcription and replication, but DNA cannot restore the proteome without pre-existing relevant protein activity. The results of this study–that single TBI causes many oxidative modifications to serum albumin in a dose-dependent manner–suggest that other proteins in the body undergo similar oxidative modifications. This means that, as Rithidech et al. postulated, changes in the expression levels of proteins may potentially be associated with late-occurring adverse effects [29]. Thus, protein variation and serum albumin oxidative modification responses found in exposed individuals are important indicators for considering the effects of radiation on living organisms along with DNA damage, in addition to their use as biomarkers estimation of the radiation dose.

## 5. Conclusions

Our previous report suggested that biological responses to chronic low-dose radiation in humans can be assessed by fluctuations in certain blood proteins and oxidative modification of HSA. The present results revealed significant increases or decreases in the serum levels of six proteins and demonstrated a dose-dependent oxidative modified region in serum albumin prepared from acute single TBI mice. Although the dose-dependent profiles of OMSA differed between acute single TBI in mice and chronic low-dose exposure in humans, the amino acid residues that correlate with exposure are all located in domain IB of albumin. It is interesting to note that the domains of albumin that are sensitive to oxidative reactions are consistent. These radiation responses are expected to have the potential to be used as biomarkers of acute and chronic radiation exposure in living organisms. DNA, the genetic material that holds all of the information of life phenomena, is an important biological target of ionizing radiation. Protein damage caused by ionizing radiation also needs to be considered in more detail.

**Supplementary Materials:** The following supporting information can be downloaded at: https://www.mdpi.com/article/10.3390/antiox11091710/s1, Figure S1: Correlation between the Serpin A3K expression levels with single TBI and the radiation dose.; Table S1: Oxidative modification pattern of peptide sequence consisting serum albumin in mice exposed to acute high dose/dose-rate radiation.

**Author Contributions:** Conceptualization, M.Y., S.T. and I.K.; methodology, M.Y., Y.T., E.D.N., Y.S. and T.M.; software, M.Y. and Y.T.; dose estimation, E.D.N. and M.H.; data curation, M.Y. and Y.T.; writing—original draft preparation, M.Y. and I.K.; writing—review and editing, M.Y., Y.T. and I.K.; visualization, Y.T.; project administration, M.S., S.T. and I.K.; funding acquisition, M.Y. and I.K. All authors have read and agreed to the published version of the manuscript.

**Funding:** This research was partially supported by the Japan Society for the Promotion of Science (JSPS) KAKENHI Grant Nos. JP16K15368, JP18KK0261, JP18K10023, JP18K18190, JP20H00556, JP21H02860, and Hirosaki University Institutional Research Grant.

**Institutional Review Board Statement:** The study was approved by the animal experiment committee of the CLEA Japan (Tokyo, Japan) (approval number: G17001).

**Informed Consent Statement:** Not applicable.

**Data Availability Statement:** All raw data for proteomics experiments are provided in supplementary information Table S1. The proteomics data are also available online using accession numbers "PXD025948, PXD025949, PXD025950" for Proteome Xchange [41] and accession numbers "JPST001166, JPST001167, JPST001168" for jPOST Repository [42]. Any additional data that support the findings of this study are available from the corresponding author upon reasonable request.

**Acknowledgments:** The authors are grateful to Miyu Miyazaki at the Center for Scientific Equipment Management, Hirosaki University Graduate School of Medicine, for help with the LC-MS/MS analysis.

**Conflicts of Interest:** The authors declare no conflict of interest.

## References

1. Yamaguchi, M.; Tatara, Y.; Nugraha, E.D.; Ramadhani, D.; Tamakuma, Y.; Sato, Y.; Miura, T.; Hosoda, M.; Yoshinaga, S.; Syaifudin, M.; et al. Detection of biological responses to low-dose radiation in humans. *Free Radic. Biol. Med.* **2022**, *184*, 196–207. [CrossRef] [PubMed]
2. UNSCEAR. *Effects of Ionizing Radiation*; UNSCEAR 2006 Report, Volume I: Report to the General Assembly, Scientific Annexes A and B; United Nations Publication: New York, NY, USA, 2006.
3. UNSCEAR. *United Nations Scientific Committee on the Effects of Atomic Radiation: Sources, Effects and Risks of ionizing Radiation*; UNSCEAR 2017, Vol I. Annex B: Epidemiological Studies of cancer risk Due To Low-Dose-Rate Radiation From Environmental. Sources Volume 1; United Nations Publication: New York, NY, USA, 2017.
4. Tang, F.R.; Loganovsky, K. Low dose or low dose rate ionizing radiation-induced health effect in the human. *J. Environ. Radioact.* **2018**, *192*, 32–47. [CrossRef] [PubMed]
5. Hosoda, M.; Nugraha, E.D.; Akata, N.; Yamada, R.; Tamakuma, Y.; Sasaki, M.; Kelleher, K.; Yoshinaga, S.; Suzuki, T.; Rattanapongs, C.P.; et al. A unique high natural background radiation area—Dose assessment and perspectives. *Sci. Total Environ.* **2021**, *750*, 142346. [CrossRef] [PubMed]
6. Nugraha, E.D.; Hosoda, M.; Kusdiana; Untara; Mellawati, J.; Nurokhim; Tamakuma, Y.; Ikram, A.; Syaifudin, M.; Yamada, R.; et al. Comprehensive exposure assessments from the viewpoint of health in a unique high natural background radiation area, Mamuju, Indonesia. *Sci. Rep.* **2021**, *11*, 14578. [CrossRef] [PubMed]
7. Dainiak, N.; Sorba, S. Early identification of radiation accident victims for therapy of bone marrow failure. *Stem Cells* **1997**, *15* (Suppl. 2), 275–285. [CrossRef]
8. Tang, F.R.; Loke, W.K.; Khoo, B.C. Low-dose or low-dose-rate ionizing radiation-induced bioeffects in animal models (Review). *J. Radiat. Res.* **2017**, *58*, 165–182. [CrossRef]
9. Shin, E.; Lee, S.; Kang, H.; Kim, J.; Kim, K.; Youn, H.; Jin, Y.W.; Seo, S.; Youn, B. Organ-Specific Effects of Low Dose Radiation Exposure: A Comprehensive Review. *Front. Genet.* **2020**, *11*, 566244. [CrossRef]
10. Guipaud, O.; Benderitter, M. Protein biomarkers for radiation exposure: Towards a proteomic approach as a new investigation tool. *Ann. Ist. Super. Sanità* **2009**, *45*, 278–286.
11. Guipaud, O. Serum and plasma proteomics and its possible use as detector and predictor of radiation diseases. *Adv. Exp. Med. Biol.* **2013**, *990*, 61–86. [CrossRef]
12. Sharma, M.; Moulder, J.E. The urine proteome as a radiation biodosimeter. *Adv. Exp. Med. Biol.* **2013**, *990*, 87–100. [CrossRef]
13. Pannkuk, E.L.; Laiakis, E.C.; Authier, S.; Wong, K.; Fornace, A.J., Jr. Gas chromatography/mass spectrometry metabolomics of urine and serum from nonhuman primates exposed to ionizing radiation: Impacts on the tricarboxylic acid cycle and protein metabolism. *J. Proteome Res.* **2017**, *16*, 2091–2100. [CrossRef] [PubMed]
14. Wathen, L.K.; Eder, P.S.; Horwith, G.; Wallace, R.L. Using biodosimetry to enhance the public health response to a nuclear incident (Review). *Int. J. Radiat. Biol.* **2021**, *97* (Suppl. 1), S6–S9. [CrossRef] [PubMed]
15. Satyamitra, M.; Turcu, F.E.R.; Pantoja-Galicia, N.; Wathen, L. Challenges and strategies in the development of radiation biodosimetry tests for patient management. *Radiat. Res.* **2021**, *196*, 455–467. [CrossRef] [PubMed]
16. Saberi, A.; Khodamoradi, E.; Birgani, M.J.T.; Makvandi, M. Gene expression biodosimetry: Quantitative assessment of radiation dose with total body exposure of rats. *Asian Pac. J. Cancer Prev.* **2015**, *16*, 8553–8557. [CrossRef] [PubMed]
17. Miura, S.; Yamaguchi, M.; Yoshino, H.; Nakai, Y.; Kashiwakura, I. Dose-dependent increase of Nrf2 target gene expression in mice exposed to ionizing radiation. *Radiat. Res.* **2019**, *191*, 176–188. [CrossRef]
18. Yao, Y.; Li, L.; Huang, X.; Gu, X.; Xu, Z.; Zhang, Y.; Huang, L.; Li, S.; Dai, Z.; Li, C.; et al. SERPINA3K induces apoptosis in human colorectal cancer cells via activating the Fas/FasL/caspase-8 signaling pathway. *FEBS J.* **2013**, *280*, 3244–3255. [CrossRef]

19. Shu, Z.; Wan, J.; Read, R.J.; Carrell, R.W.; Zhou, A. Angiotensinogen and the Modulation of Blood Pressure. *Front. Cardiovasc. Med.* **2021**, *8*, 645123. [CrossRef]
20. Brito, N.F.; Oliveira, D.S.; Santos, T.C.; Moreira, M.F.; Melo, A.C.A. Current and potential biotechnological applications of odorant-binding proteins. *Appl. Microbiol. Biotechnol.* **2020**, *104*, 8631–8648. [CrossRef]
21. Moataz, R.; Alexander, F.B.; Husam, Y.Z.; Wassana, Y. Augmenting the therapeutic window of radiotherapy: A perspective on molecularly targeted therapies and nanomaterials. *Radiother. Oncol.* **2020**, *150*, 225–235. [CrossRef]
22. Seshacharyulu, P.; Ponnusamy, M.P.; Haridas, D.; Jain, M.; Ganti, A.K.; Batra, S.K. Targeting the EGFR signaling pathway in cancer therapy. *Expert Opin. Ther. Targets* **2012**, *16*, 15–31. [CrossRef]
23. Dietz, A.; Boehm, A.; Mozet, C.; Wichmann, G.; Giannis, A. Current aspects of targeted therapy in head and neck tumors. *Eur. Arch. Otorhinolaryngol.* **2008**, *265* (Suppl. 1), 3–12. [CrossRef]
24. Lee, H.C.; An, S.; Lee, H.; Woo, S.H.; Jin, H.O.; Seo, S.K.; Choe, T.B.; Yoo, D.H.; Lee, S.J.; Hong, Y.J.; et al. Activation of epidermal growth factor receptor and its downstream signaling pathway by nitric oxide in response to ionizing radiation. *Mol. Cancer Res.* **2008**, *6*, 996–1002. [CrossRef]
25. Chen, D.J.; Nirodi, C.S. The epidermal growth factor receptor: A role in repair of radiation-induced DNA damage. *Clin. Cancer Res.* **2007**, *13*, 6555–6560. [CrossRef] [PubMed]
26. Moustafa, E.M.; Thabet, N.M. Beta-sitosterol upregulated paraoxonase-1 via peroxisome proliferator-activated receptor-γ in irradiated rats. *Can. J. Physiol. Pharmacol.* **2017**, *95*, 661–666. [CrossRef] [PubMed]
27. Serhatlioglu, S.; Gursu, M.F.; Gulcu, F.; Canatan, H.; Godekmerdan, A. Levels of paraoxonase and arylesterase activities and malondialdehyde in workers exposed to ionizing radiation. *Cell Biochem. Funct.* **2003**, *21*, 371–375. [CrossRef]
28. Schreuder, M.; Reitsma, P.H.; Bos, M.H.A. Blood coagulation factor Va's key interactive residues and regions for prothrombinase assembly and prothrombin binding. *J. Thromb. Haemost.* **2019**, *17*, 1229–1239. [CrossRef]
29. Rithidech, K.N.; Honikel, L.; Rieger, R.; Xie, W.; Fischer, T.; Simon, S.R. Protein-expression profiles in mouse blood-plasma following acute whole-body exposure to $^{137}$Cs gamma rays. *Int. J. Radiat. Biol.* **2009**, *85*, 432–447. [CrossRef]
30. Roche, M.; Rondeau, P.; Singh, N.R.; Tarnus, E.; Bourdon, E. The antioxidant properties of serum albumin. *FEBS Lett.* **2008**, *582*, 1783–1787. [CrossRef]
31. Zaias, J.; Mineau, M.; Cray, C.; Yoon, D.; Altman, N.H. Reference values for serum proteins of common laboratory rodent strains. *J. Am. Assoc. Lab. Anim. Sci.* **2009**, *48*, 387–390.
32. Gonos, E.S.; Kapetanou, M.; Sereikaite, J.; Bartosz, G.; Naparło, K.; Grzesik, M.; Sadowska-Bartosz, I. Origin and pathophysiology of protein carbonylation, nitration and chlorination in age-related brain diseases and aging. *Aging* **2018**, *10*, 868–901. [CrossRef]
33. Zsila, F. Subdomain IB is the third major drug binding region of human serum albumin: Toward the three-sites model. *Mol. Pharm.* **2013**, *10*, 1668–1682. [CrossRef] [PubMed]
34. Mavragani, I.V.; Laskaratou, D.A.; Frey, B.; Candéias, S.M.; Gaipl, U.S.; Lumniczky, K.; Georgakilas, A.G. Key mechanisms involved in ionizing radiation-induced systemic effects. A current review (Review). *Toxicol. Res.* **2015**, *5*, 12–33. [CrossRef] [PubMed]
35. Shuryak, I.; Brenner, D.J. Review of quantitative mechanistic models of radiation-induced non-targeted effects (NTE). *Radiat. Prot. Dosim.* **2020**, *192*, 236–252. [CrossRef]
36. Morgan, W.F.; Sowa, M.B. Non-targeted bystander effects induced by ionizing radiation (Review). *Mutat. Res.* **2007**, *616*, 159–164. [CrossRef]
37. Prise, K.M.; O'Sullivan, J.M. Radiation-induced bystander signalling in cancer therapy (Review). *Nat. Rev. Cancer* **2009**, *9*, 351–360. [CrossRef]
38. Du, Y.; Du, S.; Liu, L.; Gan, F.; Jiang, X.; Wangrao, K.; Lyu, P.; Gong, P.; Yao, Y. Radiation-induced bystander effect can be transmitted through exosomes using miRNAs as effector molecules. *Radiat. Res.* **2020**, *194*, 89–100. [CrossRef] [PubMed]
39. Krisko, A.; Radman, M. Phenotypic and Genetic Consequences of Protein Damage. *PLos Genet.* **2013**, *9*, e1003810. [CrossRef]
40. Krisko, A.; Radman, M. Protein damage, ageing and age-related diseases (Review). *Open Biol.* **2019**, *9*, 180249. [CrossRef]
41. Deutsch, E.W.; Csordas, A.; Sun, Z.; Jarnuczak, A.; Perez-Riverol, Y.; Ternent, T.; Campbell, D.S.; Bernal-Llinares, M.; Okuda, S.; Kawano, S.; et al. The ProteomeXchange consortium in 2017: Supporting the cultural change in proteomics public data deposition. *Nucleic Acids Res.* **2017**, *45*, D1100–D1106. [CrossRef]
42. Okuda, S.; Watanabe, Y.; Moriya, Y.; Kawano, S.; Yamamoto, T.; Matsumoto, M.; Takami, T.; Kobayashi, D.; Araki, N.; Yoshizawa, A.C.; et al. jPOSTrepo: An international standard data repository for proteomes. *Nucleic Acids Res.* **2017**, *45*, D1107–D11011. [CrossRef]

antioxidants

MDPI

*Review*

# Targeting Mitochondrial Metabolism to Reverse Radioresistance: An Alternative to Glucose Metabolism

**Chenbin Bian [1,2,3], Zhuangzhuang Zheng [1,2,3], Jing Su [1,2,3], Huanhuan Wang [1,2,3], Sitong Chang [1,2,3], Ying Xin [4,*] and Xin Jiang [1,2,3,*]**

[1] Jilin Provincial Key Laboratory of Radiation Oncology & Therapy, The First Hospital of Jilin University, Changchun 130021, China
[2] Department of Radiation Oncology, The First Hospital of Jilin University, Changchun 130021, China
[3] NHC Key Laboratory of Radiobiology, School of Public Health, Jilin University, Changchun 130021, China
[4] Key Laboratory of Pathobiology, Ministry of Education, Jilin University, Changchun 130021, China
* Correspondence: xingy@jlu.edu.cn (Y.X.); jiangx@jlu.edu.cn (X.J.); Tel.: +86-135-0431-0452 (Y.X.); +86-158-0430-2750 (X.J.)

**Abstract:** Radiotherapy failure and poor tumor prognosis are primarily attributed to radioresistance. Improving the curative effect of radiotherapy and delaying cancer progression have become difficult problems for clinicians. Glucose metabolism has long been regarded as the main metabolic process by which tumor cells meet their bioenergetic and anabolic needs, with the complex interactions between the mitochondria and tumors being ignored. This misconception was not dispelled until the early 2000s; however, the cellular molecules and signaling pathways involved in radioresistance remain incompletely defined. In addition to being a key metabolic site that regulates tumorigenesis, mitochondria can influence the radiation effects of malignancies by controlling redox reactions, participating in oxidative phosphorylation, producing oncometabolites, and triggering apoptosis. Therefore, the mitochondria are promising targets for the development of novel anticancer drugs. In this review, we summarize the internal relationship and related mechanisms between mitochondrial metabolism and cancer radioresistance, thus exploring the possibility of targeting mitochondrial signaling pathways to reverse radiation insensitivity. We suggest that attention should be paid to the potential value of mitochondria in prolonging the survival of cancer patients.

**Keywords:** radioresistance; reactive oxygen species; oxidative phosphorylation; oncometabolites; apoptosis

**Citation:** Bian, C.; Zheng, Z.; Su, J.; Wang, H.; Chang, S.; Xin, Y.; Jiang, X. Targeting Mitochondrial Metabolism to Reverse Radioresistance: An Alternative to Glucose Metabolism. *Antioxidants* **2022**, *11*, 2202. https://doi.org/10.3390/antiox11112202

Academic Editors: Elena Obrador, Alegria Montoro and Stanley Omaye

Received: 20 September 2022
Accepted: 2 November 2022
Published: 7 November 2022



## 1. Introduction

Cancer is a serious problem that threatens human life, and the number of cancer-related deaths and incidences are increasing annually. According to the 2020 World Cancer Report, 4.57 million new cancer cases and 3 million cancer-related deaths have occurred in China, ranking it first in the world for cases and deaths [1]. As a traditional cancer treatment, radiotherapy causes nuclear DNA damage directly via ionizing radiation (IR) or indirectly via the production of reactive oxygen species (ROS), pushing cancer cells with high levels of DNA damage over the threshold for cell death [2]. As some tumors, such as malignant lymphoma, testicular seminoma, and nephroblastoma, are highly sensitive to IR, an explosion of interest in the role of radiotherapy in eradicating tumor cells has been observed in recent decades [3–5]. Mitochondria exist in most cells and are the main sites of cellular aerobic respiration, adapting to rapid tumor growth demands by regulating the process of energy production [6]. It is worth noting that mitochondria are the most important targets of IR damage aside from the nucleus [7]. Radiation-induced mitochondrial DNA mutations and electron transport chain (ETC) disruption activate oxidative stress and eventually trigger the mitochondrial apoptosis pathway, which seriously affects the survival of tumor cells [8]. However, tumor cell resistance to IR remains an important obstacle that hinders the clinical application of radiotherapy, potentially leading to poor

prognosis, tumor recurrence, and metastasis [9,10]. In addition, radioresistance increases the incidence of radiation-induced damage to normal tissue cells surrounding the tumor and the disruption of homeostasis, mainly manifesting as radiation pneumonitis, intestinal dysbiosis, hemorrhage, and cardiac-related complications [11,12]. Fractionated treatment regimens have been established for radiotherapy. As fractionation is the process of dividing a radiation dose into multiple fractions, fractionated radiotherapy ensures as much tumor cell death as possible while reducing normal tissue complications. However, IR has been shown to activate epithelial–mesenchymal transition transcription factors such as Snail, Slug, Twist, ZEB1/2, hypoxia-inducible factor 1 (HIF1), and signal transducer and transcriptional activator 3 (STAT3); interfere with glucose and mitochondrial metabolism; promote metastatic potential; and increase the likelihood of radioresistance [13–15].

Metabolic disorders have long been recognized as carcinogenic factors [16]. Metabolic reprogramming, the alteration in metabolic pathways by which cancer cells can proliferate rapidly, survive under conditions of nutrient depletion and hypoxia, and evade the immune system, is considered a hallmark of cancer [17].

Glucose is the primary energy source that drives the rapid proliferation of cancer cells, and cancer starvation therapy based on glucose deprivation to induce oxidative stress has become an effective method for inhibiting tumor growth and survival [18]. 2-Deoxy-D-glucose (2DG), a glucose analog, targets glucose metabolism to deplete energy in cancer cells [19]. For most cancer cells, 2DG treatment alone does not significantly induce cell death, but renders cells more vulnerable to the oxidative stress induced by radio- or chemotherapy [20]. For example, 2DG combined with cisplatin or radiation enhances the cytotoxicity of head and neck squamous cell carcinoma through metabolic oxidative stress [21]. Furthermore, inhibition of glycolysis (2DG) and intracellular redox metabolism (glutathione/thioredoxin) improves the radiation response of radioresistant cervical cancers [22]. Unexpectedly, glucose deprivation promotes the death of malignant cells and induces colorectal cancer migration, invasion, and epithelial–mesenchymal transition (EMT). Knockdown of thioredoxin-1 can decrease G6PD protein expression and activity thereby reducing NADPH production, increasing ROS levels, enhancing glucose-starvation-induced cell death, and reversing aggressive or metastatic potential during cancer progression [23]. Rapidly proliferating cells tend to have high G6PD activity, while the pentose phosphate pathway (PPP) is the main pathway for glucose catabolism, and its reductant NADPH can be used to detoxify intracellular ROS, thus acting as an antioxidant defense [24]. During oxidative stress, cancer cells selectively shut down the glycolytic pathway, thereby increasing the glucose flux through PPP to meet the need for NADPH synthesis [25]. Snail, a key transcriptional repressor of EMT, regulates the glucose flux between glycolysis and PPP by inhibiting the platelet isoform of phosphofructokinase (PFKP) expression, which plays an important role in cancer cell survival [26]. Thus, interfering with the PPP to disrupt NADPH homeostasis not only enhances radiotherapy-induced immunogenic cell death but also overcomes cisplatin resistance [27,28].

Because of these classical conclusions, it was erroneously believed that malignant cells met their bioenergetic and anabolic needs primarily through glucose metabolism, and the role of mitochondrial metabolism in all steps of tumorigenesis was ignored [29]. However, the latest research has indicated that malignant transformation, tumor progression, and evasion of exogenous stress are influenced by mitochondria metabolism [30,31]. In addition, although the effect of radiation therapy is primarily dependent on glucose metabolism, there is growing awareness that changes in mitochondrial metabolism, such as mitochondrial function associated with antiradiation effects, also contribute to the development of radioresistance in head and neck squamous cell carcinomas and gliomas (Figure 1) [32,33]. Changes in mitochondrial size and shape or mutations in mitochondrial DNA interfere with the normal physiological function of mitochondria, thereby enhancing their adaptability to radiation [34]. Therefore, it is necessary to understand the molecular mechanisms underlying these changes caused by mitochondria to improve the efficacy of radiotherapy. Here, we briefly review the research progress on the relationship between mi-

tochondrial metabolism and radioresistance from four aspects: regulating oxidative stress, participating in oxidative phosphorylation (OXPHOS), producing oncometabolites, and triggering apoptosis (Figure 1), with a focus on the possibility of targeting mitochondrial metabolism for cancer therapy.

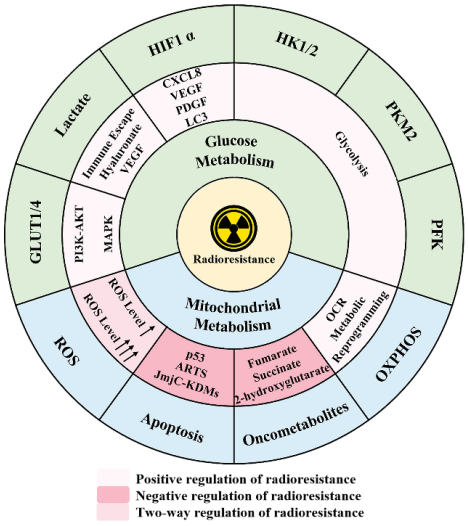


**Figure 1.** A schematic model illustrating the effects of two major metabolisms on radioresistance. Six targets in glucose metabolism have the most significant impact on radiation resistance, regulating their corresponding molecules or processes to intervene in the therapeutic effect. In general, small-molecule inhibitors can be used to help IR restore the expected efficacy, and there are several approved drugs currently available for clinical treatment. The effects of mitochondrial metabolism on radiation resistance can be summarized in four aspects, the details of which are presented below. Abbreviations: GLUT1/4—glucose transporter 1/4, PFK—phosphofructokinase, HK1/2—hexokinase 1/2, PKM2—pyruvate kinase M2, HIF1 α—hypoxia-inducible factor 1 α, OXPHOS—oxidative phosphorylation, ROS—reactive oxygen species.

## 2. ROS and Radioresistance

Reactive oxygen species are products of normal cellular metabolism and mainly include superoxide anions ($O_2^-$), hydrogen peroxide ($H_2O_2$), and hydroxyl radicals ($^-OH$) [35]. Multiple lines of evidence indicate that there are three main sources of ROS in vivo, namely macrophages, the mitochondrial respiratory chain, and mitochondrial polyunsaturated membrane lipid peroxidation, a process during which ROS from mitochondrial polyunsaturated membranes pose the greatest threat to cells [36]. Under normal physiological conditions, cells tend to maintain redox homeostasis, that is, the balance between the production of free radicals and reactive metabolites (oxidants, ROS, or reactive nitrogen species) and their elimination through protective mechanisms (antioxidant systems) [37]. When the balance between ROS and antioxidants is disrupted, the body is in a state of oxidative stress, resulting in damage to important biomolecules and cells with potential effects on the entire organism [38]. It is worth noting that oxidative stress is generally present in tumor cells, and data show that the concentration of ROS is usually 10 times higher than that in normal cells, which may further lead to DNA mutation, genomic instability, and tumor cell proliferation [39].

Most ROS in mammalian cells are generated by the mitochondrial oxidative respiratory chain [40]. Furthermore, an inextricable relationship exists between ROS production and radioresistance. Mitochondrial $H_2O_2$ can trigger the accumulation of potential oncogenic DNA or activation of potential oncogenic signaling pathways, including the mitogen-activated protein kinase (MAPK) and epidermal growth factor receptor (EGFR) signaling

pathways, thereby promoting cell proliferation and malignant transformation [41,42]. Experiments have demonstrated that activation of the MAPK and EGFR signaling pathways can increase the resistance of cervical and lung cancer cells to radiation, respectively, and knockout of thyroid hormone receptor interactor 4 (TRIP4) promotes the inactivation of MAPK signaling, which effectively improves the sensitivity of the former to radiation [43,44]. It has also been reported that activated $O_2^-$- and $H_2O_2$-mediated cell survival in non-small-cell lung cancer (NSCLC) occurs via the c-Met-PI3K-Akt and c-Met-Grb2/SOS-Ras-p38 pathways [45]. Interestingly, acidosis is a common characteristic of the tumor microenvironment. Under such acidic conditions, the specific mitogen reaction of cancer cells reduces extracellular acidification and increases $O_2^-$ production by switching from glycolysis to OXPHOS, which promotes tumor invasiveness and insensitivity to radiation therapy [31]. However, the mechanism appears to be different in endothelial cells, where mitochondrial ROS (mtROS) can stimulate the activity of NAD(P)H oxidases (NOXs), resulting in a positive feedback loop of ROS-induced ROS generation [46]. Recent studies have also shown that NOXs significantly contribute to $H_2O_2$ and $O_2^-$ production in gastrointestinal and pancreatic cancers [47,48]. Kim etal. reported that the novel PPARɣligand PPZ023 can lead to NOX4-derived mtROS generation to induce death of radioresistant NSCLC cells via exosomal endoplasmic reticulum stress [49].

The reason for these diametrically opposite results may be the dual role of ROS, in which the difference in the level of ROS is dominant (Figure 2). In normal cells, ROS are produced at low concentrations and are effectively neutralized by the potent antioxidant systems of the cells. A moderate increase in ROS levels as in states of chronic oxidative stress induces random mutations in cells and promotes tumor cell proliferation, metastasis, and radioresistance. If ROS levels continue to increase beyond the antioxidant capacity of cells, this will cause apoptosis, ferroptosis, or cuproptosis, thereby significantly improving the efficacy of radiotherapy [38,50]. Sublethal levels of ROS stimulate tumor cell proliferation by inhibiting tumor suppressors such as redox-sensitive phosphatase and tensin homologues (PTEN), thereby promoting the PI3K-Akt signaling pathway or stabilizing HIF1 α, and are associated with chemotherapy resistance and prevention of tumor cell death [51]. In addition, a slight increase in superoxide can activate signal transduction pathways related to metastasis, including the mtROS-Src-SMAD-Pyk2 signaling pathway; in particular, Src can also promote radiation resistance in glioblastoma (GBM) [52,53]. Combining the novel Src inhibitor Si306 with radiotherapy represents a promising approach to increasing the therapeutic effect on GBM [54]. Importantly, moderately elevated ROS levels increase the resistance of cancer cells to radiotherapy by triggering an adaptive hormetic response and promoting autophagy activation [55,56]. Conversely, in the case of severe oxidative stress, ROS cause regulated cell death (RCD) or trigger apoptosis independently of DNA damage, thereby increasing the sensitivity to radiotherapy (Figure 2) [57]. For example, elesclomol (STA-4785) targets tumor ROS, which can further increase ROS levels in tumor cells, induce cytotoxicity in tumor cells, and selectively induce apoptosis in melanoma cells [58]. Unexpectedly, elesclomol did not show a significant radiosensitization effect on prostate cancer cells, indicating that there was no clear linear relationship between the specific ROS dose and radioresistance [59]. Of course, we should not ignore the fact that early and late ROS accumulation can lead to opposite carcinogenic effects. Radiation-induced early ROS signaling is responsible for the activation of Jak3-Erk-STAT3, which leads to a cell survival response, whereas late ROS production is different [60].

In cells, ROS production is counterbalanced by cellular antioxidant defense systems. Superoxide dismutases (SODs), the most potent antioxidant enzymes in mitochondria, can catalyze $O_2^-$ to $H_2O_2$ [61]. SOD-produced $H_2O_2$ can be subsequently reduced to $H_2O$ by catalases (CATs), glutathione peroxidases (GPXs), and peroxiredoxins (Prxs) [31]. To date, an increasing amount of evidence has suggested that the antioxidant stress system is responsible for radio- and chemoresistance [38]. Furthermore, ROS induced by chemoradiotherapy activate the Keap1-Nrf2 and PI3K-AKT pathways, which regulate several antioxidant enzymes in downstream signaling, ultimately triggering both radio- and chemoresistance [62,63]. The

inhibitors of these two signaling pathways, trigonelline and delicaflavone, can significantly reverse radioresistance and enhance radiosensitivity, further demonstrating the detrimental effects of the antioxidant stress system on cancer therapy [64,65]. Studies have shown an important relationship between an increase in the survival rate of pancreatic cancer cells after γ-ray irradiation and enhancement of the activity of manganese superoxide dismutase (Mn-SOD), the main antioxidant enzyme in the body, which also indicates that MnSOD significantly increases the resistance of pancreatic cancer to radiotherapy [66]. CuZn-SOD overexpression confers radioresistance on human glioma cells by suppressing irradiation-induced late ROS accumulation (superoxide) [67]. GPX4 inhibition promotes lipid peroxidation and re-sensitizes radioresistant cancer cells to IR-induced ferroptosis, resulting in radiosensitization [68]. In addition, redox-active metal ions are involved in antioxidant reactions, such as $O_2^-$- and $H_2O_2$-mediated disruption of Fe metabolism, sensitizing NSCLC and GBM to pharmacological ascorbate [69]. However, recent studies have yielded conflicting results that antioxidant supplementation is detrimental to patients with adequate antioxidant status (lung, gastrointestinal tract, head and neck, and esophagus), whereas individuals with deficient antioxidant systems respond positively [47].

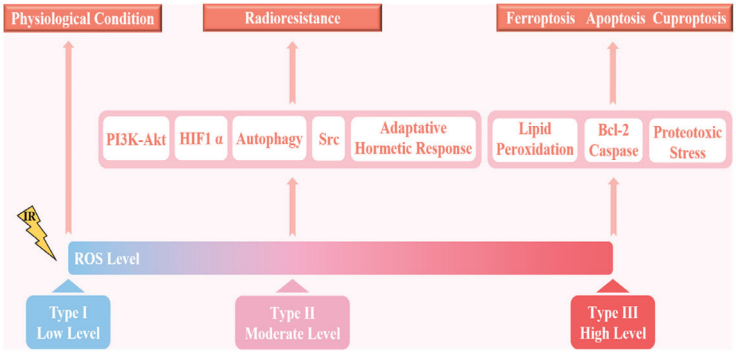


**Figure 2.** A schematic diagram of the different physiological effects of varying ROS concentrations. Under physiological conditions, ROS levels are maintained at a low state under the regulation of antioxidant systems, which ensures the survival of normal cells. Moderate levels of ROS tend to promote tumor initiation and progression, and to some extent interfere with the efficacy of radiotherapy. A continued rise in ROS levels to high levels will lead to cell death.

Based on the above studies, it can be concluded that ROS is a double-edged sword; it is one of the ways in which radiotherapy can eradicate tumor cells, yet even moderate intracellular concentrations may lead to radioresistance. Although the dual role of ROS is a major challenge in cancer therapy, it presents a promising strategy to differentiate normal cells from cancer cells using specific cellular signals to target tumor killing. An in-depth understanding of the dynamic balance between ROS and antioxidant levels and the role of ROS in different stages of the disease will help researchers to develop personalized therapies for different tumor types. Both disabling cellular antioxidants and adding specific ROS inducers provide new ideas for the precise treatment of tumors and the improvement in radiosensitivity.

## 3. OXPHOS and Radioresistance

Carbohydrates are the main source of cellular energy and are involved in the oxidative breakdown of glucose including glycolysis and OXPHOS [70]. Normally, cells favor the application of the mitochondrial OXPHOS, which is more efficient at producing ATP; however, the rate of glucose metabolism by aerobic glycolysis is 10–100 times faster than that of the complete oxidation of glucose in the mitochondria [71]. Therefore, Warburg initially believed that cancer cells could have an active glycolytic phenotype even in the presence of adequate oxygen supply and completely functioning mitochondria [72].

Warburg later proposed that this phenomenon was due to a developmental defect in the mitochondria of tumor cells that resulted in impaired aerobic respiration and reliance on glycolysis, hypothesizing that this event was the primary cause of cancer [73,74]. In contrast, Koppenol et al. offered a more plausible explanation, emphasizing the impairment of glycolytic regulation rather than mitochondrial respiration. There are clear indications that glycolysis is upregulated in most tumors without mitochondrial dysfunction. In these cancers, OXPHOS continues normally, even producing as much ATP as normal tissue at the same partial pressure of oxygen [75]. Notably, Weinhouse also strongly criticized the Warburg effect for his finding that well-differentiated Morris hepatomas do not produce lactic acid in aerobiosis [76]. At the same time, metabolic changes and adaptations occurring in tumors have been demonstrated to extend well beyond the Warburg effect and are seen as a secondary effect of tumorigenesis [77]. Subsequent studies have further revealed that certain types of tumors such as ovarian cancer and acute myeloid leukemia can also rely on mitochondria-specific OXPHOS to maintain biosynthesis and bioenergetics in addition to glycolysis [78]. Furthermore, in B16 melanoma the Warburg effect has been shown to be dispensable owing to the upregulation of mitochondrial metabolism [79].

Based on the above findings, we can conclude that metabolic reprogramming endows cancer with the ability to utilize multiple metabolic modalities to rapidly progress in vivo [80]. Some studies indicate that metabolic plasticity allows cells to efficiently produce energy through multiple metabolic pathways, thereby conferring on cancer cells a high degree of adaptability to a wide range of stresses and harsh tumor microenvironments [31]. In other words, tumor tissues are less sensitive to conventional chemoradiotherapy. In cancer cells that rely on glycolytic metabolism, OXPHOS can promote resistance to therapy through both the cancer-cell-intrinsic and -extrinsic pathways. In contrast, tumor cells that primarily utilize OXPHOS for energy production can become resistant to ETC inhibitors because they gain partial glycolytic metabolism (Figure 3) [81]. For example, recent studies have shown that acquired radioresistance is associated with a switch from glycolytic to oxidative metabolism in laryngeal squamous cell carcinoma cancer cells [32]. Similarly, a switch from glycolysis to OXPHOS was observed in glioma cells that developed acquired resistance to PI3K inhibitors [82]. In addition, glycolytic-dependent BRAF-mutant melanoma cells are more sensitive to the BRAF inhibitor vemurafenib, while resistant cells display upregulation of the mitochondrial biogenesis co-activator PGC1$\alpha$ through the melanocyte master regulator microphthalmia-associated transcription factor (MITF), leading to resistance to the original treatment and sensitivity to OXPHOS inhibitors [83]. Interestingly, glucose deprivation significantly promotes mitochondrial elongation, thereby inducing a metabolic shift from glycolysis to OXPHOS during energy stress in tumor cells, which is critical for hepatocellular carcinoma (HCC) survival [84]. Additionally, Dynamin-related protein 1 (DRP1) is necessary for mitochondrial elongation in HCC cells. Elongated mitochondria amplify OXPHOS through facilitating cristae formation and assembly of respiratory complexes and in turn, exerting a feedback inhibitory effect on glycolysis through NAD-dependent SIRT1 activation [84]. Consistent with this, nutrient-deprivation-related OXPHOS/glycolysis interconversion has also been observed in glioma cell lines, although the role of mitochondrial dynamics has not been investigated [85]. The only exception is that dichloroacetate, which activates OXPHOS by reversing aerobic glycolysis, improves the radiosensitivity of high-grade gliomas [86]. In conclusion, the vast majority of malignant cells can switch freely between the two metabolic modes, simply inhibiting glycolysis or OXPHOS as a reasonable therapeutic candidate. The combination of a glycolysis inhibitor (2-DG) with an OXPHOS inhibitor (metformin) significantly enhances the radiosensitization of neuroblastoma and glioma cells, suggesting that dual metabolic targeting may be a good strategy to control tumor progression and eliminate radioresistance [87]. Unfortunately, the cytotoxic effect of this combination on normal tissue remains the biggest obstacle to its clinical application.

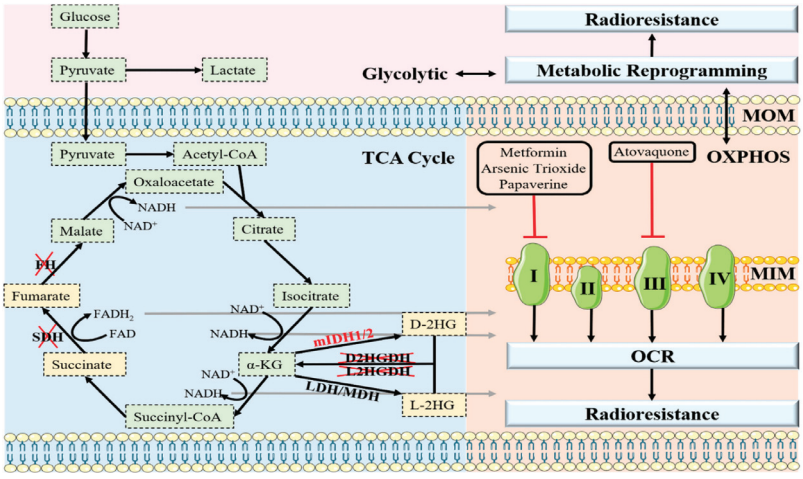


**Figure 3.** A schematic summary of glycolysis, TCA cycle, and OXPHOS in regulating radioresistance. (1) In the cytoplasm, pyruvate produced by glycolysis crosses the outer mitochondrial membrane and participates in the TCA cycle, and the subsequently produced NADH and $FADH_2$ are oxidized by a stepwise, continuous enzymatic reaction on the ETC located in the inner mitochondrial membrane, thereby releasing energy for the body to utilize. (2) Inactivation of FH, SDH, D2HGDH, and L2HGDH, mutation of IDH1/2, or promiscuous activity of MDH/LDH can induce accumulation of oncometabolites. On the one hand, oncometabolites promote tumorigenesis; on the other hand, they also amplify the benefits of radiotherapy. (3) Enhancing OCR or favoring the reprogramming of tumor cells' metabolic pathways induces radioresistance. Abbreviations: TCA cycle—tricarboxylic acid cycle, ETC—electron transport chain, OCR—oxygen consumption rate, FH —fumarate hydratase, SDH—succinate dehydrogenase, D2HGDH—D-2-hydroxyglutarate dehydrogenase, L2HGDH—L-2-hydroxyglutarate dehydrogenase, IDH1/2—isocitrate dehydrogenase-1/-2, LDH/MDH—lactate dehydrogenase/malate dehydrogenase, α-KG—α-ketoglutarate, D-2HG—D-2-hydroxyglutarate, L-2HG—L-2-hydroxyglutarate.

Another mitochondrial condition of interest is hypoxia, which poses a problem for radiation therapists because the scarcity of oxygen induces radioresistance [88]. Efforts to increase oxygen delivery to tumors have not shown positive clinical effects because of poor tumor vascularization [89]. This implies that attempts to target tumor hypoxia should focus on normalizing oxygen levels in remote tumor regions by reducing the oxygen consumption rate (OCR). Therefore, an attractive strategy is to achieve this by inhibiting mitochondrial OXPHOS as it reduces the OCR, increases oxygenation, and thus improves the radiation response [90,91]. Several clinical trials are underway to repurpose FDA-approved drugs to curb mitochondrial function and reverse radioresistance. The antidiabetic drugs metformin and phenformin have been shown to increase the partial pressure of oxygen ($pO_2$) in local tumors by inhibiting mitochondrial complex I, thereby significantly improving the effect of radiotherapy on colorectal cancer cells [92]. Another complex I inhibitory molecule, arsenic trioxide ($As_2O_3$), has shown strong superiority in the treatment of acute promyelocytic leukemia. However, in recent years, more attention has been paid to the potential of $As_2O_3$ to overcome radioresistance in solid tumors [93]. Both OXPHOS levels and the OCR are impaired by $As_2O_3$ to varying degrees in liver and lung cancer cells, with enhanced radiosensitivity [94]. Papaverine, a smooth muscle relaxant used as a vasospasm and erectile dysfunction agent, not only leads to reduced hypoxia and an increased response to radiotherapy in NSCLC and breast cancer by blocking complex I, but also has significantly fewer side effects than other OXPHOS inhibitors [95]. Atovaquone was originally used to treat and prevent parasitic infections; however, in hypopharyngeal, colorectal, and lung cancer cell lines, it significantly increased oxygenation and sensitized tumors to radiotherapy by inhibiting electron transport complex III (Table 1) [96].

**Table 1.** List of OXPHOS inhibitors under clinical trials or potential.

| OXPHOS Inhibitor | Identifier | Phase | Cancer Type | ECT Target | Ref. |
|---|---|---|---|---|---|
| Metformin | NCT04275713, NCT04414540, NCT04945148, NCT04387630 | II, II, II, II | Cervical cancer, head and neck squamous cell carcinoma, glioblastoma (IDH-wildtype), breast cancer | Complex I | [92] |
| Phenformin | NCT03026517 | I | Melanoma | Complex I | [92] |
| Arsenic Trioxide | NCT02066870, NCT03503864 | I, II | Non-small-cell lung cancer, neuroblastoma | Complex I | [93] |
| Papaverine | NCT05136846, NCT03824327 | I, I | Locally advanced or unresectable non-small-cell lung cancer | Complex I | [95] |
| Atovaquone | NCT04648033, NCT02628080 | I, I | Locally advanced non-small-cell lung cancer, non-small-cell lung cancer | Complex III | [96] |
| Proguanil | N.A. | N.A. | Acts synergistically with atovaquone | Complex I | [97] |
| Pyrvinium Pamoate | NCT05055323 | I | Resectable pancreatic ductal adenocarcinoma | Complex I | [98] |
| Vitamin E | NCT01871454 | II | Non-small-cell lung cancer | Complex II | [99] |
| ONC201 | NCT04055649 | II | Platinum-resistant epithelial ovarian, fallopian tube, or primary peritoneal cancer, diffuse midline gliomas | Complex I, II | [100] |
| Mitoxantrone | NCT04927481, NCT03839446, NCT03258320, NCT04718402 | II, II, I, I | Breast cancer, acute myeloid leukemia, prostate cancer patients, advanced gastric carcinoma | Complex V | [101] |
| Ivermectin | N.A. | N.A. | Induces the death of renal cancer cells, chronic myeloid leukemia cells, and glioblastoma cells * | Complex I | [102] |
| Anonacin | N.A. | N.A. | Delays the growth of pancreatic cancer cells * | Complex I | [103] |
| Trifluoperazine | N.A. | N.A. | Induces pancreatic ductal adenocarcinoma cell death in combination with bortezomib * | Mitochondrial Stress | [104] |

* indicates that the drug has not been validated by clinical trials but has been confirmed in in vitro cell experiments and in vivo xenograft models.

In addition to the above-mentioned drugs that have been investigated in clinical trials as hypoxia regulators, there has also been an explosion of interest in small molecules that have the potential to overcome radioresistance. For instance, since annonacin is a natural lipophilic inhibitor of complex I, in addition to its known ability to promote selective cancer cell death through NKA- and SERCA-dependent pathways, it is reasonable to speculate that annonacin may also act as a radiosensitizer through its potential ability to target OXPHOS [103,105]. In addition, experiments have shown that the anthelmintic pyrvinium pamoate inhibits the proliferation of myeloma, erythroleukemia, and pancreatic cancer cells by targeting mitochondrial respiratory complex I [98,106]. Considering this, IR combined with pyrvinium pamoate is a promising future direction for addressing the unsatisfactory effects of radiotherapy on radioresistant pancreatic cancer cells (Table 1). However, further clinical research is needed to clarify various issues that may be overlooked by new treatments, such as balancing the relationship between therapeutic effects and toxic side effects.

Given that OXPHOS involves two distinct modalities that interfere with the radiation response along with active metabolic reprogramming activity or persistent local hypoxia in some tumors, targeting mitochondrial respiration to overcome radioresistance has attracted

attention. Indeed, as the therapeutic index is the decisive factor for the utility of any therapy, those targeting OXPHOS are often limited by side effects rather than a lack of efficacy; therefore, there is an urgent need to find novel and more specific radiosensitizers.

## 4. Oncometabolites and Radioresistance

Oncometabolites, defined as metabolites that accumulate abnormally from distorted metabolic pathways, play pivotal roles in tumor transformation, cancer progression, invasiveness, and therapy resistance [107]. Mutations in the genes encoding isocitrate dehydrogenase 1/2 (IDH1/2) or promiscuous activity of lactate dehydrogenase/malate dehydrogenase (LDH/MDH) leads to the synthesis of D-2-hydroxyglutarate (D-2HG) and L-2-hydroxyglutarate (L-2HG), respectively [108]. Furthermore, loss of function of the tricarboxylic acid cycle enzymes succinate dehydrogenase (SDH) and fumarate hydratase (FH) results in the accumulation of succinate and fumarate (Figure 3) [109]. Oncometabolites act as structural mimics of α-ketoglutarate (α-KG) and thus competitively interfere with α-KG-dependent dioxygenases, which are involved in regulating the demethylation status of histones, RNA, and DNA, and targeting HIF-α degradation [110,111]. For example, oncometabolites lead to extensive hypermethylation of histone 3 lysine 9 (H3K9me3) by inhibiting histone lysine demethylase (KDM), which hinders the recruitment of DNA repair factors, leading to genomic instability that promotes tumor growth [112]. Thus, fumarate, succinate, D-2HG, and L-2HG have been characterized as bona fide tumor metabolites and have become pathognomonic hallmarks of a growing number of cancers (Figure 3), including neuroendocrine tumors, gliomas, leukemia, renal cell carcinomas, and head and neck squamous cell carcinomas [113–116]. In recent years, there has been great interest in the possible role of oncometabolites in cancer cell resistance to radiation, and numerous clinical trials have been conducted.

Furthermore, IDH1/2 mutations have been predicted in clinical trials and retrospective analyses to improve the response to radiotherapy in low-grade gliomas, showing significantly prolonged progression-free survival and overall survival [117]. However, mutated IDH1, when co-expressed with inactivating TP53 and alpha thalassemia/mental retardation syndrome X-linked gene mutations in gliomas, induces genome stability and enhances the DNA damage response, triggering resistance to IR [118]. Thus, pharmacological inhibition of the DNA repair pathway is necessary if radiotherapy demonstrates superior therapeutic advantages in IDH1/2-mutated glioma cells. Studies have shown that FH expression in gastric cancer cells is significantly higher than that in nearby normal cells and is negatively correlated with patient prognosis. In addition, cisplatin is the first-line treatment for gastric cancer, and FH can significantly inhibit the cytotoxicity of cisplatin. Recent experiments have concluded that miconazole nitrate enhances the effects of cisplatin in vitro and in vivo by inhibiting FH activity [119]. Given that activated FH restrains sensitivity to traditional chemotherapy drugs, it could have the same adverse effects on radiation therapy. Patients with hereditary leiomyomatosis, renal cell cancer (HLRCC), and a substantial accumulation of fumarate are susceptible to kidney cancer with type 2 papillary morphology, which is refractory to current radiotherapy [120,121]. Interestingly, fumarate can covalently modify GPX4 and inhibit its activity, thereby activating ferroptosis-selective HLRCC cell death [122]. Furthermore, SDH5 is required for the activity of the SDH complex, and its rapid depletion inhibits p53 degradation through the ubiquitin/proteasome pathway, thereby promoting apoptosis and enhancing NSCLC radiosensitivity [123].

Taken together, it is not difficult to see this as an interesting phenomenon, and while oncometabolites are beneficial for cancer progression, they also appear to significantly reverse the resistance of tumor tissue to IR, likely because tumors that accumulate high levels of oncometabolites are more vulnerable to therapies that cause DNA damage [124]. Moreover, it has been demonstrated that KDM induces transforming growth factor (TGF)-β2 transcriptional activation by downregulating the enrichment of H3K9me3 at its promoter region. Activated TGF-β2 further enhances Smad/ATM/Chk2 signaling, which confers radioresistance in lung cancer [125]. Therefore, oncometabolites may be suitable signals

indicative of radiosensitivity, providing new insights into possible methods for predicting radiotherapy responses in patients who cannot tolerate biopsy.

## 5. Apoptosis and Radioresistance

Apoptosis is a tightly controlled mode of programmed cell death that plays an essential role in development, tissue homeostasis, and defense against unwanted, redundant, and potentially dangerous cells, particularly in the regulation of tumorigenesis [126,127]. The mitochondrial apoptotic pathway initiated by caspases and regulated by members of the Bcl-2 family of proteins or inhibitors of apoptotic proteins may have particularly relevant roles in radiation signal transduction. In differential expression analysis of related genes in cervical cancer cell lines, 33 genes have shown changes in expression after radiation induction, which may have potential effects on the apoptosis of cervical cancer cells after radiotherapy [128]. These findings suggest that IR can lead to significant changes in the expression of apoptosis-related genes, thereby inducing radioresistance. Some genetic dysregulation, as commonly observed in apoptotic signaling pathways in aggressive cancer cells, greatly limits the efficacy of anticancer treatments such as radiotherapy, which relies on these pathways to eradicate tumors [129]. Enhancing apoptosis to improve the therapeutic effect in cancer can be accomplished in two ways: by upregulating pro-apoptotic genes or by interfering with anti-apoptotic protein function [130].

We have summarized the apoptotic molecules associated with radiation resistance, and insights into the mechanisms involved can guide subsequent therapeutic approaches as follows. (1) NF-κB is increasingly recognized as a key player in many steps from cancer initiation to progression, with some degree of activation in various tumors, such as gastric, colorectal, lung, nasopharyngeal, and prostate carcinomas [131–134]. The activity of NF-κB is often enhanced by radiation and plays a central role in the resistance of cancer cells to radiation through the activation of the pro-survival proteins Bcl-2 and Bcl-XL in downstream signaling pathways [135]. Curcumin, one of the most important inhibitors of NF-κB, significantly delays tumor regeneration in irradiated mice [136]. (2) p53, a tumor suppressor gene, also has a diametrically opposite significance in the development of radioresistance. Downregulation of p53-induced death-domain-containing protein expression and inhibition of ataxia–telangiectasia-mutated protein (ATM) directly silence NF-κB, which inhibits DNA damage repair and ultimately increases the radiosensitivity of tumor cells [129]. Conversely, radiation-induced DNA damage can also activate the downstream effector kinase Chk2 of ATM, which contributes to further activation of p53 and pro-apoptotic proteins PUMA and BAX to induce apoptosis [137]. A study showed that the loss of components in the ATM/Chk2/p53 pathway was associated with radioresistance in a glioma mouse model [138]. Radiotherapy, the standard treatment for patients with nasopharyngeal carcinoma (NPC), induces DNA methyltransferase 3B, which greatly contributes to radioresistance in NPC by methylating p53 and p21 [139]. (3) Apoptosis-related proteins in the TGF-β signaling pathway (ARTS) are alternative spliceosomes of the Sept4 gene located in the outer mitochondrial membrane [140]. As the only dual pro-apoptotic protein in vivo, ARTS directly bind to and restrain XIAP and Bcl-2 and assist p53 in inhibiting Bcl-XL [141]. Therefore, targeting the ARTS-mediated degradation of anti-apoptotic proteins may represent an effective way of sensitizing tumor cells to radiotherapy. (4) Most patients with breast cancer treated with radiotherapy are completely cured, but in partial IR-induced triple-negative breast cancer, activated STAT3 and Bcl-2 and reduced ROS promote cell proliferation, reduce apoptosis, increase angiogenesis, and increase immune evasion, thus severely compromising the effectiveness of radiotherapy [142]. Niclosamide, a small-molecule STAT3 inhibitor, leads to a significant decrease in the protein levels of downstream anti-apoptotic target genes (such as Bcl-XL and survivin) by inhibiting Tyr-705 phosphorylation and nuclear translocation of STAT3, thereby improving the survival of patients with radioresistant breast cancer [142,143]. (5) Recent studies have shown that amplification of the cancer-associated gene YWHAZ is an indicator of poor prognosis in patients with urothelial carcinoma of the bladder (UCUB) [144]. Upregulation of YWHAZ

resulted in insufficient expression of pro-apoptotic proteins (BAK and BAX) and several caspases (CASP 3, 7, and 10) involved in mitochondrial apoptotic cascade reactions, with an emphasis on radiation insensitivity [145]. Notably, gene knockdown using a specific shRNA triggered a significant increase in cell death after radiation therapy, providing a new therapeutic target for YWHAZ-overexpressing UCUB [145].

In addition, Jumonji C domain histone lysine demethylases (JmjC-KDMs), Wnt1-inducible-signaling protein 1 (WISP1), and Caveolin-1 can also interfere with apoptosis and further induce radioresistance [146–148] (Figure 4). Therefore, elucidating the precise mechanism underlying the interaction between mitochondrial apoptosis and radioresistance would benefit the development of novel radiosensitizers. Although drugs developed based on this principle still require more clinical experiments to verify their indications and safety, they undoubtedly provide a promising starting point for the treatment of tumors with high target gene expression levels.

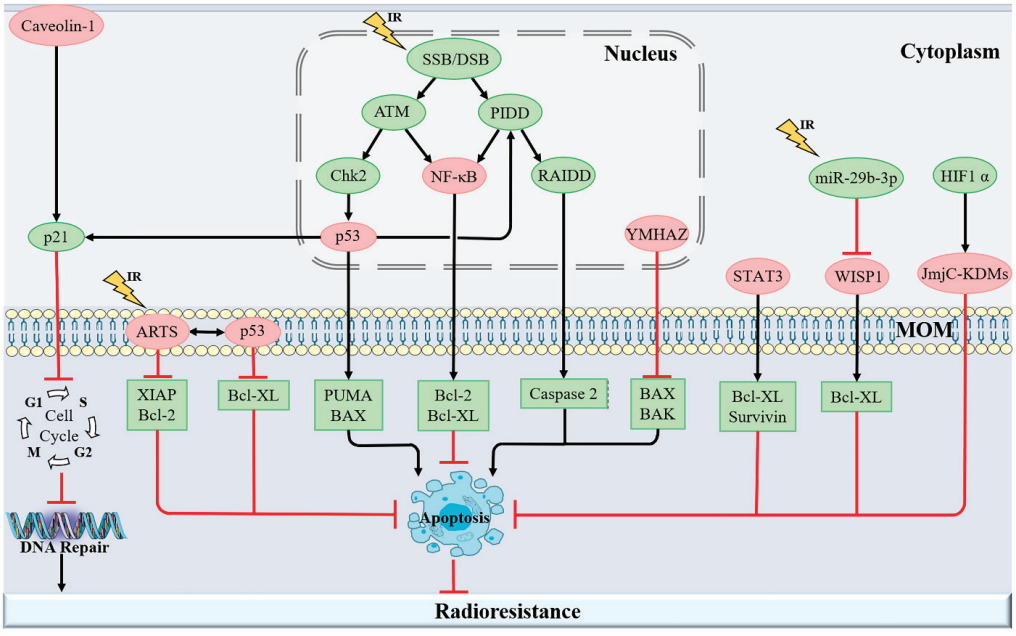


**Figure 4.** A schematic representation of the signaling mechanism of apoptosis-related molecules. IR induces DNA damage, leading to abnormal expression of mitochondria-related proteins, or directly regulates apoptosis-related genes, thereby promoting DNA damage repair and inhibiting mitochondrial apoptosis, ultimately causing the occurrence of radioresistance. Abbreviations: SSB/DSB—single-strand breaks/double-strand breaks, ATM—ataxia–telangiectasia-mutated protein, PIDD—p53-induced death-domain-containing protein, Chk2—checkpoint kinase 2, NF-κB—nuclear factor-κB, RAIDD—receptor-interacting protein (RIP)-associated ICH-1/CED-3-homologous protein with a death domain, ARTS—apoptosis-related proteins in the TGF-β signaling pathway, STAT3—signal transducer and transcriptional activator 3, WISP1—Wnt1-inducible-signaling protein 1, JmjC-KDMs—Jumonji C domain histone lysine demethylases.

## 6. Conclusions and Perspectives

Acquired radioresistance is the main clinical obstacle for patients with tumors receiving radiotherapy and is affected by several factors. Since the Warburg effect was proposed, glucose metabolism has received unprecedented attention. However, a considerable number of studies point to the development of radioresistance closely related to mitochondrial metabolism, not only because mitochondria predominate in the tolerance of malignant

cells to radiation-induced RCD, but also because it underlies metabolic reprogramming. Maintaining the normal physiological function of the mitochondria is an important factor that improves the effect of radiotherapy. To date, many small-molecule inhibitors have been developed against ROS and oncometabolites or to regulate OXPHOS and apoptosis, which can target specific receptors and enhance the radiation response of tumor tissue. However, owing to the lack of high specificity, the indiscriminate attack of radiosensitizers on non-tumor cells can have unwanted effects, which also hinders their generalization. Due to different tumor types and specific metabolic processes or molecules, we need to individualize the treatment of tumors, so the development of more effective and specific sensitizers has become an irreplaceable solution. Despite these challenges, with a deeper understanding of the mechanism of radioresistance, targeting mitochondrial metabolism to reverse radiation insensitivity may be a safe and efficient radiosensitizing method in the future and thus deserves more attention.

**Author Contributions:** Conceptualization, X.J. and Y.X.; methodology, C.B., Z.Z., J.S., and H.W.; software, C.B., J.S., H.W., and S.C.; formal analysis, Z.Z.; data curation, C.B., J.S., and S.C.; writing—original draft preparation, C.B. and Z.Z.; writing—review and editing, X.J. and Y.X.; visualization, S.C.; supervision, Y.X.; funding acquisition, X.J. All authors have read and agreed to the published version of the manuscript.

**Funding:** This research was supported by the Jilin Provincial Science and Technology Foundations (20210509003RQ and 20210402002GH), Health Talents Special Project of the Jilin Provincial Finance Department (JLSWSRCZX2021-065), Changchun Science and Technology Development Plan (21ZY29), and Achievement Transformation Guiding Foundations of the First Hospital of Jilin University (CGZHYD202012-029).

**Conflicts of Interest:** The authors declare no conflict of interest.

## References

1. Clinton, S.K.; Giovannucci, E.L.; Hursting, S.D. The World Cancer Research Fund/American Institute for Cancer Research Third Expert Report on Diet, Nutrition, Physical Activity, and Cancer: Impact and Future Directions. *J. Nutr.* **2020**, *150*, 663–671. [CrossRef] [PubMed]
2. Liu, Y.; Yang, M.; Luo, J.; Zhou, H. Radiotherapy targeting cancer stem cells "awakens" them to induce tumour relapse and metastasis in oral cancer. *Int. J. Oral Sci.* **2020**, *12*, 19. [CrossRef] [PubMed]
3. Wong, J.Y.C.; Filippi, A.R.; Dabaja, B.S.; Yahalom, J.; Specht, L. Total Body Irradiation: Guidelines from the International Lymphoma Radiation Oncology Group (ILROG). *Int. J. Radiat. Oncol. Biol. Phys.* **2018**, *101*, 521–529. [CrossRef] [PubMed]
4. Sinicrope, K.D.; Kaplan, A.B.; Brastianos, P.K. Seminoma with Neoplastic Meningitis Treated with Craniospinal Irradiation. *Oncologist* **2018**, *23*, 1385–1387. [CrossRef]
5. Demoor-Goldschmidt, C.; Chiavassa, S.; Josset, S.; Mahé, M.A.; Supiot, S. Respiratory-gated bilateral pulmonary radiotherapy for Ewing's sarcoma and nephroblastoma in children and young adults: Dosimetric and clinical feasibility studies. *Cancer Radiother.* **2017**, *21*, 124–129. [CrossRef]
6. Lee, J. Mitochondrial drug targets in neurodegenerative diseases. *Bioorg. Med. Chem. Lett.* **2016**, *26*, 714–720. [CrossRef] [PubMed]
7. Kam, W.W.; Banati, R.B. Effects of ionizing radiation on mitochondria. *Free Radic. Biol. Med.* **2013**, *65*, 607–619. [CrossRef]
8. Averbeck, D.; Rodriguez-Lafrasse, C. Role of Mitochondria in Radiation Responses: Epigenetic, Metabolic, and Signaling Impacts. *Int. J. Mol. Sci.* **2021**, *22*, 11047. [CrossRef]
9. Biau, J.; Chautard, E.; De Koning, L.; Court, F.; Pereira, B.; Verrelle, P.; Dutreix, M. Predictive biomarkers of resistance to hypofractionated radiotherapy in high grade glioma. *Radiat. Oncol.* **2017**, *12*, 123. [CrossRef]
10. Huang, R.; Xiang, J.; Zhou, P. Vitamin D, gut microbiota, and radiation-related resistance: A love-hate triangle. *J. Exp. Clin. Cancer Res.* **2019**, *38*, 493. [CrossRef]
11. McBride, W.H.; Schaue, D. Radiation-induced tissue damage and response. *J. Pathol.* **2020**, *250*, 647–655. [CrossRef] [PubMed]
12. Śliwińska-Mossoń, M.; Wadowska, K.; Trembecki, Ł.; Bil-Lula, I. Markers Useful in Monitoring Radiation-Induced Lung Injury in Lung Cancer Patients: A Review. *J. Pers. Med.* **2020**, *10*, 72. [CrossRef] [PubMed]
13. Porporato, P.E.; Filigheddu, N.; Pedro, J.M.B.; Kroemer, G.; Galluzzi, L. Mitochondrial metabolism and cancer. *Cell Res.* **2018**, *28*, 265–280. [CrossRef] [PubMed]
14. Tang, Y.; He, Y.; Zhang, P.; Wang, J.; Fan, C.; Yang, L.; Xiong, F.; Zhang, S.; Gong, Z.; Nie, S.; et al. LncRNAs regulate the cytoskeleton and related Rho/ROCK signaling in cancer metastasis. *Mol. Cancer* **2018**, *17*, 77. [CrossRef]
15. Huber, S.M.; Butz, L.; Stegen, B.; Klumpp, D.; Braun, N.; Ruth, P.; Eckert, F. Ionizing radiation, ion transports, and radioresistance of cancer cells. *Front. Physiol.* **2013**, *4*, 212. [CrossRef]
16. Fernández, L.P.; Gómez de Cedrón, M.; Ramírez de Molina, A. Alterations of Lipid Metabolism in Cancer: Implications in Prognosis and Treatment. *Front. Oncol.* **2020**, *10*, 577420. [CrossRef]

17. Wettersten, H.I.; Aboud, O.A.; Lara, P.N., Jr.; Weiss, R.H. Metabolic reprogramming in clear cell renal cell carcinoma. *Nat. Rev. Nephrol.* **2017**, *13*, 410–419. [CrossRef]
18. Yu, J.; Wei, Z.; Li, Q.; Wan, F.; Chao, Z.; Zhang, X.; Lin, L.; Meng, H.; Tian, L. Advanced Cancer Starvation Therapy by Simultaneous Deprivation of Lactate and Glucose Using a MOF Nanoplatform. *Adv. Sci.* **2021**, *8*, e2101467. [CrossRef]
19. Laussel, C.; Léon, S. Cellular toxicity of the metabolic inhibitor 2-deoxyglucose and associated resistance mechanisms. *Biochem. Pharmacol.* **2020**, *182*, 114213. [CrossRef]
20. Zhang, D.; Li, J.; Wang, F.; Hu, J.; Wang, S.; Sun, Y. 2-Deoxy-D-glucose targeting of glucose metabolism in cancer cells as a potential therapy. *Cancer Lett.* **2014**, *355*, 176–183. [CrossRef]
21. Sobhakumari, A.; Orcutt, K.P.; Love-Homan, L.; Kowalski, C.E.; Parsons, A.D.; Knudson, C.M.; Simons, A.L. 2-Deoxy-d-glucose Suppresses the In Vivo Antitumor Efficacy of Erlotinib in Head and Neck Squamous Cell Carcinoma Cells. *Oncol. Res.* **2016**, *24*, 55–64. [CrossRef] [PubMed]
22. Rashmi, R.; Huang, X.; Floberg, J.M.; Elhammali, A.E.; McCormick, M.L.; Patti, G.J.; Spitz, D.R.; Schwarz, J.K. Radioresistant Cervical Cancers Are Sensitive to Inhibition of Glycolysis and Redox Metabolism. *Cancer Res.* **2018**, *78*, 1392–1403. [CrossRef] [PubMed]
23. Lu, F.; Fang, D.; Li, S.; Zhong, Z.; Jiang, X.; Qi, Q.; Liu, Y.; Zhang, W.; Xu, X.; Liu, Y.; et al. Thioredoxin 1 supports colorectal cancer cell survival and promotes migration and invasion under glucose deprivation through interaction with G6PD. *Int. J. Biol. Sci.* **2022**, *18*, 5539–5553. [CrossRef] [PubMed]
24. Rather, G.M.; Pramono, A.A.; Szekely, Z.; Bertino, J.R.; Tedeschi, P.M. In cancer, all roads lead to NADPH. *Pharmacol. Ther.* **2021**, *226*, 107864. [CrossRef] [PubMed]
25. Jiang, P.; Du, W.; Wu, M. Regulation of the pentose phosphate pathway in cancer. *Protein. Cell* **2014**, *5*, 592–602. [CrossRef] [PubMed]
26. Kim, N.H.; Cha, Y.H.; Lee, J.; Lee, S.H.; Yang, J.H.; Yun, J.S.; Cho, E.S.; Zhang, X.; Nam, M.; Kim, N.; et al. Snail reprograms glucose metabolism by repressing phosphofructokinase PFKP allowing cancer cell survival under metabolic stress. *Nat. Commun.* **2017**, *8*, 14374. [CrossRef]
27. Wang, Y.; Chen, J.; Duan, R.; Gu, R.; Wang, W.; Wu, J.; Lian, H.; Hu, Y.; Yuan, A. High-Z-Sensitized Radiotherapy Synergizes with the Intervention of the Pentose Phosphate Pathway for In Situ Tumor Vaccination. *Adv. Mater.* **2022**, *34*, e2109726. [CrossRef]
28. Giacomini, I.; Ragazzi, E.; Pasut, G.; Montopoli, M. The Pentose Phosphate Pathway and Its Involvement in Cisplatin Resistance. *Int. J. Mol. Sci.* **2020**, *21*, 937. [CrossRef]
29. Danhier, P.; Bański, P.; Payen, V.L.; Grasso, D.; Ippolito, L.; Sonveaux, P.; Porporato, P.E. Cancer metabolism in space and time: Beyond the Warburg effect. *Biochim. Biophys. Acta Bioenerg.* **2017**, *1858*, 556–572. [CrossRef]
30. Tan, Y.Q.; Zhang, X.; Zhang, S.; Zhu, T.; Garg, M.; Lobie, P.E.; Pandey, V. Mitochondria: The metabolic switch of cellular oncogenic transformation. *Biochim. Biophys. Acta Rev. Cancer* **2021**, *1876*, 188534. [CrossRef]
31. Payen, V.L.; Zampieri, L.X.; Porporato, P.E.; Sonveaux, P. Pro- and antitumor effects of mitochondrial reactive oxygen species. *Cancer Metastasis Rev.* **2019**, *38*, 189–203. [CrossRef]
32. Grasso, D.; Medeiros, H.C.D.; Zampieri, L.X.; Bol, V.; Danhier, P.; van Gisbergen, M.W.; Bouzin, C.; Brusa, D.; Grégoire, V.; Smeets, H.; et al. Fitter Mitochondria Are Associated With Radioresistance in Human Head and Neck SQD9 Cancer Cells. *Front. Pharmacol.* **2020**, *11*, 263. [CrossRef]
33. Gao, X.; Yang, Y.; Wang, J.; Zhang, L.; Sun, C.; Wang, Y.; Zhang, J.; Dong, H.; Zhang, H.; Gao, C.; et al. Inhibition of mitochondria NADH-Ubiquinone oxidoreductase (complex I) sensitizes the radioresistant glioma U87MG cells to radiation. *Biomed. Pharmacother.* **2020**, *129*, 110460. [CrossRef]
34. Tomita, K.; Kuwahara, Y.; Igarashi, K.; Roudkenar, M.H.; Roushandeh, A.M.; Kurimasa, A.; Sato, T. Mitochondrial Dysfunction in Diseases, Longevity, and Treatment Resistance: Tuning Mitochondria Function as a Therapeutic Strategy. *Genes* **2021**, *12*, 1348. [CrossRef]
35. Wei, J.; Fang, T.; Wong, C.; Lakey, P.S.J.; Nizkorodov, S.A.; Shiraiwa, M. Superoxide Formation from Aqueous Reactions of Biogenic Secondary Organic Aerosols. *Environ. Sci. Technol.* **2021**, *55*, 260–270. [CrossRef] [PubMed]
36. Prasad, S.; Gupta, S.C.; Tyagi, A.K. Reactive oxygen species (ROS) and cancer: Role of antioxidative nutraceuticals. *Cancer Lett.* **2017**, *387*, 95–105. [CrossRef] [PubMed]
37. Tretter, V.; Hochreiter, B.; Zach, M.L.; Krenn, K.; Klein, K.U. Understanding Cellular Redox Homeostasis: A Challenge for Precision Medicine. *Int. J. Mol. Sci.* **2021**, *23*, 106. [CrossRef] [PubMed]
38. Chen, Y.; Li, Y.; Huang, L.; Du, Y.; Gan, F.; Li, Y.; Yao, Y. Antioxidative Stress: Inhibiting Reactive Oxygen Species Production as a Cause of Radioresistance and Chemoresistance. *Oxid. Med. Cell. Longev.* **2021**, *2021*, 6620306. [CrossRef]
39. Liu, J.; Liu, M.; Zhang, H.; Guo, W. High-Contrast Fluorescence Diagnosis of Cancer Cells/Tissues Based on β-Lapachone-Triggered ROS Amplification Specific in Cancer Cells. *Angew. Chem. Int. Ed. Engl.* **2021**, *60*, 12992–12998. [CrossRef]
40. Zhao, R.Z.; Jiang, S.; Zhang, L.; Yu, Z.B. Mitochondrial electron transport chain, ROS generation and uncoupling (Review). *Int. J. Mol. Med.* **2019**, *44*, 3–15. [CrossRef]
41. Weinberg, F.; Hamanaka, R.; Wheaton, W.W.; Weinberg, S.; Joseph, J.; Lopez, M.; Kalyanaraman, B.; Mutlu, G.M.; Budinger, G.R.; Chandel, N.S. Mitochondrial metabolism and ROS generation are essential for Kras-mediated tumorigenicity. *Proc. Natl. Acad. Sci. USA* **2010**, *107*, 8788–8793. [CrossRef] [PubMed]

42. Cheng, C.W.; Kuo, C.Y.; Fan, C.C.; Fang, W.C.; Jiang, S.S.; Lo, Y.K.; Wang, T.Y.; Kao, M.C.; Lee, A.Y. Overexpression of Lon contributes to survival and aggressive phenotype of cancer cells through mitochondrial complex I-mediated generation of reactive oxygen species. *Cell Death Dis.* **2013**, *4*, e681. [CrossRef] [PubMed]
43. Lee, S.L.; Ryu, H.; Son, A.R.; Seo, B.; Kim, J.; Jung, S.Y.; Song, J.Y.; Hwang, S.G.; Ahn, J. TGF-β and Hypoxia/Reoxygenation Promote Radioresistance of A549 Lung Cancer Cells through Activation of Nrf2 and EGFR. *Oxid. Med. Cell. Longev.* **2016**, *2016*, 6823471. [CrossRef] [PubMed]
44. Che, Y.; Li, Y.; Zheng, F.; Zou, K.; Li, Z.; Chen, M.; Hu, S.; Tian, C.; Yu, W.; Guo, W.; et al. TRIP4 promotes tumor growth and metastasis and regulates radiosensitivity of cervical cancer by activating MAPK, PI3K/AKT, and hTERT signaling. *Cancer Lett.* **2019**, *452*, 1–13. [CrossRef] [PubMed]
45. Liu, Y.; Shi, Q.F.; Ye, Y.C.; Tashiro, S.; Onodera, S.; Ikejima, T. Activated $O2^{\bullet -}$ and $H_2O_2$ mediated cell survival in SU11274-treated non-small-cell lung cancer A549 cells via c-Met-PI3K-Akt and c-Met-Grb2/SOS-Ras-p38 pathways. *J. Pharmacol. Sci.* **2012**, *119*, 150–159. [CrossRef]
46. Dan Dunn, J.; Alvarez, L.A.; Zhang, X.; Soldati, T. Reactive oxygen species and mitochondria: A nexus of cellular homeostasis. *Redox. Biol.* **2015**, *6*, 472–485. [CrossRef]
47. Assi, M.; Rébillard, A. The Janus-Faced Role of Antioxidants in Cancer Cachexia: New Insights on the Established Concepts. *Oxid. Med. Cell. Longev.* **2016**, *2016*, 9579868. [CrossRef]
48. Roy, K.; Wu, Y.; Meitzler, J.L.; Juhasz, A.; Liu, H.; Jiang, G.; Lu, J.; Antony, S.; Doroshow, J.H. NADPH oxidases and cancer. *Clin. Sci. (Lond)* **2015**, *128*, 863–875. [CrossRef]
49. Kim, T.W.; Hong, D.W.; Kang, C.M.; Hong, S.H. A novel PPARγligand, PPZ023, overcomes radioresistance via ER stress and cell death in human non-small-cell lung cancer cells. *Exp. Mol. Med.* **2020**, *52*, 1730–1743. [CrossRef]
50. Tsvetkov, P.; Coy, S.; Petrova, B.; Dreishpoon, M.; Verma, A.; Abdusamad, M.; Rossen, J.; Joesch-Cohen, L.; Humeidi, R.; Spangler, R.D.; et al. Copper induces cell death by targeting lipoylated TCA cycle proteins. *Science* **2022**, *375*, 1254–1261. [CrossRef]
51. Sena, L.A.; Chandel, N.S. Physiological roles of mitochondrial reactive oxygen species. *Mol. Cell* **2012**, *48*, 158–167. [CrossRef] [PubMed]
52. Porporato, P.E.; Payen, V.L.; Pérez-Escuredo, J.; De Saedeleer, C.J.; Danhier, P.; Copetti, T.; Dhup, S.; Tardy, M.; Vazeille, T.; Bouzin, C.; et al. A mitochondrial switch promotes tumor metastasis. *Cell Rep.* **2014**, *8*, 754–766. [CrossRef]
53. Torrisi, F.; Vicario, N.; Spitale, F.M.; Cammarata, F.P.; Minafra, L.; Salvatorelli, L.; Russo, G.; Cuttone, G.; Valable, S.; Gulino, R.; et al. The Role of Hypoxia and SRC Tyrosine Kinase in Glioblastoma Invasiveness and Radioresistance. *Cancers* **2020**, *12*, 2860. [CrossRef] [PubMed]
54. Torrisi, F.; Minafra, L.; Cammarata, F.P.; Savoca, G.; Calvaruso, M.; Vicario, N.; Maccari, L.; Pérès, E.A.; Özçelik, H.; Bernaudin, M.; et al. SRC Tyrosine Kinase Inhibitor and X-rays Combined Effect on Glioblastoma Cell Lines. *Int. J. Mol. Sci.* **2020**, *21*, 13917. [CrossRef] [PubMed]
55. Galluzzi, L.; Bravo-San Pedro, J.M.; Levine, B.; Green, D.R.; Kroemer, G. Pharmacological modulation of autophagy: Therapeutic potential and persisting obstacles. *Nat. Rev. Drug Discov.* **2017**, *16*, 487–511. [CrossRef] [PubMed]
56. Hausenloy, D.J.; Yellon, D.M. Ischaemic conditioning and reperfusion injury. *Nat. Rev. Cardiol.* **2016**, *13*, 193–209. [CrossRef]
57. Piskounova, E.; Agathocleous, M.; Murphy, M.M.; Hu, Z.; Huddlestun, S.E.; Zhao, Z.; Leitch, A.M.; Johnson, T.M.; DeBerardinis, R.J.; Morrison, S.J. Oxidative stress inhibits distant metastasis by human melanoma cells. *Nature* **2015**, *527*, 186–191. [CrossRef]
58. O'Day, S.; Gonzalez, R.; Lawson, D.; Weber, R.; Hutchins, L.; Anderson, C.; Haddad, J.; Kong, S.; Williams, A.; Jacobson, E. Phase II, randomized, controlled, double-blinded trial of weekly elesclomol plus paclitaxel versus paclitaxel alone for stage IV metastatic melanoma. *J. Clin. Oncol.* **2009**, *27*, 5452–5458. [CrossRef]
59. Rae, C.; Mairs, R.J. Evaluation of the radiosensitizing potency of chemotherapeutic agents in prostate cancer cells. *Int. J. Radiat. Biol.* **2017**, *93*, 194–203. [CrossRef]
60. Ryu, J.Y.; Oh, J.; Kim, S.M.; Kim, W.G.; Jeong, H.; Ahn, S.A.; Kim, S.H.; Jang, J.Y.; Yoo, B.C.; Kim, C.W.; et al. SOCS1 counteracts ROS-mediated survival signals and promotes apoptosis by modulating cell cycle to increase radiosensitivity of colorectal cancer cells. *BMB Rep.* **2022**, *55*, 198–203. [CrossRef]
61. Zhao, H.; Zhang, R.; Yan, X.; Fan, K. Superoxide dismutase nanozymes: An emerging star for anti-oxidation. *J. Mater. Chem. B* **2021**, *9*, 6939–6957. [CrossRef] [PubMed]
62. Singh, B.; Patwardhan, R.S.; Jayakumar, S.; Sharma, D.; Sandur, S.K. Oxidative stress associated metabolic adaptations regulate radioresistance in human lung cancer cells. *J. Photochem. Photobiol. B* **2020**, *213*, 112080. [CrossRef] [PubMed]
63. Hoxhaj, G.; Ben-Sahra, I.; Lockwood, S.E.; Timson, R.C.; Byles, V.; Henning, G.T.; Gao, P.; Selfors, L.M.; Asara, J.M.; Manning, B.D. Direct stimulation of NADP(+) synthesis through Akt-mediated phosphorylation of NAD kinase. *Science* **2019**, *363*, 1088–1092. [CrossRef] [PubMed]
64. Pirpour Tazehkand, A.; Salehi, R.; Velaei, K.; Samadi, N. The potential impact of trigonelline loaded micelles on Nrf2 suppression to overcome oxaliplatin resistance in colon cancer cells. *Mol. Biol. Rep.* **2020**, *47*, 5817–5829. [CrossRef]
65. Yao, W.; Lin, Z.; Shi, P.; Chen, B.; Wang, G.; Huang, J.; Sui, Y.; Liu, Q.; Li, S.; Lin, X.; et al. Delicaflavone induces ROS-mediated apoptosis and inhibits PI3K/AKT/mTOR and Ras/MEK/Erk signaling pathways in colorectal cancer cells. *Biochem. Pharmacol.* **2020**, *171*, 113680. [CrossRef]
66. Fisher, C.J.; Goswami, P.C. Mitochondria-targeted antioxidant enzyme activity regulates radioresistance in human pancreatic cancer cells. *Cancer Biol. Ther.* **2008**, *7*, 1271–1279. [CrossRef]

67. Gao, Z.; Sarsour, E.H.; Kalen, A.L.; Li, L.; Kumar, M.G.; Goswami, P.C. Late ROS accumulation and radiosensitivity in SOD1-overexpressing human glioma cells. *Free Radic. Biol. Med.* **2008**, *45*, 1501–1509. [CrossRef]
68. Lei, G.; Zhang, Y.; Koppula, P.; Liu, X.; Zhang, J.; Lin, S.H.; Ajani, J.A.; Xiao, Q.; Liao, Z.; Wang, H.; et al. The role of ferroptosis in ionizing radiation-induced cell death and tumor suppression. *Cell Res.* **2020**, *30*, 146–162. [CrossRef]
69. Schoenfeld, J.D.; Sibenaller, Z.A.; Mapuskar, K.A.; Wagner, B.A.; Cramer-Morales, K.L.; Furqan, M.; Sandhu, S.; Carlisle, T.L.; Smith, M.C.; Abu Hejleh, T.; et al. O(2)(·-) and H(2)O(2)-Mediated Disruption of Fe Metabolism Causes the Differential Susceptibility of NSCLC and GBM Cancer Cells to Pharmacological Ascorbate. *Cancer Cell* **2017**, *31*, 487–500.e488. [CrossRef]
70. Li, Z.; Zhang, H. Reprogramming of glucose, fatty acid and amino acid metabolism for cancer progression. *Cell Mol. Life Sci.* **2016**, *73*, 377–392. [CrossRef]
71. Liberti, M.V.; Locasale, J.W. The Warburg Effect: How Does it Benefit Cancer Cells? *Trends Biochem. Sci.* **2016**, *41*, 211–218. [CrossRef] [PubMed]
72. Icard, P.; Shulman, S.; Farhat, D.; Steyaert, J.M.; Alifano, M.; Lincet, H. How the Warburg effect supports aggressiveness and drug resistance of cancer cells? *Drug Resist. Updat.* **2018**, *38*, 1–11. [CrossRef]
73. Potter, M.; Newport, E.; Morten, K.J. The Warburg effect: 80 years on. *Biochem. Soc. Trans.* **2016**, *44*, 1499–1505. [CrossRef] [PubMed]
74. Warburg, O. On the origin of cancer cells. *Science* **1956**, *123*, 309–314. [CrossRef] [PubMed]
75. Vaupel, P.; Multhoff, G. Revisiting the Warburg effect: Historical dogma versus current understanding. *J. Physiol.* **2021**, *599*, 1745–1757. [CrossRef]
76. Weinhouse, S. Hepatomas. *Science* **1967**, *158*, 542–543. [CrossRef]
77. Wu, W.; Zhao, S. Metabolic changes in cancer: Beyond the Warburg effect. *Acta Biochim. Biophys. Sin. (Shanghai)* **2013**, *45*, 18–26. [CrossRef]
78. Zhang, C.; Liu, T.; Luo, P.; Gao, L.; Liao, X.; Ma, L.; Jiang, Z.; Liu, D.; Yang, Z.; Jiang, Q.; et al. Near-infrared oxidative phosphorylation inhibitor integrates acute myeloid leukemia-targeted imaging and therapy. *Sci. Adv* **2021**, *7*, eabb6104. [CrossRef]
79. Ždralević, M.; Brand, A.; Di Ianni, L.; Dettmer, K.; Reinders, J.; Singer, K.; Peter, K.; Schnell, A.; Bruss, C.; Decking, S.M.; et al. Double genetic disruption of lactate dehydrogenases A and B is required to ablate the "Warburg effect" restricting tumor growth to oxidative metabolism. *J. Biol. Chem.* **2018**, *293*, 15947–15961. [CrossRef]
80. Faubert, B.; Solmonson, A.; DeBerardinis, R.J. Metabolic reprogramming and cancer progression. *Science* **2020**, *368*, eaaw5473. [CrossRef]
81. Sancho, P.; Burgos-Ramos, E.; Tavera, A.; Bou Kheir, T.; Jagust, P.; Schoenhals, M.; Barneda, D.; Sellers, K.; Campos-Olivas, R.; Graña, O.; et al. MYC/PGC-1α Balance Determines the Metabolic Phenotype and Plasticity of Pancreatic Cancer Stem Cells. *Cell Metab.* **2015**, *22*, 590–605. [CrossRef] [PubMed]
82. Havas, K.M.; Milchevskaya, V.; Radic, K.; Alladin, A.; Kafkia, E.; Garcia, M.; Stolte, J.; Klaus, B.; Rotmensz, N.; Gibson, T.J.; et al. Metabolic shifts in residual breast cancer drive tumor recurrence. *J. Clin. Investig.* **2017**, *127*, 2091–2105. [CrossRef] [PubMed]
83. Labrie, M.; Brugge, J.S.; Mills, G.B.; Zervantonakis, I.K. Therapy resistance: Opportunities created by adaptive responses to targeted therapies in cancer. *Nat. Rev. Cancer* **2022**, *22*, 323–339. [CrossRef]
84. Li, J.; Huang, Q.; Long, X.; Guo, X.; Sun, X.; Jin, X.; Li, Z.; Ren, T.; Yuan, P.; Huang, X.; et al. Mitochondrial elongation-mediated glucose metabolism reprogramming is essential for tumour cell survival during energy stress. *Oncogene* **2017**, *36*, 4901–4912. [CrossRef]
85. Liu, Z.; Sun, Y.; Tan, S.; Liu, L.; Hu, S.; Huo, H.; Li, M.; Cui, Q.; Yu, M. Nutrient deprivation-related OXPHOS/glycolysis interconversion via HIF-1α/C-MYC pathway in U251 cells. *Tumour. Biol.* **2016**, *37*, 6661–6671. [CrossRef] [PubMed]
86. Cook, K.M.; Shen, H.; McKelvey, K.J.; Gee, H.E.; Hau, E. Targeting Glucose Metabolism of Cancer Cells with Dichloroacetate to Radiosensitize High-Grade Gliomas. *Int. J. Mol. Sci.* **2021**, *22*, 7265. [CrossRef] [PubMed]
87. Nile, D.L.; Rae, C.; Walker, D.J.; Waddington, J.C.; Vincent, I.; Burgess, K.; Gaze, M.N.; Mairs, R.J.; Chalmers, A.J. Inhibition of glycolysis and mitochondrial respiration promotes radiosensitisation of neuroblastoma and glioma cells. *Cancer Metab.* **2021**, *9*, 24. [CrossRef] [PubMed]
88. Zhou, X.; You, M.; Wang, F.; Wang, Z.; Gao, X.; Jing, C.; Liu, J.; Guo, M.; Li, J.; Luo, A.; et al. Multifunctional Graphdiyne-Cerium Oxide Nanozymes Facilitate MicroRNA Delivery and Attenuate Tumor Hypoxia for Highly Efficient Radiotherapy of Esophageal Cancer. *Adv. Mater.* **2021**, *33*, e2100556. [CrossRef]
89. Harrison, D.K.; Vaupel, P. Heterogeneity in tissue oxygenation: From physiological variability in normal tissues to pathophysiological chaos in malignant tumours. *Adv. Exp. Med. Biol.* **2014**, *812*, 25–31. [CrossRef]
90. Kim, B.; Lee, J.J.; Shin, J.S.; Suh, J.W.; Jung, S.; Hwang, G.S.; Lee, H.Y.; Lee, K.J. Nm23-H1 activator phenylbutenoid dimer exerts cytotoxic effects on metastatic breast cancer cells by inducing mitochondrial dysfunction only under glucose starvation. *Sci. Rep.* **2021**, *11*, 23549. [CrossRef]
91. Boreel, D.F.; Span, P.N.; Heskamp, S.; Adema, G.J.; Bussink, J. Targeting Oxidative Phosphorylation to Increase the Efficacy of Radio- and Immune-Combination Therapy. *Clin. Cancer Res.* **2021**, *27*, 2970–2978. [CrossRef] [PubMed]
92. de Mey, S.; Jiang, H.; Corbet, C.; Wang, H.; Dufait, I.; Law, K.; Bastien, E.; Verovski, V.; Gevaert, T.; Feron, O.; et al. Antidiabetic Biguanides Radiosensitize Hypoxic Colorectal Cancer Cells Through a Decrease in Oxygen Consumption. *Front. Pharmacol.* **2018**, *9*, 1073. [CrossRef] [PubMed]

93. Huang, W.; Zeng, Y.C. A candidate for lung cancer treatment: Arsenic trioxide. *Clin. Transl. Oncol.* **2019**, *21*, 1115–1126. [CrossRef] [PubMed]
94. Diepart, C.; Karroum, O.; Magat, J.; Feron, O.; Verrax, J.; Calderon, P.B.; Grégoire, V.; Leveque, P.; Stockis, J.; Dauguet, N.; et al. Arsenic trioxide treatment decreases the oxygen consumption rate of tumor cells and radiosensitizes solid tumors. *Cancer Res.* **2012**, *72*, 482–490. [CrossRef] [PubMed]
95. Benej, M.; Hong, X.; Vibhute, S.; Scott, S.; Wu, J.; Graves, E.; Le, Q.T.; Koong, A.C.; Giaccia, A.J.; Yu, B.; et al. Papaverine and its derivatives radiosensitize solid tumors by inhibiting mitochondrial metabolism. *Proc. Natl. Acad. Sci. USA* **2018**, *115*, 10756–10761. [CrossRef]
96. Mudassar, F.; Shen, H.; O'Neill, G.; Hau, E. Targeting tumor hypoxia and mitochondrial metabolism with anti-parasitic drugs to improve radiation response in high-grade gliomas. *J. Exp. Clin. Cancer Res.* **2020**, *39*, 208. [CrossRef]
97. Bridges, H.R.; Jones, A.J.; Pollak, M.N.; Hirst, J. Effects of metformin and other biguanides on oxidative phosphorylation in mitochondria. *Biochem. J.* **2014**, *462*, 475–487. [CrossRef]
98. Harada, Y.; Ishii, I.; Hatake, K.; Kasahara, T. Pyrvinium pamoate inhibits proliferation of myeloma/erythroleukemia cells by suppressing mitochondrial respiratory complex I and STAT3. *Cancer Lett.* **2012**, *319*, 83–88. [CrossRef]
99. Yan, B.; Stantic, M.; Zobalova, R.; Bezawork-Geleta, A.; Stapelberg, M.; Stursa, J.; Prokopova, K.; Dong, L.; Neuzil, J. Mitochondrially targeted vitamin E succinate efficiently kills breast tumour-initiating cells in a complex II-dependent manner. *BMC Cancer* **2015**, *15*, 401. [CrossRef]
100. Pruss, M.; Dwucet, A.; Tanriover, M.; Hlavac, M.; Kast, R.E.; Debatin, K.M.; Wirtz, C.R.; Halatsch, M.E.; Siegelin, M.D.; Westhoff, M.A.; et al. Dual metabolic reprogramming by ONC201/TIC10 and 2-Deoxyglucose induces energy depletion and synergistic anti-cancer activity in glioblastoma. *Br. J. Cancer* **2020**, *122*, 1146–1157. [CrossRef]
101. Rossato, L.G.; Costa, V.M.; Dallegrave, E.; Arbo, M.; Silva, R.; Ferreira, R.; Amado, F.; Dinis-Oliveira, R.J.; Duarte, J.A.; de Lourdes Bastos, M.; et al. Mitochondrial cumulative damage induced by mitoxantrone: Late onset cardiac energetic impairment. *Cardiovasc. Toxicol.* **2014**, *14*, 30–40. [CrossRef] [PubMed]
102. Juarez, M.; Schcolnik-Cabrera, A.; Dueñas-Gonzalez, A. The multitargeted drug ivermectin: From an antiparasitic agent to a repositioned cancer drug. *Am. J. Cancer Res.* **2018**, *8*, 317–331. [PubMed]
103. Yiallouris, A.; Patrikios, I.; Johnson, E.O.; Sereti, E.; Dimas, K.; De Ford, C.; Fedosova, N.U.; Graier, W.F.; Sokratous, K.; Kyriakou, K.; et al. Annonacin promotes selective cancer cell death via NKA-dependent and SERCA-dependent pathways. *Cell Death Dis.* **2018**, *9*, 764. [CrossRef]
104. Huang, C.; Lan, W.; Fraunhoffer, N.; Meilerman, A.; Iovanna, J.; Santofimia-Castaño, P. Dissecting the Anticancer Mechanism of Trifluoperazine on Pancreatic Ductal Adenocarcinoma. *Cancers* **2019**, *11*, 1869. [CrossRef]
105. Rottscholl, R.; Haegele, M.; Jainsch, B.; Xu, H.; Respondek, G.; Höllerhage, M.; Rösler, T.W.; Bony, E.; Le Ven, J.; Guérineau, V.; et al. Chronic consumption of Annona muricata juice triggers and aggravates cerebral tau phosphorylation in wild-type and MAPT transgenic mice. *J. Neurochem.* **2016**, *139*, 624–639. [CrossRef]
106. Schultz, C.W.; McCarthy, G.A.; Nerwal, T.; Nevler, A.; DuHadaway, J.B.; McCoy, M.D.; Jiang, W.; Brown, S.Z.; Goetz, A.; Jain, A.; et al. The FDA-Approved Anthelmintic Pyrvinium Pamoate Inhibits Pancreatic Cancer Cells in Nutrient-Depleted Conditions by Targeting the Mitochondria. *Mol. Cancer Ther.* **2021**, *20*, 2166–2176. [CrossRef]
107. Vasan, K.; Werner, M.; Chandel, N.S. Mitochondrial Metabolism as a Target for Cancer Therapy. *Cell Metab.* **2020**, *32*, 341–352. [CrossRef] [PubMed]
108. Nadtochiy, S.M.; Schafer, X.; Fu, D.; Nehrke, K.; Munger, J.; Brookes, P.S. Acidic pH Is a Metabolic Switch for 2-Hydroxyglutarate Generation and Signaling. *J. Biol. Chem.* **2016**, *291*, 20188–20197. [CrossRef] [PubMed]
109. Linehan, W.M.; Schmidt, L.S.; Crooks, D.R.; Wei, D.; Srinivasan, R.; Lang, M.; Ricketts, C.J. The Metabolic Basis of Kidney Cancer. *Cancer Discov.* **2019**, *9*, 1006–1021. [CrossRef]
110. Xu, W.; Yang, H.; Liu, Y.; Yang, Y.; Wang, P.; Kim, S.H.; Ito, S.; Yang, C.; Wang, P.; Xiao, M.T.; et al. Oncometabolite 2-hydroxyglutarate is a competitive inhibitor of α-ketoglutarate-dependent dioxygenases. *Cancer Cell* **2011**, *19*, 17–30. [CrossRef]
111. Han, S.; Liu, Y.; Cai, S.J.; Qian, M.; Ding, J.; Larion, M.; Gilbert, M.R.; Yang, C. IDH mutation in glioma: Molecular mechanisms and potential therapeutic targets. *Br. J. Cancer* **2020**, *122*, 1580–1589. [CrossRef] [PubMed]
112. Sulkowski, P.L.; Oeck, S.; Dow, J.; Economos, N.G.; Mirfakhraie, L.; Liu, Y.; Noronha, K.; Bao, X.; Li, J.; Shuch, B.M.; et al. Oncometabolites suppress DNA repair by disrupting local chromatin signalling. *Nature* **2020**, *582*, 586–591. [CrossRef] [PubMed]
113. Dona, M.; Neijman, K.; Timmers, H. MITOCHONDRIA: Succinate dehydrogenase subunit B-associated phaeochromocytoma and paraganglioma. *Int. J. Biochem. Cell Biol.* **2021**, *134*, 105949. [CrossRef] [PubMed]
114. Pirozzi, C.J.; Yan, H. The implications of IDH mutations for cancer development and therapy. *Nat. Rev. Clin. Oncol.* **2021**, *18*, 645–661. [CrossRef]
115. Yong, C.; Stewart, G.D.; Frezza, C. Oncometabolites in renal cancer. *Nat. Rev. Nephrol.* **2020**, *16*, 156–172. [CrossRef] [PubMed]
116. Terra, X.; Ceperuelo-Mallafré, V.; Merma, C.; Benaiges, E.; Bosch, R.; Castillo, P.; Flores, J.C.; León, X.; Valduvieco, I.; Basté, N.; et al. Succinate Pathway in Head and Neck Squamous Cell Carcinoma: Potential as a Diagnostic and Prognostic Marker. *Cancers* **2021**, *13*, 1653. [CrossRef]
117. Buckner, J.C.; Shaw, E.G.; Pugh, S.L.; Chakravarti, A.; Gilbert, M.R.; Barger, G.R.; Coons, S.; Ricci, P.; Bullard, D.; Brown, P.D.; et al. Radiation plus Procarbazine, CCNU, and Vincristine in Low-Grade Glioma. *N. Engl. J. Med.* **2016**, *374*, 1344–1355. [CrossRef]

118. Núñez, F.J.; Mendez, F.M.; Kadiyala, P.; Alghamri, M.S.; Savelieff, M.G.; Garcia-Fabiani, M.B.; Haase, S.; Koschmann, C.; Calinescu, A.A.; Kamran, N.; et al. IDH1-R132H acts as a tumor suppressor in glioma via epigenetic up-regulation of the DNA damage response. *Sci. Transl. Med.* **2019**, *11*, eaaq1427. [CrossRef]
119. Yu, H.E.; Wang, F.; Yu, F.; Zeng, Z.L.; Wang, Y.; Lu, Y.X.; Jin, Y.; Wang, D.S.; Qiu, M.Z.; Pu, H.Y.; et al. Suppression of fumarate hydratase activity increases the efficacy of cisplatin-mediated chemotherapy in gastric cancer. *Cell Death Dis.* **2019**, *10*, 413. [CrossRef]
120. Tomlinson, I.P.; Alam, N.A.; Rowan, A.J.; Barclay, E.; Jaeger, E.E.; Kelsell, D.; Leigh, I.; Gorman, P.; Lamlum, H.; Rahman, S.; et al. Germline mutations in FH predispose to dominantly inherited uterine fibroids, skin leiomyomata and papillary renal cell cancer. *Nat. Genet.* **2002**, *30*, 406–410. [CrossRef]
121. Forde, C.; Lim, D.H.K.; Alwan, Y.; Burghel, G.; Butland, L.; Cleaver, R.; Dixit, A.; Evans, D.G.; Hanson, H.; Lalloo, F.; et al. Hereditary Leiomyomatosis and Renal Cell Cancer: Clinical, Molecular, and Screening Features in a Cohort of 185 Affected Individuals. *Eur. Urol. Oncol.* **2020**, *3*, 764–772. [CrossRef] [PubMed]
122. Kerins, M.J.; Milligan, J.; Wohlschlegel, J.A.; Ooi, A. Fumarate hydratase inactivation in hereditary leiomyomatosis and renal cell cancer is synthetic lethal with ferroptosis induction. *Cancer Sci.* **2018**, *109*, 2757–2766. [CrossRef] [PubMed]
123. Zong, Y.; Li, Q.; Zhang, F.; Xian, X.; Wang, S.; Xia, J.; Li, J.; Tuo, Z.; Xiao, G.; Liu, L.; et al. SDH5 Depletion Enhances Radiosensitivity by Regulating p53: A New Method for Noninvasive Prediction of Radiotherapy Response. *Theranostics* **2019**, *9*, 6380–6395. [CrossRef] [PubMed]
124. Chen, L.L.; Xiong, Y. Tumour metabolites hinder DNA repair. *Nature* **2020**, *582*, 492–494. [CrossRef]
125. Jie, X.; Fong, W.P.; Zhou, R.; Zhao, Y.; Zhao, Y.; Meng, R.; Zhang, S.; Dong, X.; Zhang, T.; Yang, K.; et al. USP9X-mediated KDM4C deubiquitination promotes lung cancer radioresistance by epigenetically inducing TGF-β2 transcription. *Cell Death Differ.* **2021**, *28*, 2095–2111. [CrossRef] [PubMed]
126. Dhuriya, Y.K.; Sharma, D.; Naik, A.A. Cellular demolition: Proteins as molecular players of programmed cell death. *Int. J. Biol. Macromol.* **2019**, *138*, 492–503. [CrossRef]
127. Kesavardhana, S.; Malireddi, R.K.S.; Kanneganti, T.D. Caspases in Cell Death, Inflammation, and Pyroptosis. *Annu. Rev. Immunol.* **2020**, *38*, 567–595. [CrossRef]
128. Liu, S.S.; Cheung, A.N.; Ngan, H.Y. Differential gene expression in cervical cancer cell lines before and after ionizing radiation. *Int. J. Oncol.* **2003**, *22*, 1091–1099. [CrossRef]
129. Seshacharyulu, P.; Baine, M.J.; Souchek, J.J.; Menning, M.; Kaur, S.; Yan, Y.; Ouellette, M.M.; Jain, M.; Lin, C.; Batra, S.K. Biological determinants of radioresistance and their remediation in pancreatic cancer. *Biochim. Biophys. Acta Rev. Cancer* **2017**, *1868*, 69–92. [CrossRef]
130. Hafezi, S.; Rahmani, M. Targeting BCL-2 in Cancer: Advances, Challenges, and Perspectives. *Cancers* **2021**, *13*, 1292. [CrossRef]
131. Yu, H.; Lin, L.; Zhang, Z.; Zhang, H.; Hu, H. Targeting NF-κB pathway for the therapy of diseases: Mechanism and clinical study. *Signal. Transduct. Target Ther.* **2020**, *5*, 209. [CrossRef] [PubMed]
132. Rasmi, R.R.; Sakthivel, K.M.; Guruvayoorappan, C. NF-κB inhibitors in treatment and prevention of lung cancer. *Biomed. Pharmacother.* **2020**, *130*, 110569. [CrossRef] [PubMed]
133. Thomas-Jardin, S.E.; Dahl, H.; Nawas, A.F.; Bautista, M.; Delk, N.A. NF-κB signaling promotes castration-resistant prostate cancer initiation and progression. *Pharmacol. Ther.* **2020**, *211*, 107538. [CrossRef] [PubMed]
134. Huang, W.; Zhang, L.; Yang, M.; Wu, X.; Wang, X.; Huang, W.; Yuan, L.; Pan, H.; Wang, Y.; Wang, Z.; et al. Cancer-associated fibroblasts promote the survival of irradiated nasopharyngeal carcinoma cells via the NF-κB pathway. *J. Exp. Clin. Cancer Res.* **2021**, *40*, 87. [CrossRef] [PubMed]
135. Haselager, M.; Thijssen, R.; West, C.; Young, L.; Van Kampen, R.; Willmore, E.; Mackay, S.; Kater, A.; Eldering, E. Regulation of Bcl-XL by non-canonical NF-κB in the context of CD40-induced drug resistance in CLL. *Cell Death Differ.* **2021**, *28*, 1658–1668. [CrossRef]
136. Mortezaee, K.; Salehi, E.; Mirtavoos-Mahyari, H.; Motevaseli, E.; Najafi, M.; Farhood, B.; Rosengren, R.J.; Sahebkar, A. Mechanisms of apoptosis modulation by curcumin: Implications for cancer therapy. *J. Cell. Physiol.* **2019**, *234*, 12537–12550. [CrossRef]
137. Janssens, S.; Tinel, A.; Lippens, S.; Tschopp, J. PIDD mediates NF-kappaB activation in response to DNA damage. *Cell* **2005**, *123*, 1079–1092. [CrossRef]
138. McCann, E.; O'Sullivan, J.; Marcone, S. Targeting cancer-cell mitochondria and metabolism to improve radiotherapy response. *Transl. Oncol.* **2021**, *14*, 100905. [CrossRef]
139. Wu, C.; Guo, E.; Ming, J.; Sun, W.; Nie, X.; Sun, L.; Peng, S.; Luo, M.; Liu, D.; Zhang, L.; et al. Radiation-Induced DNMT3B Promotes Radioresistance in Nasopharyngeal Carcinoma through Methylation of p53 and p21. *Mol. Ther. Oncolytics* **2020**, *17*, 306–319. [CrossRef]
140. Maimon, N.; Zamir, Z.Z.; Kalkar, P.; Zeytuni-Timor, O.; Schif-Zuck, S.; Larisch, S.; Ariel, A. The pro-apoptotic ARTS protein induces neutrophil apoptosis, efferocytosis, and macrophage reprogramming to promote resolution of inflammation. *Apoptosis* **2020**, *25*, 558–573. [CrossRef]
141. Bian, C.; Su, J.; Zheng, Z.; Wei, J.; Wang, H.; Meng, L.; Xin, Y.; Jiang, X. ARTS, an unusual septin, regulates tumorigenesis by promoting apoptosis. *Biomed. Pharmacother.* **2022**, *152*, 113281. [CrossRef] [PubMed]
142. Wang, Y.; Shen, Y.; Wang, S.; Shen, Q.; Zhou, X. The role of STAT3 in leading the crosstalk between human cancers and the immune system. *Cancer Lett.* **2018**, *415*, 117–128. [CrossRef] [PubMed]

143. Lu, L.; Dong, J.; Wang, L.; Xia, Q.; Zhang, D.; Kim, H.; Yin, T.; Fan, S.; Shen, Q. Activation of STAT3 and Bcl-2 and reduction of reactive oxygen species (ROS) promote radioresistance in breast cancer and overcome of radioresistance with niclosamide. *Oncogene* **2018**, *37*, 5292–5304. [CrossRef]
144. Liu, S.; Jiang, H.; Wen, H.; Ding, Q.; Feng, C. Knockdown of tyrosine 3-monooxygenase/tryptophan 5-monooxygenase activation protein zeta (YWHAZ) enhances tumorigenesis both in vivo and in vitro in bladder cancer. *Oncol. Rep.* **2018**, *39*, 2127–2135. [CrossRef] [PubMed]
145. Yu, C.C.; Li, C.F.; Chen, I.H.; Lai, M.T.; Lin, Z.J.; Korla, P.K.; Chai, C.Y.; Ko, G.; Chen, C.M.; Hwang, T.; et al. YWHAZ amplification/overexpression defines aggressive bladder cancer and contributes to chemo-/radio-resistance by suppressing caspase-mediated apoptosis. *J. Pathol.* **2019**, *248*, 476–487. [CrossRef]
146. Macedo-Silva, C.; Miranda-Gonçalves, V.; Lameirinhas, A.; Lencart, J.; Pereira, A.; Lobo, J.; Guimarães, R.; Martins, A.T.; Henrique, R.; Bravo, I.; et al. JmjC-KDMs KDM3A and KDM6B modulate radioresistance under hypoxic conditions in esophageal squamous cell carcinoma. *Cell Death Dis.* **2020**, *11*, 1068. [CrossRef]
147. Mao, A.; Tang, J.; Tang, D.; Wang, F.; Liao, S.; Yuan, H.; Tian, C.; Sun, C.; Si, J.; Zhang, H.; et al. MicroRNA-29b-3p enhances radiosensitivity through modulating WISP1-mediated mitochondrial apoptosis in prostate cancer cells. *J. Cancer* **2020**, *11*, 6356–6364. [CrossRef]
148. Codenotti, S.; Marampon, F.; Triggiani, L.; Bonù, M.L.; Magrini, S.M.; Ceccaroli, P.; Guescini, M.; Gastaldello, S.; Tombolini, V.; Poliani, P.L.; et al. Caveolin-1 promotes radioresistance in rhabdomyosarcoma through increased oxidative stress protection and DNA repair. *Cancer Lett.* **2021**, *505*, 1–12. [CrossRef]

MDPI
St. Alban-Anlage 66
4052 Basel
Switzerland
Tel. +41 61 683 77 34
Fax +41 61 302 89 18
www.mdpi.com

*Antioxidants* Editorial Office
E-mail: antioxidants@mdpi.com
www.mdpi.com/journal/antioxidants

Academic Open
Access Publishing

www.mdpi.com

ISBN 978-3-0365-8189-7